THE PREDICTION OF VIBRATION IN LARGE ELECTRIC MACHINES

SEAMUS GARVEY

Doctor of Philosophy

THE UNIVERSITY OF ASTON IN BIRMINGHAM

OCTOBER 1988

Acknowledgements

I wish to thank the Department of Mechanical and Production Engineering at Aston University and GEC Large Machines Ltd., Rugby without whose participation the investigation would not have taken place.

I wish also to express particular thanks to Dr. J. E. Penny of the University for his assistance in the work and his tolerance. Special thanks must also go to Mr. A. J. Gilbert, formerly of GEC Large Machines, Rugby. It was his foresight and organisational skill which launched the project.

The contributions of Mr. I. McShane, and Mr. P. E. Clarke (both of GEC Large Machines Ltd.) and Mr. J. Sherlock (of GEC Electrical Projects Ltd., Rugby) are also gratefully acknowledged.

Seamus D. Garvey

October 1988.

To my family and Antonia.

The University of Aston in Birmingham

THE PREDICTION OF VIBRATION IN LARGE ELECTRIC MACHINES

Seamus Garvey.

Thesis submitted for the degree of Doctor of Philosophy.

1988

This thesis reports the development of a reliable method for the prediction of the vibration of large electric machines resulting from electromagnetic forces. The machines of primary interest are DC ship-propulsion motors but much of the work reported has broader significance. The investigation has involved work in five principal areas.

(1) The development and use of dynamic substructuring methods.
(2) The development of special elements to represent individual machine components
(3) Laboratory scale investigations to establish empirical values for properties which affect machine vibration levels.
(4) Experiments on machines on the factory test-bed to provide data for correlation with prediction.
(5) Reasoning with regard to the effect of various design features.

The limiting factor in producing good models for machines in vibration is the computation time required for an analysis to take place. Dynamic substructuring methods were adopted early in the project to maximise the efficiency of the analysis. A review of existing substructure representation and composite-structure assembly methods includes comments on which are most suitable for this application. In three appendices to the main volume methods are presented which were developed by the author to accelerate analyses. Despite significant advances in this respect, the limiting factor in machine analyses is still computation time.

The representation of individual machine components was addressed as another means by which the time required for an analysis could be reduced. This has resulted in the development of special elements which are more efficient than their finite-element counterparts.

The laboratory scale experiments reported were undertaken to establish empirical values for the properties of three distinct features - lamination stacks, bolted-flange joints in rings and cylinders and the shimmed pole-yoke joint. These are central to the preparation of an accurate machine model.

The theoretical methods are tested numerically and correlated with tests on two machines (running and static).

A system has been devised using which the general electromagnetic forcing may be split into its most fundamental components. These components are considered individually in order to draw some conclusions about the probable effects of various machine design features.

Key-Words: Vibration; Response; DC Machines; Component-Modes; Finite-Element.

CONTENTS

LIST OF FIGURES

LIST OF TABLES

Chapter 1.

INTRODUCTION

§1.1 Background.

This research project began in October 1984 as the mechanical half of a coordinated electromagnetic and mechanical investigation into the prediction and potential supression of vibration in large electrical machines. The project was instigated by Mr. M. Wright, the Managing Director of GEC Large Machines Ltd., Rugby at the time, and was handled as an autonomous contract for MOD(N). The machines of specific interest were propulsion motors - an area in which GEC Large Machines has considerable experience and expertise.

Two graduates - the author and Mr. A N Wignall were recruited by GEC to undertake the work. The project was managed by Mr. A. J. Gilbert.

§1.2 Objectives.

The project brief initially covered many possible areas of study and was condensed in the early stages of the investigation according to timescale and importance.

The electromagnetic part of the project was directed at establishing a means by which a reliable prediction of the electromagnetic forces

acting on the stators of machines could be made. This objective has been fulfilled in the electromagnetic study Wignall (A.1987).

The mechanical objectives were specified as:

(1) To establish a method by which the response to forcing of a large electrical machine stator could be predicted and investigated.

(2) To examine the effects of various controllable features on the response and thereby produce criteria for design decisions in order to minimise vibration.

The original intention was that both DC and synchronous AC machines would be examined if the timescale allowed. The priority was with DC machines. Where possible, work has been concentrated on aspects which are common to both machines. It has only been possible to include experimentation and verification for DC machines.

§1.3 Scope of the Work.

In the course of this work a number of different areas have been encountered. Initially, to acquire some experience with the dynamic modelling of machines and structures in general, a number of finite-element models were prepared and solved. The use of finite element models to represent the entire machine was abandoned for reasons outlined in chapter 3. Attention was turned to the combined use of dynamic substructuring techniques and single-element component

models. Even with the use of dynamic substructuring, the times for analyses of realistic three-dimensional models were prohibitive and the author has spent some effort in optimising the substructuring processes used. This optimisation accounts for a worthwhile fraction of the outcome of the research and the topic of dynamic substructuring is given proportionate attention in chapter 3. The use of single-element component models has proved one of the more powerful aspects to finding a suitable prediction method. The mass and stiffness matrices were derived using assumptions appropriate to the relative dimensions of the beam/cylinder/disc etc. The derivations are from first principles and the matrices will inevitably resemble matrices created by previous authors on the topic of finite-element derivations. The emphasis in this case has been on finding reliable elements suitable to the application rather than doing an exhaustive study. Thus, in chapter 4, which presents the derivations, a full review of related literature is not attempted. Instead, one or more verification examples are included for each element which prove the element.

The experimental work has included both laboratory-scale investigations and tests on machines on the factory testbed. The laboratory work was directed at finding useable values for some of the hitherto undetermined properties which clearly influence machine response. Three separate investigations of this sort have been carried out. The work on the properties of laminated components was conducted entirely by the author. The experiments relating to the properties of the bolted-flange joint in cylinders and pole-root flexibility were designed and partly done by the author. The greater

part of the actual experimental work was done by Masters degree students as four-month research projects. The author (and A. N. Wignall) contributed to the design and execution of the tests on machines on the factory testbed.

§1.4 Two distinct forms of stator.

Rotating electrical machines in general fall into two categories, AC and DC. The stators of each are vastly different in some respects, similar in others. This investigation is concentrated on the DC machine but many of the concepts and techniques developed apply equally well to both DC and AC machines. The common factors and differences in these machines are explained briefly here to clarify which aspects of the work reported in the body of the thesis are applicable to which machines.

The construction of both types of stator is described briefly in the relevant sections to follow. It is appropriate to itemise the principal features which they have in common and the principal differences here to clarify which analysis techniques are applicable to both and which are useful in one case but not the other.

Both the AC and DC stators may be approximately represented as cylinders with additional components affixed to the inner and outer surfaces. The cylinders may be split or complete. In both cases, the dominating mass and stiffness for small oscillations derives from the flux-carrying circuit. Levels of stator vibration are primarily determined by the radial thickness of this circuit compared with the

magnitude of the forcing. Both stators generally include some laminated portions and a number of types of joint which features can dramatically influence the vibrational behaviour of the machine.

The contrasting details of the stators include the following. The AC stator is relatively uniform in the circumferential and axial planes whereas the DC stator is not - having a relatively small number of discrete poles which behave as concentrated masses at the low end of the frequency spectrum. The AC stator core is invariably built into a frame which provides support and becomes an integral part of the transmission path between the airgap - where electromagnetic forces act - and the external support structure, unlike most DC machines. The magnetic circuit of the AC machine must be laminated to reduce eddy-current losses whilst the yoke of the DC machine which provides the magnetic path and the strength of the machine, is more usually solid and theoretically sees no alternating flux. The windings of the AC stator may be considered to be intimately fixed to the stator for all frequencies over the range for which one might reasonably expect to model the machines. The coils of the DC machine have been found in the course of this work to oscillate relatively independently of the yoke.

Both the AC and DC stators can be modelled to arbitrary degrees of accuracy given sufficient computing resources and reliable values for the properties of those features which cannot be modelled directly (bolted joints and interlaminar properties for stacks of laminations are examples). Some idea of the required computing power can be obtained from the early sections of chapter 3.

§1.5 Calculation of Response or Resonance.

Ultimately, the engineer concerned with the vibration of a machine is only interested in knowing the levels of motion which will occur. The response of any structure to a sinusoidal force can be considered to be the sum of the responses of the individual modes of the structure to that forcing. If the forcing is known, then for many structures, it is necessary to study only a limited subset of the modes of the system with regard to estimating the response.

This concept is the kingpin of all of the papers on the mechanical response of machine frames except some of those which report the use of the finite-element method. The way in which it is applied differs slightly from case to case. One possibility is to compute the natural frequencies of presumed shapes of deformation for which it is known that there will be some forcing. Then if the frequency of the forcing does not lie near any of the natural frequencies, the machine will at least be free from catastrophic vibrations. The response of the frame cannot be known unless the amplitude of the forcing is known but the design can be optimised to some extent by maximising the detuning. One problem here is that the accurate calculation of natural frequencies - other than those of the most fundamental modes - is notoriously difficult for any structure other than the most simple one. The scatter of values for some parameters in machines contributes to the difficulty. In some circumstances, the most fundamental modes are worthy of consideration. In the case of the DC machine in particular, the

first-order excitation of these modes can be designed out so that the modes of real interest have associated resonances lying well up the frequency spectrum. As machine size increases, more and more resonances will be found to occur in a given range. The avoidance of all resonances in a machine whose running-speed is constant is a difficult design task. It is impossible to avoid all resonances of a machine for which the running speed is a variable.

The alternative and more satisfactory approach is to calculate both the frequency and a mass-normalised shape of deformation for all of the modes which may be excited and to have values for the magnitudes of the applied forces. This data may be combined to yield figures for the vibration at every point on the machine at any frequency including the resonant frequencies. Two factors will govern the actual resonant response.

(1) The value of the damping for that mode.

(2) The range of linearity of the various deforming portions of the structure.

Structures with virtually zero damping often have finite response at resonance governed by the limited range of linearity of the force-displacement relations. We shall see that this is not a useful fact in the vibration of large machines under normal circumstances, since the vibration levels aimed at fall well below those which would be likely to cause significant nonlinearity in the joints and components.

Compared with the technique of simply attempting to ensure that resonances are avoided as much as possible, the alternative of designing to ensure that the vibration levels themselves are kept within a band has a number of obvious advantages.

(1) Some modes can be allowed to be excited to resonance if their peak amplitude is sufficiently small where the specification is concerned.

(2) The engineer has a much better idea of the comparitive value of two designs as regards vibration merit.

§1.6 Damping in machine stators.

It is to be expected that the success of studying the response of a machine stator over a broad band of frequencies is quite dependent on having available reliable values for the damping present in the frame. One technique common in the literature for AC machines is to estimate a single damping coefficient for all modes based (one presumes) on past experience. This is less than satisfactory. The materials from which machine stators are built have - for the most part - characteristic damping levels considerably lower than the damping figures which are actually used in some calculations. There is sufficient evidence to demonstrate that much of the damping apparent in machine stators is not accountable by considering internal material damping alone. Some damping is inevitably contributed by those joints of the machine which have sufficient flexibility to store and dissipate energy. The pole-yoke

joint and the joint occuring between two halves of a yoke have been studied experimentally for damping properties and damping figures are found which are considerably higher than the coefficients for the materials involved. It is possible to further increase these damping coefficients by selecting special shim materials in the case of the pole-yoke joint and applying a viscous 'lubricant' to the faces of the flanges in the bolted-flange joint.

Damping can be modelled in a number of ways. In the context of machine vibration, the 'hysteretic' or 'structural' damping model is most appropriate in virtually all cases. The other principal option is the 'viscous' model. 'Hysteretic' damping dissipates the same energy per cycle regardless of frequency whilst the energy dissipated per cycle by 'viscous' damping is proportional to the square of the frequency. The mechanisms of energy dissipation most prevalent in large electrical machines are material damping, slip-with-friction and plastic deformation. For all of these mechanisms, a hysteretic damping model is known to be more appropriate than a viscous model.

§1.7 Forces Common to All Rotating Electrical Machines.

The force patterns experienced by DC machines in operation differ substantially from those experienced by AC machines. All rotating machines are subject to the following categories of forcing and some procedures for controlling the resulting vibration levels are well established.

(i) Imbalance forces due to the revolution of the armature. Virtually all rotors of electrical or other machines are balanced to reduce the presence of these forces. However, some degree of imbalance must always exist and this will cause a once-per-revolution force to occur at the bearings of the machine.

(ii) Bearing forces. Rolling-element bearings have characteristic frequencies related to the rotational speed of the shaft which they support. Rolling element bearings have finite life and a lower load-bearing capacity than journal bearings and the latter are generally preferred despite being significantly more expensive. Journal bearings produce a wide spectrum of relatively random forcing frequencies in which no one frequency is predominant under normal conditions. Rotor instability such as oil-whip or oil-whirl can generate large components of forcing at frequencies around one-half of rotational speed. If the rotor and bearings have been designed correctly, this will not occur within the rated speed-range. More elaborate hydrodynamic bearings such as tilting-pad bearings are available for duties where high stiffness and stability is required.

(iii) Fan-generated forces. When machines have independently driven fans mounted on the frame, forces due to either imbalance of the fan, instability of the fan rotor, vortex-shedding at some position in the airpath or pulsation due to the passing of individual fan-blades in front of fan inlets or outlets can all

cause forces on the machine frame. It is common for some fans to be shaft-mounted. These too, can cause air-forces to exist on the machine stator.

(iv) Electromagnetic forces. These are quite different for the DC machine and the two forms of rotating AC machines and are discussed separately in the relevant sections to follow.

Nevelsteen (B.1978) discusses the various ways in which different machine forcings may be identified using simple tests. The proportion in which these forcings occur varies from case to case depending on the machine design and the particular running conditions. Electromagnetic forces are of most interest where vibration of the frame itself is concerned.

§1.8 Construction of the AC machine.

Rotating AC electrical machines can be subdivided into two categories - synchronous and induction. The stators of these machines are very similar if not identical. Windings set into the core produce a rotating electrical field with which the flux of the rotor interacts. The difference between induction and synchronous machines arises from the method by which rotor currents are caused to flow. The general AC machine comprises:

(i) The Stator-Core. This is the stationary flux-carrying member. Because of the sinusoidally-varying field the core is always

produced as a stack of laminations. The punchings may form the complete circuit if the core outside-diameter is not too large, or they may only be segments of the circle assembled in a staggered fashion. Endplates are normally fitted to either end of the core to spread the load of clamping bolts/rivets. Fig.1.1a shows a typical views of a stator-core before winding. Pressure is retained on some cores by means of a line of weld run down the back of the core which may or may not fix on a set of straight key bars. These bars then form the interface between core and frame. Slots are punched to accomodate the winding. These may vary in profile depending on the individual machine design but are usually simple parallel-sided gaps. The core laminations are each coated with some thin insulating substance. The stator cores of most large machines are composed of packets of laminations interspersed regularly with ducts for cooling air to pass through (Fig 1.1.b).

(ii) Stator-Winding. The stator may be wound using individual wire filaments but more commonly for large machines, bars containing thick copper conductors are formed and then inserted radially into the slots. They are retained by slot wedges. The winding projects beyond the end of the core where some supporting arrangement holds it in place (Fig. 1.1b). When the conductors are in place in the slots and the wedges driven-in, the core-plus-winding is usually consolidated with varnish or resin.

(iii) Frame. The frames of the AC machine varies considerably from case to case. In the most simple cases, the frame is a solid cylinder shrunk onto the core. This may be flush with the back-of-core but more commonly, a set of ribs integral with the frame are present introducing a gap between back-of-core and frame. The number of ribs can have a profound effect on determining whether certain modes of vibration of the core have significant effect in deflecting the frame. The frames of these machines are normally finned on the outside surface to maximise the heat transfer. More common for large machines is the construction where the core is supported directly by the endplates. In these machines the "frame" can be considered to be a baseplate plus a set of covers. It is usual that both baseplate and covers are fabricated from flat sheet steel.

(iv) Rotor. The rotor of the induction machine is either wire-wound or has a cage of aluminium or copper. The synchronous machine rotor may be of the 'salient-pole' type or 'cylindrical' type. A cross section of a typical salient-pole machine (from a finite-element analysis) is pictured in Fig. 1.2a and Fig. 1.2b shows a complete salient-pole rotor with onboard fans. The cylindrical synchronous machine rotor has windings in slots similar to the stator windings deployed regularly about its periphery. The details of these rotors is not relevant here except to note that when the rotor is slotted, care is taken at the design stage to ensure that the combination of rotor and stator slots is such that undesireable force-waves do not occur on the stator

when the machine is in operation.

§1.9 Electromagnetic Forces Acting on AC Machines.

The evaluation of forces on the stator cores of AC machines is an established science of its own. Binns (B.1964), Jordan & Rothert (B.1953), Yang (B.1981) and others use the concept of permeance harmonics (with respect to both space and time) to predict what frequencies of forcing may exist for given numbers of pole-pairs, rotor-slots and stator slots in the case of induction machines and synchronous machines of the 'cylindrical' rotor construction. The forces predicted are of the form ...

$$f(q,t) = F.\sin(wt+f).\ [a.\sin(nq) + b.\ \cos(nq)] \qquad (1.1)$$

Here, q denotes the physical angle of any position on the stator core relative to some arbitrary datum, w is the angular frequency of the individual force component, t refers to time, n is the order of the space-harmonic of the force and f is a constant phase angle.

The amplitude F of the individual components is difficult to calculate using the space-harmonics since they are dramatically affected by saturation and hence, the magnitude of each one depends to some extent on the presence of the otner components.

In large AC machines (induction and synchronous cylindrical-rotor) the

rotor may be skewed by one slot-pitch over the length of the core. That is to say, there is a twist set in the rotor slots and the circumferential position of one slot at one of the rotor is identical to the circumferential position of its neighbour at the other end. An exaggerated illustration of skewing is presented in Fig. 1.3b. The reasons for skewing can be twofold. Usually the prime motivation behind this measure is to prevent "cogging" torques. Another benefit is that the total force on any axial line on the inner bore of the stator core in both the radial or circumferential directions is, in theory, zero. Clearly, this significantly affects the vibration levels anticipated for a machine.

§1.10 Construction of the DC machine.

The large DC machine comprises the following elements:

(i) The yoke. This is a magnetically-continuous loop which carries the main field flux between main-poles. It is most often made as a rolled steel cylinder. In this case, it may be made of two halves bolted together (usually at a horizontal plane) or as a single cylinder rolled from flat plate and welded along the seam. Fig. 1.4a shows one half of a DC magnet frame. Rolled-steel yokes (Fig. 1.5a) provide strength as well as a magnetic path and no other framework is necessary. The yoke may also be built-up as a stack of laminations. In the case of large DC stators, it is rarely possible to use complete-loop punchings due to limitations in the size of punch presses and in the widths of sheet-steel available from suppliers. Laminated yokes of large machines are

therefore invariably built-up from segments (Fig. 1.5b). Clamping of these yokes is provided by a separate frame to which feet, cover-plates and cooling-apparatus etc. are attached. On some occasions it is possible to form a DC yoke-with-poles from specially shaped laminations (Fig. 1.5c) but this is rare in large machines.

(ii) Main-poles and coils. Poles are prismatic lumps of steel which direct the main field flux onto the armature of the machine. The "body" of the mainpole has sides parallel to the radial central plane and the main field coil is wound around this (Fig. 1.6a). The coil is normally restricted from moving radially inward by the pole-face which is wider than the pole-body, and it is restricted from moving radially-outward either by some small plates or bars which are fixed directly to the pole-body or by the yoke. For cooling reasons, the main coil is never designed to have intimate contact with the yoke over large areas, so it is normally reasonable to assume that motion of the main coil is independent of that of the yoke. The mainpoles of larger machines (other than permanent-magnet machines) are usually laminated. DC machines may have compensating windings present to maintain a more constant flux-density under the face of the mainpole. Slots are punched in the pole-laminations of compensated poles to accomodate the conducting bars. Figs. 1.6b and 1.6c illustrate the difference in profile between compensated and uncompensated pole laminations. Mainpoles are normally bolted to the yoke over a number of shims which are inserted or

removed to allow accurate control of the airgap.

(iii) Compoles and coils. These are similar to the mainpoles. Their shape is usually less complex than that of the mainpoles. They may be laminated or solid. Compoles are located between mainpoles and serve to reduce voltage-differences between successive commutator slots to near zero at the point of commutation. Compoles have coils and like the mainpoles, these may be assumed to be supported totally on the compole. Fig.1.7 shows a typical compole with its coil and one method of coil retension.

(iv) Armature. The armature is the rotating part of the machine. The main machine current is fed onto the armature via brushes pressing against the commutator. A typical large DC armature is shown in Fig. 1.4b. The armature normally has a number of equally-spaced slots in which the current-carrying copper bars are held. (There are slotless-armature machines in which the conductors are simply glued to the surface of a smooth cylindrical rotor).

In order to support the machine, feet must be attached to the frame/yoke capable of carrying the machine weight and opposing the torque generated. Every electrical machine must have some facility for cooling. It is normal for DC machines to use coolers fixed to the frame. Independent motor-driven fans are also mounted on the frame to circulate air through the machine and coolers. Endbrackets on the DC

machine provide a cover for the commutator, brushgear and connections. Some machines have pedestals for the bearings which have no direct connection to the machine frame, but it is more common that the bearings are supported on the endbrackets. All of the above "additional features" have the effect of considerably complicating the process of estimating the machine response.

§1.11 Electromagnetic Forces Acting on the DC stator.

The DC frame experiences a number of electromagnetic forces enumerated below.

(i) Electromagnetic forces on the mainpoles and compoles at bar-passing frequency. As the armature rotates, the mainpoles and compoles experience a pulsating force at bar-passing frequency as bundles of flux enter and leave each pole (Fig. 1.8a). The number of slots on the armature is always designed to be an integer multiple of the number of pole-pairs of the machine. If the number is an odd integer, then the forces experienced by adjacent mainpoles (and compoles) are in-antiphase. Otherwise, these forces are in phase.

(ii) Electromagnetic forces on the mainpoles and compoles at harmonics of bar-passing. The force-against-time pattern produced by the flux bundles is not sinusoidal. Therefore, harmonics of the bar-passing frequency also exist. Wignall (A.1987) has shown that harmonics up to the fourth

are significant in relation to the fundamental. The method of calculation for the pole fluxes used meshes in two planes (Fig. 1.8) to approximate the full three-dimensional field. Wignall computes the forces on the poles by integrating the Maxwell stresses over the entire surface of the pole-face.

(iii) Electromagnetic forces due to eccentricity of the armature with respect to the shaft-centers at bearings. Ideally, the shaft of the machine is perfectly straight and the laminated core of the armature is exactly concentric with the shaft-center all along its length. In practice, this can only be assured by machining the core while the entire armature is turning on its journals. The effect of this eccentricity is a once-per-revolution forcing on each of the poles. Most machines have 'equalising windings' which act to reduce the level of this forcing.

(iv) Electromagnetic forces due to segmentation of the armature core. When a core is segmented, a small clearance must be provided between adjacent segments to facilitate construction. If there are n segments in a full circle, there will be 2n locations around the periphery of the core at which the reluctance of the magnetic path is increased. This results in a pulsation of frequency 2n times rotational-speed.

In large DC machines for which the supression of vibration is important, the armature is invariably skewed i.e. the armature slots have a twist. The twist may be one or two slot-pitches or in some cases, it may be

herringbone. As with the AC machines whose rotors are skewed, the total force on any axial line of the DC machine in the circumferential and radial directions is, in theory, zero.

FIg. 1.1a View showing slots, clamping plates and keybars.

Fig. 1.1b View showing ducts, and one arrangement of feet.

Fig. 1.1 The AC Machine Stator Core.

FIg. 1.2a Cross section used for analysis.

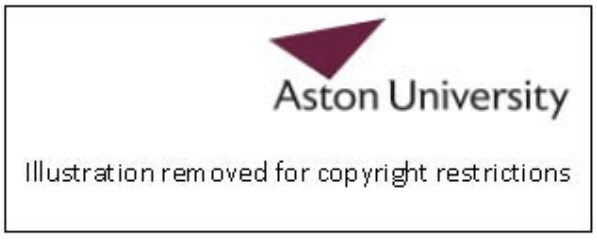

Fig. 1.2b View of complete rotor with fan.

Fig. 1.2 The Synchronous AC Rotor.

FIg. 1.3a Complete rotor showing endrings, and fans.

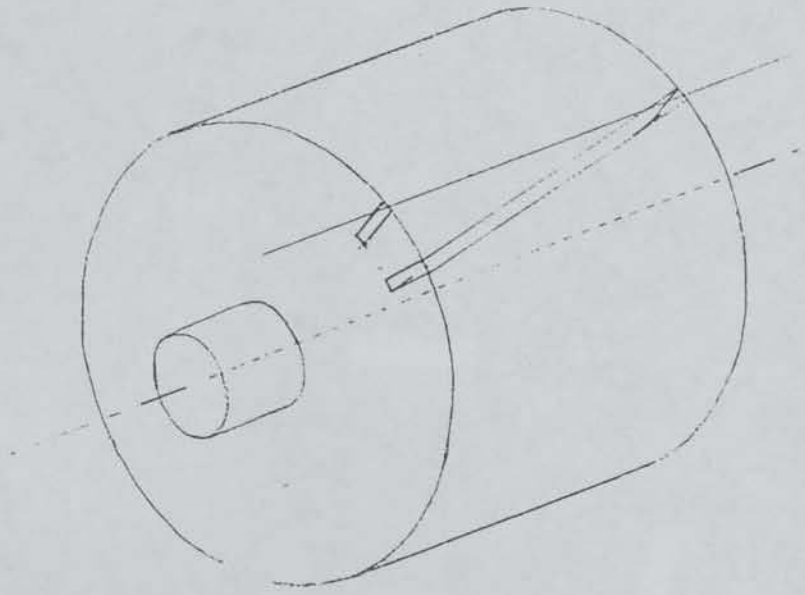

Fig. 1.3b Rotor with skew (Exaggerated).

Fig. 1.3 The Induction Rotor.

FIg. 1.4a Assembled half of magnet-frame.

Fig. 1.4b DC armature showing commutator.

Fig. 1.4 The DC machine.

FIg. 1.5a Simple rolled cylinder.

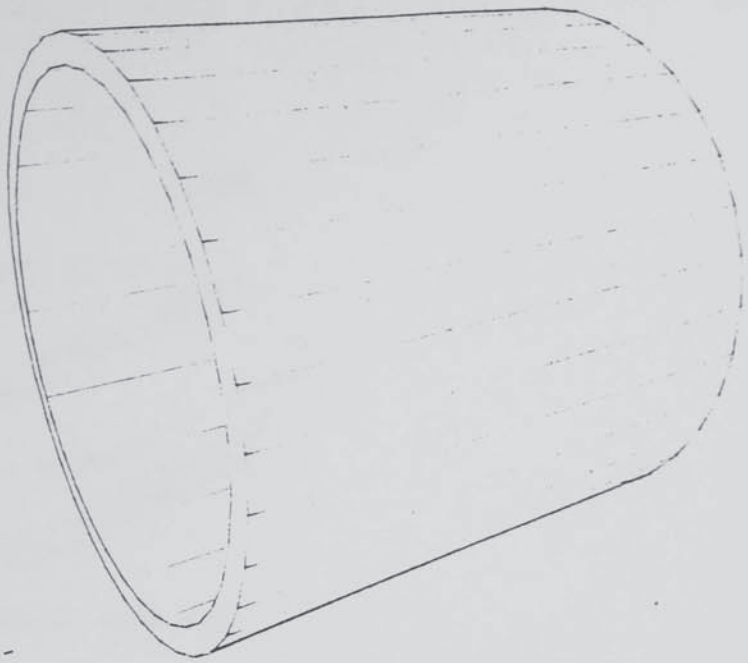

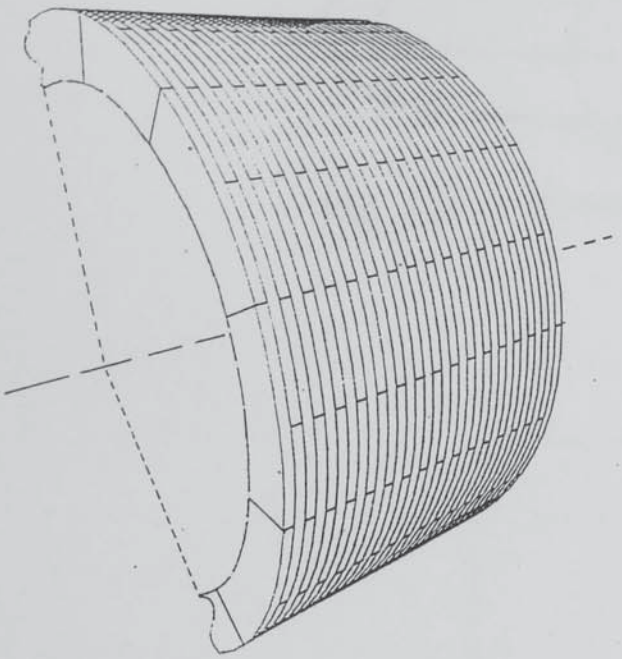

Fig. 1.5b Segmented yoke (thickness of laminations exaggerated).

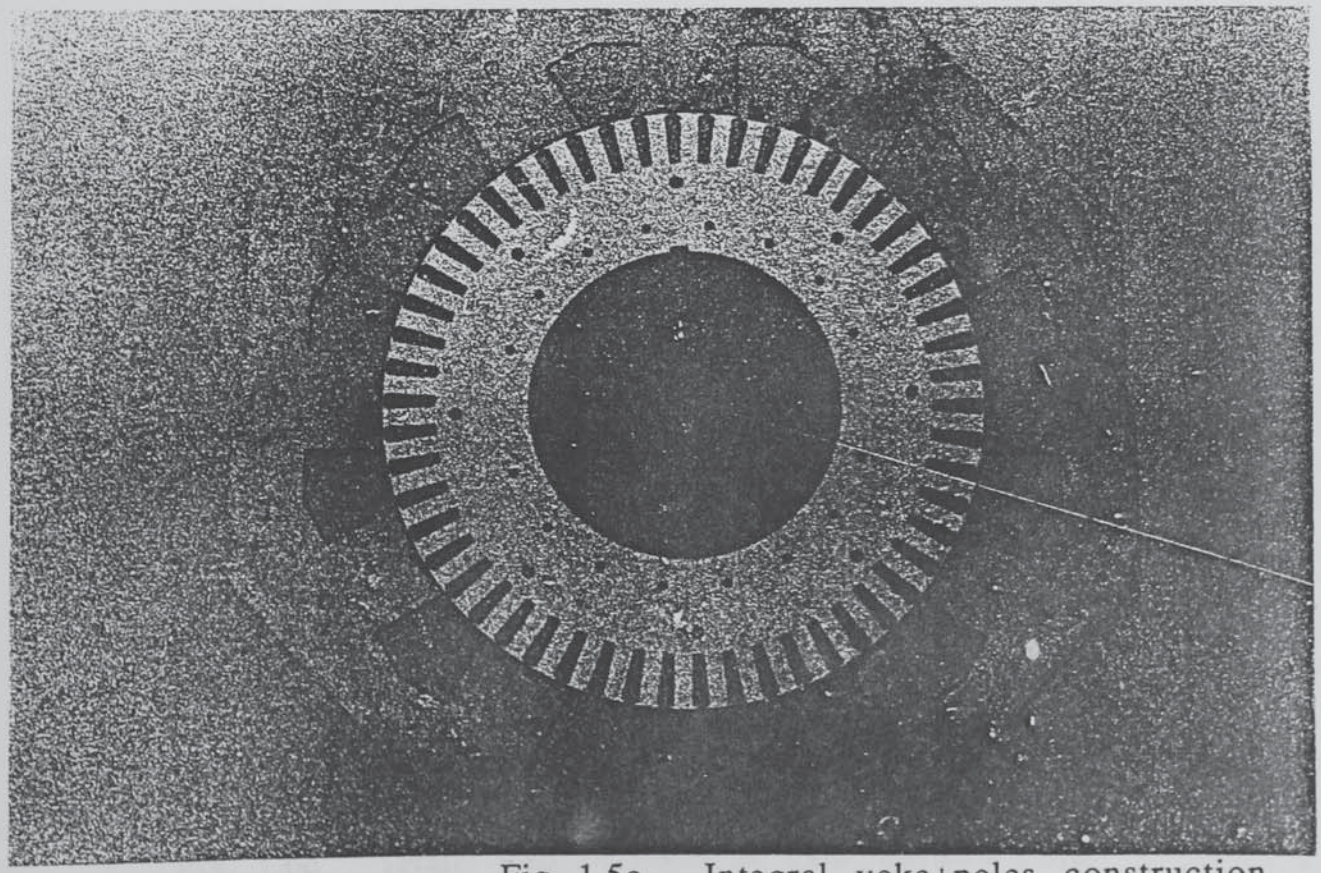

Fig. 1.5c Integral yoke+poles construction.

Fig. 1.5 The DC machine yoke.

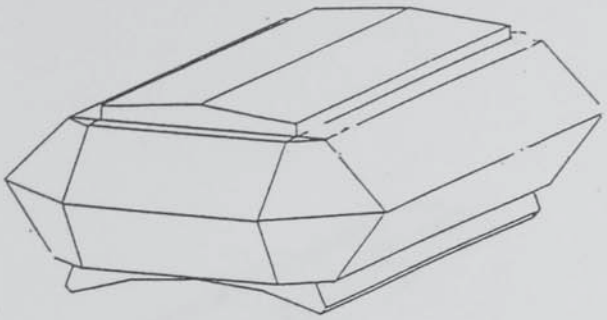

FIg. 1.6a Mainpole wıth coil.

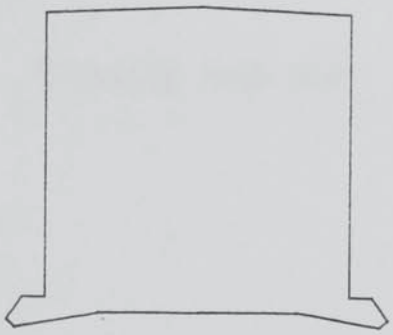

Fig. 1.6b Cross-section of uncompensated pole.

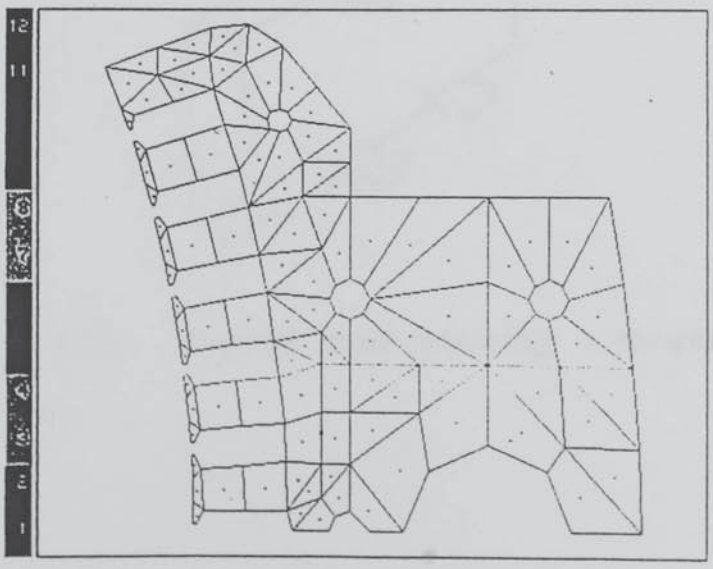

Fig. 1.6c (Half) Cross-section of Compensated Pole.

Fig. 1.6 The DC machine mainpole.

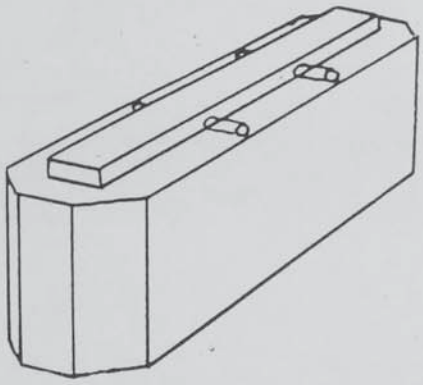

FIg. 1.7a Compole with coil.

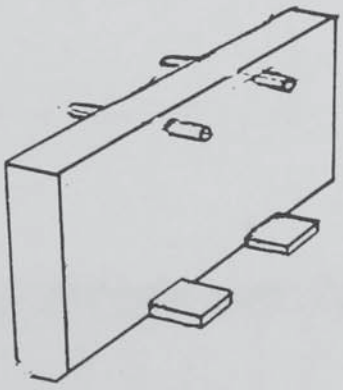

Fig. 1.7b Typical coil-retaining arrangement.

Fig. 1.7 The DC machine compole.

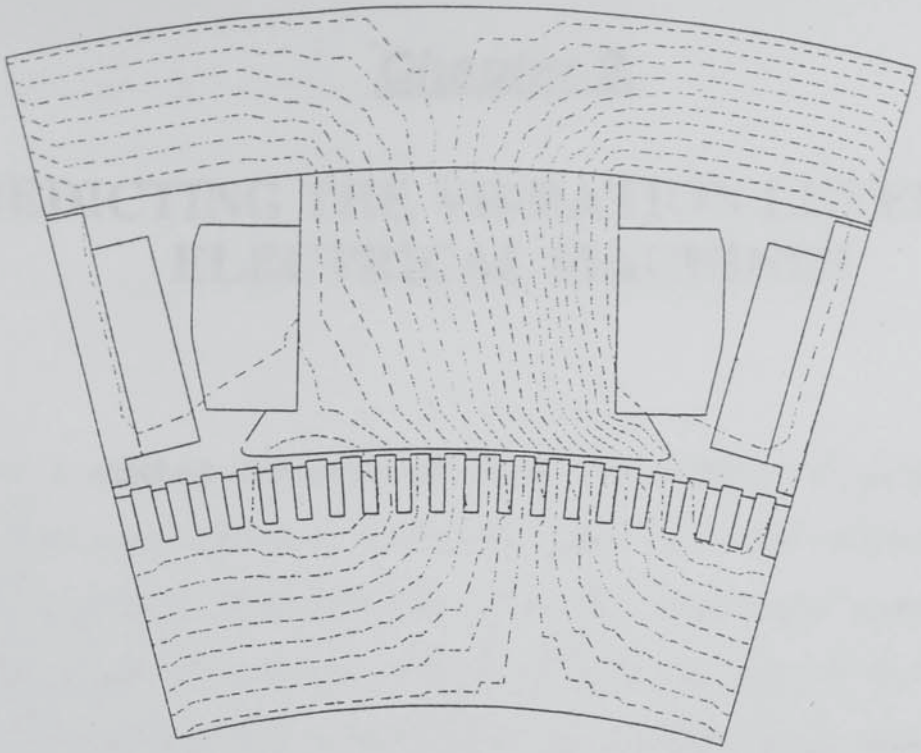

FIg. 1.8a Circumferential Mesh. (On load)

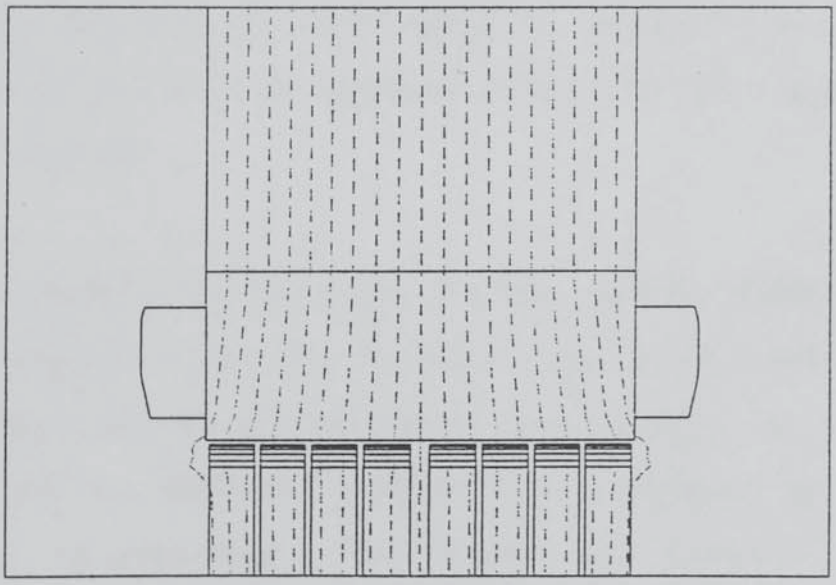

Fig. 1.8b Axial Mesh.

Fig. 1.8 DC Electromagnetic Analysis.

Chapter 2.

PREDICTING THE VIBRATION LEVELS OF ELECTRICAL MACHINES

There is a marked difference between the number of published papers which deal with vibration in DC machines and the number which deal with AC machines. The difficulty of dealing with small numbers of poles which are relatively massive compared with the rest of the machine has clearly posed prohibitive difficulty to authors who attempt to find closed-form expressions for the resonant frequencies and mode shapes of DC magnet frames. If a closed form expression is not required (i.e. if one is prepared to solve the eigenproblem arising from matrices of non-trivial dimensions or apply Gaussian elimination to such matrices to evaluate response) then the analyses of AC and DC machine stators have much in common.

It is not immediately obvious how the various published methods of machine analysis ought be classified. The categorisation used here is neither chronological nor according to the degree of sophistication or accuracy of the analyses. Instead, it is according to the geometrical generality incorporated. The following divisions are discussed individually:

(1) Circumferentially Uniform In-Plane Models.- (Ring Theories).

(2) Other In-Plane Models.

(3) Limited three-dimensional analyses.

(4) Finite-element analyses.

§2.1 Circumferentially Uniform In-Plane Models (Ring Theories).

The simplest and earliest of mechanical analyses of machine stators are those which represent the stator as a single uniform ring freely suspended. The effects of many features such as teeth, windings, wedges, frame assemblies etc. are incorporated by modifying the constants which would apply to the normal steel ring. It was observed earlier that the bulk of the potential and kinetic energies of vibrating machines is usually attributed to the stator-core/magnet-frame for the AC and DC machines respectively. Thus, by representing only the stator-core/magnet-frame, it is to be expected that a meaningful prediction of the lower natural frequencies and low frequency response is possible. Modes are classified into groups each one distinguished by an integer n. Displacements for a mode within the group characterised by n vary with the position angle θ according to $\sin(n\theta)$.

Alger (B.1954) proposes one of the simplest of these models for the AC stator in which the teeth and windings are considered to be simple added mass. The rotational inertia of the teeth and windings is ignored. The ring is assumed to be inextensional, shear is ignored and rotational inertia of the ring itself is also ignored. The result is a simple if inaccurate formula for the resonant frequency for a given n.

Jordan & Uner (B.1964) improve upon this by incorporating the effects of the tooth and winding inertia and finds improved results (Finch (B.1976)). Pavlovsky (B.1971) allows that the windings may move slightly differently to the teeth and that the ring fibres which were originally radial need not necessarily remain straight since tangential and radial deflections are functions of the radius. Similarly, teeth in the Pavlovsky model are allowed to flex. Holzman (B.1972) uses a less sophisticted model but also allows for tooth flexure and demonstrates that a break in natural resonance frequencies occurs at the tooth resonant frequency. In the Holzman model each n (except n=0) has two associated modes. In the first of these modes, the teeth rock in phase with the core and in the second, the teeth rock in antiphase. Finch (B.1976) proposes a ring model which allows for non coincidence of the ring neutral layer and its radius of gravity, and incorporates the possibility of tooth flexure by using frequency-dependent inertia terms.

A general ring model incorporating the features of all of the above analyses would involve five degrees of freedom provided that:

$$(n_{max}.t/r) < 1 \qquad (2.1)$$

Here, n_{max} is the maximum value of n which will be used, t is the radial thickness of the ring and r is the mean radius. These five features are summarised as:

(1) Radial translation at the ring neutral layer.

(2) Circumferential translation at the ring neutral layer.

(3) Shear angle within the ring.

(4) Swing of the teeth relative to the core.

(5) Motion of the winding relative to the teeth.

If the ring is thick with respect to its mean radius and reliable answers are required for high values of n, then the radial and circumferential translations must be allowed to vary with the radius as Pavlovsky proposes.

Ring type models of the AC machine are still in use for the prediction of vibration levels. Even in machines which have skewed rotors, these models can be used to good effect because the high shear-flexibility of the packets of laminations allows individual packets to deform relatively independently of their neighbours. Thus, while the total force on an axial line of the stator core is zero, the assumption that packets can move independently allows a value for the response of the stator-core to rotor slot-passing forces to be computed to reasonable accuracy.

The AC machine is more suited to this form of analysis than the DC machine, since AC stator-core teeth are invariably deployed much more evenly than DC mainpoles. Also, the nature of the attachment between stator-core and frame in the AC machine is such that any inertia or stiffness added to the core, is distributed relatively uniformly. The authors cited above ignore the frame. The presence of feet on the DC

magnet-frame tends to destroy the similarity between the machine and a simple ring. Nonetheless, an approximate formula for resonance frequencies and mode shapes of the DC machine for each n can be evolved. Mikina (A.1934) and Rothert (A.1957) discuss the excitation of those modes which would be associated with this simplified DC model but go no way towards quantifying the stiffness of inertia associated with these modes. The model presented here was developed by the author and includes some features of a GEC Standard Design Calculation procedure (A.1970) and some features from the analysis by Delves (A.1964). The depth of the mainpoles is considered equal to that of the yoke in this analysis. Generally the yoke is marginally longer than the poles so the mass-per-metre of the poles should be adjusted by a suitable factor.

Basic Notation.

θ,r	Position coordinates.
$u(\theta)$, $v(\theta)$	Translation coordinates of cylinder (Defined at cylinder inner radius).
$\alpha(\theta)$, $\beta(\theta)$	Angular deflection coordinate. (Shear of cylinder and rock of poles respectively)
U,V,A,B	Scalar coefficients which multiply either *sin* or *cos* functions to determine $u(\theta)$,$v(\theta)$,$\alpha(\theta)$,$\beta(\theta)$ resp.
E, G, ρ	Material constants for the cylinder steel. (Youngs modulus, the shear modulus and the density).
R_i, R_o	Inner and outer radii of the cylinder respectively.
n	Number of circumferential displacement waves.
m	Number of poles (must be greater than 2).
M, J, S	Mainpole mass polar inertia and root stiffness per m.
d	Distance between pole c.o.g. and cylinder inner surface.

Fig. 2.3c clarifies some of the above terms.

X_0 to X_9 are integrals through the radial depth of the ring.

$$X_0 = \int_{R_i}^{R_o} 1 . dr \qquad X_1 = \int_{R_i}^{R_o} r^{-1} . dr \qquad X_2 = \int_{R_i}^{R_o} (r-R_i) . r^{-1} . dr$$

$$X_3 = \int_{R_i}^{R_o} (r-R_i)^2 . r^{-1} . dr \qquad X_4 = \int_{R_i}^{R_o} (r-R_i) . dr \qquad X_5 = \int_{R_i}^{R_o} r . dr$$

$$X_6 = \int_{R_i}^{R_o} r . (r-R_i)^2 . dr \qquad X_7 = \int_{R_i}^{R_o} r^2 . (r-R_i) . dr \qquad X_8 = \int_{R_i}^{R_0} r^3 . dr$$

Y_1, Y_2 are the integrals of $\cos^2(n\theta)$ and $\sin^2(n\theta)$ with respect to θ over the interval $[-\pi, \pi]$. If $n = 0$, $Y_1 = 2\pi$, otherwise $Y_1 = \pi$. If $n = 0$, $Y_2 = 0$, otherwise $Y_2 = \pi$.

Z_1, Z_2 are constants which determine the significance of the pole. Z_1, Z_2 depend on the relation between n and m. If $n \in \{0, m/2, m, 3m/2, ...\}$, then $Z_1 = 1$, otherwise $Z_1 = 1/2$. If $n \in \{0, m/2, m, 3m/2, ...\}$, then $Z_2 = 0$, otherwise $Z_2 = 1/2$.

$\theta = 0$ at the center line of pole 1 and for each value of n, two distinct groups of modes will be found - either symmetrical or antisymmetrical with respect to the cylinder diameter $\theta = 0$, $\theta = 180$. Normally each group of modes contains four distinct modes.

2.1.1 Case 1. Modes Symmetrical about the Center-line of Mainpole 1.

$u(\theta) = U.\cos(\theta)$ $v(\theta) = V.\sin(\theta)$ $a(\theta) = A.\sin(\theta)$ $b(\theta) = B.\sin(\theta)$

Vector {W} is expressed below.

$$\{W\} = \begin{Bmatrix} U \\ V \\ A \\ B \end{Bmatrix}$$

The potential energy of the frame per meter of axial length is given by S.E. = $0.5*\{W\}^t.[K].\{W\}$ where [K] is equal to the matrix below.

$$
\begin{bmatrix}
\begin{array}{c} E.X_1.Y_1 \\ +2n^2.R_i^{-1}.E.X_2.Y_1 \\ +n^4.R_i^{-2}.E.X_3.Y_1 \\ +n^2.R_i^{-2}.mZ_2.S \end{array} & n.E.X_0.Y_1 + n^3.R_i^{-1}.E.X_4.Y_1 & n.E.X_2.Y_1 + n^3.R_i^{-1}.E.X_3.Y_1 & n.R_i^{-1}.mZ_2.S \\
\begin{array}{c} n.E.X_0.Y_1 \\ +n^3.R_i^{-1}.E.X_4.Y_1 \end{array} & n^2.E.X_5.Y_1 & n^2.E.X_4.Y_1 & R_i^{-1}.mZ_2.S \\
\begin{array}{c} n.R_i^{-1}.E.X_2.Y_1 \\ +n^3.E.X_3.Y_1 \end{array} & n^2.E.X_4.Y_1 & \begin{array}{c} n^2.E.X_3.Y_1 \\ +R_i^2G.X_1.Y_2 \end{array} & 0 \\
n.R_i^{-1}.mZ_2.S & R_i^{-1}.mZ_2.S & 0 & mZ_2.S
\end{bmatrix}
$$

Matrix [K] for modes symmetrical about the center-line of mainpole 1.

The kinetic energy of the frame per metre length is given by K.E. = $0.5*\{W\}^t.[M].\{W\}$ where [M] is the matrix below.

$$\begin{bmatrix} \rho.X_5.Y_1 + n^2.\rho.R_i^{-2}.X_6.Y_1 + mZ_1.M & n.\rho.R_i^{-1}.X_7.Y_1 & n.\rho.R_i^{-1}.X_6.Y_1 & 0 \\ n.\rho.R_i^{-1}.X_7.Y_1 & \rho.X_8.Y_2 + mZ_2.M & \rho.X_7.Y_2 & mZ_2.Md \\ n.\rho.R_i^{-1}.X_6.Y_1 & \rho.X_7.Y_2 & \rho.X_6.Y_2 & 0 \\ 0 & mZ_2.Md & 0 & mZ_2.(J+Md^2) \end{bmatrix}$$

Matrix [M] for modes symmetrical about the center-line of mainpole 1.

2.2.2 Case 2. Modes Anti-Symmetrical About Center-line of Mainpole1.

$u(\theta) = U.\sin(\theta)$ $v(\theta) = V.\cos(\theta)$ $a(\theta) = A.\cos(\theta)$ $b(\theta) = B.\cos(\theta)$

Vector {W} is expressed below.

$$\{W\} = \begin{Bmatrix} U \\ V \\ A \\ B \end{Bmatrix}$$

The potential energy of the frame per meter of axial length is given by S.E. = $0.5*\{W\}^t.[K].\{W\}$ where [K] is equal to the matrix below.

$$
\begin{bmatrix}
\begin{matrix} E.X_1.Y_2 \\ +2n^2.R_i^{-1}.E.X_2.Y_2 \\ +n^4.R_i^{-2}.E.X_3.Y_2 \\ +n^2.R_i^{-2}.mZ_2.S \end{matrix} & -n.E.X_0.Y_2 & -n.E.X_1.Y_2 & -n.R_i^{-1}.mZ_1.S \\
\begin{matrix} -n.E.X_0.Y_2 \\ -n^3.R_i^{-1}.E.X_4.Y_2 \end{matrix} & n^2.E.X_5.Y_2 & n^2.E.X_4.Y_2 & R_i^{-1}.mZ_1.S \\
\begin{matrix} -n.E.X_1.Y_2 \\ -n^3.R_i^{-1}.E.X_3.Y_2 \end{matrix} & n^2.E.X_4.Y_2 & \begin{matrix} n^2.E.X_3.Y_2 \\ +R_i^{-2}.G.X_4.Y_1 \end{matrix} & 0 \\
-n.R_i^{-1}.mZ_1.S & R_i^{-1}.mZ_1.S & 0 & mZ_1.S
\end{bmatrix}
$$

Matrix [K] for modes anti-symmetrical about center-line of mainpole 1.

The kinetic energy of the frame per metre length is given by K.E. = $0.5*\{W\}^t.[M].\{W\}$ where [M] is the matrix below.

$$\begin{bmatrix}
\rho.X_5.Y_2 + n^2.\rho.R_i^{-2}.X_6.Y_1 + mZ_2.M & -n.\rho.R_i^{-1}.X_7.Y_1 & -n.\rho.R_i^{-1}.X_6.Y_1 & 0 \\
-n.\rho.R_i^{-1}.X_7.Y_1 & \rho.X_8.Y_1 + mZ_1.M & \rho.X_7.Y_1 & mZ_1.Md \\
-n.\rho.R_i^{-1}.X_6.Y_1 & \rho.X_7.Y_1 & \rho.X_6.Y_1 & 0 \\
0 & mZ_1.Md & 0 & mZ_1.(J+Md^2)
\end{bmatrix}$$

Matrix [M] for modes anti-symmetrical about the center-line of mainpole 1.

Using the normal eigenvalue/eigenvector solution routines (see Chapter 4) modes and frequencies can be found for this ring-type DC frame model. There are a few special cases for which the above cases are most useful when considering the fundamental and harmonics of slot-passing frequencies. They are: $n = 0$, $n = m/2$, $n = m$.

This model is quite adequate for DC machines having no skew and enables the response of the frame in such cases to be calculated with satisfactory accuracy. The occurrance of unskewed armatures is, however, rare if the machine is required to have low vibration levels in operation. In the light of the balanced nature of the electromagnetic forces which can be caused to exist on the DC stator, the ring-type model needs to be replaced by a much more comprehensive one. The measures used to control the forcing on the DC stator are discussed separately in §2.5.

The methods of those authors who have used the simple ring model to represent the AC stator-core and ring-type methods which might be used to represent the DC magnet frame can be classified according to which features from table 2.1 are included. The DC model presented above includes effects 1,2,7,8,9 from the table over.

	AC	DC
1	Teeth considered simple masses.	Mainpoles considered simple masses.
1a		Compoles included as simple masses.
2	Root flexibility of teeth acknowledged.	Root flexibility of poles acknowledged.
2a	- - - - - - - - - - - - - - - - - -	Shear root-flexibility acknowledged.
3	Flexure of teeth allowed.	In-plane deformation of poles allowed.
3a	Wedge-stiffening effect included.	- - - - - - - - - - - - - - - - - -
4	Windings included as simple mass.	Windings included as simple mass.
5	Windings flexibly connected.	Windings flexibly connected.
6	Ring stiffening effect of teeth included.	Ring stiffening by mainpole included.
7	Shear allowed within ring.	Shear allowed within ring.
8	Extension of the ring included.	Extension of the ring included.
9	Rotatory inertia of ring included.	Rotatory inertia of ring included.

Table 2.1 Features of In-Plane Models of AC and DC stators.

§2.2 Other In-Plane Models of Machines.

Erdelyi (B.1955) discusses the case of an induction motor having core and frame. Fig 2.2a. The core is positioned relative to the frame by means of ribs which may bend and extend/compress. The frame is not circumferentially uniform and the modes are not divided into convenient groups according to n as was previously the case. Erdelyi uses ring models to represent both the core (plus teeth and windings) and the frame. Simple beam elements are used to represent the ribs and supports. The feet of the machine are considered to be free. The deflections of the stator are expressed using finite series and the number of coordinates used depends on the exact nature of the stator and the number of reliable modes required. Openings in the frame for ventilation and connection are ignored, and the endshields are also ignored. The connection of components is achieved by assigning coordinates to both the core and the frame and expressing the deflections of the other members directly in terms of these coordinates.

Erdelyi does point out that the modes of the core plus frame are significantly different from those of the core alone and that inclusion of the frame is especially important in computing the noise radiated by the machine.

Ellison and Yang (B.1974), deal with a similar arrangement of machine (Fig. 2.2b), but use a more powerful model (still a ring) for the frame in which the shear, extensional and rotatory inertia effects are included. Teeth and windings are once again considered to be strongly fixed to

the core.

Models in this category appropriate to the analysis of DC machines include those presented by Den Hartog (A.1928) and Fertman (B.1952). Both deal with evaluating natural frequencies for rings with prescribed boundary conditions. Den Hartog produces formulae for the first resonance of a ring arch with feet which may be either pinned or rigidly constrained against both translation and rotation (Fig. 2.2a). Fertman uses a differential equation approach to produce an indirect frequency equation which is more useful for evaluating whether a particular frequency is close to a resonance than it is for evaluating the frequency associated with the resonance itself. Fertman's three boundary conditions for the ring are illustrated in Fig. 2.2b. Den Hartog uses a mass correction factor to compute the reduction in natural frequency of a cylinder arch with mainpoles fixed compared with that of the cylinder arch having no mainpoles fixed.

These DC motor representations are only useful if the feet have a profound effect on the vibration. Normally, propulsion motors are mounted upon rubber pads to further attentuate the vibrations produced. In this case, the effect of the feet is as an added inertia rather than as an added stiffness and is relatively minor except that the feet modify some mode-shapes in such a way that the excitation experienced by them is no longer zero.

§2.3 Models Incorporating Variation of Displacements Along the Axis.

Verma and Girgis (B.1973) present a model for a induction machine stator of encased construction (Fig. 2.2c). Teeth and windings are assumed to move with the stator core which is modelled using the cylinder theory of Flugge. The materials of the core and case are assumed to elastic and isotropic though the core is laminated. Other authors (Watenabe, Kenjo *et al* (B.1983), White (D.1955)), Delves (A.1964), Walker *et al* (D.1964)) have discovered that laminated cores are cannot be considered isotropic and this author has performed a set of tests to establish equivalent elastic properties for various cases of lamination stacks. Extension, shear and rotational inertia are implicitly included in the calculations since displacements within the back-of-core are allowed to vary with radial position. A double power series is used to represent each of the displacements (radial, circumferential and axial translations in the core and case) for each value of n - the number of waves about the circumference. A simplified frequency searching routine is employed to find the natural frequencies and modes. Verma and Girgis use the term 'mode' where mode-group is more appropriate in that they state that for each mode (meaning for each value of n), three frequencies are found. In the methods developed during this investigation, those applicable to the prediction of vibration in AC stators are most akin to the Verma and Girgis analysis. Verma and Girgis explicitly represent the teeth and fins whereas in DMS, 'cylinders' having specially adjusted material properties have been used to collectively represent all teeth or fins.

The closest analysis of this type for DC machines is that due to Delves (A.1964). Delves' analysis considers that the variation of deflections may have a sinusoidal component superimposed on a linear component (Fig 2.3a). The frame is implicitly assumed to be rotationally-periodic and the only mode of interest is that described below.

(1) All deflections are symmetrical about the axial center of the machine.

(2) Axial nodal lines occur on the yoke behind the mainpoles so that mainpoles can swing but not translate.

(3) Poles may deflect relative to the yoke in the r-θ plane.

The analysis yields the 'exact' axial profile and the frequency for the mode. The machines to which this analysis is applied have laminated yokes with stiff endplates. This analysis has very limited value now except in pointing to the effects which must be catered-for in a good DC frame model. In particular, Delves states that the pole-root flexibility is of fundamental importance. He also allows for a more general variation of 'in-plane' deflections with respect to the axial position coordinate albeit for only one class of mode. The importance of the flexibility of laminations in both shear and normal strain is emphasised.

Delves' single mode shape is symmetrical with respect to the axial position coordinate. Mikina (A.1934) presents a discussion on the use of

pole spacing and armature skewing so as to reduce the excitation on what he refers to as the "four principal modes" of DC machines. Three of the modes he decribes are axially-uniform. In Mikina's "third principal mode" (mode (c) in Fig 2.3b) displacements vary linearly with the axial position coordinate but they are antisymmetrical. Mikina shows that a single slot-pitch skew provides a significant excitation of this mode. Ellison and Moore (B.1968) state for induction machines that if the axial length of a machine is greater than about the square root of the product of the radial thickness and the mean radius, it is necessary to consider the axially non-uniform modes. A similar criterion is appropriate to DC machines.

The Delves, Fertman, Den Hartog and Mikina analyses are all deficient because of their simplicity. However, together they indicate the ingredients which should be combined to generate a valuable analysis method for the prediction of vibration in DC machines in particular. These have been incorporated without exception into the method presented in this thesis (which is the method programmed into DMS.)

§2.4 Measures for Controlling the Excitation of Important Modes in DC Machines.

A number of methods have evolved in the context of DC machine design for the reduction of electromagnetically produced machine vibration. These include:

(a) Choosing the number of slots to be an even or odd integer multiple of the number of pole pairs.

(b) Choosing the width of the pole face to approximately "cover" an integer number of armature slots.

(c) Designing the armature to have an optimum skew.

Item (a) above is invariably done. The choice of whether to use an even or odd integer multiplier has previously been made on the basis of past experience alone. A rational criterion for choosing one or the other has been developed by the author and is given in chapter 9. If the DC machine is considered to be rotationally periodic, then only a limited subset of its modes will experience any excitation due to the slot-passing flux ripple.

It is impossible to achieve either (b) or (c) for all load and field conditions of the machine. Theoretically, if (b) above could be achieved, the distribution of force (both radial and circumferential) on the mainpole face would be an integer number of sinusoids and the summation of this forcing would then be zero. Lee Boon Chong (A.1976) discusses the effectiveness of controlling the mainpole width and concludes that it is limited. The fact that on quiet machines the airgap is frequently "graded" further complicates matters in this respect. Wignall (A.1987) has investigated the effectiveness of (b)&(c) and finds that armature reaction has a significant effect on (b). It is evident from the flux plot in Fig1.7a that the flux lines leaving the armature are not

radial and straight. It is nonetheless possible to choose an optimum pole-face width given the allowable profile based on finite-element analysis and the most typical load condition.

Wignall (A.1987) finds that magnetic saturation together with fringing about the ducts plays a strong role in reducing the effectiveness of skewing and proposes that real skew values of other than unity are optimal. Skewing does significantly reduce the axially-uniform component of forcing and this reduction is such that in some cases, the response of the machine to the sinusoidally varying pattern exceeds the response to the diminished axially uniform pattern.

§2.5 Finite Element Models of Machines.

For generality, the best models of both the AC and DC machines are finite-element models. (The method proposed in this thesis may be regarded as a finite element method in which some of the elements are specialised). All assumptions regarding rotational perodicity, axial uniformity and specific mode shapes can be relaxed. However many of the features of machines cannot be modelled directly without empirical determination of properties. In particular, special spring-damper elements must be used for joints such as that between back-of-core and keybars, the shimmed joint between pole and yoke etc.

Results from a small number of F.E. (mechanical) analyses have been published. Fig. 1.8 shows some recent models. (Electromagnetic F.E. models of machines are commonplace now. These are generally simpler

than the mechanical models since rotational periodicity is invariably present and frequently, the field of interest is axially uniform so that the problem reduces to a two-dimensional analysis.) Some modellers consider only the in-plane vibration of machines (Chen & Zhu (B.1986)) and others use full three dimensional models (Belmans (B.1986)). At present, the accuracy of these models is limited by the power of the methods being used and the capacity of the computing hardware being used to implement them.

A number of cautions ought be heeded with regard to use of FE models.

Firstly, the mesh used must be sufficient but not over-detailed. Elements should not be allowed to be badly distorted except when they are present only to add mass. Tips of stator teeth are not critical elements and distortion of these will not cause serious errors.

The elements should have suitable properties. Verma & Girgis (B.1978) and Belmans (B.1986) have assumed that the core of their stator models was composed of uniform isotropic steel. Watenabe, Kenjo *et al.* (B.1986), Delves (A.1962) and the present author have found that the laminations cause significant flexibilities to be introduced particularly for normal and shear strains out of the plane of lamination.

Elements having offsets must be used in some circumstances. A difficulty which arose early in the course of this work was connected with the fact that nodes can only be located on the central (neutral) plane of some elements - particularly plate and shell elements. When a support

structure is attached to a cylinder along a continuous weld, the circumferential stretching and compression of the support when the cylinder attempts to flex accounts for significant quantities of stored energy. If the support is attached to the neutral plane of the cylinder in the theoretical model, the support plates need not compress or extend when the cylinder flexes.

The use of automatic selection of master degrees of freedom must be treated with care. Most commercial packages choose some or all of the master degrees of freedom in one sweep. The only failsafe method of choosing master degrees of freedom is to eliminate slave freedoms one by one carrying out the reduction process as the condensation proceeds. The master degrees of freedom are those which are left over when the desired number of slaves have been identified and reduced out. Structures which have many nodes with identical stiffness and inertia properties (for example the nodes defining the solid yoke of a DC stator) are prone to poor results owing to the fact that the routines selecting the 'next' master degree of freedom may not allow for the fact that the 'last' master degree of freedom may have been physically very close. The provision of steering data or explicit identification of suitable master degrees of freedom is a possible solution.

Special elements can be derived to complement the existing library within most commercial packages. Chen and Zhu (B.1984) mention the notion of a generalised tooth/slot. It is not clear what is meant by this but it suggest that the stator core could be divided into as many elements as there are teeth. This idea is particularly applicable to AC

machines but a similar notion can be applied to DC.

In-plane models of machines should take account of the Poisson coupling between normal strains. This effect is dramatically reduced for laminated components. Appendix 6 includes a derivation of some factors which should be applied to plane models to correct for the Poisson coupling.

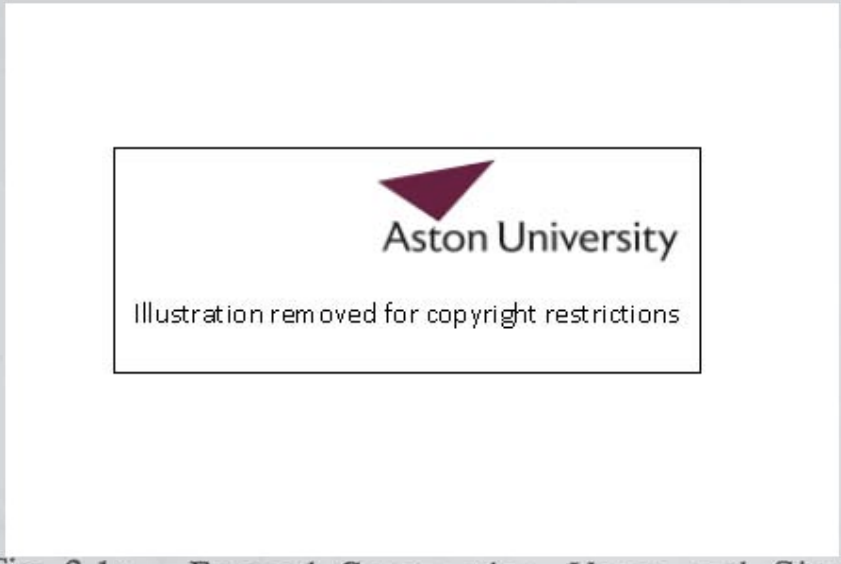

Fig. 2.1a Encased Construction. Verma and Girgis

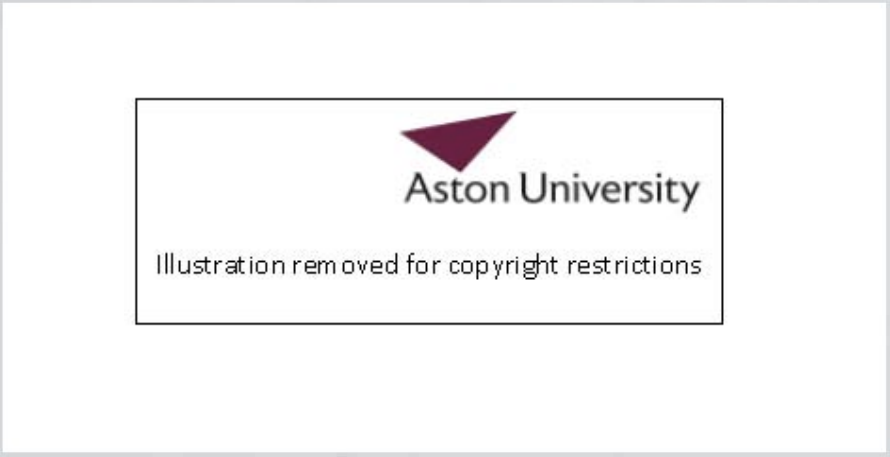

Fig. 2.1b Ribbed Construction. Ellison and Yang(B.1978).

Fig. 2.1c Ribbed Construction. Erdelyi(B.1974).

Fig. 2.1 Three Different Forms of Stator Analysed.

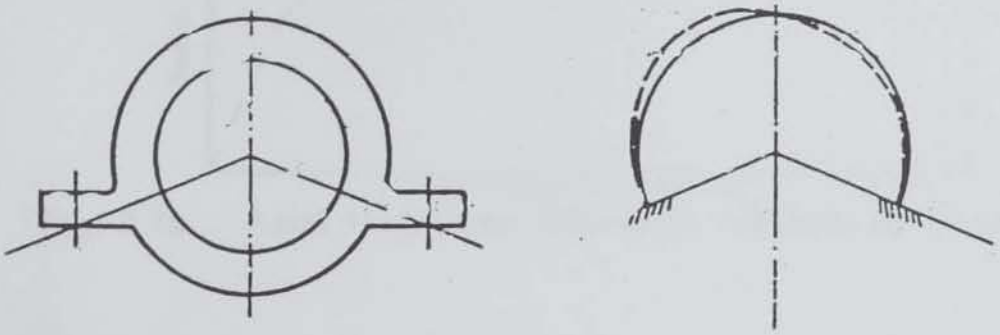

Fig. 2.2a Constrained ring model considered by Den Hartog

Fig. 2.2b Constrained ring model considered by Fertman. (A.1956)

Fig. 2.2 Two "Incomplete" Ring Models.

Fig. 2.3a Axial Generating Functions Allowed by Delves (A.1962)

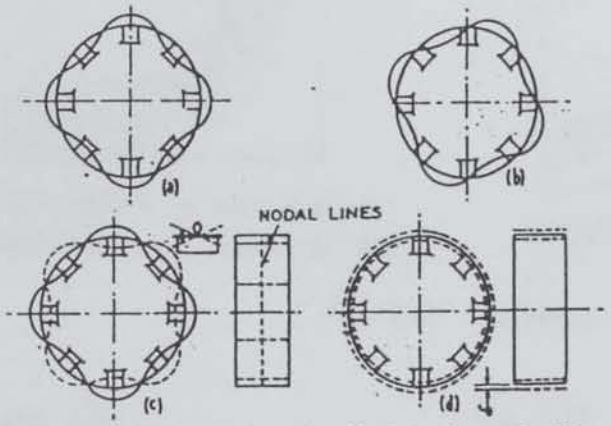

Fig. 2.3b Four 'Principal' Modes Defined by Mikina.

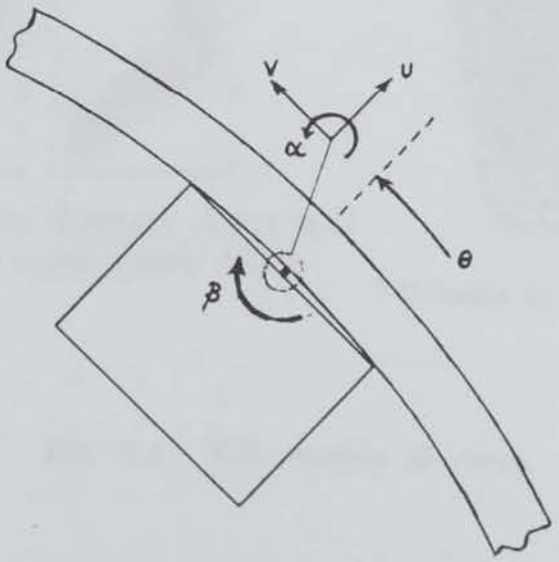

Fig. 2.3c Notation for Simple In-Plane Analysis

Fig. 2.3 Particular DC Frame Modes and Notation for In-Plane Analysis

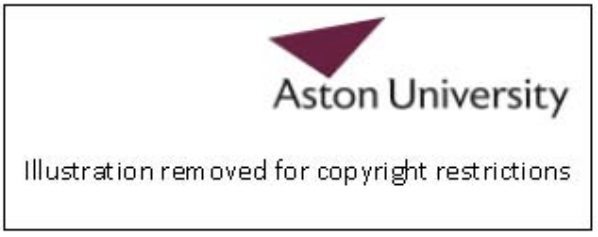

Fig. 2.4a In-plane model to test against measurements by Finch (B.1976)

Fig. 2.4b In-Plane model by Chen & Zhu

Fig. 2.4c

Fig. 2.4d

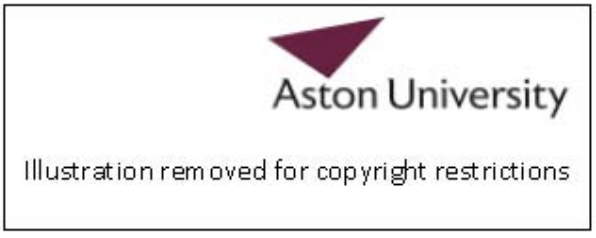

In-Plane model by Watenabe, Kenjo *et al.* (B.1986) with superimposed modes.

3-D model by Belmans *et al.* (1986).

Fig. 2.4 F.E. models of cores.

Chapter 3.

STRUCTURE-SYNTHESIS USING COMPONENT MODES.

In the previous chapter, the usefulness of employing purely analytical methods to the prediction of vibration in large machines was examined. It has been shown that current design practices eliminate virtually all of the vibration forms which might be predicted with these methods. To progress from the current state-of-the-art it is necessary to employ numerical solutions of some description in order that the assumptions of perfect symmetry can be relaxed and the less simple mode-shapes considered.

Two quite different approaches have been examined. One possibility would be to create a single large finite-element model to represent the entire machine. The alternative is to use the natural subdivisions occurring in the machine and the closeness-to-symmetry to advantage using substructuring techniques. The choice of which of these was more appropriate was based on an assessment of the relative speed and ease of use bearing in mind the following considerations.

(i) The analysis must consider a broad range of frequencies.

(ii) The emphasis is to be on the evaluation of system response rather than on the location of natural frequencies and solution

for mode-shapes.

(iii) Damping is to be included as accurately as possible.

(iv) It is desireable that the effects of various changes can be assessed with a minimum of human and computational effort.

(v) Non-linearity can occur at some joints but the individual subsystems may be considered to have linear force-deflection relations.

The substructuring approach was found to be the more appropriate. A suite of programs has been written to implement this approach. It comprises a set of programs pertaining to the assembly of subsystems to form a composite-system, programs to automatically generate the data for some elementary forms of subsystem, a basic display facility and programs which deal with the generation of models of DC machines (composite- and sub- systems thereof). It is referred to as DMS in the remainder of the thesis which initials stand for "a Dynamic Modelling System".

§3.1 Comparison of methods :- Full F.E. versus Substructuring.

The following example illustrates the relative merits of the two possible approaches. The test structure comprises a cylinder having a horizontal axis and to which seven other substructures are attached (Fig. 3.1a). It is supported upon two short pillars whose bases are rigidly affixed to

the ground. The cylinder has a circular disc fitted to one end and contains four identical lumps attached rigidly to the middle surface. The auto-response of this structure to a point forcing (as shown in Fig. 3.1a) is required and the non symmetrical (and non antisymmetrical) nature of the forcing makes the problem fully general.

Fig. 3.1b presents the finite-element model of this structure. This structure contains most of the features of the typical DC machine analysis. The response was evaluated for 250 frequencies varying logarithmically between 5 Hz and 500 Hz. Fig. 3.2 compares the response traces predicted by the two methods and gives total-time figures as required by the two methods. Both programs were run on a DOMAIN 550 workstation rated at 1.8 mips. The number of coordinates used in preparing each of the individual subsystems of the substructured models and the number of degrees of freedom in the F.E. model are summarised in Fig. 3.3a and the computation times taken for various parts of the job for are quoted in Fig. 3.3b for both the DMS and PAFEC analyses.

Considering this job alone, a factor of 12 is realised in time saving if it is required that the effects of a number of structural modifications be investigated. Most of the computational time involved in the DMS analysis is tied up with the preparation of modal data for the substructures. Once prepared, this data can be retained for use of the substructure as part of any composite system.

Based on this experience, the notion of creating whole F.E

representations of DC motors for response calculations was abandoned in favour of the substructuring approach.

§3.2 Two Aspects to Substructuring.

It is useful here to distinguish between two separable features of this type of analysis.

(i) The means by which each individual substructure is represented.

(ii) The procedures used to effect the synthesis.

In dynamic-substructuring literature at present it is possible to differentiate between a number of methods due to various authors. In this chapter, it is not proposed to enumerate the individual details of each one. Generally, the differences occur either in the modified coordinate-set used to model the allowable displacement patterns in the individual substructures for a given frequency span, or in the way in which the connections/constraints are imposed to form the composite-system from the complete unconnected system. In some instances the actual order-of-computation or computational-technique employed for some of the fundamental operations is the chief discriminating factor. This can have some impact on making some methods more efficient or accurate than others though they be mathematically identical. It is the authors' impression that there are significantly more "different methods" than there are "differences between each method and every-other-method". It is sensible therefore, to present the general principles first and discuss the variations rather

than attempt to deal with individual methods.

The details of order and technique of computational are given least emphasis in this discussion. They tend to be specific to the exact combination of component representation and synthesis methods. Instead, attention is concentrated mainly on the representation of components where the principle variations published to date are reviewed for suitability to the particular application of the analysis of machine vibration. The various methods of synthesis are discussed towards the end of this chapter and a single general method is extracted which is both suitable for use with <u>any</u> component representation and necessary for the particular representation favoured in this investigation.

§3.3 Representing Subsystems Generally.

The general subsystem in dynamics has n displacement coordinates assigned to it at the creation of a model. They may correspond to point displacements in the case of a lumped-mass model, displacements distributed over a finite span of the subsystem in the case of a finite-element model or distributed displacements spanning the entire subsystem in the case of the models used for beams, rings, cylinders, discs etc. in chapter 4. It is implicitly assumed that the subsystem can only deflect in shapes which are linear combinations of the above displacement shapes. The vector of coefficients for this linear combination is $\{\mathbf{q}(t)\}$. Since the primary interest is in the steady-state response of the composite-structure, $\{\mathbf{q}(t)\}=\{q\}.\sin(\omega t)$. Forces acting on the subsystem are symbolised as $\{\mathbf{Q}(t)\}=\{Q\}.\sin(\omega t)$ with respect to the "q"

coordinate-system. The equation-of-motion governing the behaviour of the undamped subsystem in steady-state conditions is

$$[[k]-\omega^2[m]]\ \{q\} = \{Q\} \qquad (3.1)$$

There is some set of m point displacements which are of special interest for a given substructure. The coordinate-vector associated with these is denoted $\{\mathbf{r}(t)\}$ and has associated vector $\{\mathbf{R}(t)\}$. In finite-element models, these displacements are simply a subset of the complete set of point displacements for the structure. In order to retain compatibility with the use of single-element representation of components as developed in chapter 4, we state that in general there is some coordinate transformation matrix [E] such that $\{\mathbf{r}(t)\}$ is related to $\{\mathbf{q}(t)\}$ by (3.2). For F.E. models E is a sparse matrix containing only ones and zeros.

$$\{\mathbf{r}(t)\} = [E]\ \{\mathbf{q}(t)\}$$

$$\{r\} = [E]\ \{q\} \qquad (3.2)$$

It is straightforward to show by virtual work arguments that if (3.2) holds, the force vectors $\{\mathbf{Q}(t)\}$ and $\{\mathbf{R}(t)\}$ are related by (3.3).

$$\{\mathbf{Q}(t)\} = [E]^t\ \{\mathbf{R}(t)\}$$

$$\{Q\} = [E]^t\ \{R\} \qquad (3.3)$$

The coordinates $\{\mathbf{r}(t)\}$ are described as *terminal freedoms* throughout this

work using jargon from electrical network analysis in which the concept of substructuring has its roots. Other terms have been used by various authors including *boundary, attachment, junction* and *interface freedoms.* This author prefers the term *terminal freedoms* to the alternatives since it does not preclude those point displacements at which response data might be required or forces applied but which are not directly used for the attachment of other substructures and do not occur on an obvious composite-structure interface or boundary.

The representation which is sought for each individual subsystem may be expressed in the most general form as (3.4) below.

$$\{r\} = [f]\{R\} \qquad (3.4a)$$

$$\{R\} = [d]\{r\} \quad \text{(sometimes)} \qquad (3.4b)$$

Matrix [f] is the dynamic flexibility matrix. This matrix is dependent on frequency and the way in which it is built-up is discussed for the each of the substructure representation methods discussed. Garvey *et al.* (C.1988.1) demonstrate for one method of substructuring that it is the formation of these matrices which consumes virtually all of the required computation time. Matrix [d] of (3.4b) above is the subsystem dynamic stiffness matrix if it exists. This proviso must be stated since it is possible that some subsystems can have more terminal freedoms than they had generalised coordinates. The effect is that certain combinations of the terminal freedoms will always sum to zero and so the elements of {r} are not independent. Thus [f] of (3.4a) will be singular in such cases and [d]

- the inverse of [f] - does not exist.

Generally, matrix [f] is built-up (at least in part) from component modes. This has the following advantages;

(a) The effects of the internal displacements of the subsystems are accounted for though data specifically relating to them is not retained.

(b) The total number of coordinates can be reduced by discarding generalised coordinates (modes) whose natural frequency is very much higher than the highest frequency in the range of interest. The process of truncating the modal series requires considerable care and is discussed further in the context of the various substructure representations.

For the purposes of using software to automatically connect substructures and to create images of the substructures, it is also necessary to store the physical positions of the nodes of the substructures but compared with the modal data, the storage required for this information is very small. The volume of node-position data is proportional to n (n being the number of degrees of freedom in the substructure) while the volume of modal data is roughly proportional to n^2. In DMS, a set of five datafiles is used to completely represent each of the substructures stored. A full description of these files is given in the DMS manual - Garvey (C.1987)

§3.4 Structure Representation Using Free-Free Component Modes.

This is the simplest of the methods which will be discussed. Only one class of mode is required - considering rigid-body modes to be zero-frequency natural modes of vibration. The proponents of this method include Goldman (C.1969), Hou (C.1970) and Simpson (C.1984). It is intuitively evident that the behaviour of a subsystem is completely known if the modeller has details of the frequency, mode-shape and associated modal-mass of all free-modes of the structure. Dealing with substructures in the free-free state has strong advantages when data is to be experimentally derived and when details of the remainder of the composite-system are not available to the numerical modeller. Goldman points out that one of the disadvantages is that simple truncation of the modal series can result in significant error and that reliable upper-bounds for this error cannot be formulated. Convergence of the subsystem internal forces/stresses at forced or restrained terminal freedoms with increasing numbers of retained modes is predictably poor.

Equation (3.1) is the equation of motion of a single undamped subsystem originally having n independent displacmement coordinates. The eigen-problem corresponding to the search for free-free modes is concisely stated in (3.5). Solving this yields the n natural frequencies ω and associated modes $\{u\}$ of the free-free substructure. We assume for the present that all of the natural frequencies and modes are explicitly evaluated.

$$[[k] - \omega^2[m]]\ \{u\} = \{0\} \qquad (3.5)$$

It is convenient to scale the modes so that they are mass-normalised according to (3.6).

$$\{u\}_i^t[m]\{u\}_i = 1.0 \qquad (3.6)$$

Now, we can use the coordinate-transformation matrix [E] defined in (3.2) to find the modal displacements at the terminal freedoms $\{v\}_i$ using (3.7).

$$\{v\}_i = [E]\ \{u\}_i \qquad (3.7)$$

Forces

$$\{U\}_i = [E]^t\ \{V\}_i \qquad (3.8)$$

The various $\{v\}_i$ (ordered according to increasing frequency) are the columns of the coordinate-transformation matrix [V]. The eigenvalues λ_i are placed along the diagonal of an n x n matrix of zeros to form $[\Lambda]$.

The transient response of any of the substructure terminal freedoms to forcing applied at terminal freedoms can be computed by (3.9). The steady state response is computed using (3.10) as shown by Garvey, Penny & Gilbert (C.1988).

$$\{r(t)\} = \int_0^t \int_0^t [V].\left[[\Lambda] + D_t^2[I]\right]^{-1}.[V]^t.\{R(t)\}.dt.dt \qquad (3.9)$$

$$\{r\} = [V].\left[[\Lambda] - \omega^2[I]\right]^{-1}.[V]^t\{R\} \qquad (3.10a)$$

If [V] is invertible, we can also write {R} directly in terms of {r} as (3.10b).

$$\{R\} = [V]^{-t}.\left[[\Lambda] - \omega^2[I]\right].[V]^{-1}\{r\} \qquad (3.10b)$$

The advantage of using the component modes as coordinates is evident here. It is possible to express (3.10a) without using component modes as (3.11a) below.

$$\{r\} = [E].\left[[k] - \omega^2[m]\right]^{-1}.[E]^t\{R\} \qquad (3.11a)$$

Clearly, (3.10a) involves inverting a diagonal matrix which involves only n floating-point divisions in the case where no truncation of the modal series has taken place. Fewer operations are required if some of the higher modes are discarded. On the other hand, the number of floating-point operations required to solve (3.11a) is approximately $n^2/2$.

If [E] is invertible, then {R} may be written directly in terms of {r} as (3.11b) and the free-free component mode representation of the substructure can be used in the direct method of substructure assembly

discussed in §3.10.

$$\{R\} = [E]^{-t}.\left[[k] - \omega^2[m]\right].[E]^{-1}\{r\} \qquad (3.11b)$$

§3.5 Structure Representation Using "Fixed-Constraint" Component Modes.

An alternative to using free-free component modes is to consider that all terminal freedoms which will occur at subsystem interfaces within the composite system are fully restrained. The terminal coordinates $\{r\}$ are partitioned into internal and boundary coordinates $\{r_i\}$ and $\{r_b\}$.

$$\{r\} = \begin{Bmatrix} \{r_i\} \\ \{r_b\} \end{Bmatrix} \qquad (3.12)$$

A subsystem which initially had n coordinates to define its displacement is reduced to having n-l coordinates if l is the number of boundary terminal coordinates. There are then n-l natural modes of vibration of the component referred to as the *fixed-constraint,* or *fixed-terminal modes.* The l suppressed freedoms must be explicitly reintroduced into the subsystem by including another category of coordinates which Hurty (C.1965), Benfield & Hruda (C.1971) and MacNeal (C.1971) refer to as *attachment modes* or *constraint modes.* Now, the attachment modes are not natural modes of vibration in so far as they are generally <u>not</u> uncoupled from one another (either inertially or elastically). Neither are these modes inertially uncoupled from the natural *fixed-constraint* modes though they are shown here to be elastically uncoupled. The use of

attachment modes is frequently referred to as *generalised inertial coupling* because of the off-diagonal terms $[m_{ib}']$ and $[m_{bi}']$ which will be seen to occur in equations (3.20) to (3.26).

The inertial coupling of the so-called *attachment-modes* has a significant impact on the time required to form [f] of (3.4a) because of the necessity to invert (or perhaps apply Gaussian elimination to) a non-diagonal dynamic-stiffness matrix for the composite-system generalised coordinates. However, if the modal series is to be truncated for an individual subsystem, significantly more of the normal modes may be discarded here than in the case of the free-free component mode series when substantial forces are required to exist at the component boundaries. The advantage in computation time is reviewed after the equations are developed.

The development of the fixed-terminal representation is most straightforward when the vector of boundary terminal freedoms $\{r_b\}$ is simply a subset of the complete set of substructure coordinates $\{q\}$ in which case, some coordinate transformation matrices can be avoided by simply using partitioning.

$$\{q\} = \begin{Bmatrix} q_i \\ r_b \end{Bmatrix} \tag{3.13}$$

The matrices [k] and [m] are partitioned to correspond.

$$[k] = \begin{bmatrix} [k_{ii}] & [k_{ib}] \\ [k_{ib}]^t & [k_{bb}] \end{bmatrix} \quad , \quad [m] = \begin{bmatrix} [m_{ii}] & [m_{ib}] \\ [m_{ib}]^t & [m_{bb}] \end{bmatrix} \qquad (3.14)$$

Now, the eigenproblem corresponding to the search for *fixed-terminal* modes is written as (3.15) below.

$$[[k_{ii}] - \omega^2 [m_{ii}]] \{u_i\} = \{0\} \qquad (3.15)$$

The n-l eigenvectors are mass-normalised for convenience and arranged in columns of the matrix $[V_i]$ so that (3.16a) holds. Equation (3.16b) then follows. (Matrix $[\Lambda]$ is the (n-l) x (n-l) diagonal matrix with the individual ω_n^2 placed in order).

$$[U_i]^t [m_{ii}] [U_i] = [I] \qquad (3.16a)$$

$$[U_i]^t [k_{ii}] [U_i] = [\Lambda] \qquad (3.16b)$$

Now, the attachment-modes are defined as the static deformed shapes of the structure which occur when one of the terminal freedoms is displaced by one unit while the other terminal freedoms are constrained to be zero. No forces are applied to the internal coordinates, thus when $\omega=0$:

$$[k_{ii}] \{q_i\} + [k_{ib}] \{r_b\} = \{Q_i\} = \{0\} \qquad (3.17)$$

If j be the index for the terminal freedoms, then the attachment modes

$\{u_b\}^j$ can be derived from (3.17) by setting the j^{th} entry of $\{r_b\}$ equal to 1.0, setting all other entries equal to 0.0, and solving the equation to find $\{q_i\}$ (= $\{u_b\}^j$). The vectors $\{u_b\}^j$ are arranged as columns of the matrix $[U_b]$. There is no benefit in normalising this matrix with respect to either $[k_{bb}]$ or $[m_{bb}]$.

A coordinate-transformation is now set up. The new coordinates $\{s\}$ express the subsystem displacement in terms of the fixed-constraint normal-modes and the attachment modes according to (3.18).

$$\{q\} = \begin{Bmatrix} q_i \\ r_b \end{Bmatrix} = \begin{bmatrix} U_i & U_b \\ 0 & I \end{bmatrix} \begin{Bmatrix} s_i \\ s_b \end{Bmatrix} = [U]\{s\} \qquad (3.18)$$

The stiffness and mass matrices with respect to $\{s\}$ are $[k']$ and $[m']$ as defined below.

$$[k'] = \begin{bmatrix} \begin{bmatrix} U_i^t k_{ii} U_i \end{bmatrix} & \begin{bmatrix} U_i^t k_{ii} U_b \\ + U_i^t k_{ib} \end{bmatrix} \\ \begin{bmatrix} U_b^t k_{ii} U_i \\ + k_{bi} U_i \end{bmatrix} & \begin{bmatrix} U_b^t k_{ii} U_b \\ + k_{ib} U_b \\ + U_b^t k_{bi} \\ + k_{bb} \end{bmatrix} \end{bmatrix} = \begin{bmatrix} [\Lambda] & [0] \\ [0] & [k'_{bb}] \end{bmatrix} \qquad (3.19)$$

$$[m'] = \begin{bmatrix} [U_i^t . m_{ii} . U_i] & [U_i^t . m_{ii} . U_b + U_i^t . m_{ib}] \\ [U_b^t . m_{ii} . U_i + m_{bi} U_i] & [U_b^t . m_{ii} . U_b + m_{ib} . U_b + U_b^t m_{bi} + m_{bb}] \end{bmatrix} = \begin{bmatrix} [I] & [m'_{ib}] \\ [m'_{bi}] & [m'_{bb}] \end{bmatrix} \qquad (3.20)$$

Using standard coordinate-transformation techniques, we can now write a direct relation between forces and displacements as (3.21)

$$\begin{Bmatrix} q_i \\ r_b \end{Bmatrix} = \begin{bmatrix} U_i & U_b \\ 0 & I \end{bmatrix} \left[\begin{bmatrix} [\Lambda] & 0 \\ 0 & [k'_{bb}] \end{bmatrix} - \omega^2 \begin{bmatrix} [I] & [m'_{ib}] \\ [m'_{bi}] & [m'_{bb}] \end{bmatrix} \right]^{-1} \begin{bmatrix} U_i^t & 0 \\ U_b^t & I \end{bmatrix} \begin{Bmatrix} Q_i \\ R_b \end{Bmatrix} \qquad (3.21)$$

Now the 'internal' terminal coordinates $\{r_i\}$ are related to $\{q_i\}$ by (3.22) - a substatement of (3.2) - and thus (3.21) can be transformed to have the same form as (3.4a) - equation (3.23).

$$\{r_i\} = [E_{ii}] \{q_i\} \qquad (3.22)$$

$$\begin{Bmatrix} r_i \\ r_b \end{Bmatrix} = \begin{bmatrix} V_i & V_b \\ 0 & I \end{bmatrix} \left[\begin{bmatrix} [\Lambda] & 0 \\ 0 & [k'_{bb}] \end{bmatrix} - \omega^2 \begin{bmatrix} [I] & [m'_{ib}] \\ [m'_{bi}] & [m'_{bb}] \end{bmatrix} \right]^{-1} \begin{bmatrix} V_i^t & 0 \\ V_b^t & I \end{bmatrix} \begin{Bmatrix} R_i \\ R_b \end{Bmatrix} \quad (3.23)$$

Matrices $[V_i]$ and $[V_b]$ are given as (3.24) and (3.25).

$$[V_i] = [E_{ii}]\,[U_i] \quad (3.24)$$

$$[V_b] = [E_{ii}]\,[U_b] \quad (3.25)$$

Now, if $[U_i]$ is invertible, it is possible to write $\{R\}$ directly in terms of $\{r\}$ as (3.26). This is a prerequisite for the use of the direct method of structure assembly discussed later.

$$\begin{Bmatrix} R_i \\ R_b \end{Bmatrix} = \begin{bmatrix} V_i^t & 0 \\ V_b^t & I \end{bmatrix}^{-1} \left[\begin{bmatrix} [\Lambda] & 0 \\ 0 & [k'_{bb}] \end{bmatrix} - \omega^2 \begin{bmatrix} [I] & [m'_{ib}] \\ [m'_{bi}] & [m'_{bb}] \end{bmatrix} \right] \begin{bmatrix} V_i & V_b \\ 0 & I \end{bmatrix}^{-1} \begin{Bmatrix} r_i \\ r_b \end{Bmatrix} \quad (3.26)$$

The portion of (3.23) which must be inverted has the form shown below

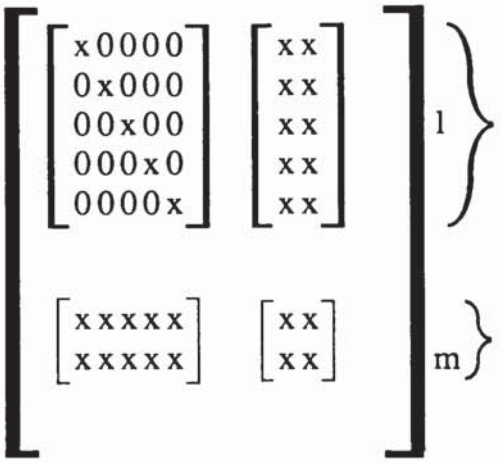

Form of the portion of (3.23) which must be inverted.

Let l be the number of fixed-terminal normal modes retained in the fixed-terminal component mode representation, let m be the number of terminal coordinates and let n be the number of free-terminal normal modes retained in the free-free component mode representation. Then, if the program being used to invert this matrix can utilise the fact the top left portion is already diagonalised, the number of operations required for the inversion is approximately $m^2 + 2.(l \times m)$. A further m^2 operations is needed to evaluate {r}. Comparing this with the n operations necessary to invert the generalised dynamic stiffness matrix of (3.11) and 2.(n x m) operations to evaluate {r} indicates the extra number of component modes which must be removed by modal truncation from the fixed-terminal representation compared with the number removed from a free terminal representation in order that the two representations should be equally effective.

Some of the components used in this investigation are modelled as single elements (chapter 4) and the basic set of coordinates used for these components does not relate to the point displacements so conveniently as

the coordinates of a finite-element model would. (Considering the example presented earlier in §3.1, the F.E. cylinder model of a had 432 degrees of freedom each of which was associated either with unit translation or rotation at one of the nodes. The DMS model, by comparison, used 20 smooth shape-functions for each of the mode-groups.) Some of these involved translation in one direction and rotation about two axes at each of the nodes of the component.) Thus, instead of (3.12) which stated that the vector of boundary terminal coordinates $\{r_b\}$ was a sub-vector of $\{q\}$, the terminal freedoms are related to the subsystem generalised coordinates, $\{q\}$, by (3.27) - an expanded version of equation (3.2).

$$\begin{Bmatrix} \{r_i\} \\ \{r_b\} \end{Bmatrix} = \begin{bmatrix} [E_i] \\ [E_b] \end{bmatrix} \{q\} \qquad (3.27)$$

Previously, we assumed that $\{q\}$ could be partitioned into $\{q_i\}$ and $\{r_b\}$ so that the matrix $[E_i]$ of (3.27) would have been partitioned as $[[E_{ii}],[0]]$.

If vector $\{q\}$ has n entries and $\{r_b\}$ has 1 entries, then $[E_b]$ is 1 x n. A prerequisite to the use of the fixed-constraint mode representation of any substructure is that a matrix [D] (n-1) x n exists such that ..

$$[E_b]\,[D]^t = [0] \qquad (3.28)$$

.. and ..

$$[D]\,[D]^t = [I] \qquad (3.29)$$

These conditions can be restated as $n \leq l$ and row-rank $([E_b]) = l$. If they are satisfied, then we can set up a coordinate-transformation according to (3.30).

$$\{q'\} = \begin{Bmatrix} q_i \\ r_b \end{Bmatrix} = \begin{bmatrix} D \\ E_b \end{bmatrix} \{q\} \qquad (3.30)$$

Now, by the simple expedient of replacing the original coordinate set $\{q\}$ with the modified set $\{q'\}$, we have the situation stated by equation (3.13). The subsystem stiffness and mass matrices [k] and [m] would be modified to [k'] and [m'] according to (3.31).

$$[k'] = \begin{bmatrix} D \\ E_b \end{bmatrix} [k] \left[D^t E_b^t \right] \quad , \quad [m'] = \begin{bmatrix} D \\ E_b \end{bmatrix} [m] \left[D^t E_b^t \right] \qquad (3.31)$$

It has often been the case in the course of this investigation that the number of boundary terminal coordinates l has exceeded the number of generalised coordinates being used to model the subsystem for a particular case of symmetry, especially where the substructure has properties of rotationally-periodicity and one particular mode-group is being examined.

The fixed-terminal mode representation of substructures has not therefore been used at all. (The desirablity of programming this case was mitigated against by the fact that it could not be applied generally to all

substructures prepared).

§3.6 Hybrid Substructure Representation.

MacNeal (C.1971) formally presents a method in which the natural component modes used for the representation have some free interface freedoms and some constrained. Attachment modes need only be added for each of the terminals which was fixed during the computation of the natural component modes. Theoretically, the method is only a minor extrapolation from the pure fixed-constraint component mode representation. In fact, because of the general approach taken with terminal coordinates (i.e. that they need not necessarily be boundary coordinates) the extension is quite trivial. Instead of considering the vector $\{r_b\}$ to include literally all of the boundary terminals, the hybrid method allows that some of the boundary terminals can be included in the vector $\{r_i\}$ instead. If this substitution is made mentally, the mathematics for the substructure representation is then unchanged from that presented above.

The choice between whether to allow a given terminal coordinate to be free or constrained when computing the component modes is a powerful expedient in controlling the number of coordinates which must ultimately be retained to approximate the behaviour of a subsystem. If a large stiff component has a small flexible component attached to it at a particular terminal, then that coordinate is best dealt-with in the free condition in the context of the large subsystem and as a fixed terminal in the context of the smaller subsystem.

In the previous section, it was stated that the fixed-terminal representation of substructure was rejected for use in this investigation because it was not generally applicable to the special substructures analytically developed by the methods of chapter 4. It is always possible to fix some of the terminal freedoms of any substructure without causing problems of over-constraint, and so it would be possible in general to use the hybrid method of substructure representation for all substructures encountered in this investigation. This has not been done, however, because techniques have been developed which overcome the problems of the free-free representation in a more convenient way.

§3.7 Free-Free Component Mode Representation with Interface Loading.

Gladwell (C.1964) does not treat the individual subsystems independently of the other subsystems within the composite system. This removes one of the principle advantages of substructuring as enumerated by Hurty *et al.* (C.1971) and makes it more difficult to separate the processes of substructure representation and composite structure assembly. Instead of dividing the composite system into distinct subsystems, Gladwell forms "branches". In each branch one of the subsystems is free to move and distort while the others are constrained so that they can either move as rigid bodies or not at all (the decision being left to the discretion of the modeller). Thus the component modes take some account of the adjoining subsystems and so the more closely resemble the modes of the composite system. Gladwells' method caters

only for statically determinate interfaces. Benfield & Hruda (C.1971), propose a similar but more generalised method by which the effects of adjoining subsystems are included to some extent in the formation of the 'component modes' for a given subsystem. As with the Gladwell method, the representation for one subsystem requires knowledge of the others. The effects of the adjoining subsystems are included by "interface loading" - both inertial and elastic.

Let [m], [k] be the mass and stiffness matrices for the subsystem of interest. Vector {q} is the vector of generalised coordinates for the subsystem. Matrices [$\underline{m}$], [$\underline{k}$] are the mass and stiffness matrices for the remainder of the system and {$\underline{q}$} is the vector of generalised coordinates. The vectors of terminal coordinates for the subsytem and remainder-of-the-composite-system are {r} and {$\underline{r}$} respectively and these relate to {s}, {$\underline{s}$} by coordinate transformation matrices [E] and [$\underline{E}$] as in equation (3.2). Now, the connection between the subsystem and the remainder-of-the-composite-system is expressed by (3.32) below. It is convenient for purposes of explanation to define a set of tie coordinates {t}.

$$[C]\{r\} = \{t\} = [\underline{C}]\{\underline{r}\} \qquad (3.32)$$

$$[D]\{q\} = \{t\} = [\underline{D}]\{\underline{q}\} \qquad (3.33)$$

... where ...

$$[D] \doteq [C]\,[E] \qquad (3.34a)$$

$$[\underline{D}] = [\underline{C}]\,[\underline{E}] \qquad (3.34b)$$

Benfield & Hruda apply standard static reduction techniques in order to find approximate mass and stiffness matrices for the remainder of the composite system. In their paper, the generalised cordinates are the same as the terminal coordinates. Here, we require to maintain as general a view as possible. Thus, we suppose that some matrix $[\underline{F}]$ is found as defined below.

$$[\underline{F}] = [\underline{D}]\,[\underline{k}]^{-1}\,[\underline{D}]^{t} \qquad (3.35)$$

Matrix $[\underline{F}]$ relates the vector of deflections of the remainder of the composite system $\{\underline{q}\}$ to forces at connections for a forcing frequency of zero. Thus we arrive at mass and stiffness "interface-loading" matrices $[\underline{m'}]$, $[\underline{k'}]$.

$$[\underline{m'}] = [\underline{F}]^{t}\,[\underline{m}]\,[\underline{F}] \qquad (3.36a)$$

$$[\underline{k'}] = [\underline{F}]^{t}\,[\underline{k}]\,[\underline{F}] \qquad (3.36b)$$

If the subsystem of interest is oscillating at angular frequency ω with a given set of deflections $\{q\}$, we can establish values for the vector of tie coordinates $\{t\}$ from (3.33). The contribution to kinetic energy, K.E., from the remainder of the composite system is then $0.5\ \omega^2\ \{t\}^t\ [\underline{m'}]\ \{t\}$ and the contribution to strain energy, S.E., from the remainder of the composite system is $0.5\ \{t\}^t\ [\underline{k'}]\ \{t\}$, if the frequency, ω, is significantly less than

the first resonance of the remainder of the composite system. The interface loading matrices [m'], [k'] above apply to the tie coordinates {t}. The equivalent interface loading matrices [m"], [k"] which apply to the subsystem generalised coordinates {q} are defined as ...

$$[m''] = [C]^t [m'] [C] = [C]^t [F]^t [m] [F] [C] \qquad (3.37a)$$

$$[k''] = [C]^t [k'] [C] = [C]^t [F]^t [k] [F] [C] \qquad (3.37b)$$

These matrices have the same dimension as [m], [k]. Benfield and Hruda simply add [m"], [k"] to [m],[k] before solving the subsystem eigenvalue problem. The 'component modes' which result are generally more similar to the component deflections within composite-system modes than either the free-free modes of the subsystem or the fixed-attachment modes. Consequently, it is generally possible to eliminate more coordinates from the individual subsystems.

The selection of a coordinate-transformation for each subsystem requires the solution of a statics problem of the entire remainder of the composite structure. Furthermore, the 'component modes' obtained are neither mutually inertially uncoupled nor mutually elastically uncoupled with respect to the subystem mass and stiffness matrices [m],[k]. Consequently the amount of data which must be retained for the individual subsystem is frequently increased relative to a more straightforward substructure representation though the numbe. of coordinate actually used in the representation is less.

The free-free component mode representation of substructures with interface loading is not a suitable technique for use with the indirect method of substructure assembly. Because this has been the preferred assembly method, interface loading has not been used.

§3.8 Hybrid Component Mode Representations with Redundancy

Bamford (C.1966) presents a method in which the complete set of free-free subsystem modes is augmented by a set of fixed-constraint normal modes. The result, initially, is a coordinate transformation from a set of n original generalised coordinates to a set of more than n 'component modes'. Truncation of the modal series must be applied before to reduce the number of 'component modes' back to n before the substructure can be incorporated into a composite system. A number of variants of this method are conceivable. Once again, the need to solve for fixed-constraint normal modes for the subsystems has dictated that these methods are not suitable for use with the motor component elements of Chapter 4.

§3.9 Composite Structure Assembly.

Two distinct methods for composite-structure assembly exist within the literature. We shall refer to these are the "direct" and "indirect" methods. Both are suitable for the calculation of response to forcing over a range of frequencies and for the solution of modes and natural frequencies. It is not necessary for either approach that component

mode representations of the subsystems exist though there can be a serious impact on the computation time required if the original generalised coordinates of the subsystems are used. For generality, we shall call the vector of generalised coordinates being used for subsystem i $\{q"\}_i$. The associated vector of forces is $\{Q"\}_i$ and the mass and stiffness matrices are $[m"]_i$ and $[k"]_i$. The vector of terminal coordinates for subsystem i is termed $\{r\}_i$ and the vector of terminal forces is $\{R\}_i$. These vectors have the same meaning as before. The transformation between $\{q"\}_i$ and $\{r\}_i$ is expressed by (3.38).

$$\{r\}_i = [V"]_i \{q"\}_i \qquad (3.38a)$$

$$\{Q"\}_i = [V"]_i^t \{R\}_i \qquad (3.38b)$$

The coordinate transformations for free-free, fixed-constraint and hybrid component mode representations have been developed in previous sections and the substitutions necessary are summarised here.

<u>For Free-Free Component mode representation.</u>

$[m"] = [I]$ .. equations (3.5) and (3.6)

$[k"] = [\Lambda]$ .. equations (3.5) and (3.6)

$[V"] = [V]$ .. equations (3.7) and (3.8).

For Fixed-Constraint Component Mode Representation.

$$[m''] = [m'] \qquad \text{.. equation (3.20).}$$

$$[k''] = [k'] \qquad \text{.. equation (3.19).}$$

$$[V''] = \begin{bmatrix} V_i & V_b \\ 0 & I \end{bmatrix} \qquad \text{.. equations. (3.15) and (3.17)}$$

For Hybrid Component Mode Representation.

The partitioning of the terminal coordinates is different to that used for the *Fixed-Constraint* modes but otherwise the substitutions are identical.

$$[m''] = [m'] \qquad \text{.. equation (3.20).}$$

$$[k''] = [k'] \qquad \text{.. equation (3.19).}$$

$$[V''] = \begin{bmatrix} V_i & V_b \\ 0 & I \end{bmatrix} \qquad \text{.. equations. (3.15) and (3.17)}$$

For Direct use of the Original Subsystem Generalised Coordinates.

$$[m''] = [m]$$

$$[k''] = [k]$$

$$[V''] = [E] \qquad \text{.. equation (3.2).}$$

In the "direct" method, the set of constraints representing the connections between subsystems is used to form another new set of coordinates. If the total number of coordinates in the unconnected composite system is n and the total number of connection coordinates is l, then the new set contains n–l coordinates. The stiffness and mass matrices are then formed directly and used in the usual way.

This contrasts with the "indirect" method in which all† of the subsystem

---

† *Footnote:* Approximations used in conjunction with either the "direct" or "indirect" methods of composite structure assembly can result in a reduction in the number of coordinates for the composite system. In strict terms, it is correct to consider that such approximations are actually made in the process of creating the individual substructure representations. Then, the statement made above is generally true.

coordinates are retained and the joining of subsystems is enforced by applying connection forces to the unconnected composite system which are exactly sufficient to prevent the joints from separating.

Both methods have merits and shortcomings and these are listed with the respective discussions below. The preclusion of flexibility of connections in the case of the direct method is not as severe a drawback as might first be imagined. It is possible to model connection flexibility by including it in one of the substructures using notional masses as illustrated below. However, in machines, the flexibility of some of the joints has been shown to be controllable and in modelling a number of different cases of flexibility, it is not practicable to regenerate the data for those subsystems with which the flexibility was associated.

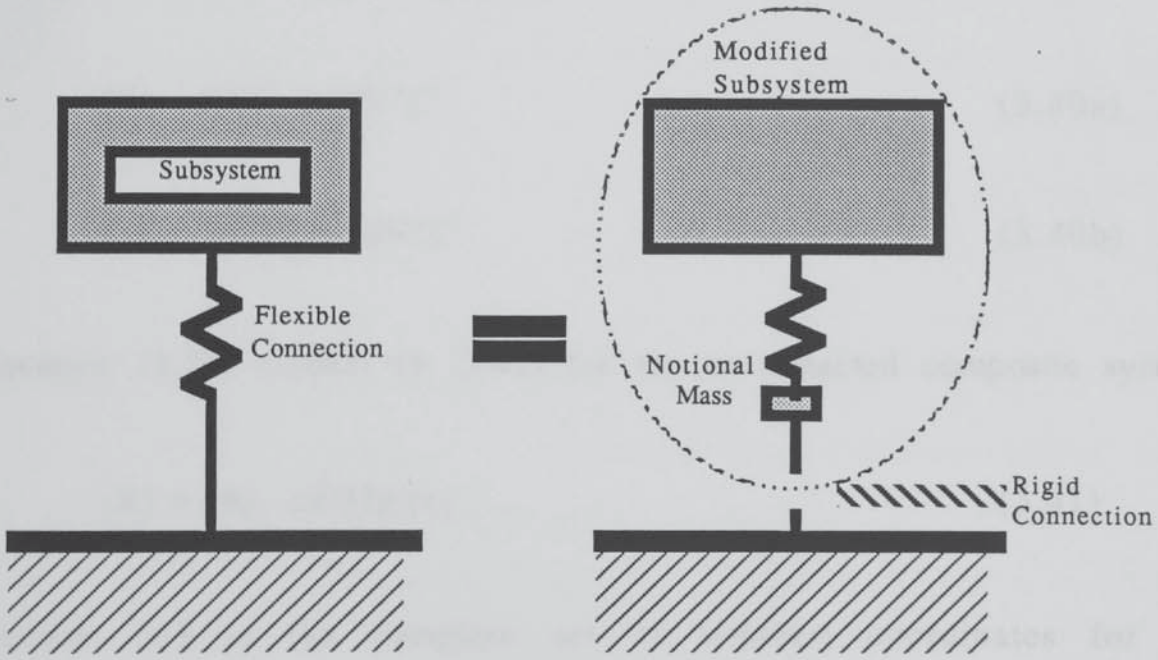

Incorporating Connection Flexibility into a Substructure.

§3.10 The "Direct" Method of Structure Assembly.

In the direct method of structure assembly, we require to form stiffness matrix [K] and mass matrix [M] for each subsystem i such that the vector of terminal forces $\{R\}_i$ is related to the vector of terminal displacements $\{r\}_i$ by (3.39).

$$\{R\}_i = [[K]_i - \omega^2 [M]_i] \{r\}_i \qquad (3.39)$$

In general, this is only possible if the transformation matrix [V"] is square and well conditioned since $[K]_i$ and $[M]_i$ are related to [k"] and [m"] by (3.40a) and (3.40b) below.

$$[K] = [V"]^{-t} [k"][V"]^{-1} \qquad (3.40a)$$

$$[M] = [V"]^{-t} [m"][V"]^{-1} \qquad (3.40b)$$

Equation (3.39) extends to (3.41) for the unconnected composite system.

$$\{\mathbf{R}\} = [[\mathbf{K}] - \omega^2[\mathbf{M}]] \{\mathbf{r}\} \qquad (3.41)$$

Vector $\{\mathbf{r}\}$ is the complete set of terminal coordinates for the unconnected composite system comprising vectors $\{r_1\}$, $\{r_2\}$, $\{r_3\}$ etc. - the vectors of terminal coordinates for each of the subsystems. Similarly, vector $\{\mathbf{R}\}$ is the complete set of terminal forces for the

unconnected composite system comprising vectors $\{R_1\}$, $\{R_2\}$, $\{R_3\}$ etc. - the vectors of terminal forces for each of the subsystems. Matrices [**K**] and [**M**] are formed by placing the individual $[K]_i$ and $[M]_i$ along diagonals.

Now, when the subsystems are rigidly connected, the displacements at the various interfaces must always match. In general, there is some constraint matrix [C] for every composite structure which expresses the conditions at the subsystem interfaces as (3.42).

$$[C]\{\mathbf{r}\} = \{0\} \qquad (3.42)$$

Normally, the connection matrix [C] is a sparse matrix each row of which contains a single "1" and a single "-1". It is trivial in this case to produce a reduced set of coordinates $\{\underline{r}\}$ for the connected composite system which automatically satisfies the connection equation matrix by simply eliminating some coordinates. A workable algorithm is to proceed through the matrix [C] removing the coordinate which corresponds to each column which has either a single "1" or "-1". In more complex cases of [C], individual coordinates are successively written in terms of the remaining coordinates and then struck from the list. Let n be the total number of coordinates in the unconnected composite-system and l the number of constraints. Matrix [C] is then l x n. Whichever technique applies, it is possible in general to find some matrix [G] (n x (n-l)) such that (3.43) and (3.44) are true.

$$[C][G] = [0] \qquad (3.43)$$

$$[G]^t [G] = [I] \tag{3.44}$$

The number of rows of [G] equals the total number of unconnected composite-system coordinates. The number of columns is less than the number of rows by the number of independent connections which have been applied to the collection of subsystems. If [G] has been found, a coordinate transformation can immediately be effected to produce $\{\underline{\mathbf{r}}\}$ using (3.45) which inherently satisfies the constraint equations [C].

$$\{\mathbf{r}\} = [G] \{\underline{\mathbf{r}}\} \tag{3.45}$$

The mass and stiffness matrices for the connected composite system $[\underline{\mathbf{M}}]$ and $[\underline{\mathbf{K}}]$ are derived using standard coordinate-transformation techniques - equations (3.46) and (3.47).

$$[\underline{\mathbf{M}}] = [G]^t [\mathbf{M}] [G] \tag{3.46}$$

$$[\underline{\mathbf{K}}] = [G]^t [\mathbf{K}] [G] \tag{3.47}$$

Thus, the procedure of substructure assembly is - in the end - reduced to a single coordinate transformation. Now eigenvalues and eigenvalue and response calculations can be performed directly for the composite structure using well established methods. This is the first option for structure assembly and is proposed by most of the papers in the literature including Goldman (C.1969), Gladwell (C.1964), Benfield & Hruda (C.1972), Craig & Bampton (C.1968) and MacNeal (C.1971). Its

limitations as far as the investigation into machines is concerned are threefold.

(1) The matrix [V"] must be square and well-conditioned. This is particularly difficult to ensure with non finite-element subsystems such as the RING, BEAM and CYLINDER elements developed in chapter 4.

(2) The procedure relies on the use of only rigid constraints. We shall see that the particular problem associated with the DC frame must incorporate joint flexibility.

(3) The matrices [**M**] and [**K**] being dealt-with are very large though they are only partly populated.

§3.11 The "Indirect" method of Structure assembly.

The alternative approach to structure assembly is that originally adopted by Kron (C.1963) for use with electrical networks and developed towards mechanics applications by Simpson (C.1984). Simpson does not include the facility for flexible connections though other authors applying the same method (Turner *et al.* (C.1985)) do include mention of flexibility at interfaces.

In this case, we do not require to produce [**M**] and [**K**]. Instead, the subsystems are represented in the dynamic-flexibility form of (3.4a). The relation between $\{r\}_i$ and $\{R\}_i$ for subsystem i is (3.48).

$$\{r\}_i = [V''] \, [\, [k''] - \omega^2 [m''] \,]^{-1} \, [V'']^t \, \{R\}_i = [f]_i \, \{R\}_i \qquad (3.48)$$

Once again, a set of connection equations exists in the form of [C]. In the indirect assembly method, an auxiliary set of coordinates $\{\mathbf{t}\}$ is defined for the composite system (equation (3.49)) which represents the separation of the joints (the separation may be non-zero if the joints are flexible).

$$\{\mathbf{t}\} = [C] \, \{\mathbf{r}\} \qquad (3.49)$$

A set of connection forces $\{\mathbf{T}\}$ exist which are proportional to $\{\mathbf{t}\}$ according to (3.50). The matrix constant $[k_t]$ is the stiffness of the connections and is usually diagonal in form. Infinite entries are allowable for those connections which are completely rigid.

$$\{T\} = - [k_t] \, \{t\} \qquad (3.50)$$

The minus sign comes about because we define $\{\mathbf{T}\}$ as the vector of forces exerted <u>by</u> the connections <u>on</u> the subsystems rather than vice-versa. Now, using the principle of virtual work, it is simple to show that $\{\mathbf{R}_{conn}\}$ - the vector of forces acting on the terminals of the unconnected composite-system - is related to $\{T\}$ by (3.51).

$$\{\mathbf{R}_{conn}\} = [C]^t \, \{T\} \qquad (3.51)$$

The total force acting on the individual subsystems of the composite system is the sum of two components $\{\mathbf{R}_{conn}\}$ and $\{\mathbf{R}_{ext}\}$ (3.52).

$$\{\mathbf{R}\} = \{\mathbf{R}_{conn}\} + \{\mathbf{R}_{ext}\} \tag{3.52}$$

Combining (3.48) with (3.50) thru' (3.52) enables us to write $\{\mathbf{T}\}$ in terms of $\{\mathbf{R}_{ext}\}$ as (3.53).

$$\left[[\mathbf{I}] + [\mathbf{k}_t][\mathbf{C}][\mathbf{f}][\mathbf{C}]^t\right]\{\mathbf{T}\} = -[\mathbf{k}_t][\mathbf{C}][\mathbf{f}]\{\mathbf{R}_{ext}\} \tag{3.53}$$

The total composite-system response $\{\mathbf{r}\}$ is evaluated using the same equations and can be written as (3.54) or (3.55).

$$\{\mathbf{r}\} = [\mathbf{f}]\,[[\mathbf{C}]^t\{\mathbf{T}\} + \{\mathbf{R}_{ext}\}] \tag{3.54}$$

$$\{\mathbf{r}\} = [\mathbf{f}]\left[[\mathbf{I}] - [\mathbf{C}]^t\left[[\mathbf{I}] + [\mathbf{k}_t][\mathbf{C}][\mathbf{f}][\mathbf{C}]^t\right]^{-1}[\mathbf{k}_t][\mathbf{C}][\mathbf{f}]\right]\{\mathbf{R}_{ext}\} \tag{3.55}$$

In practice, (3.53) and (3.54) are used in preference to the single closed form (3.55). It is sometimes impossible to find the inverse included in (3.55) but it is always possible to find some $\{\mathbf{T}\}$ (not unique when there are redundant connections) by Gaussian elimination which satisfies (3.53).

Resonances of the subsystem are located by searching for frequencies at which the determinant of $[[\mathbf{I}] + [\mathbf{k}_t][\mathbf{C}][\mathbf{f}][\mathbf{C}]^t]$ is zero. Simspon (C.1984) has

extended the Sturm sequence observations of Wittrick and Williams (C.1971) to enable the modeller to count the number of composite-system resonances whose frequencies are below the trial frequency and developed a searching algorithm based on the Gaussian reduction of the matrix which does not involve the explicit calculation of the determinant.

The "indirect" method does not suffer the limitations enumerated above for the "direct" method. Its principle shortcoming is the relative high amount of computation time necessary to solve for the vector of connection forces {T} for each trial frequency. The time compares favourably with the direct method when the number of composite system coordinates is very large with respect to the number of connections.

(1) The matrix [E] can have any form and any condition without loss of accuracy to the computed displacements.

(2) Flexibility of connections can be included without penalty.

(3) The amount of core storage is minimal.

§3.12 An Optimised "Direct" Approach to the Solution of the Constrained Eigenvalue Problem.

The author has developed a method by which the eigenvalues and eigenvectors of a rigidly connected composite structure can be found by

directly forming banded stiffness and mass matrices for a set of coordinates which inherently satisfy the constraints of connection. The method is many times more efficient than the "indirect" method described above (and by previous authors) for typical problem dimensions and does not suffer from the two major (as far as the investigation of the vibration of motors is concerned) shortcomings of the "direct" method:

(1) The matrix [E] of (3.2) can have any form and any condition.

(2) The full (n-l) x (n-l) mass and stiffness matrices are never formed (where (n-l) is the total number of composite system degrees of freedom after connection). Instead, the mass and stiffness matrices are banded.

The procedure is designed around the use of free-free component mode representations but can be extended for any subsystem representations including the fixed-constraint and hybrid varieties. The method is developed and explained in appendix 3.

§3.13 Approximations To Accelerate Analysis.

In all branches of numerical analysis it is possible to trade exactness for increased speed of computation. In the context of dynamic substructuring and dynamic modelling in general, the most powerful method of achieving increased speed is to reduce the numbers of coordinates (degrees of freedom) involved in various stages of the

computation. In some cases, the coordinates are discarded completely. More usually, assumptions are made regarding the way in which some coordinates may vary with frequency. The approximation techniques are categorised as follows:

(1) Approximations made at the substructure representation stage.

(2) Approximations during composite-structure assembly.

  (a) Those applicable in the "direct" method of assembly.

  (b) Those applicable in the "indirect" method of assembly.

We deal first with the approximations made at the substructure representation stage. Every substructure model is approximate. In applying the Rayleigh-Ritz method, the first step taken by the modeller is to assume that the general deflection pattern of the substructure must be some linear combination of a finite number of shape-functions. Generally, if more shape-functions are used, the quality of the approximation is improved. Also, if the individual shape-functions can be made to be more similar to the system eigenstates, the quality of approximation for a given number of shape-functions improves. (Each shape-function is associated with one coordinate). The latter point is one of the two main reasons for using component-mode representations. By finding subsystem modes and associated resonant frequencies, a coordinate transformation is effected and the new coordinates are elastically and inertially uncoupled. The associated frequencies can be used to discern to some extent whether various coordinates need to be retained. If the frequency is very high compared with the highest

frequency in the range of interest, it is likely that the coordinate can be discarded.

Goldman (C.1969) discusses the use of free-free component mode representation and points out that serious errors can arise if high frequency component modes are discarded from the mode series. This can be justified intuitively. In a low-frequency free-free mode, the locations of maximum stress/internal-force are towards the center of the structure and stress/internal-force decreases steadily with proximity to the boundary. Thus, if a low frequency subset of the free-free modes is retained and all other modes discarded, the modeller has implicitly assumed that stresses/internal-forces must be small near the boundaries. However, connection forces are applied at boundaries when the subsystem is a part of a composite system. Hence, some finite error is expected.

The substructure representation proposed by Hurty (C.1965) uses fixed-constraint natural modes and a set of attachment modes. The number of attachment modes is equivalent to the number of degrees of freedom at the subsystem boundaries and it is not possible to reduce this number before the substructure is incorporated into a composite system. The fixed-constraint natural modes are shown (above as well as by other authors) to be elastically uncoupled from the attachment modes but there is some inertial coupling. The series of fixed-constraint natural modes can be truncated based on frequency comparisons without the risk of serious error so long as no forces are required to be applied to the subsystem except at its boundaries and no responses are

required except at the boundaries.

The components used in this investigation have had relatively large numbers of terminals at which forces might be applied or responses computed. Frequently, the number of terminal coordinates has equalled or exceeded the number of generalised coordinates which were used to model the component. The fixed-constraint representation of subsystems was rejected because it was not generally possible to ensure that the boundary terminals would be independent. Had it been possible to do so, the principle advantage of the method (i.e. the straightforward reduction in the numbers of subsystem coordinates) would still have been of little value because of the relative magnitudes of the number of subsystem generalised coordinates and the number of subsystem terminal coordinates.

Truncation of the modal series in the case of the free-free component mode representation with interface loading ought lead to fewer coordinates being used for the individual subsystems than in the case of either the free-free of fixed-constraint representations for the same quality of approximation since the 'component modes' (more correctly called 'branch modes' in this case) ought generally be more similar to the composite system modes than the component modes in either of the other two cases. If there are a number of resonances of the remainder of the composite system below the highest frequency of the range of interest, then it becomes questionable whether a free-free component mode representation is superior to a fixed-constraint component mode representation.

An alternative to discarding coordinates from a substructure representation is to replace many of them with matrix terms which collectively account for the "residual" mass, energy dissipation (if damping is being used), and stiffness of the coordinates or component modes removed. A static analysis can be used to determine the contribution from high-frequency component modes by neglecting the inertia terms. MacNeal (C.1971) suggests that the correction matrices be derived from the difference between the true subsystem receptance matrix at very low frequencies and the approximate subsystem receptance matrix derived from the truncated set of component modes. MacNeal takes no account of the inertia effects of the removed modes. (His 'residual mass' matrix corrects for inertia terms associated with the retained component modes which are originally omitted in his formulation. The fixed-constraint component mode representation by Hurty includes these effects). Rubin (C.1975) proceeds one step further in correcting for the discarded modes. As with MacNeal, Rubin derives a flexibility correction matrix based on a static analysis at frequencies which are low compared with the lowest frequency of the discarded modes. Then, based on the receptance correction matrix, inertia terms are derived. Rubin demonstrates that this formulation is an order of approximation better than the MacNeal approximation which is in turn one order of approximation better than the traditional method of simply discarding component modes on the basis of frequency. The three levels of approximation are summarised here. Matrix [f] of (3.4a) is the true flexibility matrix for the substructure at angular frequency ω. Matrix $[f_m]$ is the contribution to [f] of the retained subsystem modes. Matrix

$[f_d]$ is the contribution to [f] of the discarded modes. $[U_d]$ is the modal matrix expressing the discarded modes in terms of the subsytem generalised coordinates.

The zeroth order approximation (simply discarding modes) reads ...

$$[f] \approx [f_m] \tag{3.56}$$

The first order approximation (MacNeal) reads ...

$$[f] \approx [f_m] + [f_d] \tag{3.57}$$

The second order approximation (Rubin) reads ...

$$[f] \approx [f_m] + [f_d] - \omega^2[h_d] \tag{3.58}$$

The matrices $[f_d]$ and $[h_d]$ are derived according to (3.59) and (3.60).

$$[f_d] = [U_d]^t\,[k]^{-1}\,[U_d] \tag{3.59}$$

$$[h_d] = [[U_d]^t\,[k]^{-t}]\,[m]\,[[k]^{-1}\,[U_d]] \tag{3.60}$$

Rubin observes that higher order approximations can be devised but suggests that the law of diminishing returns quickly comes into play.

Kuhar & Stahle (C.1974) propose that a Guyan type dynamic reduction in the number of subsystem coordinates be effected <u>before</u> the

eigenvalue problem is solved for the subsystem. "Slave" freedoms can be chosen by comparing the frequency obtained from dividing the associated diagonal stiffness and mass terms with the highest frequency of the range of interest. Then when the component modes are being evaluated, all resulting modes are retained as the new subsystem coordinates. Turner, Milsted and Hanks (C.1985) note that in such a process, none of the terminal freedoms themselves should be allowed to be "slave" freedoms. This approximation method is highly effective insofar as it ensures that the subsystem deflection patterns which are suppressed by the removal of coordinates elastically uncoupled from deflections of the terminal freedoms just as the fixed-constraint modes were elastically (but not inertially) uncoupled from the terminal freedoms in the fixed-constraint representation.

The method of Kuhar & Stahle has been employed directly when finite-element models of components have been prepared. The DMS system automatically labels the selected terminal freedoms of the substructure as master degrees of freedom.

For machine components which are modelled semi-analytically as single elements, the Kuhar & Stahle method poses difficulties. Since the matrix [E] of (3.2) relating the terminal freedoms {r} to the subsystem generalised coordinates is not generally square it is difficult to ensure that by removing any one generalised coordinate, a constraint has not been placed on {r}.

A different method has been used for these components. Because it is

possible in most cases to divide the modes of these components into separate groups it is usually convenient to solve for all the modes. Thus, one might typically find 700 modes of a cylinder having solved many eigenvalue problems of degree 20. Then modes are discarded one by one if their frequency is sufficiently far removed from the range of interest. (Garvey, Penny and Gilbert (C.1988) include the case in which the bottom of the frequency range of interest may be above some of the subsystem modes.) A frequency-independent receptance correction matrix is built up representing the entire set of discarded modes. The result is the same as the Kuhar & Stahle appoach but avoids the danger of inadvertently constraining the subsystem implicitly. The receptance correction matrix being independent of frequency is a first order approximation. By using higher orders of approximations it would be possible to remove more modes while retaining the same quality of approximation. The relative magnitudes of the various problem dimensions encountered within this investigation are such that it is not effective to use any order higher than the first. Some substructures have had such large numbers of terminal coordinates compared with the numbers of modes which might be discarded that it has not even been effective to use the first order approximation and in these cases, all of the computed modes have been retained.

Having removed all of those subsystem coordinate which can be discarded on the basis of high characteristic frequencies, (or replaced them using first, second or third order receptance matrix quantities etc.) any further approximation/increase-in-computational speed must come about by some economisation in the number of connections used or the

manner in which these connections are handled in programs.

For the "direct" method of composite-structure assembly (ie. a coordinate transformation which produces a set of coordinates implicitly satisfying the constraints), Craig & Chang suggest that a reduction be applied to the interface coordinates. Three different forms of reduction are proposed. They propose that the Rayleigh quotient be examined for each of the interface coordinates and if the corresponding characteristic frequency is significantly higher than the highest frequency of the range of interest, the coordinate should be reduced out either by simply striking it from the list of coordinates of using a Guyan-type reduction process to remove the coordinate and modify the mass and stiffness matrices acordingly.

The equivalent operation in the 'indirect' (Kron) method of assembly is more difficult. In this case, the connections have no unique corresponding stiffness and mass since both are functions of frequency. Garvey, Penny & Gilbert (C.1988) suggest a method by which this process can be effected by assigning an approximate receptance for the connections based on the minimum modal receptance figures for each of the subsystem modes of the composite system. The 'responsiveness' of the composite-system to connection forces is compared with the flexibility of the connections themselves. If the responsiveness of the composite-system to a given connection force is significantly less than the flexibility of the connection, the connection may be discarded. For example, if the composite system is a single degree of freedom mass of 100 kg, and the only connection joins this mass to ground with a

stiffness of 1N/m, the connection may be ignored for angular frequencies greater than (let us say) 1 rad/sec because above 1 rad/sec, the receptance of the composite system never exceeds 0.01 m/N which is much less than the connection flexibility (1 m/N). Normally, the modeller would not include such a connection in any case. However, it possible is in realistic cases to solve a "mini" eigenvalue problem to find a new set of connection coordinates some of which have high associated flexibility compared with the 'responsiveness' of the composite system over the frequency range of interest. This has frequently been the case in the connection sets joining DC machine mainpoles to the yoke. A number of connections are used to represent a smooth join and then by "reblending" these, a large proportion of the connections can be removed. The procedure is explained in more detail in appendix 1.

An entirely different approach has also been used which relates to the formation of the matrix product $[C][f][C]^t$ known as Kron's matrix. No connections are discarded. Instead, the contributions made to this matrix by some of the subsystem modes (whose frequencies are well removed from the frequency range of interest) are represented by a matrix power series in ω^2. This process was developed by the author and is explained in detail in appendix 1. It has been found to be the single most useful approximate method for accelerating analyses.

§3.14 A Special Case of Composite-Structure:- Rotational Periodicity.

In the previous chapter, the term rotational periodicity occurred frequently in conjunction with simplifications made by authors in order to produce close-form analytical expressions for natural frequency. Thomas (C.1979) shows that if a structure possesses the property of rotational periodicity, the modes fall into distinct groups each of which is characterised by n - the number of "waves" of displacement about the circumference of the structure. If there are m subsections in the R.P. structure, then n can have values between 0 and m/2.

In the analysis of DC frames in this study, the general method of modelling is to deal with the yoke using pure cylinder theory and use substructuring concepts later to attach the poles individually along with all other subsystems involved in the model. Simpson (C.1984) points out that the solution of a very large composite system is best done by pyramiding solutions (ie. forming the ultimate composite-system from a number of sub-composite-systems and forming each of these from sub-sub-composite systems etc.). The final solution process is much faster if the number of connections involved is small.

A powerful alternative to the general modelling method - if the yoke is not split - is to find all modes and frequencies of the sub-composite system comprising just the yoke, mainpoles and compoles using the techniques associated with rotational periodicity.

One way of performing this analysis is to divide the frame into l identical subsystems, (l being the number of mainpoles on the frame) each one of which contains a fraction of the cylinder, one mainpole, and one compole (Fig. 3.4b) and use the properties of R.P. structures to economically solve for the modes and frequencies of the yoke-with-poles. The time taken to obtain a 'complete' set of free modes for the whole frame is significantly less using this method compared with the general method described above since the usual processes of structure assembly (formation of the matrix [f] of (3.4a) etc.) need not be used. Instead, l separate eigenvalue problems each of dimension 2p are solved (where p is the number of degrees of freedom used to model the individual sections). The larger commercial finite-element analysis packages include facilities to perform analyses of R.P. structures from a model of the repeated substructure.

A more subtle method again has been used in practice (Fig. 3.4c). Instead of considering the mainpoles to be l separate subsystems, they are considered to a single subsystem which - being R.P. - has modes divided into groups characterised by the integer n. Since there is no connection whatsoever between these subsystems, the solution for the modes of this structure for each n involves only p coordinates (p being the usual number of coordinates which would be used to represent the pole) instead of the usual 2p .

Conventional substructuring methods (employing only free-free component modes) are then used to find the modes of the composite structure for each n. Only a subset of cylinder modes needs to be

considered for each n. Thus, for n =2, cylinder modes having {0,2,4,6 ... } waves about the periphery are considered. The case n=0 is special. Cylinder modes {0, 1, 21, 31, 41 ... } are used.

The power of this method lies in the fact that only <u>one</u> of the poles need be connected to the cylinder and the presence of only a limited subset of the modes of both the cylinder and the set-of-mainpoles ensures that the connections are maintained for all of the other poles. Thus, when an unsplit-yoke with mainpoles is being prepared as a substructure in a larger analysis, only two substructures and one set of connections are considered for each mode-group n. If compoles are included also, this becomes three substructures and two sets of connections for each n.

It is somewhat unfortunate in the light of the economy afforded by this method that the occurance of unsplit yokes in very large machines is virtually nil because of the practicalities of rolling the steel and assembling/dissembling the machine. In small and medium-size machines (< 1 MW) most solid yokes are made as a single piece.

§3.15 A Special Case of Composite-Structure:- "Periodic Structures".

The author uses the term "periodic" structure to mean a composite-structure comprising a number of identical substructures identically connected. This regularity-of-form is not quite so useful as the property of rotational-periodicity in terms of the amount of computation time which may be saved. It is, however, a more general

occurrance. (A structure having rotational periodicity may be regarded as a special case of a periodic structure).

There are instances of such structures within electrical machines. Examples include AC stator-cores, DC machine half-yokes with poles and compoles, and finned casings. The author has developed a procedure whereby full use is made of the fact that a "periodic" structure has that particular form. The reader is referred to Garvey & Penny (C.1988). The method is particularly powerful when the number of connection coordinates between successive subsystems is small with respect to the number of generalised coordinates use to describe the behaviour of the subsystem itself and the number of subsytems in the composite system is significantly greater than three.

The method has been tried in the context of analysing a DC machine half-yoke as a periodic structure rather than as a composite-structure comprising half-cylinder and pole-models. It is not an effective alternative in this instance for reasonable numbers of poles. The number of connection coordinates is too great compared with the number of generalised coordinates. It has been estimated that stator cores can also be modelled more effectively using the RING or CYLINDER elements (derived in chapter 4) with special material properties.

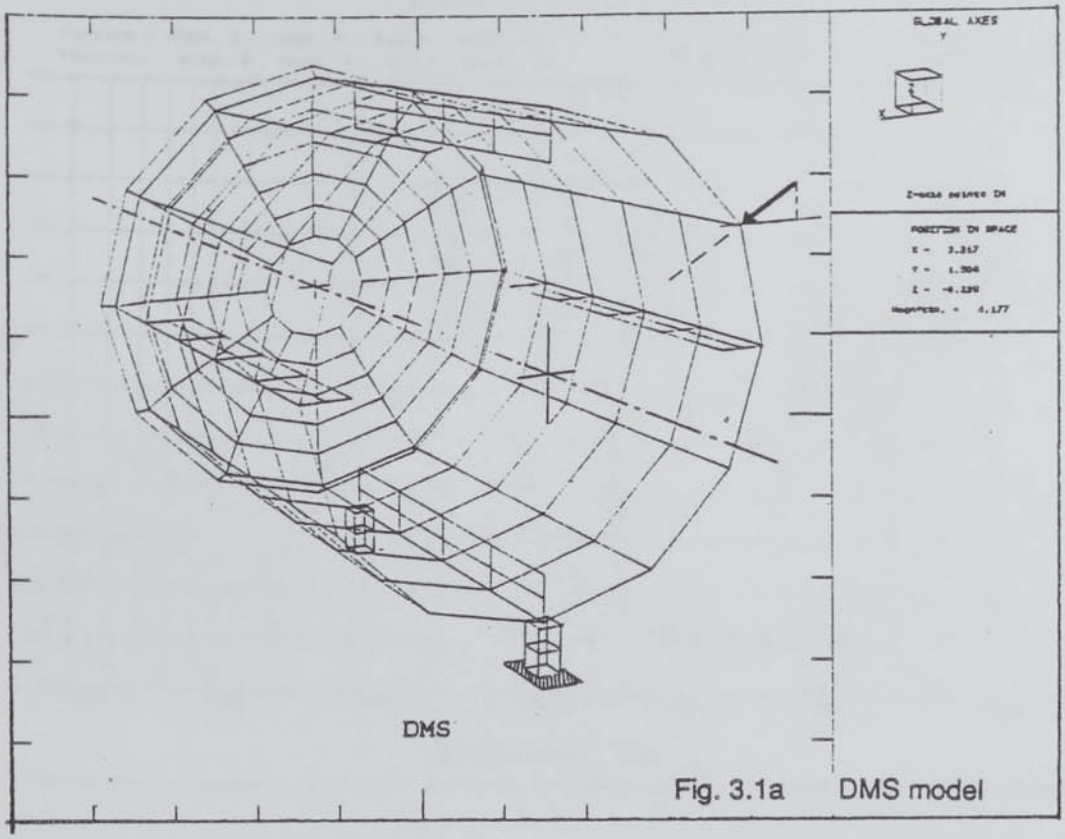

Fig. 3.1a DMS model

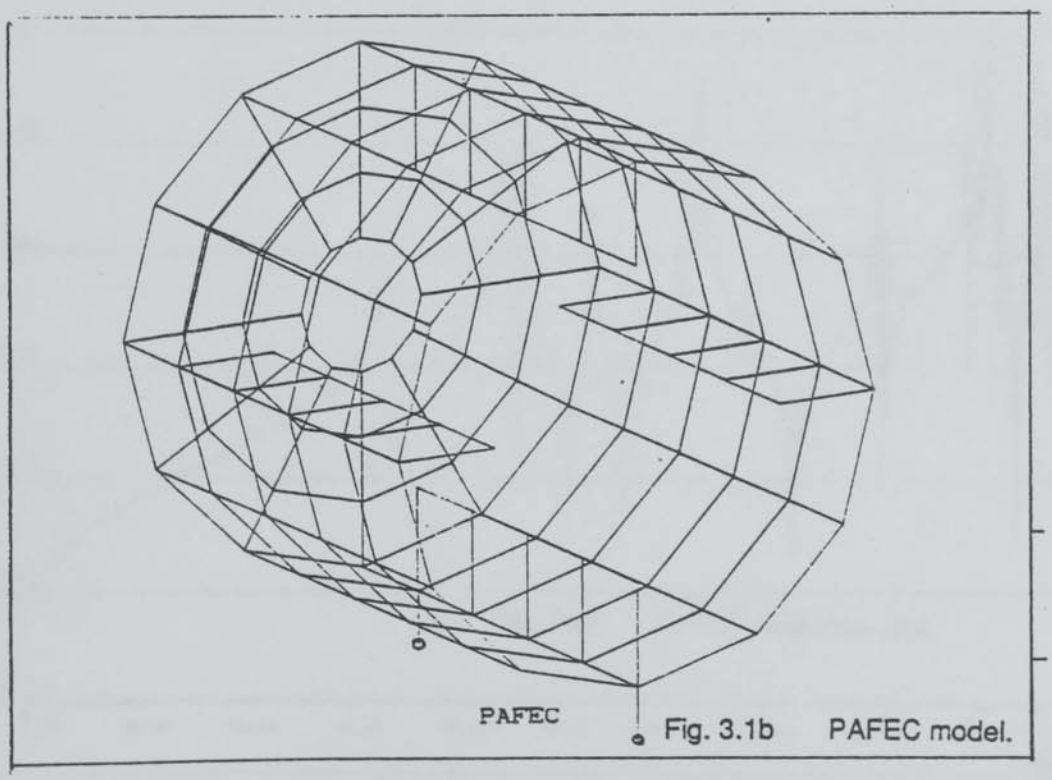

Fig. 3.1b PAFEC model.

Fig. 3.1 DMS and PAFEC models of Test Structure.

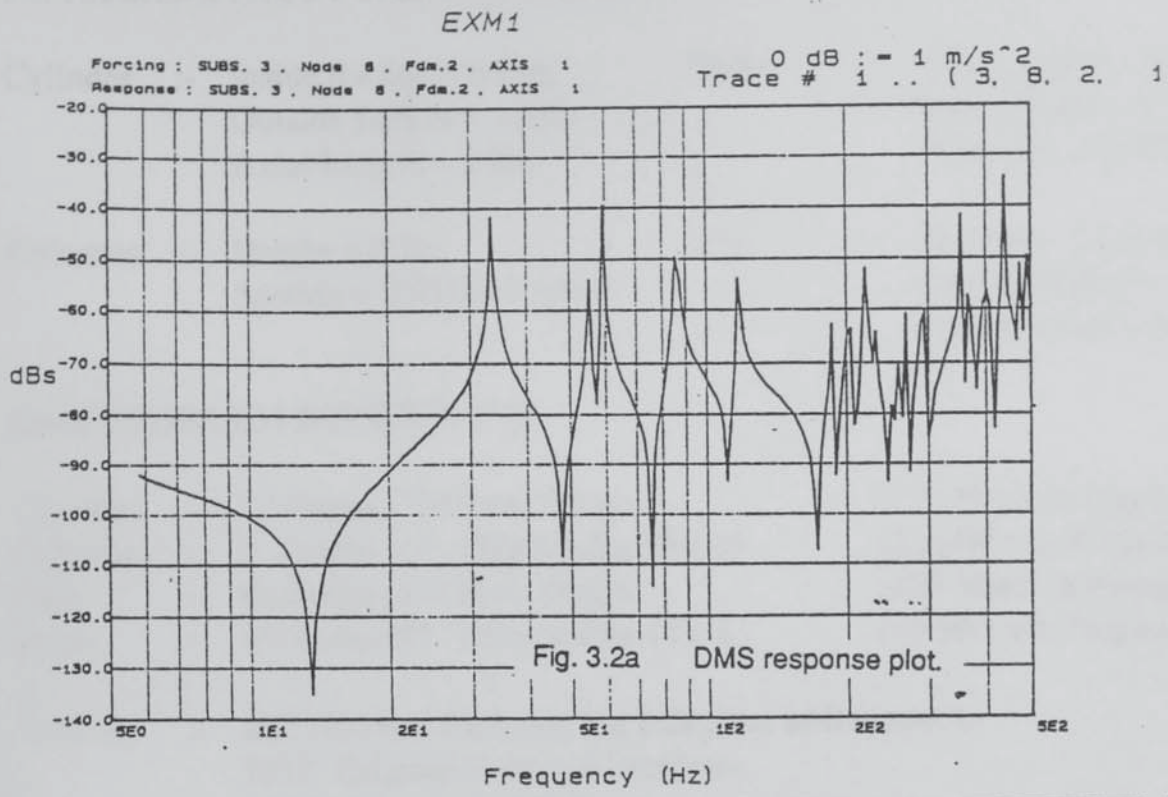

Fig. 3.2a DMS response plot.

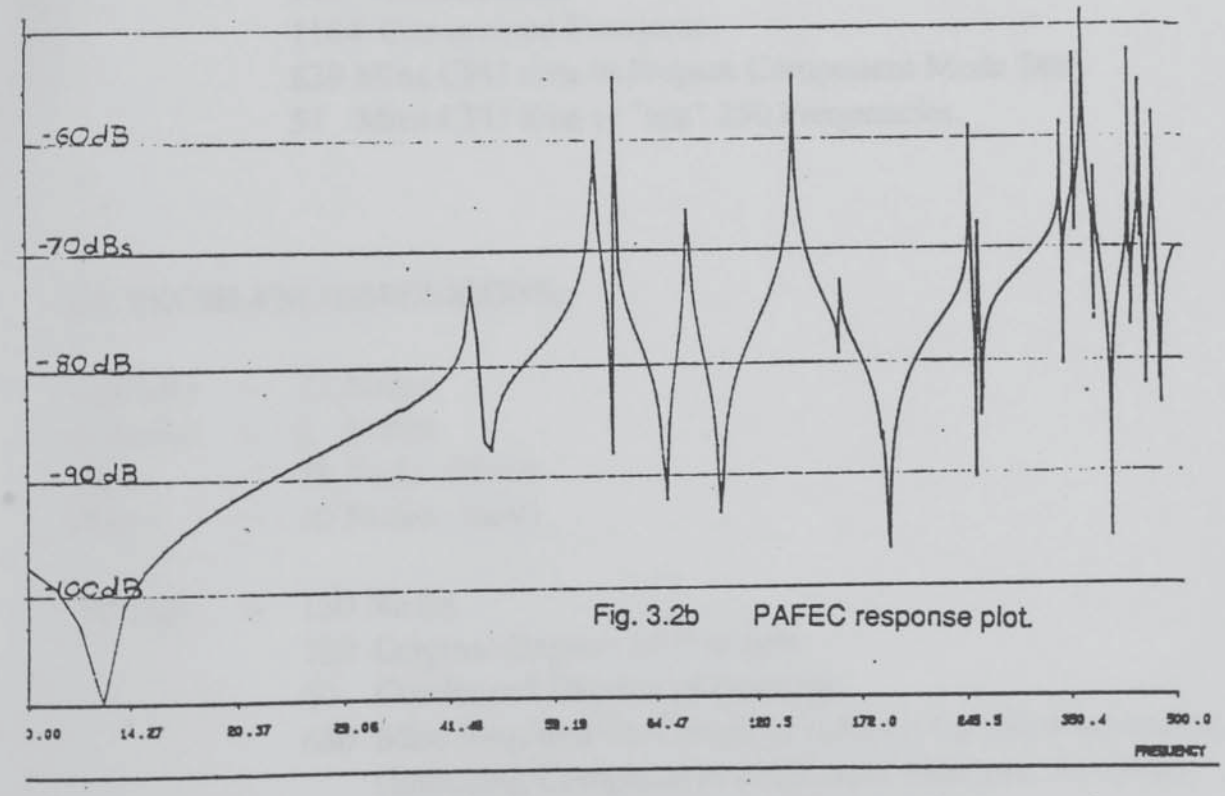

Fig. 3.2b PAFEC response plot.

Fig. 3.2 DMS and PAFEC results for Test Structure.

PHYSICAL STRUCTURE DIMENSIONS.

Cylinder :- Inside Radius = 0.95m
Outside Radius = 1.05m
Axial Length = 2.0m.

Columns :- Height = 0.3m
Section = 0.05m x 0.05m.

Plates :- Axial Length = 1.6m
Radial Depth = 0.2m
Thickness = 0.05m.

Disc :- Thickness = 0.05m
Outside Radius = 1.05m
Inside Radius = 0.2m.

DMS PROBLEM DIMENSIONS.

Cylinder	:-	72 Nodes, 700 Free Modes.	(370 Min.s to Prepare)
Columns	:-	3 Nodes, 14 Free Modes. (Each)	(11 Min.s to Prepare)
Disc	:-	84 Nodes, 478 Free Modes.	(409 Min.s to Prepare)
Plates	:-	15 Nodes, 88 Free Modes. (Each)	(49 Min.s to Prepare)

TOTAL :- 222 Nodes. (Each one has 6 degrees of freedom.).
1332 Original Terminal Freedoms.
1558 Component Modes.
148 Connections.
1184 Constrained Freedoms.
839 Mins CPU time to Prepare Component Mode Sets.
51 Mins CPU time to "test" 250 Frequencies.

FE PROBLEM DIMENSIONS.

Cylinder :- 72 Nodes
Columns :- 2 Nodes
Disc :- 36 Nodes (New)
Plates :- 20 Nodes (New)

TOTAL :- 130 Nodes.
780 Original Degrees of Freedom.
60 Condensed Degrees of Freedom.
650 Mins Required for Complete Solution for 250 Frequencies.
(Including Computation of Element Matrices, Assembly and reduction of Structure Matrices).

Fig. 3.3 Structure and Problem Dimensions for Test Structure.

Fig. 3.4a Complete Magnet-Frame.

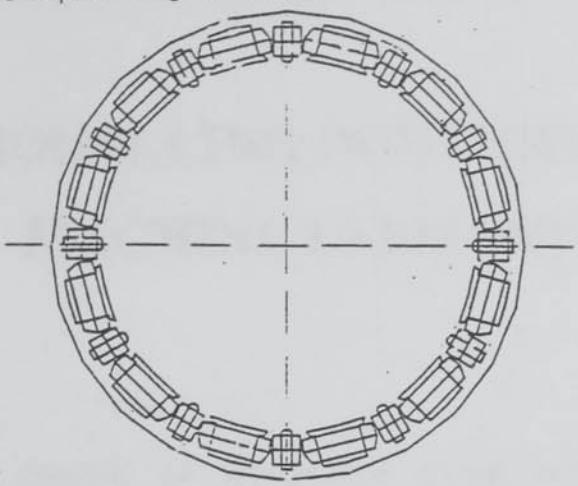

Fig. 3.4b One method.

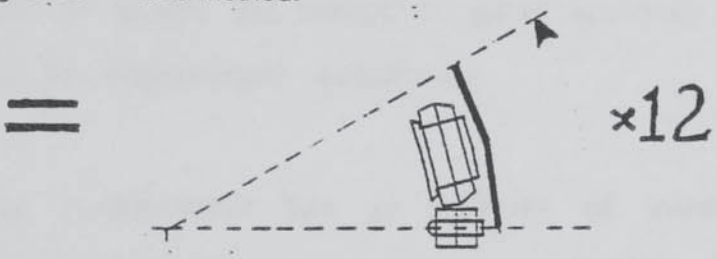

Fig. 3.4c A better method.

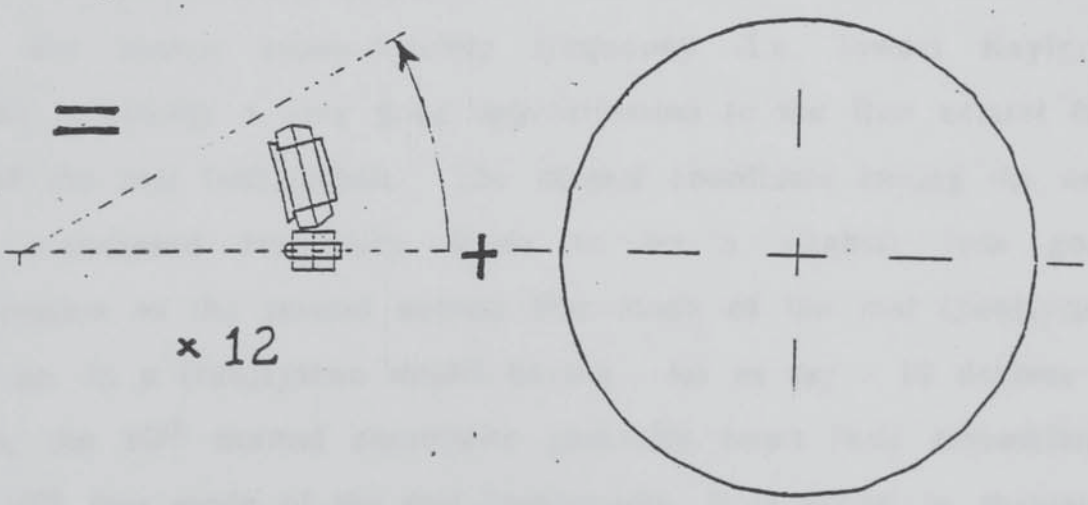

Fig. 3.4 Use of Rotational Periodicity in Unsplit Frame.

Chapter 4.

MODELLING INDIVIDUAL MACHINE ELEMENTS

In chapter 3, the process of component mode synthesis was presented as an ideal means by which the stator of any electrical machine could be modelled. In order that the ultimate composite-system model is sufficient in detail to model the reality to good accuracy, the subsystems themselves must be represented accurately.

In reality, every (sub)system has an infinity of modes. If a finite number of degrees of freedom is used in a model, it will only be possible to find the same number of normal modes and associated frequencies. Using the Rayleigh-Ritz technique, the normal coordinate having the lowest corresponding frequency (i.e. lowest Rayleigh Quotient) is usually a very good approximation to the first natural free mode of the real (sub)system. The normal coordinate having the next lowest associated frequency tends to be a slightly less good approximation to the second natural free mode of the real (sub)system and so on. In a (sub)system model having - let us say - 10 degrees of freedom, the 10^{th} normal coordinate generally bears little resemblence to the 10^{th} free mode of the real (sub)system. It is shown in chapter 3 that when modelling a subsystem, we are not directly concerned with

how well the free modes can be approximated. Instead, we require to find a set of coordinates which can accurately approximate the deflection patterns which would be experienced by the real subsystem connected into the composite-system and vibrating at any frequency within the range of interest.

§4.1 Distributed Versus Discrete Coordinates And Choosing How Many to Use for a Given (Sub)System.

In general, it may be stated that using more coordinates in a given (sub)system model results in a better representation. Clearly, there comes a point when the increase in accuracy is not sufficient to justify the increase in computation time which is associated with having one extra coordinate. In fact, the number of coordinates necessary to model a given (sub)system to a certain degree of accuracy is a function of the frequency range over which response calculations are to be performed (or natural-frequencies found). This point is illustrated with the simple example of a beam system of cross-section d x d and length l for which $l \gg d$ which is to be rigidly attached at one end to a much stiffer member as shown in Fig 4.1a. Coordinates for the beam are chosen from the set of Legendre polynomials. $\Phi_1 = 1$, $\Phi_2 = 2z/l$, $\Phi_3 = 3/2(z/l)^2 - 1/2$, and so on. (illustrated in Fig. 4.1b. A minimum of three coordinates is necessary since two degrees of freedom are constrained at the point of attachment. The question is, *how many more coordinates are necessary to model the beam over a given frequency range ?*. A frequency can be associated with each coordinate of the beam by computing its Rayleigh quotient and dividing the square-root of this by 2π. For a given

frequency range $[f_1,f_2]$, it is possible to assess whether the fourth coordinate is necessary by comparing the f_2 with the frequency associated with Φ_4.

If it is known from the outset that the beam is to be rigidly constrained at one end, we can simply choose a different set of coordinates, Ψ, all of which satisfy the constraints, and it follows that over frequency ranges $[f_1,f_2]$ where f_2 is significantly less than the characteristic frequency of the second coordinate Ψ_2, the behaviour of the beam could be well-modelled using one coordinate only. Fig 4.1c illustrates a suitable set of constrained coordinates.

If it is the case that the beam is to have substantial structures rigidly attached to each end, a minimum of four coordinates is necessary (there are two angular freedoms and two translational freedoms).

In general, the remarks made with regard to the fixed-constraint representation of subsystems in chapter 3 apply here and can be used to specify the number of generalised coordinates which would ideally be used for a given object as follows:

For a given object, there should be sufficient generalised coordinates that one independent "attachment mode" can be found for each freedom at which force may be applied - the other such freedoms being constrained against motion. Further coordinates are necessary to introduce the first normal mode of the constrained object (none of the

freedoms which may be forced is allowed to move) if its frequency is not high above the highest frequency of interest and similarly for the second, third such normal modes etc..

This criterion can only be applied approximately. Where connections are to be flexible (ie between pole and yoke) it is not necessary to ensure that each freedom which may be forced has one associated independent 'attachment mode'.

§4.2 Assumptions Relating to the Variation of Displacements Within a Continuous (Sub)System.

Displacements internal to a continuum can vary continuously in all three directions. Where it has been appropriate to generate models of continuous (sub)systems in the context of this work, the displacement pattern has been described by sets of functions of the position coordinates. In setting-up coordinates for a given continuous subsystem it is advantageous to recognise that when one physical dimension is small, the variation of point translations with respect to the relevant position coordinate may be assumed to be zeroth, first or second order etc. depending on the actual proportions of the object. For example, in modelling a membrane or film it would be justifiable to assume that a point on one side of the film would move in exactly the same way as the point on the exact opposite side i.e. the variation of displacements with respect to depth in the film is zeroth order. For thin plates and shells, one may asume that while points on opposite surfaces (but on the same normal) may translate by differing amounts (tangential to the plane of

the plate/shell) at any one instant, the variation of translations (in all three directions) between these two points is linear.

There are identifiable limits to the use of these assumptions. In the section before this, approximate criteria by which the number of displacement coordinates necessary were developed. Choosing a finite set of coordinates is entirely analogous to imposing the assumptions in question here and similar techniques can be employed to evaluate validity. If the thickness of a given isotropic shell is d and it has a shear modulus G, we can state that the assumption of linear variation of displacement between its surfaces will be quite valid at all frequencies significantly less than f_1, where f_1 is the characteristic frequency at which the middle layer might oscillate in antiphase with both the outer surfaces. Similarly, the assumption that normal strain out of the plane of the paper is zero can be tested by computing a natural frequency f_2, at which the plate would have a comprexxion/extension resonance out of the plane. Formulae for f_1, f_2 are presented and illustrated in Fig. 4.2.

The assumption of linear variation of point translations with respect to position through the depth has been used for all of the elements which will be discussed.

§4.3 Damping matrices for the subsystems.

Damping values for metals and most other materials used in large machines - where they exist - tend to be given as hysteretic damping

factors. That is, unlike the viscous damping mechanism, the energy dissipated in a given cycle of strain is independent of the time-span in which the cycle occurred.

Hysteretic damping can be represented explicitly as a matrix of real numbers having the same units as the stiffness matrix. It is common practice in finite-element packages to combine the (real) stiffness matrix with the hysteretic damping matrix to form a complex stiffness matrix. The imaginary part of this complex matrix is the hysteretic damping matrix.

The hysteretic damping matrix is derived in exactly the same way as the pure stiffness matrix except that instead of using elastic modulii E and G, (representing the material Young's and Shear modulii respectively) quantities representing the energy dissipated per unit volume for unit strain are substituted. In compiling the complex stiffness matrices, therefore, one may simply use complex values of E and G to include damping effects. This has been done throughout this investigation. Where material constants are used they are considered to have both real and imaginary components. Damping matrices do not then have to be derived separately.

Damping is significant in the context of the vibration of machines, but generally, the greatest contributions to damping derive from various mechanisms at the joints between components. Since damping is so small within the components themselves, it has been ignored for the purposes of performing the coordinate transformations necessary to

model the components as substructures. Then having chosen a set of generalised coordinates, a damping ratio is computed for each one. This method would be completely free from error if the condition of "proportional" damping obtained. A more complete treatment of the damping within components is not worthwhile since it would effectively double the storage requirements for the substrutures. The errors introduced by this approximation are completely dwarfed by uncertainties in other areas.

§4.4 Derivation of the General Mass and Stiffness Expressions.

In the case of all of the elements used in this investigation, the outline procedure for establishing these quantities has been the same. The number of coordinates actually used for each object depends of the dimensions of the object and the number of nodes assigned to it. Instead of dealing with specific coordinates as the general finite-element derivations do, we adopt the more general approach that the coordinates are each particular distributions of the relevant "coordinate types". (Two coordinate types for a beam are lateral-translation-of-the-section and shear-angle-of-the-section.)

The general derivation follows the format outlined below:

(1) Choose the set of coordinate types which are to be used to represent the deflection state of the element based on assumptions relating to the proportions of the element.

(2) Create expressions (zeroth- or first- order differential equations) relating the translation (local frame) of each particle of the element to the coordinate types.

(3) Create expressions (zeroth-, first- or second- order differential equations) which relate strains at each point (in terms of the local coordinates) in the element to the coordinate types.

(4) Formulate expressions relating translations and strains in the local frame to those in the global frame.

(5) The stiffness and damping matrices are derived by integrating the product of strain-squared and the appropriate modulus of elasticity (or modulus of energy dissipation) over the entire volume of the element. Mass matrices are found by integrating the product of translation-squared and density over the volume.

The procedure is illustrated below for a limited beam model.

§4.5 Stiffness and Mass Terms - Simple Beam in Flexure.

In the context of modelling DC machines, the beam element is especially useful in representing mainpoles and compoles of the machine and various stiffening elements. In this section, we consider only the case of a rectangular-section beam in flexure to illustrate the procedures used in the more complex cases to follow. The beam occupies the volume $x \in [-b/2,b/2]$, $y \in [-b/2,b/2]$, $z \in [-l/2,l/2]$. A much more general

beam model is discussed in §4.6 allows for a general cross-section beam. The derivation is outlined in the following section.

For simplicity, the effects of shear are neglected. Then, only one type of coordinate is necessary to fully describe the translations of all particles of the beam. This is defined as the translation in the y direction (other definitions could be used to equal effect) and is symbolised as V(z). The "y" translation, v(x,y,z), for all particles on a given beam cross-section is identical. Thus:

$$v(x,y,z) = V(z) \tag{4.1}$$

The translation of individual particles of one section in the z direction is dependent on the y (position) coordinate of the respective particles as expressed in (4.2).

$$w(x,y,z) = -y.D_z(V(z)) \tag{4.2}$$

Individual particles of a section will translate in the x direction by some small amount when there is a finite strain ε_{zz} present, as a result of the Poisson coupling between normal stresses/strains. The strain ε_{xx} is accounted-for implicitly insofar as the constant, E, relating ε_{zz} and σ_{zz} is lower than it would be if strains ε_{xx} and ε_{yy} were constrained to be zero. The x -translation of individual particles is then set to zero though this is not strictly true.

$$u(x,y,z) = 0 \tag{4.3}$$

Equations (4.1) to (4.3) are more concisely expressed by table 4.1 whose dimensions are trivial in this case but for the elements to come, the corresponding tables will be seen to be much larger.

COORDINATE TYPE	TRANSLATION		
	u	v	w
V	0.0	1.0	$-y.D_z$

Table 4.1 Mapping between coordinate types and point translations (BEAM)

The only strain to contribute to the stored-energy of this beam in flexure is ε_{zz}. given by (4.4) and stress σ_{zz}. is related to ε_{zz}. by (4.5).

$$\varepsilon_{zz} = D_z(w) = -y.D_z^2(V(z)) \tag{4.4}$$

$$\sigma_{zz}. = E.\ \varepsilon_{zz}. \tag{4.5}$$

Equation (4.4) is best expressed in tabular form for the more complex cases discussed later but for this beam, the tabular form of (4.4) is trivial.

COORDINATE TYPE	STRAIN ε_{zz}
V	$-y.D_z^2$

Table 4.2 Mapping for strains (BEAM).

Now, in order to obtain a numerical model of finite dimension, V(z) is assumed to be a linear combination of n functions $v_i(z)$, $1 \leq i \leq z$ as (4.6).

$$V(z) = \Sigma v_i(z).\ a_i \qquad (4.6)$$

The choice of these functions and the number of them which should be used is discussed later. What we require here is to formulate expressions for the general (complex) stiffness term k_{ij} and the inertia term m_{ij} corresponding to v_i and v_j. The general stiffness term is defined by Przemienecke (D.1968) in energy terms by (4.7).

$$k_{ij} = \left[\frac{d^2(S.E.)}{d\,a_i.d\,a_j}\right] \qquad (4.7)$$

.. where a_i and a_j are coefficients. This extrapolates exactly to the case where damping is included in the stiffness term as the imaginary part. The general inertia term takes on a similar form shown in (4.8).

$$m_{ij} = \left[\frac{d^2(K.E.)}{\dot{da}_i.\dot{da}_j}\right] \qquad (4.8)$$

Now, the stored energy S.E. in simple continuous elements can in general be expressed as the convolution of stress and strain over the volume of the element. The formulation is simple for the beam in flexure.

$$S.E. = \frac{1}{2}\iiint \sigma_{zz}.\varepsilon_{zz}.dVol$$

$$= \frac{1}{2} E \frac{bd^3}{12} \int_{-\frac{1}{2}}^{\frac{1}{2}} \left[D_z^2(V)\right]^2 . dz \qquad (4.9)$$

E above is a complex constant whose real part is the elastic modulus of the material and whose imaginary part is the damping constant for the element. Combining (4.6), (4.7) and (4.9) gives a formula for k_{ij}.

The kinetic energy is expressed using (4.10).

$$K.E. = \frac{1}{2}\iiint \rho.\left(\dot{v}^2 + \dot{w}^2\right).dVol$$

$$= \frac{1}{2}\rho.bd\int_{z_1}^{z_2}\left(\dot{V}\right)^2 . dz \; + \frac{1}{2}\rho.\frac{bd^3}{12}\int_{z_1}^{z_2}\left[D_z\left(\dot{V}\right)\right]^2 . dz \qquad (4.10)$$

Section-Translation Section-Rotation

... where ρ is the material density for the beam. Combining (4.6), (4.8)

and (4.10) gives a formula for m_{ij}.

The functions v_i might typically be Legendre polynomials. It is useful for this beam to observe the condition of symmetry and solve for symmetrical and antisymmetrical modes separately.

§4.6 Stiffness and Inertia Terms - BEAM element.

In the beam element used throughout this investigation, flexure in two planes is catered-for together with twist of the beam, shear deflection (in two planes) and section warp. Seven distinct coordinate types are used, each one being a function of z only. Table 4.3 below relates the symbols to their definitions.

U	Translation of the section in the x direction.
V	Translation of the section in the y direction.
W	Translation of the section in the z direction.
α	Shear angle of the section... +x- axis $\rightarrow$ +z- axis
β	Shear angle of the section... +y- axis $\rightarrow$ +z- axis
χ	Twist angle of section (positive rotn. about z- axis)
δ	Section warp.

Table 4.3. Definitions of coordinate-types for the beam element.

Now the translations u, v and w (representing translations in the x, y and z directions of the global frame) of the individual particles of the beam are linearly related to the generalised motions by the mapping given in table 4.4 below.

COORDINATE TYPE	TRANSLATION		
	u	v	w
U	1.0	0.0	$-x.D_z$
V	0.0	1.0	$-y.D_z$
W	0.0	0.0	1.0
α	0.0	0.0	x
β	0.0	0.0	y
χ	–y	x	0.0
δ	0.0	0.0	xy

Table 4.4 Mapping for point translations (BEAM).

The stiffness and damping matrices are derived on the basis of energy stored/dissipated due to the strains. Assuming that our beam is narrow, it is justifiable to assert that the stresses σ_{xx}, σ_{yy}, and σ_{xy} are all zero. In this case, contributions to the stored energy can only be made by the strains ε_{xz}, ε_{yz} and ε_{zz}. A mapping of these strains may be written directly relating them to the coordinate types. The term $-x.D_z^2$ (beneath ε_{zz} and horizontally across from U indicates that the normal strain ε_{zz} acting in the z direction depends on the second derivative of U - the lateral translation of the beam cross-sections in the x direction.

COORDINATE TYPE	STRAIN		
	ε_{xz}	ε_{yz}	ε_{zz}
U	0.0	0.0	$-x.D_z^2$
V	0.0	1.0	$-y.D_z^2$
W	0.0	0.0	D_z
α	1.0	0.0	xD_z
β	0.0	1.0	yD_z
χ	$-yD_z$	xD_z	0.0
δ	y	x	$xy.D_z$

Table 4.5 Mapping for strains (BEAM).

The elemental stored energy, dS.E., in the elemental length of the BEAM between z and z+dz is given as the integration of the energy per unit volume over the beam cross-sectional area. Equation (4.11) expresses this formally.

$$2.dS.E. = (U,V,W,\alpha,\beta,\chi,\delta) \int\int [T_B]\, dx.dy\, (U,V,W,\alpha,\beta,\chi,\delta)^t\, dz \qquad (4.11)$$

where $[T_B]$ is the matrix of operators shown in Fig 4.3. (Matrix $[T_B]$ of Fig. 4.3 is loosely called the "stiffness" matrix for convenience but would be more accurately described as the half-strain-energy-density matrix since it requires to be integrated over the entire volume of the beam before it resembles a proper stiffness matrix. Note that the double integration over the cross-sectional area is a constant for a given cross-section. Each part of each of the terms in $[T_B]$ has the form (Operator_1).Scalar.(Operator_2). The first of these operators applies to

the pre-multiplying coordinate and the second to the post-multiplying coordinate. Thus, term $T_B(1,4)$ written in full would read $E.x^2.D_z^2(U).D_z(\alpha)$. (U, α are the first and fourth coordinates respectively as defined in tables 4.3 and 4.4 above).

The mass matrix is ultimately determined from the kinetic energy of the BEAM. The elemental kinetic energy, dK.E., in the elemental length of the BEAM between z and z+dz is given in terms of the time-derivatives of the coordinate-types (U' V' etc.) by (4.12) below.

$$2.dK.E.=(U',V',W',\alpha',\beta',\chi',\delta').\int\int[S_B]dx.dy.(\ U',V',W',\alpha',\beta',\chi',\delta')^t\ dz \quad (4.12)$$

where $[S_B]$ is the matrix of operators shown in Fig. 4.4. ($[S_B]$ is called the BEAM "mass" matrix for convenience but would be more properly termed the half-kinetic-energy-density matrix.)

The actual stiffness and mass matrices are determined by the set of functions which the coordinates (U V W α β χ δ) are allowed to follow. Generally, if there are n functions used for the beam, there are 7n generalised coordinates. Nodes are allowed to occur anywhere on the outside surface of the beam or on the central fibre and there is no restriction on the axial distance between sections at which nodes are defined. Indeed, two or more nodes may be located on the same axial section.

This particular formulation of a beam element has been derived

especially for use in the context of modelling machines. Apart from the generality of this model (allowing it to have any number of nodes deployed randomly), it is distinguished from the usual formulation in F.E. packages by the inclusion of the section warp coordinate type, δ - particularly useful in the modelling of beams in torsion having sections which are significantly narrower in one dimension than in the other. At each node, three translations are defined and two rotations. (Rotation at any node about an axis parallel to the beam axis has no associated stiffness and no associated mass. This freedom must not therefore be used to connect the beam.

The verification example chosen for the beam is a cantilevered "T" piece comprising two identical rectangular-section beam pieces (Fig. 4.5). The substructuring programs of DMS are used to connect the two pieces but all approximations are suppressed. A PAFEC FE model is used for comparison purposes.

The "T" piece is subjected to a harmonic point force acting obliquely at the corner shown in Fig 4.5 and the response of the same freedom was computed for 250 frequency intervals geometrically spaced between 5 Hz and 1000 Hz. The responses computed by PAFEC and DMS are compared in Fig. 4.6.

§4.7 Stiffness and Inertia terms - RING element.

The ring element serves to represent a number of machine components including simplistic models of the complete stator frame, ring stiffeners,

flanges and brushgear-support rings. The treatment presented below allows for flexure in and out of the plane, extension of the ring, shear in two planes, section twisting and, as with the beam, section warp. The ring cross-section may assume any shape (but the same provisos apply as are applicable to the beam element).

The RING element as it has been used most often occurs as a full 360° of material but this is not necessarily the case in the formulation given here. All section deflections are computed at the radius R which may be anywhere between the inside and outside radii of the ring.

The coordinate-types for the ring U,V,W,α,β,χ,δ are defined in table 4.6 similar to table 4.3 for the beam.

U	Radial translation of the section.
V	Circumferential translation of the section.
W	Axial translation of the section.
α	Shear angle of the section... rotn. in direction +θ.
β	Shear angle of the section... postv. rotn. about radius
χ	Twist angle of the section... postv. rotn. about +θ axis.
δ	Section warp.

Table 4.6. Coordinate-types for the RING element.

A mathematical definition of each of these coordinate-types is given in table 4.7 in the form of the diaplacement map. Note that the local point deflections u,v and w are now related to the cylindrical polar frame r,θ,z rather than the local cartesian set. (Deflection "u" is radially outward, "v" is circumferential in the direction of +θ, and w is the usual deflection

in the z direction). R is the radius at which deflections are defined.

COORDINATE TYPE	TRANSLATION		
	u	v	w
U	1	$-(r-R)D_\theta$	0.0
V	0.0	r	0.0
W	-z	$-z.D_\theta$	r
α	0.0	(r-R)	0.0
β	0.0	z	0.0
χ	z	0.0	-(r-R)
δ	0.0	z.(r-R)	0.0

Table 4.7 Mapping for point translations (RING).

A mapping of the strains may be written directly using the relations between deflections in polar coordinates and strains in polar coordinates derived in appendix 5. The relevant equations are summarised here.

$$\varepsilon_{\theta\theta} = (u+(dv/d\theta))/r \qquad (4.13a)$$

$$\varepsilon_{\theta r} = (r.(dv/dr)-v+(du/d\theta))/r \qquad (4.13b)$$

$$\varepsilon_{\theta z} = ((dv/dz) + (dw/d\theta)/r) \qquad (4.13c)$$

COORD	STRAIN		
	$\varepsilon_{\theta\theta}$	$\varepsilon_{\theta r}$	$\varepsilon_{\theta z}$
U	$(1-(r-R)D_\theta^2)/r$	0.0	0.0
V	D_θ	0.0	0.0
W	$-z.(1+D_\theta^2)/r$	0.0	0.0
α	$(r-R)D_\theta/r$	R/r	0.0
β	zD_θ/r	-z/r	1.0
χ	z/r	zD_θ/r	$-(r-R)D_\theta/r$
δ	$z(r-R)D_\theta/r$	zR/r	(r-R)

Table 4.8 Mapping for strains (RING).

The elemental strain-energy, dS.E., contained in the elemental arc of the ring between θ and $\theta+d\theta$, is defined as by (4.14) below.

$$2.dS.E = (U,V,W,\alpha,\beta,\chi,\delta).\int\int [T_R]\ drdz.(U,V,W,\alpha,\beta,\chi,\delta)^t\, d\theta \qquad (4.14)$$

... where $[T_R]$ is the matrix of operators shown in Fig 4.7. The convention used is the same as before.

The mass matrix is determined from the kinetic energy expression. The elemental kinetic energy, dK.E., is given in terms of the time-derivatives of the coordinate-types (U' V' etc.) by (4.15) below.

$$2.dK.E. = (U',V',W',\alpha',\beta',\chi',\delta')\int\int [S_R]\ drdz.(U',V',W',\alpha',\beta',\chi',\delta')^t\, d\theta \qquad (4.15)$$

where $[S_R]$ is the matrix of operators shown in Fig. 4.8.

The actual stiffness and mass matrices are determined by the set of functions which the coordinates $(U,V,W,\alpha,\beta,\chi,\delta)$ are allowed to follow. Generally, if there are n functions used for the ring, there are 7n generalised coordinates. Nodes are allowed to occur anywhere on the outside surface of the beam or on the central fibre and there is no restriction on the circumferential distance between sections at which nodes are defined.

Like the beam element of §4.6, the DMS element RING is distinguished from normal FE models in that any number of nodes can be randomly deployed and section warp (coordinate type- δ) is specifically included. At each node, three translations are defined and two rotations. (Rotation at any node about an axis parallel to the tangent lines has no associated stiffness and no associated mass and must not be used to connect the ring.

The verification example chosen for the beam is a quarter ring having rectangular cross section. (Fig. 4.9). The DMS substructuring programs are used to rigidly fix one end, and none of the approximations available are used. A PAFEC FE model is again used for comparison purposes.

The ring piece is subjected to a harmonic point force acting obliquely at the end shown in Fig 4.9 and the response of the same freedom was computed for 250 frequency intervals geometrically spaced between 5 Hz and 500 Hz. Fig. 4.10 shows the responses computed by PAFEC

and DMS.

§4.8 Stiffness and Inertia terms - PLATE element.

The flat-plate is the most common sort of component modelled in the dynamic representation of machines having covers. Instances include the base-plates of machines (fabrications of a number of distinct plates) covers for machines, terminal-boxes, machine-feet, cooler-sides and baffles. In the context of the vibration of machines, the bending behaviour of plate members needs to be considered as well as the membrane behaviour.

The plates discussed here are of uniform-thickness and it is assumed that properties do not vary through the thickness of the plate. It can be shown by simple symmetry arguments that the membrane (in-plane) behaviour of such plates is entirely uncoupled from the bending (out-of-plane) behaviour. This uncoupling is clear in the inertia and stiffness matrix definitions. For conciseness, the in-plane behaviour is examined simultaneously with the out-of-plane behaviour of the uniform plate. The plate is considered to lie in the x-y plane so that the z axis is normal to it.

The representation presented implicitly assumes that material fibres originally normal to the plane of the plate remain straight and that the plate is free to strain normal to the plane. Shear and rotatory inertia effects are included. Five coordinate-types are used, three translations and two rotations. Each one corresponds to the motion of the individual

fibres of material normal to the plane of the plate. The coordinate-type symbols used are defined below in table 4.9.

U	Translation of the fibre in the x direction.
V	Translation of the fibre in the y direction.
W	Translation of the fibre in the z direction.
α	Shear angle of the fibre ... rotn. +z -axis $\rightarrow$ +x- axis
β	Shear angle of the fibre ... rotn. +z -axis $\rightarrow$ +y- axis

Table 4.9. Coordinate-types for the PLATE element.

The relation between point translations within the PLATE and the coordinate types is given as table 4.10 below.

COORDINATE TYPE	TRANSLATION		
	u	v	w
U	1.0	0.0	0.0
V	0.0	1.0	0.0
W	$-z.D_x$	$-z.D_y$	1.0
α	z	0.0	0.0
β	0.0	z	0.0

Table 4.10 Mapping for point translations (PLATE).

The strains are defined in the usual way and related to the coordinate-types by table 4.11.

	U	V	W	α	β
ε_{xx}	D_x	0	$-z.D_x^2$	$z.D_x$	0
ε_{xy}	D_y	D_x	$-2z.D_xD_y$	$z.D_y$	$z.D_x$
ε_{yy}	0	D_y	$-z.D_y^2$	0	$z.D_y$
ε_{xz}	0	0	0	1	0
ε_{yz}	0	0	0	0	1

Table 4.11. Strains related to coordinates (PLATE).

The elemental stored energy dS.E. of the PLATE in the elemental area [(x,x+dx), (y,y+dy)] is written in matrix form as (4.16) below.

$$2.dS.E = (U,V,W,\alpha,\beta) \int [T_P]\, dz\, (U,V,W,\alpha,\beta)^t\, dx.dy \qquad (4.16)$$

where $[T_P]$ is the matrix given in Fig. 4.11.

The elastic modulii E_{xx}, E_{xy} and E_{yy}, relate normal stresses σ_{xx} and σ_{yy} to the normal strains ε_{xx} and ε_{yy} by (4.17). Derivations for these can be found in standard stress & strain textbooks.

$$\sigma_{xx} = E_{xx}.\varepsilon_{xx} + E_{xy}.\varepsilon_{yy} \qquad (4.17a)$$

$$\sigma_{yy} = E_{xy}.\varepsilon_{xx} + E_{yy}.\varepsilon_{yy} \qquad (4.17b)$$

The elemental kinetic energy, dK.E., in the elemental area [(x,x+dx), (y,y+dy)] is derived from the translation map of table 4.10 and is expressed as (4.18).

$$2.dK.E. = (U',V',W',a',b') \int [S_p]\, dz\, (U',V',W',a',b')^t\, dx.dy \qquad (4.18)$$

where $[S_p]$ is given for the plate element in Fig. 4.12.

The plate element presented here is identical to that normally used in conventional FE packages except that any number of nodes may be used and they may be randomly deployed on the top, bottom or middle surfaces of the plate. (Normal F.E. plate elements only allow nodes to be located on the central - or "neutral" - plane). Three translations and two rotations are defined - rotation about a normal to the plane of the plate has no associated mass or stiffness.

The example used to verify the plate element is an "L" shape as shown in Figs. 4.13a and 4.13b. Once again, the PAFEC FE and DMS results are compared.

A harmonic force acts on one corner of the "L" shape and response is measured at the same point and in the same direction. The DMS substructuring programs are used to appropriately constrain the two DMS plate elements and no approximations are allowed. Frequencies between 5Hz and 500Hz have been scanned using 250 frequency intervals geometrically spaced and the resulting response from both PAFEC and DMS is compared in Fig. 4.14.

§4.9 Stiffness and Inertia terms for the DISC element.

In §4.8 above, the stiffness and inertia matrix terms corresponding to deflection coordinates of a uniform plate were derived with respect to Cartesian position coordinates. Depending on the nature of the plate-boundaries or the directionality of non-isotropy in the plate material, it is sometimes more convenient to use polar coordinates throughout. One such circumstance is the end-plate of machines which often comprises either a single complete disc or a pair of half-discs joined together at a bolted-flange joint. The DISC element as described here may occur as a full 360° span or any partial span.

As with the "plate" element, five coordinate-types are used - three translations and two rotations. Each one corresponds to the motion of an the individual fibres of material normal to the plane of the disc. It is implicitly assumed that these fibres remain straight and that the disc is free to strain normal to the plane to minimise stresses within the plane. Rotation of any node about the normal-to-the-disc has no associated stiffness or mass. The coordinate-type symbols used are defined below in table 4.12.

U	Radial translation of the fibre.
V	Circumferential translation of the fibre.
W	Axial translation of the fibre.
α	Shear angle of the fibre... rotn. +z -axis $\rightarrow$ + r- axis
β	Shear angle of the fibre... rotn. +z -axis $\rightarrow$ + θ axis

Table 4.12 Definitions of the coordinate-types for the DISC element.

The coordinate-types are mathematically defined by the translations map given as table 4.13 for the DISC.

COORDINATE TYPE	TRANSLATION		
	u	v	w
U	1.0	0.0	0.0
V	0.0	1.0	0.0
W	$-z.D_r$	$-zD_\theta/r$	1.0
α	z	0.0	0.0
β	0.0	z	0.0

Table 4.13 Mapping for point translations (DISC).

A mapping of the strains may be written directly using the relations between deflections in polar coordinates and strains in polar coordinates presented in appendix 5. The relevant equations are summarised here.

$$\varepsilon_{\theta\theta} = (u+(dv/d\theta))/r \qquad \varepsilon_{rr} = (du/dr) \qquad (4.19a)$$

$$\varepsilon_{qr} = (r.(dv/dr)-v+(du/d\theta))/r \qquad \varepsilon_{rz} = ((du/dz)+(dw/dr)) \qquad (4.19b)$$

$$\varepsilon_{\theta z} = ((dv/dz) + (dw/d\theta)/r) \qquad (4.19c)$$

\	U	V	W	α	β
ε_{rr}	D_r	0	$-zD_r^2$	zD_r	0
$\varepsilon_{\theta r}$	$\left(\frac{1}{r}\right)D_\theta/r$	$D_r-\frac{1}{r}$	$-\left(\frac{2z}{r}\right)\left(D_\theta D_r-\left(\frac{1}{r}\right).D_\theta\right)$	$\left(\frac{z}{r}\right).D_\theta$	$z.\left(D_r-\frac{1}{r}\right)$
$\varepsilon_{\theta\theta}$	$\left(\frac{1}{r}\right)$	$\left(\frac{1}{r}\right).D_\theta$	$-\left(\frac{z}{r}\right)\left(D_r+\left(\frac{1}{r}\right).D_\theta^2\right)$	$\left(\frac{z}{r}\right)$	$\left(\frac{z}{r}\right).D_\theta$
ε_{rz}	0	0	0	1.0	0
$\varepsilon_{\theta z}$	0	0	0	0	1.0

Table 4.14 Mapping for strains (DISC).

The elemental stored energy, dS.E., in the elemental area [(r,r+dr), (θ,θ+dθ)] of the DISC is written in matrix form as (4.20)

$$2.dS.E = (U,V,W,\alpha,\beta) \int\int [T_D]\, dz\ (U,V,W,\alpha,\beta)^t\, dr.d\theta \qquad (4.20)$$

... where $[T_D]$ is the matrix defined in Fig. 4.15. The convention used is that established in §4.6.

The elemental kinetic energy, dK.E., in the elemental area [(r,r+dr), (θ,θ+dθ)] of the DISC is written in terms of the velocities (U',V' etc) as (4.21)

$$2.dK.E. = (U',V',W',\alpha',\beta') \int\int [S_D]dz\ (\ U',V',W',\alpha',\beta')^t\, dr.d\theta \qquad (4.21)$$

... where $[S_D]$ is defined in Fig. 4.16 Again, the convention used is that

established in §4.6.

The DMS element DISC is distinct from FE plate elements in that the boundaries, material constants and nodal positions are expressed in polar coordinates and as usual, any number of nodes can be assigned to the object randomly placed on either the top, bottom or middle surfaces.

The verification example presented here analyses one half of a 'disc' whose geometry is depicted in Fig. 4.17 and whose inner radius is built-in. PAFEC and DMS models of the constrained disc are compared. DMS substructuring programs are used to constrain the disc appropriately and no approximations are used. An oblique harmonic force is applied to a single point (Fig 4.17) and response is calculated at the same freedom for 100 frequency intervals geometrically spaced between 5 Hz and 500 Hz. Fig. 4.18 presents the results from both the PAFEC FE analysis and the DMS analysis.

§4.10 Stiffness and Inertia terms - CYLINDER element.

The cylinder is the single most powerful element in the context of this work. Modelling a cylinder (or portion thereof) as a single element having many nodes can save a considerable amount of computation time compared with a conventional F.E representation. The cylinder is used primarily in representing the yoke of DC machines but can be used to approximately represent stator cores of AC machines by adjusting the material modulii.

Five coordinate-types are used for the cylinder - three translations and two rotations. Each one corresponds to the motion of the individual fibres of material normal to the central membrane of the cylinder. It is implicitly assumed that these fibres remain straight and that the cylinder is free to strain normal to the central membrane i.e in the radial direction. The coordinate-type symbols used are defined below in table 4.15.

U	Radial translation of the fibre.
V	Circumferential translation of the fibre.
W	Axial translation of the fibre.
α	Shear angle of section... rotation +z -axis $\rightarrow$ + r- axis
β	Shear angle of section... rotation +z -axis $\rightarrow$ + θ- axis

Table 4.15. Definitions of coordinate-types for CYLINDER element.

The coordinate-types are mathematically defined by the translations map given as table 4.16. The symbols u,v and w represent translations of individual particles of the cylinder in the three polar directions r,θ,z. The coordinates are assumed to be evaluated at some membrane of the cylinder whose radius is R.

COORDINATE TYPE	TRANSLATION		
	u	v	w
U	1.0	$-(r-R)D_\theta/R$	$-(r-R)D_z$
V	0.0	r	0.0
W	0.0	0.0	1.0
α	0.0	(r-R)	0.0
β	0.0	0.0	(r-R)

Table 4.16 Mapping for point translations (CYLINDER).

The polar strains $\{ \varepsilon_{\theta\theta}, \varepsilon_{\theta z}, \varepsilon_{zz}, \varepsilon_{\theta r}, \varepsilon_{zr}\}$ are now related directly to the coordinates U,V,W,α,β by substitution of the entries of table 4.16 above into the equations for polar stresses & strains.

$$\varepsilon_{\theta\theta} = (u+(dv/d\theta))/r \qquad \varepsilon_{\theta r} = (r.(dv/dr)-v+(du/d\theta))/r \qquad (4.22a)$$

$$\varepsilon_{\theta z} = ((dv/dz) + (dw/d\theta)/r) \qquad \varepsilon_{zr} = ((du/dz) +(dw/dr)) \qquad (4.22b)$$

$$\varepsilon_{zz} = (dw/dz) \qquad (4.22c)$$

The resulting mapping for cylinder strains is presented as table 4.17 below.

\	U	V	W	A	B
ε_{rr}	$\left(\frac{1}{r}\right)\left(1-\frac{(r-R)}{R}.D_\theta^2\right)$	D_θ	0	$\left(\frac{r-R}{r}\right).D_\theta$	0
$\varepsilon_{\theta z}$	$-(r-R)\left(\frac{1}{r}+\frac{1}{R}\right).D_\theta D_z$	$r.D_z$	$\left(\frac{1}{r}\right).D_\theta$	$(r-R).D_z$	$\left(\frac{r-R}{r}\right).D_\theta$
ε_{zz}	$-(r-R).D_z^2$	0	D_z	0	$(r-R).D_z$
ε_{rz}	0	0	0	$\left(\frac{R}{r}\right)$	0
$\varepsilon_{\theta z}$	0	0	0	0	1.0

Table 4.17 Mapping for strains (CYLINDER).

The stiffness matrix is found using (4.7) from the strain energy. The elemental strain energy, dS.E., contained in the elemental area of CYLINDER $[(\theta,\theta+d\theta), (z,z+dz)]$ is given as (4.23) below.

$$2.dS.E. = (U,V,W,\alpha,\beta).\int [T_C]\, dr\, .(U,V,W,\alpha,\beta)^t\, d\theta.dz \qquad (4.23)$$

Matrix $[T_C]$ is defined in Fig. 4.19 using the same conventions as explained in §4.6.

The mass matrix is found from the expression for kinetic energy. The elemental kinetic energy, dK.E., contained in the elemental area of CYLINDER $[(\theta,\theta+d\theta), (z,z+dz)]$ is expressed in terms of the velocities (U',V' etc.) as (4.24) below.

$$2.dK.E. = (U',V',W',\alpha',\beta'). \int [S_C]\, dr. (U',V',W',\alpha',\beta')^t\, d\theta.dz \qquad (4.24)$$

Matrix $[S_C]$ appears in Fig. 4.20 using the established conventions. The CYLINDER - like the DISC and PLATE elements - can have an arbitrary number of nodes arbitrarily located on any of three layers inside-radius, middle-radius or outside-radius.

One verification example for the CYLINDER has been to compare results for the computed response-to-forcing of a constrained half-cylinder in a fashion similar to the verification examples presented for the other elements.

Fig. 4.21 shows the physical model chosen and Fig. 4.22 gives the frequency response traces computed by DMS and PAFEC respectively.

A further piece of corroborative evidence for this cylinder element is the comparison of predicted and measured frequency response traces for one of the cylinders used in the study on bolted-joints in cylinders. These curves are presented as Figs. 7.7 and 7.8.

§4.11 Generating Functions for the Elements.

In the preceding sections, the mass and stiffness matrices were not given directly for the elements derived since the coordinates used for each of these elements is chosen to best model the particular case. Instead, the strain energy and the kinetic energy were expressed for

each element using a matrix of differential operators.

The coordinates for each one of these elements are created by combining a set of generating functions with the coordinate types. For example, with the BEAM element, seven coordinate types are defined {U, V, W, α, β, χ, δ}. all of which are allowed to vary with respect to the position coordinate of the beam section - z. A set of coordinates for a particular case of the BEAM element might be defined as:

$$
\begin{aligned}
U(z) &= u_1\Phi_1(z) + u_2\Phi_2(z) + u_3\Phi_3(z) + u_4\Phi_4(z) \\
V(z) &= v_1\Phi_1(z) + v_2\Phi_2(z) + v_3\Phi_3(z) + v_4\Phi_4(z) \\
W(z) &= w_1\Phi_1(z) + w_2\Phi_2(z) + w_3\Phi_3(z) + w_4\Phi_4(z) \\
\alpha(z) &= 0 \\
\beta(z) &= 0 \\
\chi(z) &= 0 \\
\delta(z) &= 0
\end{aligned}
\qquad (4.25)
$$

Functions $\Phi_1(z)$, $\Phi_2(z)$, $\Phi_3(z)$, $\Phi_4(z)$ are the generating functions for the beam and they are used to define a total of twelve generalised coordinates $\{ u_1, u_2, u_3, u_4, v_1, v_2, v_3, v_4, w_1, w_2, w_3, w_4\}$.

For the "surface" elements CYLINDER, DISC and PLATE, the generating functions are functions of two variables. In this investigation, functions of two variables have always been constructed as products of two functions of one variable. The principal reason for this is that the boundaries of the PLATE element have generally been lines of constant x and lines of constant y. Similarly, the CYLINDER is usually bounded by lines of constant θ and circles/circular-arcs of constant z, and the DISC

boundaries are generally arcs of constant r and lines of constant θ. It is then possible to use the result of equation (4.26) below to simplify integrations necessary for forming the mass and stiffness matrices.

$$\int_{y1}^{y2}\int_{x1}^{x2} F(x).dx.G(y).dx.dy = \int_{x1}^{x2} F(x).dx.\int_{y1}^{y2} G(y).dy \qquad (4.26)$$

For the "surface" elements, therefore, two distinct sets of functions are chosen whilst only one set of functions is chosen for the "line" elements BEAM and RING.

Now, the sets of functions used for any element must satisfy four principal requirements.

(1) The set must contain a sufficient number of functions that some linear combination of the functions can be found to produce a good approximation to any of the possible deflection shapes of the object being modelled within the frequency range of interest.

(2) It should be possible to convolute each one of the functions in the set and its first and second derivatives with each of the other functions of the set and its first and second derivatives. A numerical integration procedure is incorporated in the DMS package but it requires inordinate amounts of computer time.

(3) The functions ought be divisible into groups in cases where this is useful. Two cases in particular are important for some of the elements. If symmetry is present with respect to the position

coordinate, then the functions should be divided into symmetrical and antisymmetrical sets. If axi-symmetry obtains, then the set should contain only trigonometric terms with integer numbers of waves about the periphery.

(4) The function set should be as independent as possible. For example, over the span $z \in [-1,1]$, one might choose symmetrical functions $\cos(0.01z)$, $\cos(0.02z)$, $\cos(0.03z)$. These functions are independent insofar as one cannot find a linear combination of the three functions which will be zero for all z. However, in order to find a linear combination which resembles $\cos(\pi z)$, large coefficients would be required and the classic computing syndrome of "small differences of large numbers" becomes a problem.

Two distinct sets of functions have been employed for the elements. These are referred to as the Line/Trigonometric/Hyperbolic set and the Legendre polynomial set. These are discussed separately.

§4.12 The Line/Trigonometric/Hyperbolic function set.

This family of functions was originally the only set in the software developed. A correct choice of the coefficients results in a set fulfilling all of the requirements of §4.11. The independent variable (i.e. the position coordinate) is x for the purposes of this discussion and the interval over which the functions are to be defined is $x \in [-1,1]$ by applying suitable constants. (This interval is exact if the boundaries are "regular" as defined

above. If not, the interval is set to be approximately $x \in [-1,1]$)

It is well known that the functions $\cos(0x)$, $\cos(\pi x)$, $\cos(2\pi x)$, $\cos(n\pi x)$ etc. form a uniformly convergent approximation to any symmetrical function defined over the interval $x \in [-1,1]$ if the function and its derivatives are continuous over the interval and if the derivative of the function at $x=1$ is zero. (If the function is symmetrical, the derivative at $x=-1$ must also be zero.) Clearly, any function (be it symmetrical, antisymmetrical or neither) which describes the variation of displacements within a continuous body must be continuous. The same applies to all the derivatives of such a function. However, the slope at the interval ends is generally not zero. (Consider the first flexural mode of a beam defined over the interval.) In order that a finite first-derivative of displacement be allowed at the ends of the various elements, a single hyperbolic function is added to the set. The set of cosine functions defined above are independent when convoluted with a weighting factor of 1 over the interval $x \in [-1,1]$, but they are not independent of the hyperbolic-cosine function $\cosh(nx)$. However, by choosing a relatively large coefficient m for the hyperbolic cosine, the dependence is kept to a minimum. Too large a coefficient leads to precision and overflow errors in the programs and a rule-of-thumb has been developed in which the coefficient, m, chosen for the cosh function is twice the largest coefficient in the trigonometric cosines n. This has proved a satisfactory solution and it has been shown that small changes in the value of the coefficient of the hyperbolic-cosine have little effect on the results produced for any of the elements which use the line/trig./hyp. function set.

The number of functions used for a given element on any occasion is arbitrary but it is a simple matter to determine the maximum "waviness" of the element for which the assumptions of the element still hold good. For the BEAM element in flexure in one plane, the minimum wavelength should not be less than three times the maximum depth of the beam in that plane as a rough guideline. The minimum wavelength is considered to be determined by the cosine function having the highest coefficient. Strictly, a shorter "wave" could occur in the beam because of the hyperbolic-cosine but it generally holds that since stiffness terms tend to be dominated by the first and second derivatives of displacement, greater "waviness" corresponds to higher stiffness. Deflection patterns which have high "waviness" have correspondingly high stiffnesses and consequently, contribute little to the behaviour of the element.

The function $f(x)=1$ can either be regarded as a "line" function or a trigonometric function, $f(x)=\cos(0x)$. It is convenient for programming to pair symmetrical and antisymmetrical functions where the element has some symmetry with respect to a position coordinate. There is no antisymmetrical equivalent to $\cos(0x)$ except the trivial case $\sin(0x)=0$. Thus, the function $f(x)=1$ is invariably considered as the line function whose antisymmetrical partner is $f(x)=x$.

A typical set of symmetrical functions from the line/trig./hyp. family is shown in Fig. 4.23a.

The antisymmetrical functions of the line/trig./hyp. family comprise trigonometric and hyperbolic sin functions and the antisymmetrical line

function y = x. We observed above that a single hyperbolic function was useful for the symmetrical function to provide for a non-zero derivative at the boundaries x=1, x=-1. The trigonometric sinusoids $\sin(\pi x)$, $\sin(2\pi x)$, $\sin(3\pi x)$ etc have zero values but finite first-derivatives at x =1, x=-1. The inclusion of the line function y = x provides for a non-zero value at the boundaries. Thus, there is often no need to include a hyperbolic sin function in the set. The need sometimes arises when the second derivative of the displacement coordinate is also important. For example, in a beam in flexure (neglecting shear effects), the moment at any section is dependent on the second derivative of the transverse translation with respect to the axial position coordinate. If we are modelling the antisymmetrical set of modes for a beam and do not include a hyperbolic sin function with the line function and the trigonometric sin functions, then we are implicitly imposing the constraint that the moment at the beam ends will always be zero. This is useful if we are only interested in the free modes of the beam but when the beam is to be used as a substructure, significant errors can be caused. Thus, if the diagonal stiffness entry for a given coordinate-type involves second derivates of the coordinate-type, then the hyperbolic sin is used. In order to keep dependence of the functions to a minimum without causing numerical problems, the rule-of-thumb stated above for the coefficient of the hyperbolic cosine related to the highest coefficient of the trigonometric cosines is applied to the antisymmetrical functions also.

A typical set of symmetrical functions from the line/trig./hyp. set is presented in Fig. 4.23b.

Sometimes, it has been appropriate to include trigonometric sin and cosine functions not having an integer number of wavelengths within the span of the object. Consider the case of a RING element spanning $\theta \in [-\pi/2,\pi/2]$. Suppose that we are interested in the symmetrical modes of the ring vibrating in its own plane. We might begin by assigning the four functions $y=1$, $y=\cos(2\theta)$, $y=\cos(4\theta)$, $y=\cosh(8\theta/\pi)$ to the radial displacement coordinate U. When the RING element moves in a symmetrical rigid-body mode, the radial displacement actually varies as $\cos(\theta)$. Now, no linear combination of the four functions above is an exact match for $\cos(\theta)$. Thus, when the free modes of the RING portion are evaluated, a non-zero frequency will be evaluated for the "rigid-body" mode. This is not a serious drawback if the ring portion is fixed to more substantial members in a composite structure, but it is generally desireable that the rigid body modes should have associated natural frequencies of zero. The situation can be rectified by introducing the function $y=\cos(\theta)$ to the set. Then, the rigid body mode can be modelled exactly. This can cause some difficulty since the dependency within the function set then becomes large. A method of circumventing the problems caused by dependency within the sets of functions has been developed and is presented in §4.14.

The convolutions of the various functions from this set symmetrical and antisymmetrical over a symmetrical interval are presented in appendix 4. The DMS programs forming the stiffness and mass matrices for the various elements call a common routine to perform the integrations. If the boundaries are "regular", the integrations take place extremely quickly.

§4.13 The Legendre Polynomial set of functions.

The Legendre polynomials were introduced especially to model the radial variation of displacements within the element DISC. It can be seen from Figs. 4.15 and 4.16 that both the mass and stiffness matrices for an elemental volume of the DISC contain powers of r - the radius. The convolution integrals (with respect to r) required to form complete mass and stiffness matrices for the DISC involve three functions whereas all other convolutions for other elements and for the circumferential direction of the DISC involve only two functions. It is entirely inappropriate to use the line/trig./hyp. family to represent the radial variation of displacements within the DISC element since the convolutions are so difficult to evaluate analytically. The convolution of three polynomials requires no more than the multiplication of the three polynomials and the integration of the single polynomial product.

Legendre polynomials are chosen in preference to other forms since the polynomials themselves and their derivatives are relatively independent for monotonic weighting functions over the interval $x \in [0,1]$.

Problems arise due to the size of the coefficients in the convolutions. The coefficients of the first six Legendre polynomials over the interval $x \in [0,1]$ which have a value of +1 at $x = 0$, and a value of ± 1 at $x = 1$ are presented in table 4.19 below. The curves corresponding to these functions are displayed in Fig. 4.24. Since the precision of modern computing machines in single-precision variables is limited to about 1 part in 10^7, it is not generally possible to perform the convolutions to

acceptable precision for more than 6 Legendre polynomials without resorting to the use of double-precision.

Polynomial	COEFFICIENTS					
	X^0	X^1	X^2	X^3	X^4	X^5
1	1	0	0	0	0	0
2	1	-2	0	0	0	0
3	1	-6	6	0	0	0
4	1	-12	30	-20	0	0
5	1	-20	90	-140	70	0
6	1	-30	210	-560	630	-252

Table 4.18 Coefficients of the Legendre polynomials - $x \in [0,1]$

The problem with precision is the central reason for choosing the line/trig./hyp. family of functions in preference to the Legendre polynomials in all cases possible.

§4.14 Symmetry with Respect to a Position Coordinate.

Consider the BEAM element whose axis is coincident with the z axis and whose center is at the origin. Coordinate type U(z) describes the transverse deflection of the sections in the direction of the x axis. Coordinate type $\alpha(z)$ describes the shear angle in the x-z plane. In symmetrical modes, U(z) is a symmetrical function and $\alpha(z)$ is an antisymmetrical function. (Consider the first flexure mode. The

transverse displacement at z=0 is finite while the shear angle at z=0 is zero).

Coordinates fall into groups if the element possesses some symmetry with respect to a position coordinate. Some are symmetrical with respect to the position coordinate in symmetrical modes (and antisymmetrical in antisymmetrical modes) and the others are antisymmetrical with respect to the position coordinate in symmetrical modes (and symmetrical in antisymmetrical modes). For example, if the boundaries of the PLATE element are symmetrical with respect to both the x and y axes (x-y being the plane of the PLATE), the symmetry case of each of the five coordinate types is shown in table 4.18 below for modes symmetrical with respect to both x and y.

COORD.	Defn.	Symmetrical w.r.t X.	Symmetrical w.r.t Y.
U	X - Translation	NO	YES
V	Y - Translation	YES	NO
W	Z - Translation	YES	YES
α	Rotation $z \rightarrow x$	NO	YES
β	Rotation $z \rightarrow y$	YES	NO

Table 4.19 Symmetry properties of the coordinates - PLATE.

Thus, when dividing the modes of a symmetrical element into groups,

symmetrical or antisymmetrical sets of function are used to represent the various coordinates as appropriate.

§4.15 Dealing with Dependency in Coordinates.

It was observed earlier in §4.12 that functions are sometimes included in sets to model special cases of deflection which cause a relatively high degree of dependency in the coordinates. A method has been developed by which this dependency can be identified and dealt-with in the solution of the eigenvalue problem.

The identification is based on an automated inspection of the stiffness matrix [k] for the element. Each coordinate i is examined in turn as follows. Firstly, a quantity R(i) - related to the minimum stored energy contribution for a unit value of the coordinate - is computed as (4.27).

$$R(i) = k(i,i) - \Sigma\, k(i,j)^2 / k(j,j) \qquad (4.27)$$

Then, R(i) (this has the dimensions of a stiffness) is compared with k(i,i). If R(i)/k(i,i) is less than the precision being used in the computer, then the set has one totally redundant coordinate. The coordinate q(i) is removed from the set by expressing it as a linear combination of the other coordinates using the Guyan reduction method. Generally, coordinates are specifically included to cater for the rigid-body modes. For these coordinates R(i) is zero but k(i,i) is zero also and they are not considered redundant.

The same check is performed on the mass matrix. In general, because the mass matrix involves zeroth and first derivatives and the stiffness matrix involves zeroth, first and second derivatives, it is possible to find redundancy with respect to either the mass or stiffness matrix and not the other.

If the mass matrix exhibits a coordinate redundancy, the Cholesky factorisation of the mass matrix is likely to fail because it may detect that the matrix is not positive definite. If the factorisation does not fail, the inversion of the Cholesky factor (see §4.15) will produce very large numbers and the presence of these numbers destroys precision when this inverse is multiplied by the Cholesky factor of the stiffness matrix.

If the stiffness matrix has a redundancy not shared by the mass matrix and it is allowed to remain during the solution of the eigenproblem, the solver will find more rigid-body modes than it ought.

If both matrices share a redundancy, then there are more eigenvalues than independent eigenvectors in the problem. This can cause totally erroneous results to be generated by the eigenproblem solver, because of the attempts the program makes to ensure that eigenvectors are mutually orthogonal with respect to both the mass and stiffness matrices (§4.15).

§4.15 Solving the eigenvalue problem for the substructures.

In order to find the set of normal coordinates for each individual

substructure, an n x n eigenvalue problem must be solved where n is the number of displacement coordinates used to represent the general deflected shape of the substructure. If the substructure were being represented as an assembly of individual finite-elements, the "original" coordinates would be nodal displacements and the mass and stiffness matrices for the system would be sparse. Suitable "front-ordering" would reduce these to banded form and the resulting computation time is considerably diminished. When the original coordinates are smooth displacement functions, the number of original coordinates required for a given quality of representation is fewer but the mass and stiffness matrices resulting are normally fully-populated. It should be noted that a Guyan reduction performed on a normal finite-element model of say a plate will result in mass and stiffness matrices very similar to those produced in DMS. The methods used to solve the eigenvalue problem for the substructures are briefly summarised here.

The first step in solving the problem is to factorise the mass and stiffness matrices using the Cholesky decomposition technique for symmetrical matrices. Since, [m] and [k] are both positive-definite, the Cholesky factors $[l_m]$ and $[l_k]$ should contain only real entries.

$$[m] = [l_m].[l_m]^t \tag{4.28}$$

$$[k] = [l_k].[l_k]^t \tag{4.29}$$

It is worth noting at this point that matrix [m] has no zero-eigenvalues but matrix [k] normally has six zero-eigenvalues corresponding to the

six rigid-body-modes of every free object. In ideal circumstances, one single coordinate corresponds to each of these modes. To avoid the possibility of complex values occurring in $[l_k]$, it is common practice to shift the eigenvalues by some minimum prescribed amount d. Thus, [k'] is formed using (4.27) below before the Cholesky decomposition and the eigenvalues finally computed are shifted back to their correct values by subtracting d from each one again when they have been computed.

$$[k'] = [k] + d.[m] \tag{4.30}$$

For convenience, the distinction between [k'] and [k] is ignored for the rest of of this section. It can be shown Gourlay & Watson (D.1984) that the eigenvalues, of the matrix [r] are the same as those of the matrix-pair [k], [m] where [r] is given by (4.31).

$$[r] = [[l_m]^{-1}.[l_k]] \; . \; [[l_k]^t.[l_m]^{-t}] = [[l_r].[l_r]^t] \tag{4.31}$$

Matrix [r] is formed from its factor $[l_r]$ which in turn is formed from $[l_k]$, $[l_m]$ by a direct Gaussian operation rather than by explicit matrix inversion and matrix multiplication. The eigenvectors {w} of [r] are related to the eigenvectors {u} of [k],[m] by $[l_m]^{-t}$ in equations (4.32) and it is useful to observe that if $\{w\}^t.\{w\}=1$, then $\{u\}^t.[m].\{u\}=1$ also. That is to say, the mode shapes have been mass-normalised.

$$\{w\} = [l_m]^t.\{u\} \tag{4.32a}$$

$$\{u\} = [l_m]^{-t}.\{w\} \qquad (4.32b)$$

Having formed [r], a real symmetric tridiagonal matrix [t] having the same eigenvalues as [r] can be formed by a series of pre- and post-multiplications by Householder matrices. The eigenvalues themselves are then found using a version of the QR (or QL) algorithm, with temporary shifts, specifically for the solution of eigenvalues of symmetric tridiagonal matrices.

The eigenvectors of [r] can be found for the individual eigenvalues using the highly convergent inverse-iteration algorithm. Once found, each vector {w} is normalised. The convergence rate for a given eivenvector depends on the difference between the corresponding eigenvalue and the next closest eigenvalue. Convergence is accelerated by shifting individual eigenvalues, λ, to be marginally negative once the associated eigenvector, {w}, has been found – if the next-largest eigenvalue is too close. This is achieved by forming [r'] from [r] using (4.31).

$$[r']=[r]-\{w\}.\{w\}^t.\lambda \qquad (4.31)$$

All of the transformations used are very stable and the combination has proved to be an effective one in solving problems up to 200 x 200 on the Appollo 550 workstation. Above this size, in-core storage of the matrices becomes a problem.

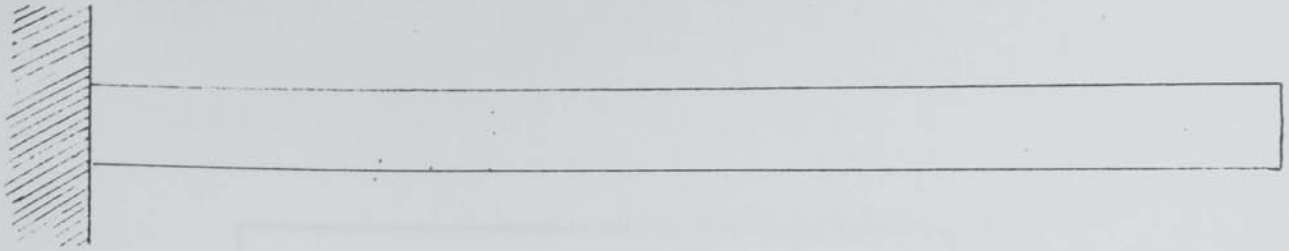

Fig 4.1a Cantilever Beam.

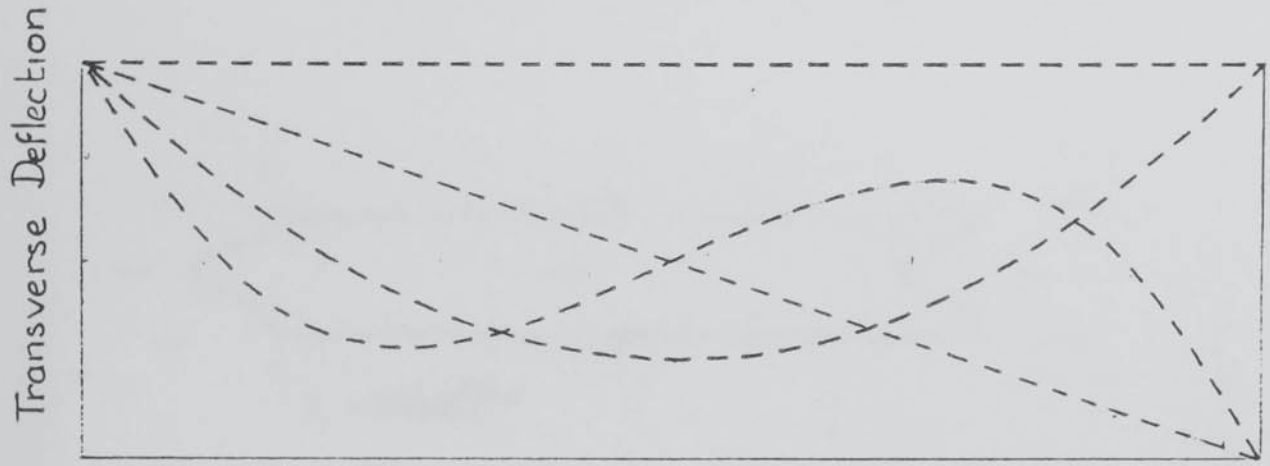

Fig 4.1b Coordinate Set for Free Beam.

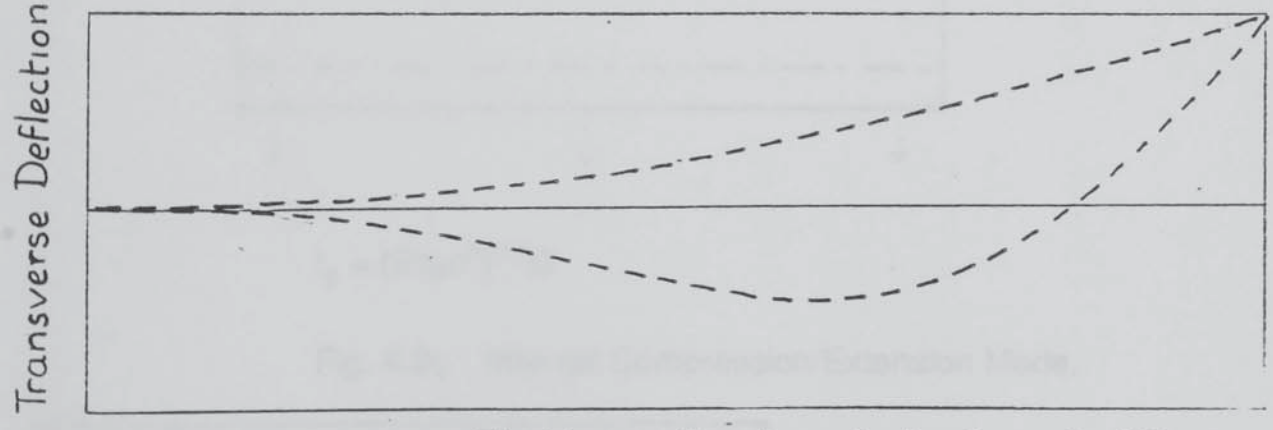

Fig 4.1c Coordinate Set for Constrained Beam.

Fig 4.1 Cantilever Beam for Illustration of Derivations.

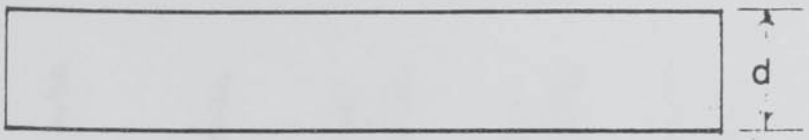

Fig. 4.2a Undeformed Portion of Plate.

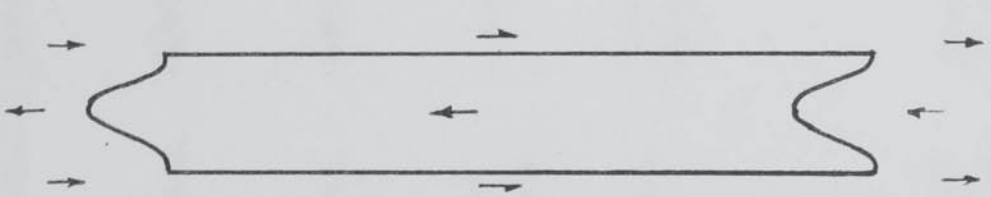

$f_1 = (G/\rho d^2)^{0.5}$

Fig. 4.2b. Internal Shear Mode of Plate.

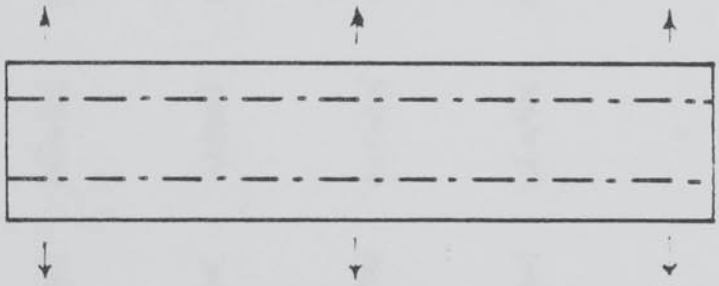

$f_2 = (E'/\rho d^2)^{0.5}/2$

Fig. 4.2c. Internal Compression/Extension Mode.

E'	=	E.(1-ν)/((1-2ν).(1+ν))
E	=	Young's Modulus for the Material.
G	=	Shear Modulus for the Material.
ν	=	Poisson's Ratio for the Material.
ρ	=	Material Density.

Fig. 4.2 Use of Frequency Criteria for Testing Assumptions

$D_z^2.(Ex^2).D_z^2$	$D_z^2.(Exy).D_z^2$	$D_z^2.(-Ex).D_z$	$D_z^2.(-Ex^2).D_z$	$D_z^2.(-Exy).D_z$	0	$D_z^2.(-Ex^2y).D_z$
$D_z^2.(Exy).D_z^2$	$D_z^2.(Ey^2).D_z^2$	$D_z^2.(-Ey).D_z$	$D_z^2.(-Exy).D_z$	$D_z^2.(-Ey^2).D_z$	0	$D_z^2.(-Exy^2).D_z$
$D_z(-Ex).D_z^2$	$D_z(-Ey).D_z^2$	$D_z(E).D_z$	$D_z(Ex).D_z$	$D_z(Ey).D_z$	0	$D_z(Exy).D_z$
$D_z(-Ex^2).D_z^2$	$D_z(-Exy).D_z^2$	$D_z(Ex).D_z$	$1.(G_{xz}).1$ + $D_z(Ex^2).D_z$	$D_z(Exy).D_z$	0	$1.(G_{xz}y).1$ + $D_z(Ex^2y).D_z$
$D_z(-Exy).D_z^2$	$D_z(-Ey^2).D_z^2$	$D_z(Ey).D_z$	$D_z(Exy).D_z$	$1.(G_{yz}).1$ + $D_z(Ey^2).D_z$	0	$1.(G_{xz}x).1$ + $D_z(Exy^2).D_z$
0	0	0	0	0	$D_z(G_{xz}y^2).D_z$ + $D_z(G_{yz}x^2).D_z$	$D_z(-G_{xz}y^2).1$ + $D_z(G_{yz}x^2).1$
$D_z(-Ex^2y).D_z^2$	$D_z(-Exy^2).D_z^2$	$D_z(Exy).D_z$	$1.(G_{xz}y).1$ + $D_z(Ex^2y).D_z$	$1.(G_{xz}x).1$ + $D_z(E(xy^2)).D_z$	$1.(-G_{xz}y^2).D_z$ + $1.(G_{yz}x^2).D_z$	$1.(G_{xz}y^2).1$ + $1.(G_{yz}x^2).1$ + $D_z(Ex^2y^2).D_z$

Fig 4.3 Stiffness Matrix of General "BEAM".

$1.(\rho).1 + D_z(\rho x^2).D_z$	$D_z(\rho xy).D_z$	$D_z(-\rho x).1$	$D_z(-\rho x^2).1$	$D_z(-\rho xy).1$	$1.(-\rho y).1$	$D_z(-\rho x^2 y).1$
$D_z(\rho xy).D_z$	$1.(\rho).1 + D_z(\rho y^2).D_z$	$D_z(-\rho y).1$	$D_z(-\rho xy).1$	$D_z(-\rho y^2).1$	$1.(\rho x).1$	$D_z(-\rho xy^2).1$
$1.(-\rho x).D_z$	$1.(-\rho y).D_z$	$1.(\rho).1$	$1.(\rho x).1$	$1.(\rho y).1$	0	$1.(\rho xy).1$
$1.(-\rho x^2).D_z$	$1.(-\rho xy).D_z$	$1.(\rho x).1$	$1.(\rho x^2).1$	$1.(\rho xy).1$	0	$1.(\rho x^2 y).1$
$1.(-\rho xy).D_z$	$1.(-\rho y^2).D_z$	$1.(\rho y).1$	$1.(\rho xy).1$	$1.(\rho y^2).1$	0	$1.(\rho xy^2).1$
$1.(-\rho y).1$	$1.(\rho x).1$	0	0	0	$1.(\rho x^2).1 + 1.(\rho y^2).1$	0
$1.(-\rho x^2 y).D_z$	$1.(-\rho xy^2).D_z$	$1.(\rho xy).1$	$1.(\rho x^2 y).1$	$1.(\rho xy^2).1$	0	$1.(\rho x^2 y^2).1$

Fig 4.4 Mass Matrix of General "BEAM".

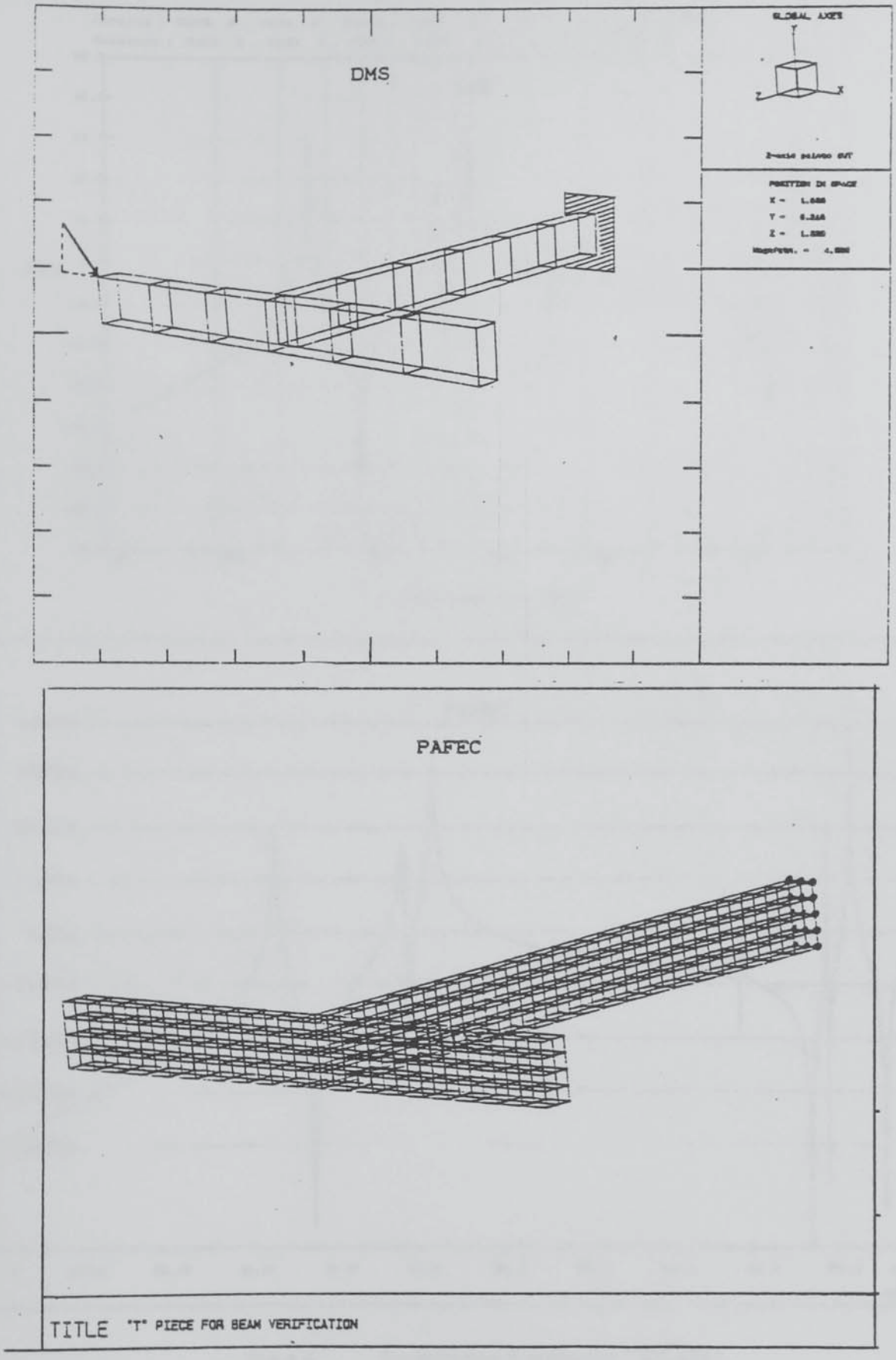

Fig 4.5 Verification Model for "BEAM".

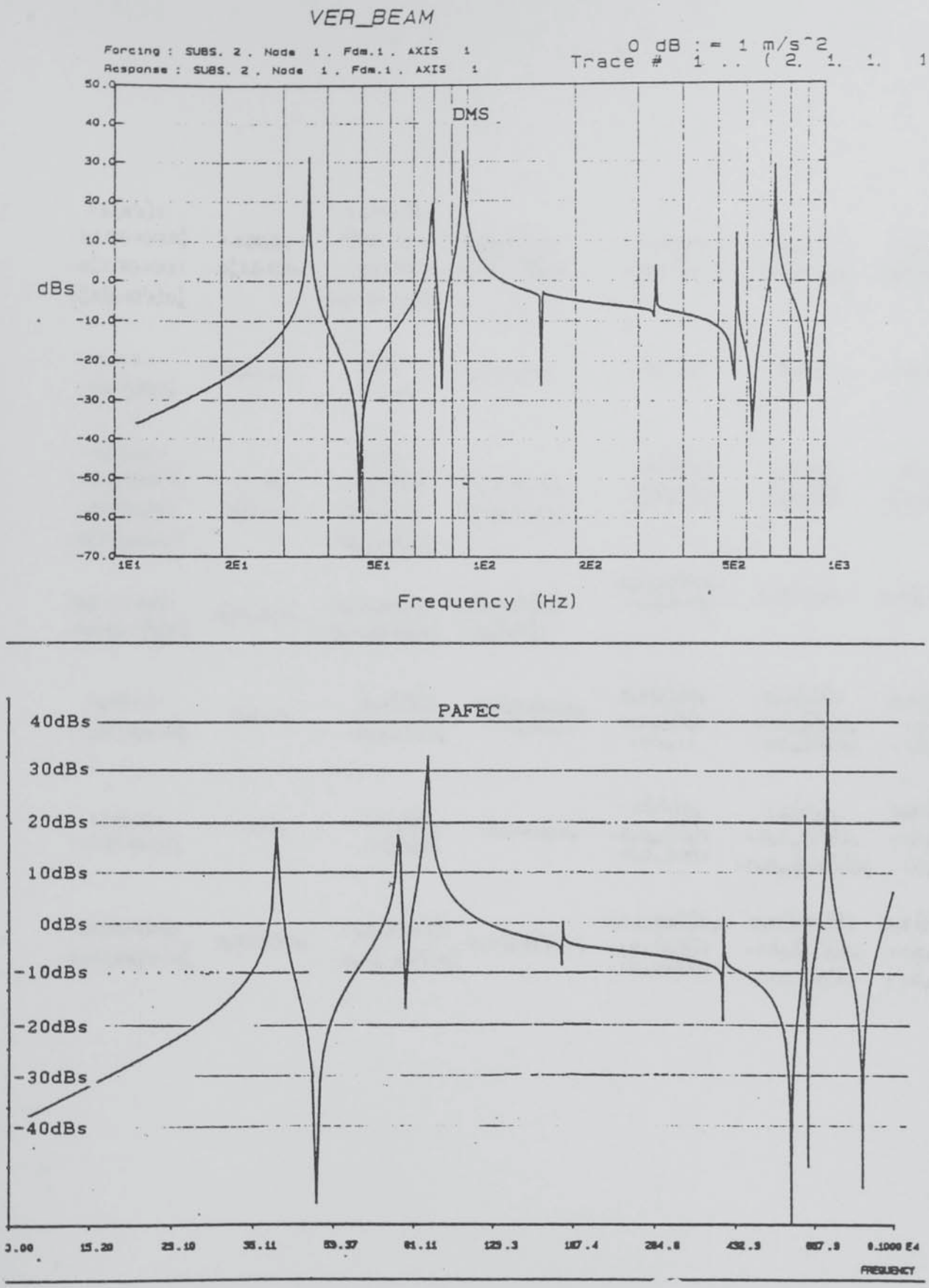

Fig 4.6 Verification Results for "BEAM".

Fig. 4.7 Stiffness Matrix for the RING.

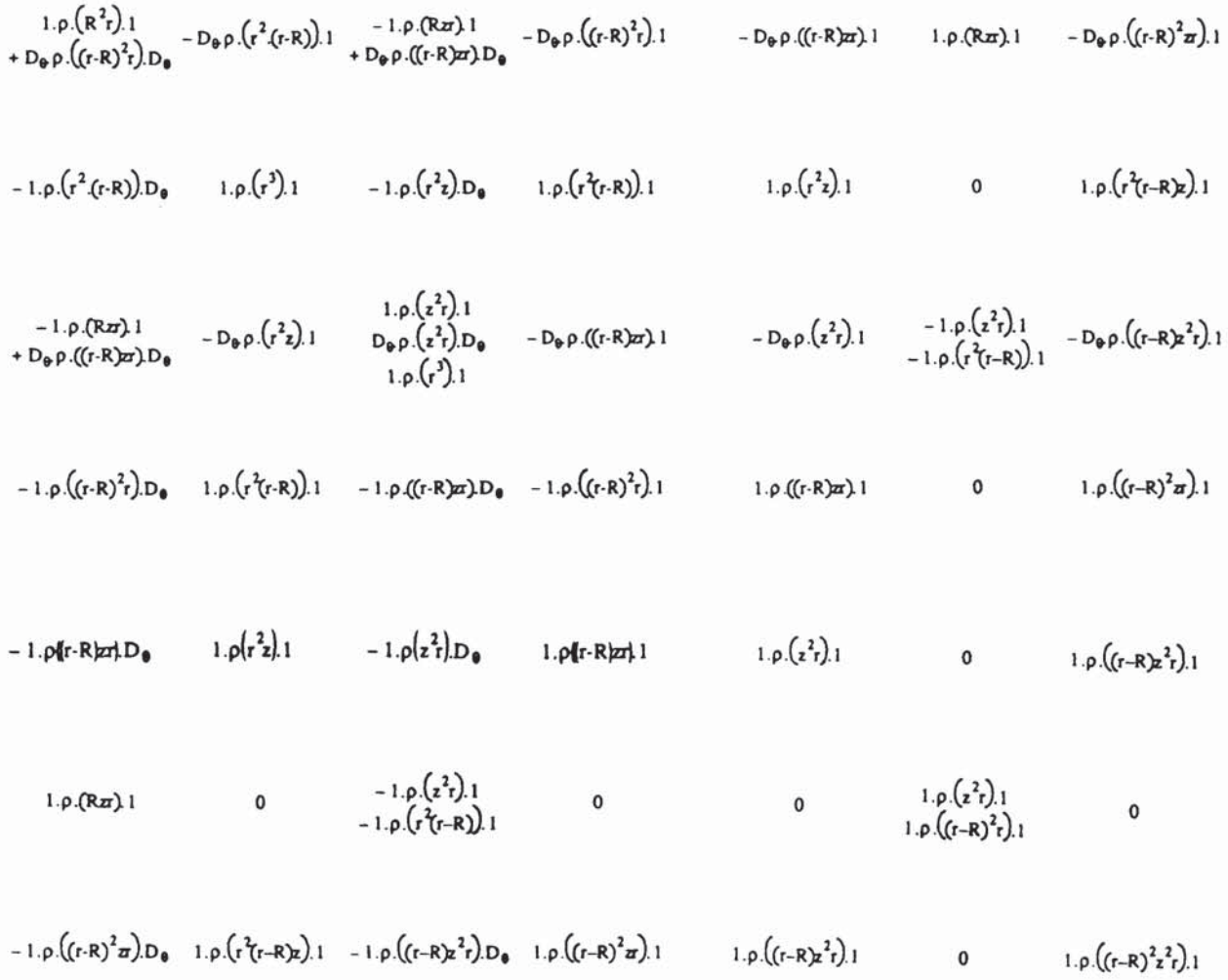

Fig. 4.8 Mass Matrix for the RING.

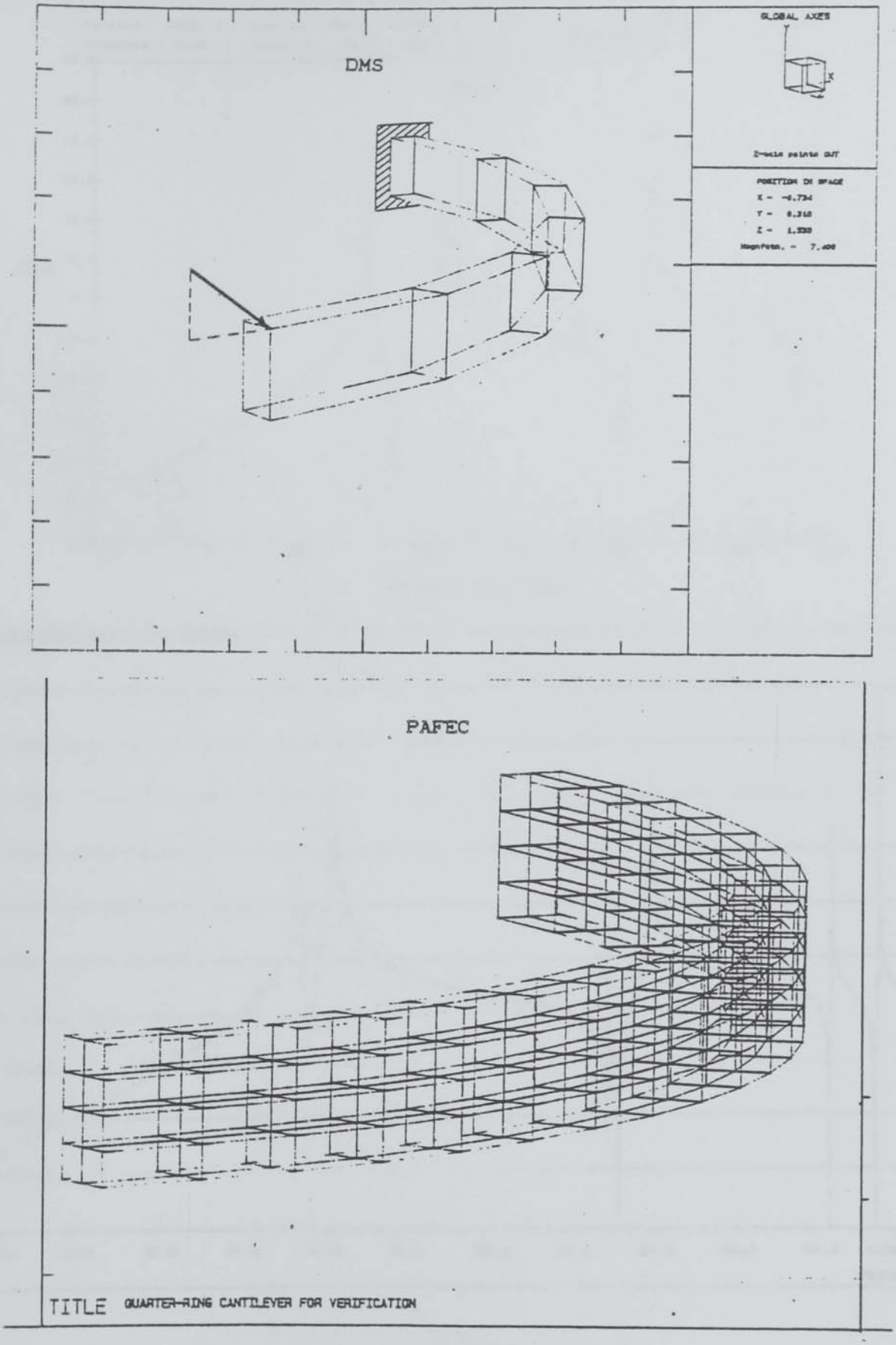

Fig 4.9 Verification Model for "RING".

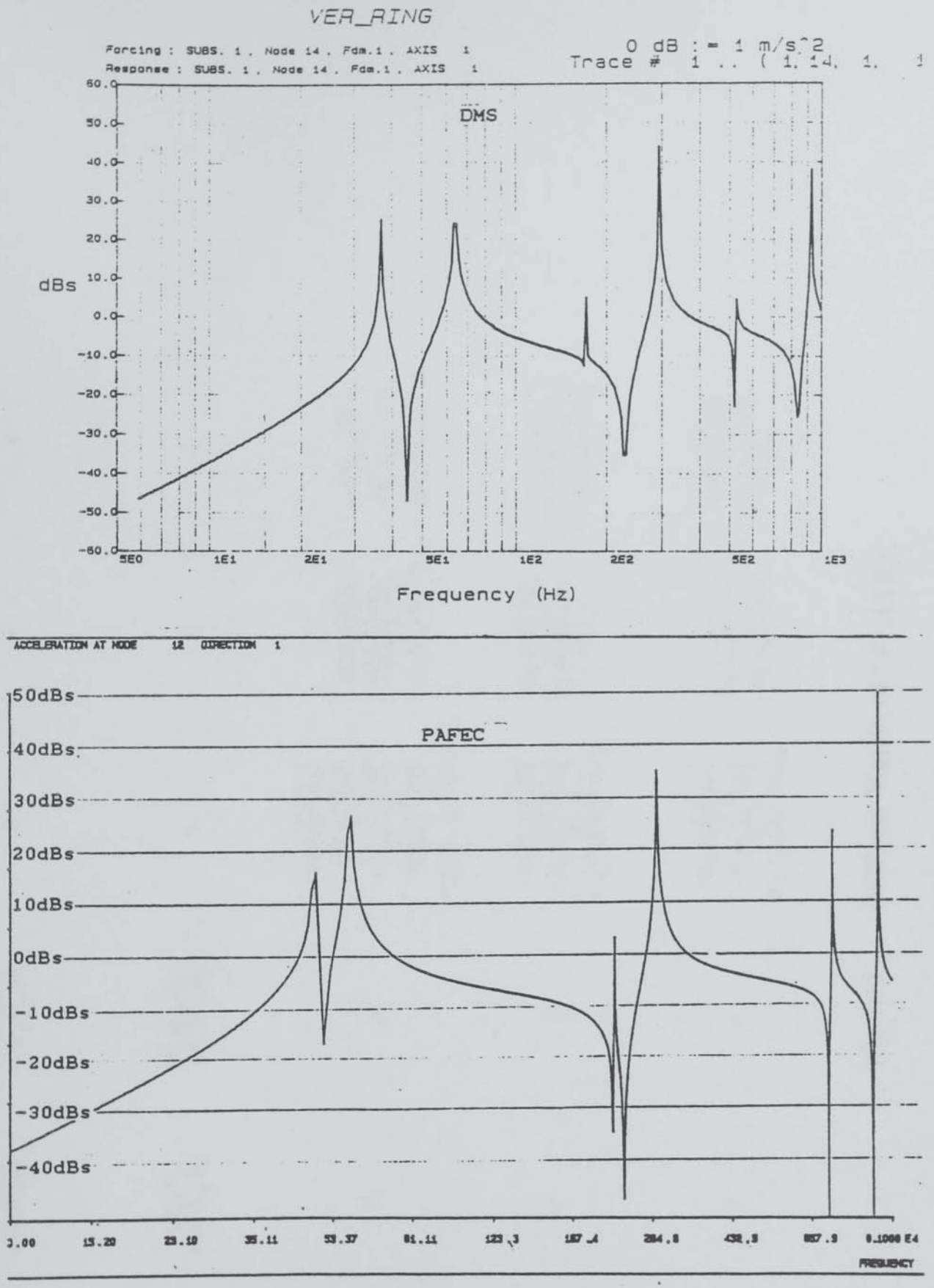

Fig 4.10 Verification Results for "RING".

$D_x.E_{xx}D_x$ $+ D_y.G_{xy}D_y$	$D_x.E_{xy}D_y$ $+ D_y.G_{xy}D_x$	0	0	0
$D_y.E_{xy}D_x$ $+ D_x.G_{xy}D_y$	$D_y.E_{yy}D_y$ $+ D_x.G_{xy}D_x$	0	0	0
0	0	$D_x^2.E_{xx}(z^2).D_x^2$ $D_x^2.E_{xy}(z^2).D_y^2$ $D_y^2E_{xy}(z^2).D_x^2$ $D_y^2E_{yy}(z^2).D_y^2$ $+ D_xD_y.G_{xy}(4z^2).D_xD_y$	$-D_x^2.E_{xx}(z^2).D_x$ $-D_y^2E_{yx}(z^2).D_x$ $-D_xD_y.G_{yx}(2z^2).D_y$	$-D_x^2.E_{xy}(z^2).D_y$ $-D_y^2E_{yy}(z^2).D_y$ $-D_xD_y.G_{yx}(2z^2).D_x$
0	0	$-D_x.E_{xx}(z^2).D_x^2$ $-D_x.E_{xy}(z^2).D_y^2$ $-D_y.G_{yx}(2z^2).D_xD_y$	$-D_x.E_{xx}(z^2).D_x$ $D_y.G_{yx}(z^2).D_y$ $-1.G_{xz}1$	$D_x.E_{xy}(z^2).D_y$ $+ D_y.G_{xy}(z^2).D_x$
0	0	$-D_y.E_{xy}(z^2).D_x^2$ $-D_y.E_{yy}(z^2).D_y^2$ $-D_x.G_{yx}(2z^2).D_xD_y$	$D_y.E_{xy}(z^2).D_x$ $+ D_x.G_{xy}(z^2).D_y$	$D_y.E_{xx}(z^2).D_y$ $+ D_x.G_{xy}(z^2).D_x$ $+ 1.G_{yz}1$

Fig 4.11 Stiffness Matrix of "PLATE".

$$
\begin{bmatrix}
1.\rho.1 & 0 & 0 & 0 & 0 \\
0 & 1.\rho.1 & 0 & 0 & 0 \\
0 & 0 & \begin{matrix}1.\rho.1 \\ +D_x.\rho(z^2).D_x \\ +D_y.\rho(z^2).D_y\end{matrix} & -D_x.\rho(z^2).1 & -D_y.\rho(z^2).1 \\
0 & 0 & -1.\rho(z^2).D_x & 1.\rho(z^2).1 & 0 \\
0 & 0 & -1.\rho(z^2).D_y & 0 & 1.\rho(z^2).1
\end{bmatrix}
$$

Fig 4.12 Mass Matrix of "PLATE".

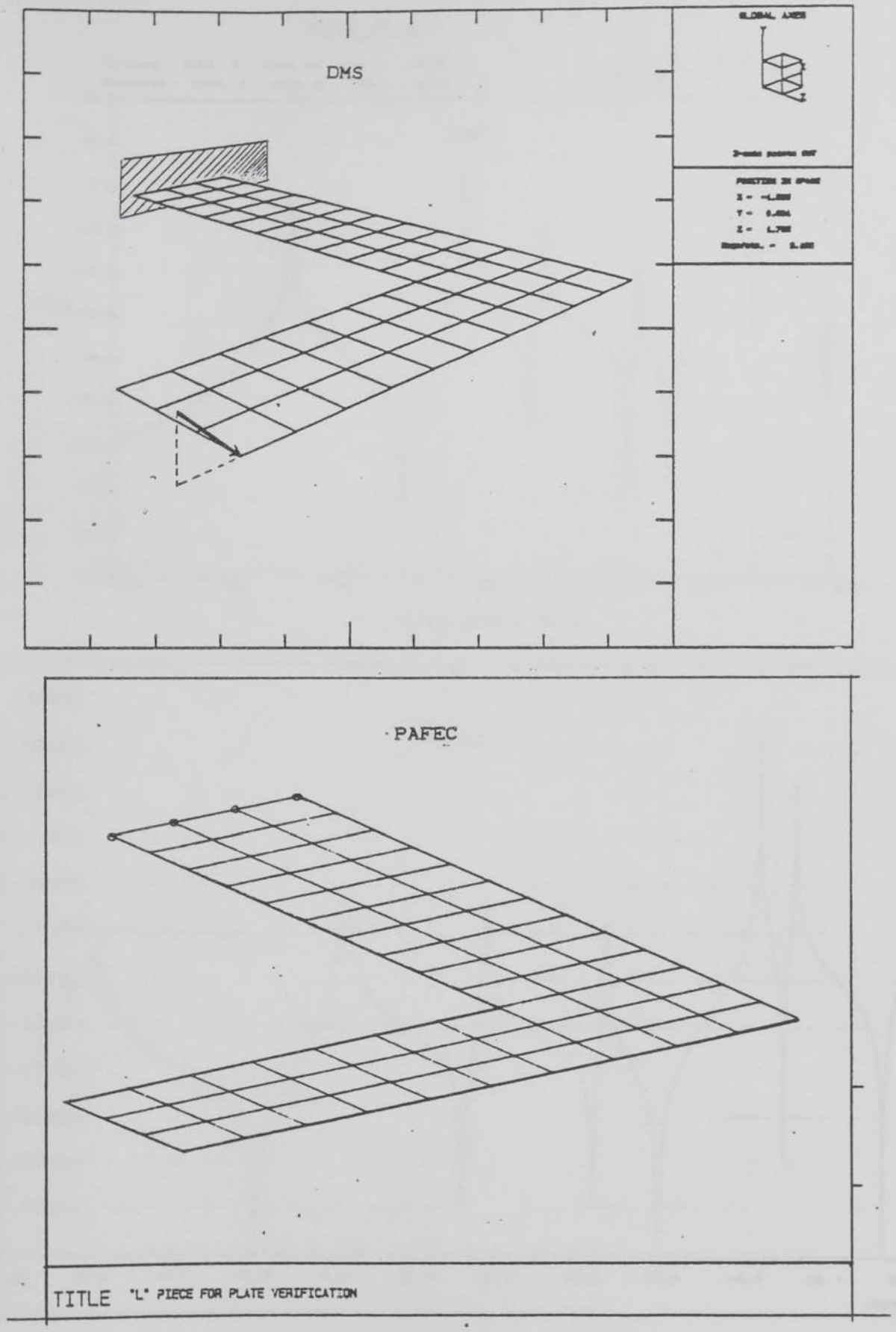

Fig 4.13 Verification Model for "PLATE".

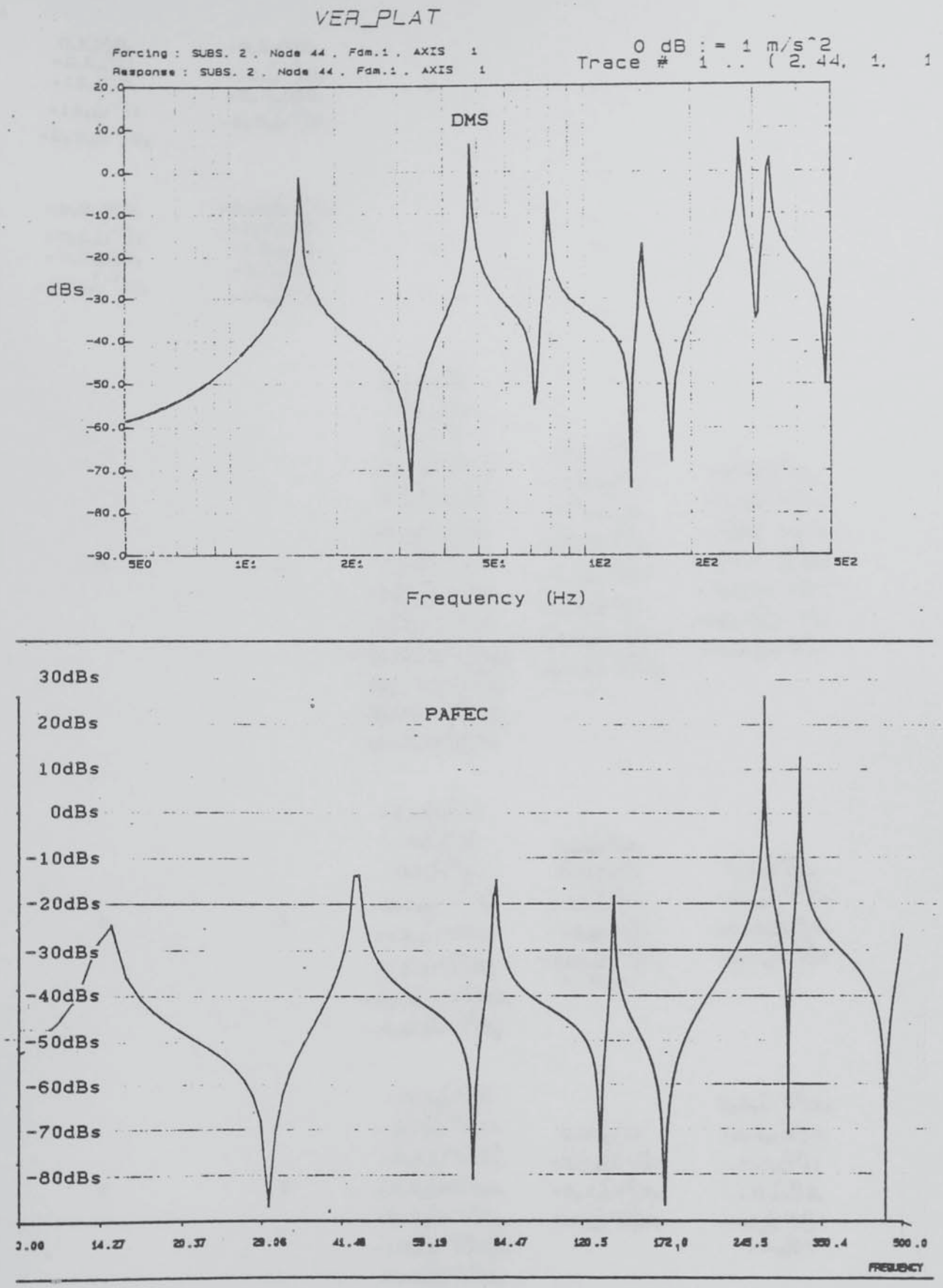

Fig 4.14 Verification Results for "PLATE".

$D_r E_{rr}(r).D_r$ $+ D_r E_{r\theta}(1).1$ $+ 1.E_{r\theta}(1).D_r$ $+ 1.E_{\theta\theta}(r^{-1}).1$ $+ D_\theta G_{r\theta}(r^{-1}).D_\theta$	$+ D_r E_{r\theta}(1).D_\theta$ $+ 1.E_{r\theta}(r^{-1}).D_\theta$ $+ D_\theta G_{r\theta}(1).D_r$ $- D_\theta G_{r\theta}(r^{-1}).D_r$	0	0	0
$+ D_\theta E_{r\theta}(1).D_r$ $+ D_\theta E_{r\theta}(r^{-1}).1$ $+ D_r G_{r\theta}(1).D_\theta$ $- D_r G_{r\theta}(r^{-1}).D_\theta$	$+ D_\theta E_{\theta\theta}(r^{-1}).D_\theta$ $+ D_r G_{r\theta}(r).D_r$ $- 1.G_{r\theta}(1).D_r$ $- D_r G_{r\theta}(1).1$ $+ 1.G_{r\theta}(r^{-1}).1$	0	0	0
0	0	$D_r^2.E_{rr}(rz^2).D_r^2$ $+ D_r^2.E_{r\theta}(z^2).D_r$ $+ D_r E_{r\theta}(z^2).D_r^2$ $+ D_r^2.E_{r\theta}(r^{-1}z^2).D_\theta^2$ $+ D_\theta^2 E_{r\theta}(r^{-1}z^2).D_r^2$ $+ D_r E_{\theta\theta}(r^{-1}z^2).D_r$ $+ D_r E_{\theta\theta}(r^{-2}z^2).D_\theta^2$ $+ D_\theta^2 E_{\theta\theta}(r^{-2}z^2).D_r$ $+ D_\theta^2 E_{\theta\theta}(r^{-3}z^2).D_\theta^2$ $+ D_\theta D_r G_{r\theta}(4r^{-1}z^2).D_\theta D_r$ $- D_\theta D_r G_{r\theta}(4r^{-2}z^2).D_\theta$ $- D_\theta G_{r\theta}(4r^{-2}z^2).D_\theta D_r$ $+ D_\theta G_{r\theta}(4r^{-3}z^2).D_\theta$	$- D_r^2.E_{rr}(rz^2).D_r$ $- D_r^2.E_{r\theta}(z^2).1$ $- D_r E_{r\theta}(z^2).D_r$ $- D_\theta^2 E_{r\theta}(r^{-1}z^2).D_r$ $- D_r E_{\theta\theta}(r^{-1}z^2).1$ $- D_\theta^2 E_{\theta\theta}(r^{-2}z^2).1$ $+ D_\theta D_r G_{r\theta}(2r^{-1}z^2).D_\theta$ $- D_\theta G_{r\theta}(2r^{-2}z^2).D_\theta$	$- D_r^2.E_{r\theta}(z^2).D_\theta$ $- D_r E_{r\theta}(r^{-1}z^2).D_\theta$ $- D_\theta^2 E_{r\theta}(r^{-2}z^2).D_\theta$ $- D_\theta D_r G_{r\theta}(2z^2).D_r$ $+ D_\theta G_{r\theta}(2r^{-1}z^2).D_r$ $- D_\theta D_r G_{r\theta}(2r^{-1}z^2).1$ $+ D_\theta G_{r\theta}(2r^{-2}z^2).1$
0	0	$- D_r E_{rr}(rz^2).D_r^2$ $- 1.E_{r\theta}(z^2).D_r^2$ $- D_r E_{r\theta}(z^2).D_r$ $- D_r E_{r\theta}(r^{-1}z^2).D_\theta^2$ $- 1.E_{\theta\theta}(r^{-1}z^2).D_r$ $- 1.E_{\theta\theta}(r^{-2}z^2).D_\theta^2$ $+ D_\theta G_{r\theta}(2r^{-1}z^2).D_\theta D_r$ $- D_\theta G_{r\theta}(2r^{-2}z^2).D_\theta$	$D_r E_{rr}(rz^2).D_r$ $+ D_r E_{r\theta}(z^2).1$ $+ 1.E_{r\theta}(z^2).D_r$ $+ 1.E_{\theta\theta}(r^{-1}z^2).1$ $+ D_\theta G_{r\theta}(r^{-1}z^2).D_\theta$ $+ 1.G_{z\theta}(r).1$	$D_r E_{r\theta}(z^2).D_\theta$ $+ 1.E_{\theta\theta}(r^{-1}z^2).D_\theta$ $+ D_\theta G_{r\theta}(1z^2).D_r$ $- D_\theta G_{r\theta}(r^{-1}z^2).1$
0	0	$- D_\theta E_{r\theta}(z^2).D_r^2$ $- D_\theta E_{r\theta}(r^{-1}z^2).D_r$ $- D_\theta E_{r\theta}(r^{-2}z^2).D_\theta^2$ $- D_r G_{r\theta}(2z^2).D_\theta D_r$ $+ D_r G_{r\theta}(2r^{-1}z^2).D_\theta$ $- 1.G_{r\theta}(2r^{-1}z^2).D_\theta D_r$ $+ 1.G_{r\theta}(2r^{-2}z^2).D_\theta$	$D_\theta E_{r\theta}(z^2).D_r$ $+ D_\theta E_{\theta\theta}(r^{-1}z^2).1$ $+ D_r G_{r\theta}(1z^2).D_\theta$ $- 1.G_{r\theta}(r^{-1}z^2).D_\theta$	$D_\theta E_{\theta\theta}(r^{-1}z^2).D_\theta$ $+ D_r G_{r\theta}(rz^2).D_r$ $- D_r G_{r\theta}(z^2).1$ $- 1.G_{r\theta}(z^2).D_r$ $- 1.G_{r\theta}(r^{-1}z^2).1$ $- 1.G_{\theta z}(r).1$

Fig 4.15 Stiffness Matrix of "DISC".

$$
\begin{array}{ccccc}
1.\rho(r).1 & 0 & 0 & 0 & 0 \\
0 & 1.\rho(r).1 & 0 & 0 & 0 \\
0 & 0 & \begin{matrix} D_r\rho(rz^2).D_r \\ D_\theta\rho(r^{-1}z^2).D_\theta \\ 1.\rho(r).1 \end{matrix} & -D_r\rho(rz^2).1 & -D_\theta\rho(z^2).1 \\
0 & 0 & -1.\rho(rz^2).D_r & 1.\rho(rz^2).1 & 0 \\
0 & 0 & -1.\rho(z^2).D_\theta & 0 & 1.\rho(rz^2).1
\end{array}
$$

Fig 4.16 Mass Matrix of "DISC".

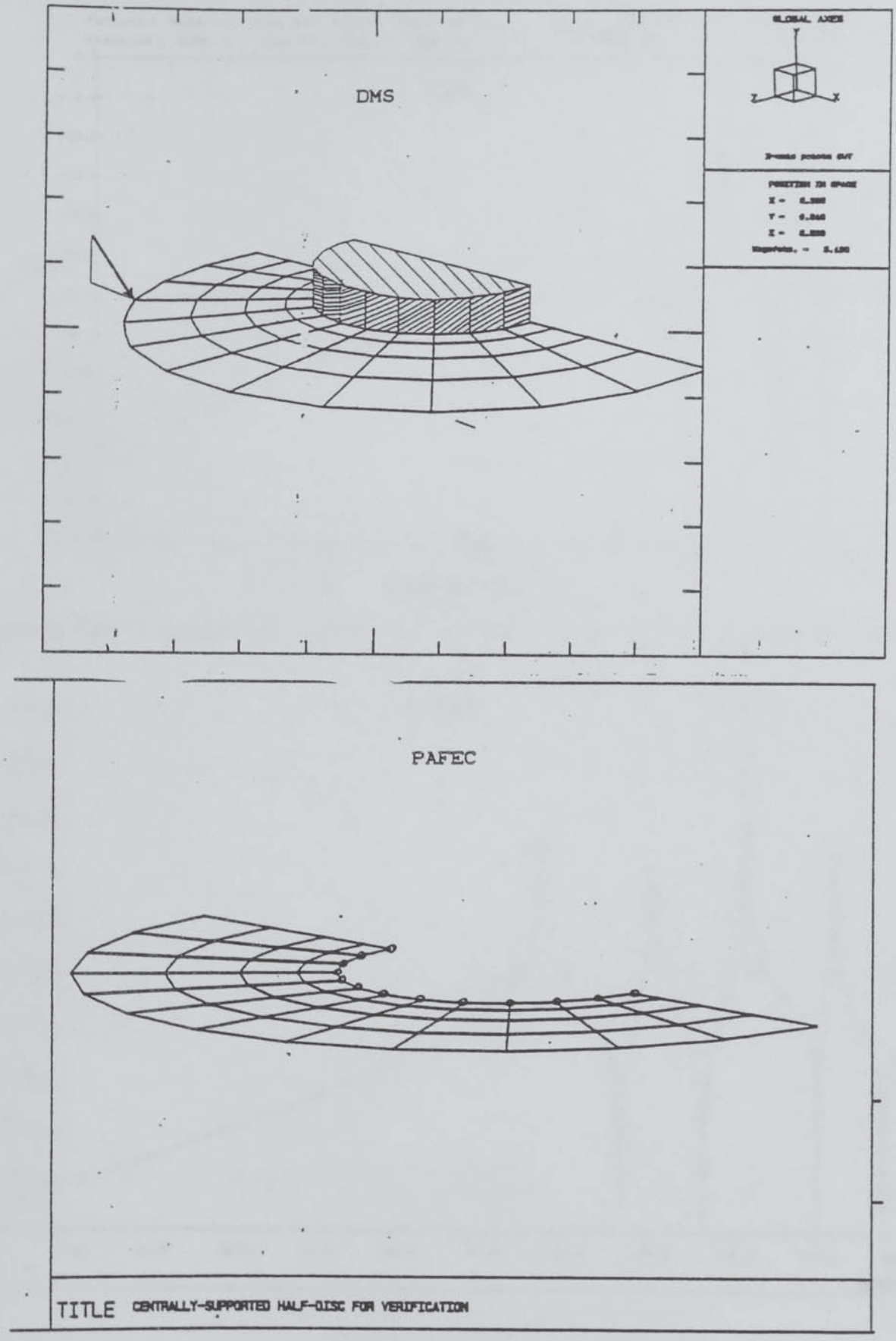

Fig 4.17 Verification Model for "DISC".

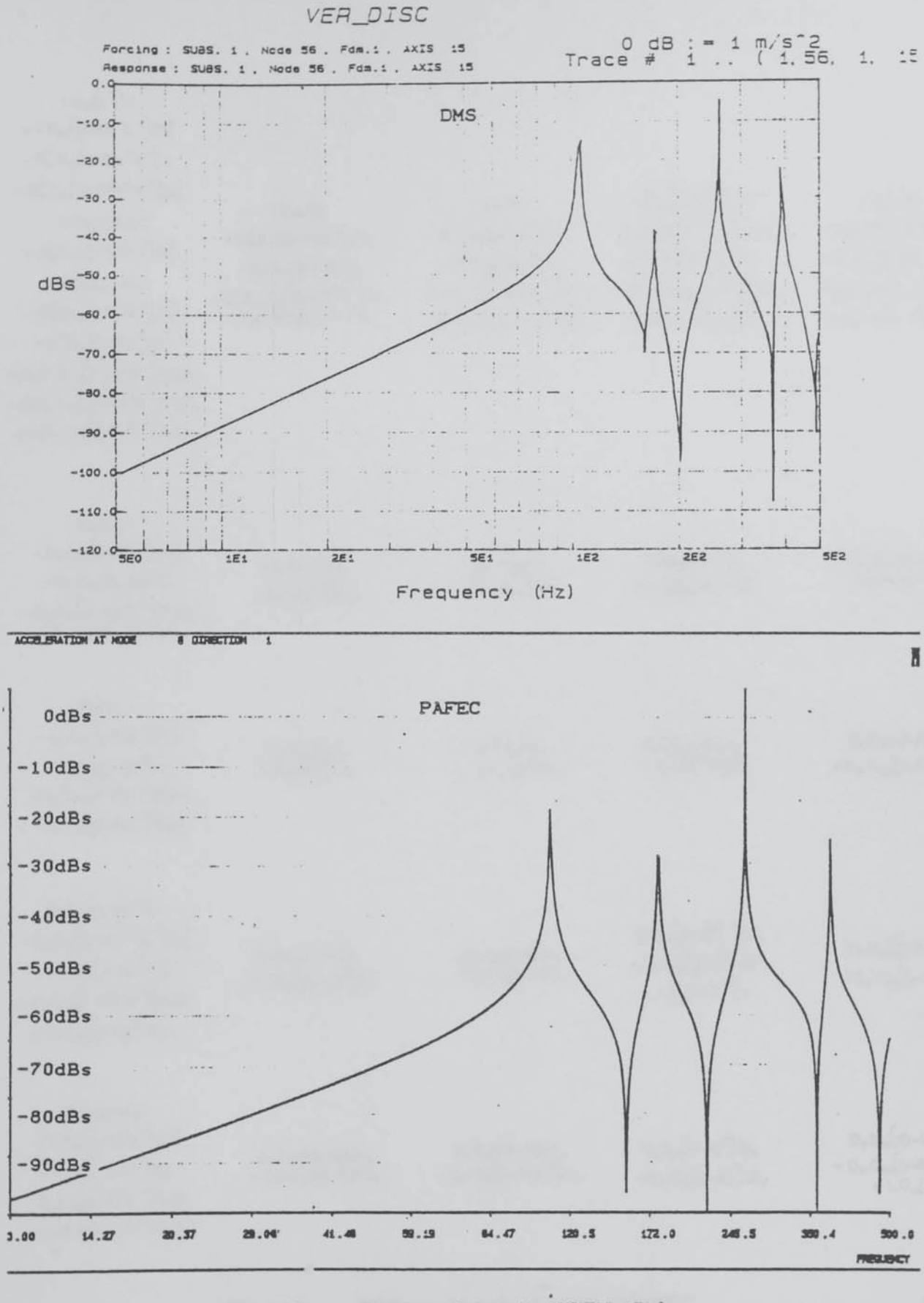

Fig 4.18 Verification Results for "DISC".

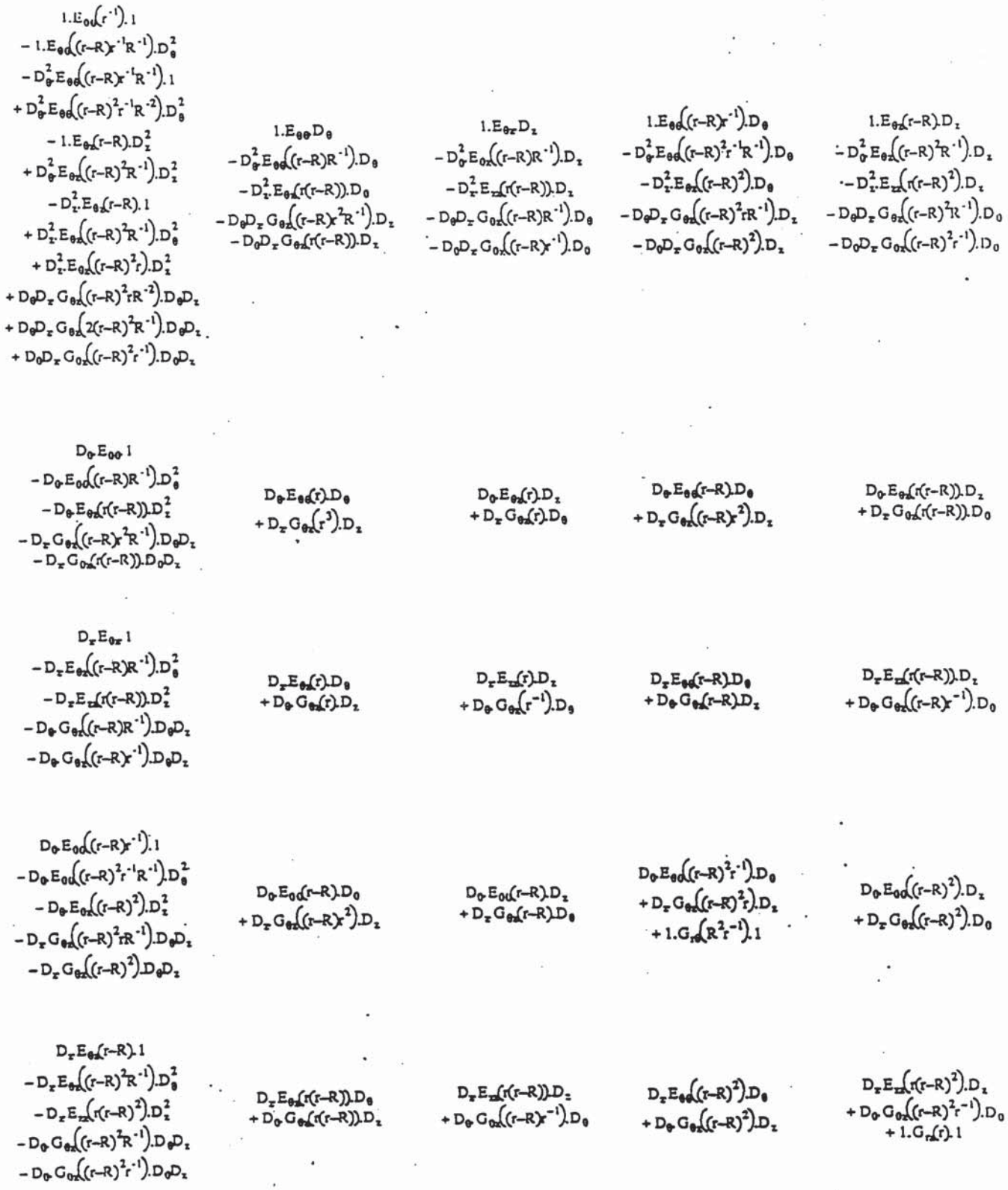

Fig 4.19 Stiffness Matrix of "CYLINDER".

$1.\rho(r).1$ $+ D_\theta.\rho\left(r(r-R)^2R^{-2}\right).D_\theta$ $+ D_z\rho\left(r(r-R)^2\right).D_z$	$-D_\theta\rho\left((r-R)r^2R^{-1}\right).1$	$-D_z\rho((r-R)r).1$	$-D_\theta.\rho\left((r-R)^2rR^{-1}\right).1$	$-D_z\rho\left((r-R)^2r\right).1$
$-1.\rho\left((r-R)r^2R^{-1}\right).D_0$	$1.\rho\left(r^3\right).1$	0	$1.\rho\left((r-R)r^2\right).1$	0
$-1.\rho((r-R)r).D_z$	0	$1.\rho(r).1$	0	$1.\rho((r-R)r).1$
$-1.\rho\left((r-R)^2rR^{-1}\right).D_\theta$	$1.\rho\left((r-R)r^2\right).1$	0	$1.\rho\left((r-R)^2r\right).1$	0
$-1.\rho\left((r-R)^2r\right).D_z$	0	$1.\rho((r-R)r).1$	0	$1.\rho\left((r-R)^2r\right).1$

Fig 4.20 Mass Matrix of "CYLINDER".

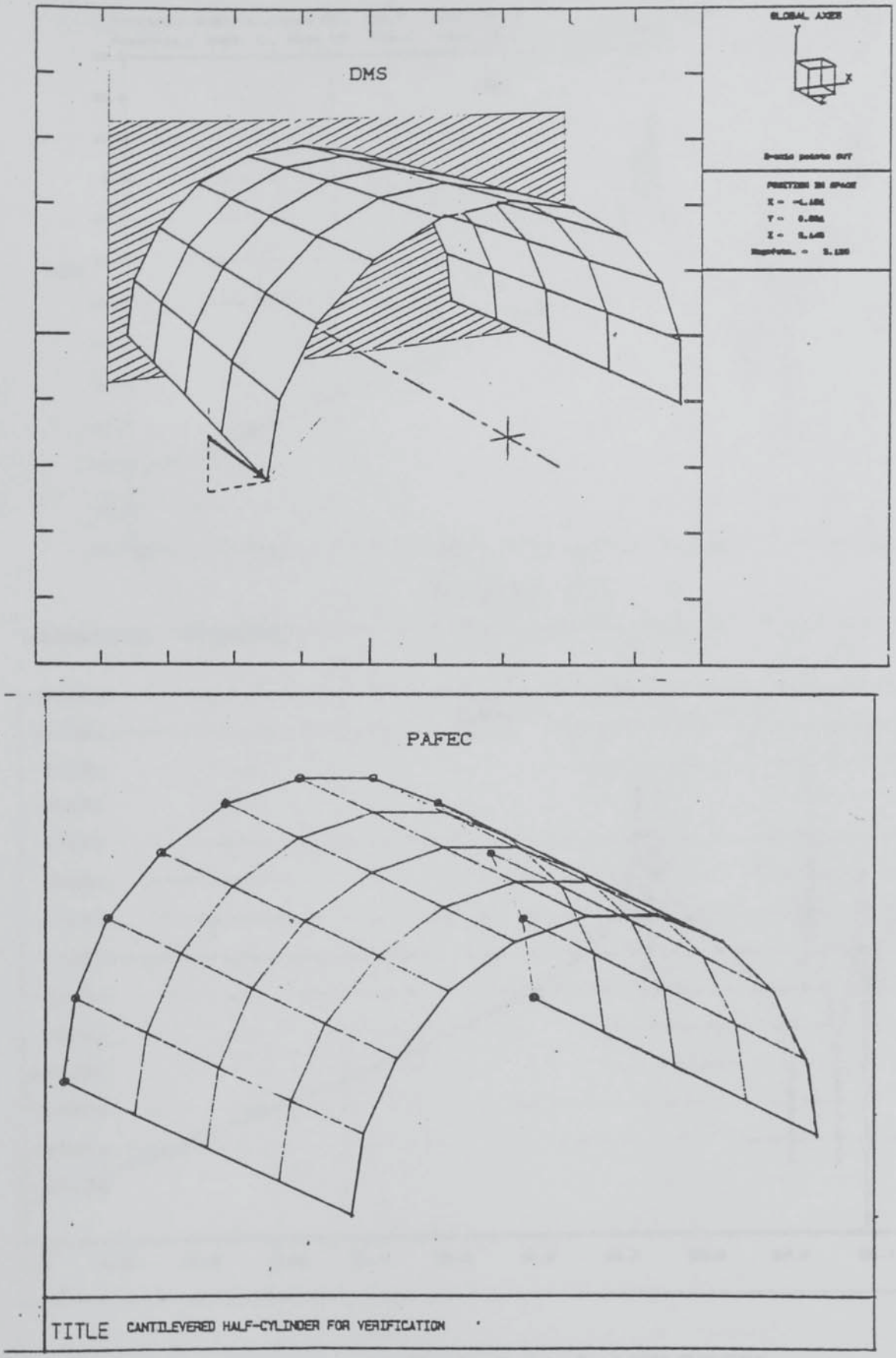

Fig 4.21 **Verification Model for "CYLINDER".**

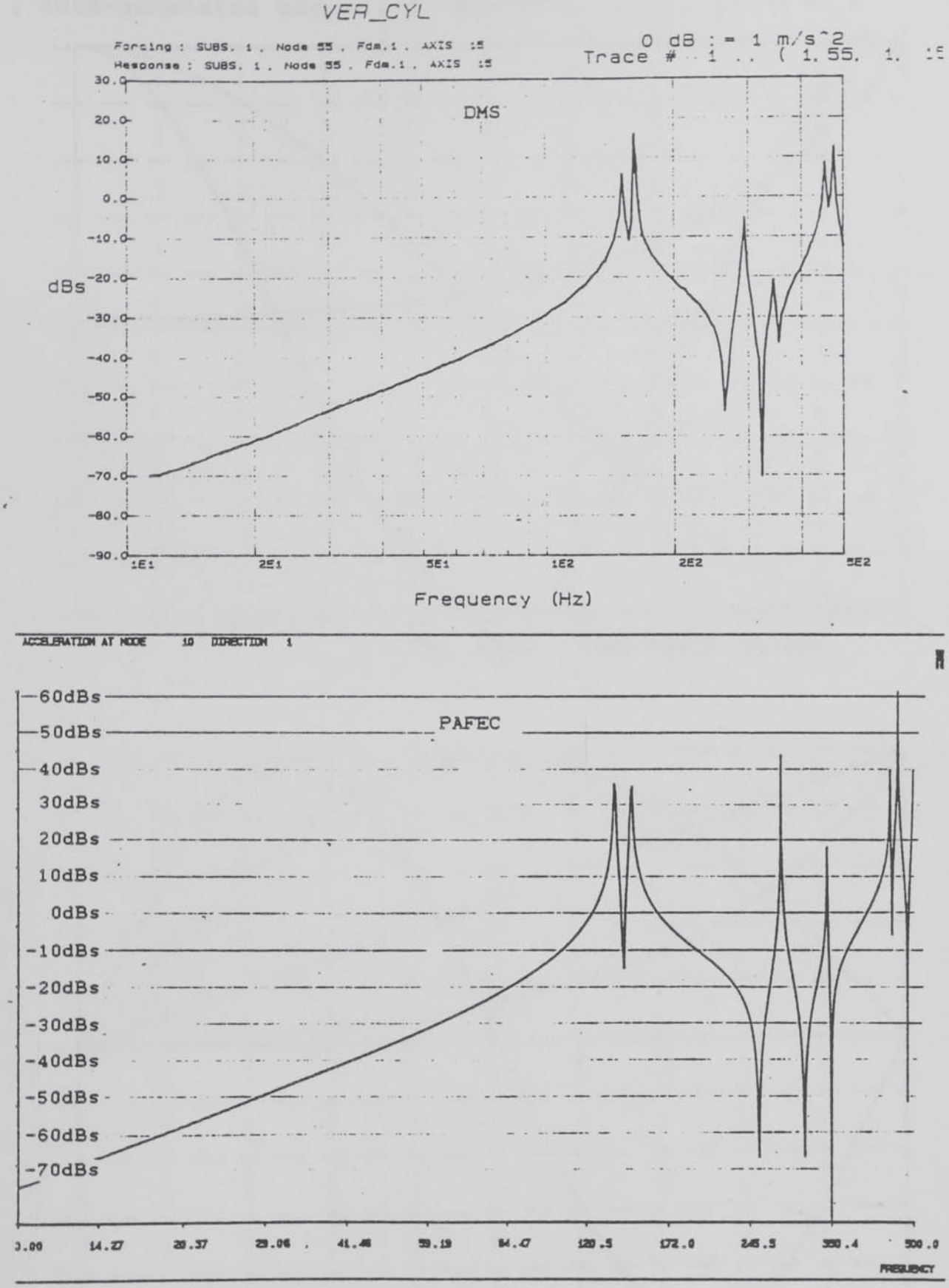

Fig 4.22 Verification Results for "CYLINDER".

GENERATING functions -type LINE/TRIG/HYP
Auto-generated set ..1 to 4 step 1

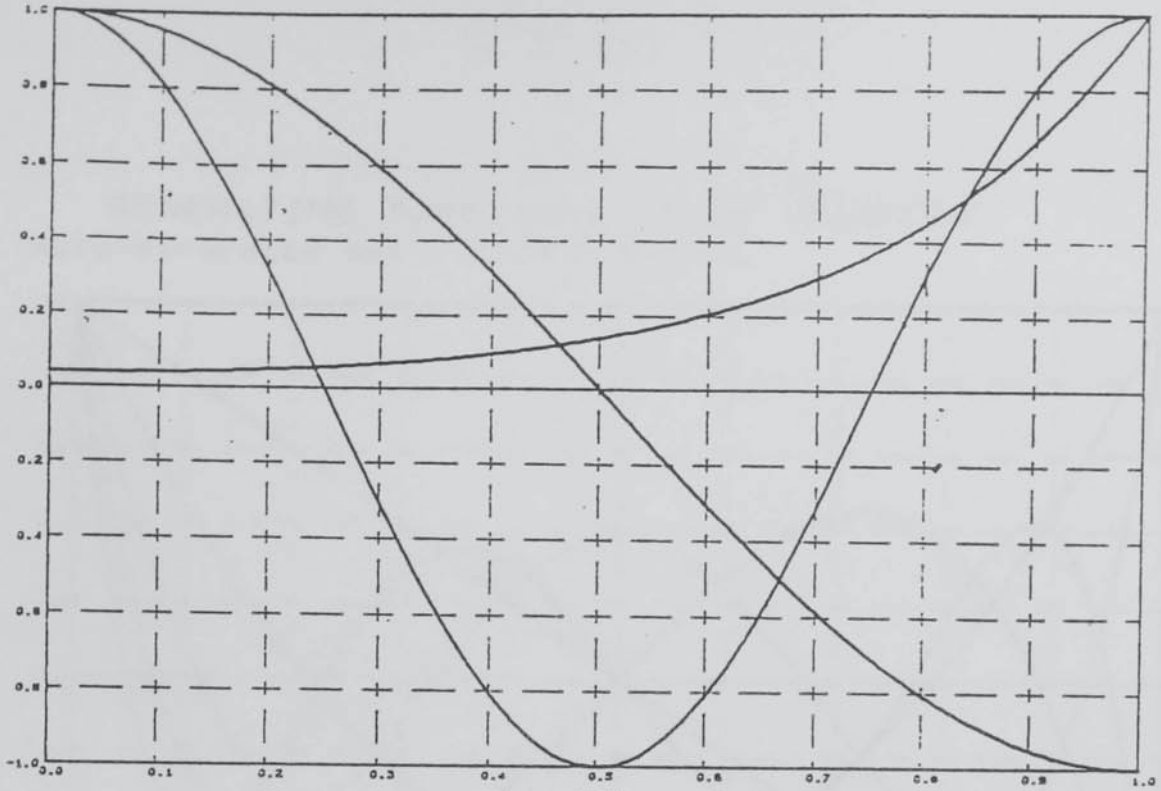

Fig. 4.23a Symmetrical Functions.

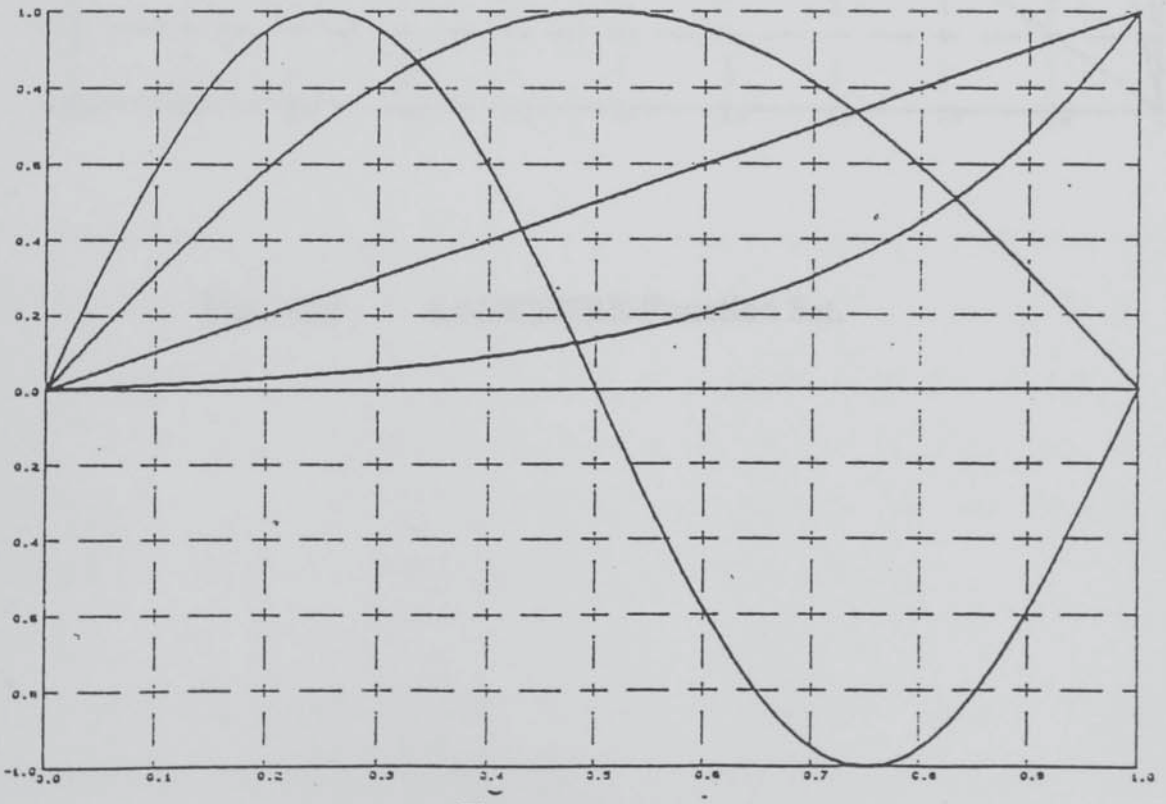

Fig. 4.23b Antisymmetrical Functions.

Fig. 4.23 LINE/TRIGONOMETRIC/HYPERBOLIC Function Set.

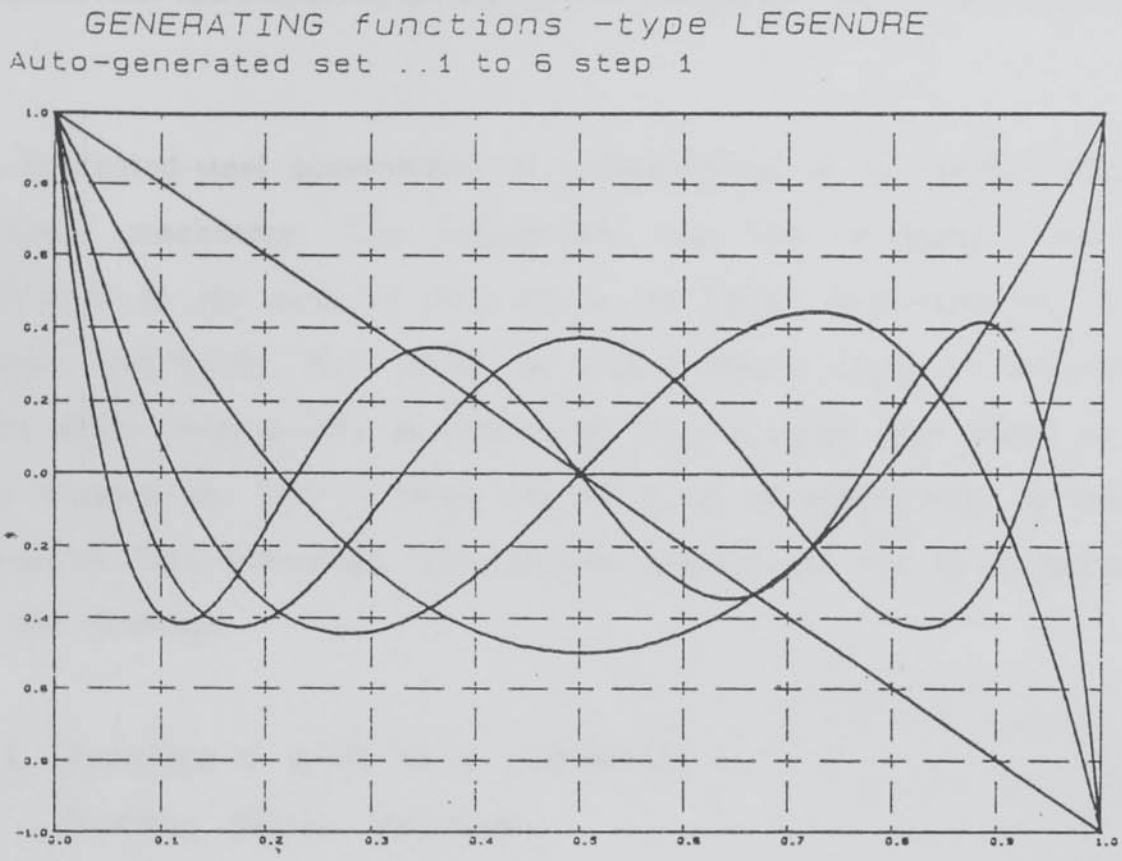

Fig. 4.24 LEGENDRE Function Set.

Chapter 5.

LAMINATED COMPONENTS IN MACHINES

The laminated-steel construction is commonplace in the environment of electrical machinery. The laminations vary in thickness from one application to the next as they do in the finish and treatment of the surfaces. Intuitively, one would be expect that a stack of laminations might differ substantially in behaviour from a solid steel piece of the same dimensions. This is borne out by a set of experiments devised to investigate this behaviour. This chapter reports the set of experiments and the findings.

§5.1 Treating a stack as a continuum :- Normal Stress Relations.

It is convenient to treat a pack of laminations as a continuum for the purpose of extrapolating the characteristics of a laminated body from the bulk properties of the pack itself. We establish a set of stress-strain relations for the general stack. Using these, it is possible to draw conclusions about the general bulk properties of the stack from observations about the behaviour of particular objects.

It is possible make some simp'e statements about 'laminated' stresss-strain relations before any experimentation. Firstly, we note that there are three principal directions in every laminated body. One is

necessarily the normal to the plane of lamination and will be referred to as the 'z' direction. The other two ('x' and 'y') can be any convenient orthogonal directions in the plane of lamination. Consider the cube in Fig. 5.1. It is usual for the density of packing of the steel to be of the of the order of 0.96-0.99 in the current context. The interposing material may be air, varnish, resin or any combination of these. Asperities (or a coating as the case may be) on the surface of each lamination prevent a completely flush fit. We would expect that the interposing layers would contribute some extra flexibility to compression in the axial direction and that shear strains in the x-z and y-z planes would have significantly lower energy per unit volume associated with them than if the same strains were to occur in solid steel.

The behaviour of the laminated continuum can be split into two areas - behaviour with respect to normal stresses and behaviour with respect to shear stresses.

For normal stresses within the stack a relation of the form of 5.1 will hold between the normal stresses σ_{xx}, σ_{yy}, and σ_{zz} in the x, y, and z directions.

$$\begin{Bmatrix} \sigma_{xx} \\ \sigma_{yy} \\ \sigma_{zz} \end{Bmatrix} = E \begin{bmatrix} 1 & \mu_1 & \mu_2 \\ \mu_1 & 1 & \mu_2 \\ \mu_2 & \mu_2 & \alpha \end{bmatrix} \begin{Bmatrix} \varepsilon_{xx} \\ \varepsilon_{yy} \\ \varepsilon_{zz} \end{Bmatrix} \qquad (5.1)$$

The constant **E** in (5.1) is derived directly from the properties of the lamination steel. If we use E_{steel} for the usual Young's modulus of the

lamination steel, μ_{steel} for the lamination steel Poisson's ratio and SF for the stacking factor, then **E** from (5.1) above may clearly be expressed as (5.2) below.

$$\mathbf{E} = SF \,.\, E_{steel} /(1 - \mu_{steel}^2) \qquad (5.2)$$

The constant α will be much less than 1, thereby dictating that the stiffness of the stack in compression/extension in the 'z' direction is low. The constant μ_1 can be shown to be related to μ_{steel} as (5.3).

$$\mu_1 = \frac{(1 - \mu_{steel})}{(1 - 2\mu_{steel})(1 + \mu_{steel})} \qquad (5.3)$$

It is difficult to deduce the exact value of constant μ_2, using (5.1) directly. However, it is simple to show from (5.1) using the argument that the matrix must be positive-definite (i.e. that no state of strain can have a negative associated stored-energy per unit volume) that must μ_2 is bounded as expressed in (5.4).

$$2.\mu_2^2 \leq \alpha \qquad (5.4)$$

We can proceed further by finding the inverse relation to (5.1). It is convenient to define the following constants.

$$\chi = \frac{1}{\left(1 - \mu_1^{\,2}\right)}, \qquad \delta = \frac{\mu_2}{\left(1 + \mu_1\right)} \tag{5.5}$$

$$\lambda = \alpha - \mu_2^{\,2}\left(1 + \frac{\left(1 - \mu_1\right)}{\left(1 + \mu_1\right)}\right) \tag{5.6}$$

We can form the inverse relation to (5.1) by performing a Gauss-Doolittle inversion on the matrix. The result is given as (5.7).

$$\begin{Bmatrix} \varepsilon_{xx} \\ \varepsilon_{yy} \\ \varepsilon_{zz} \end{Bmatrix} = \frac{1}{E}\begin{bmatrix} \chi + \frac{\delta^2}{\lambda} & -\chi.\mu_1 + \frac{\delta^2}{\lambda} & -\frac{\delta}{\lambda} \\ -\chi.\mu_1 + \frac{\delta^2}{\lambda} & \chi + \frac{\delta^2}{\lambda} & -\frac{\delta}{\lambda} \\ -\frac{\delta}{\lambda} & -\frac{\delta}{\lambda} & \frac{1}{\lambda} \end{bmatrix} \begin{Bmatrix} \sigma_{xx} \\ \sigma_{yy} \\ \sigma_{zz} \end{Bmatrix} \tag{5.7}$$

Now, we can come to a conclusion about the cross-coupling terms (δ/λ) by reasoning that the strains in ε_{xx} and ε_{yy} would be the same in a solid steel continuum as they would be in a laminated stack for a given state of stress σ_{xx}, σ_{yy}, σ_{zz}. Equation (5.8) gives the relation (δ/λ).

$$(\delta/\lambda) = \mu_{steel} \tag{5.8}$$

Thus, for normal stress/strain relations within a laminated stack, we find that there is only one true degree of freedom. The most simple

variable to measure is the quantity $(1/E\lambda)$ which is the 'longitudinal' flexibility of the stack given zero stress values for σ_{xx}, σ_{yy}.

§5.2 Treating a stack as a continuum :- Shear Stress Relations.

The shear stress relations are significantly simpler than those for developed for the normal stresses above. We begin as before by expressing the stresses explicitly in terms of the strains as (5.9)

$$\begin{Bmatrix} \sigma_{xz} \\ \sigma_{yz} \\ \sigma_{xy} \end{Bmatrix} = \begin{bmatrix} G_{xz} & 0 & 0 \\ 0 & G_{yz} & 0 \\ 0 & 0 & G_{xy} \end{bmatrix} \begin{Bmatrix} \varepsilon_{xz} \\ \varepsilon_{yz} \\ \varepsilon_{xy} \end{Bmatrix} \qquad (5.9)$$

Now, for shear stress/strain within the x-y plane, the behaviour of the stack must be very similar to that of the equivalent solid steel body. If we use G_{steel} to represent the shear modulus of the solid steel and SF as before to represent the lamination stacking factor, then we can write (5.10) by inspection.

$$G_{xy} = SF \,.\, G_{steel} \qquad (5.10)$$

The other properties G_{xz}, G_{yz} must be identical unless the lamination surfaces have a strong directionality which is not usually the case. Thus, as we found with the normal stress relations, there is only one parameter to be empirically determined for the shear stress/strain relations.

§5.3 Effect of the "Laminated" Properties on the Behaviour of machines.

It is to be expected that the properties discussed above will not significantly influence the axially-uniform modes of stators, hence it has been possible for previous authors to produce good solutions for the vibration modes and frequencies for these modes. With these modes, virtually no interlaminar shear takes place so the shear modulii are of no significance. The normal stress-strain relations do have an impact which some authors have failed to recognise. Laminated cylinders of finite length vibrating in "axially-uniform" shapes have resonances which are relatively insensitive to the cylinder length. Correction factors are developed in appendix 6 which are applied to the modulii of cylinder materials (based on the length of the cylinders) which accomodate in an approximate way the effects of the Poisson coupling between circumferential and axial normal strains. Laminated cylinders will not experience the same stiffening effects due to the Poisson coupling except a much greater cylinder lengths. Hence a plane-stress model can be justified in the case of these cylinders for the axially-uniform modes.

Another consequence of the properties is that the mode having (say) two wavelengths about the circumference (n= 2) and zero 'wavelengths' in the axial direction (m= 0) will be lower in frequency than the mode (n=2 , m=1) by some amount which would be much greater if the cylinder were solid. In other words *axial waviness will not contribute greatly to the stiffness of modes of laminated cylinders.* This is an

important observation. More than one author (Verma & Girgis (B.1986) and Watenabe *et al.* (B.1983)) has reported difficulty in identifying some modes of the machine stators which they examined. The effect mentioned here regarding the small increment in energy for increased axial waviness makes the clear identification of modes difficult.

§5.4 Design of Models to Investigate the Behaviour.

The reasoning behind the dimensions, geometry and nature of the models used in this work is outlined here in order to clarify for the reader, the material to follow.

Terms of reference:

a) Produce a model whose behaviour depends on the relevant properties of the laminated construction.

b) The model should have a set of identifiable well separated resonances.

c) The model should be amenable to analysis either numerical or analytic.

d) The model should be scaled so that results obtained from it apply to the components of interest.

e) It should have a system of clamping which can:-

(i) Produce a range of pertinent clamping pressures to acceptable accuracy.

(ii) Spread the load so that the outer laminations experience a reasonably uniform pressure.

(iii) Not interfere with a b or c above.

The range of clamping pressures investigated is 0-2MPa. The laminated cores of small AC machines are sometimes compressed higher than this but generally, this represents the whole spectrum of pressure. In such cases, extrapolation of the results presented here will have to be relied upon. Surface finishes vary dramatically with application from proprietrary mineral treatments for withstanding high temperatures to none whatsoever in the case of DC mainpoles. (The primary reason for laminating these is for ease of manufacture). Only a small subset of these has been addressed because of time restrictions. The following surface conditions have been examined . . .

(1) Clean plain steel surfaces.
(2) Varnished surfaces.
(3) Clean steel surfaces having been vacuum-pressure-impregnated.
(4) Varnished surfaces having been vacuum-pressure-impregnated.

The results show a considerable scatter in the properties derived though the trends in each case are steady.

§5.5 The Dependence of Beam Resonances on the Material Properties

The models chosen were rectangular-section beams in all cases. It is appropriate to note the following about the modes of these beams.

(1) The modes occur in four distinct groups; torsion about the beam-axis, extension along the beam-axis and flexure in two orthogonal planes.

(2) The resonances of extension modes are determined solely by the modulus of compression of the material in the direction of the beam-axis..

(3) The resonances of the torsional modes are determined primarily by the shear modulii of the beam material in the two planes which contain the z-axis. If the beam is square in section and relatively narrow, an accurate determination of the relation between the torsional resonances and the shear modulii in the two planes may be made.

(4) The frequencies of the flexure modes in either of the two orthogonal planes are determined by both the modulus of compression of the beam material in the direction of the beam axis and the shear modulus of the material in that plane. For a thick beam with a small shear-modulus in one plane, the resonant frequencies of flexure of the beam in that plane will be

governed primarily by the shear modulus. The mode-shapes in this case will look like sinusoids. Fig. 5.2a shows one such mode. For a narrow beam in which the shear modulus is not small relative to the modulus of compression in the direction of the beam-axis, the frequencies are determined primarily by the modulus of compression and virtually no shear strain occurs within the beam. A mode of this type is shown in Fig. 5.2b. When designing a model to investigate one of the modulii mentioned above, the proportions can be chosen so the frequencies of the flexure modes will have a strong dependence on that modulus.

(5) The damping contributions from shear and compression strains are uncoupled. The damping inherent in one mode can be considered to be the sum of the components from shear and compression. If the stiffness of one mode is determined mostly by one modulus, then the damping coefficient of that mode will be approximately equal to the damping coefficient associated with that type of strain.

§5.6 Outline of Experimental Procedure.

All of the tests preformed involved examining the response-to-forcing of the models over a suitable frequency range which included one or more of the first resonant conditions of the model. All information extracted is based upon the shape of the frequency-response curves and in particular, the position and "width" of the resonance peaks. For

speed, the excitation was 'white-noise' after preliminary investigations revealed a satisfactory degree of linearity of the relation between stiffness and deflection. Records of the forcing amplitude were kept in order that the amplitude of motion at every frequency sould be obtained directly from the frequency response plots.

The models were all flexibly supported to approximate the "free" condition. The first models were suspended from a light steel cable which allowed completely free flexure of the beam though motion in the direction of the beam axis would have been constrained.

The 'white-noise' was generated by the spectrum analyser and consequently had frequency components only within the range of frequencies being measured. The force signal was amplified before being passed to an exciter where the force input was measured.

Damping figures are estimated on the basis of the resonance bandwidths. In all cases, the damping is sufficiently large in comparison withn the coefficients for solid steel that the energy-dissipation may be considered to be due entirely to the relative motion of lamination surfaces. The careful design of the models resulted in a set of well-separated resonances. Because of the relative coarseness of the traces which had to be accepted in order to allow find more than one resonance in the frequency range, not all of the peaks will have been well represented. (ie. the frequency band which includes the true resonant frequency is a finite fraction of the 3dB bandwidth). Therefore, use of the 3dB bandwidth method to estimate damping did not seem the

optimm means of estimating damping. Instead, a method was devised which involves comparing the response levels measured at two different prescribed bandwidths (for example $f_n/10$ and $f_n/20$). The bandwidths can be chosen arbitrarily to best suit the individual response traces being examined. The consistency of results obtained using this method indicated that it was satisfactory.

Where the pressure of clamping was being adjusted for models 5.1, 5.2 and 5.5, (these relied on the measurement of compression in springs to set the pressure) each increment was divided in two and the bolts were tightened to half tension starting from one end and proceeding upward and then the tensioning was finished working the other way. The resulting pressure distribution should have been quite even as a result. The rate of compression of the laminations themselves at lower pressures was sufficient to make this tightening procedure necessary.

On models 5.3 and 5.4, the bolt tension could be measured absolutely at any time.

§5.7 Model 5.1 and Tests 5.1.1-5.1.2

The first model tested was a beam of dimensions 1.5m x 0.2m x 0.2m (Figs. 5.3 and 5.4). The similarity of the dimensions in the x and y directions was intentional in order that the flexure modes in these two planes could be compared and contrasted. It was expected that the resonant frequencies of modes of flexure in the y-z plane would be

slightly lower than those of the modes-of-flexure in the x-z plane (these modes should be totally unaffected by the fact that the beam is laminated since both the stiffness-in-flexure and the linear density of the stack are proportional to SF - the stacking factor).

Tests 5.1.1 involved suspending model 5.1 from a light steel cable so that it was free to vibrate in flexure in the x-z plane (Fig. 5.3a). A shaker was attached at the low end and the response measured at the high end. Various amplitudes of forcing were supplied so that the motion at the ends of the beam was varied between 0.0m and 1.0e-7m. No dependence on the amplitude was observed over this range either in the value of the resonant frequency or the hysteretic damping coefficient calculated (5.1e-3).

A model of this beam was prepared using DMS. The properties of solid steel (scaled by the stacking-factor (0.94 at low clamping pressures) were used in this model and the response of transverse motion at one end of the beam to forcing at the other was computed over the range 0-3kHz. The mass of the clamping gear (plates, springs, bolts etc.) was 'smeared' over the length of the beam for simplicity. Fig 5.5 compares the calculated response for the beam with the measured. The slight discrepancy in the natural frequency of the second and third modes can be accounted for by the "smearing" of the inertias of the clamping bolts and plates. The conclusion is that for laminations vibrating within their own plane (configured so that they cannot buckle), the material constants which should be used are simply those of solid steel scaled down by the stacking factor for the laminations. There is no detectable

variation in the parameters of the principal modes of flexure in this plane as the clamping pressure is increased.

Tests 5.1.2 on this model consisted of exciting the beam to vibrate in flexure in the y-z plane. The resonant frequencies encountered here differed substantially from those measured and calculated for tests 5.1.1. Fig.s 5.6 and 5.7 are sample response curves from tests 5.1.2 for clamping pressures of 250kPa and 750kPa resp. See table 5.1 for the first resonant frequencies and the damping coefficients measured. These values are for the low amplitude oscillations of the beam ends. The values for the shear modulus are found by comparing the resonances calculated using a special beam flexure model for high shear (allowing linear and quadratic variation of the axial point translation across the section) in which a number of values for shear modulus were tried. In the report on the behaviour of laminated components in vibration, (Garvey (A.1986)) the r.m.s. shear strain in the beam is related to the translation at the beam ends and the effective shear modulus for the first three modes.

It should be noted that the first natural frequency of flexure out of the plane of lamination of this beam transpired to be satisfactorily sensitive to the effective shear modulus of the stack for confidence in the results. This was somewhat fortunate. There was no way of knowing in advance what shear modulii could be expected and values closer to the figure for solid mild steel (81.3 GPa) would have meant that the first resonance was almost totally insensitive to the shear modulus.

Pressure (kPa)	First Resonance (Hz)	Resolved 3dB Bandwidth (Hz)	Shear Modulus(GPa)	Damping Factor
250	148.	6.20	0.42	4.2e-2
313	164.	5.75	0.61	3.5e-2
375	180.	5.60	0.76	3.1e-2
437	192.	5.00	0.93	2.6e-2
500	202.	5.05	1.04	2.5e-2
563	212.	5.10	1.11	2.4e-2
625	218.	4.80	1.20	2.2e-2
687	222.	4.35	1.31	2.0e-2
750	228.	4.35	1.33	1.9e-2

Table 5.1 Results from test 5.1.2. (Low amplitude).

Amplitudes of vibration at the ends were varied continuously up to approximately 3e-6m. The trend was that damping values increased dramatically with increased amplitude above some (slightly indefinite) threshold. The stiffness of the mode, on the other hand, decreases in a second-order relation with increased amplitude. Both these trends are illustrated for one clamping pressure in Fig. 5.8. The range-of-linearity of the stack for a given clamping pressure is obviously slightly arbitrary, but order-of-magnitude figures are presented in table 5.2.

Since the variation of stiffness with amplitude is smooth and quite

gradual up to 5 times the strains mentioned below, a linear model for the behaviour of a laminated component will probably be quite adequate up to at least 5 times these values if suitable corrections are made.

Pressure (kPa)	Range of Linearity (Shear Strain)
250 - 460	2.0×10^{-7}
460 - 580	2.5×10^{-7}
580 - 690	3.0×10^{-7}

Table 5.2 Range of Linearity for the Laminations of Model 5.1.

§5.8 Model 5.2 and Tests 5.2.1

Model 5.2 (Fig. 5.9) was similar to model 5.1, the only difference being that fewer laminations were used. The depth of the stack in this case was approximately half that used previously. This beam was to serve as a check on the results obtained from the previous beam. In particular, it should immediately show up any error in the theoretical model.

Experiments 5.2.1 took the same form as tests 5.1.2 in which the beam was suspended vertically on a light steel cable. Excitation was applied at the low end and response measured at the high end for flexure modes

out of the plane of lamination. The amplitudes of vibration were kept below the ranges of linearity outlined in table 5.2.

The results were not completely consistent with those of tests 5.1.2. The deduced values of the shear modulus were lower for model 5.2 than those found for model 5.1 by a factor of about 0.75 and at the same time, the damping factors were increased by a factor of almost 2. The results are presented in table 5.3 below. There are a number of reasons why this may have been the case. The theoretical model was re-examined and found to be correct - agreeing very closely with a "plane sections remain plane" model both at very high and very low values of shear modulus where the simple "p.s.r.p" model should give good answers.

The principle reason for the discrepancy is most likely to be the increased insensitivity of the beam resonances to the shear modulus (due to the beam being thin). Other influences are discussed in the dedicated report (Garvey (A.1986)). The results at least show the same trend as those from tests 5.1.2 both in damping and effective shear modulus.

Pressure (kPa)	First Resonance (Hz)	Resolved 3dB Bandwidth (Hz)	Shear Modulus (GPa)	Damping Factor
250	101.	8.68	0.33	8.6e-2
313	109.	7.95	0.41	7.3e-2
375	117.	7.95	0.50	6.8e-2
437	127.	7.62	0.62	6.0e-2
500	131.	7.20	0.68	5.5e-2
563	136.	6.93	0.76	5.1e-2
625	142.	6.81	0.88	4.8e-2
687	146.	6.57	0.94	4.5e-2
750	150.	6.15	0.97	4.1e-2

Table 5.3 Results from test 5.2.1. (Low amplitude).

§5.9 Model 5.3 and Tests 5.3.1-5.3.3

Model 5.3 was a relatively thick beam laminated along the axis (Fig 5.10) The geometry of this model is at least similar to that of some DC machine mainpoles whereas models 5.1 and 5.2 bore no obvious relation to any machine component. The sections of model 5.3 are square as this enables us to make good sense of the results from a torsion test.

Clamping is achieved by four pieces of M12 threaded-rod running through the laminations and holding two square 12mm mild-steel endplates together. The measurement of the pressure was achieved by measuring the extension of each of the bolts using a large Vernier scale. Pressures as high as 2.4 MPa could be achieved.

All four of the "types" of beam mode discussed in §5.5 are strongly dependent upon some properties of the lamination for this particular beam. Since the sections are square, the modes-of-flexure should be identical in both flexure planes. Flexure tests have been performed in one plane only.

The beam was rested on two foam supports lying approximately under the locations where "nodes" of vibration would occur for the flexure modes. The extension and torsion modes would not be significantly stiffened by this support.

Tests 5.3.1 comprised exciting model 5.3 to vibrate in axial compression/extension. These tests give a direct impression of the effective Youngs modulus of the stack. The first such resonance has a very simple associated mode-shape. A number of preliminary tests indicated that for clamping pressures above 300kPa, sufficient force could not be supplied by the power-amplifier + shaker arrangement being used to drive the system into detectable non-linearity. Thus, the stack was assumed to be linear for all tests performed.

For each stage of tightness, a response-curve was recorded from which

was extracted the first resonant frequency and the resolved 3dB bandwidth (using suitable bandwidths). The Youngs modulus deduced from the stack depends on the first resonant frequency as well as the stack-length and stacking factor. (Both of these quantities vary slightly with increased pressure.)

Delves (A.1962) quotes a single figure of 0.26e6 lb/in^2 for the Youngs modulus measured on a stack forming the flux-carrying yoke of a DC machine. This converts to 1.8 GPa. Delves' laminations may have had a different thickness and the clamping pressure used is unspecified but the value is nonetheless similar to the values being found by the experiments here.

Tests 5.3.2 were a set of torsion tests on model 5.3. The beam was excited transversely at a point near one edge at one end. Response was measured at the same position on the other end. This excitation caused the torsional resonances of the beam to be forced as well as the flexural vibrations. The first resonant frequency of torsional oscillation consistently fell below the first resonance of the flexural vibrations so at least one resonance was obtained for each bolt-tightness which could be identified as torsional. The torsional stiffness of a square section is not simply the product of the shear modulus for the material and the second moment of area of the section about the torsional axis. However, this approximation suffices for our purposes. The error introduced here depends largely on the ratio between compression and shear modulii. A large ratio minimises the error. The comparing results from these tests (table 5.5 below) with the results of the pure compression test (table

5.4) shows that the shear modulus for the stack is consistently less that 15% of the Youngs modulus at the same clamping pressure. The approximation is thus justified.

Pressure (kPa)	First Resonance (Hz)	Resolved 3dB Bandwidth Hz	Youngs Modulus (Gpa)	Damping Factor
300	490.	21.3	3.51	4.3e-2
600	557.	17.7	4.54	3.2e-2
950	582.	12.5	4.96	2.1e-2
1300	600.	8.5	5.27	1.4e-2
1700	616	6.9	5.64	1.1e-2
2000	630.	6.3	5.80	1.0e-2

Table 5.4 Results from test 5.3.1.

Pressure (kPa)	First Torsion. Resonance (Hz)	Resolved 3dB Bandwidth (Hz)	Shear Modulus (GPa)	Damping Factor
300	178.	16.4	0.46	9.2e-2
600	188.	10.9	0.52	5.8e-2
950	220.	9.24	0.71	4.2e-2
1300	226.	8.61	0.74	3.8e-2
1700	230.	8.06	0.77	3.5e-2
2000	232.	8.12	0.79	3.5e-2

Table 5.5 Results from tests 5.3.2. (Torsion)

Tests 5.3.3 were then conducted in which model 5.3 was again shaken transversely but in this case, the line of action of the forcing passed through the axis of the beam so that no torsional modes would be excited. The resulting resonances are all transverse flexure in which both the compression and shear modulii of the laminations influence the behaviour. Figures have already been found for these modulii under the various conditions of clamping pressure from the direct compression/extension tests and torsion tests respectively. These flexure tests serve as a test that the resonant frequencies measured for the beam coincide with the frequencies which would be calculated for the beam given the properties of shear and compression. The theoretical model for flexure is thus validated. The comparison of measured and

calculated first resonant frequency is presented in table 5.6.

The agreement found is indicative that both the shear and compression modulus have been correctly assessed since the resonant frequency of the first mode of 'flexure' of the model has a strong dependence on both modulii

Pressure (kPa)	Measured Resonance (Hz)	Calculated Resonance (Hz)
300	170	174
600	200	207
950	240	244
1300	255	258
1650	260	263
2000	265	268

Table 5.6 First Flexural Resonances Of Model 5.3.

§5.10 Model 5.4 and Tests 5.4.1-5.4.2

Model 5.3 was dissembled and the individual laminations varnished to standard coat specifications, then reassembled to produce model 5.4 (Fig. 5.11). The same number of laminations was used and the same system of clamping and monitoring the pressure. The direct contrast

with model 5.3 produces immediate information on the effect of the varnish.

Tests 5.4.1 were performed exactly as tests 5.3.1. The beam was excited into compression/extension vibration along its own axis by a shaker fixed to one end face. Response was measured at the other end face. The range of pressures covered was 0 - 2.0Mpa.

The results from these tests are presented below in table 5.7.

Pressure (KPa)	First Compression Resonance (Hz)	Resolved 3dB Bandwith (Hz)	Youngs Modulus (GPa)	Damping. Factor
300	314	35.6	1.45	11.3e-2
600	346	30.9	1.77	8.9e-2
950	376	27.6	2.06	7.4e-2
1300	390	25.6	2.23	6.5e-2
1650	399	23.1	2.34	5.8e-2
2000	407	22.5	2.42	5.5e-2
2400	415	22.0	2.52	5.3e-2

Table 5.7 Results from tests 5.4.1

Continuing the comparison with the unvarnished laminations, tests 5.4.2 were carried out. These tests were identical to tests 5.3.2. Torsional

modes were excited by shaking the beam transversely at one end. Response was measured at the other. Flexure modes were found again as expected but as before, the lowest resonance was the first torsional resonance. The shear modulus is calculated directly from the torsional frequency by assuming that the torsional stiffness equals the shear modulus times the second moment of area about the beam axis.

Pressure (kPa)	First Torsion Resonance (Hz)	Resolved 3dB Bandwith (Hz)	Shear Modulus (MPa)	Damping Factor
300	-	-	-	-
600	73	8.1	77.4	11.0e-2
950	91	5.9	120.2	6.0e-2
1300	107	5.6	166.2	5.2e-2
1700	122	6.6	216.1	5.3e-2
2000	136	6.5	268.5	4.8e-2
2400	150	6.5	326.7	4.3e-2

Table 5.8. Results from tests 5.4.2. (Torsion)

§5.11 Model 5.5 and Tests 5.5

Model 5.5 is similar to model 5.2 in all dimensions, (Fig. 5.12) but the length of the the beam is built up from segments of laminations rather than whole laminations. There are 6 x 2mm gaps in half of the layers of this beam and 7x2mm gaps in the other half. The laminations are staggered in the usual fashion. The pressure control system for model 5.5 is the same as that used for models 5.1 and 5.2. It seems likely to be acceptable to deduce "bulk" properties for the segmented stack from the first mode when the gaps are spread quite evenly over the deformed shape.

Tests 5.5 comprised exciting the model at one end so that the beam vibrated out of the plane of lamination and measuring response at the other. It was expected that the resonant frequencies measured for model 5.5 would be very slightly less than those found for model 5.2. In actual fact they were slightly higher, but given the uncertainty associated with the surface conditions they are sufficiently close to be considered as supportive evidence. The surfaces of the laminations used in building model 5.5 had not been exposed to air and moisture while those of model 5.2 had been for short periods. The damping figures obtained were not discernably different from those obtained in test 5.2. The comparison of frequencies between test 5.2.1 and 5.5 is presented below.

Pressure (kPa)	First Resonance (Segmented) (Hz)	First Resonance (Whole) (Hz)
250	102.	101.
313	111.	109.
375	120.	117.
437	131.	127.
500	136.	131.
563	144.	136.
625	152.	142.
687	155.	146.
750	167.	150.

Table 5.9. Resonant frequencies for Model 5.5.

§5.12 Tests on the Impregnated Beams.

Model 5.4 was tightened to a clamping pressure of 5.0MPa. Model 5.5 was torqued up to the maximum giving a pressure of approx. 800kPa. Both beams were vacuum pressure impregnated to investigate the effects of this treatment on the properties. The bolts were left at their maximum tension and the following three discrete tests were done.

(1) Flexure Vibration of the impregnated Model 5.5.

(2) Compression/Extensional Vibration of Impregnated model 5.4.

(3) Torsional Vibration of Impregnated model 5.4.

The results are summarised in the table below.

Model	Test	Previous First Resonance (Hz)	New First Resonance (Hz)	Damping Factor
5.4	Compression	415.	576.	1.2e-2
5.4	Torsion	150.	288.	2.3e-2
5.5	Flexure	167.	242.	1.6e-2

Table 5.10. Effects of Impregnation.

§5.13 Discussion of Results.

A number of different combinations of surface condition and clamping pressures have been investigated in the set of tests reported here. For lamination thickness of 0.65mm, it has been found that the effective shear modulus varies between zero and 1.5 GN/m^2. The maximum shear modulus was present when clean untreated laminations were clamped-up to 750 kPa. The maximum Youngs modulus for the laminations was also found for the case when clean plain surfaces were clamped up and was found to be 5.4 GPa.

There is quite a high degree of uncertainty associated with the prooerties of any one stack. Generally the stacks themselves exhibit very consistent behaviour but reassembling the stack or beginning tests again from a zero pressure value tends to produce a different set of results to the one found previously. The difficulty of realising the same tightness twice contributes to this.

In all cases investigated, the shear and compression modulii vary continuously with respect to the clamping pressure. The full extent of this smooth relation could not be found, but it certainly lies well above the range of pressures utilised in this study. As pressure increases, so the modulii increase also, but they rise in ever-decreasing amounts.

An approximate range of linearity has been established for the shear behaviour. It seems reasonable to assume that the beam behaviour in compression/extension will be linear with respect to the amplitude of strain until such time as the laminations begin to separate.

Damping for laminated components in deformations (other than those in the plane of lamination itself) is generally much higher than it would be for a solid steel component. For shear strains, the minimum associated damping found was 3.5% while for normal strains, the minimum damping found was 1.0%.

Varnish on the surfaces reduces the effective shear modulus considerably. There is a reduction in the compression modulus also but

it is not so marked. The damping values increase when the laminations are varnished.

Impregnation has a significant stiffening effect. Together with this, the effective damping is reduced. The stiffening is most prevalent on the shear modulus where the value is increased by a factor of more than 2.

Segmentation can be accounted for using suitable theory and reliable values for the modulii. Multiplying constants for the extensional and flexural stiffneses of a segmented core/yoke are derived and presented in appendix 7. The formulae indicate that for most normal situations, the ratio between the half-area of contact between successive segments is so large compared with the cross-sectional area of the segments themselves that the core/yoke behaviour is virtually unaffected by the segmentation.

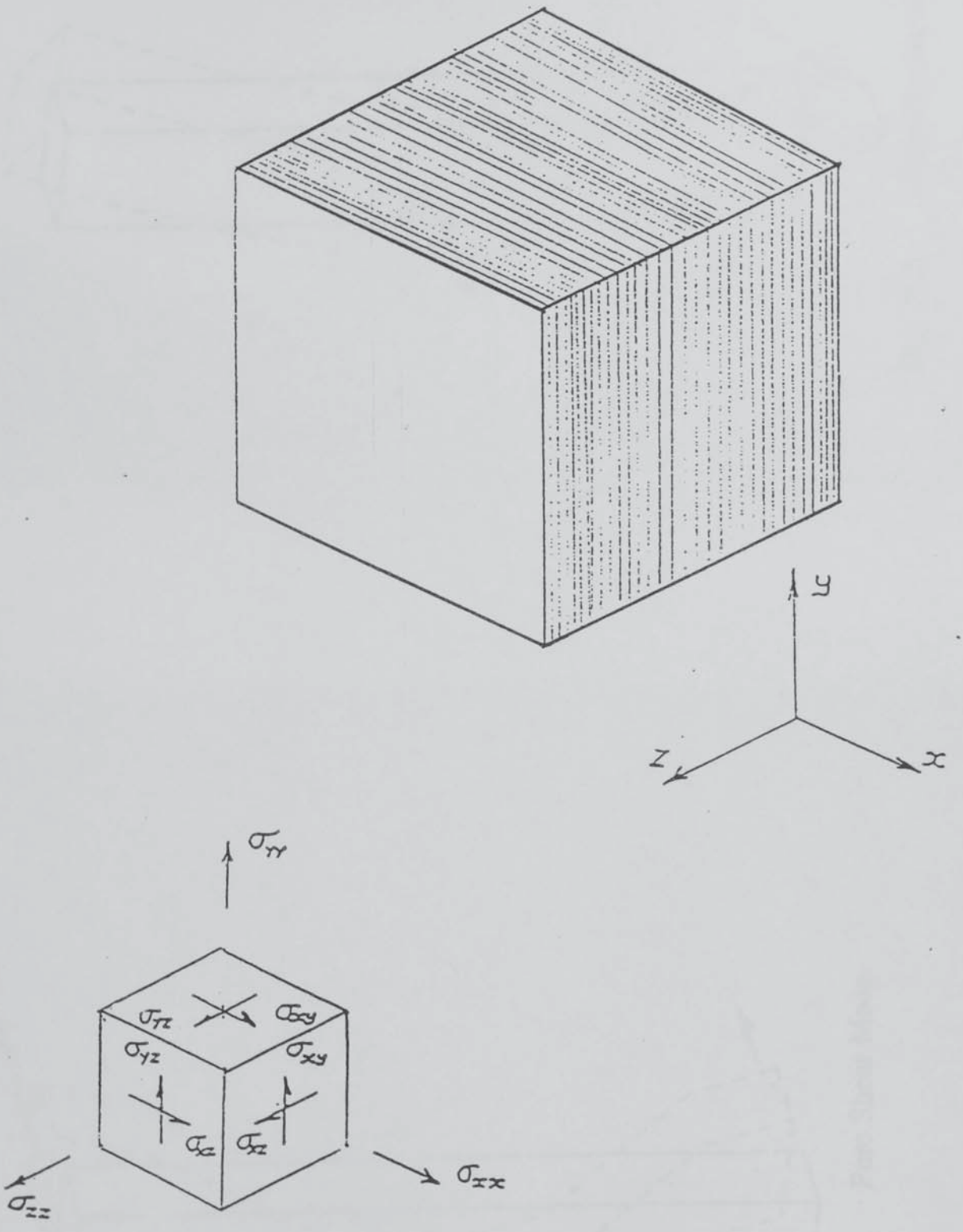

Fig. 5.1 Principle Directions and Stresses

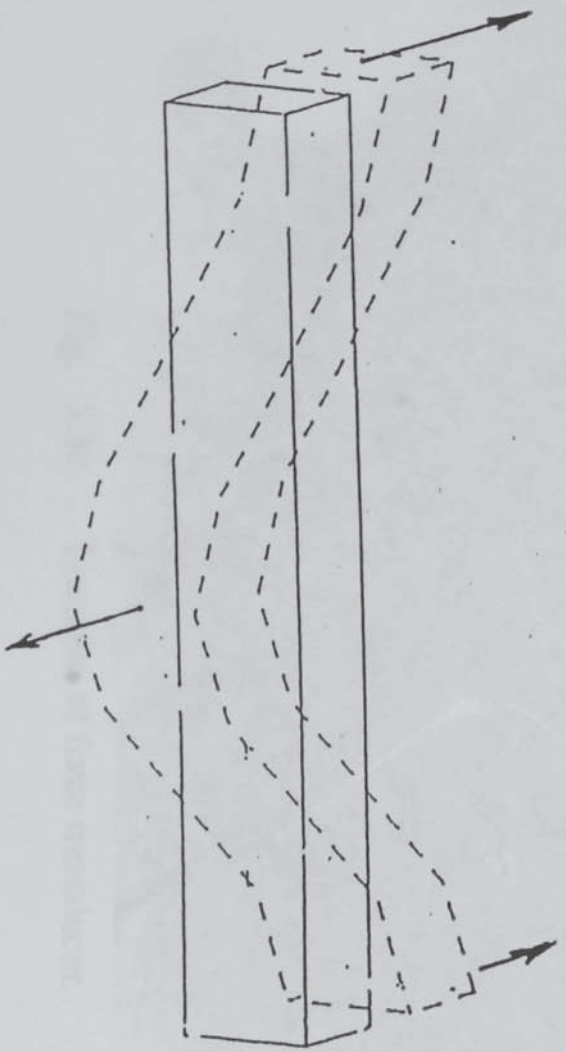

Fig. 5.2a Pure Shear Mode.

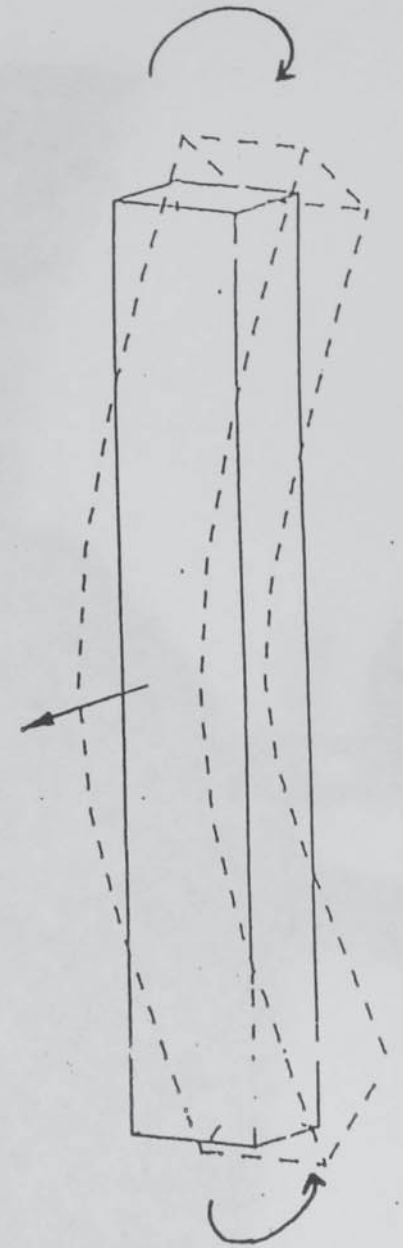

Fig. 5.2b Pure Flexure Mode.

Fig. 5.2 Comparison of Pure Shear and Pure Flexure Modes.

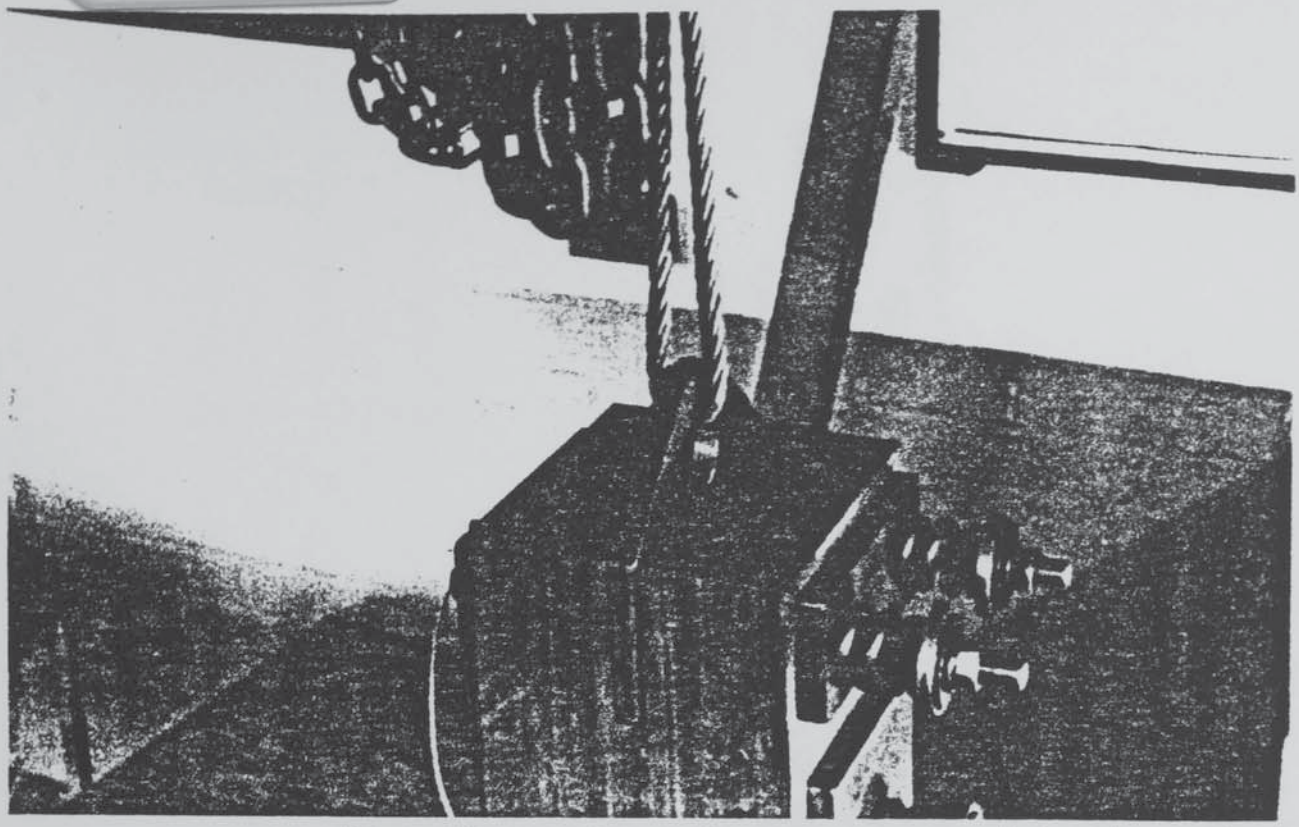

Fig. 5.3a Suspension arrangement and clamping method.

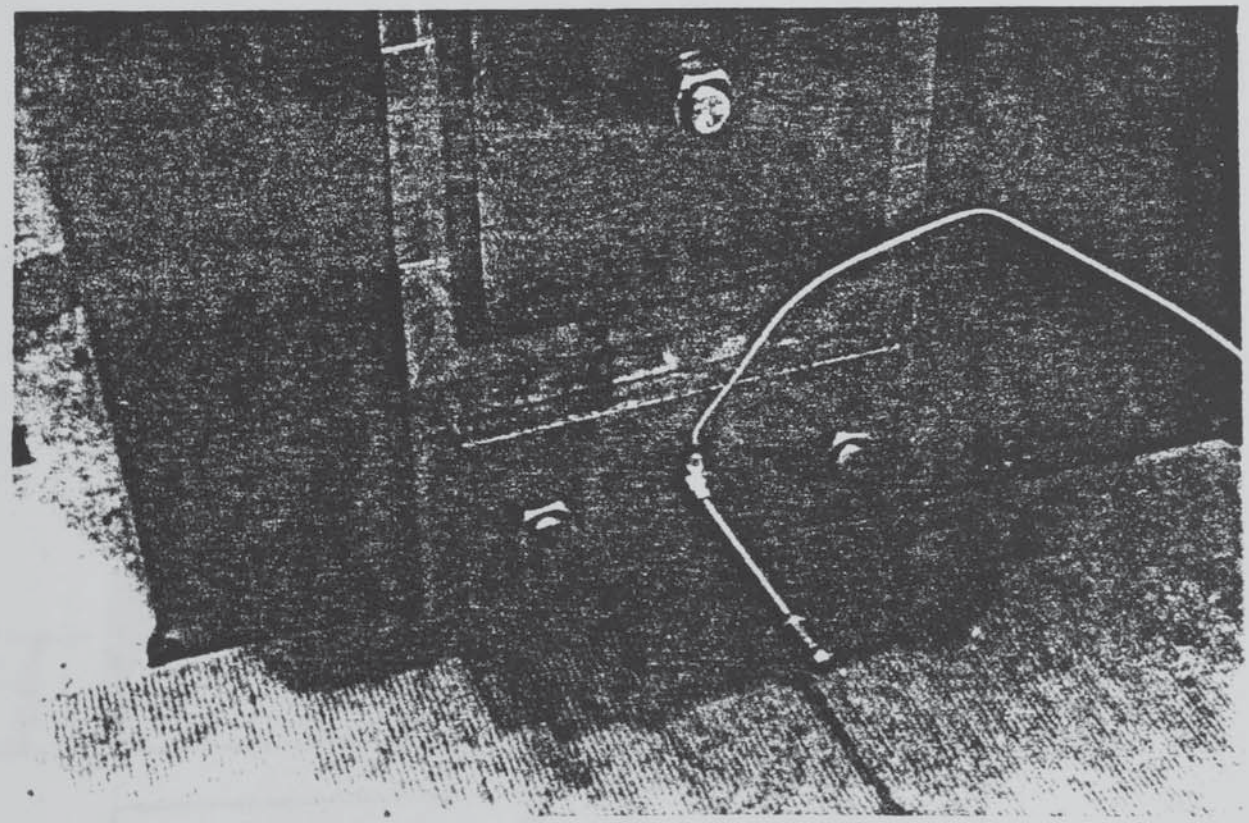

Fig. 5.3b Location of force transducer.

Fig. 5.3 Model 5.1. Suspension and Measurement Methods.

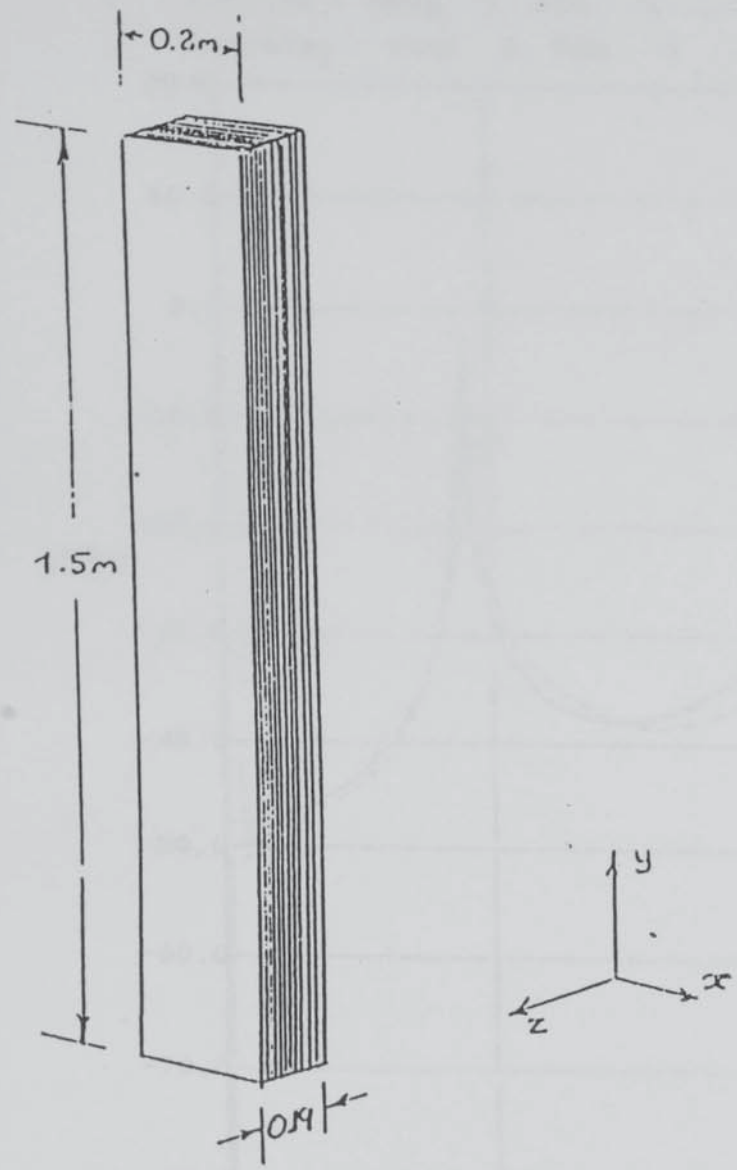

Surface	:-	Plain
Max. Pressure	:-	750 kPa
Pressure Steps	:-	62.5 kPa
No. of Laminations	:-	278 (Continuous)
Thickness of Laminations	:-	0.65 mm
Total Mass	:-	440 kg.
Parameters Investigated	:-	Shear Modulus

Fig. 5.4 Model 5.1.

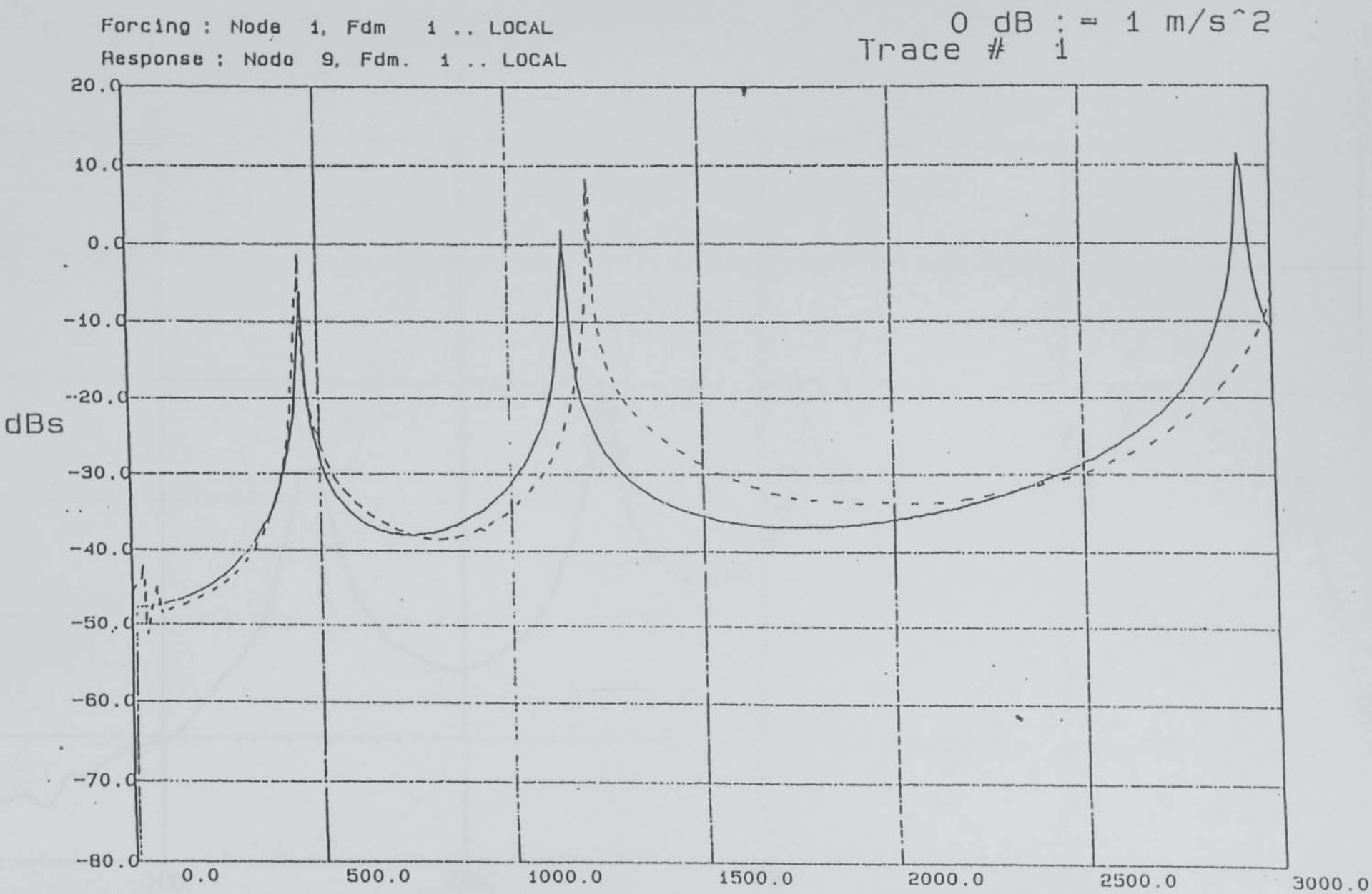

Fig. 5.5 **Calculated and Measured Response of Model 5.1 (Test 5.1.1)**

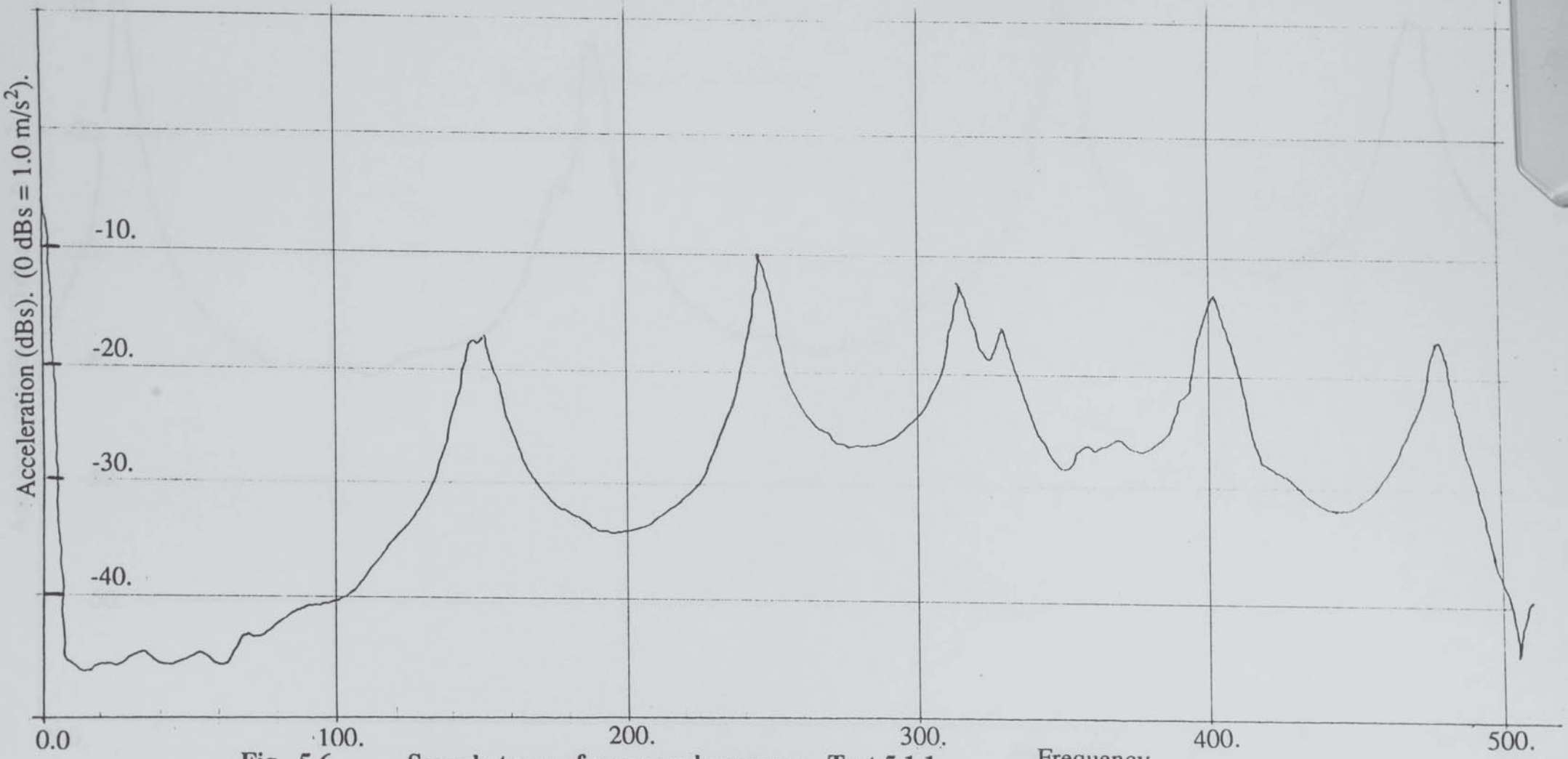

Fig. 5.6 **Sample trace of measured response. Test 5.1.1. Clamp. Pressure = 250 kPa.**

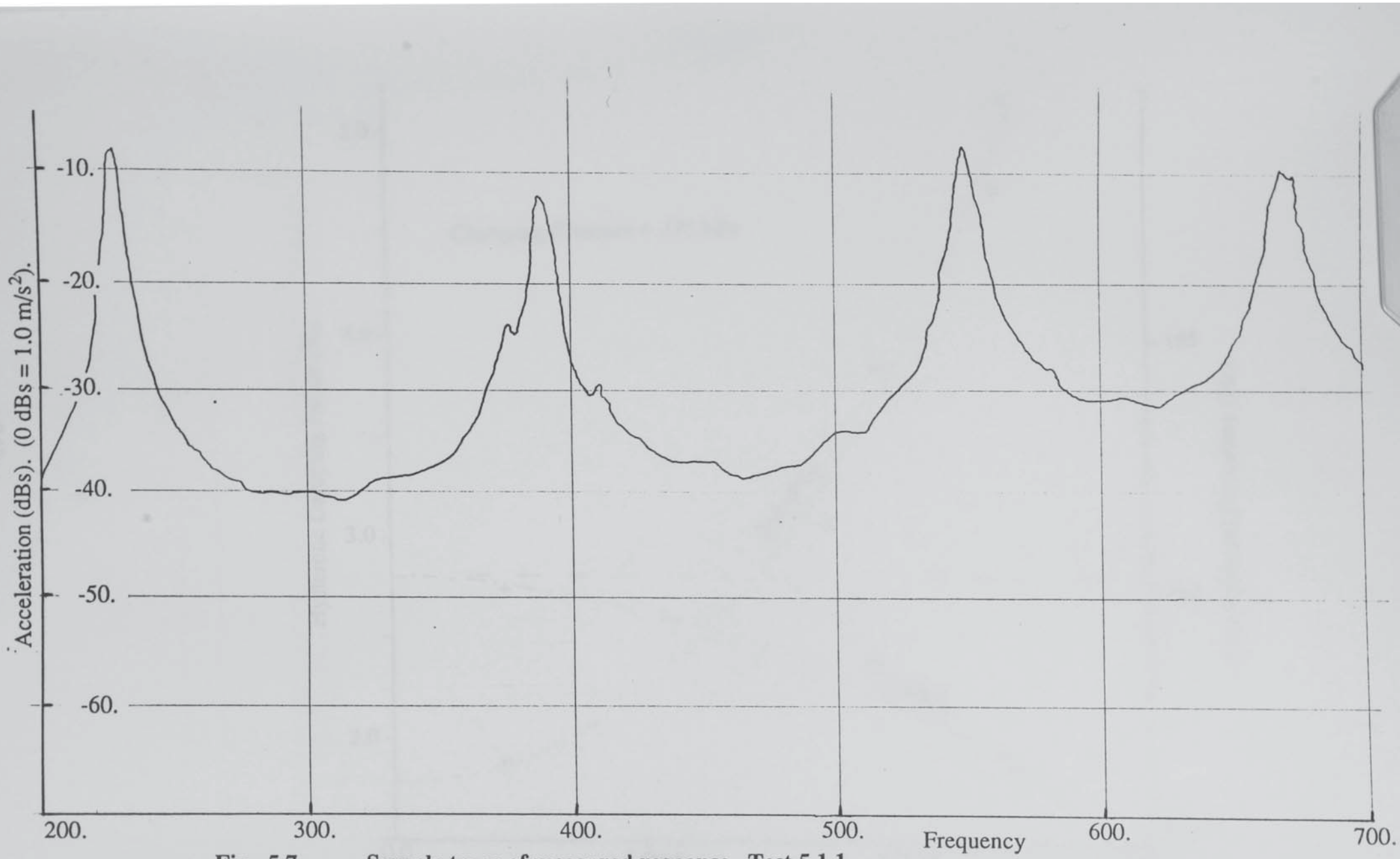

Fig. 5.7 **Sample trace of measured response. Test 5.1.1. Clamp. Pressure = 750 kPa.**

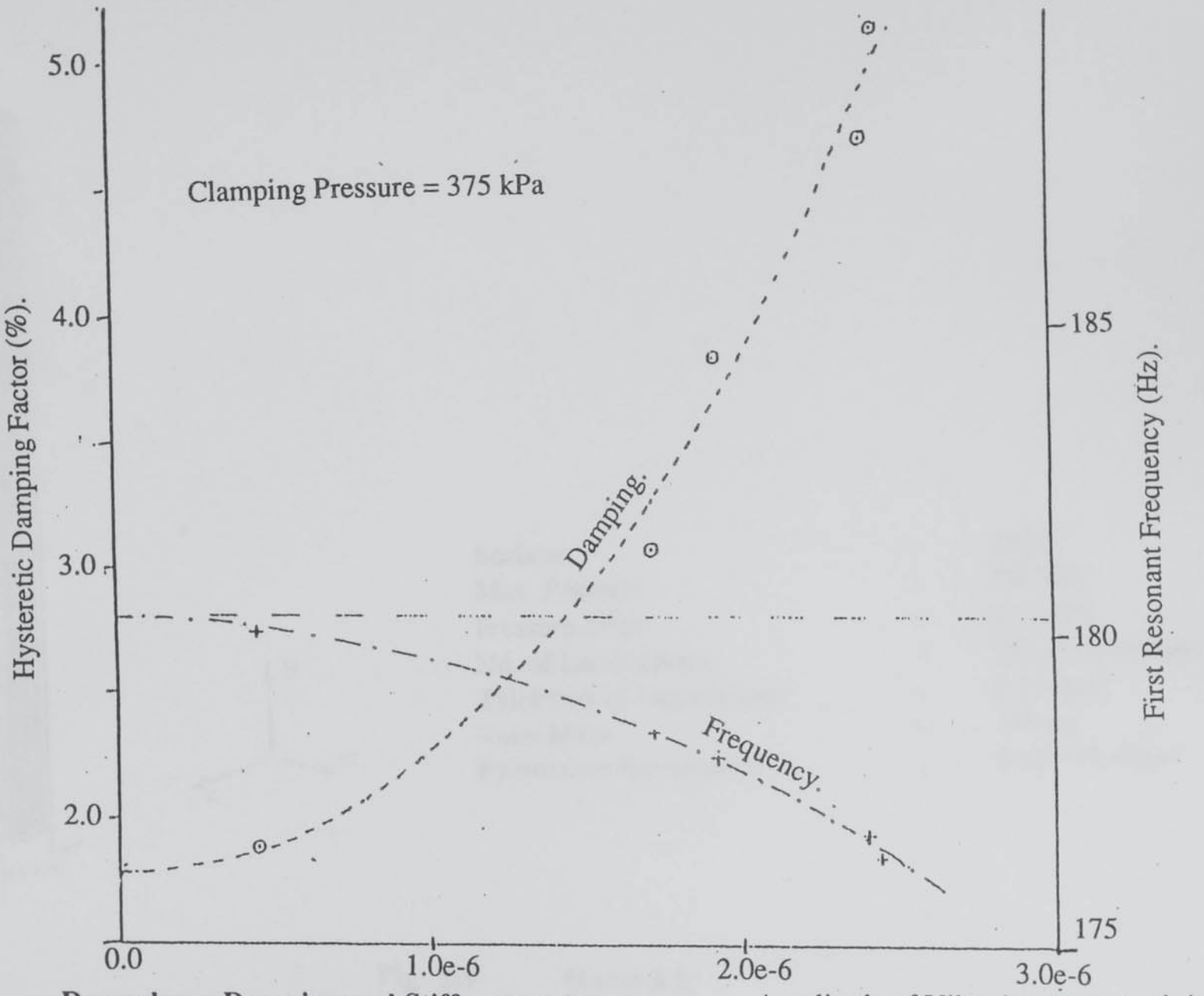

Fig. 5.8 **Dependence Damping and Stiffness on Amplitude. (Test 5.1.2.)**

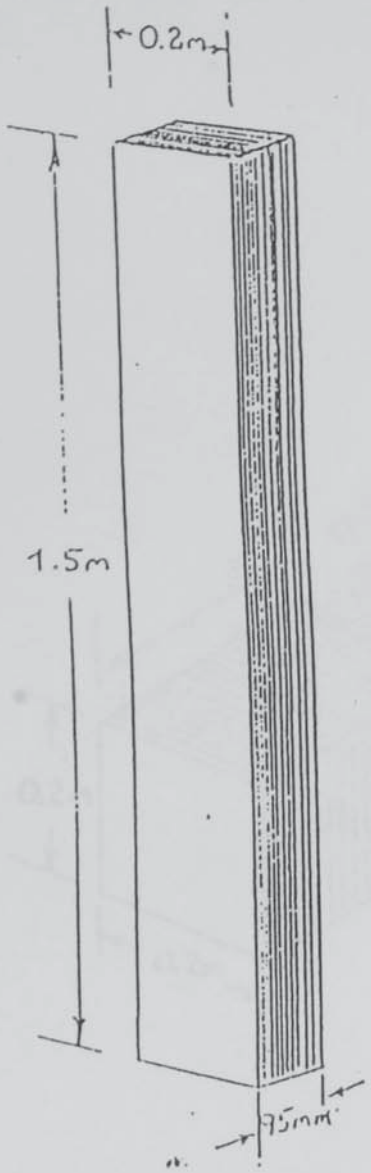

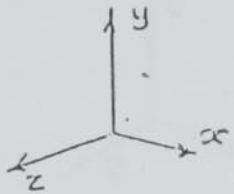

Surface	:-	Plain
Max. Pressure	:-	750 kPa
Pressure Steps	:-	62.5 kPa
No. of Laminations	:-	137 (Continuous)
Thickness of Laminations	:-	0.65 mm
Total Mass	:-	246 kg.
Parameters Investigated	:-	Shear Modulus

Fig. 5.9 Model 5.2.

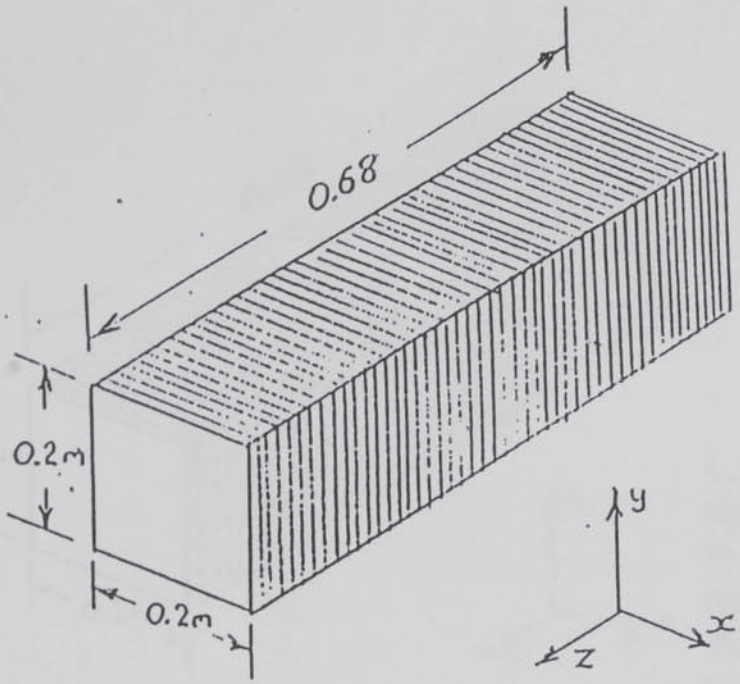

Surface	:-	Plain
Max. Pressure	:-	2 MPa
Pressure Steps	:-	300 kPa
No. of Laminations	:-	1000 (Squares)
Thickness of Laminations	:-	0.65 mm
Total Mass	:-	202 kg.
Parameters Investigated	:-	Shear Modulus & Young's Modulus

Fig. 5.10 Model 5.3.

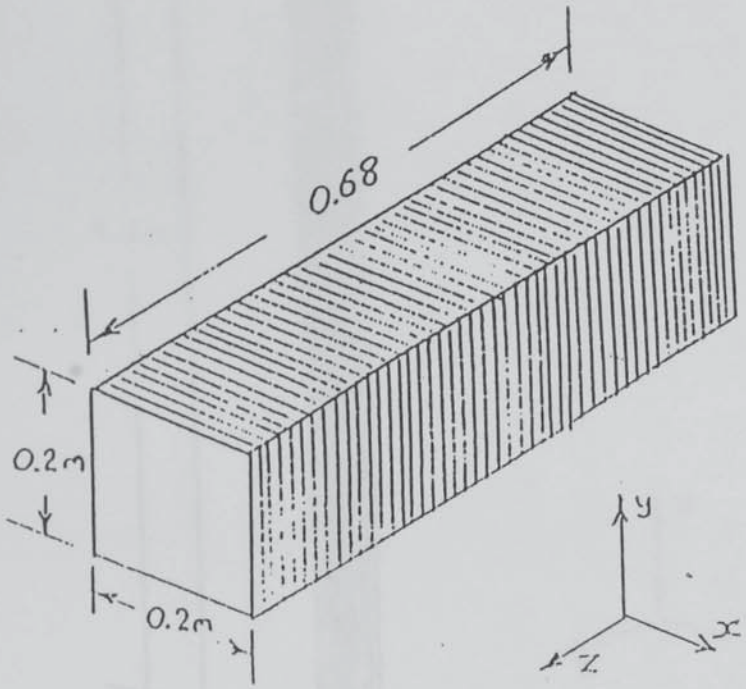

Surface	:-	Varnished
Max. Pressure	:-	2 MPa
Pressure Steps	:-	300 kPa
No. of Laminations	:-	1000 (Squares)
Thickness of Laminations	:-	0.65 mm
Total Mass	:-	205 kg.
Parameters Investigated	:-	Shear Modulus & Young's Modulus

Fig. 5.11 Model 5.4.

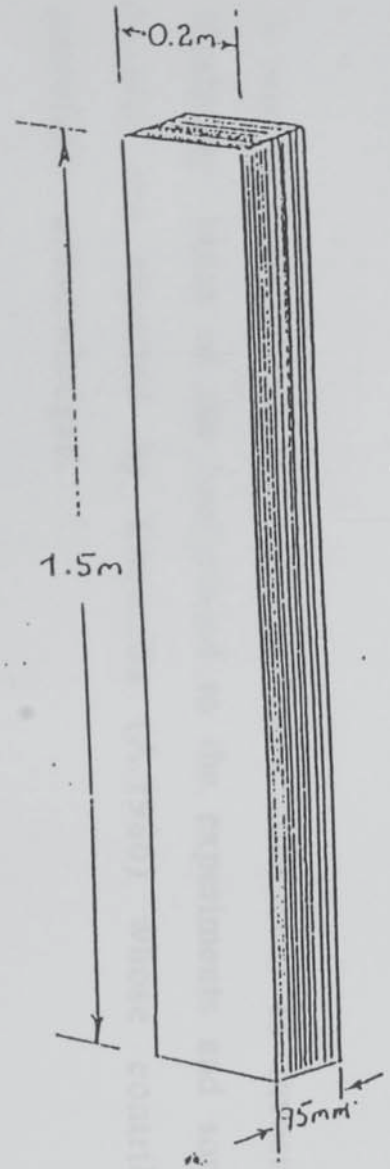

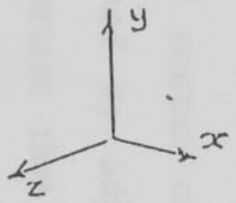

Fig. 5.12 **Model 5.5.**

Surface	:-	Plain
Max. Pressure	:-	750 kPa
Pressure Steps	:-	62.5 kPa
No. of Laminations	:-	287 (Segmented)
Thickness of Laminations	:-	0.65 mm
Total Mass	:-	440 kg.
Parameters Investigated	:-	Shear Modulus

Chapter 6.

THE SHIMMED POLE - TO - YOKE JOINT

In D.C. machines having a rolled-steel yoke, it is the practice to bolt on the main poles and compoles over a number of shims to allow control of the airgap for commutation purposes. The shim material used varies from case to case. Sometimes it is non-magnetic and there is no reason for it to be electrically conductive though in most machines, metal shims are used.

It has been determined that this joint is sufficiently flexible to make a considerable difference to the values of vibration computed for the machine. Delves (A.1962) made some account of this effect in his analysis. The figures used for his pole-root flexibility were retrospectively chosen to fit the results to the measurements. Later in this text, it is shown that some degree of control of the vibrational behaviour of the machine can be achieved by adjustment of the pole-root flexibility. It is therefore important that the values be established for this flexibility and the dependence on various factors be examined.

A set of experiments were devised and conducted to investigate this flexibility. Much of the background to the experiments and some of the results are reported by Cocotelis (A.1986) whose contribution is gratefully acknowledged.

Delves catered-for the existence of only one form of pole-root flexiility where in fact, there are three. The pole may move relative to the yoke in the following ways . . .

(1) The pole may rock relative to the yoke (about a line down the center of the pole-back).

(2) The pole may translate circumferentially relative to the yoke. In this case, the shims experience a shearing action.

(3) The pole may translate radially relative to the yoke in which case the shims experience compression/extension.

The experiments described here were aimed primarily at establishing the rocking flexibility which is undoubtedly the most significant. The stiffness of the joint was such that the other two flexibilities could not be quantified directly, since the modes to which they corresponded lay in a frequency range well populated with other resonances. However, it is shown later in §6.9 that a reasonable order-of-magnitude estimate of these quantities can be made based on the rocking flexibility.

§6.1 The Models Used.

A system incorporating the shimmed joint was devised to have the following attributes.

(1) The system is extremely simple as far as dynamic analysis is concerned over the anticipated range of frequencies of interest.

(2) The system has one or more principal modes which are primarily dependent on the behaviour of the joint.

(3) The number of shims, shim-material and pre-load at the joint are all variable.

The system designed is shown in Fig. 6.1. It comprises two mild-steel blocks one of which is to represent the yoke and the other represents the pole. The blocks are dimensioned so that the lowest non-rigid-body resonances are well above the anticipated range of frequencies of interest. 0-2kHz. (The first resonance at the 'yoke'-block lies at 2.52 kHz). Two separate pieces were prepared for the "pole" block - one twice as thick as the other. The thickness of the narrower "pole" piece (hereafter referred to as pole-1) is the same order of magnitude as that of a large DC compole. The broader pole (pole-2) is less wide than typical large DC mainpoles. However, it enables us to establish the scaling relationships. These are not as obvious as they might seem.

The tension on the bolts was monitored using the strain-gauges on the surface of a bridge-beam between two fulcrums. This arrangement may seem unnecessarily elaborate but the following two facts combine to justify it:

(1) The sensitivity of the joint to bolt tightness was not known in advance and so a relatively accurate measurment facility was desired.

(2) Two different thicknesses of 'pole' were to be examined - one twice as thick as the other. The same degree of accuracy could be achieved in each case by simply adjusting the distance between the fulcrums.

Four shim materials were tested. These are presented in table 6.1 below.

Material	Thickness
Electrical Steel	0.5mm
Stainless Steel	0.16mm
Half-Hard Brass	0.85mm
Copper	0.5mm

Table 6.1 Shim Materials Used.

§6.2 Two 'Contact' types.

It is common practice in the design of large DC machines to specify a larger radius-of-curvature on the backs of main poles than the internal radius of the yoke. This causes a small angle of relief to exist at the

edges of the pole back. Pressure on the shims is then concentrated more at the edges and the joint stiffness is increased.

Pole-1 and pole-2 each had two machined faces which could be bolted over the shims. In each case, one of these faces was flat and the other was machined into a "vee" shape with angle 2.5° (Fig. 6.2). The surface of the yoke-piece which faced the shims was skimmed on a milling machine to be quite flat and smooth. By using the "vee" side of the poles, the effect of concentrating the preload at the edges of the pole was simulated.

Clearly, there is no fine line which determines whether a pole-yoke joint is effectively "vee" or flat. If the angle of relief is extremely small, it will be completely masked by the compression of the shims and no appreciable concentration of the preload force will occur. The angle of relief actually found in machines is somewhat lower than the 2.5% used. The steel mill motor studied in this investigation has a 0.7^{o} angle and the propulsion motor has 0.1^{o}. Tests on the steel mill motor frame (motor **B** of chapter 8) have revealed that main pole rocking frequency (with 4 electrical-steel shims similar to those used in the tests in chapter 8 and no coils attached) lies in the region of 550 Hz with the poles in a tight condition. This is actually consistent with a <u>flat</u> contact type according to the measurements made. (See the example calculation presented later in this chapter). By examining the cases of 0° and 2.5° relief, the two extremes of joint contact are catered-for.

§6.3 Values for the Joint Preload.

The model was designed to be able to represent a realistic range of tightness values for both Pole-1 and Pole-2. The values considered to be 'realistic' were obtained as follows. For a number of different machine designs, the ratio of the area of the back of the pole to the total area of bolts used to fix the poles to the yoke was calculated. The average of these ratios was 0.024. With pole-2 fitted, the ratio of bolt area to the area of the pole-back is 0.03.

Pole-bolts are generally torqued-up to some large fraction of their yield strength. This depends to some extent on the threaded part into which the bolt is screwed. For the poles of some machines, the laminations are drilled and tapped directly. For such cases, the diameter of the bolt would need to be suitably large to spread the load over some minimum number of laminations. For larger machine poles, the pole-laminations have a rectangular or circular hole punched in each so that a bar may be passed lengthwise through the poles. The pole bolts are then screwed into this bar. (Some of the laminations in this case have more material punched from them to allow access to the bar from the pole-back). In the case of solid mainpoles and compoles, the bolt holes are simply drilled and tapped straight into the pole-back. Whichever configuration obtains, the material from which the bolts are made together with the bolt dimensions will determine the maximum bolt torque and load.

Bolt-tightness has been varied over a range 0 - 12 kN, for 'pole' 1 and 0 - 20 kN on each of the two bolts for pole-2. This does not nearly

exploit the full capability of the bolts but practical limitations prevailed (in particular - the difficulty of holding the model down when large torques were applied). The smooth variation of joint stiffness with tightness actually measured on these models indicates that some extrapolation to higher values may be carried out if necessary without introducing significant errors.

A fact to note is that there is a significant force of magnetic attraction between the mainpoles and the yoke of a machine operating at full field. It can been shown that this force would be sufficient to overcome the gravitational forces on the mainpoles of one machine. The amount of armature flux will also have some effect in that there will be a static force of considerable magnitude acting to push the pole to one side. Thus, to some extent, the mechanical properties of the DC machine frame are dependent on the operating conditions of the machine.

§6.4 Form of the Tests

The tests all took the form of measuring response-to-forcing by analysing the outputs from one force transducer and one accelerometer at the same position on the edge of the 'yoke' piece (Labelled "P" in Fig. 6.1). Translation at this position is the freedom most responsive in the first rocking mode.

Impulse tests were attempted at first. The yoke-piece was struck at point "P" and response measured there. A number of averages were taken. It soon became apparent by the variation in the amplitude of the

frequency response being measured and the shifting of the resonance, that the joint was being excited into non-linearity. The remainder of the tests were carried out under conditions where the amplitude of the vibration was controllable at all times during the measurements.

The first successful set of tests (on "pole-1") were done using a frequency-sweep technique enabling a relatively high injection of force to be realised at one frequency. The amplitude-dependence of the resonance demonstrated in Fig. 6.3 by using different input force levels is a clear indication of the non-linear behaviour. Amplitudes of forcing were maintained in the linear range from then on.

The tests on the broader 'pole' used the spectrum analyser to inject 'white' forcing to the system. The force input at each of the discrete bands was considerably less than the forces which had caused the joint to behave nonlinearly in the previous tests in the region of the first resonance. These tests were concentrated on establishing the new joint stiffnesses (natural frequencies) of the system and verifying the damping figures obtained earlier.

The significant figures for each test were simply the first resonant frequency and the damping - expressed as before as a hysteretic damping factor. Damping was estimated using a bandwidth method. In the series of tests on pole-1 (the narrower pole) two frequency sweeps were performed. The first sweep simply located the resonant frequency to a good approximation and recorded the proximity of the next. The second sweep was a zoom-up on the first resonance which enabled a

good estimation of the 3dB bandwidth to be made. In the series of tests on pole-2, only one "sweep" per test was made. This produced adequate values for the resonant frequencies but damping estimates were necessarily poor quality.

§6.5 Derivation of Stiffness Values from the First Resonance of the Jig.

The dimensions of the jig are such that under the excitation supplied, neither of the two pieces would have components of vibration other than in the plane of Fig. 6.4. Each of the two pieces then has three degrees of freedom (two translations and a rotation) in the horizontal plane so that the system as a whole has six. Three of the six system degrees-of-freedom can be discounted as rigid-body modes. The other three are illustrates in Fig. 6.4. Now, mode 3 from Fig. 6.4 involves compression/extension of the shims. Because this is symmetrical with respect to the central plane of the pole while the other two modes are anti-symetrical with respect to the same plane, mode 3 is uncoupled from the other two modes and need not be considered in calculations relating to the calculation of the two anti-symetrical mode-shapes and frequencies.

Measurements on the system indicate one clear unobscured resonance below the range of frequencies where the elements start to behave dynamically. Fig. 6.5 is a typical response curve obtained. Investigation of the associated mode-shape (by moving the accelerometer) showed this to be a rocking mode. Clearly, there will be some degree of

"shearing" taking place within the shims for this mode. However, the fact that the other anti-symetrical mode has a much higher resonant frequency indicates that the degree to which this shearing occurs is extremely small. For the purposes of the calculations to follow, the relative motion occurring at the joint is assumed to be pure rocking with no component of shearing.

The rocking natural frequency (assuming no significant shear at the joint) can be derived by considering the angular momentum of the system about the line running along the center of the contact between pole and yoke. Let I_a be the second moment of inertia of the "yoke" piece and I_b, the second moment of inertia of the "pole" piece. The respective moments of inertia of the two pieces about the line described above are J_a and J_b given by (6.1) and (6.2).

$$J_a = I_a + M_a d_a^2 \qquad (6.1)$$

$$J_b = I_b + M_b d_b^2 \qquad (6.2)$$

Conservation of angular momentum (or if one prefers, the "inertial orthogonality" of the modes) dictates that a_a and a_b are related by (6.3) below.

$$J_a a_a + J_b a_b = 0 \qquad (6.3)$$

From this ...

$$a_b = - a_a J_a/J_b \qquad (6.4)$$

The restoring moment on the "yoke" piece is MOM_{res} and is proportional to $(a_a - a_b)$ as (6.5).

$$MOM_{res} = T (a_a - a_b) \qquad (6.5)$$

$$= T (1 + J_a/J_b) a_a \qquad (6.6)$$

Then, by simple reasoning, the natural frequency is expressed in terms of the ratio of restoring-force to acceleration as (6.7)

$$w_n^2 = T (1 + J_a/J_b) /J_a \qquad (6.7)$$

$$T = J_a w_n^2 / (1 + J_a/J_b) \qquad (6.8)$$

For Pole-1 ..... $\omega_n^2 = 9.49\ T$ (6.9)

For Pole-2 ..... $\omega_n^2 = 7.06\ T$ (6.10)

Having derived these factors, the results for the tests are now presented in terms of natural frequencies (Hz) and hysteretic damping coefficients (dimensionless).

BOLT TENSION (kN)	NUMBER OF SHIMS 2	4	6	8	
0	150	132	102	84	
2	581	560	413	376	
4	882	861	631	635	Copper Shims
6	951	938	768	759	
8	999	996	930	855	
10	1002	1029	952	903	
12	1069	1051	972	932	
0	101	85	100	93	
2	600	393	337	291	
4	812	623	532	476	Brass Shims
6	872	784	680	600	
8	931	851	769	688	
10	966	902	845	757	
12	996	930	878	803	
0	80	81	80	80	
2	575	449	338	335	
4	783	680	546	516	Electrical Steel Shims
6	921	786	683	624	
8	972	865	779	714	
10	1025	912	826	774	
12	1033	923	868	812	
0	115	60	77	80	
2	854	807	759	678	
4	973	954	914	912	Stainless Steel Shims
6	1033	1021	997	984	
8	1077	1061	1052	1023	
10	1105	1085	1077	1057	
12	1125	1104	1100	1082	

Table 6.2 Natural frequencies of the 'rocking' mode. VEE contact. Pole 1.

BOLT TENSION (kN)	NUMBER OF SHIMS 2	4	6	8	
0	109	116	108	108	
2	382	284	233	210	
4	512	416	338	296	
6	638	533	443	351	Copper Shims
8	711	648	539	423	
10	777	726	633	491	
12	790	759	691	542	
0	103	102	97	95	
2	206	183	178	152	
4	273	268	236	191	
6	313	309	275	237	Brass Shims
8	359	348	316	280	
10	409	400	364	329	
12	498	453	418	381	
0	123	108	110	104	
2	248	223	200	160	
4	329	316	283	216	
6	401	394	355	283	Electrical Steel Shims
8	460	437	414	350	
10	525	504	456	423	
12	582	554	518	488	
0	112	110	108	94	
2	353	306	261	249	
4	474	439	345	344	
6	614	561	429	428	Stainless Steel Shims
8	707	683	528	525	
10	798	786	631	615	
12	873	884	708	676	

Table 6.3 Natural Frequencies at the Rocking Mode. FLAT CONTACT. Pole 1.

BOLT TENSION (kN)	NUMBER OF SHIMS 2	4	6	8	
0	14.10	17.05	12.74	18.09	Copper Shims
2	8.51	9.84	. 6.65	11.35	
4	4.10	4.46	4.23	7.77	
6	2.51	2.64	3.08	5.79	
8	1.20	1.10	2.91	3.41	
10	1.05	0.71	1.81	2.54	
12	0.81	0.63	1.70	1.72	
0	16.86	20.93	18.90	20.43	Brass Shims
2	4.61	6.66	5.81	6.90	
4	1.52	3.74	4.15	4.49	
6	1.39	1.72	2.93	4.17	
8	0.52	1.59	2.61	3.82	
10	0.53	1.13	2.14	2.98	
12	0.30	0.92	1.66	2.11	
0	26.91	24.87	-	-	Electrical Steel Shims
2	3.13	3.56	4.27	4.18	
4	1.30	2.26	3.07	3.23	
6	0.52	1.13	2.16	2.75	
8	0.81	0.69	1.43	2.08	
10	0.29	0.35	1.04	1.61	
12	0.51	0.40	0.86	1.26	
0	-	-	-	31.20	Stainless Steel Shims
2	2.67	2.85	5.88	7.55	
4	1.56	1.99	2.10	1.15	
6	1.18	1.25	1.90	1.88	
8	0.89	1.16	2.38	2.38	
10	0.69	0.87	1.11	1.28	
12	0.50	0.61	0.73	0.91	

Table 6.4 Damping Coefficients (%) for the Rocking Mode. VEE CONTACT 'Pole' 1.

BOLT TENSION (kN)	NUMBER OF SHIMS 2	4	6	8	
0	11.92	10.51	11.11	12.03	Copper Shims
2	4.84	8.27	5.92	7.42	
4	4.39	7.21	5.91	7.09	
6	4.07	6.37	5.41	4.55	
8	6.34	5.86	4.49	4.78	
10	4.31	5.64	3.22	3.62	
12	4.25	5.24	2.43	2.78	
0	14.27	26.66	21.85	21.79	Brass Shims
2	6.94	7.54	7.02	9.73	
4	4.65	4.55	5.17	7.12	
6	4.15	3.85	4.36	5.48	
8	4.12	3.73	4.17	4.64	
10	4.37	3.95	3.90	4.10	
12	3.80	2.78	3.82	3.36	
0	10.90	15.90	19.00	12.50	Electrical Steel Shims
2	5.32	4.88	6.10	6.87	
4	3.43	3.36	3.53	5.37	
6	2.84	2.86	3.04	3.53	
8	2.35	1.91	2.76	3.14	
10	2.22	2.03	2.45	3.07	
12	2.05	1.71	2.12	2.76	
0	19.64	19.73	-	21.50	Stainless Steel Shims
2	6.46	7.10	6.32	6.00	
4	4.75	5.72	5.62	5.46	
6	4.23	4.28	5.50	5.00	
8	3.30	4.24	4.75	4.34	
10	2.19	3.13	3.79	3.32	
12	1.35	1.30	2.97	2.49	

Table 6.5 Damping Coefficients (%) for the Rocking Mode FLAT CONTACT. 'pole' 1.

BOLT TENSION (kN)	NUMBER OF SHIMS 2	5	8	
5	1660	1500	1360	Copper Shims
10	2080	1980	1780	
15	2120	2020	1860	
20	2160	2060	1980	
5	1300	1220	1100	Brass Shims
10	1780	1640	1560	
15	1920	1800	1740	
20	2020	1960	1800	
5	880	820	740	Electrical Steel Shims
10	1400	1340	1280	
15	1760	1540	1400	
20	1960	1800	1680	
5	1680	1440	1300	Stainless Steel Shims
10	1960	1860	1740	
15	2040	1980	1920	
20	2100	2060	2000	

Table 6.6 Resonant Frequencies (Hz) for Pole-2 VEE contact.

BOLT TENSION (kN)	NUMBER OF SHIMS 2	5	8	
5	480	420	350	Copper Shims
10	940	800	600	
15	1180	1080	920	
20	1540	1320	1200	
5	350	300	280	Brass Shims
10	700	700	620	
15	1220	1000	920	
20	1540	1340	1260	
5	320	300	300	Electrical Steel Shims
10	720	680	550	
15	1240	1120	1000	
20	1600	1440	1320	
5	720	640	440	Stainless Steel Shims
10	1000	860	700	
15	1480	1220	1140	
20	1700	1520	1450	

Table 6.7 Resonant Frequencies (Hz) for Pole-2, FLAT contact.

§6.6 Summary of Findings

A set of stiffness and damping values has been evaluated for four different shim materials over a full range of preload and contact-type conditions.

6.6.1 Effects on the Joints

As one might expect, it is not possible to completely isolate the effects of the various independent variables on the resultant joint characteristics. However, the following comments apply;

(1) The principle determinant of joint stiffness and damping for the "vee" contact is the preload. The indications are that at high values of preload on the "vee" contact, and with few shims, virtually all of the rocking flexibility might be derived from local internal deformation of the pole and the yoke at the points (lines) of contact since there is not much variation of the stiffness with respect to the shim material. It is not possible to model this accurately using ordinary finite-element methods or others since the area of contact is theoretically zero. However a simple hand-calculation below (6.7.1) indicates that the local internal deformations are not of sufficient order to account for the flexibility. Another possible explanation is that the two lines of contact become virtually rigid and all rocking flexibility is due to one side of the 'poles' lifting off the yoke each half-cycle. This

possibility is dismissed by arguments presented in 6.7.2. The only conclusion satisfactory to this author at this time is that the deformation does occur at the shim surfaces.

Increasing the preload invariably increases the joint stiffness and decreases the damping coefficient. For the flat contact, the relation between stiffness and preload rises with a linear dependence (after the initial portion where the relation appears quadratic) over the range of preloads tested. The "vee" contact on the other hand, begins linearly and displays a definite levelling-off at higher preloads.

(2) Increasing the number of shims invariably decreases the joint stiffness and usually increases the damping coefficient.

(3) Damping coefficients have been found to be between 0.5% and 2.5% in the realistic range of conditions. Brass displays the best damping coefficients allowing for the inevitable scatter which occurred in the readings.

(4) The dependence (of the stiffness particularly) on the shim material is not as marked as one might have expected. The dependence is quite visible for the "flat" contact type. In this instance, it appears that the surface finish probably has more effect on the properties than the bulk properties of the shim material itself. For the "vee" contact, the maximum difference in stiffness due to the material is about 10%.

6.6.2 Comparison of Joints

The behaviour at a "Vee" contact joint differs markedly from that of a flat contact in the following ways:

(1) The stiffness of the flat contact joint may be quite dependent on the shim surfaces. The measurements from pole-1 suggest that this is the case (Brass and electrical-steel shims with coarse surfaces yield lower joint-stiffness than copper shims with a smooth finish) while those from pole-2 suggest that it is not.

(2) The dependence of the stiffness and damping figures on the preload differs considerably. See point (1) from §6.6.1 above.

(3) The stiffness of the flat joint is very much less than that of the Vee contact joint, over the range tested.

(4) The damping coefficients of the flat contact joint are generally much higher than that of the Vee-contact joint. Typically, the ratio of 3 applies. Moreover the energy dissipation per radian of joint motion is the same or higher for the flat joint. This is an unexpected result. (Energy dissipation is proportional to the product of stiffness and the damping coefficient).

6.6.3 Comparison of Results from Different Poles- Scaling.

For the "flat" contact type, the pressure in the joint for pole-1 at a bolt-tension of 10 kN would be the same as the pressure in the joint for pole-2 at a bolt-tension of 20 kN. If the shims were acting as a uniform matress, one would expect that the 'rocking' stiffness of the joint would be eight times as great for pole-2. (The area is twice as large and the second moment of area is four times greater). At a bolt-tension of 10 kN acting on 8 stainless-steel shims under pole-1, the measured resonance was 615 Hz. The corresponding torsional stiffness is . . .

$$T=(615*6.283)^2/9.49 = 1.57e6 \text{ Nm/rad} \qquad (6.11)$$

Eight times this torsional stiffness at the joint between pole-2 and the yoke-piece would cause the resonant frequency to be

$$F_n= (1.57e6 \times 8 \times 7.05)^{0.5} / 6.283 = 1498 \text{ Hz.} \qquad (6.12)$$

In fact, the measured frequency was 1450 Hz (table 6.7). Allowing for the scatter in the readings which is evident throughout the set, this is corroborative. Similar calculations for all of the other combinations of materials and numbers-of-shims shows that the scaling of stiffness according to the cube of the pole-width is generally true. One anomaly which appeared was that for flat contact with pole-1, the resonant frequency was substantially lower with brass and electrical steel shims than with the other materials. This was not the case for "pole-2".

With regard to the vee configuration, we would expect that the same conditions would prevail under the edges of pole-2 at any given bolt-tension as would have prevailed under the edges of pole-1 at the same bolt-tension. Therefore, when examining how the torsional stiffness scales up, we compare the results at 10kN per bolt from the measurements on both poles. There is a simple increase in resonant frequency by a factor of approximately 2 for all materials when pole-1 is exchanged for pole-2 in the jig. This corresponds to an increase in torsional stiffness by a factor of 4 x (9.49/7.05) = 5.4. We would have expected that this factor come out as exactly 4. Again, there seems to be no obvious explanation.

The results for both poles are combined to smooth-out some of the scatter, and graphically presented for a pole-back width of 0.1 m as stiffness per meter of length. It is recommended that the theoretical factors be applied to scale these results up to real pole dimensions and this process is illustrated by an example in §6.8. Fig. 6.7 shows the envelope of likely pole root torsional stiffnesses (per meter of axial length) for a "flat" contact configuration. There is not sufficient difference between the figures produced by the various materials tested to warrent producing individual bands for each one. Fig. 6.8 shows the same results for a "vee" contact. Again, there is no differentiation between the materials. Fig. 6.9 shows the dependence of damping coefficients on the pressure for the flat joint and Fig. 6.10 shows the same dependence for the "vee" joint.

§6.7 Two Possible Sources of Flexibility In the Model Other Than at the Shim Surfaces - Dismissed

6.7.1 Local Internal Deformation in the Pole and Yoke- Pieces.

This is a very approximate calculation. What is done here is to demonstrate that the minimum stiffness of the edges of the pole- piece (under the conditions which would obtain with a 15kN preload of the bolts in the model) precludes the possibility that this sort of deformation could be responsible for more than a tiny part of the rocking flexibility of the joint. The stiffness of the lines on the 'yoke' piece would obviously be greater than that of the pole-edges.

We suppose, to begin, that the pole edges deform in yield until there there is a sufficiently wide band of material at each of the pole-edges to sustain a force of 15 kN distributed over the 250 mm of contact between "pole" and "yoke". We call this width d and calculate it as (6.13).

$$d=15e3 \ / \ (500e6 \ x \ 250e\text{-}3)=1.2e\text{-}4 \ m \qquad (6.13)$$

The edges are assumed to have been sharp. Then the situation below prevails. We assume that all of the tip flexibility derives from the triangular portion which is 1.3mm deep. When a force of 1N is applied downward at the flattened tip, it is causes a downward deflection of "A".

The assumption for calculating A is that each horizontal slice experiences a uniform compression and does not deviate from being flat. "A" is then given by the integral below. (Note that Tan2.5° = 1/22.9.

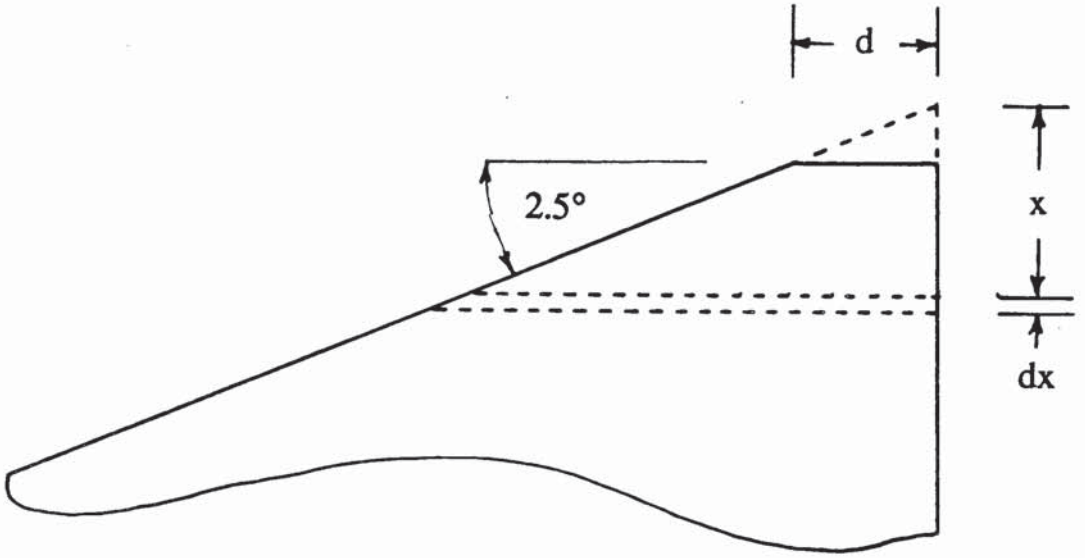

$$A = \frac{1.0}{209e9} \int_{d/22.9}^{1.3e-3} \frac{1.0}{22.9x}\, dx = 1.15e\text{-}12m \qquad (6.14)$$

It is worth noting that however crude this calculation, it is not very sensitive to the magnitude of d. If we multiply d by 10, then A=6.71e-13m and if we divide d by 10, then A=1.63e-12m.

The stiffness of the pole edges is thus in the region of 8.7e11 N/m per meter of edge.

For our pole, this is 2.18e11 N/m. The resulting torsional stiffness is 7.8e8 Nm/rad. for pole-1. Comparing this figure with the true torsional stiffness as measured (≈5.0e6) shows that allowing plenty of scope for

error in the approximation, we can be assured that the flexibility of the "vee" joints is not influenced profoundly by internal deformation at the pole-edges.

6.7.2 Torsional flexibility due to the bolts themselves.

It might be suggested that the pole-edges in the model were not moving at all with respect to the "yoke" for one half of each cycle and rising clear of the shims and "yoke" for the other half. The stiffness would then be derived from the pulling action of the pole-bolts at the center of the pole. This notion is easily dismissed. The maximum tension in the bolts for pole-1 at any time was 12kN. The tension would not be noticeably changed by movement of less than 5e-5m at the pole end with respect to the "yoke". The restoring moment would then be independent of the amplitude and clearly an amplitude-dependent resonance would result. This was not found to be the case at low amplitudes of vibration.

It is worth bearing in mind that for larger amplitudes of oscillation, the torsional stiffness of the joint is ultimately limited by the stiffness of the bolts.

§6.8 Using the Values.

Fig.s 6.7 to 6.10 present the torsional stiffness (per metre) of a cross-section of the joint conditions tested. The figures have been converted to apply to a pole-back of width 0.1m. In order to use these

figures, one must first establish whether the contact is closer to "Vee" than to the "Flat" as defined earlier in this chapter. To get bounds for the possible pole-stiffness not knowing which contact type is closest, treat both cases. (In the extreme - assuming that local joint stiffness is proportional to pressure- the "Vee" joint is three time more stiff in torsion than the "Flat" joint). Next, evaluate the mean pressure at the pole-back and the force-per-metre at the edges of the pole-back. Look up the stiffness from the appropriate graph from Fig.s 6.7 - 6.10 for the nearest combination of shims. (The number of shims is much more important than the depth). Finally, scale the results to apply to the true width of pole-back in question.

Example: A steel mill machine pole has pole-back dimensions 406mm x 140mm. It is held by three M24 bolts. In the set of impulse tests done on this frame, the pole-bolts were torqued-up tight by hand with a spanner of length 0.3m. The tension in the bolts would then be approximately 25kN. The poles were seated upon four electrical shims.

For the "vee" contact, this is equivalent to a force of 92 MN/m. Fig. 6.10a shows that the expected torsional stiffness-per-metre for a pole-back width of 0.1m would be roughly 55MNm/rad. The true width of the pole-backs for the MDX machine was 0.14. We scale the torsional stiffness figure by 1.4^2 to get 180 MNm/rad . Given the inertia of the pole per metre, the resulting rocking frequency (assuming a rigid yoke) would be 1870Hz. The expected damping coefficient is 2%. (Table 6.5)

For the "flat" contact type, 25 kN results in a pressure of 1.3 MPa.

Fig. 6.8a shows the expected torsional stiffness-per-metre for a pole-back width of 0.1m to be some 23 MNm/rad. To scale this appropriately, we must multiply by 1.4^3. The resulting torsional stiffness is 75 MNm/rad . This would have resulted in a rocking resonance (again assuming that the yoke were rigid) of 1210Hz. Damping for this joint can be estimated from table 3.4 as about 0.7%.

It is seen in chapter 8 on the correlations performed that the characteristic pole-rocking resonance was estimated at 1300 Hz. The angle of relief on these poles was 0.7°.

Delves (A.1962) presents a series of curves relating pole-root flexibility to the pole dimensions only. The curves are simply of the form $T=k.a^2b$, where "k" is some constant of proportionality, "a" is the width of the pole-back and "b" is the length of the pole. For a=0.1m, b=1m, the curves presented by Delves suggest a torsional stiffness of 185e6 lb.in/rad. This figure converts to 21.0e6 Nm/rad. The curves presented in Fig.s 3.7 to 3.10 show possible values between 15.0e6 and 70.0e6 Nm/rad. That the two analyses agree to this extent is encouraging. Delves extrapolated these curves from a small number of indirect measurements based on matching resonant pole-rocking frequencies.

§6.9 Estimation of Compression and Shear Flexibilities from the Rocking Flexibility.

For the "flat" contact, the shims behave as a uniform matress. If "a" is

the width of the pole-back, then the ratio between the stiffness of the joint in compression (we shall call this stiffness C) and that of the joint in rocking (this is called T as before) is given by . .

$$T/C = a^2/3 \qquad (6.15)$$

For a "vee" contact, the stiffness of the rocking is concentrated at the pole edges. Hence,

$$T/C = a^2 \qquad (6.16)$$

Intuitively, one would expect that the "shearing" stiffness of the joint (denoted by S) would be smaller than the stiffness in compression. The normal ratio between the shear modulus and Youngs modulus for the shim material would seem to be a sensible scaling factor. Thus . . .

$$S/T \approx 1.0/ (2(1+\mu)) \qquad (6.17)$$

No tests have been done which can give a direct indication of S. An error in the value will result in a small shift of peaks in a frequency-response curve in the region of the characteristic frequency of circumferential pole-translation. This is normally sufficiently high in the spectrum of frequencies to be of little concern.

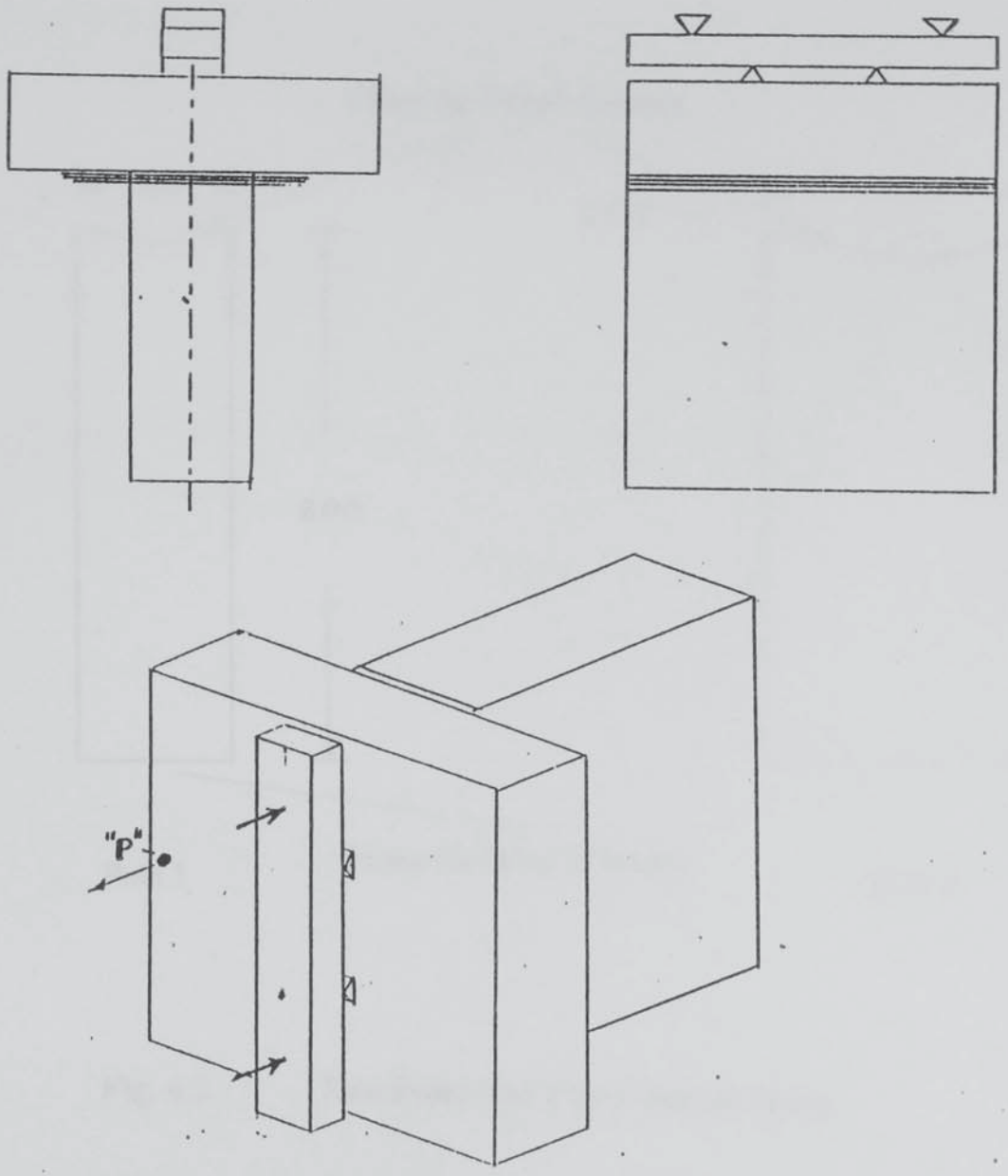

Fig. 6.1 System for measuring joint characteristics.

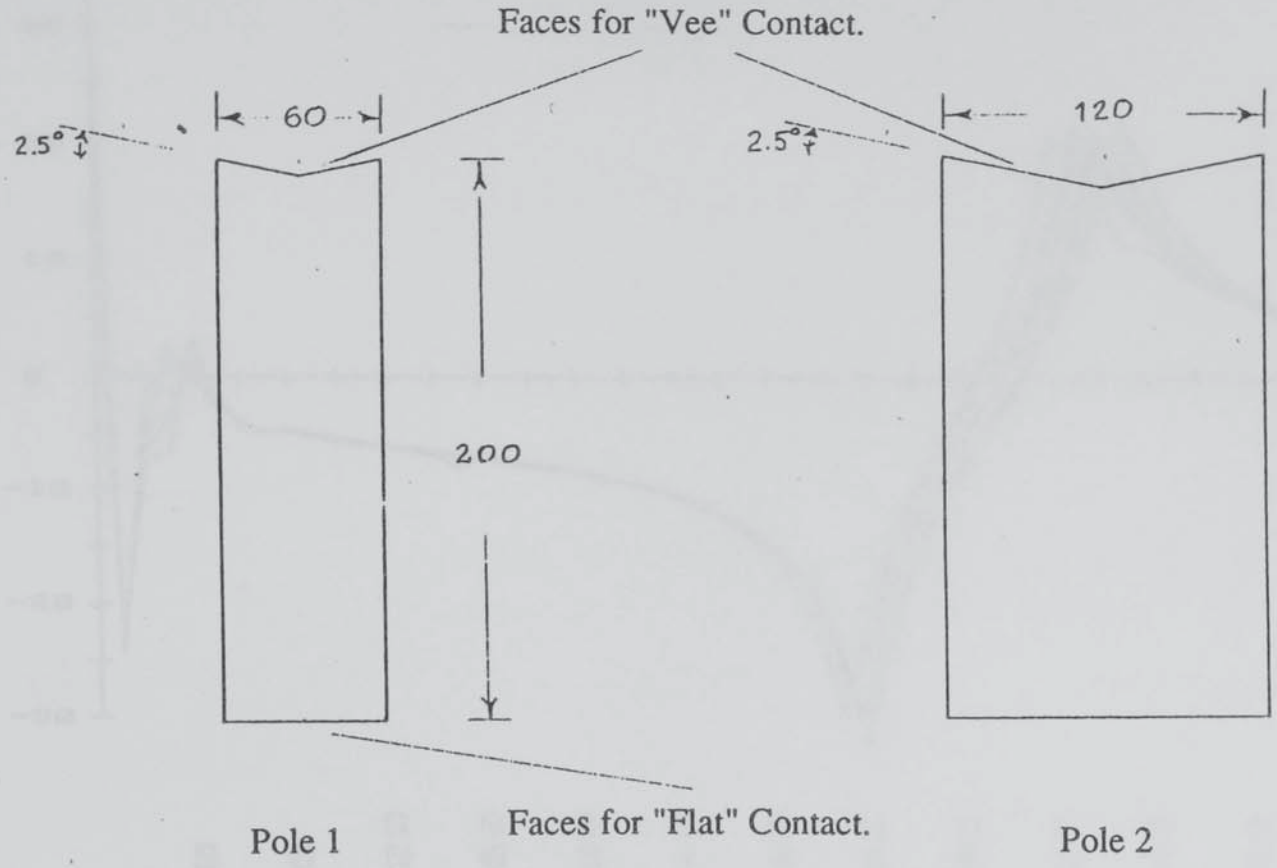

Fig. 6.2 Two Poles and Two Contact Types.

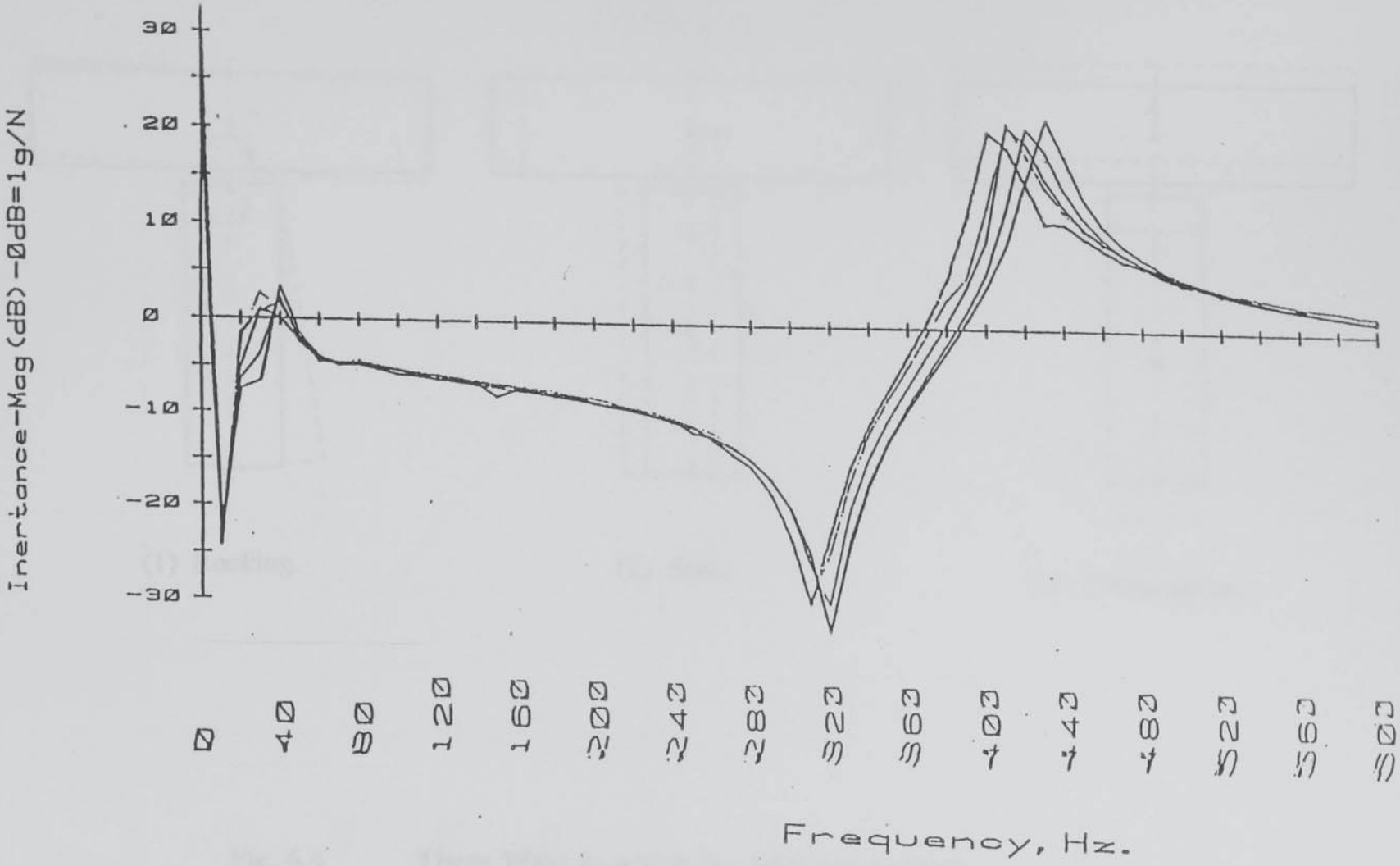

Fig. 6.3 **Amplitude Dependence of Resonance.**

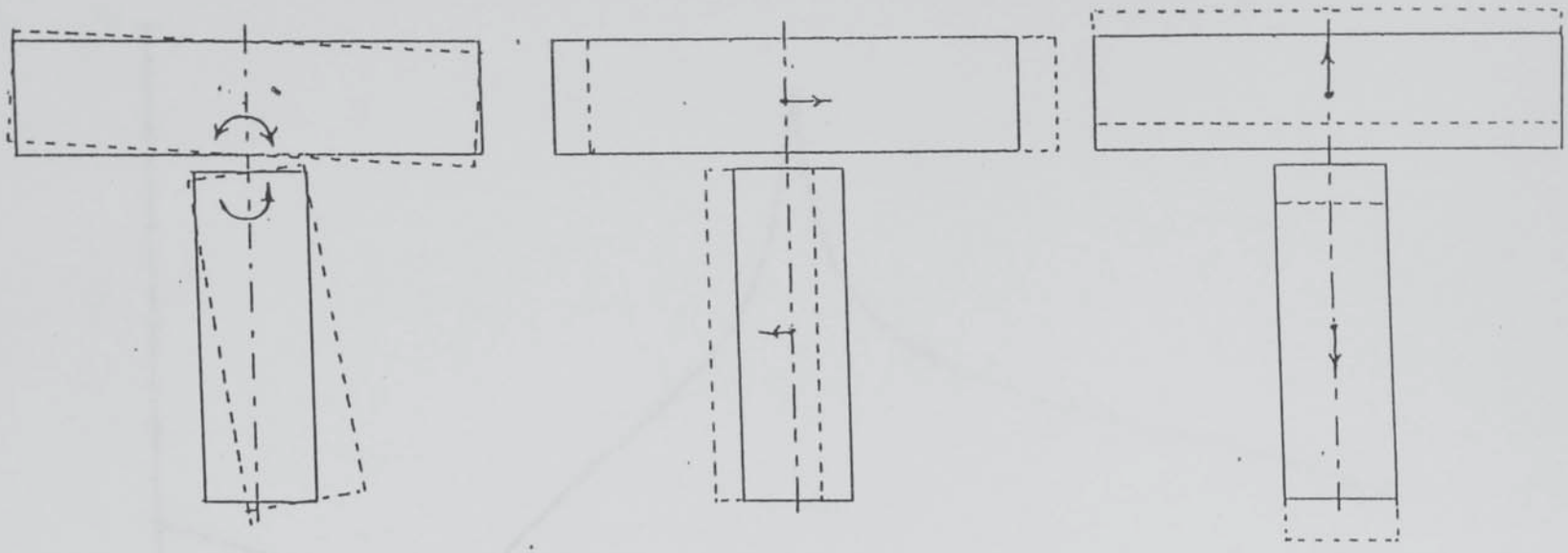

(1) Rocking. (2) Shear (3) Compression.

Fig. 6.4 Three Ways in which the Joint can Deform.

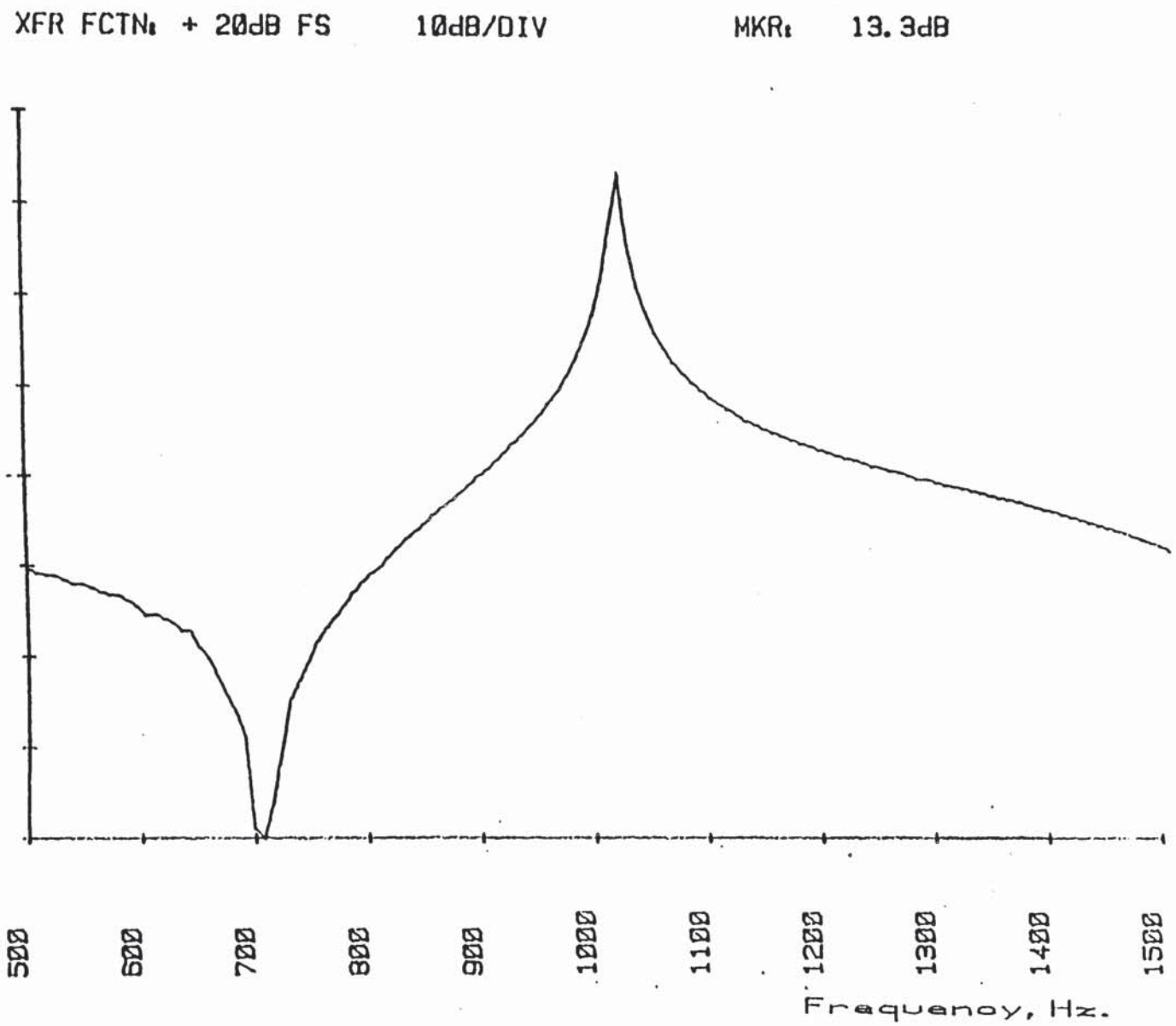

Fig. 6.5 **Typical Response Curve Measured.**

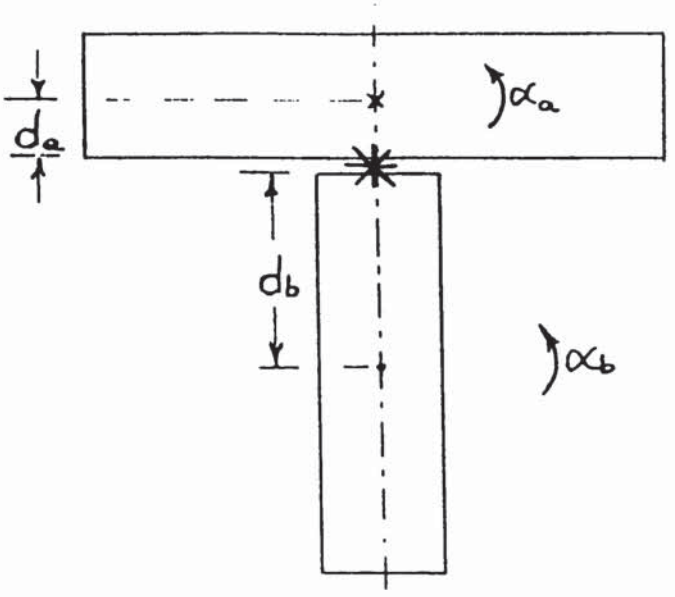

Fig. 6.6 **Notation for derivation of stiffness quantities.**

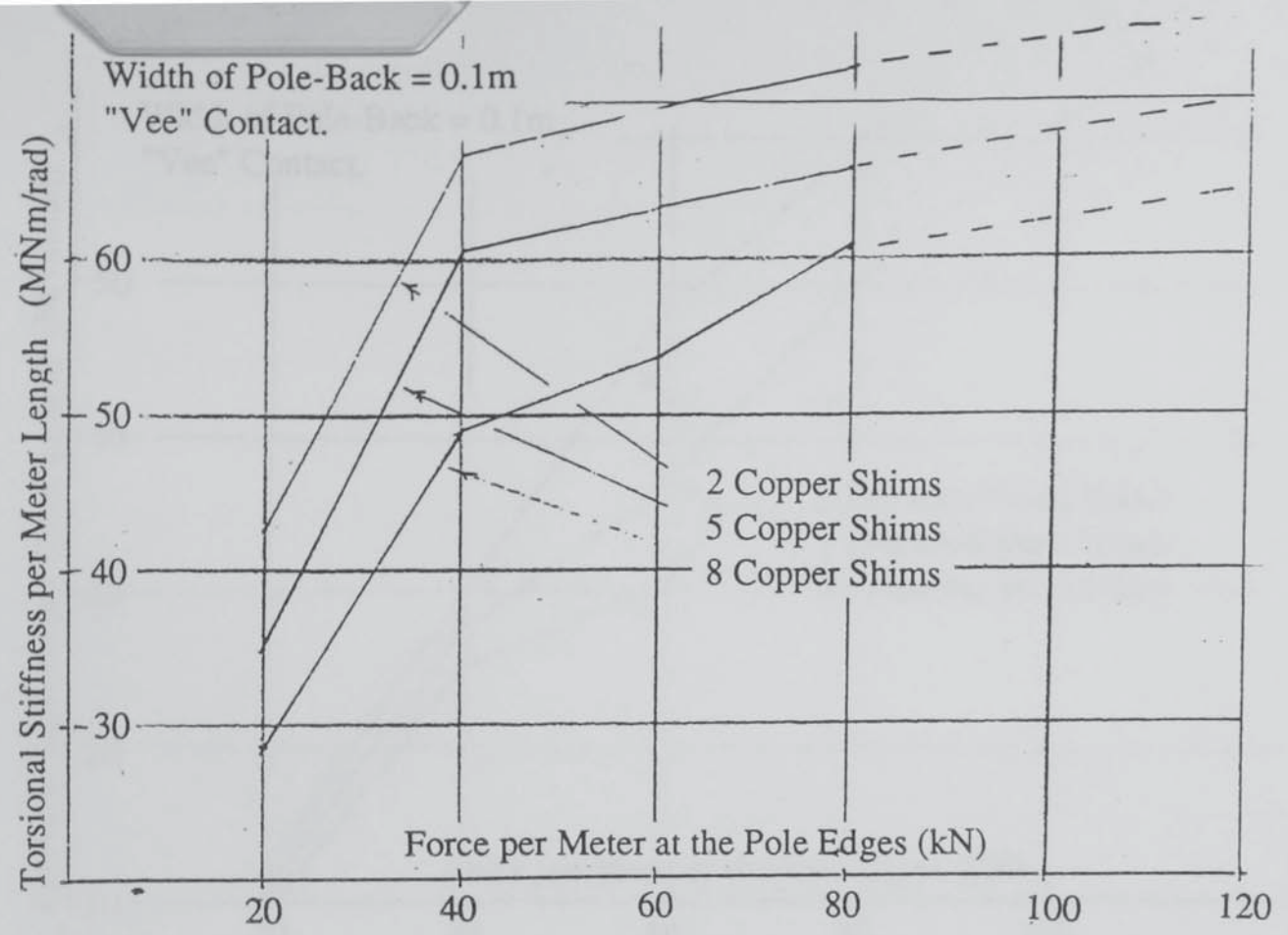

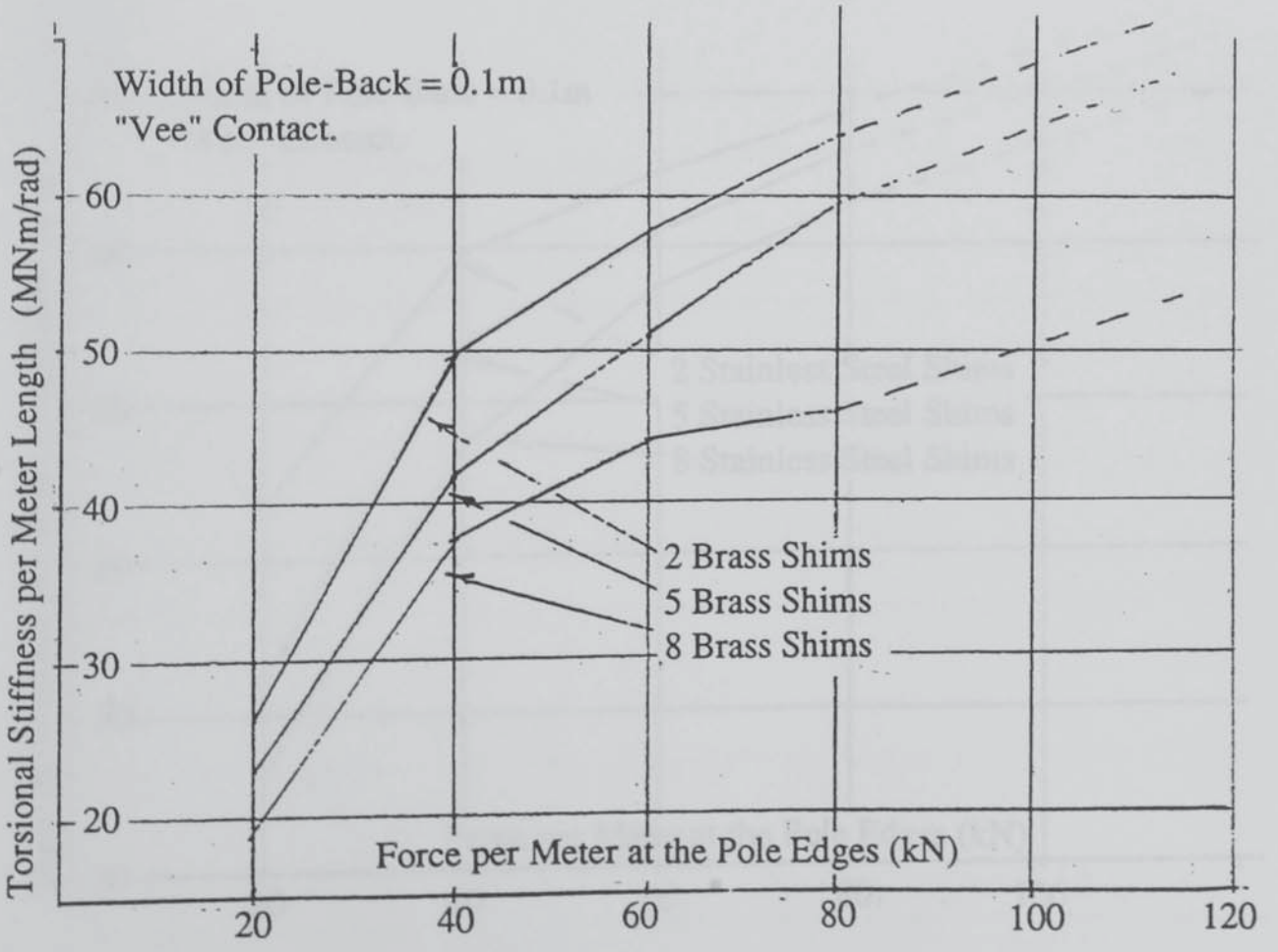

Fig. 6.7 **Joint Rocking Stiffness ("Vee") Copper and Brass Shims.**

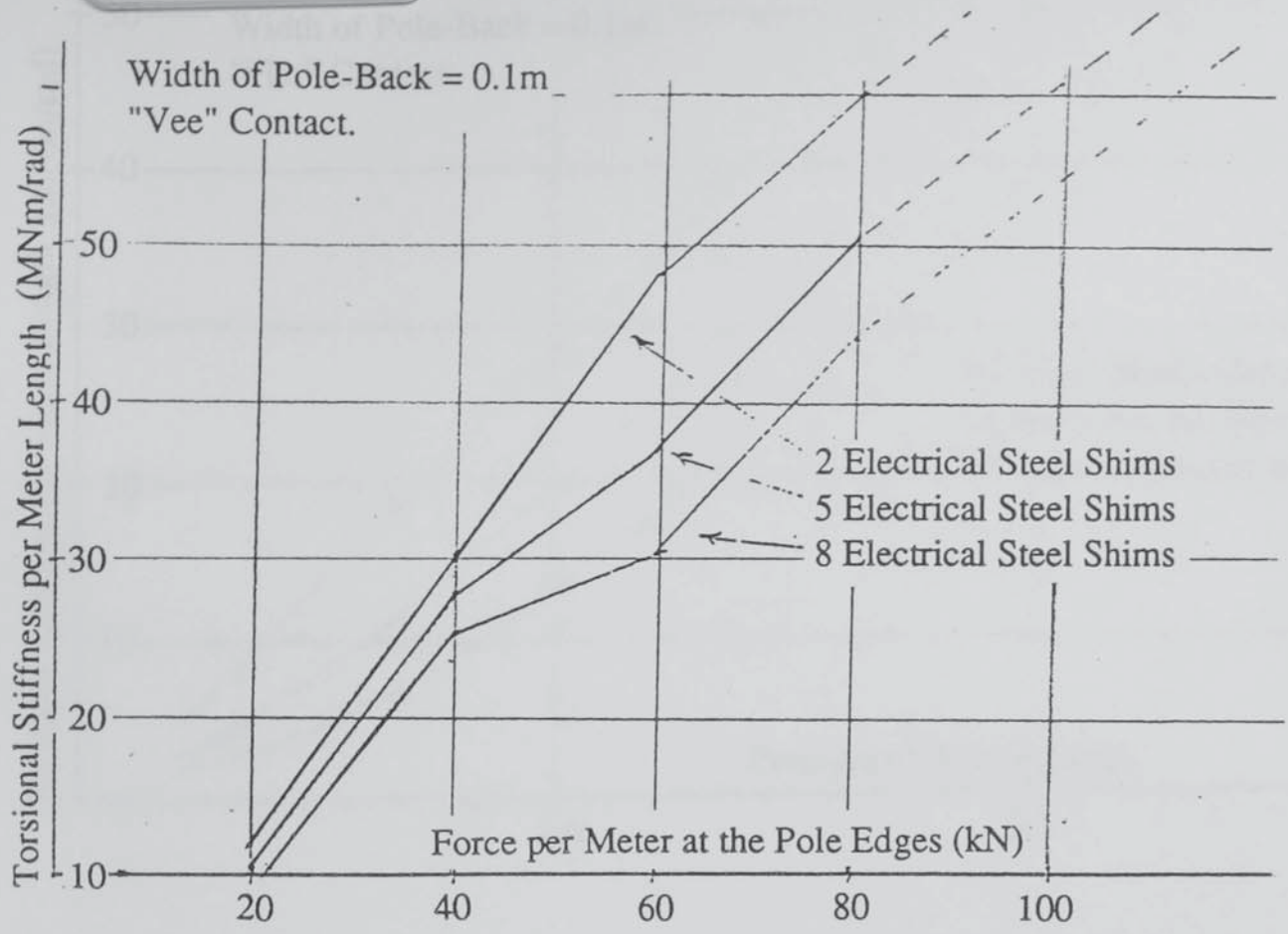

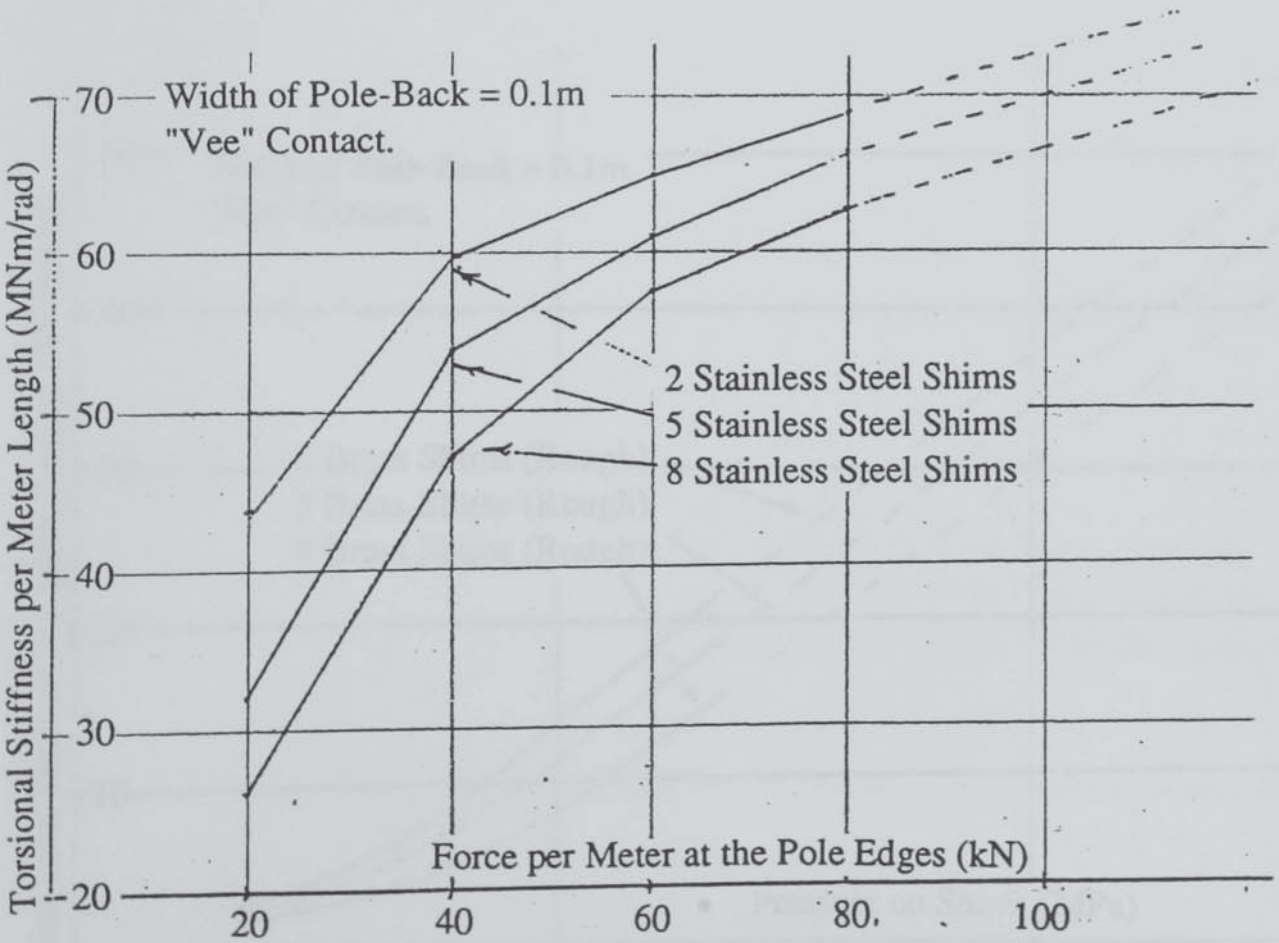

Fig. 6.8 **Joint Rocking Stiffness ("Vee") Electrical and Stainless Steel Shims**

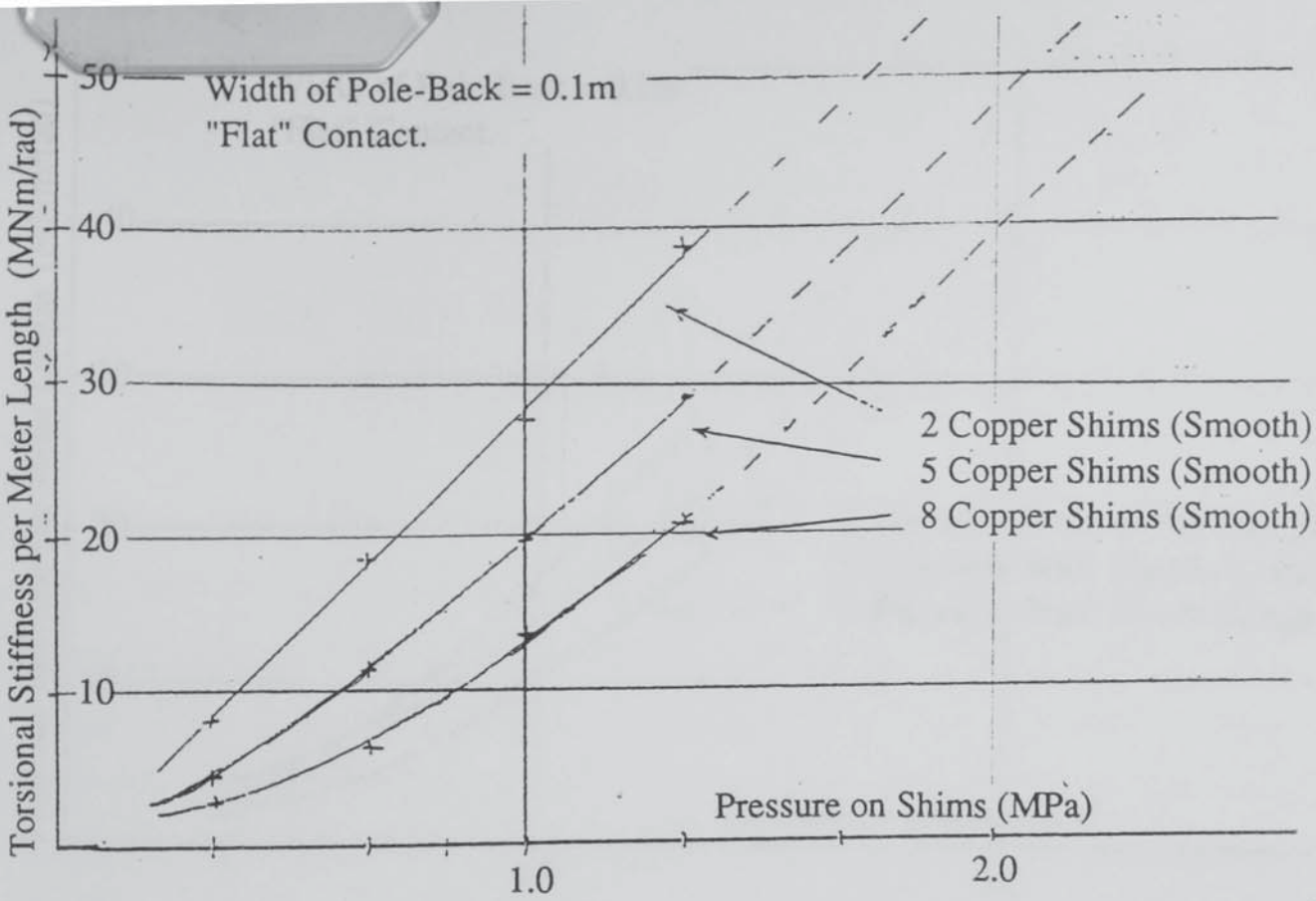

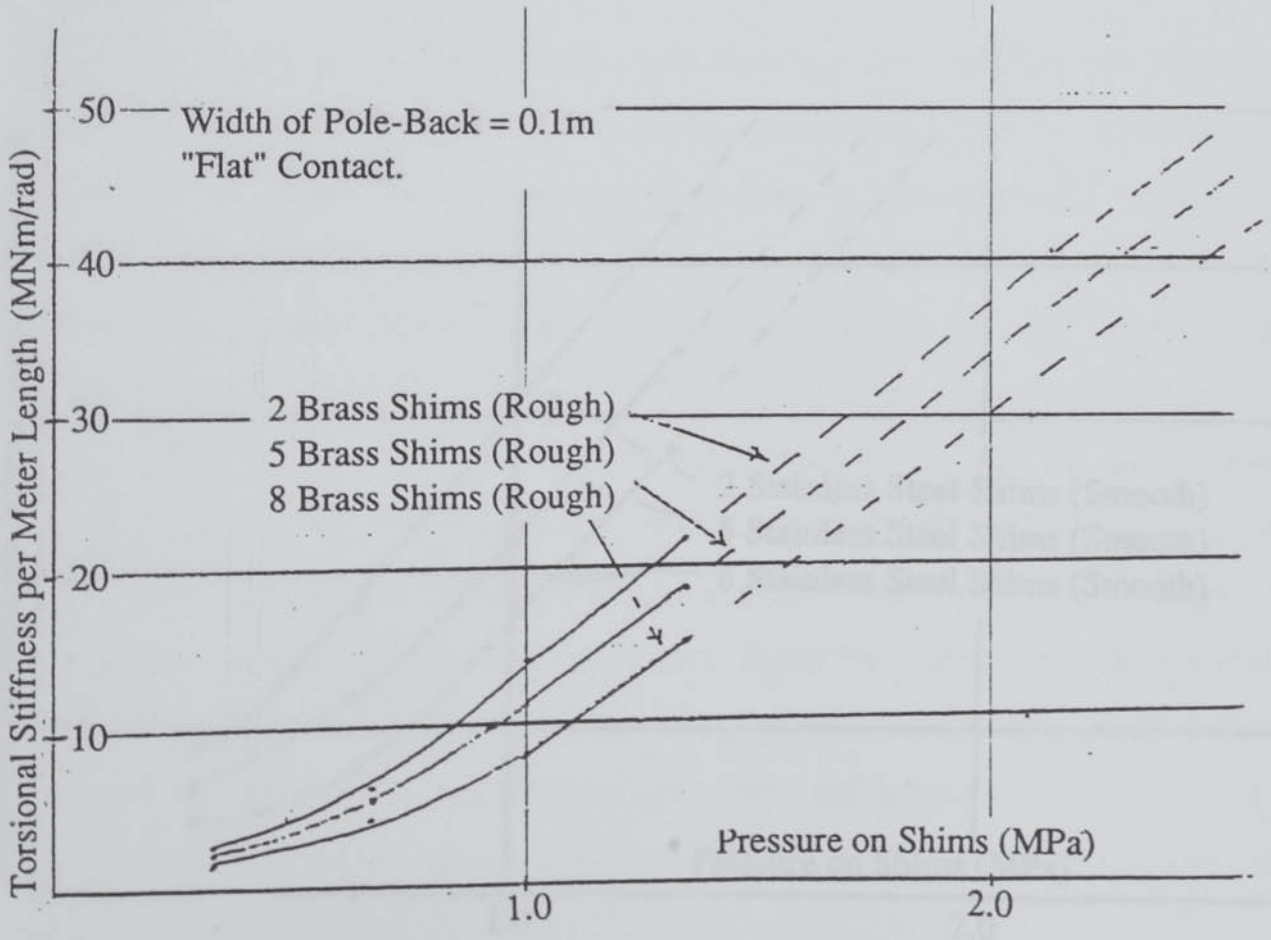

Fig. 6.9 **Joint Rocking Stiffness ("Flat") Copper and Brass Shims.**

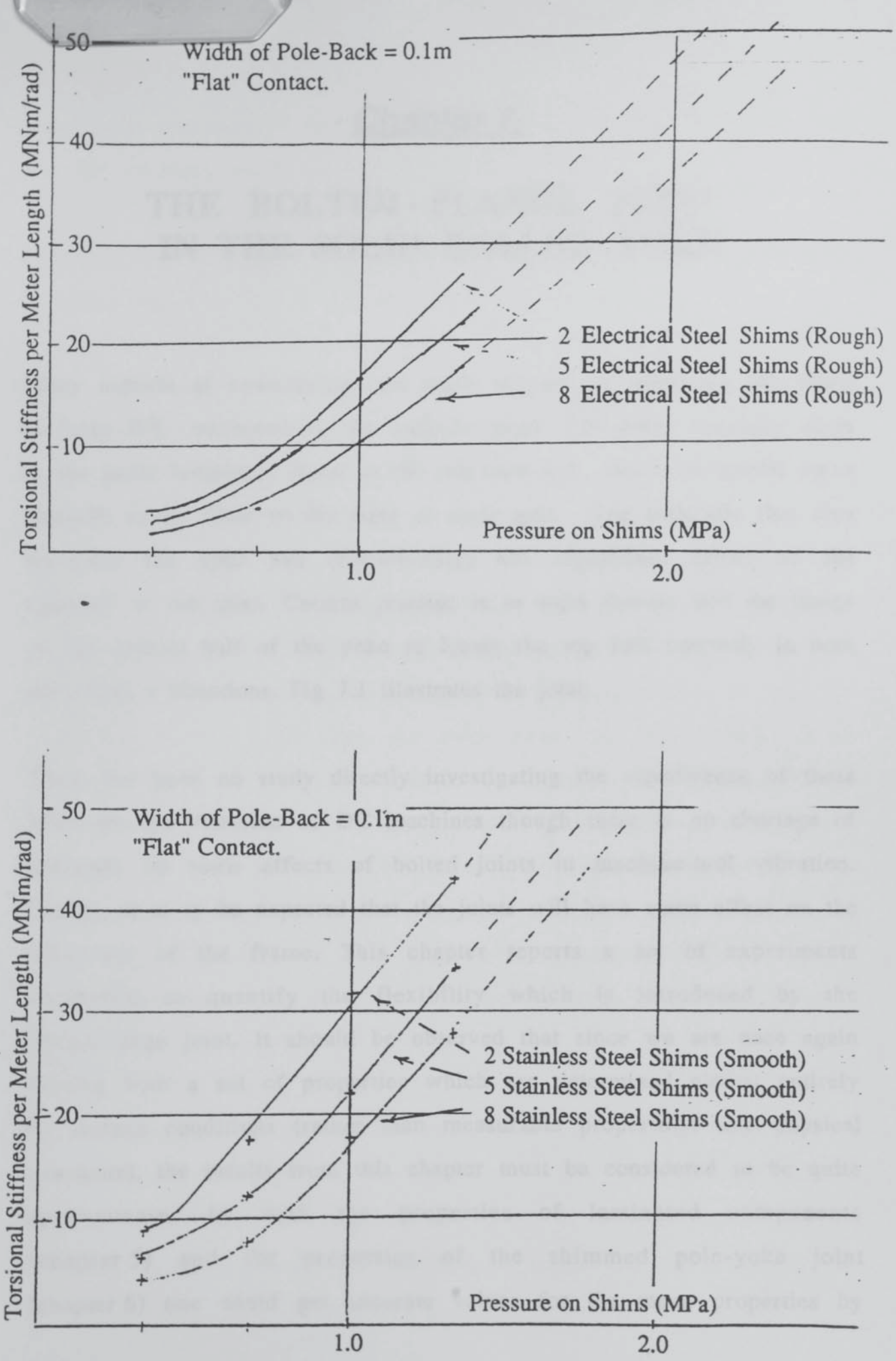

Fig. 6.10 **Joint Rocking Stiffness ("Flat") Electrical and Stainless Steel Shims.**

Chapter 7.

THE BOLTED - FLANGE JOINT IN THE SOLID ROLLED YOKE

Many aspects of construction are made simpler by preparing the yokes of large D.C. machines in two separate parts. The joints normally occur in the same horizontal plane as the armature C.L. and it is normal for a compole to be fixed to the yoke at each split. The mainpole flux then traverses the split and (fortuitously) has significant effect on the tightness at the joint. Current practise is to weld dowels into the flange on the bottom half of the yoke to locate the top half correctly in both the x and z directions. Fig 7.1 illustrates the joint.

There has been no study directly investigating the significance of these splits on the vibration of DC machines though there is no shortage of literature on some effects of bolted joints in machine-tool vibration. Clearly, it is to be expected that the joints will have some effect on the behaviour of the frame. This chapter reports a set of experiments performed to quantify the flexibility which is introduced by the bolted-flange joint. It should be observed that since we are once again dealing with a set of properties which are determined almost entirely by surface conditions (rather than measurable proportions and physical constants), the results from this chapter must be considered to be quite approximate. As with the properties of laminated components (chapter 5) and the properties of the shimmed pole-yoke joint (chapter 6) one could get accurate values for the mean properties by

doing large numbers of tests but the variance would probably be such that this accuracy would not be of any practical value.

Damping in these joints has been investigated to a limited extent. Damping figures obtained for various modes of the models tested have been of the same order of magnitude as the material damping of steel itself in low-amplitude vibration. Thus, we are content to assume that the damping is low. Obtaining accurate figures for it is impossible because of the difficulty of separating the energy dissipation at the split from that internal to the steel.

It has been the case in the course of the work reported in this chapter, that all of the modes examined on the various models have been very similar to modes of true uniform rings and cylinders. That is to say, the flexibility of the joints has not been such that mode-shapes have become dramatically altered. There is a convention for the description of the modes of pure rings and cylinder. The central notion to this convention is the use of an integer n which specifies the number of wavelengths of the displacement pattern about the circumference. In discussing the experiments done and the interpretation of the results, it is useful to retain this short notation for the mode-shapes though it is no longer strictly correct.

§7.1 Dynamic Properties of the Joint

Fig. 7.1 shows a cross-section of the joint. If it were rigid, then the rotations a_1 and a_2 would be identical as would the translations u_1, u_2

and v_1, v_2. In reality, there will be a restoring moment "M" and restoring forces P and Q, given by . . .

$$M = T\,(a_2 - a_1) \tag{7.1}$$

$$P = C\,(u_2 - u_1) \tag{7.2}$$

$$Q = S\,(v_2 - v_1) \tag{7.3}$$

We have considered only the displacements in the r-θ plane. The length of the joint is usually large in comparison with its width so that bending moments about radial and tangential axes are taken care of in the numerical models by the translational stiffnesses of the joint. The joint faces are normally finished with an end-mill. Therefore, they do not have a directionality and it is to be expected that the shear properties of the joint in the longitudinal sense are identical to those in the radial sense.

A good quality surface from the end-milling operation will have a r.m.s. height of asperity of some 6e-6 m. The vibrations with which we are concerned are generally lower than this in amplitude. Therefore, the whole vibration amplitude can normally be taken up at these joints. It will not be surprising therefore, that finite values can be measured for the quantities T,C and S above.

The following factors will obviously play a part in determining the joint

parameters.

(1) The material of the flanges.

(2) The surface-finish ot the machined faces.

(3) The flatness of the machined faces.

(4) The tightness of the joint.

(5) The surface area of the joint.

The material is always steel. The area of the joint is normally determined by the need to fit bolt-holes between the cylinder and the outside of the flange. Joint tightness is controllable to some extent though gravity and magnetic attraction play a strong role in providing a base value of pressure.

§7.2 Design of the Experimental Models

In choosing a model to investigate the behaviour, similar principles were applied to those outlined in §6.1. The original system comprised two flat rectangular plates which formed a 1m square when bolted together at the flange-joint (Fig. 7.2). This would allow the three stiffnesses C,S and M to be investigated in completely separate tests. The tests which were envisaged are shown in Fig. 7.2 also. The dimensions of this model had been obtained by proportionally scaling-down from a real machine joint. It transpired that the flange itself was too flexible in comparison with the joint interface for any very useful results to be obtained.

Two problems seemed to be present. Firstly, the weld itself appeared to be contributing to the flexibility figures being recorded. It was also noticed (as a result of a simple purely theoretical calculation) that the pressure at the joint interface caused by the bolts was not being spread very uniformly by the flanges as tends to happen in the real machine joints. Further thought reveals that it would have been more correct to have scaled the flange thickness according to the square-root and scale all other dimensions linearly. The investigation on this model was carried out by P. Swales (A.1985) and his contribution is gratefully acknowledged.

With the above experience in mind, a new system was adopted. This would directly address the problem of the behaviour of the joint in the cylinder. The scaling of these models was somewhat more realistic. In all, six distinct models were prepared. Fig.s 7.3 and 7.4 illustrate three rectangular-section ring models. Fig.s 7.5 - 7.8 illustrate three uniform cylinder models made in one, two and four pieces respectively.

The progression in behaviour observed in models 7.1-7.3 and 7.4-7.6 can be interpreted to produce figures for the three stiffnesses required. Benhafsi (A.1986) was responsible for carrying out the tests and has been very thorough in this task.

Both the rings and the cylinders have a number of well separated resonances at the low-frequency end of the spectrum (beginning near 250Hz for the first non-rigid-body mode). The cylinder dimensions chosen are such that every mode whose resonant frequency lies below

1000Hz has displacements which vary almost exactly linearly with respect to axial position. This is the case by design and only these modes are of interest for the study of the joint behaviour. If the flanges were required to twist or bend significantly in any one mode, it would be more difficult to accurately represent their effect.

§7.3 The Behaviour of Rings and Cylinders Having Symmetrically Deployed Joints

Before we proceed to describe the experiments carried out, it is appropriate to explain how the measurement of the torsional stiffness T could be isolated from the effects of the shear stiffness S and vice-versa.

Every uniform ring possesses an infinity of planes of symmetry each one containing the axis of the ring. (The z-axis). One of these planes is nominated as the y-z plane and the x axis is normal to that plane. The orthogonal plane which contains the z-axis is the x-z plane.

Now applying some knowledge about the modes of objects having one plane of symmetry, it is clear that the modes of the ring/cylinder can be divided in to four groups as...

(1) Modes Sym. w.r.t. x and Sym. w..rt. y.

(2) Modes Sym. w.r.t. x and Asym. w..rt. y.

(3) Modes Asym. w.r.t. x and Sym. w..rt. y.

(4) Modes Asym. w.r.t. x and Asym. w..rt. y.

Modes which are symmetrical with respect to the y-z plane are characterised by the following facts:

(1) Particles lying on the plane can freely translate within the plane but they cannot depart from the plane.

(2) The shear stresses σ_{xy} and σ_{xz} are zero at the plane of symmetry.

Modes which are anti-symmetrical with respect to the y-z plane are characterised by the following facts:

(1) Particles lying on the plane can freely translate normal to the plane but they can have no component of motion parallel to the plane.

(2) The normal stress σ_{xx} is zero at the plane of symmetry.

Now, if a pair of joints is positioned on the plane-of-symmetry y-z , the modes symmetrical about that plane will cause a bending moment to exist at the joints but no shear, and the anti-symmetrical modes will cause a shear force to exist at the joints with no bending moment. This reasoning applies as directly to cylinders as it does to rings. By

selectively exciting modes which are symmetrical or anti-symmetrical with respect to the plane(s) at which joins occur in the ring/cylinder, the behaviour of the joints in shear can be investigated separately from their behaviour in bending.

Compression/extension of the joints cannot be separated from bending in these models except for the breathing mode (n=0) . The stiffness of the joints in compression/extension motion is such that simple opening of the joint makes little impression on the natural frequencies of the ring compared with the bending motion. In fact, it was not possible to detect any added flexibility due to compression/extension of the joints at the low-frequency end of the spectrum. However, we can apply the same logic as used in §6.9 to deduce the stiffness of the joint in compression/extension from the bending stiffness. In the meantime, we assume that C is very large (ie. that no compression/extension occurs in the joint.)

§7.4 Tests on the Ring Models

All of the information required from this experimental study could have been obtained by considering the ring models alone. A complete set of tests was done on the rings to achieve the following:

(1) Verify a theoretical model for the rings so that results could be interpreted using this model.

(2) Check the effect of the welds independently of the splits in order

to establish whether the welds themselves contribute significant flexibility.

(3) Assess the influence of the split by examining the shift in resonances caused by it.

The plain ring was mounted in a free state and excited to vibrate in its own plane. The optimum mounting technique was chosen by comparing the first three measured resonances. The setup which returned the lowest frequencies was deduced to be the least stiff. The suspension methods tried include hanging by a rope, three-point support on softwood blocks and three-point support on rubber pads. The resulting suspension arrangement was to lay the ring on the rubber.

Natural frequencies were recorded for the flexural modes (n=2,3,4,5) and the extensional mode n=0 for the free ring. These correlated well with the ring model of DMS and verified that it is satisfactory to use this theoretical model in these circumstances. Results are presented in Table 7.1.

n	Measured Resonance (Hz)	Predicted Resonance (Hz)
2	246.4	246.7
3	684.2	684.9
4	1289.0	1291.2
5	2043.2	2046.9
0	2574.5	2576.3

Table 7.1. Measured and Predicted Resonances for Model 7.1

In order to assess the effects of the welds independently of the splits, it was decided that the models which were to become the ring-with-two-joints and the ring-with-four-joints would each be prepared first as single pieces and tested. These tests were carried out to excite both modes symmetrical and anti-symmetrical with respect to the y-z plane. The natural frequencies resulting were lower than those measured on the free ring as would have been expected because these models had two and four lumps of steel effectively added. Use of the DMS ring model with two and four added masses revealed that there had been no measurable decrease in the flexural stiffness of the ring due to the presence of the fillet-welds. Table 7.2 below gives measured and predicted frequencies for the tests on model 7.2 (two added lumps of steel) Table 7.3 gives measured and predicted frequencies for the

tests on model 7.3 (four added lumps of steel)

n	Measured Resonance (Hz)	Predicted Resonance (Hz)
2	225.0	225.5
3	633.5	634.5
4	1202.1	1205.3
5	2042.1	2048.5

Table 7.2. Measured and Predicted Resonances for Model 7.2 (Unsplit)

n	Measured Resonance (Hz)	Predicted Resonance (Hz)
2	214.3	214.9
3	628.2	630.0
4	1125.0	1128.6
5	1767.0	1776.8

Table 7.3. Measured and Predicted Resonances for Model 3 (Unsplit)

Then the splits were introduced by cutting through the two models mentioned above. A relatively small amount of material was lost in this process and the surfaces were purposely left rough (by the saw). Models 7.2 and 7.3 were then used to investigate the properties of the split in bending and shear. The pre-tension at the splits was provided by one 0.5" bolt at each split. The yield strength of these bolts is approximately 24.5 kN and this tension is achieved by a torque of some 46 lb ft (62.4 Nm). At full tension, the mean pressure at the joint interface is 6.2 MPa.

Model 7.2 was suspended on the rubber feet and shaken so that the modes n=2 and n=3 (symmetrical w.r.t. the plane of the split) were excited. Comparison of the natural frequency for the n=2 mode here with the n=2 from the unsplit version of model 7.2 shows that the extra bending flexibility of the split has had a measurable influence on the ring behaviour. On the other hand, the flexibility of the joint in shear had a negligible influence on the resonant frequencies. Table 7.5 below presents the resonances for two values of joint tightness where the surface condition of the joint was rough.

Joint-Pressure (MPa)	Resonance (Hz) (Mode n=2)	Resonance (Hz) (Mode n=3)
3.1	209.5	633.2
6.2	216.5	633.2

Table 7.5. Measured Resonant Frequencies of Model 7.2 (Rough joint surface).

By comparing the frequency shift with the shift predicted by DMS for this model - given various values of torsional stiffness - an estimate of the torsional stiffness can be obtained. Table 7.6 below shows the results of this comparison. The depth of the joint in the axial direction was 40mm and the width 100mm. The figures for torsional stiffness can be scaled to apply to other joint proportions.

Joint-Pressure (MPa)	Torsional Stiffness (MNm/rad)
3.1	1.2
6.2	2.0

Table 7.6. Deduced Torsional Stiffness For Model 7.2 (Rough joint surface).

Model 7.3 was then split in two planes and re-assembled with bolts at each split as was done for model 7.2. Tests similar to those described above were carried out. In this case, the n=2 mode (symmetrical w.r.t. both planes of split) involves pure bending at all the joints as before, but n=3 incorporates bending at two of the joints and shear at the other two joints. By using a different point of excitation, the n=2 mode (anti-symmetrical w.r.t. both planes of split) was excited. This mode causes a shear force to exist at the joints but no bending. The resonances are presented below in table 7.7.

Joint-Pressure (MPa)	Resonance (Hz) (Mode n=2)	Resonance (Hz) (Mode n=3)
3.1	201.6	610.0
6.2	206.0	612.2

Table 7.7. Measured Resonant Frequencies of Model 7.3 (Rough joint surface).

Using the same technique of comparison between theoretical model and the measurements, equivalent torsional stiffness values for the joints are obtained. Again the frequency shift due to the shear flexibility was negligible. The implied average torsional stiffnesses of the joint were of the same order as those found previously for both cases of joint tightness. Table 7.8 gives the joint bending stiffness as calculated from the ring with four splits.

Joint-Pressure (MPa)	Torsional Stiffness (MNm/rad)
3.1	1.1
6.2	1.8

Table 7.8. Deduced Torsional Stiffness For Model 7.3 (Rough joint surface).

The faces of the joints in both models 7.2 and 7.3 were then milled to represent a more typical condition for the DC machine. The tests and procedures described above were reapplied to assess the torsional stiffness of the joints again. It was found to be reduced instead of increased as was expected.. Tables 7.9 below is a record of the resonances found for the milled joints in model 7.2. The loss of material as a result of the machining operation was accounted-for in the DMS model and the corresponding torsional stiffnesses were then derived as before. (Table 7.10)

Joint-Pressure (MPa)	Resonance (Hz) (Mode n=2)	Resonance (Hz) (Mode n=3)
3.1	205.2	671.8
6.2	206.6	673.0

Table 7.9. Measured Resonant Frequencies of Model 7.2 (Milled Joint surface).

Joint-Pressure (MPa)	Torsional Stiffness (MNm/rad)
3.1	0.8
6.2	1.1

Table 7.10. Deduced Torsional Stiffness For Model 7.2 (Milled joint surface).

In summary, the tests on the rings reveal:

(1) That the welds at the flanges do not contribute significant flexibility to the joint.

(2) That the damping occurring at the joint is negligible in comparison with the damping in machines from other sources.

(3) That the flexibility of the joint in shear is immeasureably small (on the present model)

(4) That the bending flexibility of the joints is sufficient to cause a significant change in some of the resonant frequencies of the ring.The rough surface surprisingly yielded higher resonant frequencies than the milled one. Possibly, this effect could have been due to flatness errors in the sawed joint causing intimate contact between the two sides of the joint flattening down asperities etc. in one or very few areas. The sawed faces did have very poor quality where flatness was concerned.

§7.5 Tests on the Cylinder Models (7.4 - 7.6)

The cylinder models were created with two purposes in mind. Firstly, the values for the joint stiffness values found from the ring model would be supported and generalised. The other function was to demonstrate that the split cylinder could be modelled well with the DMS software. For the present, we concentrate on the former.

As commented earlier, the dimensions of the cylinders are such that in

the low-frequency modes displacements vary quite linearly with respect to the axial length. Now, each of the cylinders has a plane of symmetry normal to the axis of the cylinder as well as two planes of symmetry containing the axis. Modes symmetrical w.r.t. z - the coordinate of axial position - are very similar to the in-plane modes of the rings. Modes anti-symmetrical w.r.t. z have zero radial and circumferential displacements at the plane of symmetry. Therefore, when the cylinder models are excited radially at the axial center, none of the anti-symmetrical modes are forced. In the tables to follow, n=2,S denotes the mode shape which has two full wavelengths about the circumference of the cylinder and which is symmetrical w.r.t. z. Similarly, n=3,A denotes the mode shape which has three full wavelengths about the circumference of the cylinder and which is anti-symmetrical w.r.t. z and so forth.

The first test on the cylinders was to suspend the plain uniform cylinder on flexible rubber mats and excite the modes symmetrical wrt z by applying the forcing at a point axially half-way along the cylinder. The response was measured at the center of the cylinder also. The frequency response-trace measured compared very favourably with the trace generated by the DMS cylinder representation. (Fig. 7.8). Exciting the cylinder at one end causes the antisymmetrical (w.rt. z) modes to be excited with the symmetrical ones. Again, the measurement compares favourably with the prediction (Fig. 7.9). The theoretical model is considered to be validated.

Each of the joints in models 7.5 and 7.6 were held together by six 0.75"

bolts. Three values for the bolt torque have been used, namely 25 lbft, 50 lbft and 100 lbft. These result in mean joint pressures of 0.9 MPa, 1.8MPa and 3.6MPa respectively.

Model 7.5 was flexibly mounted and shaken so that at first, only the symmetrical (w.rt. z) modes are excited. Then all modes were excited by applying the forcing at the end of the cylinder. In each case, the force was applied in a plane perpendicular to the plane of the splits. Thus, the modes n=2,S and n=2,A will involve a bending moment at the joints while modes n=3,S and n=3,A involve a shear force at the joints. Natural frequencies were recorded for the three conditions of joint pressure 0.9 MPa, 1.8 MPa and 3.6 MPa. Table 7.12 below gives the resonances for each of the cylinder modes of model 7.2 having a resonant frequency less than 1 kHz:

Joint-Pressure (MPa)	Mode	Resonance (Hz)
0.9	n =2,S	190.0
0.9	n =2,A	284.4
0.9	n =3,S	705.0
0.9	n =3,A	880.5
1.8	n =2,S	194.0
1.8	n =2,A	289.0
1.8	n =3,S	706.4
1.8	n =3,A	883.3
3.6	n =2,S	220.0
3.6	n =2,A	302.8
3.6	n =3,S	708.6
3.6	n =3,A	894.0

Table 7.12. Measured Resonant Frequencies of Model 7.5 as a Function of Joint Pressure

Model 7.6 was flexibly mounted and excited similarly to model 7.5 to extract the resonant frequencies of the low-frequency modes. The natural frequencies were recorded for the same three conditions of joint pressure 0.9 MPa, 1.8 MPa and 3.6 MPa. Table 7.13 below gives the resonances for each of the cylinder modes of model 7.6.

Joint-Pressure (MPa)	Mode	Resonance (Hz)
0.9	n =2,S	147.2
0.9	n =2,A	255.1
0.9	n =3,S	548.7
0.9	n =3,A	776.7
1.8	n =2,S	166.8
1.8	n =2,A	267.2
1.8	n =3,S	578.8
1.8	n =3,A	797.4
3.6	n =2,S	189.0
3.6	n =2,A	277.5
3.6	n =3,S	626.4
3.6	n =3,A	816.3

Table 7.13. Measured Resonant Frequencies of Model 7.6 as a Function of Joint Pressure

Fig. 7.10 shows the representation of model 7.5 created within DMS. The second "half" of model 7.5 is simulated by imposing suitable symmetry conditions at the flanges. Depending on the stiffness of the joint in bending, the true lowest-frequency mode of the model will be between the two extremes illustrated in Fig. 7.10.

Fig. 7.11 shows the theoretical representation of model 7.6. The simulation of the whole model is built up from a one-quarter portion by imposing suitable symmetry conditions as before. Again, the two extremes of the mode-shape of the lowest-frequency mode are illustrated.

A number of joint stiffness values have been used in these theoretical models to establish how the first resonant frequency of models 7.5 and 7.6 depend on this stiffness. The results are presented graphically in Fig. 7.12.

Comparison of the measurements with the curves of Fig. 7.12 yields a set of joint torsional stiffnesses. The values are presented in table 7.13.

§7.6 Discussion of Results

The outcome of this investigation is summarised here. Compression/extension, and shear flexibilities of the joints in the models prepared has been too small to obtain reliable values. (Estimates of these quantities can be made). The flexibility of the joints in bending is sufficient to significantly influence the resonant frequencies of those modes which cause a bending moment to occur at the joints. Figures have been obtained for this flexibility. The damping estimates indicate that no very significant energy dissipation is occurring at the joints. The figures for the bending stiffness of the joints have been evaluated from two different test set-ups and found to agree within the bounds of error. These figures must be regarded as approximate. The scatter in

the figures is such that the true stiffness at any time may well be anywhere between 0.5 and 2 times the predicted figure.

The bending stiffness of the joints has been shown to depend on the joint preload and the surface condition. A better surface will increase the stiffness. Flatness errors, however, in combination with high joint pressure, leads to very intimate contact of the two sides of the joint at a small number of points and result in a stiff joint. The literature suggests that lubrication of the joints with high viscosity oil can considerably increase the stiffness and introduce a mechanism for finite energy dissipation to occur. Benhafsi (A.1986) includes an ample literature survey.

The results for bending (torsional) stiffness of the joints have been scaled to apply to a joint width of 0.1m and joint length of 1m. Fig. 7.13 shows the relation between the joint pressure and the anticipated joint stiffness in bending for these joint proportions. For other joint widths, scale the values according to the square. For other joint lengths, scale the values proportionally.

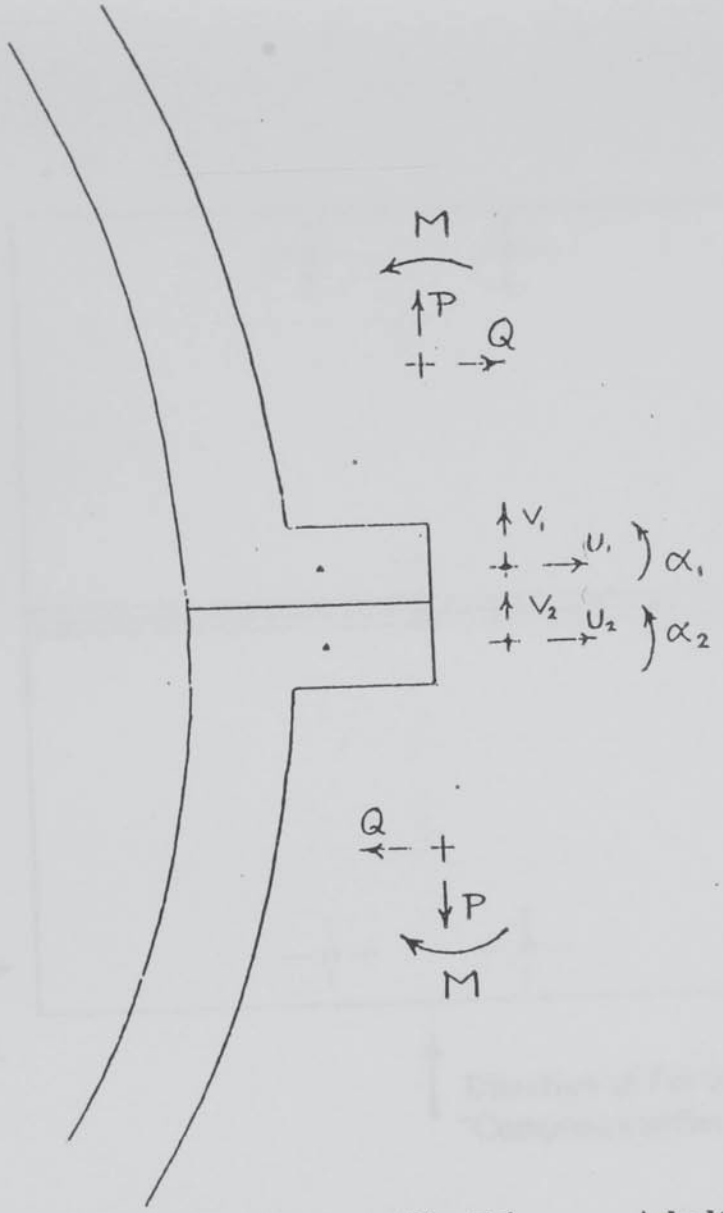

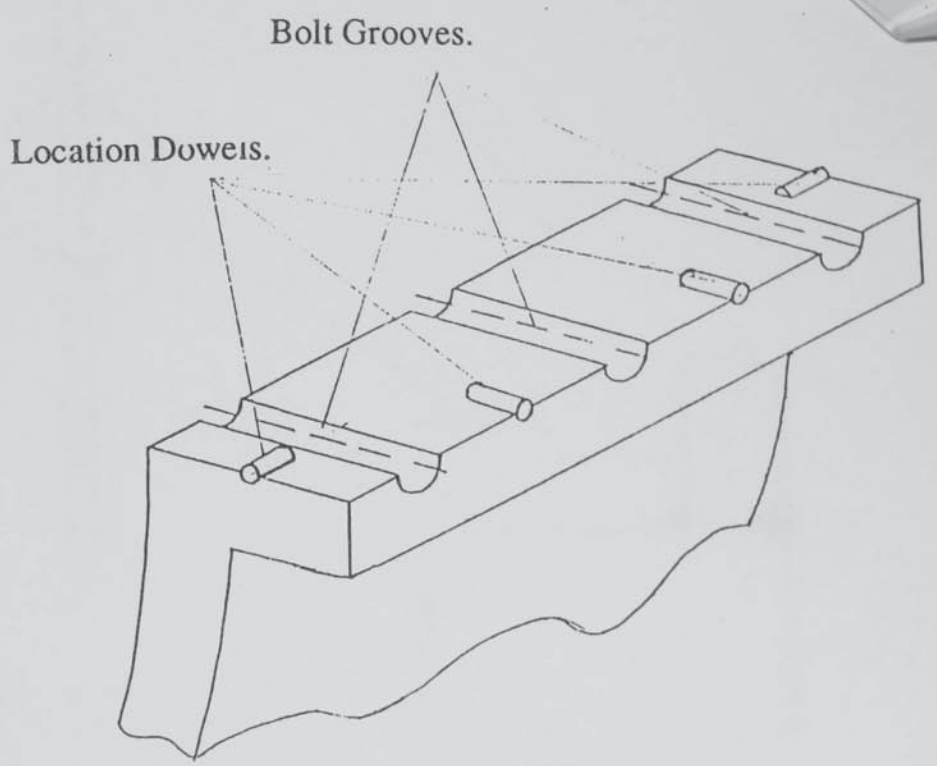

Fig. 7.1 **A bolted flange joint.**

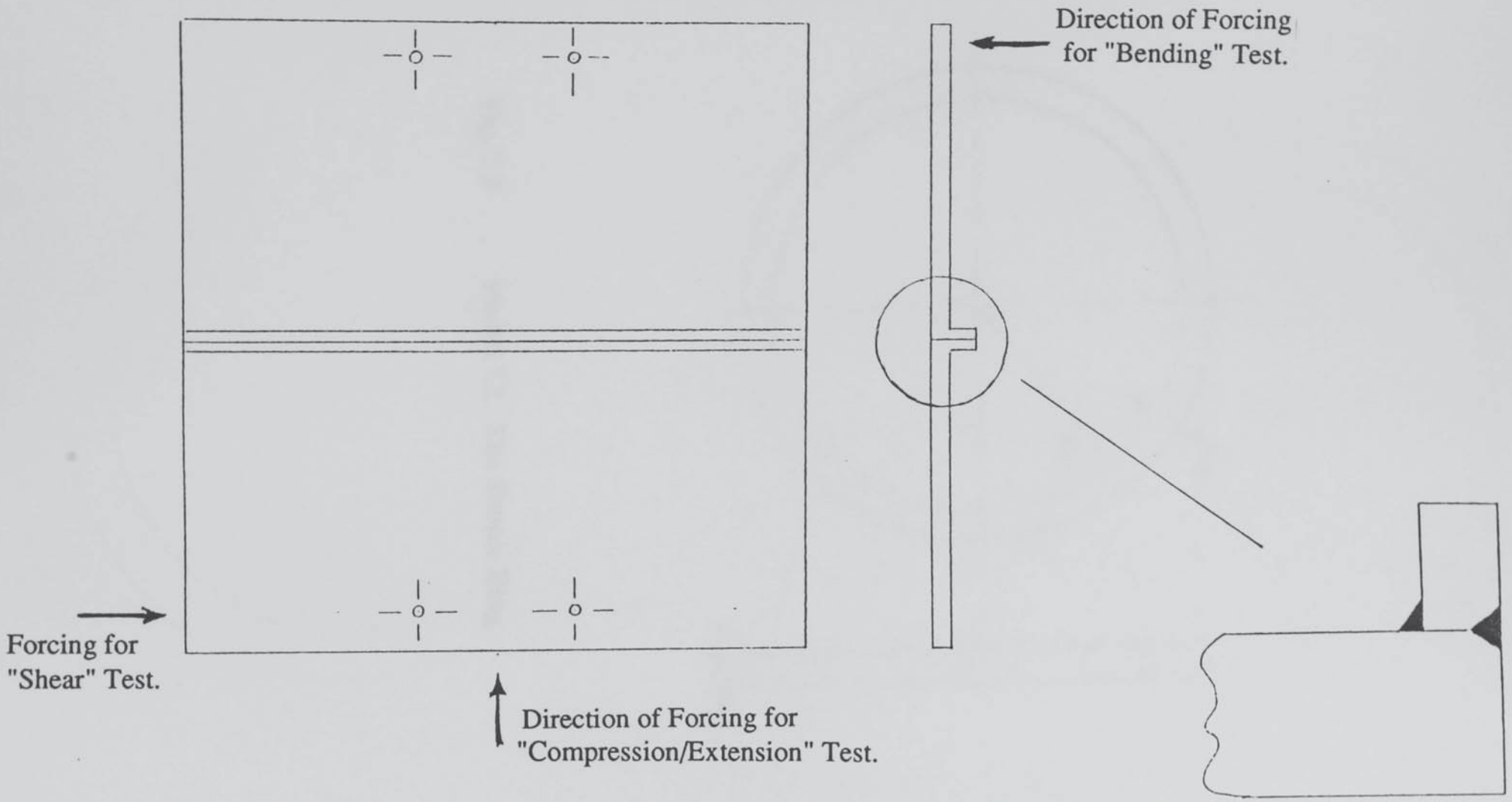

Fig. 7.2 Original 'Plate' Model to Investigate Behaviour.

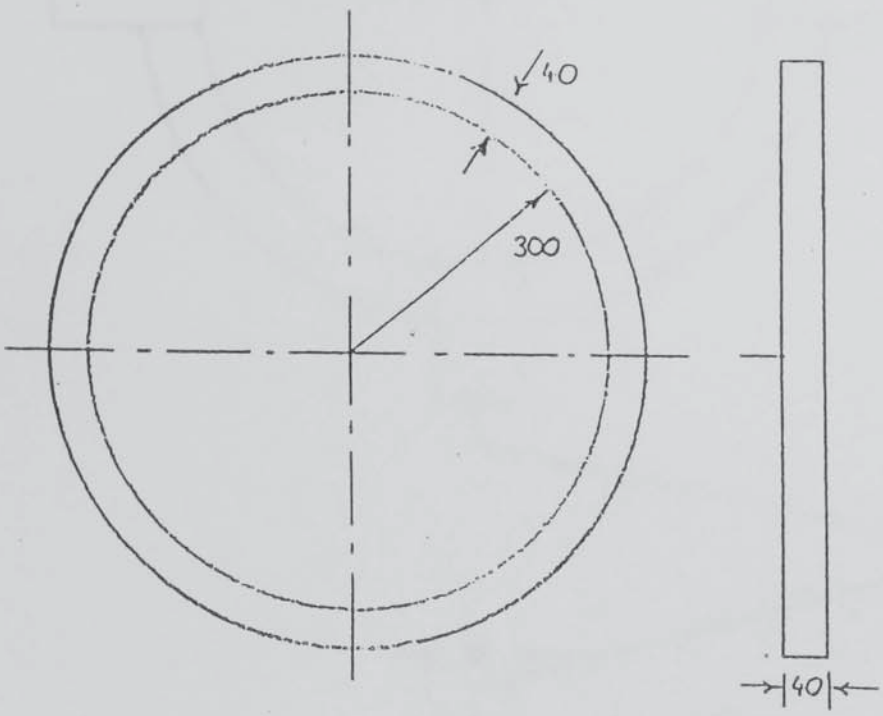

Fig. 7.3 **Model 7.1. The Simple Ring.**

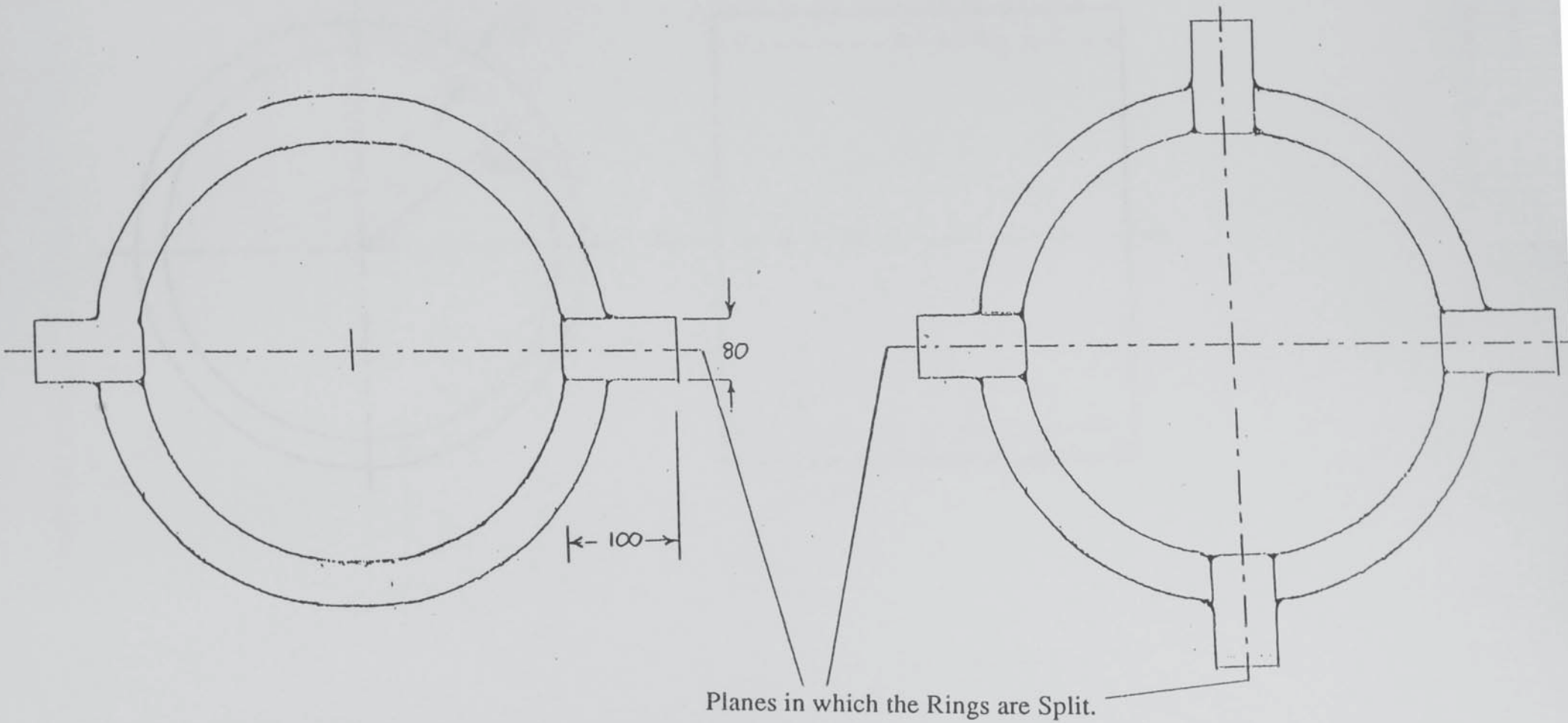

Fig. 7.4 **Models 7.2 and 7.3. Rings with "Flanges".**

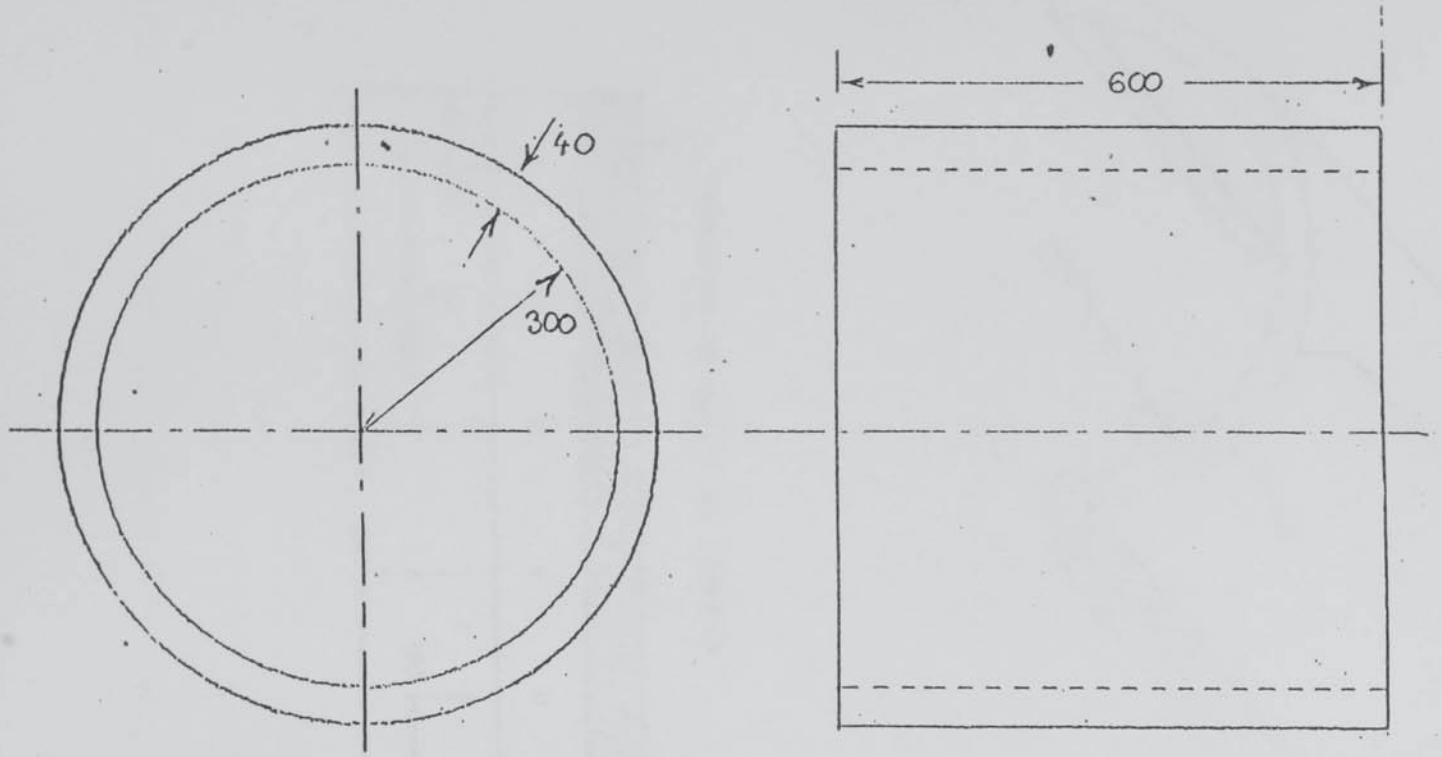

Fig. 7.5 **Model 7.4. The Plain Cylinder.**

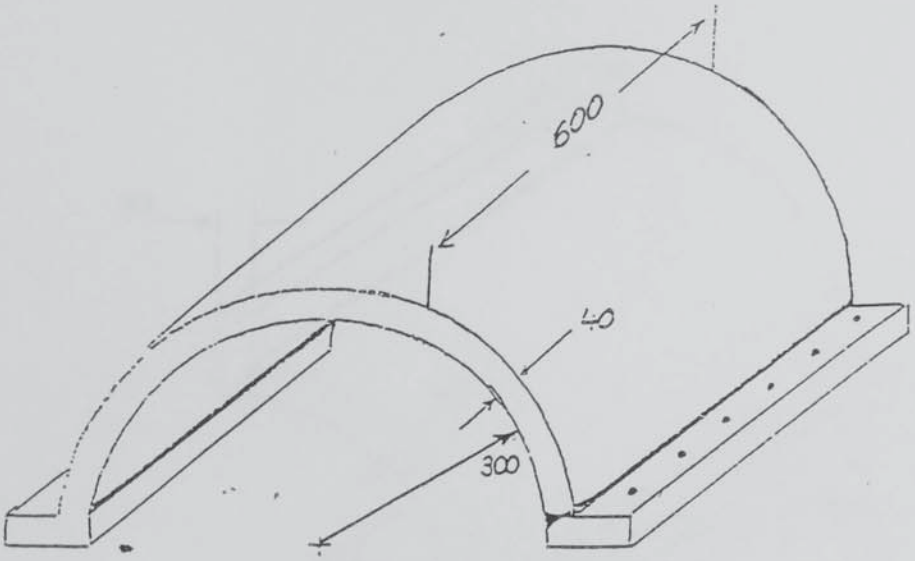

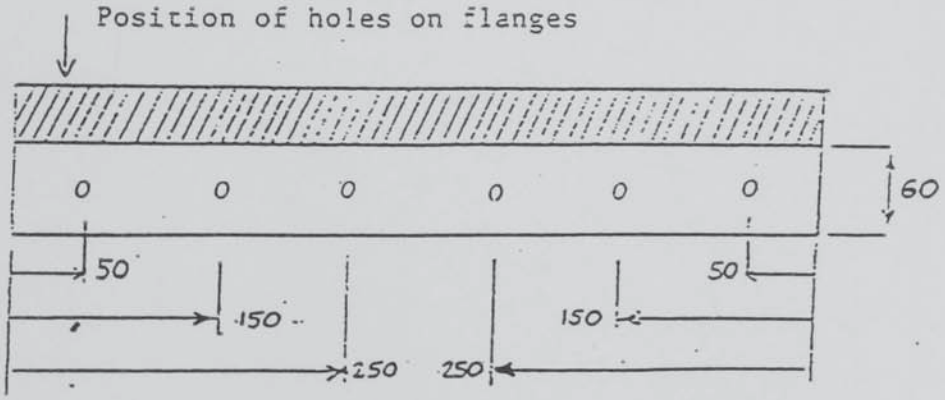

Fig. 7.6 **Model 7.5. Cylinder in two parts.**

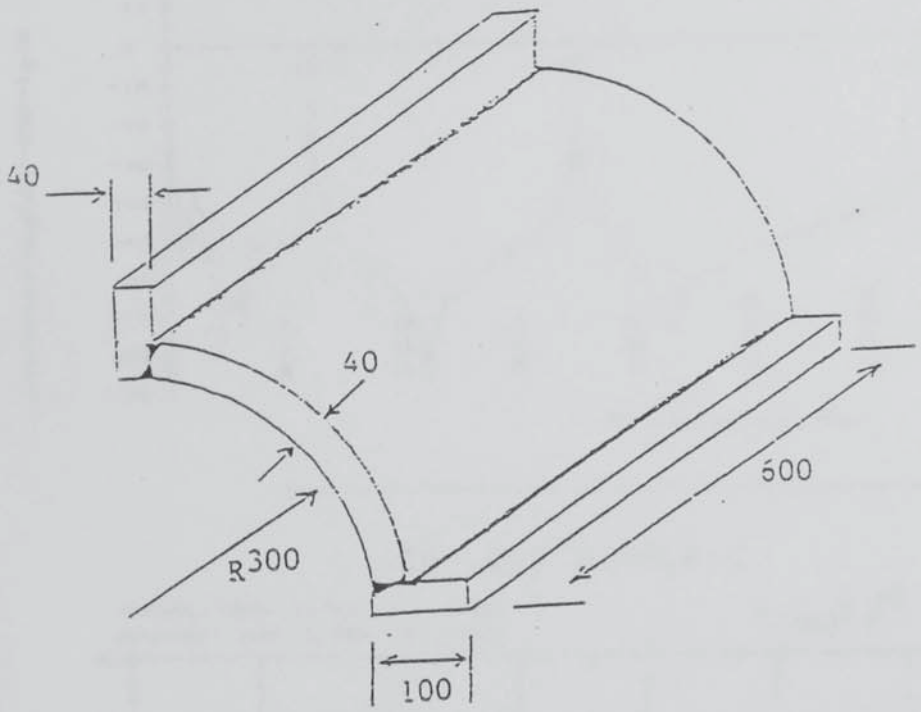

Fig. 7.7 **Model 7.6. Cylinder in 4 parts.**

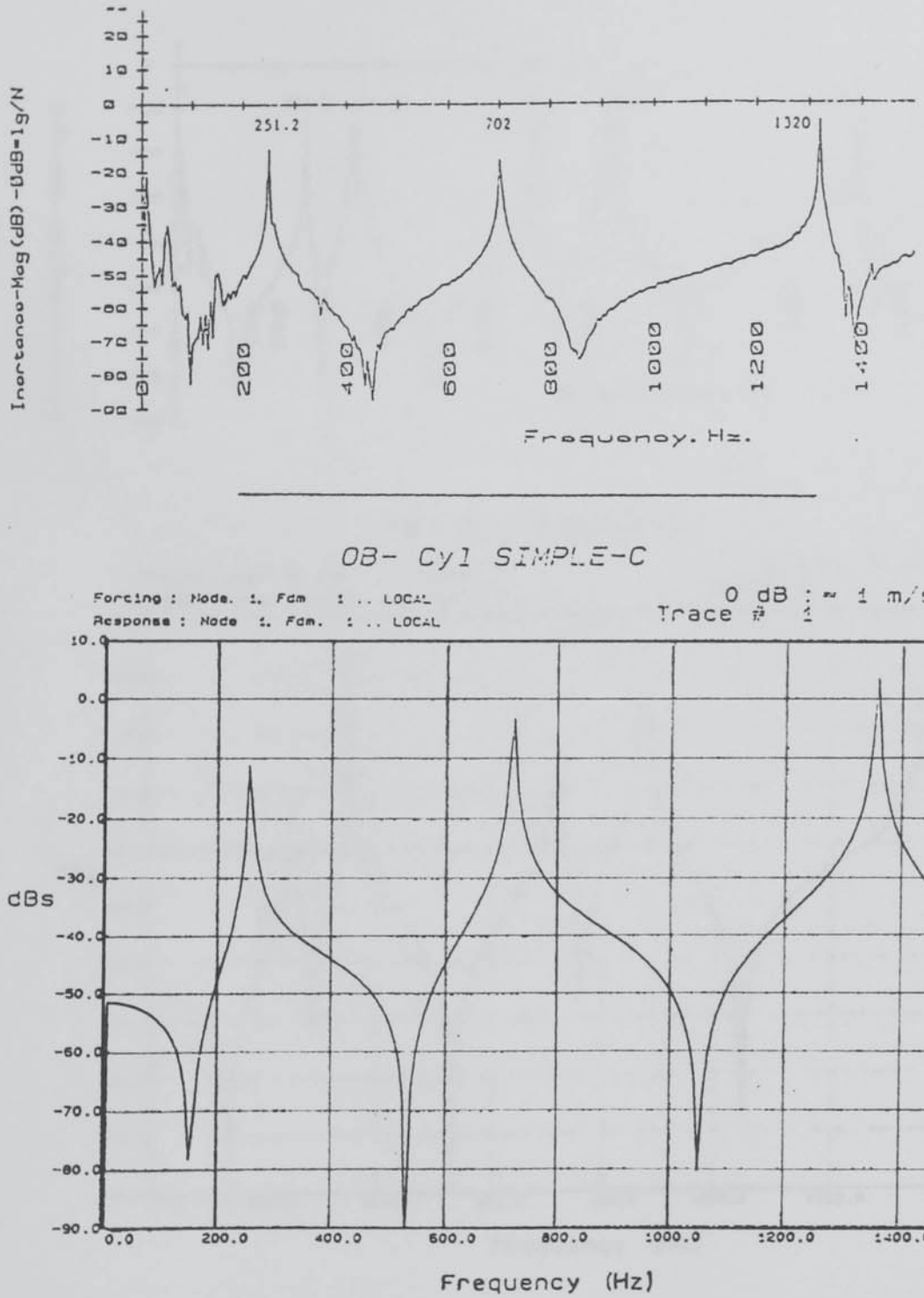

Fig. 7.8 **Measured and Predicted Response for Model 7.4 :- Axially Symmetric Modes.**

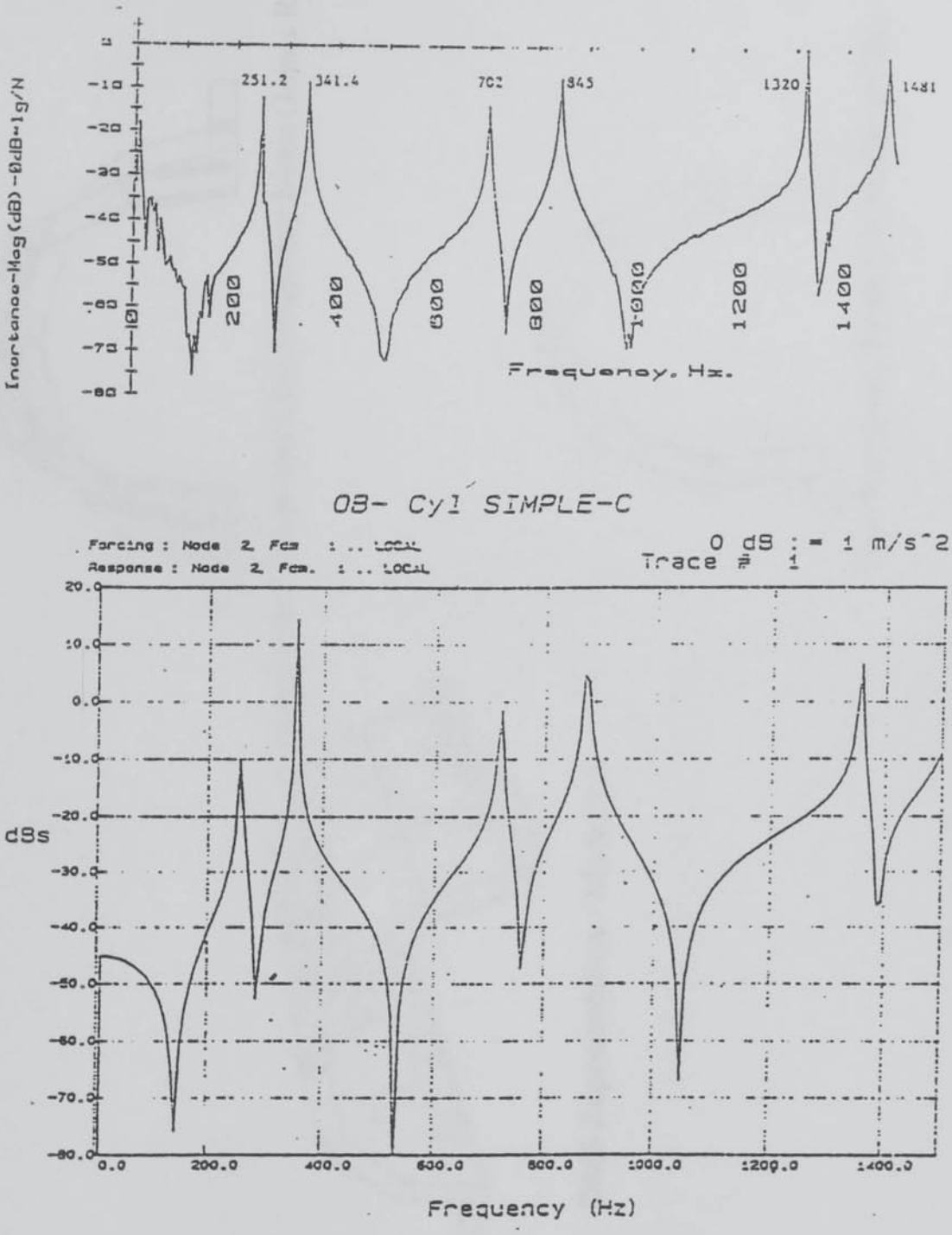

Fig. 7.9 **Measured and Predicted Response for Model 7.4 Axially Anti-Symmetric Modes.**

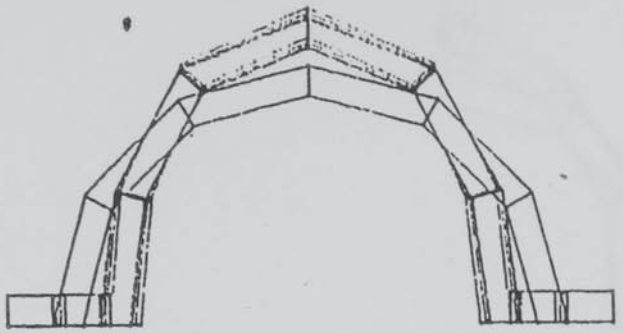

Undeformed Shape and Low-Frequency Mode (Joints Rigid)

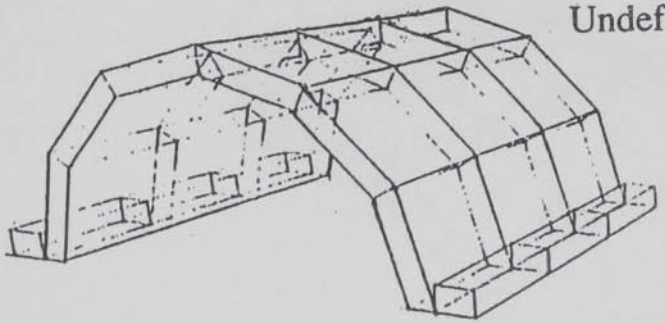

DMS Representation - Model 7.5.

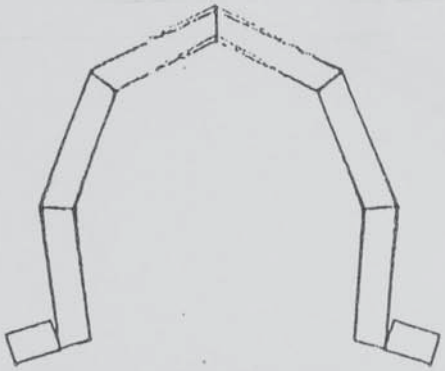

Low-Frequency Mode (Joints Flexibible).

Fig. 7.10 DMS Representation of Model 7.5

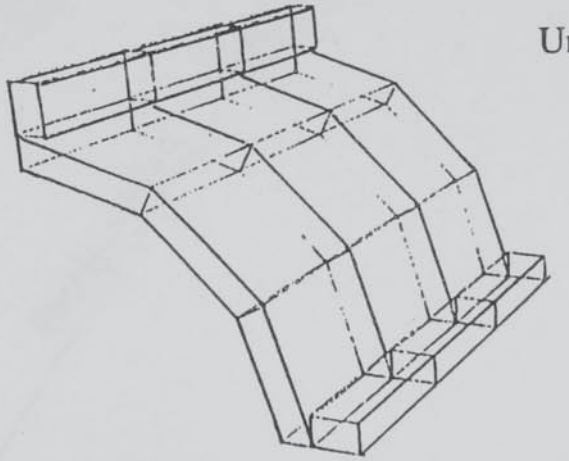

DMS Representation - Model 7.6.

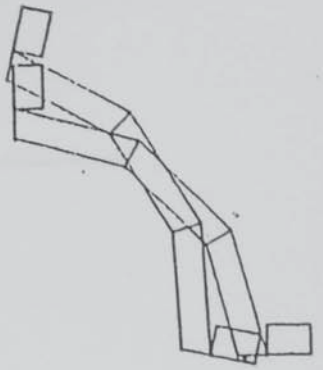

Undeformed Shape and Low-Frequency Mode (Joints Flexible)

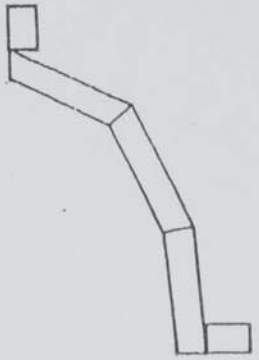

Low-Frequency Mode Shape(Joints Stiff).

Fig. 7.11 DMS Representation of Model 7.6

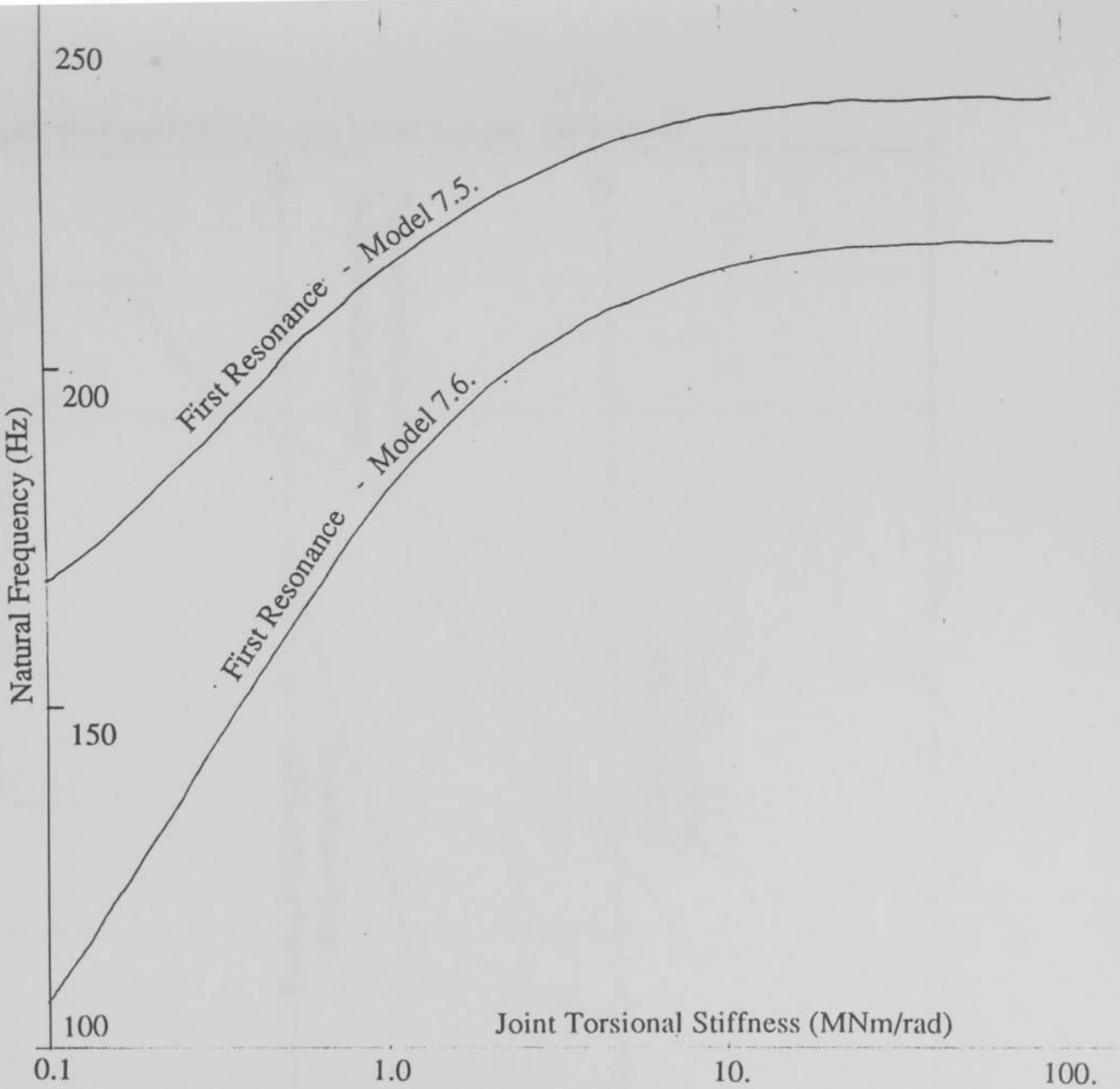

Fig. 7.12 **Derived Variation of Resonance with Joint Torsional Stiffness. (Models 7.5 and 7.6).**

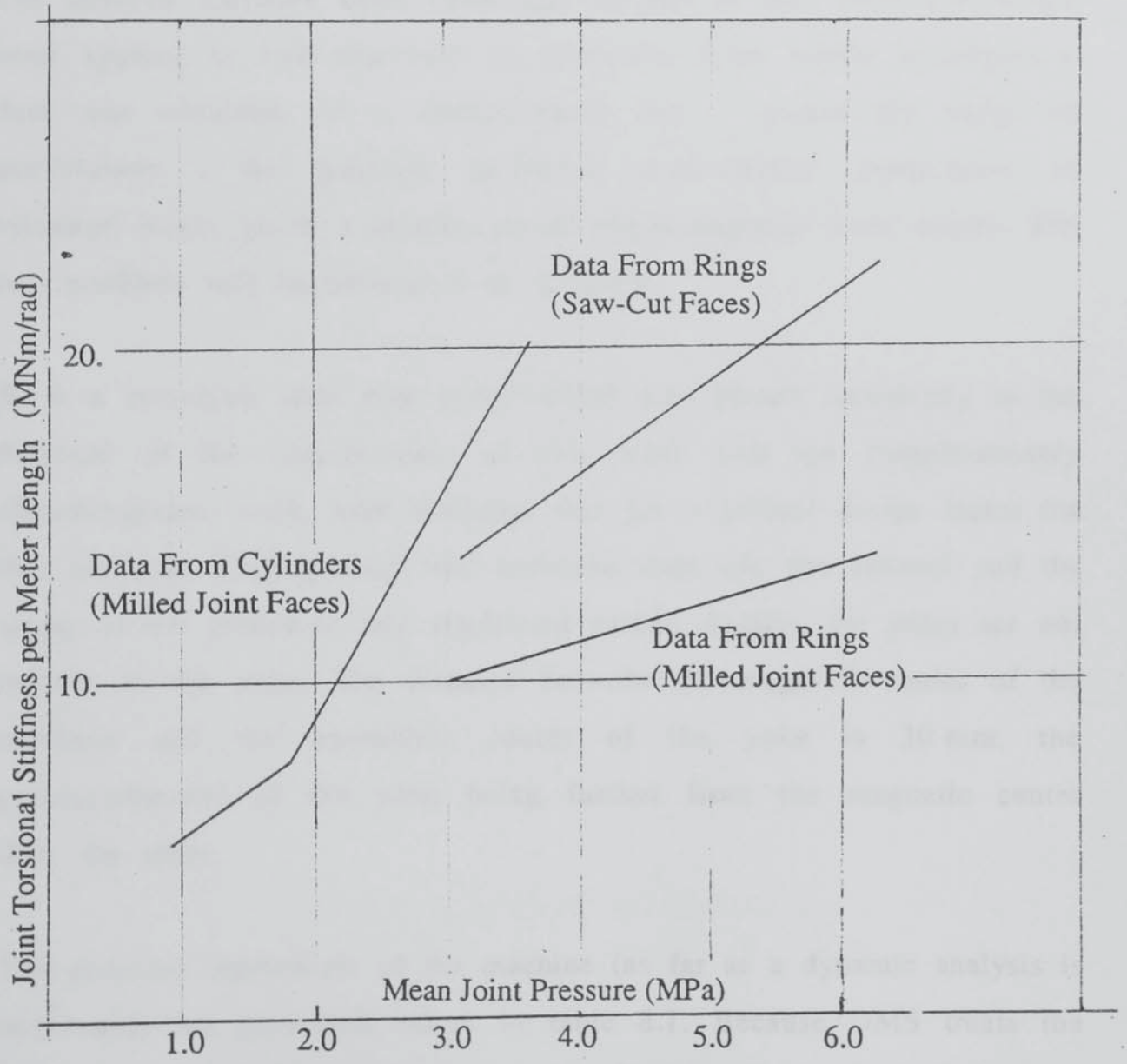

Fig. 7.13 **The Dependence of Joint Torsional Stiffness on Pressure.**

Chapter 8

CORRELATION WITH TWO MACHINES

The analysis software DMS developed as part of this investigation has been applied to two machines in particular from which experimental data was obtained. It is demonstrated that - within the range of uncertainty - the package produces good-quality predictions of vibration levels, given a reliable set of electromagnetic force values. The two machines will be referred to as **A** and **B**.

A is a prototype steel mill motor which was placed completely at the disposal of the requirements of this work and the complementary electromagnetic work. Low vibration was not a critical design factor for this machine. Consequently, the armature slots are not skewed and the airgap is not graded to any significant extent. Axially, the poles are not central on the yoke. The distance between the magnetic center of the machine and the geometric center of the yoke is 30 mm, the commutator-end of the yoke being further from the magnetic center than the other.

The principal dimensions of the machine (as far as a dynamic analysis is concerned) are presented below in table 8.1. Because DMS treats the poles as rectangular-section prisms, it is most convenient to present

only the equivalent prism dimensions for the mainpoles and compoles.

Length of Yoke	-	642 mm
Inside Radius of Yoke	-	319 mm
Outside Radius of Yoke	-	375 mm
Yoke Cylinder.	-	Complete.
Number of Poles	-	4
Mass of each Mainpole	-	62.5 kg
Axial Length of Mainpole	-	406 mm
Radius of Mainpole c.o.g.	-	251 mm
Radial Prism Dimension	-	136 mm
Ccmftl. Prism Dimension	-	170 mm
Mass of each Compole	-	15.2 kg
Axial Length of Compole	-	406 mm
Radius of Compole c.o.g.	-	259 mm
Radial Prism Dimension	-	120 mm
Ccmftl. Prism Dimension	-	40.9 mm

Table 8.1 Principal Dimensions of Machine **A**.

B is a propulsion motor on which an extensive set of tests were carried out as part of another contract. It is a double-armature machine. Only one "half" of the machine was instrumented in detail and only one half

of the stator frame is modelled since the joining section between the two yokes is relatively flexible. The airgap under the mainpoles is graded and the armature is herringbone-skewed. The machines mainpoles are laminated and the compoles are solid. The magnetic center armature coincides axially with the center of the yoke and the poles. A compole is located at the top dead center of the frame and compoles are bolted on at the splits in the yoke which occur in the same horizontal plane as the machine axis.

The principal dimensions of machine **B** are given in table 8.2 below. Again, in giving the pole dimensions, only the equivalent prism dimensions are necessary.

In the case of both machines, both static and running tests have been done. The static tests are undoubtedly the better test of the software since the forcing is such that a good many modes are excited to some measureable extent and the value of the forcing is known to very good accuracy. In the case of the running tests, it must be borne in mind that the input to the mechanical analysis is computed not measured. Some degree of error is inevitable here. Wignall (A.1987) discusses the errors in his predictions of flux ripple on the machine poles. The proportion of errors in the resulting electromagnetic forces computed will be <u>at least twice</u> the proportion of errors in the magnetic flux ripple since force is derived from flux density by a square-law. In particular, the forcing on the compoles has considerable uncertainty associated with it. The compole forces have not been used directly though their effect is demonstrated.

There are also mechanical sources of uncertainty. The stiffness and damping of the joints between the pole and yoke can be estimated for the machines from the experimental work done on the subject (reported

Length of Yoke	-	788 mm
Inside Radius of Yoke	-	1390 mm
Outside Radius of Yoke	-	1525 mm
Yoke Cylinder.	-	Split in the Horizontal Plane Containing the Machine Axis.
Number of Poles	-	12
Mass of each Mainpole	-	332 kg
Axial Length of Mainpole	-	630 mm
Radius of Mainpole c.o.g.	-	1404 mm
Radial Prism Dimension	-	243 mm
Ccmftl. Prism Dimension	-	284 mm
Mass of each Compole	-	71.5 kg
Axial Length of Compole	-	630 mm
Radius of Compole c.o.g.	-	1276 mm
Radial Prism Dimension	-	228 mm
Ccmftl. Prism Dimension	-	64 mm

Table 8.2 Principal Dimensions of Machine **B**.

in chapter 6) and a knowledge of the shim numbers and materials. However, there is a considerable uncertainty and scatter associated with these values as mentioned in chapter 6. This scatter is very apparent in the irregularity of the operating-shapes measured on machine **B**.

The properties of the laminated poles as determined by experiment (chapter 5) are quite reliable as demonstrated later in this chapter. The properties of the split in machine **B** are subject to some uncertainty also. The effect of this uncertainty is difficult to assess. It will certainly cause small shifts in the various resonant frequencies but the response of the stator over broad bands of frequency will not be seriously affected. One very important determinant of the vibration levels has been found to be the field coils and the stiffness+damping of the connection between each coils and its respective pole. Some of the tests done on machine **A** reflect approximate values for the connection between the main field coils and the mainpoles for this particular machine. The operating stiffnesses and damping values of the field coils of machine **B** are estimated for the purposes of the calculations. Apart from the measurements on machine **A**, there is no background to these estimates and the values used will inevitably have a noticeable effect on the vibration levels computed.

§8.1 Static Tests on Machine A.

Machine **A** was dismantled and tested in various stages of assembly to provide a thorough understanding and verification of the relevant quantities. The static tests done showed up a number of modes of

varying complexity in the relatively low-frequency band of 0-1 kHz. There is frequent reference in this section to the "principal" modes of the frame. These are modes in which a high proportion of the kinetic and potential energy resides in the yoke (+poles) rather than in the end-brackets.

8.1.1 Tests on the Stripped Frame of Machine A.

Initially, the armature of this machine was removed and all poles removed to leave only the all-welded assembly of the frame. The frame was stood upright on one of the end-brackets, on a softwood base to emulate approximately the free boundary condition Fig. 8.1a. There was no likely source of non-linearity and so it was appropriate to excite the structure using a hammer with calibrated force-transducer. Response was measured at a number of points using an accelerometer mounted on a magnetic base over a thin layer plasticine to accomodate the curvature of the barrel. A number of resonances were apparent and there was a clear distinction between the modes symmetrical w.r.t. the plane of symmetry of the machine and those anti-symmetrical w.r.t. this plane. Mode shapes were investigated for each of the resonances below 1000 Hz. The results of these tests were input to a small dedicated program which was used to process them and produce the visual impressions of the modes. Two of these views are presented later for comparison with the computed mode shapes.

The frame itself is not a geometrically simple structure. The rolled steel cylinder makes up some 86% of the mass. Yet the low frequency modes

are dominated by deflections at the end brackets. Originally, it was envisaged that the outcome of these tests could be used directly as a practical evaluation of the correctness of the cylinder model prepared as part of the software. The frame of machine **A** was clearly not suited to this purpose. Instead, the structure-synthesis techniques used in the software for assembling a motor model from its components have been employed to generate a representation of the bare frame of machine **A**.

The end-brackets are modelled using simple rectangular-section rings coupled to the yoke via thin-walled cylinders. The frame is not so simple in reality but use of some engineering intuition in establishing equivalent dimensions (for the thin-walled cylinders in particular) has produced relatively good results. The feet of the machine are modelled quite exactly using the triangular uniform-plate finite-element facility within DMS. The image generated for this model is shown in Fig. 8.1b. It is important to remember that this wire-frame is not the product of a finite-element analysis package and so the true boundaries of the solids are not necessarily delineated.

The DMS model was used to predict the response of four point displacements (P1-P4 on Fig. 8.1b). This forcing causes only those modes which are symmetrical w.r.t the machines' plane of symmetry to become excited. The measured frequency-response are transcribed onto similar scales for comparison purposes. Fig.s 8.2 and 8.3 show both the measured and predicted responses for the frame. There is a small discrepancy between measured and predicted responses in the resonance frequencies which can be accounted-for by the

approximation used for the end-brackets. Otherwise, the agreement is good.

Correlation of the mode-shapes is equally good. Fig.s 8.4 and 8.5 compare two measured mode-shapes with those computed.

The evidence suggests that the modelling of the components used for the frame and the structure-synthesis software is correct.

8.1.2 Tests on The Frame with two Mainpoles Attached.

Following the tests on the bare frame, two mainpoles were attached to the frame without their field-coils. The structure remained on end on top of a softwood base. The frame was again excited by striking it with a hammer. In this case, only the resonance peaks of the principal modes were of interest and sufficient details of each were manually recorded to make a good estimate of the damping of the modes using the method mentioned in chapter 6.

Again, a DMS model was prepared. This time, the feet and end-brackets were not included as attention was confined to two modes which are not significantly affected by them. An end-on view of this model is shown in Fig. 8.6 with three mode shapes. Shape 1 involves the poles rocking in the same sense as the yoke does behind them. If the pole-yoke joints were completely rigid, there would obviously be no relative motion between the poles and the yoke. The presence of some flexibility in these joints allows each pole to rock more than the yoke behind it does

in the low-frequency modes. This flexibility also introduces a mode at higher frequency similar to shape 2 of Fig. 8.6. In this mode, the pole rocks in the opposite sense to the yoke behind it. Shape 2 shows the yoke deforming in a classical n=2 fashion. This will only be the case if the joint rocking flexibility is relatively large. Shape 3 would be the second non-rigid-body mode of the assembly if the joints were rigid. In fact, shape 1 is very similar to the first of the two modes in which we are interested and shape 3 is like the second.

The two resonances of interest of the assembly were found by striking the yoke centrally between the poles and measuring at the same position. (Half-way down the axial length). The mode shapes were checked using the convenient technique of striking different points on the structure and measuring response (acceleration) at the one point all the time. The modal data for these is given below in table 8.3

Mode	Frequency (Hz)	Damping Factor (Hysteretic)
1	264	6.1e-3
2	715	9.3e-3

Table 8.3 Frequency and Damping for Two Modes of the Frame with 2 Mainpoles.

By using different joint stiffness values in the theoretical model of this assembly, the relation between the joint-stiffness and the natural

frequencies of the two modes can be established. This has been done and the relations are graphically presented in Fig.s 8.7a and 8.7b. Comparing the measured frequencies with these relations leads to a value for the effective torsional stiffness of the pole-yoke joints of 77 MNm/rad. It was shown in chapter 6 that this agrees with the values given for the joint stiffness.

8.1.3 Frame with two Mainpoles+Field Coils.

The field coils were then replaced on the mainpoles with the original packing and the mainpoles were re-attached in the same position. The resonant frequency of mode 1 was shifted down by 16 Hz from 264 to 248 Hz. The DMS model of a pole and field coil was used to represent this assembly. If the coils were rigidly mounted on the poles, the drop in the resonance would have been some 22.5 Hz. Inserting a number of different stiffness values into the theoretical model leads to an approximate figure of 1.9e8 N/m for the stiffness of the side-to-side motion of this coil on its pole. (More than one value of stiffness can be chosen for this joint which would result in a resonance at 248 Hz but knowledge of the approximate mode shape enables us to discriminate the 'correct' one). The associated characteristic resonance is 345 Hz. Thus, at frequencies above 345 Hz, the main field-coils will behave as added stiffness to the system whilst at frequencies below this threshold, they behave as added mass. It must be reiterated that the value of 1.9e8 is approximate since other changes may have occurred in the structure when the pole was removed and replaced which would account for some frequency shift.

8.1.4 Frame with two Compoles and Coils.

The next arrangement tested was the frame with two compoles attached as shown in Fig. 8.8. Again, three possible mode-shapes of the assembly are shown. Shape 1 is the lowest frequency mode if the joint between the compoles and the yoke is very flexible. Shape 2 is a low-frequency mode which is independent of the rocking flexibility of the pole-yoke joint. Shape 3 is a higher frequency mode in which the compoles rock in the opposite sense to the yoke behind them.

The coils could not easily be removed from the compoles of this particular machine as they were resin-bonded on. In the event, it was not possible to isolate the effects of the two different connections present (pole-yoke and coil-pole). Assuming that there is an intimate contact between the coil and the compole here allows a crude hand calculation to be performed to quantify the stiffness of the connection between the pole and coil based on the compressibility of the insulation layer. The resulting value is 1.9e10 N/m for the side-to-side motion. The characteristic resonance of the coil on a fixed pole would then be 4.4 kHz. For our purposes, this connection may sometimes be considered rigid. Two principle resonances of the frame with two compoles below 1 kHz occurred at 272 Hz and 706 Hz. The resonance at 272 Hz involves the compoles simply translating inwards and outwards and so tells us nothing of the torsional flexibility of the pole-yoke joint. Using the software to analyse the second principle resonance leads to a value of 11.0 MNm/rad for the torsional stiffness of the joint. This is in good

agreement with the work of chapter 6.

8.1.5 Tests on an Individual Mainpole.

A test was done on one of the mainpoles in which the pole was suspended on a rope (through an eye-bolt in the back) and struck on the end to excite both torsional and compression/extension modes. (The mainpoles are laminated and each individual lamination is nominally 1.6mm deep.) The resonances measured were 1002 Hz for the first torsional mode and 2515 Hz for the first axial compression/extension mode. Treating this pole in the same way as the beams of chapter were analysed yields values for the effective shear and Young's modulii of 0.55 GPa and 1.25 GPa respectively. These values are in good agreement with what we would have predicted based on the tests reported in chapter 5.

8.1.6 Static Tests on Complete Stator of Machine A.

All poles and field coils were replaced in the frame (Fig. 8.9) and impulse tests done to compare predicted (based on experimentally derived properties) and measured natural frequencies. The results of this comparison are presented below in table 8.4. (There were other minor resonances in the case of both models which were not matched).

Mode Number	Predicted Resonance (Hz)	Measured Resonance (Hz)	Damping. Factor
1	216.5	214.0	8.0e-3
2	412.1	416.0	4.5e-3
3	641.2	608.0	7.0e-3
4	814.0	795.0	1.0e-2
5	915.0	902.0	9.5e-3

Table 8.4 Measured and Predicted Resonances for Complete Unthreaded Stator of Machine A.

§8.2 Running Tests on Machine A.

Machine A was reassembled completely, located on a base-plate capable of withstanding the full-load torque produced by it and connected "back-to-back" with a similar motor of slightly smaller size. The machine was instrumented with accelerometers at the ten positions shown in Fig. 8.10. Measurements were taken for a number of running conditions and stored on tape. These measurements were later analysed to extract the frequency components at the fundamental slot-passing frequency and the second harmonic of this frequency. Accelerometer "R2N" measures radial acceleration on mainpole 2 at the non commutator end. Accelerometer "A1C" measures axial acceleration on mainpole 1 at the commutator end. Accelerometer "R01" is one of the

accelerometers measuring the radial vibration on the outside of the yoke.

8.2.1 Five Running Conditions for Machine A.

For five running conditions, a correlation has been done between the predicted vibration levels and those measured. The prediction of the forces was produced by Wignall using electromagnetic finite-element software. As part of a verification exercise for the electromagnetic part of the investigation, slots had been machined in the mainpoles (centrally on the faces). The forcing on the mainpoles is significantly greater than that on the compoles because of the very sudden change in airgap length caused by the slot. The mean airgap under the compole is larger in any case. Only the mainpole forces have been applied in the mechanical analysis for correlation, though the effect of the compole forces is demonstrated.

In the case of all five of the conditions presented here, the fundamental slot-passing frequency occurs between 460 Hz and 475 Hz.

Two analyses have been done.

(1) Coils are disregarded and the poles are assumed to be rigidly affixed to the yoke. No account is taken of constraints present at the machine feet. This analysis preceded the close examination of the results from the pole-yoke joint study and is useful in demonstrating the extra error incurred by

simplifying the problem in this way.

(2) The effects of the coils and that of pole-root flexibility is incorporated and constraints are introduced at the feet to simulate the conditions there. Fig.s 8.11a and 8.11b illustrate two of the operating shapes calculated for machine A using this analysis.

For each of the tests 8.2.1-8.2.5, the running conditions are summarised with the computed forces acting on the pole in a single table and the vibration levels predicted (using both the simplified analysis and the more general one) are tabulated together with the actual measured values.

Test	-	8.2.1.
Slot-passing Frequency	-	460 Hz
Field Current	-	4.0 A
Armature Current	-	130 A
Armature Voltage	-	180 V
Harmonic 1	ω^2= 8.35 e6 s^{-2}	
Computed Total Radial Force on Mainpoles	351 N	@ 0°
Computed Total Ccmftl Force on Mainpoles	190 N	@ 0°
Computed Total Moment Force on Mainpoles	3.13 Nm	@ -66°
Harmonic 2	ω^2= 33.4e6 s^{-2}	
Computed Total Radial Force on Mainpoles	45.2 N	@ -4°
Computed Total Ccmftl Force on Mainpoles	49.7 N	@ +2°
Computed Total Moment Force on Mainpoles	1.55 Nm	@ -75°

Table 8.5 Machine Conditions and Computed Forces on Mainpoles for Test 8.2.1

The comparison between predicted and measured vibration levels at the fundamental slot-passing frequency on the machine from test 8.2.1 is presented in table 8.6 below.

Acclmtr.	Measured (m)	Prediction 1 (m)	Error(dB)	Prediction 2 (m)	Error(dB)
C2N	1.31e-7	6.30e-7	13.6	1.92e-7	3.3
A2C	1.86e-8	1.24e-9	-23.5	1.10e-9	-24.6
C2C	3.71e-7	7.23e-7	5.8	4.25e-7	1.2
R1N	5.21e-7	2.89e-7	-5.1	3.31e-7	-3.9
R1C	2.08e-7	2.37e-7	1.1	2.10e-7	0.1
A1C	1.86e-7	6.49e-9	-29.1	2.20e-9	-38.5
R01	2.09e-7	4.61e-7	6.9	2.39e-7	1.2
R02	1.47e-7	1.45e-7	-0.1	1.13e-7	-2.3
R03	1.65e-7	3.41e-7	6.3	2.52e-7	3.7
R04	1.47e-7	3.62e-7	7.8	1.54e-7	0.4

Table 8.6 Measured and Predicted Vibration Levels Fundamental Slot-Passing Frequency. (Test 8.2.1).

The comparison for the second harmonic of slot-passing frequency is presented in table 8.7 below.

Acclmtr.	Measured (m)	Prediction 1 (m)	Error(dB)	Prediction 2 (m)	Error(dB)
C2N	3.30e-7	1.06e-7	-9.9	2.07e-7	-4.1
A2C	9.31e-8	2.45e-9	-31.6	1.82e-9	-34.2
C2C	1.66e-7	9.16e-8	-5.2	1.98e-7	1.5
R1N	2.61e-7	5.25e-9	-33.2	1.82e-7	-3.1
R1C	4.66e-7	1.51e-8	-29.8	2.24e-7	-6.4
A1C	3.30e-7	2.33e-9	-43.0	1.67e-9	-45.9
R01	3.29e-8	5.39e-8	4.3	4.00e-8	-0.5
R02	6.57e-8	7.55e-8	1.2	5.16e-8	-2.1
R03	3.29e-8	6.51e-8	5.9	4.08e-8	1.9
R04	5.22e-8	3.00e-8	-4.8	3.82e-8	-2.7

Table 8.7 Measured and Predicted Vibration Levels
2^{nd} Harmonic of Slot-Passing Frequency. (Test 8.2.1).

Condition	-	8.2.2.
Slot-passing Frequency	-	465 Hz
Field Current	-	4.0 A
Armature Current	-	250 A
Armature Voltage	-	180 V
Harmonic 1	ω^2= 8.54 e6 s^{-2}	
Computed Total Radial Force on Mainpoles	359 N	@ 0°
Computed Total Ccmftl Force on Mainpoles	191 N	@ 0°
Computed Total Moment Force on Mainpoles	3.05 Nm	@ -69°
Harmonic 2	ω^2= 34.1e6 s^{-2}	
Computed Total Radial Force on Mainpoles	44.3 N	@ -4°
Computed Total Ccmftl Force on Mainpoles	49.5 N	@ +2°
Computed Total Moment Force on Mainpoles	1.58 Nm	@ -73°

Table 8.8 Machine Conditions and Computed Forces on Mainpoles for Test 8.2.2

The comparison between predicted and measured vibration levels at the fundamental slot-passing frequency on the machine from test 8.2.2 is presented in table 8.9 below.

Acclmtr.	Measured (m)	Prediction 1 (m)	Error(dB)	Prediction 2 (m)	Error(dB)
C2n	1.27e-7	6.51e-7	14.2	1.89e-7	3.5
A2C	1.01e-7	1.60e-9	-36.1	1.35e-9	-37.5
C2C	3.19e-7	7.63e-7	7.6	4.21e-7	2.4
R1N	4.01e-7	3.37e-7	-1.5	3.00e-7	-2.5
R1C	1.60e-7	2.79e-7	4.8	2.02e-7	2.0
A1C	2.01e-7	6.32e-9	-30.0	1.21e-9	-45.1
R01	2.54e-7	4.02e-9	4.0	2.40e-7	-6.9
R02	2.85e-7	1.40e-7	-6.2	1.89e-7	-3.6
R03	1.60e-7	3.62e-7	7.1	2.40e-7	3.5
R04	1.43e-7	3.46e-7	7.7	1.62e-7	1.1

Table 8.9 Measured and Predicted Vibration Levels Fundamental Slot-Passing Frequency. (Test 8.2.2).

The comparison for the second harmonic of slot-passing frequency is presented in table 8.10 below.

Acclmtr.	Measured (m)	Prediction 1 (m)	Error(dB)	Prediction 2 (m)	Error(dB)
C2N	2.85e-7	1.07e-7	-8.5	1.98e-7	-3.2
A2C	8.03e-8	2.51e-9	-30.1	2.03e-9	-31.9
C2C	1.43e-7	1.17e-7	-1.7	1.82e-7	2.1
R1N	2.52e-7	5.42e-9	-33.3	1.73e-7	-3.3
R1C	5.04e-7	1.11e-8	-33.7	2.20e-7	-7.2
A1C	4.01e-7	2.62e-9	-43.7	2.61e-9	-45.7
R01	1.60e-8	5.96e-8	11.4	3.04e-8	5.6
R02	4.52e-8	8.22e-8	5.2	6.61e-8	1.0
R03	2.53e-8	7.21e-8	9.1	4.51e-8	3.9
R04	6.37e-8	3.44e-8	-5.4	4.92e-8	-4.2

Table 8.10 Measured and Predicted Vibration Levels
2^{nd} Harmonic of Slot-Passing Frequency. (Test 8.2.2).

Condition	-	3.
Slot-passing Frequency	-	465 Hz
Field Current	-	4.0 A
Armature Current	-	380 A
Armature Voltage	-	176 V
Harmonic 1	ω^2= 8.54e6 s^{-2}	
Computed Total Radial Force on Mainpoles	360 N	@ 0°
Computed Total Ccmftl Force on Mainpoles	193 N	@ 0°
Computed Total Moment Force on Mainpoles	2.67 Nm	@ -57°
Harmonic 2	ω^2= 34.1 e6 s^{-2}	
Computed Total Radial Force on Mainpoles	44.2 N	@ -4°
Computed Total Ccmftl Force on Mainpoles	49.2 N	@ +2°
Computed Total Moment Force on Mainpoles	1.62 Nm	@ -73°

Table 8.11 Machine Conditions and Computed Forces on Mainpoles for Test 8.2.3

The comparison between predicted and measured vibration levels at the fundamental slot-passing frequency on the machine from test 8.2.3 is presented in table 8.12 below.

Acclmtr.	Measured (m)	Prediction 1 (m)	Error(dB)	Prediction 2 (m)	Error(dB)
C2N	1.02e-7	6.52e-7	16.1	1.69e-9	4.4
A2C	9.70e-8	1.64e-9	-35.4	1.32e-9	-37.3
C2C	1.61e-7	7.48e-7	13.3	3.01e-7	5.4
R1N	3.59e-7	3.38e-7	-0.5	2.57e-7	-1.7
R1C	1.43e-7	2.79e-7	5.8	1.99e-7	2.9
A1C	1.61e-7	6.33e-9	-28.9	5.42e-9	-29.5
R01	2.03e-7	4.83e-7	7.5	2.45e-7	1.6
R02	2.87e-7	1.40e-7	-6.2	1.93e-7	-3.4
R03	1.61e-7	3.64e-7	7.1	2.52e-7	3.9
R04	1.61e-7	3.48e-7	6.7	1.72e-7	0.6

Table 8.12 Measured and Predicted Vibration Levels Fundamental Slot-Passing Frequency. (Test 8.2.3).

The comparison for the second harmonic of slot-passing frequency is presented in table 8.13 below.

Acclmtr.	Measured (m)	Prediction 1 (m)	Error(dB)	Prediction 2 (m)	Error(dB)
C2N	2.03e-7	9.41e-8	-6.7	1.54e-7	-2.4
A2C	1.02e-7	2.45e-9	-32.4	2.01e-9	-32.4
C2C	2.28e-7	1.08e-7	-6.5	1.75e-7	-2.3
R1N	2.02e-7	5.19e-9	-31.8	1.51e-7	-2.5
R1C	5.08e-7	1.14e-8	-33.0	2.67e-7	-5.6
A1C	4.03e-7	2.41e-9	-44.5	2.55e-9	-44.0
R01	7.20e-9	5.54e-8	17.7	2.11e-8	9.3
R02	8.08e-9	7.71e-8	19.6	4.12e-8	14.1
R03	2.03e-8	6.69e-8	10.4	3.21e-8	4.0
R04	5.41e-8	3.11e-8	-4.8	4.36e-8	-1.9

Table 8.13 Measured and Predicted Vibration Levels
2^{nd} Harmonic of Slot-Passing Frequency. (Test 8.2.3).

Condition	-	4.
Slot-passing Frequency	-	472.5 Hz
Field Current	-	1.6 A
Armature Current	-	255 A
Armature Voltage	-	85 V
Harmonic 1	ω^2= 8.81 e6 s^{-2}	
Computed Total Radial Force on Mainpoles	71.4 N	@ 0°
Computed Total Ccmftl Force on Mainpoles	29.6 N	@ 0°
Computed Total Moment Force on Mainpoles	3.10 Nm	@ -74°
Harmonic 2	ω^2= 35.3 e6 s^{-2}	
Computed Total Radial Force on Mainpoles	17.3 N	@ -10°
Computed Total Ccmftl Force on Mainpoles	12.8 N	@ +6.1°
Computed Total Moment Force on Mainpoles	1.71 Nm	@ -85.3°

Table 8.14 Machine Conditions and Computed Forces on Mainpoles for Test 8.2.4

The comparison between predicted and measured vibration levels at the fundamental slot-passing frequency on the machine from test 8.2.4 is presented in table 8.15 below.

Acclmtr.	Measured (m)	Prediction 1 (m)	Error(dB)	Prediction 2 (m)	Error(dB)
C2N	1.51e-8	1.50e-7	0.0	3.52e-8	7.8
A2C	8.51e-9	4.13e-10	-26.3	5.14e-8	-24.4
C2C	3.79e-8	1.32e-7	9.2	7.25e-8	5.6
R1N	9.55e-8	8.21e-8	-1.3	8.73e-8	-0.8
R1C	3.79e-8	6.23e-8	4.3	5.13e-8	2.6
A1C	2.40e-8	1.17e-9	-26.2	9.35e-10	-8.2
R01	3.01e-8	1.01e-7	10.5	3.13e-8	7.5
R02	1.90e-8	2.20e-8	1.3	2.61e-8	2.8
R03	3.01e-8	5.39e-8	5.1	4.89e-8	4.2
R04	2.13e-8	4.68e-8	6.8	3.35e-8	3.9

Table 8.15 Measured and Predicted Vibration Levels Fundamental Slot-Passing Frequency. (Test 8.2.3).

The comparison for the second harmonic of slot-passing frequency is presented in table 8.16 below.

Acclmtr.	Measured (m)	Prediction 1 (m)	Error(dB)	Prediction 2 (m)	Error(dB)
C2N	9.53e-8	5.33e-8	-5.0	7.72e-8	-1.8
A2C	3.39e-8	1.18e-9	-9.2	3.21e-9	-20.5
C2C	6.01e-8	4.61e-8	-2.3	4.36e-8	-2.8
R1N	1.70e-7	3.18e-8	-14.5	6.97e-8	-7.7
R1C	1.70e-7	6.68e-8	-8.1	8.65e-8	-5.9
A1C	1.20e-7	1.11e-9	-40.7	8.21e-8	-23.3
R01	7.55e-9	2.70e-8	11.1	1.93e-8	8.2
R02	1.07e-8	3.61e-8	10.6	2.52e-8	7.4
R03	8.47e-9	3.18e-8	11.5	1.53e-8	5.1
R04	2.68e-8	1.74e-8	16.2	2.97e.8	0.9

Table 8.16 Measured and Predicted Vibration Levels
2^{nd} Harmonic of Slot-Passing Frequency. (Test .8.2.3).

Condition	-	5.
Slot-passing Frequency	-	471.0 Hz
Field Current	-	1.6 A
Armature Current	-	255 A
Armature Voltage	-	85 V
Harmonic 1	ω^2= 8.76 e6 s^{-2}	
Computed Total Radial Force on Mainpoles	89.9 N	@ 0°
Computed Total Ccmftl Force on Mainpoles	43.5 N	@ 0°
Computed Total Moment Force on Mainpoles	0.45 Nm	@ +48.1°
Harmonic 2	ω^2= 35.0 e6 s^{-2}	
Computed Total Radial Force on Mainpoles	17.1 N	@ +10.5°
Computed Total Ccmftl Force on Mainpoles	14.1 N	@ +5.1°
Computed Total Moment Force on Mainpoles	2.83 Nm	@ +90°

Table 8.17 Machine Conditions and Computed Forces on Mainpoles for Test 8.2.4

The comparison between predicted and measured vibration levels at the fundamental slot-passing frequency on the machine from test 8.2.4 is presented in table 8.18 below.

Acclmtr.	Measured (m)	Prediction 1 (m)	Error(dB)	Prediction 2 (m)	Error(dB)
C2N	6.98e-9	1.91e-7	28.9	1.81e-8	8.3
A2C	6.99e-9	6.75e-10	-20.3	2.25e-10	-9.8
C2C	3.48e-8	1.66e-7	13.6	6.02e-8	6.0
R1N	9.88e-8	9.83e-8	0.0	1.05e-7	0.5
R1C	7.00e-8	8.22e-8	1.4	8.24e-8	1.4
A1C	3.51e-8	1.45e-9	-27.7	5.32e-10	-36.4
R01	4.39e-8	1.26e-7	9.2	8.21e-8	5.4
R02	2.77e-8	3.11e-8	1.0	2.51e-8	-1.9
R03	2.47e-8	8.32e-8	10.5	5.13e-8	6.3
R04	2.77e-8	7.12e-8	8.2	3.75e-8	-5.6

Table 8.18 Measured and Predicted Vibration Levels Fundamental Slot-Passing Frequency. (Test 8.2.3).

The comparison for the second harmonic of slot-passing frequency is presented in table 8.19 below.

Acclmtr.	Measured (m)	Prediction 1 (m)	Error(dB)	Prediction 2 (m)	Error(dB)
C2N	1.24e-7	4.22e-8	-9.0	9.53e-8	-2.3
A2C	3.51e-8	1.11e-9	-29.4	3.03e-9	-21.3
C2C	6.98e-8	4.73e-8	-3.4	5.21e-8	-2.5
R1N	1.57e-7	3.13e-8	-14.0	7.33e-8	-6.6
R1C	1.75e-7	8.41e-8	-8.7	9.14e-8	-5.6
A1C	1.57e-7	9.25e-10	-44.6	7.35e-9	-26.6
R01	3.11e-9	2.41e-8	17.8	1.82e-8	15.3
R02	9.83e-9	3.26e-8	10.4	2.63e-8	9.5
R03	6.20e-9	2.29e-8	11.3	1.62e-8	8.3
R04	2.77e-8	1.49e-8	-5.4	3.08e-8	0.9

Table 8.19 Measured and Predicted Vibration Levels
2^{nd} Harmonic of Slot-Passing Frequency. (Test 8.2.3).

8.2.2 Discussion of Errors. :- Running tests on Machine A.

It is clear from the tables above that the response calculations produce figures of the correct order of magnitude but there is quite a large scatter. In fact, some of the numbers cause the analysis to look deceptively inaccurate for this machine. A closer consideration of some of the operating conditions shows that the total vibration energy

indicated by the measurements differs only by a small amount from the total energy calculated. There are a number of contributors to the discrepancies between the calculated responses and those measured.

The worst errors by far occur at the axial accelerometers A1C and A2C. In the calculations the only mechanism by which the ends of the mainpoles can be caused to vibrate in the axial direction is a "bowing" of the mainpole so that the center of the pole translates radially outward more than the ends do. Then, because the length of the pole at the back tends to be held constant by the yoke, the length of the pole at the airgap decreases slightly. The mainpoles are laminated so that their stiffness in axial compression is much lower than one would expect for similar lumps of solid steel. Machine **A** has an unskewed armature and so there is no forcing which would directly incline the mainpole to deform in the manner suggested here.

In reality, the armature slots produce a ripple force on the end of the poles exciting them in the axial direction. This force is not catered for in the electromagnetic analysis and so cannot be modelled here. In the case of machine **A**, therefore, it is to be expected that the measurements of axial vibrations at the mainpoles will greatly exceed the predictions.

The circumferential measurements (C2C and C2N) and the radial measurements (R1C and R1N) on the mainpole rank next in order of errors. It is clear that the mainpole is moving significantly relative to the yoke. The exact values of the pole root flexibility are essential to

an accurate prediction of the vibrations at the ends of the mainpoles. The circumferential vibrations are dependent on the stiffness of the fixture of the coil on the mainpole. When the armature current is zero, it is to be expected that the compole forces are zero. The vibrations associated with low armature-current conditions can be computed quite well by considering only the forces acting on the mainpoles. The increase in error with armature current is evident from the tables. Radial forces acting on the compoles primarily influence the circumferential vibrations of the mainpole and vice-versa.

The best agreements between the measured and predicted vibration levels are the radial vibration figures on the outside of the yoke which are also the most important. The chief determinant of the ratios (both in magnitude and phase) between each of these radial motions is the stiffness of the yoke itself compared with the stiffness of the fixing between the feet and the base-plate. The yoke is modelled very accurately but the characteristics of the fixing of the feet are somewhat uncertain. It has been assumed in the more detailed analysis that the feet are totally free to move except that translation vertically upward is totally prohibited. There is not sufficient information in the tests done to test the validity of that assumption, but it appears to improve the estimates made compared with assuming that the feet are totally unconstrained.

The predictions made for the fundamental slot-passing frequency are substantially better than those prepared for the second harmonic. The forcing on successive poles of the machine due to the second harmonic

is in-phase, while the fundamental slot-passing forcing on successive poles is 180° out of phase. The resulting shape of deformation of the yoke is simpler for the fundamental slot-passing force and is less stiff than the deformation shape for the second harmonic. Consequently, a greater proportion of the total motion of the poles at the slot-passing frequency is taken up by deformation of the yoke itself. Under the action of the second harmonic forces, most of the motion of the poles is taken up by the less well defined relative motion between the poles and the yoke.

The correlations presented here demonstrate the effects of some of the degrees of uncertainty present in the analysis of DC machine stators. Given a reliable set of values for the parameters determining the behaviour of the pole-yoke and coil-pole connections, reasonable accuracy can be anticipated. The action of compole forces is normally sufficient to seriously detract from the quality of an analysis unless they are accurately represented. In this comparison, the presence of an axial slot in the mainpole face had the effect of generating large force components on the mainpole relative to those acting on the compole so that the exclusion of the compole forces does not seem to have adversely affected the analysis to any significant extent.

§8.3 Static Tests on Machine B. (and Deducing Certain Parameters).

A number of static tests were done on this machine using both the impulse hammer and a shaker as sources of excitation and a large number of graphs were generated depicting the response at various points to forcing at others. The principal objective was to identify natural modes of the structure which would act to magnify forcing (electromagnetic or other). In all cases, a large number of resonances were found in the range of frequencies tested. Only a few of the corresponding mode-shapes were identified. It is already well known that many of the modes of machine stators which would be apparent at the low-frequency end of the spectrum from a single-point forcing static test obtain virtually zero net excitation from the electromagnetic force pattern when the machine is running. There are many significant degrees of uncertainty in a dynamic model of the stator of machine **B** as is shown later, and it is unlikely that the resonant frequencies found in an impulse test will be matched by any analysis. Attention is confined therefore in this brief section to the approximate matching of measured and predicted levels of vibration over broad bands of the spectrum.

Machine **B** was instrumented with accelerometers about the periphery (on a plane axially halfway along the "fwd" machine) and along the bottom. The arrangement and nomenclature of these is given in Fig.s 8.12a and 8.12b.

8.3.1 Comparison of Measred and Predicted Responses to Impulse Excitation of Machine **B.**

We consider two of the results from the impulse tests in which the machine was excited at the back of the compole. These are particularly convenient to analyse since the machine will respond symmetrically to this forcing (about the vertical plane containing the machine axis). Because of the number of "connections" which must be made to create a good quality representation of this machine, the DMS model prepared uses symmetry arguments so that only half of the machine is represented at a time. The response to forcing which is either symmetrical or anti-symmetrical can be computed directly. Forcing which is neither symmetrical nor anti-symmetrical must be broken into symmetrical and anti-symmetrical components, the response to each component found and these responses added. Fig. 8.13 is the DMS representation of one half of the "fwd" machine having all mainpoles, compoles, coils and feet attached. For the symmetrical modes, the nodes on the plane of symmetry are constrained so that they may not translate out of the plane or rotate about an axis in the plane. For the antisymmetrical modes, these nodes are constrained so that they may not translate in the plane or rotate about the axis normal to the plane. The effects of the split were not incorporated into this model as the full set of data on the properties of the splits had not been analysed at the time the model was prepared.

A force of 2N was applied to the top of the DMS model of the half machine. The response of the half-machine to a force of 2N would be

the same as the response of the whole machine to 4N. Thus, we expect that the response trace computed will be consistently 12dB above the measured trace (the measured trace is the response to 1N).

Fig. 8.14 compares the predicted and measured responses for vertical translation at the foot. Fig. 8.15 compares the measured and predicted responses for upward translation of accelerometer position 11x.

8.3.2 Discussion of the Quality of the Predictions.

Over the broad range of frequencies, the agreement is good in terms of the levels. At lower frequencies the quality of the estimates of the four coil stiffnesses and damping values has a strong influence on the levels which are predicted. The trend for the response to become more smooth at higher frequencies is clear from both the measured and predicted response traces.

Clearly, the response traces are too complex to attempt to use any one resonance from them to glean data about the root stiffness of the mainpoles and compoles. The values used to produce the DMS model for the impulse tests were extrapolated from the data presented in chapter 6.

8.3.3 Derivation of Approximate Values for the Root Stiffness of the Mainpoles and Compoles for Machine B.

One part of the test programme for machine **B** was directed at

identifying the dependence of vibration levels on the operating conditions of the machine. In these tests the machine was set to run at armature currents of 0.0, 0.5 p.u and 1.0 p.u at various combinations of speed and field-current. One of the principal assumptions made in the analysis of the electromagnetic forces is that the eddy-current effects on the various iron surfaces within the machine have little effect on the flux-ripple occurring. If this is the case, we can assert that the forces acting on the poles in some of the conditions remain unchanged in magnitude though the frequency of the forces has changed. Thus, when the rotating speed is doubled and the armature voltage is also doubled, the only reason for a change in the amplitudes of vibration of the poles of the machine is the mechanical frequency-dependence. It is clear from results presented later in this chapter that the mainpoles and compoles of this machine move relative to the yoke to such an extent (compared with the motion of the yoke itself) that to assume that the yoke was entirely rigid allows one to assess the motion of the poles in a simple yet relatively accurate manner at the lower end of the frequency spectrum.

We shall not attempt a correlation between measured and predicted levels for these tests. Instead, they are used to provide us with mode accurate estimates of the root stiffness of both the main and compoles.

Table 8.20 below relates the measured amplitudes of vibration of the compole accelerometers to the rotating speed while the armature current is held at 1.0 p.u. and the field is held at aproximately 0.5 p.u so that the armature voltage is directly proportional to the running speed.

Fig. 8.12 gives details of the positions of the accelerometers. All vibration levels are given in dBs of acceleration.

Slot-Passing (Hz)	1R	1C	2R	2C
133	63	72	64	67
265	73	91	71	~
530	82	86	76	84

Table 8.20 Vibration at the Ends of the Compole at Three Speeds. [Armature Current = 1.0 p.u] (0 dBs = 10^{-5} m/s^2)

Now, we expect from the data prepared in chapter 6 that the compression/extension stiffness of the joint between the yoke and the compole is such that the mode of radial translation of the compole on the yoke lies well above 1000 Hz. Thus, at frequencies of 265 Hz and below, the acceleration of the compole ought be almost directly proportional to the frequency-squared. The mean rise in the radial vibration figures as the speed is changed from 133 to 265 Hz is 8.5 dBs. The expected rise was 12 dB. ($20.\log_{10}(4)$). We can be reasonably confident from this that the compole forcing has dropped by some amount in the region of 3.5 dB. If the compole rocking resonance were also very high in relation to 133 Hz and 265 Hz, the vibration measured by 1C would be expected to rise by 8.5 dB. Instead, it rises 19 dB!. The

clear indication is that there is a compole rocking resonance very close to 265 Hz. Without knowing the phase of the response of 1C at the two speeds it is impossible to judge whether the resonance occurs just below 265 Hz or just above it. However, based on the increase in the amplitude of the response, the compole rocking resonance can be computed to be either 232 Hz or 335 Hz.

At a much lower value of field current, the same running speeds result in lower armature voltages. Table 8.21 below gives the compole vibration figures for these conditions.

Slot-Passing (Hz)	1R	1C	2R	2C
265	75	93	76	95
530	81	89	~	86

Table 8.21 Vibration (dBs) at the Ends of the Compole at Two Speeds. Armature current=1.0 p.u (0 dBs = 10^{-5} m/s^2). Field current $\in$ [0.06, 0.112] p.u.

The same reasoning as before implies that the compole forces are reduced by some 6 dBs between the frequencies of 265 and 530 Hz. The larger vibration value for both accelerometers 1C and 2C at the frequency 265 Hz is clear evidence that compole rock is occurring just below 265 Hz. We conclude that the compole rocking resonance occurs

at approximately 230 Hz. At a frequency as low as this, it is probable that the coil moves side-to-side with the compole. The rocking stiffness of the joint can be deduced accordingly.

The rocking stiffness of the mainpole can be approached in a similar way. Table 8.22 below relates mainpole vibration to the slot-passing frequency for the operating condition in which the armature current is 1,0 p.u. and the field current is such that the armature voltage is proportional to the rotating speed of the machine.

Slot-Passing (Hz)	3C (dB)	4C (dB)
133	59	54
265	69	69
530	73	77
663	77	80

Table 8.22 The Vibration at the Ends of the Mainpole at Two speeds. Armature current = 1.0 p.u. (0 dBs = 10^{-5} m/s^2) Field current $\in$ [0.46,0.66] p.u

The figures here are less emphatic than those recorded on the compole. The vibration acceleration would have been expected to rise 12 dB each

time the frequency was doubled. Clearly, this has not been the case. However, by considering the three pairs of successive intervals, different estimates of the natural frequency of pole rocking are produced (202 Hz, 389 Hz and 596 Hz). In the case of each of these figures small deviations in the measured accelerations would lead to large deviations in the computed resonance. The reason for the indefiniteness of the figures may be that the main field coil is not stiff on the mainpole at what would be the resonance of the bare mainpole. This could have the effect of spreading the resonance considerably depending on the linearity of the coil-pole connection.

In this case, it is best to rely solely on the extrapolation from the data in chapter 6. The rocking stiffness of the joint between mainpole and yoke is extrapolated as 215 MNm/rad.

§8.4 Running Tests on Machine "B".

One set of tests from the programme originally devised for machine **B** was aimed at establishing the operating shapes of the machine under running conditions. Armature current was set to 0.5 p.u. and the field set to approximately 0.26 p.u. The armature voltage was adjusted to give the following running speeds.

55 rpm. , 62 rpm. , 83 rpm. ,92 rpm. ,133 rpm.

The armature of machine **B** has 234 slots. Slot-passing frequencies are computed from the running speeds. At each of these speeds, six sets of

thirteen accelerometer readings were recorded. One of these sets concerns axial measurements at the end plate of the machine. For the present purposes, these are disregarded since the model does not include consideration of the end assemblies. Three of these sets deal primarily with the vibration about the periphery of the machine on the central plane. Another set contains data for the vibration at the mainpoles and compoles. The final set holds the readings from the accelerometers along the line at the bottom of the machine.

8.4.1 The Measured Operating Shapes of Machine **B**.

The situation is considerably more complex than one might have expected. The fact that the armature is herringbone-skewed means that the first-order components of forcing must deform the mainpoles and compoles before thay can be transmitted to the yoke. Given the scatter in the measured properties of the laminated solids, it is inevitable that some of the mainpoles will be stiffer than others in both shear and compression/extension either due to differences in the pressure with which they are clamped-up or differences at the surfaces of the laminations. Once the poles have deformed, the force transmitted to the yoke is directly dependent on the root stiffness of the poles. We shall see here, that the root stiffness contributes relatively little to the stiffness of the poles themselves for this machine. There is also a considerable scatter in the figures for root flexibility of the poles. Given the strong dependence on properties which are indefinite, one might expect that the measured operating shapes would not be as regular as the operating shapes computed for the machine.

Fig. 8.16 shows the deformation at the central plane of the "fwd" machine at the running speed of 55 rpm for both the fundamental and second harmonic of slot-passing. For simplicity, the phase of each measurement has been adjusted to be some multiple of 90°. The translations portrayed with a broken line are approximately 90° ahead of those shown with a solid line. Fig. 8.17 shows the deformation at the central plane for the fundamental and second harmonic at the speed of 83 rpm and Fig. 8.18 shows the measured deformation of the machines' central plane at 133 rpm.

Fig. 8.19a shows how the radial displacement of the compole ends varies with the running speed and Fig. 8.19b shows how the circumferential displacement of the compole ends varies with the speed. Fig. 8.20 shows the relation between the mainpole radial vibrations and the running speed while Fig. 8.21 shows the relation between mainpole circumferential vibrations and running speed. Fig. 8.22 shows the vibration at the bottom line of the machine for each of the five conditions.

There are two points worth noting before we proceed. Firstly Fig. 8.19b bears out the assertion that the compole rocks at a natural frequency of 235 Hz. Secondly, Fig. 8.22 showing the vibration of the line at the bottom of the machine demonstrates quite clearly the components of forcing which are not axially uniform do contribute significantly to the vibration of the machine.

8.4.2 The Electromagnetic Forces Acting on the Poles of Machine **B.**

The computation of the electromagnetic forces for this running condition yields the results for the mainpole given in table 8.23 below. The electromagnetic computations take no account of the speed with which the -armature rotates so these forces apply to all of the running speeds examined.

Force	Fundametal	2nd Harmonic
Radial	111 N/m	6.4 N/m
Ccmftl.	68 N/m	6.4 N/m
Moment	16.2 Nm/m	0.29 Nm/m

Table 8.23 Electromagnetic Forces Calculated for the Mainpoles.

The mainpole forces are computed to good accuracy. The mainpole has no sharp corners, it is laminated (which will tend to reduce the eddy-current effects which might exist) and the current in the armature conductors beneath it does not change as the armature rotates. The forcing on the compole is not known with any confidence. The distribution of the fundamental slot-passing forces is such that a residual axially uniform component does exist on the poles. The figures supplied for these axially-uniform force components are as follows . . .

Force	Fundamental	2nd Harmonic
Radial	5.6 N /m	0.68 N/m
Ccmftl.	4.0 N /m	0.029 N/m
Moment	0.95 Nm /m	0.008 Nm /m

Table 8.24 Residual Axially-Uniform Force Densities on the Mainpole.

The distribution of forces over the poles is obviously not uniform whether they be radial, circumferential or moment forces. Wignall has developed a means by which the distribution can be accurately assessed. The DMS model prepared for this machine has 4 nodes on the face of each pole at which the forces may be applied. This is sufficient to model the "A0" component of the forces and the "A2" component (see §9.1). It is demonstrated in Appendix 8 that the forces due to a herringbone or straightline skew of the armature slots can be separated into components and these components are quantified.

The axially-uniform components (henceforth referred to as "A0" - see §9.1) of both the fundamental and second harmonic are residual forces caused by the deviation-from-the-ideal of the skewed flux distribution. In order to estimate the "A0" component of forces on the poles, the profile of the machine in the axial direction must be modelled using F.E methods. Wignall does this in his computations. The "A2" component of

both frequencies of forcing is first-order and can be calculated to good accuracy using techniques similar to those of appendix 8. We assume for the purposes of the calculations here that the magnetic center of the armature is perfectly coincident with the magnetic center of the stator. Because the machine is herringbone skewed, there is no component of the "A1" force distributions (see §9.1 for the meaning of "A1")

8.4.3 The Computed Operating Shapes of Machine **B** Responding to the Individual Force Components.

A procedure has been developed during the course of this work for dividing the total forcing on the machine into the most basic components. This is described in detail in §9.1. By combining the computed response data from the respective force components in the correct proportions, the response of the machine to the total forcing is computed. It is appropriate here to present this intermediate stage for reasons which become apparent later.

The set of force components applicable to the computation of the machine response is listed below in table 8.25. The force-density used for each one was 6.35 N/m in the case of the radial and circumferential forces and 6.35 Nm /m in the case of the moment forces. (For the axially-uniform distribution, "A0", this corresponds to a force of 1N applied to each of the four nodes on each of the relevant poles). Each force component was applied to the theoretical model in turn and the operating shape calculated for the appropriate frequency.

Force Component Number	Force Component Name	Fig. #	Frequency
1	"RAD_CP_C1_A0"	8.23a	2nd Harmnonic
2	"RAD_CP_C1_A0"	8.23b	2nd Harmnonic
3	"RAD_CP_C2_A0"	8.24a	Fundamental
4	"RAD_CP_C2_A0"	8.24b	Fundamental
5	"CCF_CP_C1_A0"	8.25a	2nd Harmnonic
6	"CCF_CP_C1_A0"	8.25b	2nd Harmnonic
7	"CCF_CP_C2_A0"	8.26a	Fundamental
8	"CCF_CP_C2_A0"	8.26b	Fundamental
9	"MOM_CP_C1_A0"	8.27a	2nd Harmnonic
10	"MOM_CP_C1_A0"	8.27b	2nd Harmnonic
11	"MOM_CP_C2_A0"	8.28a	Fundamental
12	"MOM_CP_C2_A0"	8.28b	Fundamental
13	"RAD_CP_C1_A2"	8.29a	2nd Harmnonic
14	"RAD_CP_C1_A2"	8.29b	2nd Harmnonic
15	"RAD_CP_C2_A2"	8.30a	Fundamental
16	"RAD_CP_C2_A2"	8.30b	Fundamental
17	"CCF_CP_C1_A2"	8.31a	2nd Harmnonic
18	"CCF_CP_C1_A2"	8.31b	2nd Harmnonic
19	"CCF_CP_C2_A2"	8.32a	Fundamental
20	"CCF_CP_C2_A2"	8.32b	Fundamental
21	"MOM_CP_C1_A2"	8.33a	2nd Harmnonic
22	"MOM_CP_C1_A2"	8.33b	2nd Harmnonic
23	"MOM_CP_C2_A2"	8.34a	Fundamental
24	"MOM_CP_C2_A2"	8.34b	Fundamental

Table 8.25. Key for Figures 8.23 - 8.34

The regularity of these shapes is in striking contrast to the irregularity of the measured shapes in Fig.s 8.16 - 8.22. The facility for combining

the operating shapes in proportion to the coefficients of each of the component forces does exist within the DMS software package. However, it is already clear that there will not be a strong resemblence. This avenue is not pursued. Instead, for the running speeds 55 rpm, 83 rpm, and 133 rpm, rms values of vibration are extracted from the measured and theoretical cases and compared for the following categories of deflection.

1	Radial Vibrations on the Yoke.
2	Radial Vibrations on the Mainpole
3	Circumferential Vibrations on the Mainpole

These computations are based on the mainpole forces only.

8.4.4 Radial Vibrations on the Yoke.

Table 8.26 below is a concise summary of the result of combining the data from table 8.23 and that on the appropriate Fig. ($\in$ [8.33,8.44]) for the running speed of 55 rpm.

Force-Pattern	Computed Force Density	Resultant Peak Yoke Vibration
"RAD_MP_C2_A0"	5.6 N/m	1.24e-9 m
"CCF_MP_C2_A0"	4.0 N/m	1.20e-9 m
"MOM_MP_C2_A0"	0.95 Nm /m	8.21e-10 m
"RAD_MP_C2_A2"	94.1 N/m	2.46e-10 m
"CCF_MP_C2_A2"	57.7 N/m	4.68e-11 m
"MOM_MP_C2_A2"	13.7 Nm /m	4.62e-11 m

Table 8.26 Prediction of the Radial Yoke Vibration of Machine B. (Fundamental Slot-Passing) Running Speed = 55 rpm.

The radial forces on the mainpoles act to create an operating shape which has peak radial vibration approximately behind the mainpoles. The circumferential forces cause a peak radial vibration to occur approximately behind each of the compoles. The moment forces have the same effect. The circumferential forces are generally phase-shifted from the moment forces by an angle close to 90°. Therefore, there is no significant cancellation. Hence, the r.m.s. value of yoke vibration which would be expected from the mainpole forces alone can be calculated as shown below.

The computed r.m.s. radial vibration of the yoke :

$$= 0.5 * (1.24^2 + 1.20^2 + 0.82^2 + 0.246^2 + 0.047^2 + 0.046^2)^{0.5} * 1.0e\text{-}9$$

$$= 9.6\ e\text{-}10\ m.$$

The measured r.m.s. value of radial vibration on the yoke = 2.1e-9.

Table 8.27 below is the equivalent of table 8.26 for the 2nd harmonic of the slot-passing frequency.

Force-Pattern	Computed Force Density	Resultant Peak Yoke Vibration
"RAD_MP_C1_A0"	0.68 N/m	1.48e-9 m
"RAD_MP_C1_A2"	2.18 N/m	3.60e-12 m

Table 8.27 Prediction of the Radial Yoke Vibration of Machine **B**. (Harmonic 2). Running Speed = 55 rpm.

The computed r.m.s. radial vibration of the yoke = 1.05 e-9 m.

The measured r.m.s. value of radial vibration on the yoke = 1.6 e-9.

The same procedure is applied for the the other two running speeds of the machine. The results for all three running speeds are tabulated in table 8.28 below.

RPM	FUNDAMENTAL		2nd HARMONIC	
	Predicted	Measured	Predicted	Measured
55	0.96 e-9	2.1 e-9	1.05 e-9	1.6 e-9
83	6.06 e-9	1.7 e-9	1.04 e-9	0.95 e-9
133	1.08 e-9	0.85 e-9	0.07 e-9	0.25 e-9

Table 8.28 Comparison of Predicted and Measured r.m.s. Yoke radial Vibration.

That the predicted levels occur both below and above the measured values ought not be a source of undue concern. The response of the yoke of the machine is very strongly dependent on the closeness of the forcing frequency to an excitable resonance. The impulse response curves demonatrate that the structure has a number of clear modes of vibration about the frequencies at which forcing has been applied. (215 Hz - 1037 Hz). A small inaccuracy in the value of one of the properties can obviously lead to a large difference in the response at one frequency. Statistical methods can probably be employed to demonstrate that the mean response over a broad band of frequencies is not sensitive to these inaccuracies. To demonstrate this in practice would necessitate the examination of an impractically large population of running speeds.

Obtaining correct values for the forces acting on the compoles should tend to improve the quality of the prediction. It is certain, however, that the improvement would not be such as to significantly affect the error ratios being obtained.

8.4.5 Radial Vibrations on the Mainpole.

Once again, the response to each of the component force patterns is summed in the correct proportion to yield the response of the mainpole to the complete force set. It can be seen from the operating shapes calculated that the mainpole can move significantly relative to the yoke in all senses. Because the mainpole radial accelerometers were mounted on the corners of the pole, they will produce a reading when the pole rocks on the yoke though the net relative radial motion between pole and yoke be zero. The "joint attributes" chosen for the mainpole-yoke joints in the theoretical model were such that the mainpole (without field coil) has a natural frequency of translation relative to the yoke of some 1.55 kHz while the natural pole rocking frequency is 370 Hz. Wignall's force predictions suggest that the circumferential force is the same order of magnitude as the radial one. Clearly, the largest contribution to radial motion at the corners of the pole may be provided by the rocking mode at forcing frequencies below 1kHz. The vector sum of the two readings at one end of the mainpole gives us the radial motion at the central plane of the mainpole at that end (assuming that the pole does not deform).

Table 8.29 lists the vibration levels at the two ends of the mainpole for

the fundamental slot-passing and the 2nd harmonic for the three running speeds 55, 83 and 133 rpm.

RPM	FUNDAMENTAL		2nd HARMONIC	
	End 1	End 2	End 1	End 2
55	5.7e-9	1.6e-9	1.1e-9	2.6e-9
83	3.0e-9	2.1e-9	5.6e-10	4.3e-10
133	1.5e-9	5.4e-10	1.63e-9	2.9e-9

Table 8.29 Measured Radial Motion at Ends of Mainpole.

There is no immediately obvious reason for the discrepancy between the ends. The particular mainpole instrumented was well removed from those locations on the yoke where the existence of other steelwork would tend to affect the way in which the yoke behaved in the region. It may well be that one end was more stiffly joined to the yoke than the other due to unevenness in the bolt torques.

The predicted levels of radial vibration of the pole are obviously the same for both ends. Predicted levels are compared with the measured in table 8.30 below.

RPM	Mean Radial Motion at Mainpole Ends.	Predicted Radial Motion at Mainpole Ends.
Fundamental		
55	3.7e-9	2.78e-9
83	2.5e-9	3.22e-9
133	1.0e-9	1.95e-9
2nd Harmonic		
55	1.9e-9	1.2e-9
83	4.5e-10	9.2e-10
133	2.27e-9	1.7e-9

Table 8.30 Comparison of Predicted and Measured Radial Motion at ends of Mainpole.

The agreement between the measured and predicted values is significantly better for the mainpoles than it was for the radial vibrations of the yoke. The reasons are twofold. Firstly, the number of resonances which significantly affect the vibration on the mainpoles is much less than the number of resonances affecting the vibration of the yoke beacuse the pole root flexibility effectively isolates the mainpole from the yoke for many of the "yoke" resonances. Secondly, the vibrations on the mainpole are not sensitive to the forcing on the compole which is not known with confidence.

It is worth noting that the contribution of the "A2" forces to the motion of the ends of the poles is the same order of magnitude as the contribution from the "A0" forces. This was not the case for the vibrations of the yoke. Again, the pole root flexibility is the cause of this difference.

8.4.6 Circumferential Vibrations on the Mainpole.

Accelerometers 3C and 4C on the mainpole recorded the circumferential motion of the poles at each of the running speeds examined. It is evident from the computed operating shapes (Fig.s 8.23 - 8.34) that the pole is much more inclined to rock on the yoke than it is to translate in the circumferential sense. Most of the circumferential motion of the mainpoles is therefore contributed by the rocking model of the pole on the yoke. The accelerometers were located on blocks close to the face of the pole face. The measured values from accelerometers 3C and 4C differ considerably for each running speed as did the radial measurements. The predictions from the theoretical model will give the circumferential vibration figures for both ends of the mainpole. Thus, as before, the mean measured vibration at he ends is compared with the the prediction. These results are presented in table 8.31 below.

RPM	Mean Ccftl. Motion at Mainpole Ends.	Predicted Ccftl. Motion at Mainpole Ends.
Fundamental		
55	7.6e-9	4.72e-9
83	3.4e-9	1.95e-8
133	2.7e-9	3.85e-9
2nd Harmonic		
55	5.2e-10	8.2e-10
83	5.1e-10	9.5e-10
133	2.6e-9	1.7e-9

Table 8.31 Comparison of Predicted and Measured Circumferential Motion at Ends of Mainpole.

Again, the agreement between the measured and predicted values here is better than it was for the radial vibrations of the yoke. The same reasons as were given in 8.4.4 apply. The pole rocking resonance of 370 Hz is directly responsible for the high value of predicted vibration at the running speed of 83 rpm when slot-passing frequency is 324 Hz.

8.4.8 Discussion of the Accuracy of the Predictions in the Running Tests of Machine **B**.

As was pointed out earlier, it is to be expected that comparing a small number of discrete-frequency measurements with the corresponding predicted levels is prone to large discrepancies owing to the difference between the true and theoretical values for the frame resonance frequencies. The damping ratios of the various modes of the frame determine the extent of the discrepancy which is expected between measured and predicted vibration levels. A brief examination of the impulse responses presented earlier shows that a small change in forcing frequency can easily lead to a change in response of the order of 10 dB at the lower frequencies of forcing. The comparison of predicted with measured levels of rms radial vibration of the yoke displays a worst discrepancy of approximately 12dB.

Compole forces have not been included in the computations here as the uncertainty associated with them renders it unlikely that they would improve the calculations significantly.

In the light of the fact that the measurements indicate such non-ideal behaviour of the frame, (opposite ends of the mainpoles and compoles display marked differences in the vibration levels and there is not the expected pattern of displacements about the periphery of the machine) the correlation between measured and predicted values of vibration must be regarded as being as good as possible in the circumstances.

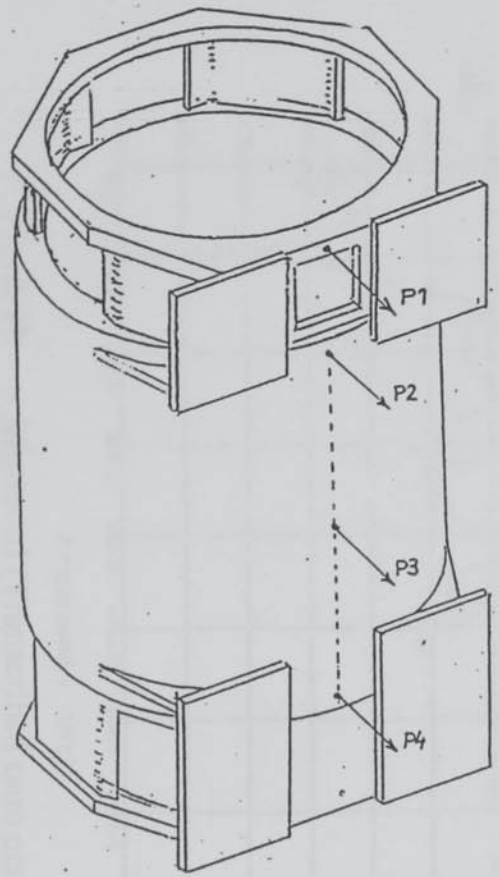

Fig. 8.1a Stripped and Unthreaded Frame of Machine "A".

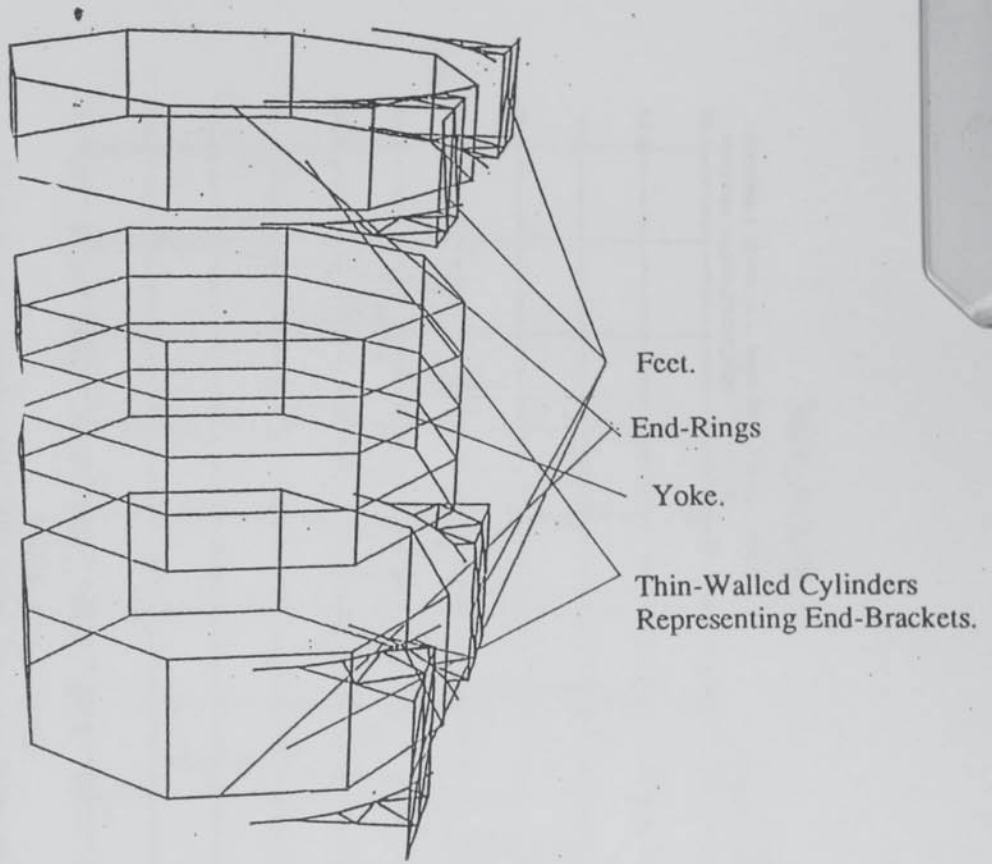

Fig. 8.1b DMS Model of the Frame of Machine "A".

Fig. 8.1 Machine "A".

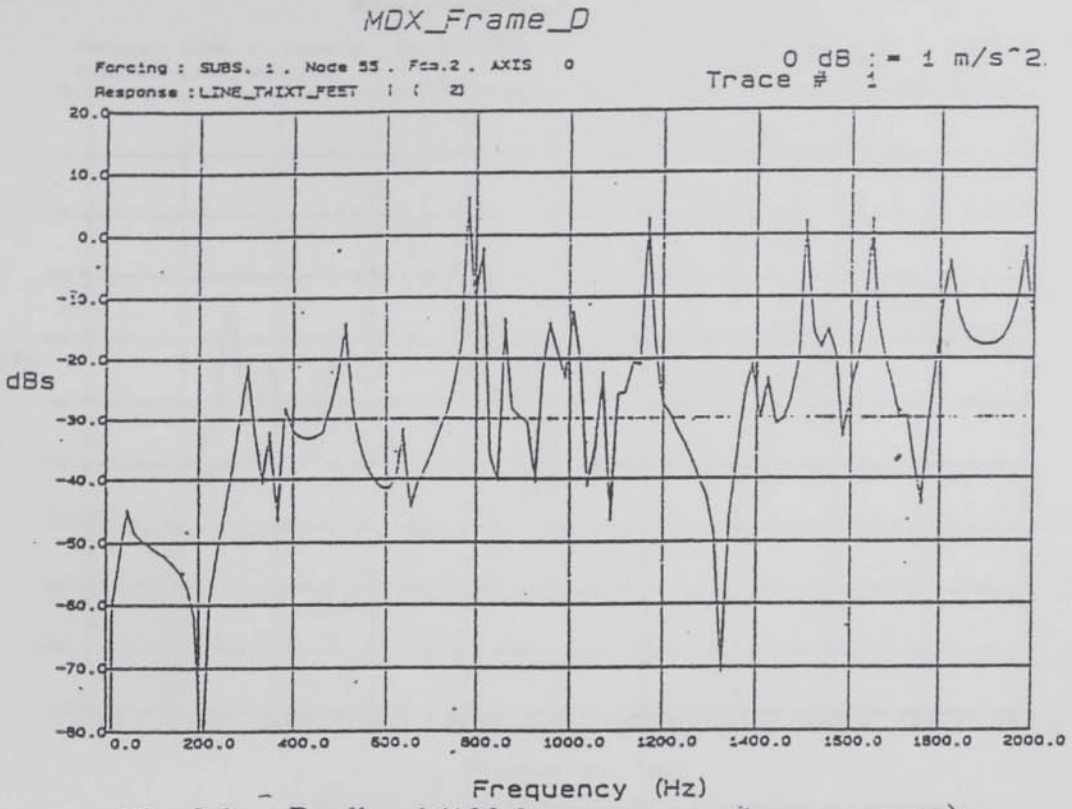

Fig. 8.2a Predicted (100 frequency samples over range)

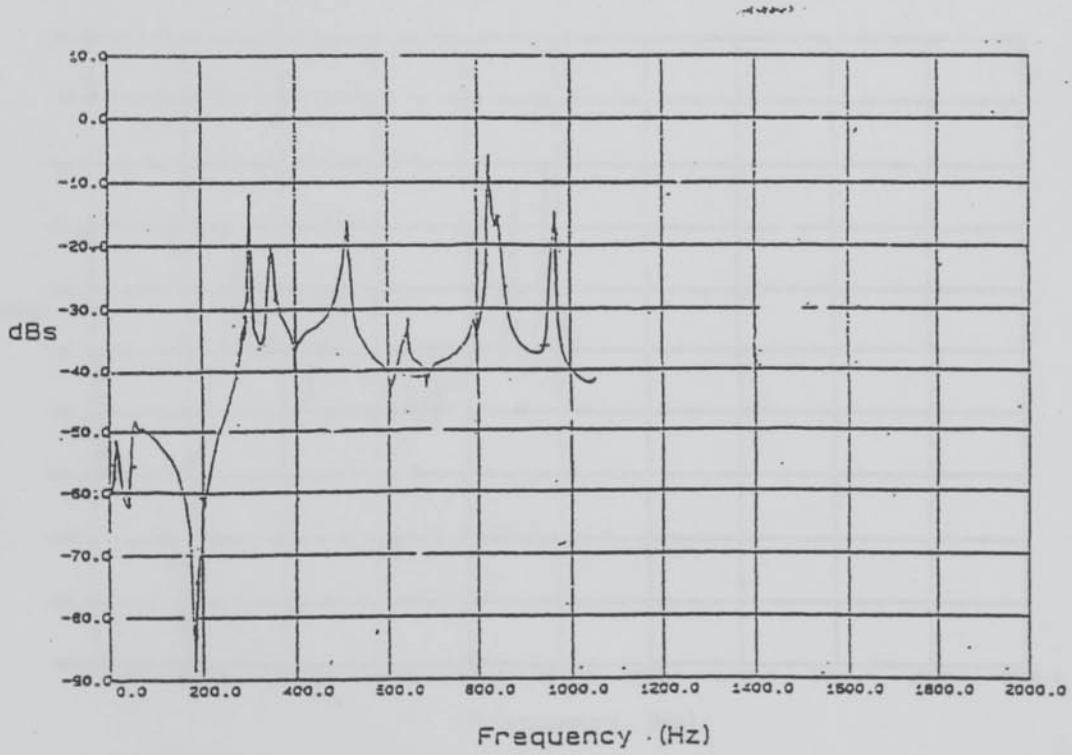

Fig. 8.2b Measured (Transcribed onto compatible scale)

Fig. 8.2 Comparison of Measured and Predicted Response Curves (P1/P1)

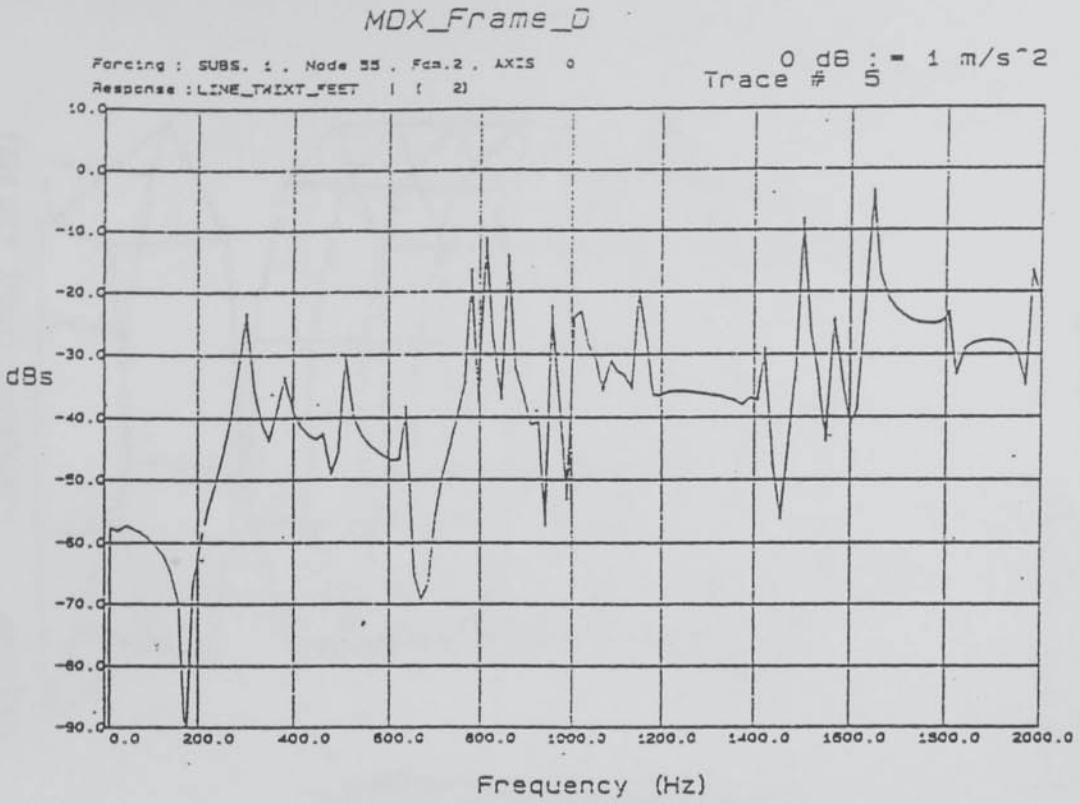

Predicted (100 frequency samples over range)

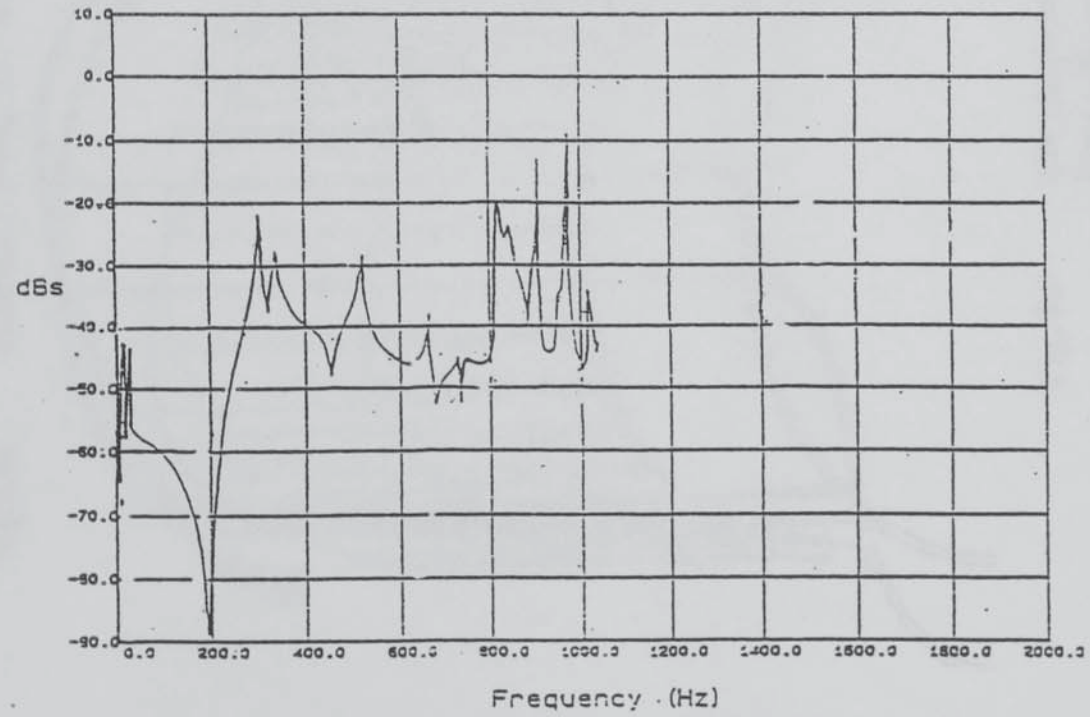

Fig. 8.3b Measured (Transcribed onto compatible scale)

Fig. 8.3 Comparison of Measured and Predicted Response Curves (P4/P1)

Fig.8.4a Measured. (Freq. 251 Hz)

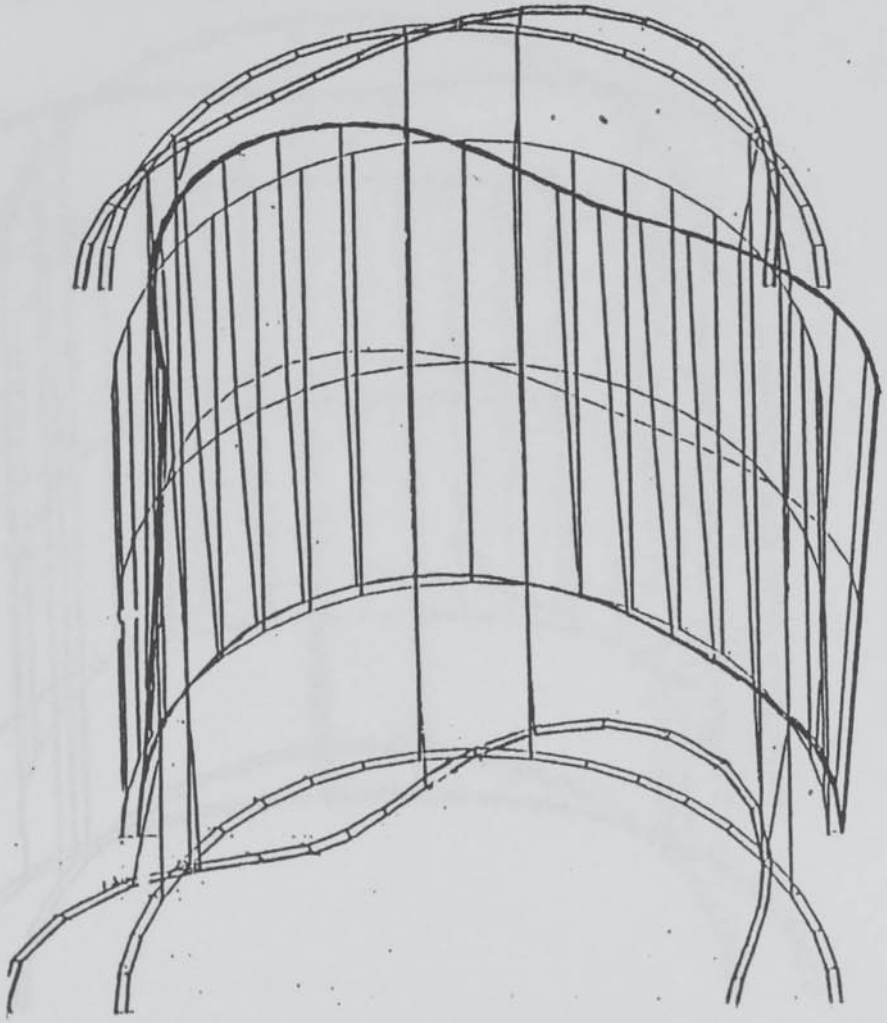

Fig.8.4b Computed. (Freq. 256 Hz)

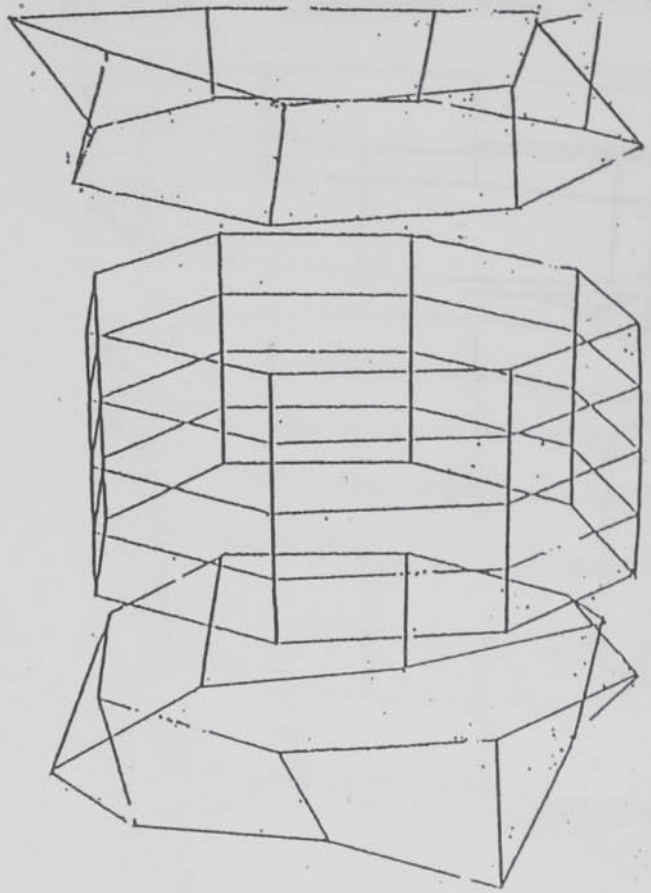

Fig. 8.4 Comparison of Measured and Computed Mode-Shapes. (Lowest frequency mode - type "n=2")

Fig. 8.5a Measured. (Freq. 946 Hz)

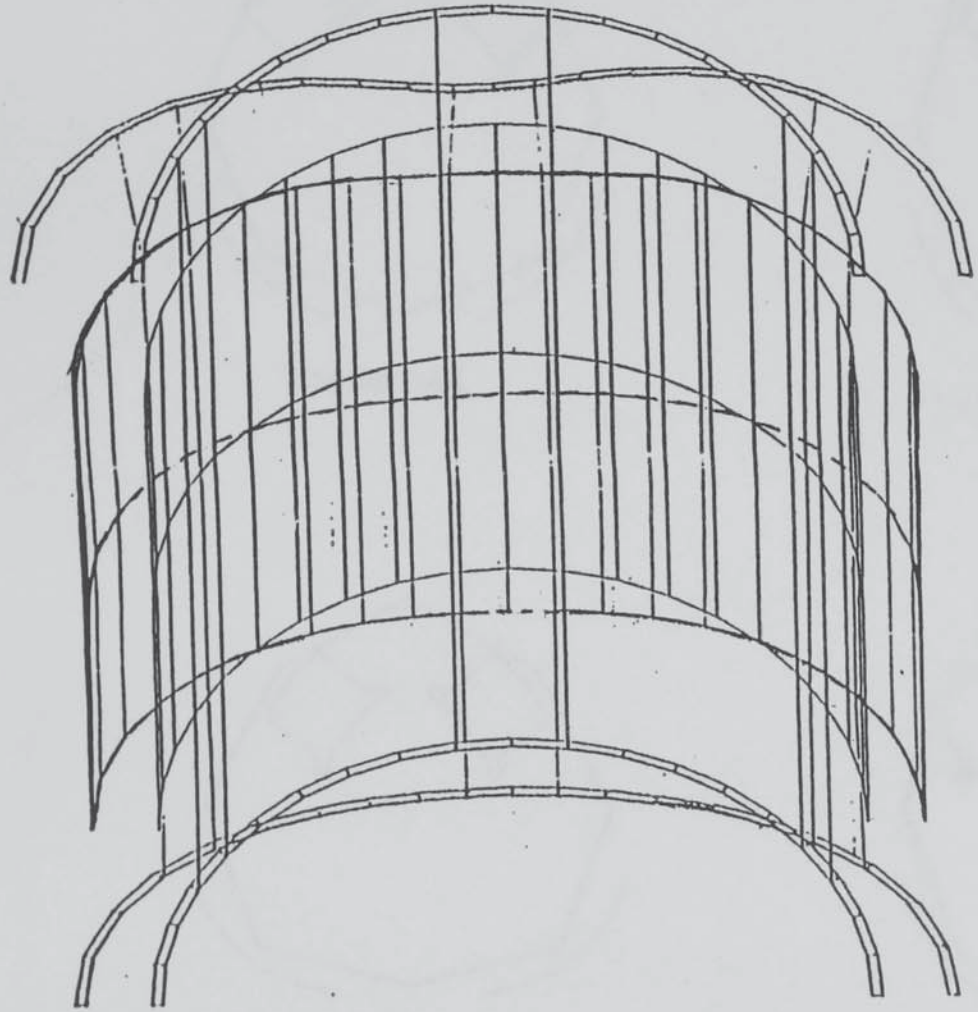

Fig. 8.5b Computed. (Freq. 960 Hz)

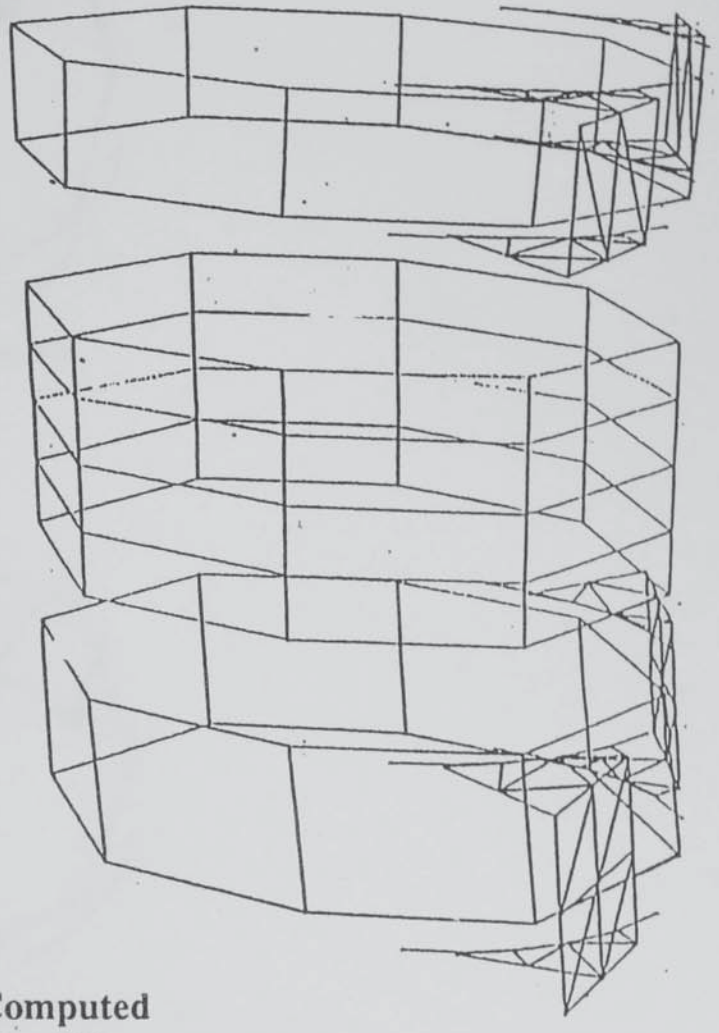

Fig. 8.5 Comparison of Measured and Computed Mode-Shapes. (A mode of type "n=3")

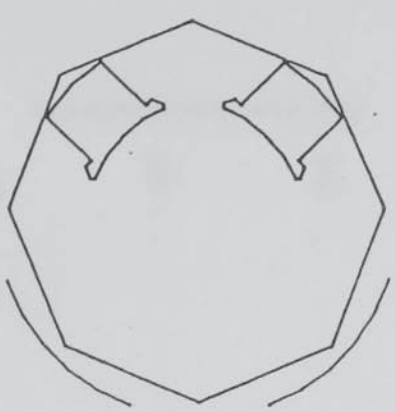

Undeformed.

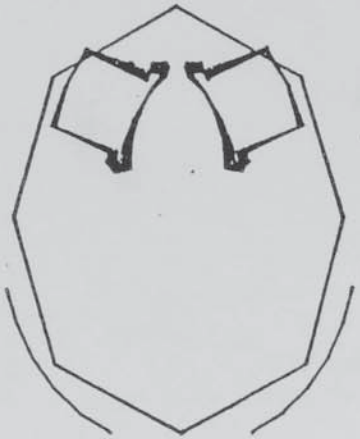

Deformed Shape #1.

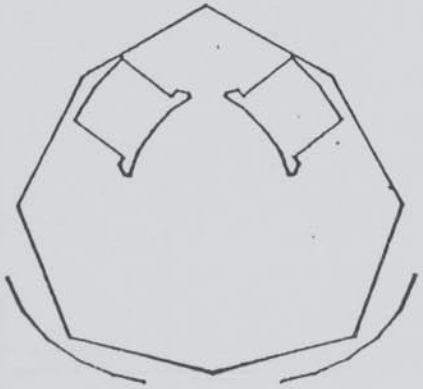

Deformed Shape #2.

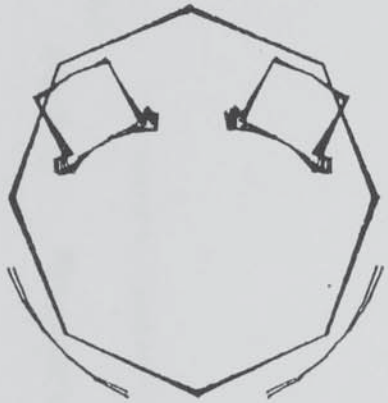

Deformed Shape #3.

Fig. 8.6 Bare Frame with Two Mainpoles.

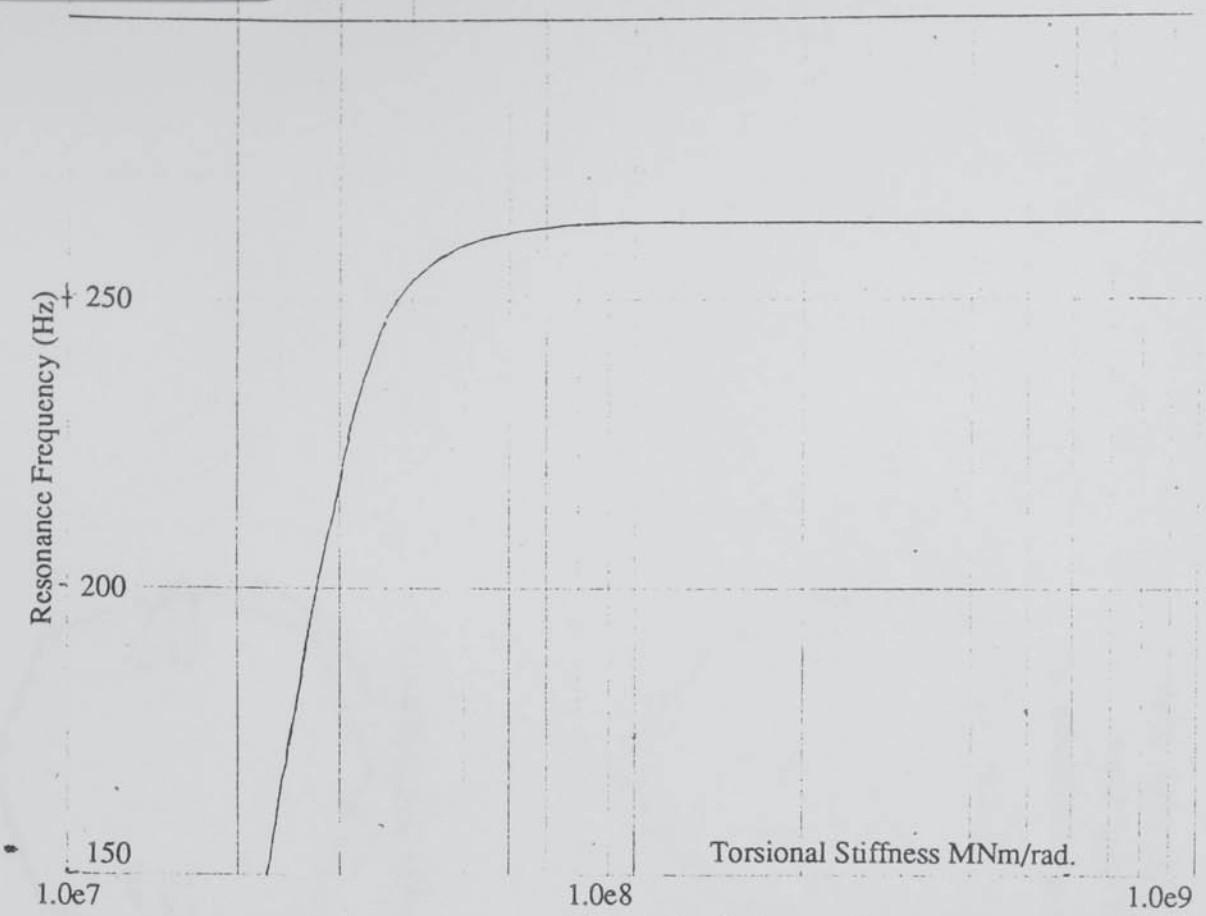

Fig. 8.7a Resonance of Mode 1.

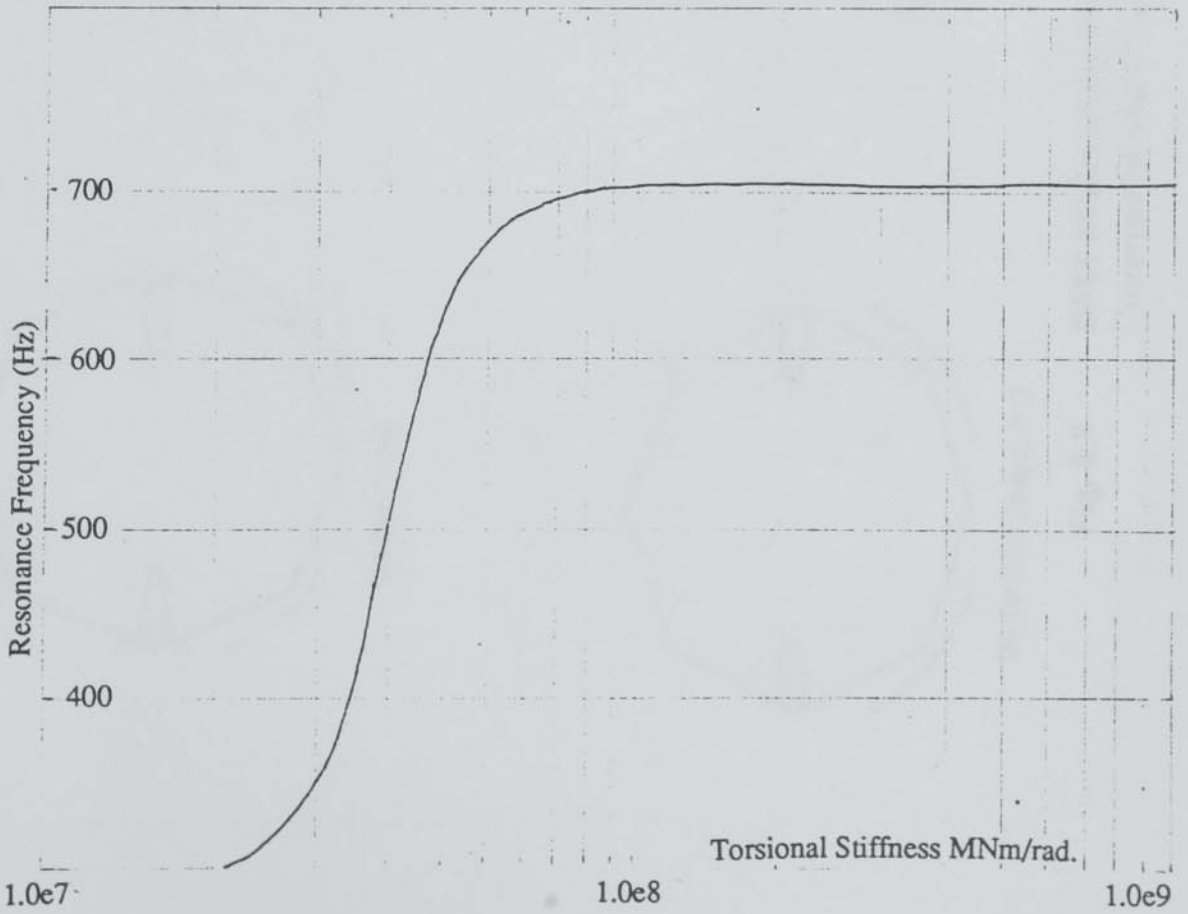

Fig. 8.7b Resonance of Mode 2

Fig. 8.7 Relation Between Resonant Frequencies and the Torsional Stiffness of the Pole-Yoke Joint.

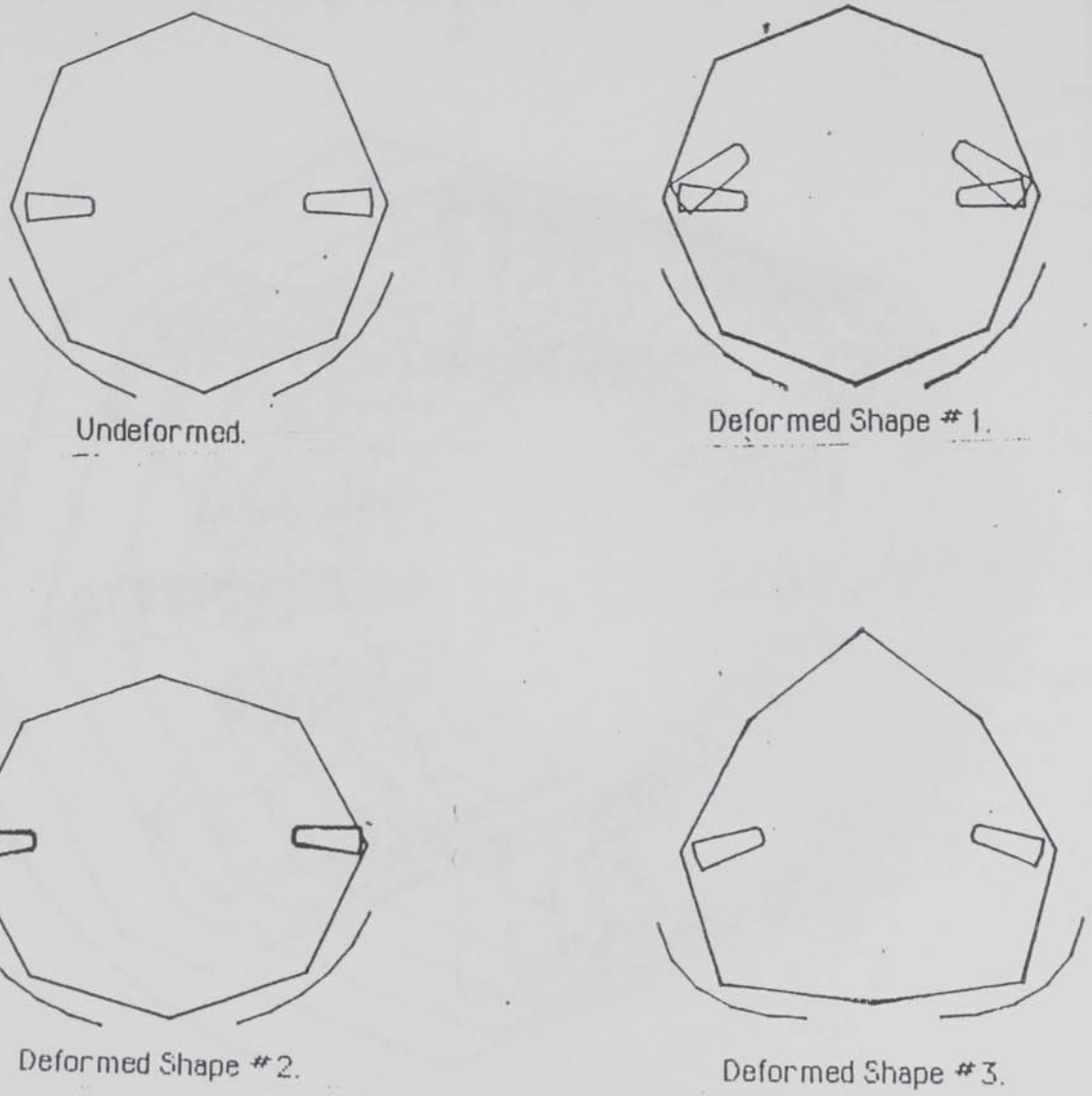

Fig. 8.8 **DMS Model of the Frame with Two Commpoles and Coils.** (Coils not shown).

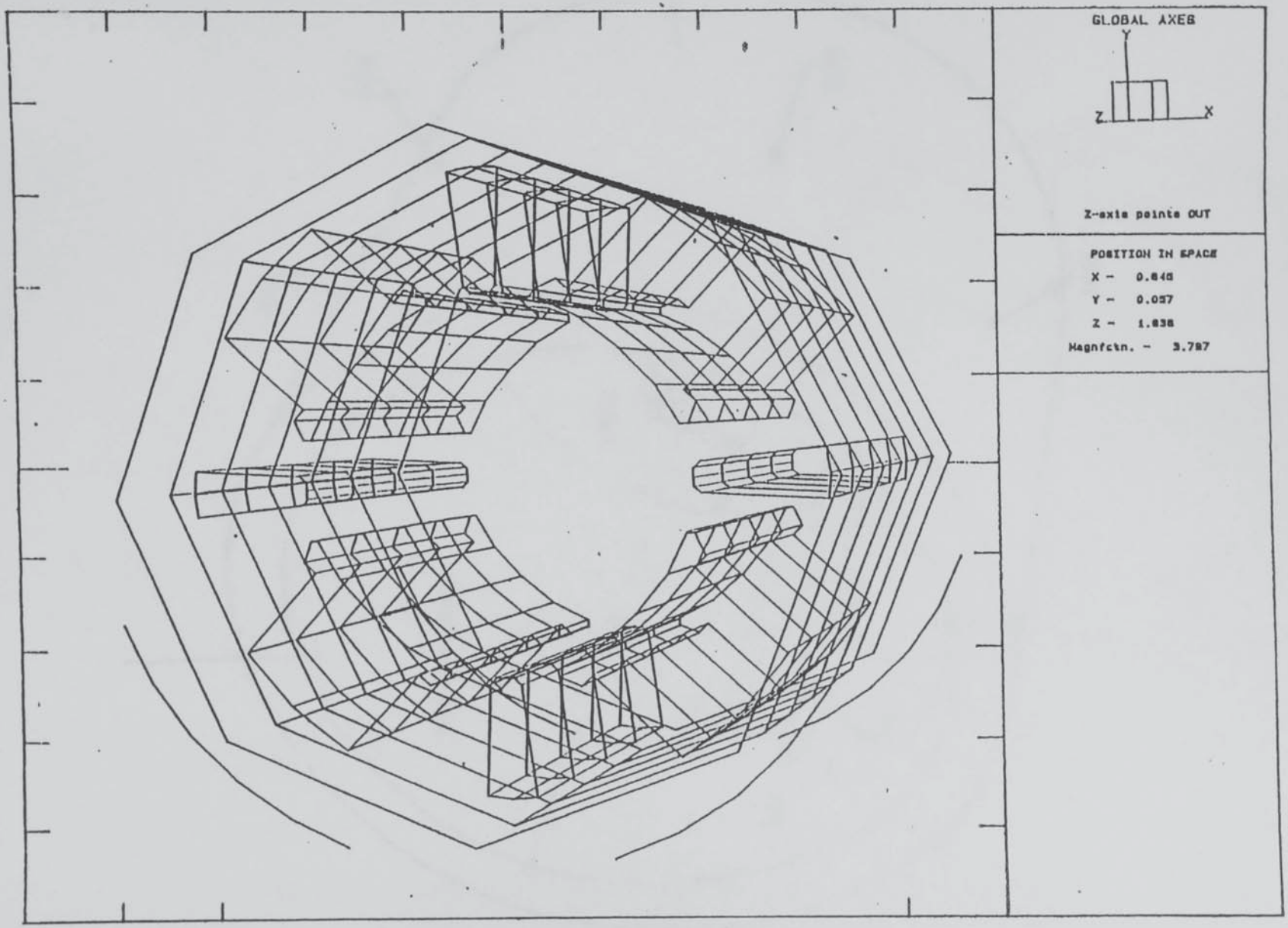

Fig. 8.9 DMS Model of Complete Stator of Machine "A".

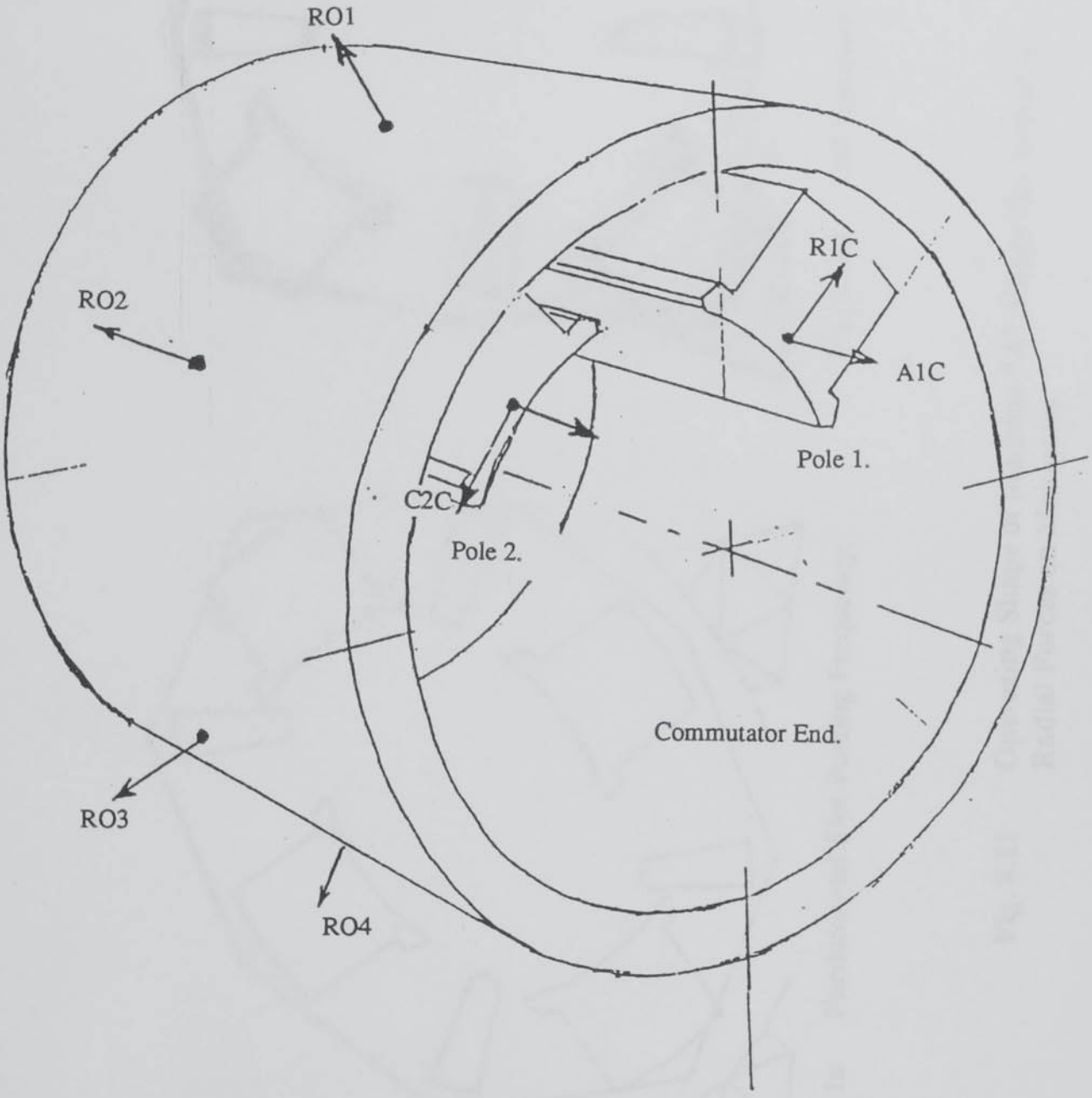

Fig. 8.10 Measurements Made during Running Tests on Machine "A".

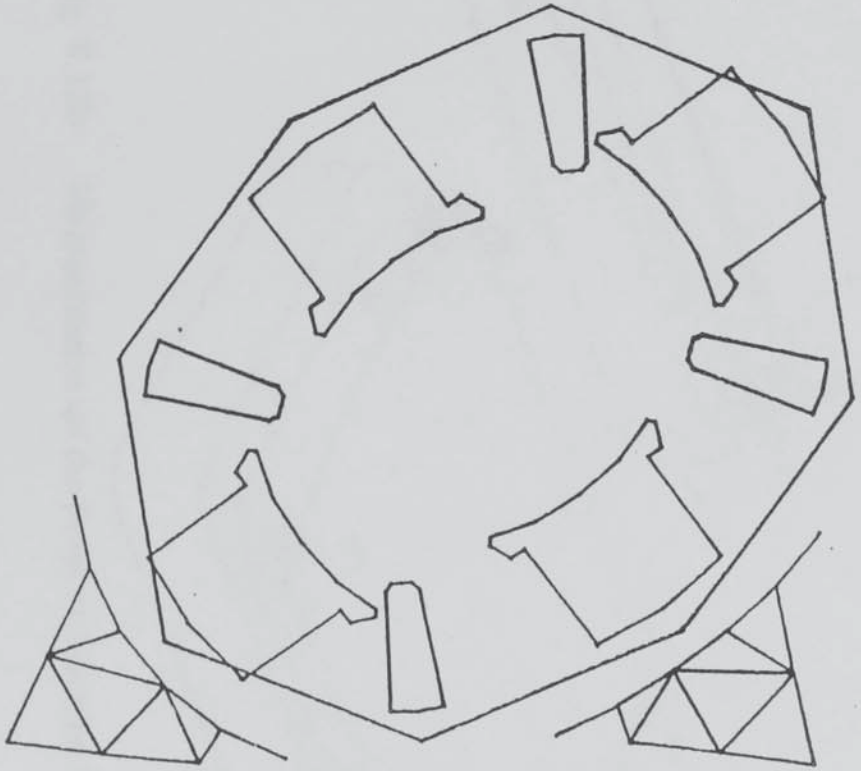

Fig. 8.11a Fundamental Slot-Passing Frequency.

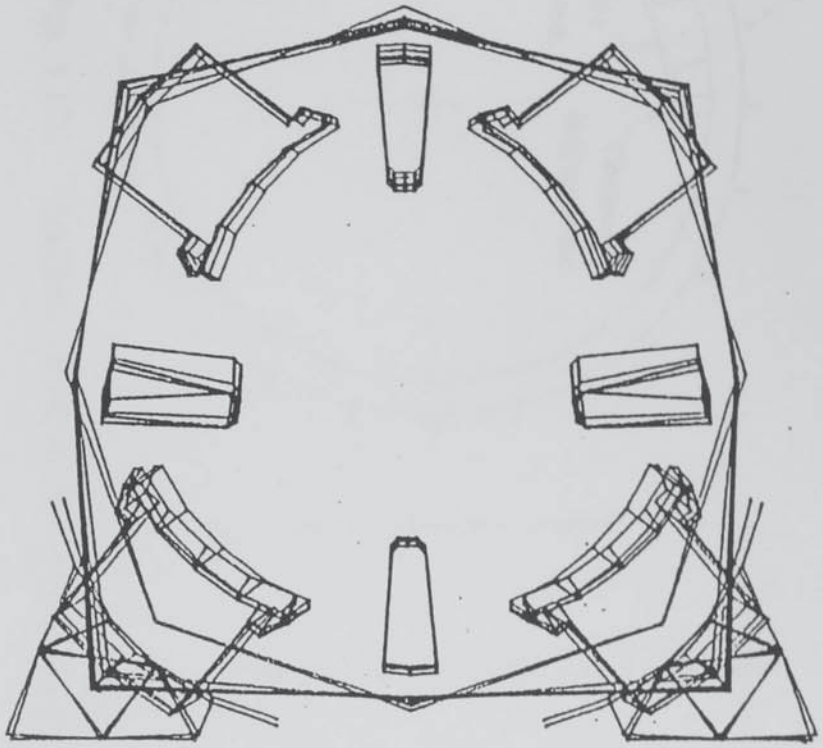

Fig. 8.11b 2nd Harmonic of Slot-Passing.

Fig. 8.11 Operating Shape of Machine "A" Under the Action of Radial Forces on Mainpoles

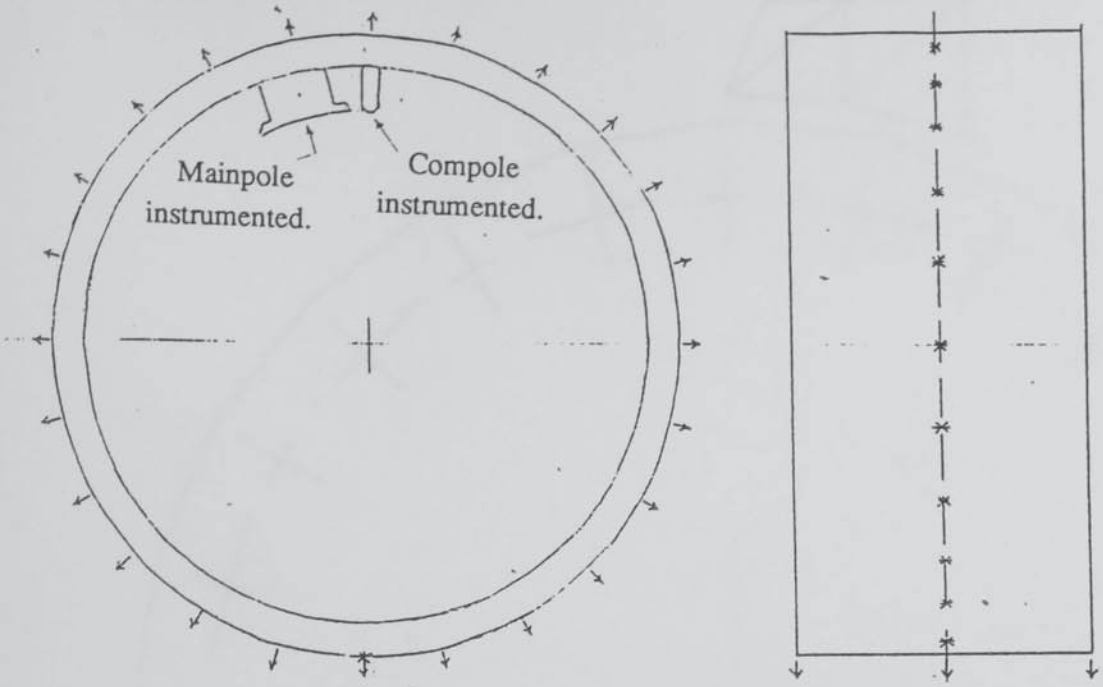

Fig. 8.12a Positions of accelerometers on the yoke.

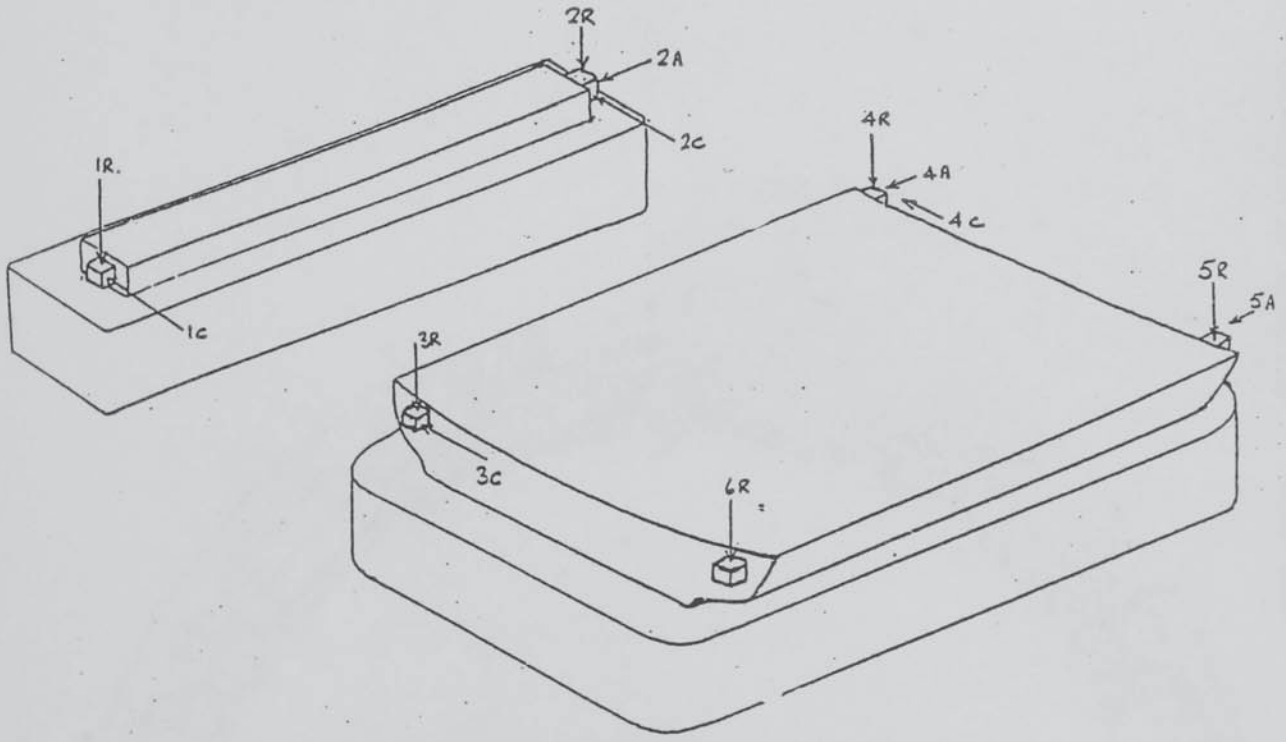

Fig. 8.12b Measurements on the Poles of Machine "B".

Fig. 8.12 Measurements on the Yoke of Machine "B".

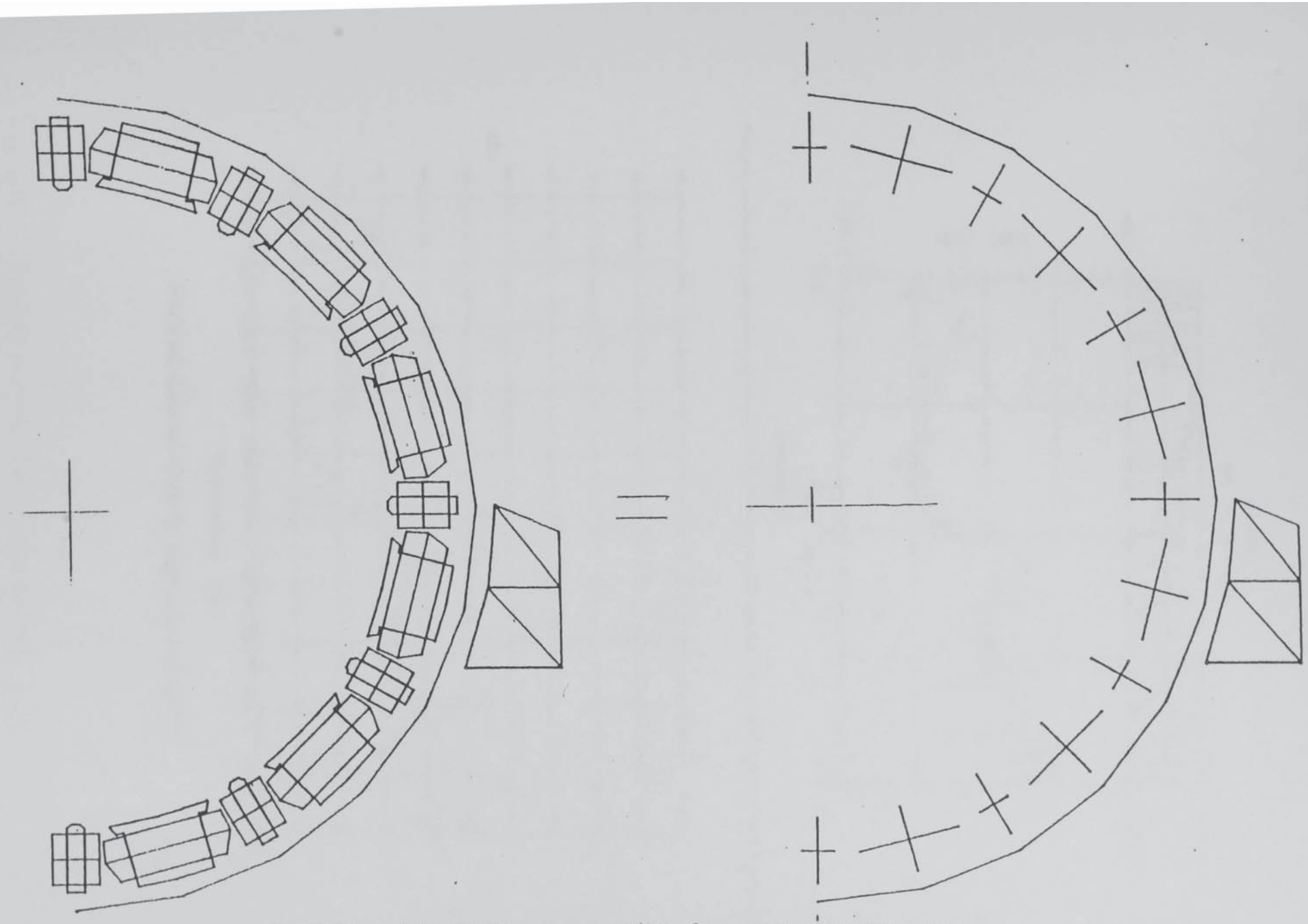

Fig. 8.13 The DMS representation of one half of Machine "B".

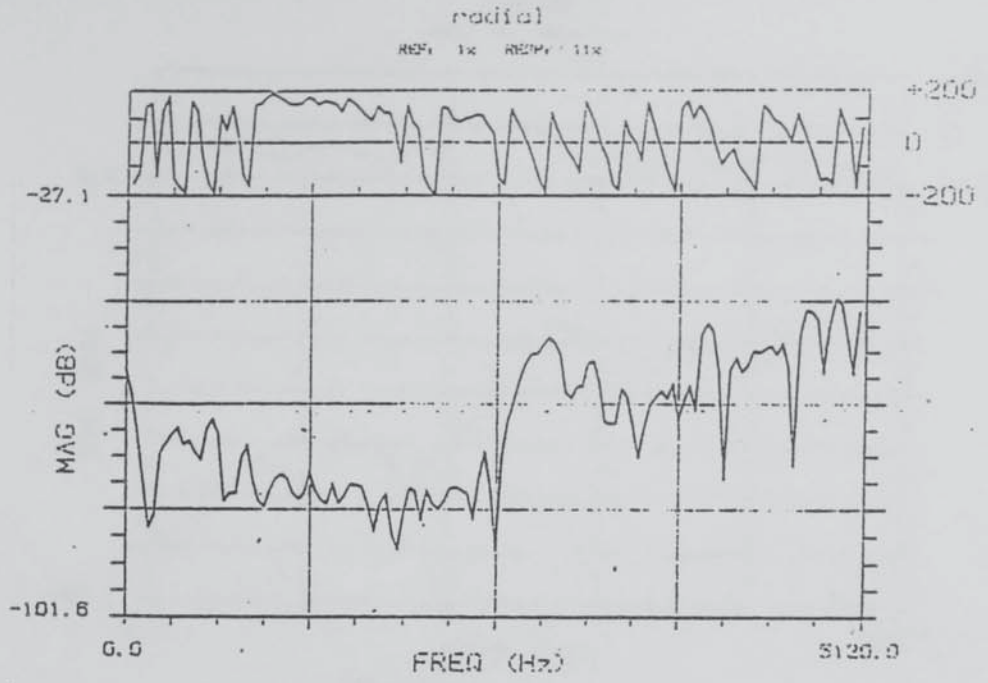

Measured.

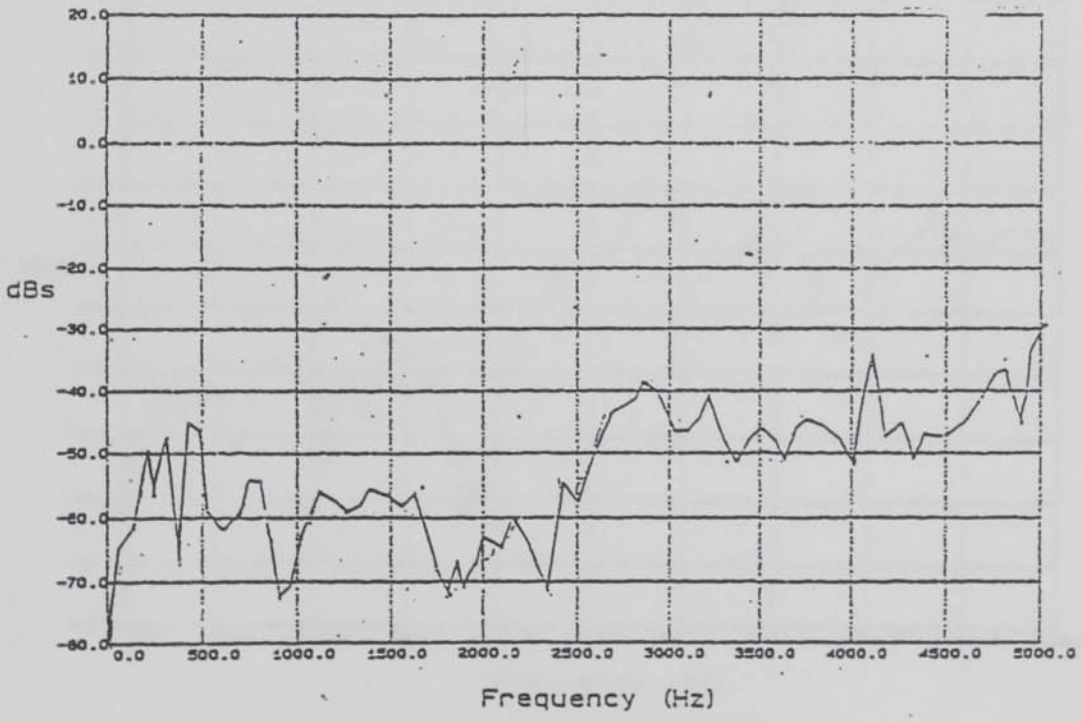

Predicted. (Subtract 12 dB for response to a 1N force)

Fig. 8.14 Predicted and Measured Impulse Response (11R/1R)

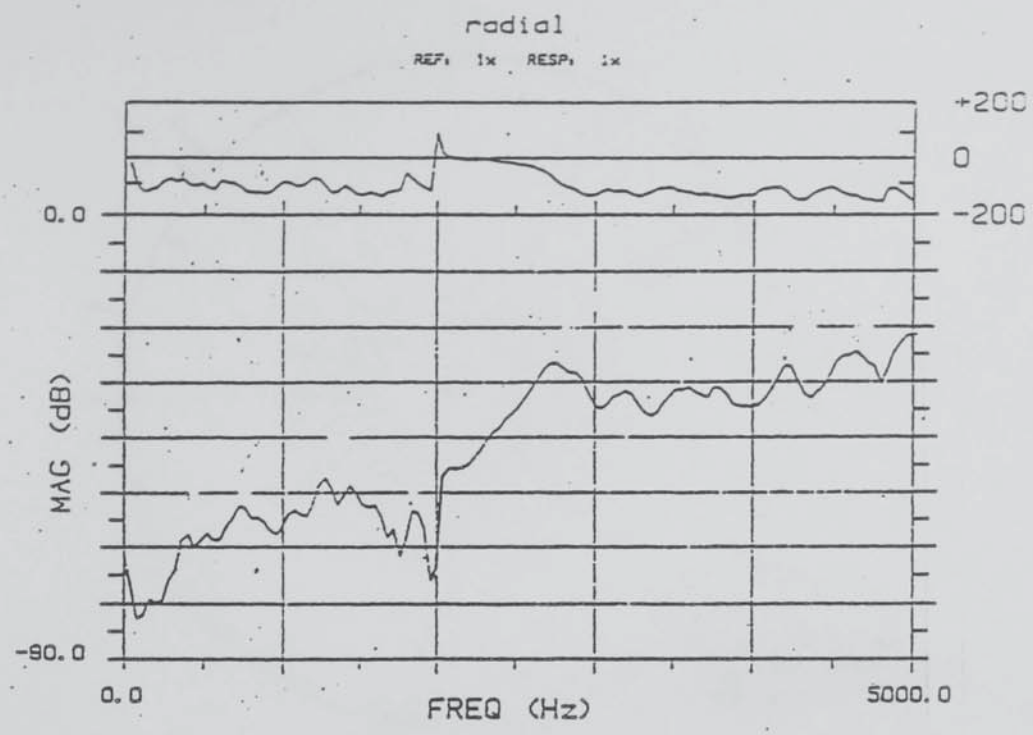

Measured.

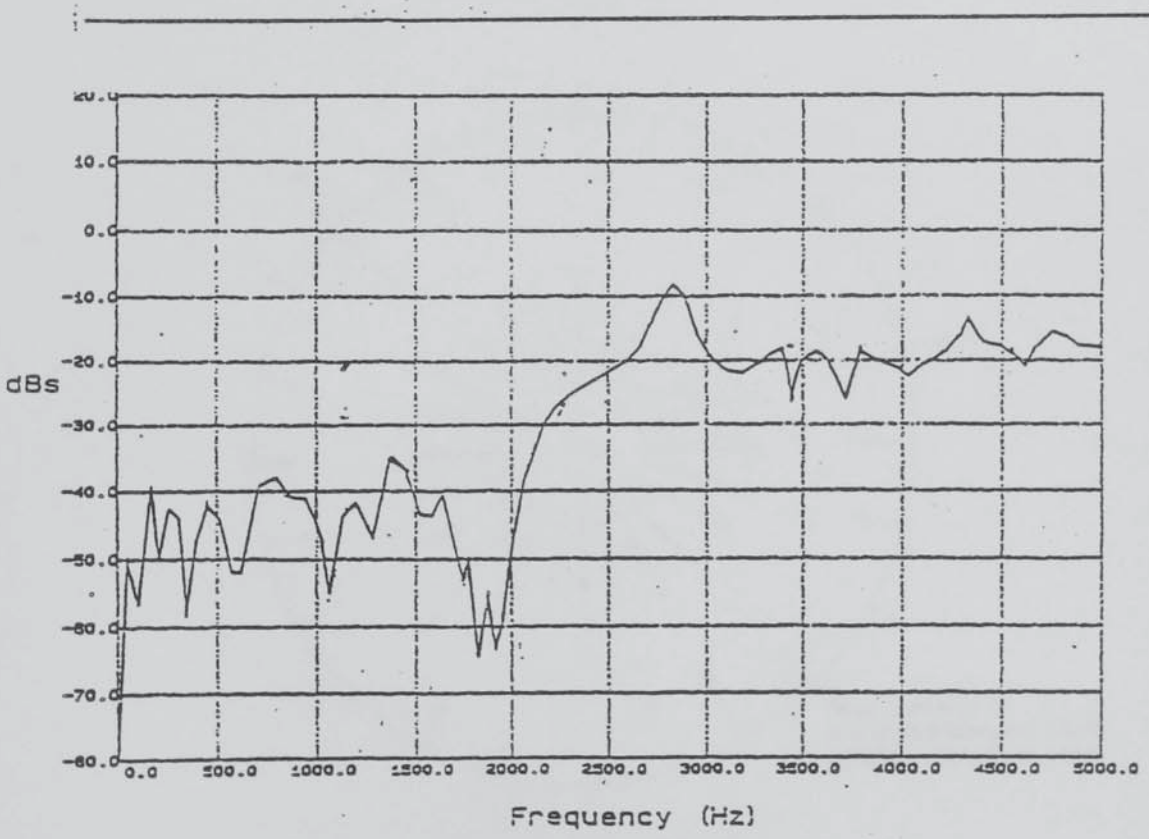

Predicted. (Subtract 12 dB for response to a 1N force)

Fig. 8.15 Predicted and Measured Impulse Response (1R/1R)

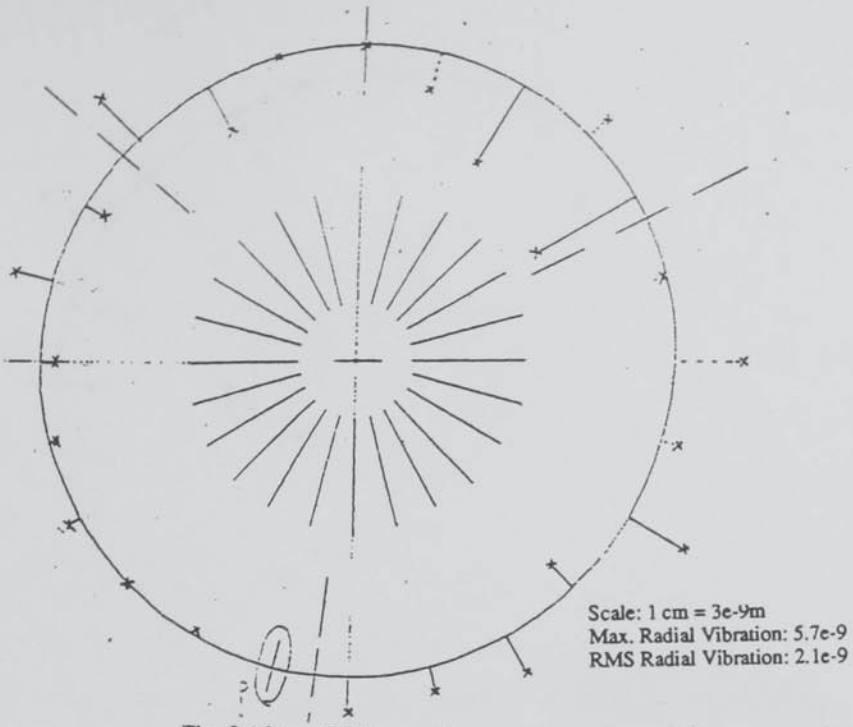

Fig. 8.16a Fundamental.

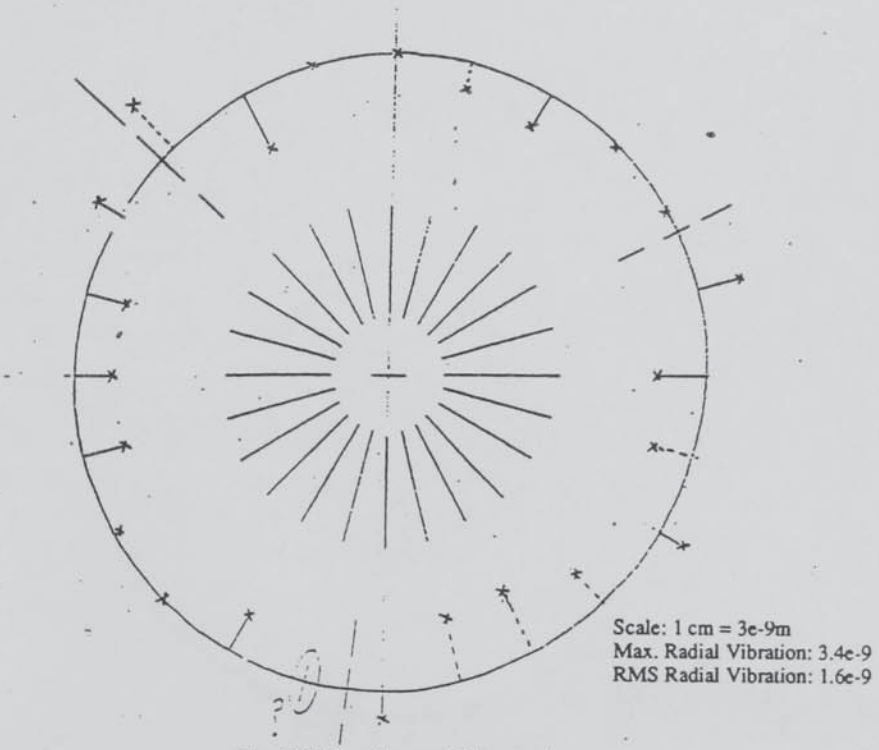

Fig. 8.16b Second Harmonic.

Fig. 8.16 Measured Operating Shape of Machine B Running at 55 rpm.

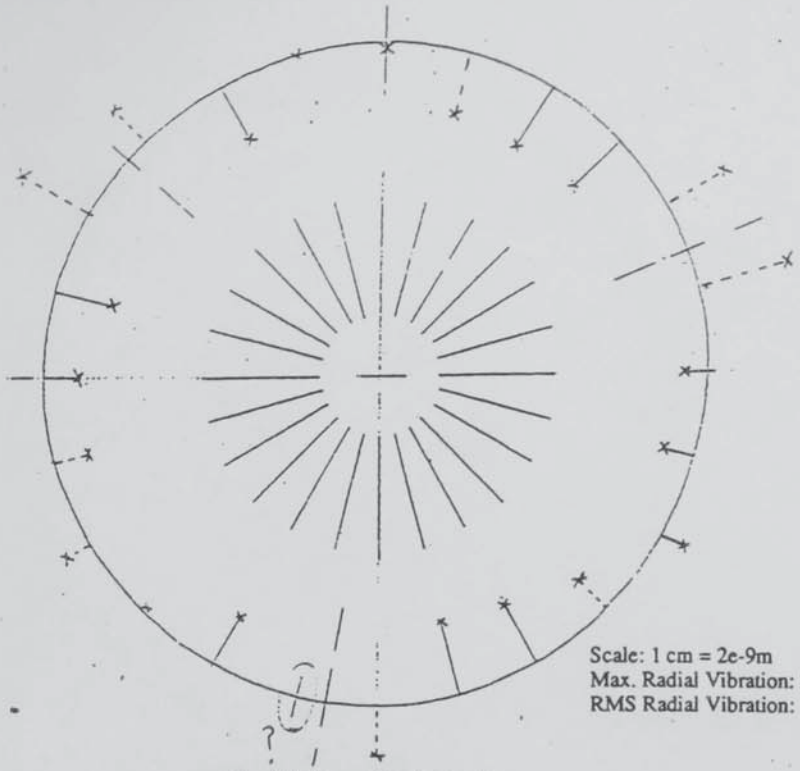

Fig. 8.17a Fundamental.

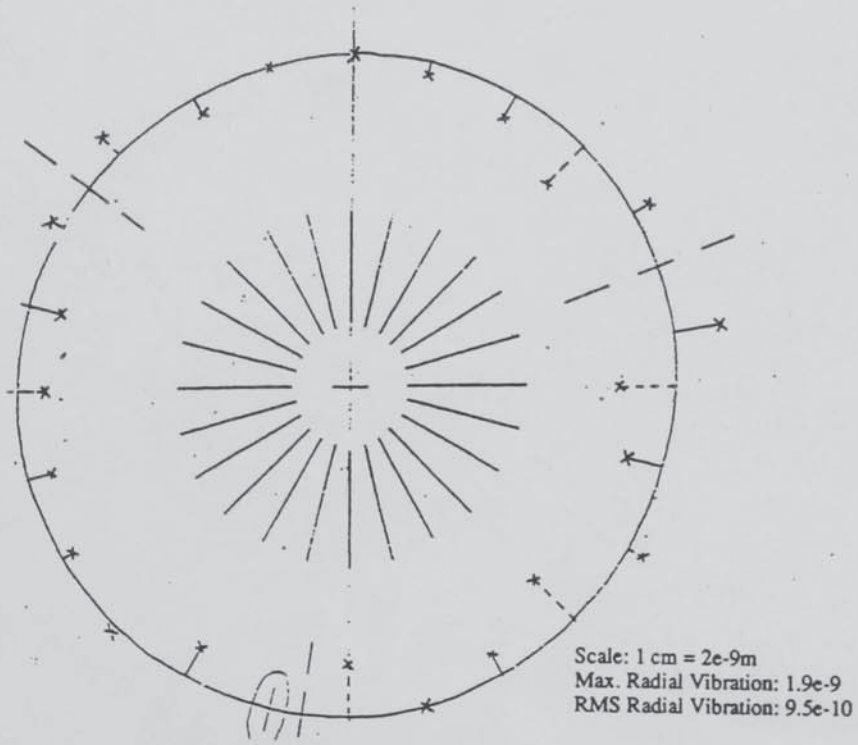

Fig. 8.17b Second Harmonic.

Fig. 8.17 Measured Operating Shape of Machine B Running at 83 rpm.

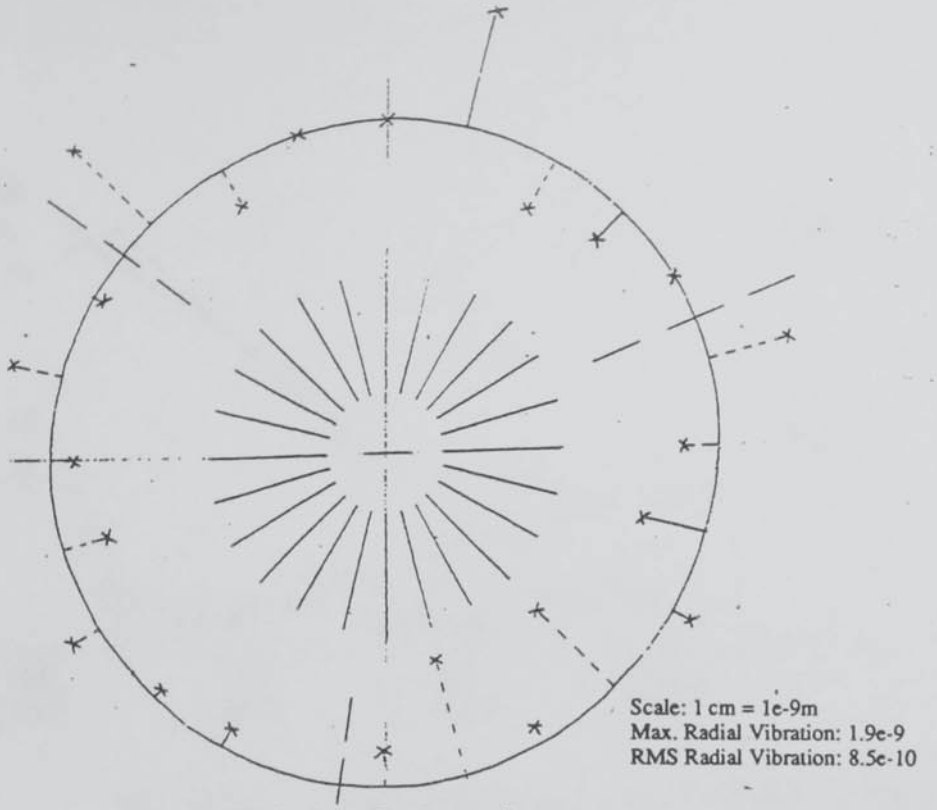

Fig. 8.18a Fundamental.

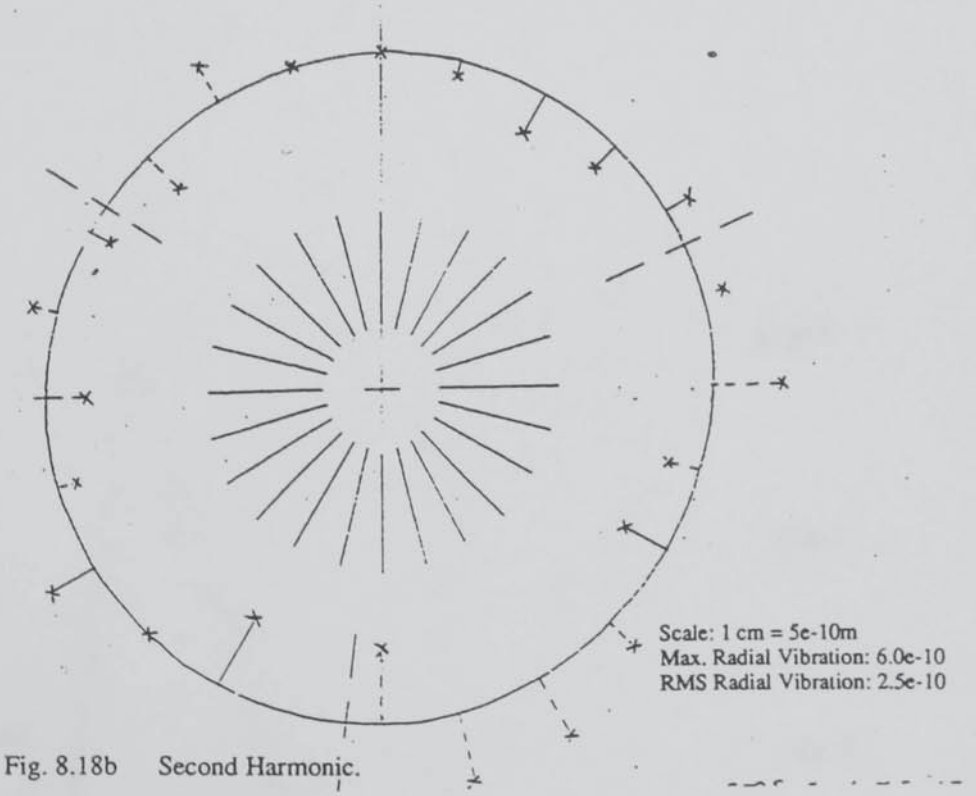

Fig. 8.18b Second Harmonic.

Fig. 8.18 Measured Operating Shape of Machine B Running at 83 rpm.

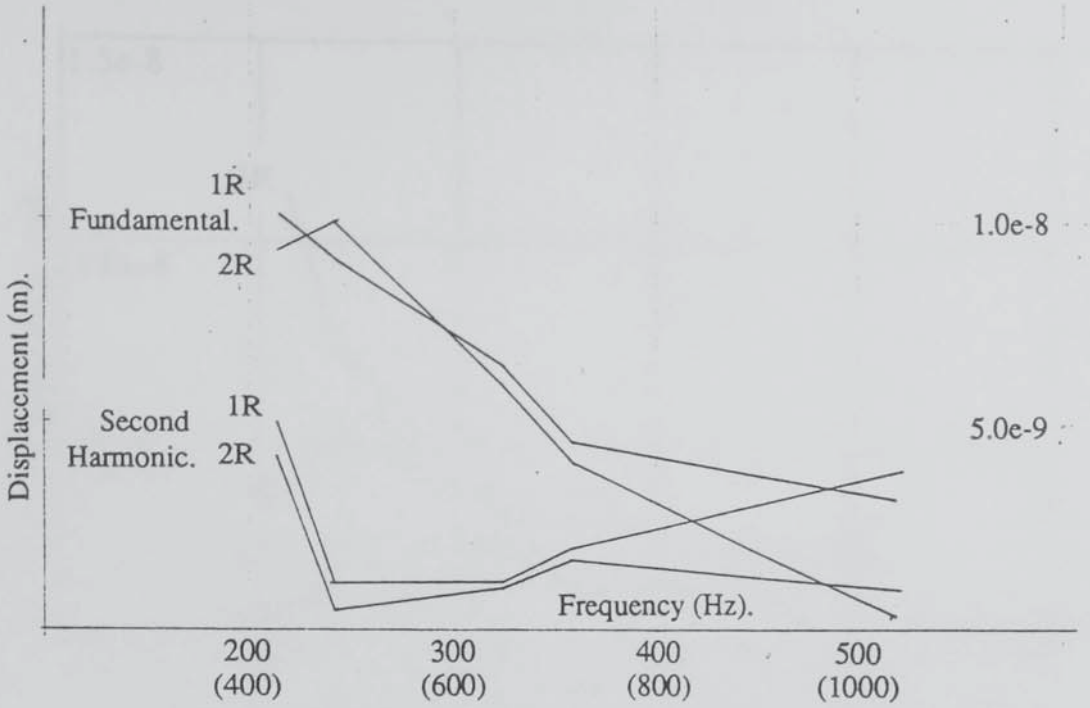

Fig. 8.19a Radial Displacements at Compole Ends

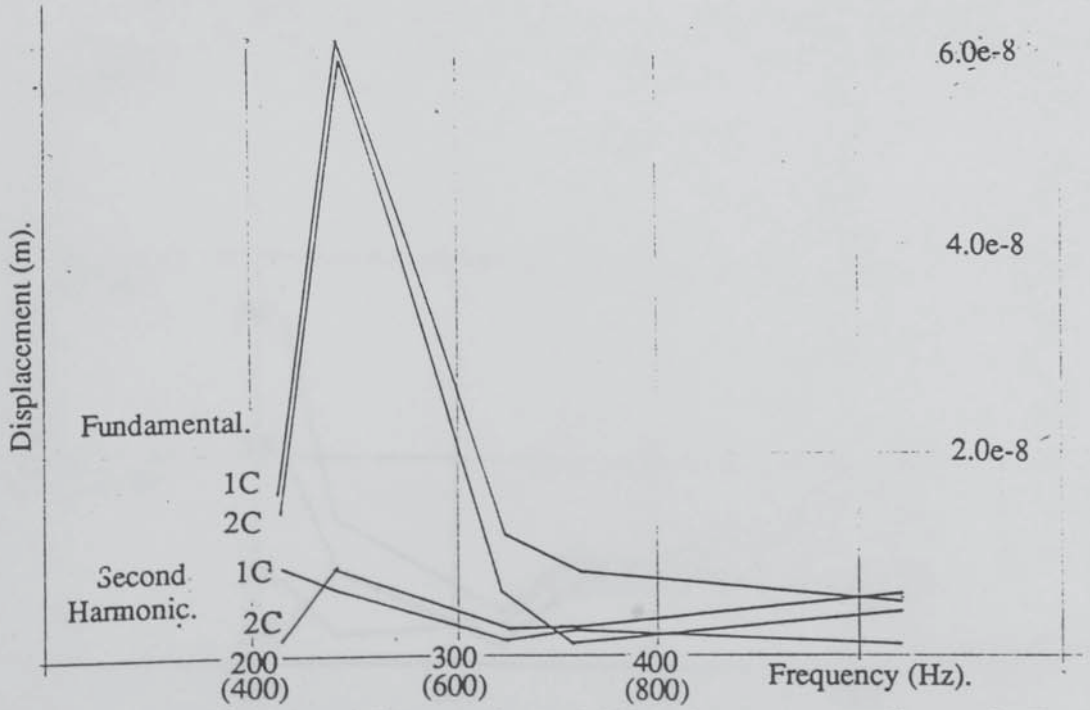

Fig. 8.19b Circumferential Displacements at Compole Ends

Fig. 8.19 Displacements at Compole Ends

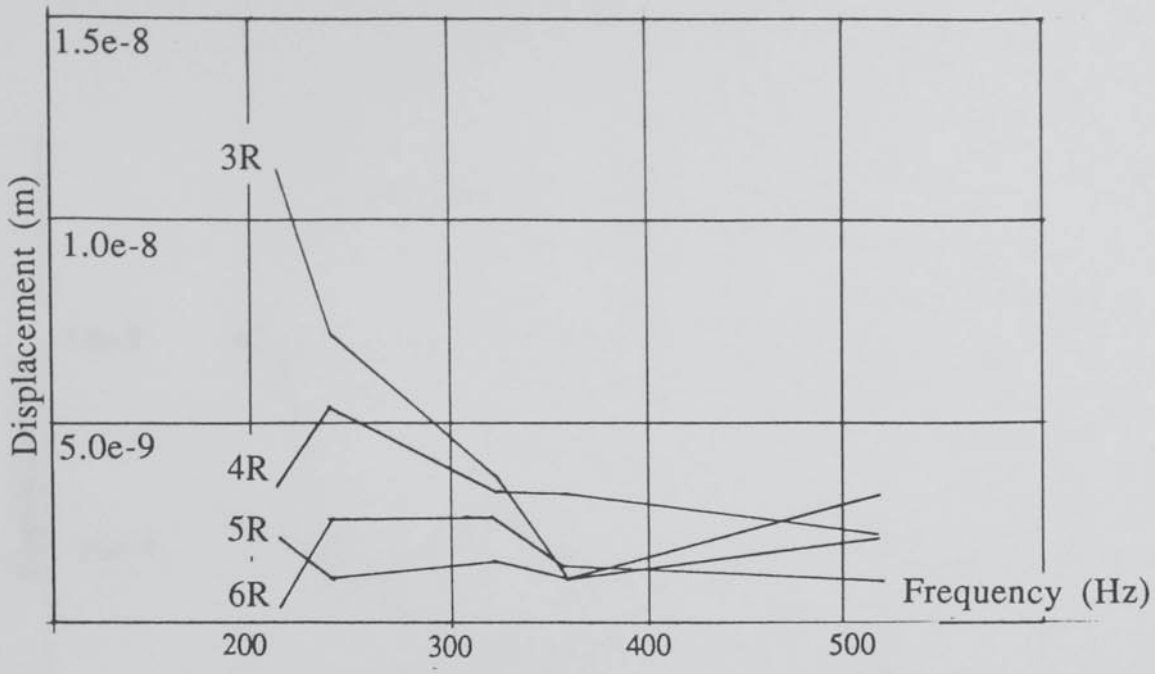

Fig. 8.20a Fundamental Slot-Passing Frequency.

Fig. 8.20b 2nd Harmonic of Slot-Passing Frequency.

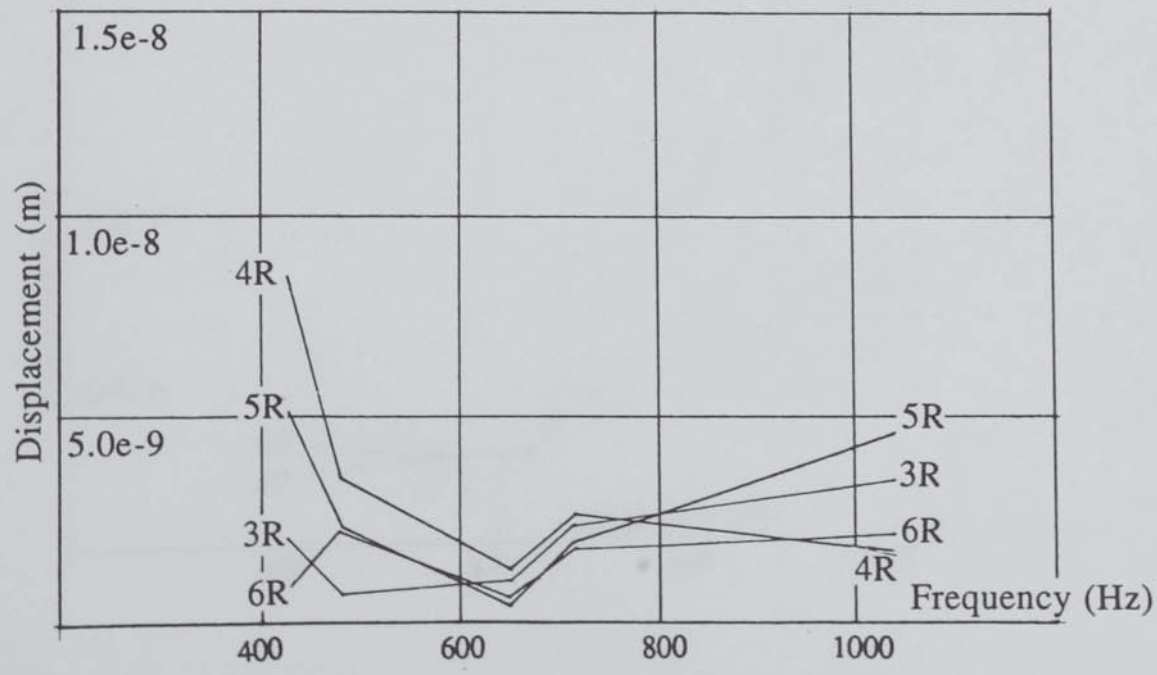

Fig. 8.20 Radial Deflections at Mainpole Ends.

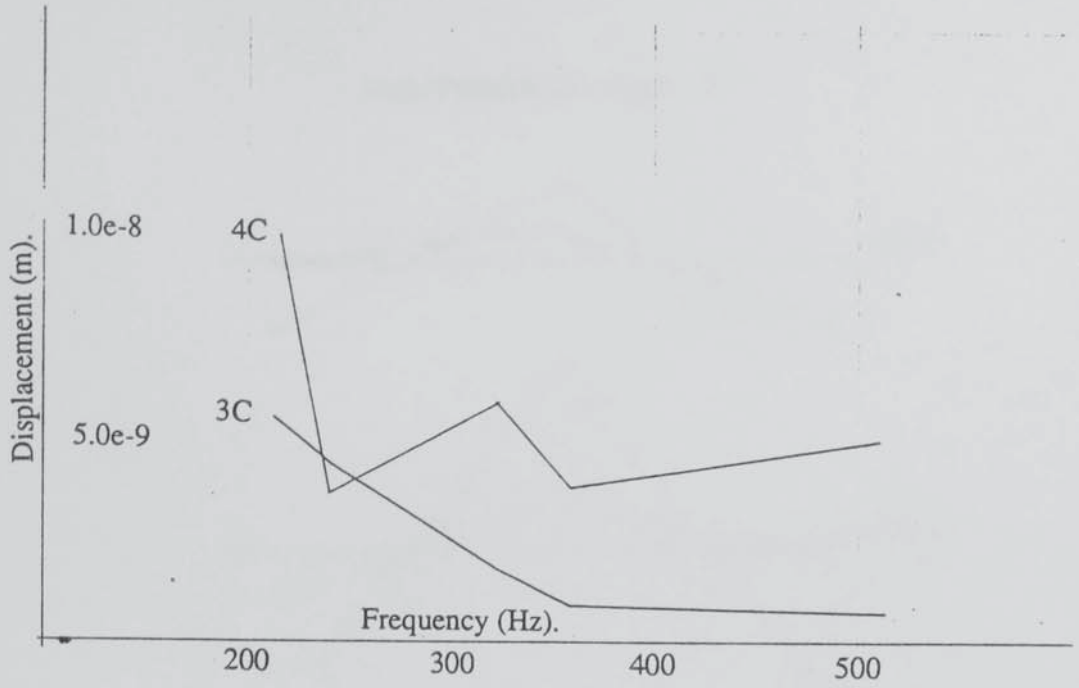

Fig. 8.21a Fundamental Slot-passing frequency.

Fig. 8.21b 2nd Harmonic of Slot-passing frequency.

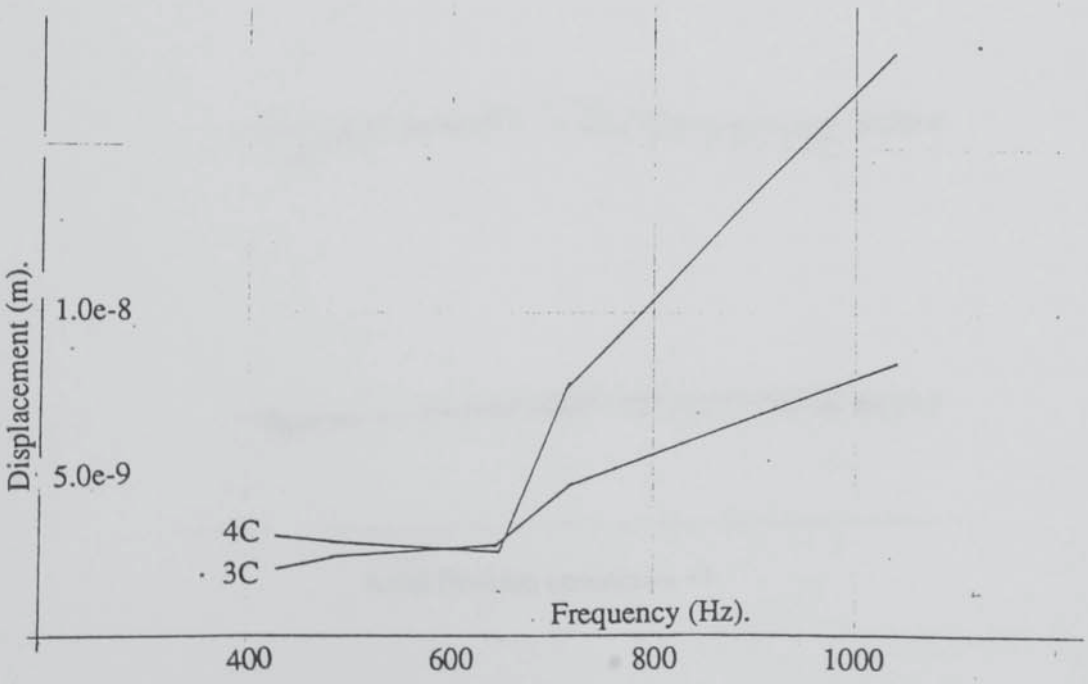

Fig. 8.21 Circumferential Displacements at Mainpole Ends

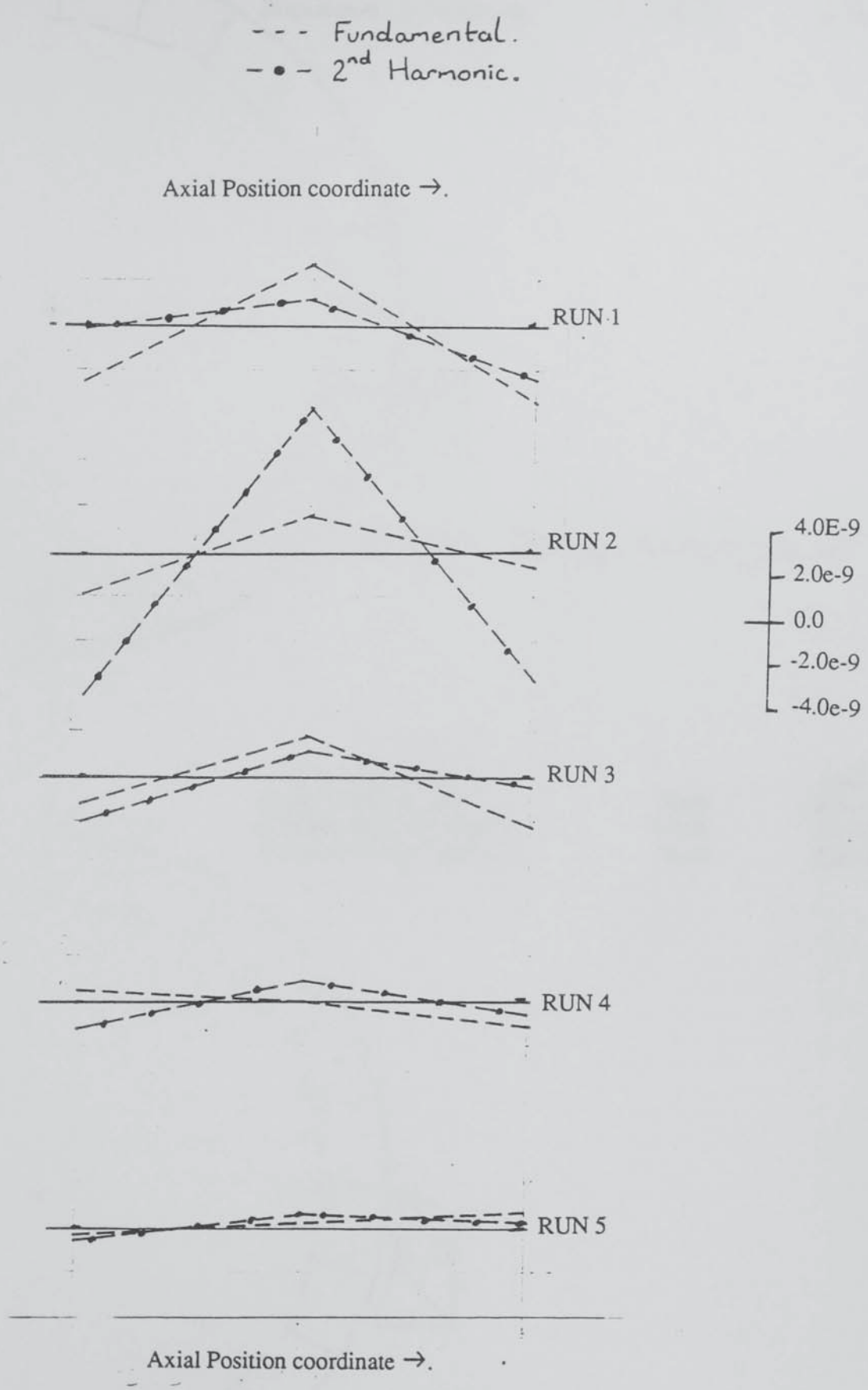

Fig. 8.22 Deflections Measured at the Bottom of the Machine.

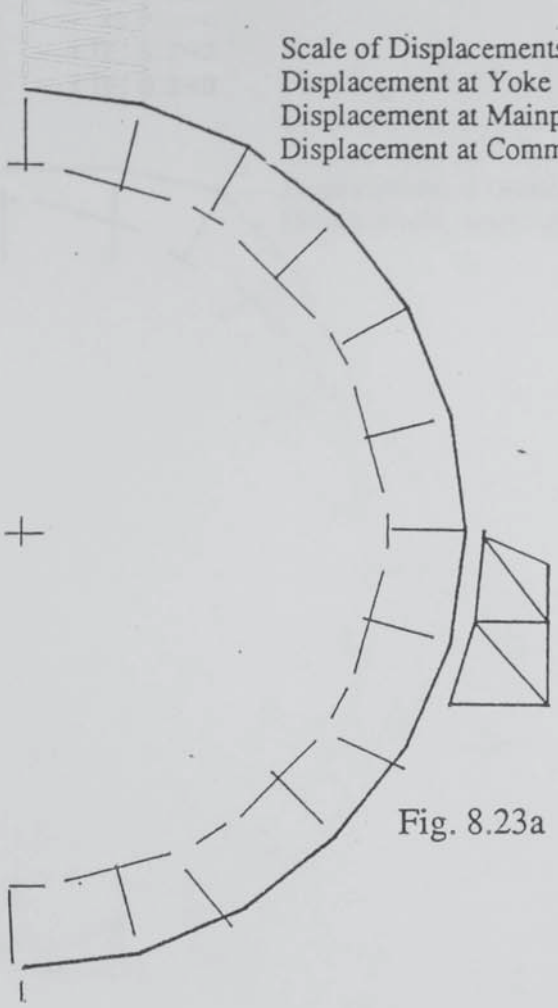

Fig. 8.23a Forcing :- RAD_CP_C1_A0

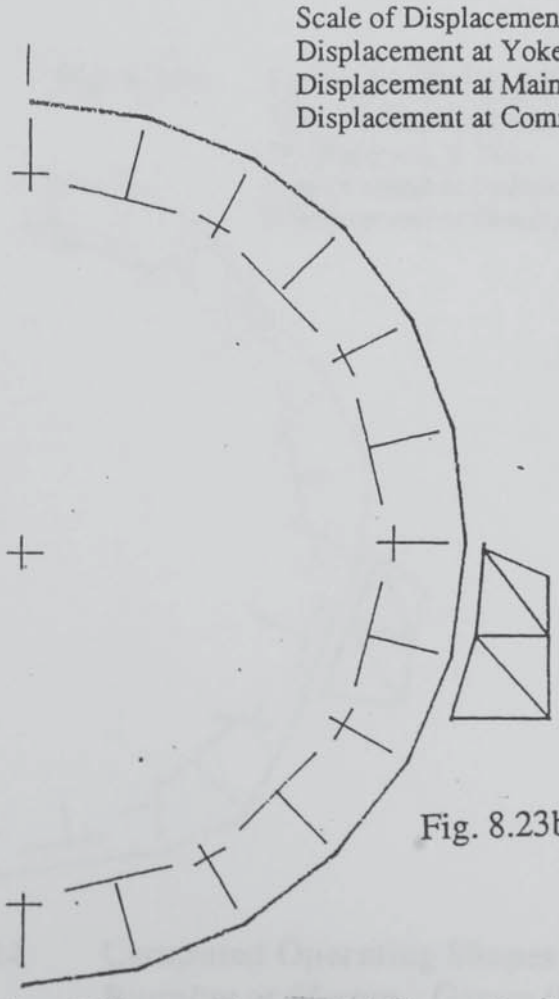

Fig. 8.23b Forcing :- RAD_MP_C1_A0

Fig. 8.23 Computed Operating Shapes for Machine B Running at 55 rpm - Group (RAD_C1_A0).

Fig. 8.24a Forcing :- RAD_CP_C2_A0

Scale of Displacements :-		5.0e7
Displacement at Yoke	(Rad)	1.42e-9
Displacement at Mainpole	(Ccf)	9.2e-10
Displacement at Commpole	(Rad)	1.96e-9

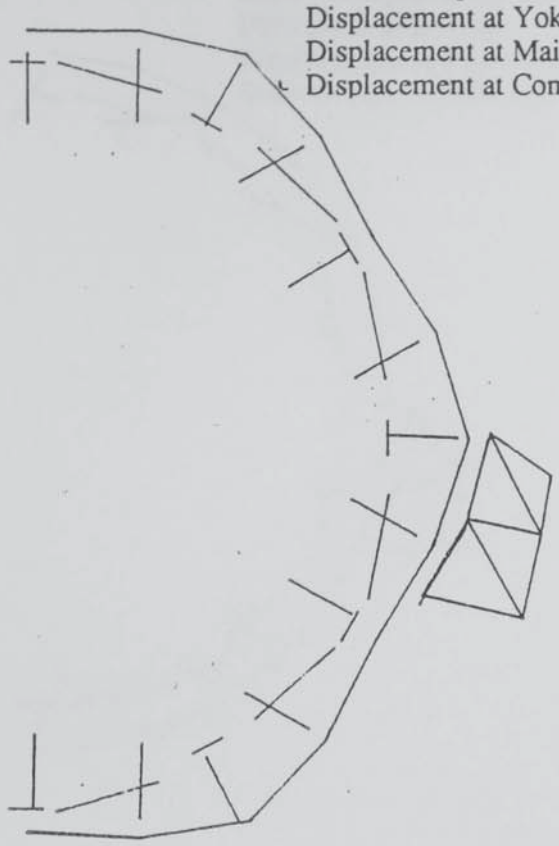

Fig. 8.24b Forcing :- RAD_MP_C2_A0

Scale of Displacements :-		5.0e7
Displacement at Yoke	(Rad)	1.43e-9
Displacement at Mainpole	(Rad)	1.54e-9
Displacement at Commpole	(Ccf)	9.2e-10

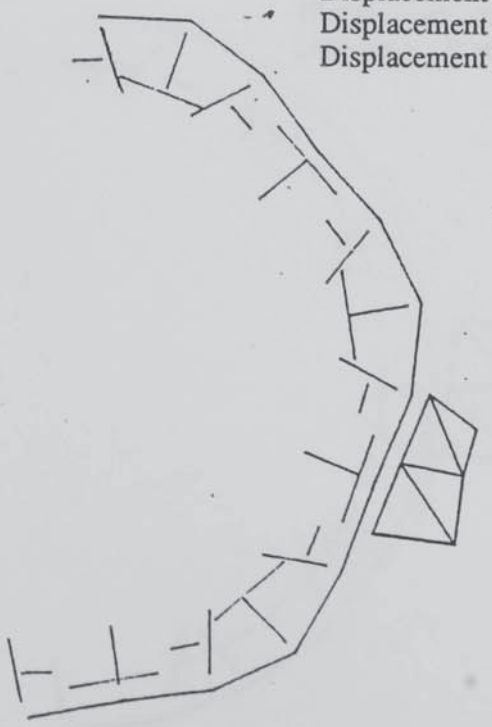

Fig. 8.24 Computed Operating Shapes for Machine B Running at 55 rpm - Group (RAD_C2_A0).

Fig. 8.25a Forcing :- CCF_MP_C1_A0

Scale of Displacements :-		1.0e7
Displacement at Yoke	(Ccf)	2.47e-9
Displacement at Mainpole	(Ccf)	1.51e-9
Displacement at Commpole	(Ccf)	3.82e-8

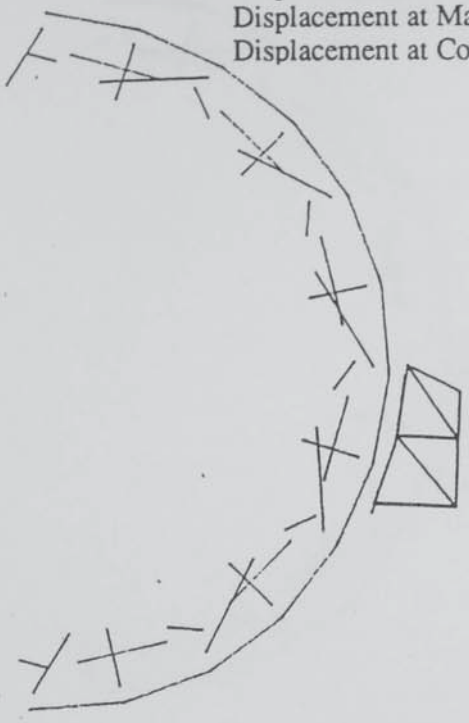

Fig. 8.25b Forcing :- CCF_MP_C1_A0

Scale of Displacements :-		5.0e7
Displacement at Yoke	(Ccf)	2.48e-9
Displacement at Mainpole	(Ccf)	2.02e-9
Displacement at Commpole	(Ccf)	2.05e-8

Fig. 8.25 Computed Operating Shapes for Machine B Running at 55 rpm - Group (CCF_C1_A0).

Fig. 8.26a Forcing :- CCF_CP_C2_A0

Scale of Displacements :-		5.0e7
Displacement at Yoke	(Rad)	3.06e-9
Displacement at Mainpole	(Rad)	3.04e-9
Displacement at Commpole	(Ccf)	4.48e-8

Fig. 8.26b Forcing :- CCF_MP_C2_A0

Scale of Displacements :-		5.0e7
Displacement at Yoke	(Rad)	2.23e-9
Displacement at Mainpole	(Ccf)	4.26e-9
Displacement at Commpole	(Rad)	1.93e-9

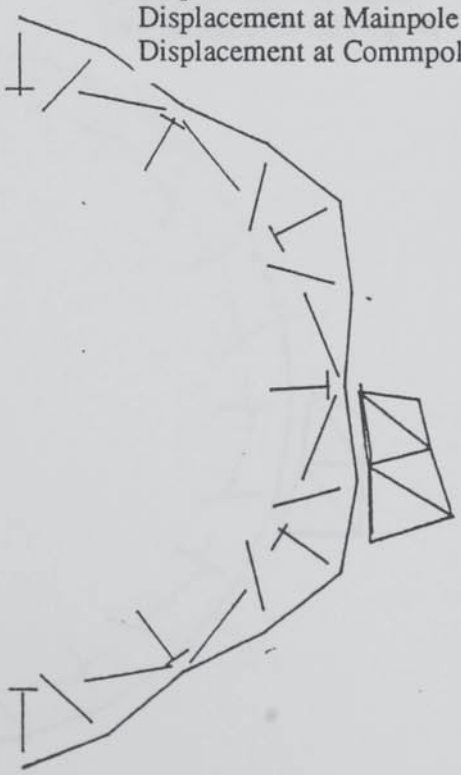

Fig. 8.26 Computed Operating Shapes for Machine B Running at 55 rpm - Group (CCF_C2_A0).

Fig. 8.27a Forcing :- MOM_CP_C1_A0

Scale of Displacements :-		2.5e7
Displacement at Yoke	(Ccf)	2.48e-9
Displacement at Mainpole	(Ccf)	1.50e-9
Displacement at Commpole	(Ccf)	1.70e-8

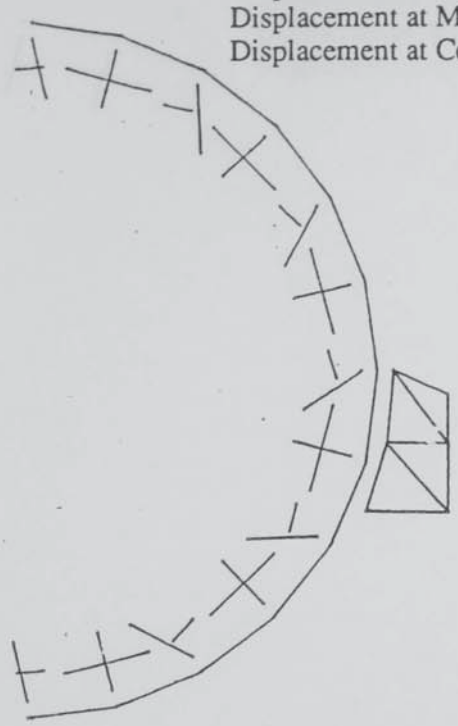

Fig. 8.27b Forcing :- MOM_MP_C1_A0

Scale of Displacements :-		2.5e7
Displacement at Yoke	(Ccf)	2.03e-9
Displacement at Mainpole	(Ccf)	6.52e-9
Displacement at Commpole	(Ccf)	1.82e-9

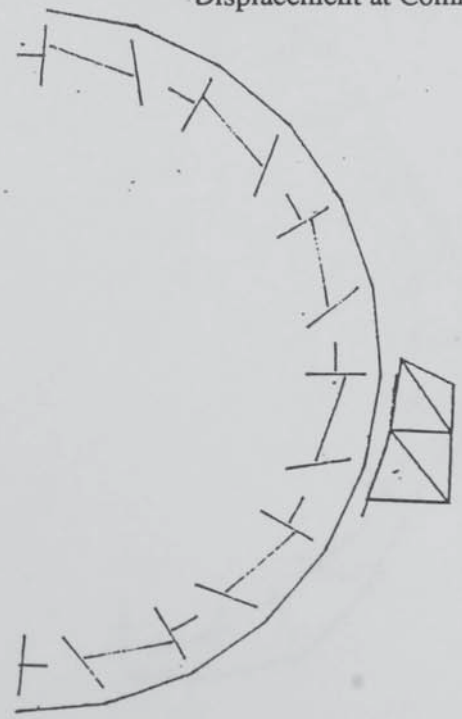

Fig. 8.27 Computed Operating Shapes for Machine B Running at 55 rpm - Group (MOM_C1_A0).

Fig. 8.28a Forcing :- MOM_CP_C2_A0

Scale of Displacements :-		1.0e6
Displacement at Yoke	(Rad)	1.13e-8
Displacement at Mainpole	(Rad)	1.04e-8
Displacement at Commpole	(Ccf)	1.78e-8

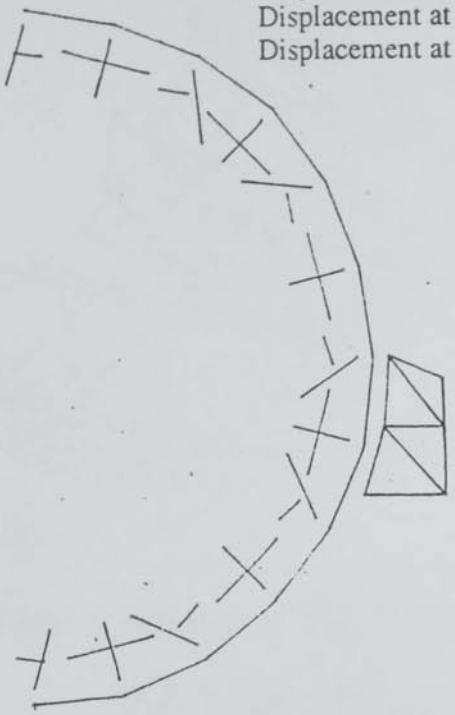

Fig. 8.28b Forcing :- MOM_MP_C2_A0

Scale of Displacements :-		1.0e7
Displacement at Yoke	(Rad)	5.71e-9
Displacement at Mainpole	(Ccf)	1.08e-8
Displacement at Commpole	(Rad)	5.53e-9

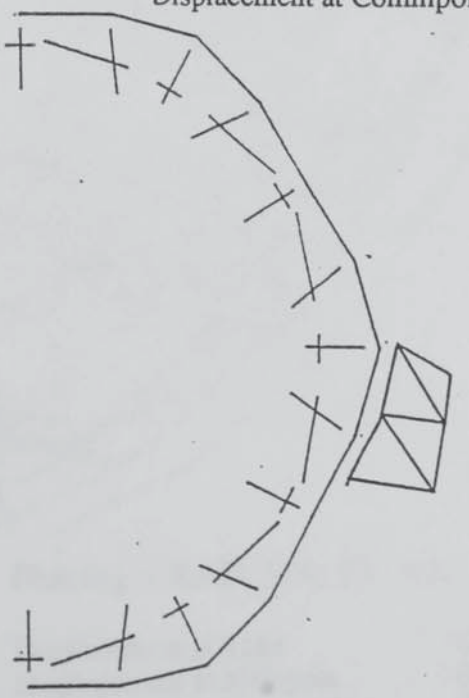

Fig. 8.28 Computed Operating Shapes for Machine B Running at 55 rpm - Group (MOM_C2_A0).

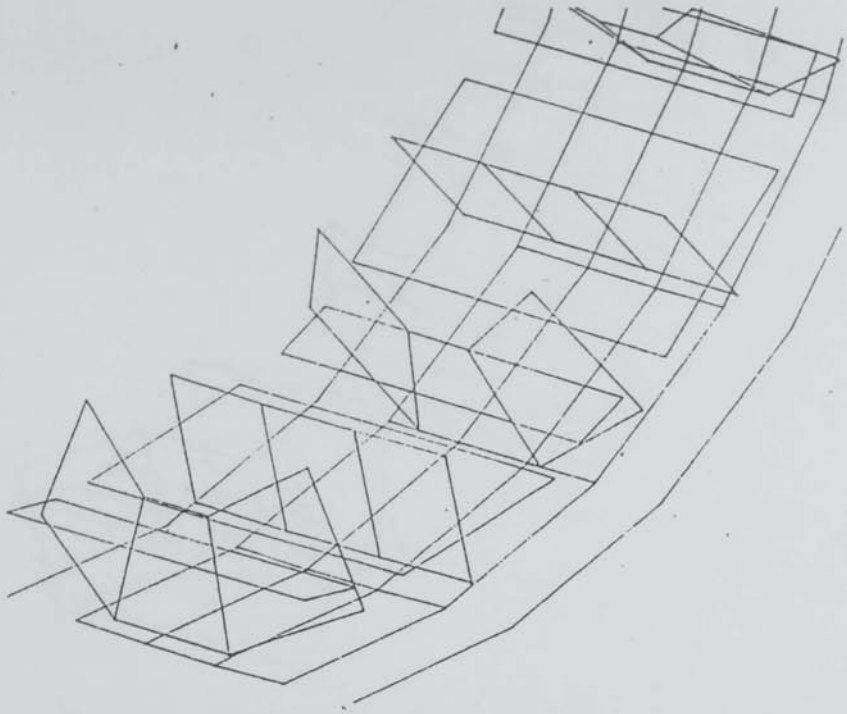

Fig. 8.29a Forcing :- RAD_CP_C1_A2 Frequency :- 430 Hz.

		Center	Edge
Displacement at Yoke	(Rad)	4.15e-12	1.50e-11
Displacement at Mainpole	(Rad)	~	~
Displacement at Commpole	(Rad)	9.34e-11	9.62e-11

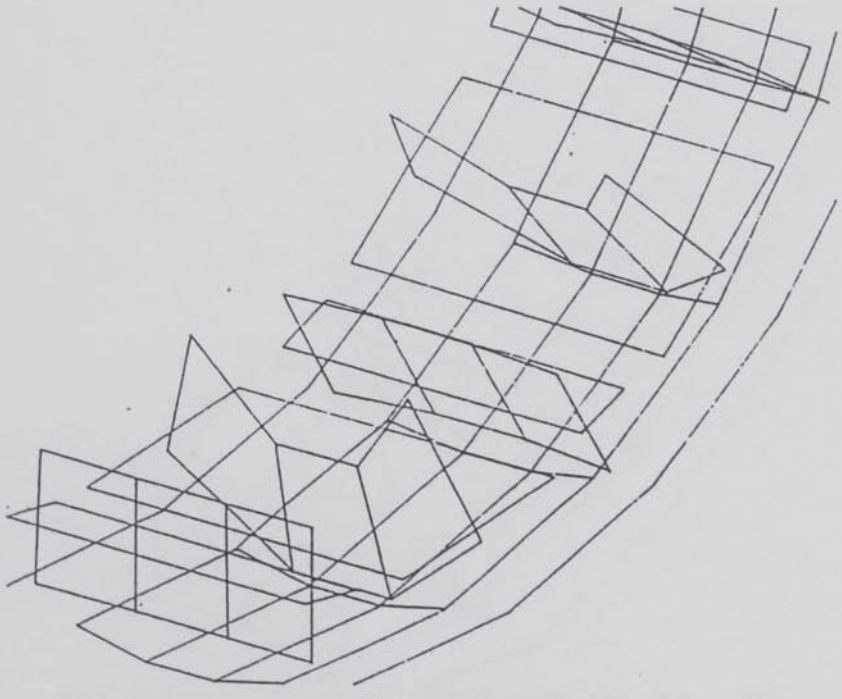

Fig. 8.29b Forcing :- RAD_MP_C1_A2. Frequency :- 430 Hz.

		Center	Edge
Displacement at Yoke	(Rad)	1.95e-11	3.81e-11
Displacement at Mainpole	(Rad)	7.18e-11	6.02e-11
Displacement at Commpole	(Rad)	~	~

Fig. 8.29 Computed Operating Shapes for Machine B Running at 55 rpm - Group (RAD_C1_A2).

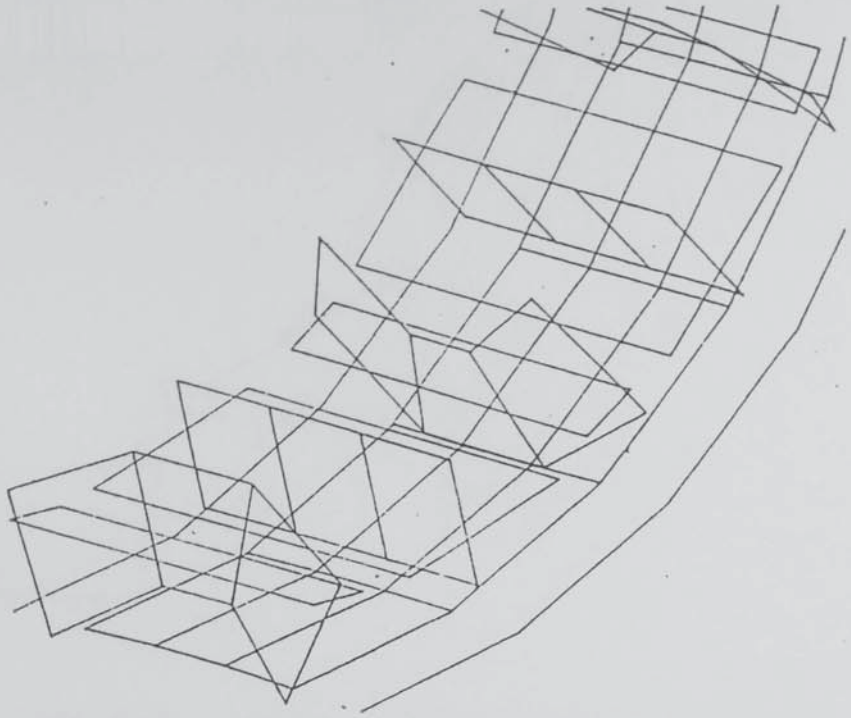

Fig. 8.30a Forcing :- RAD_CP_C2_A2 Frequency :- 430 Hz.

		Center	Edge
Displacement at Yoke	(Rad)	1.44e-12	1.79e-12
Displacement at Mainpole	(Rad)	~	~
Displacement at Commpole	(Rad)	9.30e-11	9.50e-11

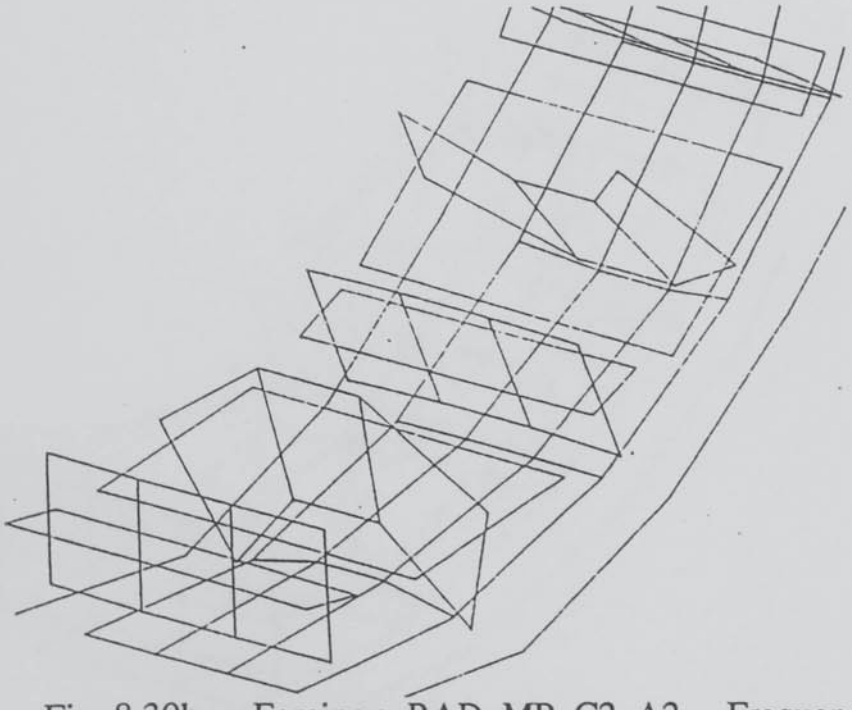

Fig. 8.30b Forcing :- RAD_MP_C2_A2 Frequency :- 430 Hz.

		Center	Edge	
Displacement at Yoke	(Rad)	1.49e-11		2.90e-11
Displacement at Mainpole	(Rad)	6.57e-11		5.92e-11
Displacement at Commpole	(Rad)	~		~

Fig. 8.30 Computed Operating Shapes for Machine B Running at 55 rpm - Group (RAD_C2_A2).

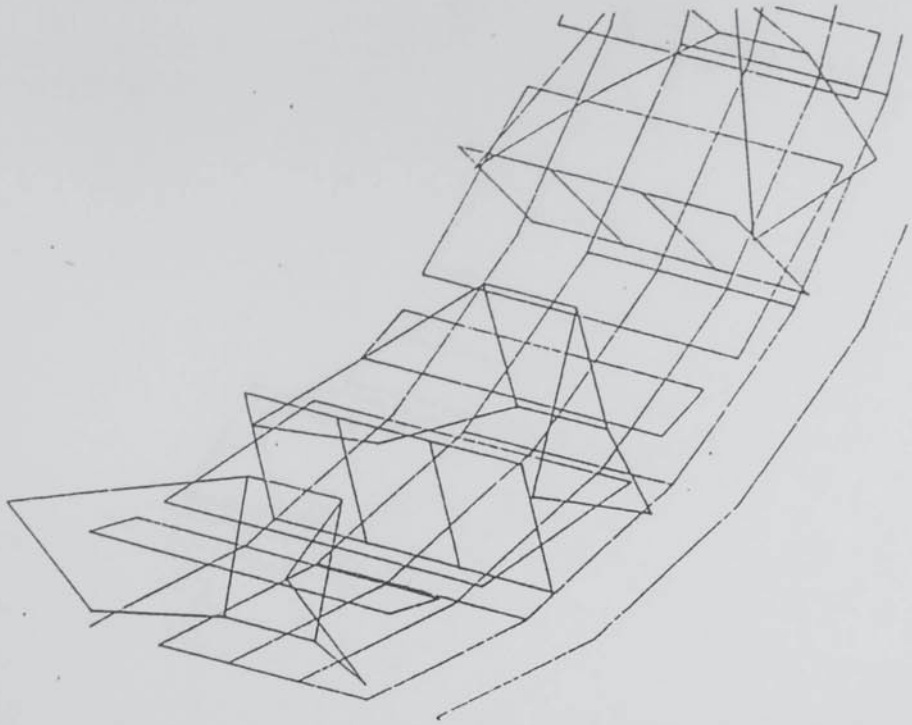

Fig. 8.31a Forcing :- CCF_CP_C1_A2 Frequency :- 430 Hz.

		Center	Edge
Displacement at Yoke	(Ccf)	1.78e-11	1.44e-11
Displacement at Mainpole	(Ccf)	3.05e-11	3.17e-11
Displacement at Commpole	(Ccf)	1.17e-9	1.76e-9

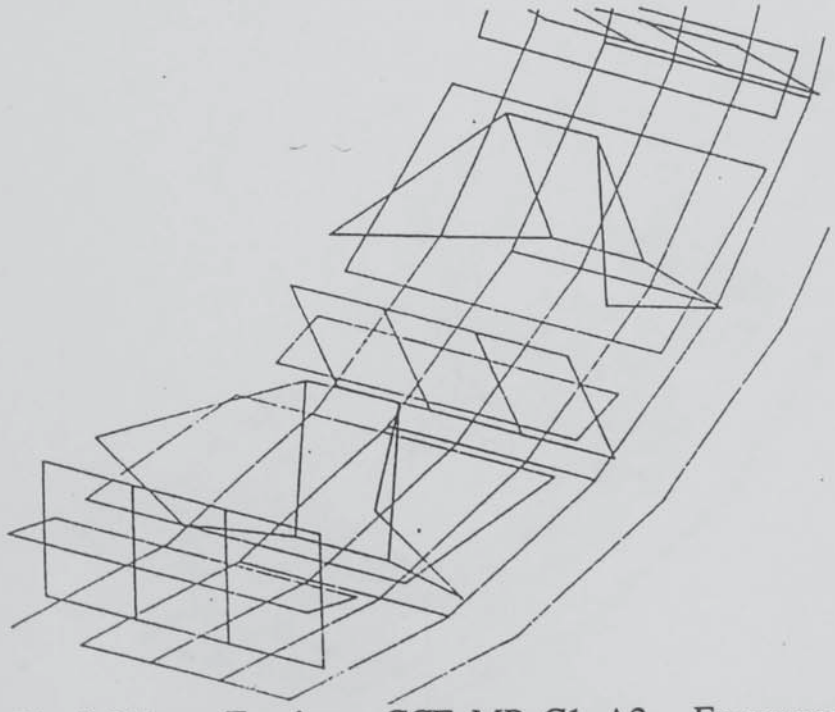

Fig. 8.31b Forcing :- CCF_MP_C1_A2 Frequency :- 430 Hz.

		Center	Edge
Displacement at Yoke	(Ccf)	3.75e-12	3.79e-12
Displacement at Mainpole	(Ccf)	2.35e-10	2.56e-10
Displacement at Commpole	(Ccf)	4.34e-11	4.38e-11

Fig. 8.31 Computed Operating Shapes for Machine B Running at 55 rpm - Group (CCF_C1_A2).

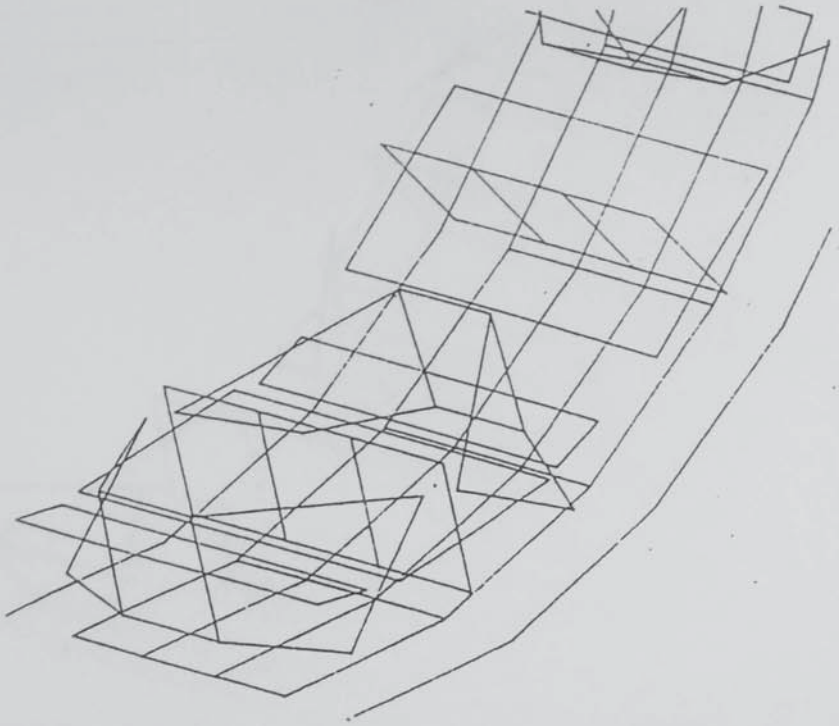

Fig 8.32a Forcing :- CCF_CP_C2_A2 Frequency :- 215 Hz.

		Center	Edge
Displacement at Yoke	(Rad)	3.28e-11	3.84e-11
Displacement at Mainpole	(Rad)	4.77e-11	4.97e-11
Displacement at Commpole	(Ccf)	9.76e-10	1.71e-9

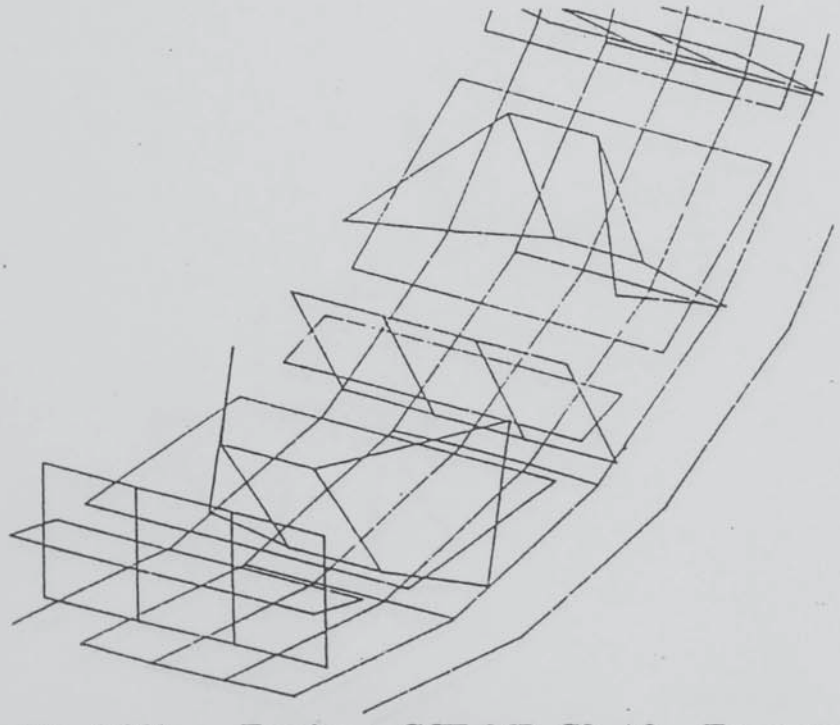

Fig. 8.32b Forcing :- CCF_MP_C2_A2 Frequency :- 215 Hz.

		Center	Edge
Displacement at Yoke	(Rad)	3.64e-12	7.36e-12
Displacement at Mainpole	(Ccf)	2.17e-10	2.21e-10
Displacement at Commpole	(Rad)	2.15e-12	2.58e-12

Fig. 8.32 Computed Operating Shapes for Machine B Running at 55 rpm - Group (CCF_C2_A2).

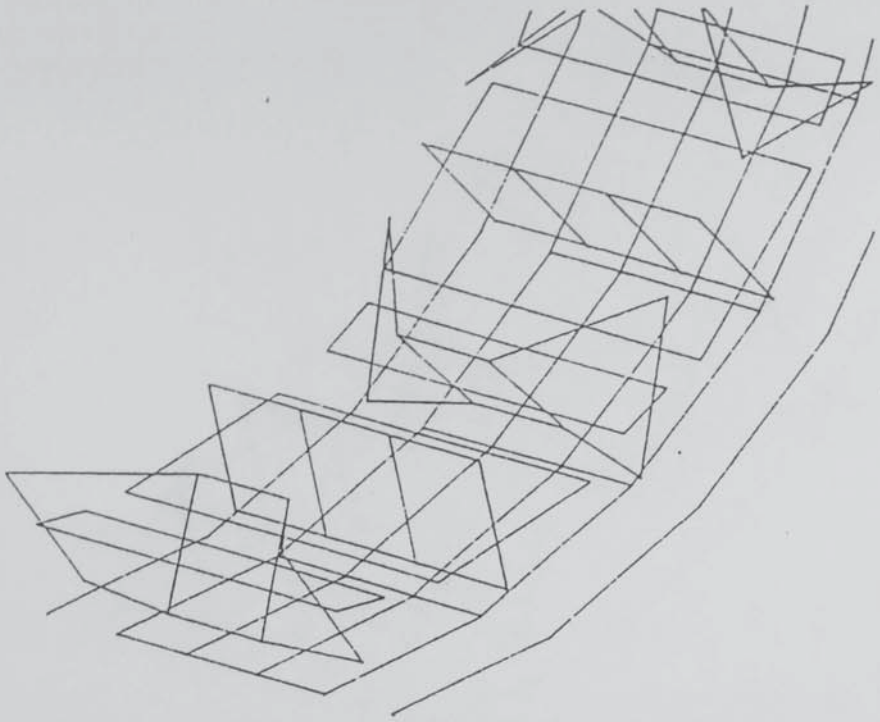

Fig. 8.33a Forcing :- MOM_CP_C1_A2 Frequency :- 430 Hz.

		Center	Edge
Displacement at Yoke	(Ccf)	2.01e-11	2.84e-11
Displacement at Mainpole	(Ccf)	4.21e-11	4.17e-11
Displacement at Commpole	(Ccf)	3.13E-9	4.15e-9

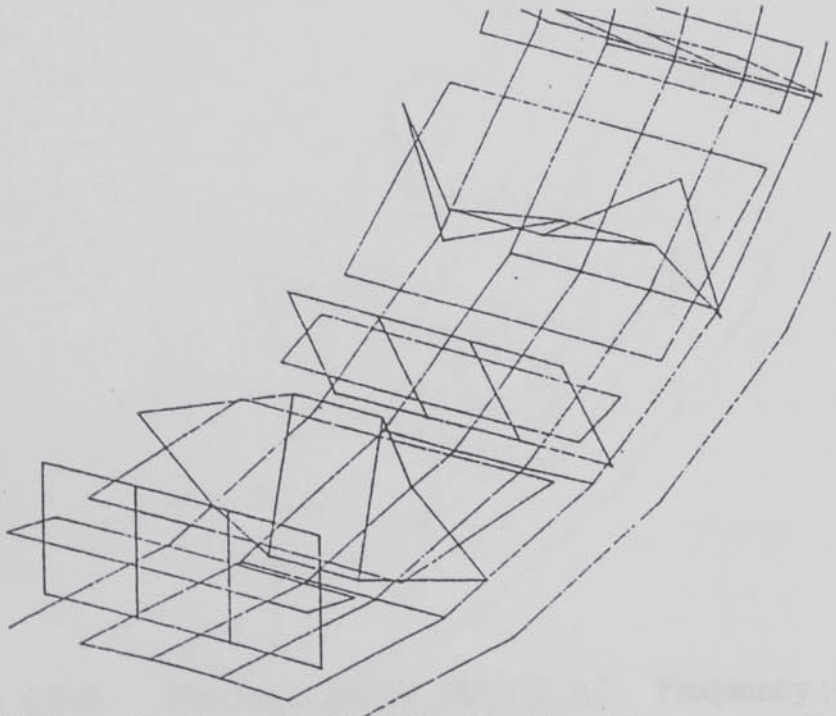

Fig. 8.33b Forcing :- MOM_MP_C1_A2 Frequency :- 430 Hz.

		Center	Edge
Displacement at Yoke	(Ccf)	6.97e-12	1.26e-11
Displacement at Mainpole	(Ccf)	8.42e-10	9.39e-10
Displacement at Commpole	(Ccf)	1.35e-11	1.65e-11

Fig. 8.33 Computed Operating Shapes for Machine B Running at 55 rpm - Group (MOM_C1_A2).

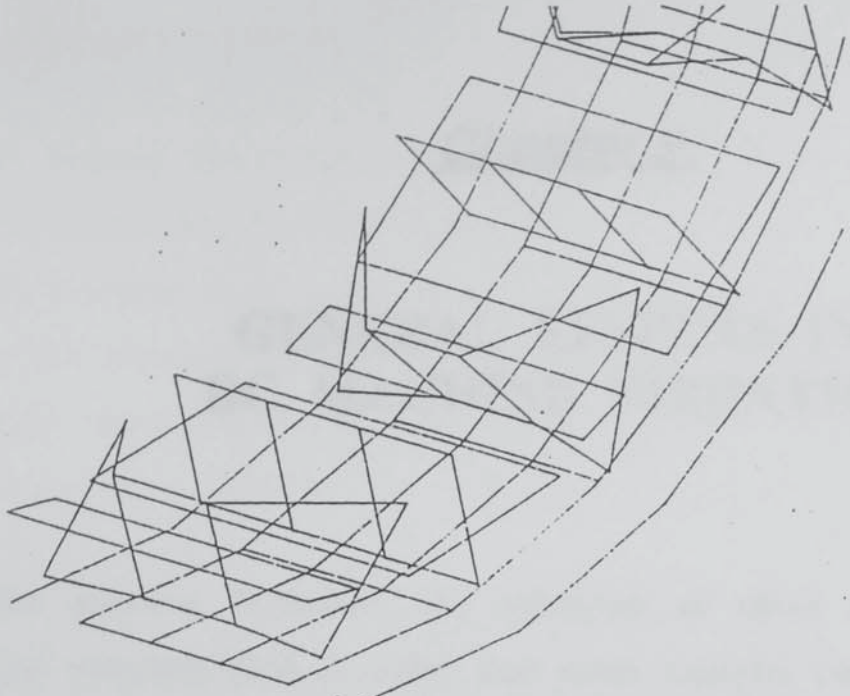

Fig. 8.34a Forcing :- MOM_CP_C2_A2 Frequency :- 215 Hz.

		Center	Edge
Displacement at Yoke	(Rad)	5.02e-11	4.86e-11
Displacement at Mainpole	(Rad)	7.15e-11	6.54e-11
Displacement at Commpole	(Ccf)	2.81e-9	4.06e-9

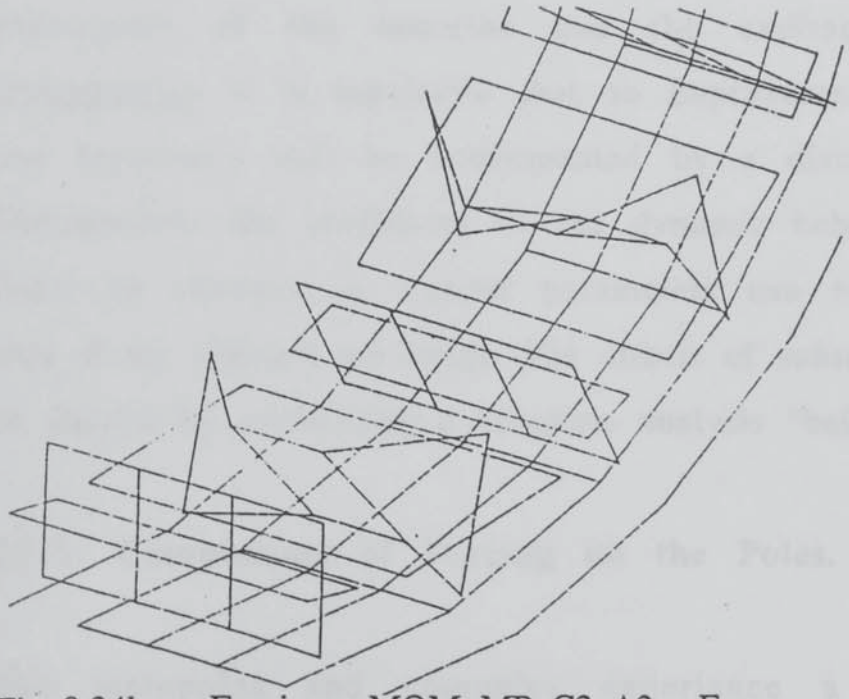

Fig. 8.34b Forcing :- MOM_MP_C2_A2 Frequency :- 215 Hz.

		Center	Edge
Displacement at Yoke	(Rad)	1.53e-11	4.33E-11
Displacement at Mainpole	(Ccf)	7.92E-10	8.24e-10
Displacement at Commpole	(Rad)	8.73E-12	1.28e-12

Fig. 8.34 Computed Operating Shapes for Machine B Running at 55 rpm - Group (MOM_C2_A2).

Chapter 9.

GENERAL EFFECTS IN DC MACHINE VIBRATION

In the existing literature, the vibration of these machines has been greatly oversimplified in order that some analysis could take place. The greater the simplification, the greater will be the uncertainty associated with the answers produced by that analysis. In this chapter, some of the mechanical determinants of the vibration levels in machines are discussed in the context of how the vibration might be reduced. The effect of any one parameter in a machine is governed by the other parameters of the machine and the excitation (both type and frequency). It is inevitable that an improvement in the behaviour at one frequency will be accompanied by a disimprovement at others. Furthermore, the sensitivity of the dynamic behaviour of the machine stator to changes in various parameters can be accurately estimated only if the changes are small. The effects of substantial changes can only be judged by performing a complete analysis "before" and "after".

§9.1 Components of Forcing on the Poles.

The mainpoles and compoles experience a complex pattern of electro-magnetic forcing from the armature. The original approach used for the analysis of the response of machines to these forces was to discretise the forces into a finite number of point forces and moments.

These discrete forces were then applied all together to the poles of the theoretical model. A more organised method is to examine the response of the machine to a "unit" of each of the contributing force components. Then the response of the machine to the working force pattern can be assessed using the principle of superposition to combine the response of the machine to each of the components in suitable proportion.

The total forcing on the poles of a machine can be subdivided according to the following criteria:

(1)	Radial, Circumferential or Moment force.	"RAD"/"CCF"/"MOM"
(2)	Action on Mainpoles or Compoles.	"MP"/"CP"
(3)	Circumferential Distribution .	"C1"/"C2"/"C3"
(4)	Axial Distribution is	"A0"/"A1"/"A2".

Items (1) and (2) above are self-explanatory.

The circumferential distribution is allowed to be one of three cases. The number of slots on the armature is always an integer multiple of the number of pole-pairs in the machine. If it were not, there would be a rotating UMP (unbalanced magnetic pull) acting on the magnet frame at slot-passing frequency. If the integer multiple is <u>even</u>, the forces on all mainpoles are in phase and similarly, the forces on all compoles are in phase. The substring "C1" references this type of circumferential distribution. If the integer multiple is <u>odd</u>, - as tends to be the case - then the forces on adjacent poles are 180° out of phase (regardless of the type of force). The substring "C2" is used to reference the circumferential distribution in which forces on adjacent mainpoles and

compoles are 180° out of phase. An error in the pole-spacing can be represented as an extra force acting with the normal forces. Fig. 9.1 shows how this error force can be computed vectorially. In a multipolar machine, there are a number of independent spacing errors possible. However, by quantifying the response to the worst error force acting on a single pole, one can normally estimate the effect of the worst combination of pole-spacing errors. The characters "C3" in the name of a force pattern indicate that the forces apply to one pole only. Depending on the extent to which the symmetry of the machine is disturbed, the response of the machine to forcing on an single pole can vary considerably according to which pole is forced.

The axial distribution of force on a pole is determined principally by the skew of the armature. An unskewed armature produces force patterns which are (for all practical purposes) axially uniform. In the nomenclature adopted for the force components, "A0" is used to identify the axially uniform force component. On machines designed for quiet operation, the armature is normally skewed. In "straight-line" skew the angular location of the center of one slot of the armature varies linearly along the axis so that at one end it is angularly displaced from the other (normally by one slot-pitch). Ideally, the distribution of the fundamental slot-passing flux-ripple along the poles should then vary sinusoidally in the axial direction. The inclusion of ducts and the existence of fringing cause the distribution to deviate from sinusoidal.

The straightline skew (with a skew factor of 1.0) causes a fundamental slot-passing frequency force to be axially distributed like one wavelength of a cosine at one instant in time. (Of course, that 'instant'

will not be the same for the radial force as it is for the circumferential force etc.) When the armature is rotated from this position by one-half of a slot-pitch, the axial distribution of the force is like one wavelenth of a sine waveform. This is explained in more detail in Appendix 8.

The 'sin' force distribution is obviously antisymmetrical w.r.t. a plane dividing the machine axially in half. At low frequencies (relative to the spectrum of resonances of the magnet frame) the 'sin' distribution tends to significantly excite modes of the machine which are antisymmetrical about the afore-mentioned plane while the 'cos' force tends to excite the symmetrical modes though rarely to the same extent. The reason for the difference is that the modes which can be excited by the 'cos' force involve flexure of the yoke in the axial direction while the modes excited by the 'sin' force do not involve this flexure. In order to remove the antisymmetrical component of the force distributions, some armatures are herringbone skewed. Appendix 8 gives a concise quantitative description of the components of force distributions from the straightline and herringbone skew.

Clearly, it is possible to Fourier-analyse the distribution of force on a pole into trigonometric components. Given the complexity of the distribution, we would require a relatively large number of terms to do this accurately although it is clear from experience that very few terms (properly chosen) can be used in the theoretical model without loss of accuracy. On relatively short machines, the yoke is very reluctant to bend in radial planes. Longer machines are more flexible where bending in radial planes is concerned. Experience shows that for the usual yoke dimensions, only three separate components of the axial force

distribution need be considered. Other components are suppressed by the stiffness of the yoke and the poles against bending in a radial plane. These components are illustrated in Fig 9.2a, 9.2b and 9.2c.

The cosine shape of "A2" (Fig. 9.2c) is not ideal. A better shape would be the quadratic form shown in Fig. 9.2d, because this is closer to the shape in which the pole and yoke naturally deform. However, the cosine shape lends itself much more easily to analysis.

The following examples illustrate the naming convention adopted in this work for the force components.

RAD_MP_C1_A0 — A radial force acting on the mainpoles. Forces on all mainpoles are in phase and the axial distribution of the forces is uniform.

CCF_CP_C2_A2 — A circumferential force acting on the compoles. Forces on adjacent compoles are 180° out of phase. The axial distribution of the force is a cosine waveform (see above).

MOM_CP_C3_A1 — A moment force acting on a single compole . The axial distribution of the force is a straight line passing through zero at the center of the pole.

By applying each of these force components in turn to the theoretical model, a full description of the behaviour of the stator is prepared. In

the case of a machine which is straightline skewed and in which the number of armature slots is an odd integer multiple of the number of pole-pairs, 54 independent force patterns exist and must be investigated. Each of these force patterns can be automatically generated within the DMS software. Occasionally some subsets of these cases can be dismissed if a simple hand calculation indicates that they will not be contributing significantly to the total vibration levels of the machine. Section 9.2 is a brief discussion of the relative importance of each of these force patterns.

Note that when the number of slots on the armature is an odd integer multiple of the number of pole-pairs, the circumferential distribution of forces for the fundamental slot-passing forces is "C2" (assuming that there are no pole-spacing errors) but the circumferential distribution of the second harmonic (and all even harmonics of the slot-passing force) is "C1".

If the number of slots on the armature of the machine is an even integer multiple of the number of pole-pairs the circumferential distribution "C1" does not occur for any force. If the machine is herringbone skewed, the axial distribution "A1" does not occur unless there is an error in the alignment of the poles.

So far we have explained only the "proportions" of each of the force components. In order to put these to practical use, each one must be quantified in a meaningful way. The convention which appears most satisfactory is to use unit force-per-metre. Thus, the force component "RAD_CP_C2_A0" corresponds to a total radial force of "1" N acting on

each of the compoles where "l" is the axial length of the compoles. Similarly, "RAD_MP_C1_A1" corresponds to a radial force on each of the mainpoles which is a dependent on z (z is the coordinate of axial position, z=0 for the axial center of the mainpoles and compoles) according to :-

$$F_r = 2\,z/\,l \quad N/m \tag{9.1}$$

The total radial force on the mainpoles is zero for "RAD_MP_C1_A1" .

The units appropriate to the force components are "N/m" for the "RAD" and "CCF" components and "Nm /m" for the "MOM" components.

If simplifying assumptions are made, it is sometimes possible to examine the force components in groups. In such cases, one or more of the elements of the force component identifiers is discarded. For example, at no-load operation of a machine which has an unskewed armature, all forces on the compole are theoretically zero (by symmetry considerations) and the axially-uniform distribution of force "A0" is only significant one. The subset of relevant force components is then collectively termed "MP_A0".

§9.2 The Relative Importance of the Various Component Force Patterns.

For the purposes of this discussion, it is assumed, to begin, that the frequency of the forcing is low relative to the various natural

frequencies of those modes of the stator which can be excited significantly by the various component force-patterns. This assumption is relaxed later for some cases, but it must be understood that any one of the 54 force patterns is capable of creating dominant vibrations on the yoke if the frequency of forcing is sufficiently close to a suitable mode of the frame.

In assessing the "importance" of any one force component, we must have a clear criterion by which the responses to different modes can be compared. The obvious basis for such a criterion is the total r.m.s vibration of the yoke (ie. the total vibration energy present). If we interested in the noise generated by the machine, a more suitable criterion would be based on the r.m.s radial vibration of the yoke. It should be understood that the conclusions drawn in this case would be quite different.

9.2.1 Forces Applied to the Yoke Only.

It is instructive to firstly examine how the yoke of the machine would respond to each of the force components in turn if they were transferred without modification via the poles to the yoke. Radial, circumferential and moment forces are considered to be applied directly to the yoke behind the poles. The yoke is considered to be a complete cylinder with no other steelwork attached. The number of poles on the machine is denoted n_p.

The "RAD_C1_A0" force components

It is straightforward to show using symmetry arguments that the force component "RAD_MP_C1_A0" will produce the same rms vibration of the yoke as "RAD_CP_C1_A0" so the differentiation is dropped for the present and these force components are collectively termed "RAD_C1_A0". These force components act to excite two classes of modes of the yoke :-

(a) Yoke "flexure" modes which have n_p wavelengths about the circumference.

(b) Yoke "extension" modes which have zero wavelengths about the circumference.

In the case of both (a) and (b) here, the axial profile of the modes is symmetrical about the center plane of the yoke (dividing the yoke axially in two). The mode from each class which has the lowest stiffness is the mode for which the axial profile is a "horizontal" line.

The chief "extensional" mode of the machine is more stiff than the chief "flexural" mode if n_p is small, and vice-versa if n_p is relatively large. That is, the force components "RAD_MP_C1_A0" and "RAD_MP_C1_A0" would be expected to produce greater radial displacement contributions from the "flexure" mode than they would from the "extensional" mode. Denoting the stiffness of the chief "extensional" mode as K_e we define it as . .

K_e = (Radial Displacement of the Yoke due to "RAD_C1_A0")$^{-1}$ (9.2)

. . . and using elementary ring theory, K_e is quantified as

$$K_e = E \cdot d / r_m \quad (9.3)$$

For the present, "d" is the radial thickness of the yoke, " r_m" is the mean radius and "E" is Young's modulus for steel following the usual convention.

The stiffness of the chief "flexural" mode is denoted K_{f1} and we define it as . .

K_{f1} = (Peak Radial Displacement of the Yoke due to "RAD_C1_A0")$^{-1}$ (9.5)

. . . and using elementary ring theory again, K_{f1} is quantified as

$$K_{f1} = (E \pi \ d^3 (n_p^2-1)^2) / (12 \ r_m^3) \quad (9.6)$$

Now, the "flexural" mode produces a r.m.s yoke vibration of approximately one half of the peak radial vibration on the yoke, so it is concluded that the flexure mode is more significant than the extensional one when the following condition obtains :-

$$\pi \; d^2 \; (n_p^2 - 1)^2 \; / (12 \; r_m^2) < \; 2 \qquad (9.7)$$

In the case where d=0.125, r_m= 1.5 and n=12, the expression above is evaluated to be 26.2 and so the extension mode will contribute virtually all of the vibration of the yoke.

The rms. vibration of the bare-yoke subjected to these force components can be readily assessed using the equations above.

The "RAD_C2_A0" force components.

These force components excite only one class of modes of the yoke (circumferential flexure) in which there are n/2 full wavelengths of vibration about the periphery of the yoke. The lowest-stiffness mode of these is again the mode in which the axial profile is a "horizontal" line. We denote the stiffness of this mode as K_{f2} and define it by (9.8) below similar to (9.5).

K_{f2}=(Peak Radial Displacement of the Yoke due to "RAD_C2_A0")$^{-1}$

$$\wedge \Diamond \wedge \Diamond \wedge \Diamond \wedge \; \Rightarrow \qquad (9.8)$$

. . . and again using elementary ring theory, K_{f2} is quantified as

$$K_{f2} = \; (E \pi \; d^3 \; ((n_p/2)^2 - 1)^2) \; / \; (12 \; r_m^3) \qquad (9.9)$$

Again, the rms vibration of the yoke is approximately one half of the peak radial vibration of the yoke. Thus the importance of these forces

can be immeditately assessed.

Now when the r.m.s. yoke vibration due to the force components "RAD_MP_C1_A0" or "RAD_CP_C1_A0" is compared with the rms yoke vibration due to the force components "RAD_MP_C2_A0" or "RAD_CP_C2_A0", there are two possible conclusions depending on the geometry of the yoke.

(1) If the "extensional" modes dominate the vibration caused by the "RAD_C1_A0" forces (as will tend to be the case for multipolar machines), the comparison of the stiffness, K_e, of the yoke with regard to the "RAD_C1_A0" forces and the stiffness, K_{f2}, of the yoke with regard to the "RAD_C2_A0" shows that the "RAD_C1_A0" forces are more significant when the condition expressed by (9.10) below obtains.

$$\pi \; d^2 \; ((\; n_p/2)^2-1)^{\;2} \; / \; (12 \; r_m^{\;2}) < \; 2 \qquad (9.10)$$

(2) If the "flexural" modes dominate the vibration caused by the "RAD_C1_A0" forces (or if they are similar-in-importance to the "extensional" modes) then it may be be stated without further ado that the "RAD_C1_A0" force components are <u>less</u> significant at the low frequency end of the spectrum than the "RAD_C2_A0" forces by a factor of approximately . . .

$$\text{"C2/C1\_Stiffness\_Ratio"} \; = \; ((\; n_p/2)^2-1)^2 \; / \; (n_p^{\;2}-1)^{\;2} \qquad (9.11)$$

Thus the "RAD_C1_A0" force components are easily compared with the "RAD_C2_A0" components using the reasoning above. Now, the "RAD_C2_A0" force components are contributed by the fundamental and odd harmonics of slot-passing if the number of armature slots is an odd integer multiple of the number of pole-pairs. "RAD_C1_A0" components are contributed by the even harmonics of such an armature.

The "CCF_A0" force components

Acting on the poles of a machine, these components are often equal in importance to the "RAD_A0" force components. They cause the poles to rock relative to the yoke to some extent and it is the resulting moment on the yoke which is primarily responsible for the contribution from these forces to the rms yoke vibration. "CCF_A0" forces acting on the yoke itself have virtually no effect at low frequencies except in one instance. The exception is the response of the yoke to "CCF_C1_A0". This force pattern tends to rotate the yoke about its own axis relative to the armature. Since the yoke is not required to deform at all, the only stiffness resisting this motion is that introduced by the feet. At all practical speeds of motor operation, the dynamic mass of the yoke for this mode is equal to the true mass of the yoke and it is the inertia rather than stiffness which determines the level of the motion.

For the yoke dimensions used before, the rms vibration of the yoke resulting from "CCF_C1_A0" at a frequency of 200Hz would be $(6.9e\text{-}11.n_p)$ m.

The "MOM_A0" force components

When these forces act on the poles of the machine, the poles tend to rock relative to the yoke and the moment is transferred to the yoke at the pole-yoke joint. The pole-yoke joint also resists relative motion between the back of the pole and the yoke in the circumferential direction and so the "MOM_A0" forces also cause a circumferential force to exist on the yoke. We have stated above that the circumferential forces on the yoke are not generally of much consequence.

The "MOM_C1_A0" forces can excite two classes of modes.

(a) Yoke "flexure" modes which have n_p wavelengths about the circumference.

(b) Torsional modes of the yoke in which the circular sections rotate about the cylinder axis

Group (a) above was discussed in the paragraph about "RAD_C1_A0" forces. The principal mode of group (a) is that whose axial profile is a "horizontal" line. We defined a stiffness K_{f1} for this mode based on the peak radial displacements caused by the "RAD_C1_A0" force. We define a new stiffness quantity K_{fm1} for this mode here based on the radial vibration resulting from <u>moment</u> forces.

K_{fm1} = (Peak Radial Displacement of the Yoke due to "MOM_C1")$^{-1}$

^◊^◊^◊^ ⇒ (9.12)

$$K_{fm1} = (E \pi d^3 (n_p^2-1)^2) / (12 r_m^2 n) = K_{f1} / (r_m n_p) \qquad (9.13)$$

Equation (9.12) gives an immediate comparison between the importance of the "RAD_C1_A0" forces and the "MOM_C1_A0" forces as applied to the yoke. Remember that the "MOM_C1_A0" forces acting on the yoke are contributed partly by the "CCF_C1_A0" forces on the poles.

The principal mode of group (b) above is the "rigid-body-mode" described in the paragraph on "CCF_A0" forces. Again it is the inertia of the yoke that determines the vibration levels achieved by this mode. Using the same yoke dimensions again, the rms vibration of the yoke resulting from "MOM_C1_A0" at a frequency of 200Hz would be (3.1e-11. n_p) m.

With the "RAD_C2_A0" forces, the only modes of the yoke being excited were the flexural modes having $n_p/2$ wavelengths about the circumference. The same applies to the "MOM_C2_A0" forces. We defined a stiffness quantity K_{f2} for this mode using (9.4) to relate peak radial displacement to the applied "RAD_C2_A0". We now define K_{fm2} for this mode.

K_{fm2} = (Peak Radial Displacement of the Yoke due to "RAD_C2_A0")$^{-1}$

$\wedge \diamond \wedge \diamond \wedge \diamond \wedge \Rightarrow$ (9.14)

$$K_{fm2} = (E \pi d^3 ((n_p/2)^2-1)^2) / (6 r_m^2 n_p) = 2 K_{f2} / (r_m n_p) \qquad (9.15)$$

The rms yoke vibration caused by the "MOM_C2_A0" can be assessed using (9.15) .

We have now considered how each of the "A0" forces being applied to the yoke influences its vibration at low frequencies. For motors running at low speed relative to the spectrum of resonances of the frame, the above arguments can be applied directly in assessing which force components will be dominant.

We now briefly consider the "A1" force components. These arise if the armature is straightline skewed or if there is an axial misalignment of the armature in the case of a herringbone skewed armature. The effect of these forces is to excite the two ends of the machine frame in opposite senses. The modes excited by the "A1" force components are the axially antisymmetric versions of the modes excited by the "A0" components. Fig. 9.3 contrasts the modes which can respond to "A0" components (called j=0) with those (j=1) which respond to "A1" and those (j=2) which respond to the "A2" components. For this picture, $n_p^2=4$ and the circumferential distribution of the forces is "C2".

The expressions for the stiffness quantities are more complex for these forces than the expressions above relating to the axially uniform modes since the shear strains of the yoke must also be taken into account. In general however, it may be stated that the stiffness of the first axially-antisymmetric flexure mode is substantially higher than the stiffness of the first axially-symmetric flexure mode. As the length of the machine increases, the ratio between the stiffnesses of the first

axially antisymmetric mode and the first axially symmetric mode decreases. Also, as i (the number of wavelengths about the periphery of the yoke) increases, the ratio in question decreases. Table 9.1 below presents the value of this ratio for the yoke geometry r_m=1.5, d=0.125 in the cases of three yoke lengths. The trends are clear from these numbers. Similar figures for different geometries are easily generated using the software.

Mode		l=0.5	l=1.0	l=1.5
i = 0	...extensional	0.872	0.970	0.997
i = 2	...flexural	18.41	17.94	10.53
i = 4	...flexural	24.75	8.78	3.84
i = 6	...flexural	14.32	3.83	2.08
i = 8	...flexural	7.73	2.36	1.54
i = 10	...flexural	4.72	1.78	1.32
i = 12	...flexural	3.28	1.50	1.21

Table 9.1 Ratio Between Stiffness of j =1 and j =0 modes.

Now a comparison between the "A0" and the "A2" forces is much more complex again. The stiffnesses of the j=0 and j=2 modes are again compared numerically for a particular cross-section geometry. Table 9.2 below shows the variation of the ratio between the mode stiffnesses for j=0 and j=2 with yoke length for the cross-section geometry in which

r_m=1.5, d=0.125

Mode	l=0.5	l=1.0	l=1.5
i = 0 ...extensional	460	6.79	1.77
i = 2 ...flexural	1.07e6	3.56e5	1.27e4
i = 4 ...flexural	1.44e5	7.86e2	124.2
i = 6 ...flexural	1.40e3	61.9	13.0
i = 8 ...flexural	277	16.0	4.96
i = 10 ...flexural	80.6	7.31	2.96
i = 12 ...flexural	33.3	4.43	2.18

Table 9.5 Ratio between stiffness of j=2 and j=0 modes.

Figures such as those presented in tables 9.1 and 9.2 are useful in considering the effectiveness of skewing (both herringbone and straightline) in reducing the vibration levels of a machine. This is considered in more detail in section 9.3.

9.2.2 Forces Applied to the Yoke With Poles

In practice, the response of the bare yoke is not necessarily indicative of the response of the whole machine. Forces acting on the poles of a machine are not directly transmitted to the yoke. The inertia of the poles, their stiffness and the properties of the joint between the poles and the yoke combine to generate a frequency-dependent relation

between the forces acting on the poles and those reaching the yoke. For a full appraisal of the vibration of any machine, the coils must be considered with the poles and yoke. The effect of the coils is dealt with separately in §9.4.

The relative "importance" of the force components in any machine will be a function of ...

(1) The frequency of the forcing.
(2) The geometry of the yoke and the poles
(3) The stiffness of the joint between the poles and the yoke.

"RAD_A0" force components

RAD_A0 forces on the mainpoles and compoles act to force the poles radially against the yoke. The joint between the poles and the yoke has flexibility and consequently, the force transmitted to the yoke is not equal to the force applied at the face of the pole. There is a characteristic frequency of pole radial translation relative to the yoke. We define this as the natural frequency at which the pole would vibrate if the yoke were perfectly rigid and static. Denoting the pole-yoke joint stiffness in the radial sense as S_r, and the pole mass as M_p, the characteristic frequency of the pole radial translation is given by ...

$$f_r = (1/2\pi).(S_r/M_p)^{0.5} \qquad (9.16)$$

The force being transmitted to the yoke is dependent on the frequency

f. If f is similar to f_r, then there will be a considerable degree of pole vibration relative to the yoke. If the yoke is considered rigid, the transmitted force could be related to the force acting on the pole as . .

$$\text{(Transmitted Force) / (Acting Force)} = (1.0 - (f_r/f)^2)^{-1} \qquad (9.17)$$

The situation is not always so simple. The stator may have modes for which the yoke vibrates significantly occurring at frequencies near f_r. A general expression for the transmitted force is not possible. However, from the simple expression above (9.16), it is apparent that there will be some set of frequencies (probably close to the f_r frequency given by (9.16) at which there is a magnification of the "RAD_A0" forces.

The "CCF_A0" and "MOM_A0" force components.

CCF_A0 and MOM_A0 forces act to rock the poles and move them circumferentially. The connection between the pole and the yoke creates a coupling of these modes. Again, there is a marked difference between the forces transmitted to the yoke and those applied at the poles. The natural frequency of pole rocking on a rigid yoke is invariably much lower than the natural frequency of pole circumferential translation on a rigid yoke, and the natural frequency of circumferential translation is in turn less than that of radial translation. In the tests on machine **B** (chapter 8) it was found that the compoles had a natural rocking frequency of 235 Hz. The rocking frequency of the compoles is normally less than that of the mainpoles. The two

translational characteristic natural frequencies (radial and circumferential) will be similar for the compoles and mainpoles.

In 9.2.1 above, we considered two separate flexure modes of the yoke $i=n_p$ and $i=n_p/2$ which are excited by "MOM_C1_A0" and "MOM_C2_A0" force components acing on the yoke. If the characteristic frequency of pole rocking is much less than the resonance of each of these, then the contribution of both "CCF" and "MOM" forces to the machine vibration will be small.

The other force distributions acting on the poles are cause by skewing of the armature and these are discussed in 9.3 below.

§9.3 The Effectiveness of Skewing in Reducing Vibration.

In the previous section, we considered the factors which influence how much vibration is caused by the "A0" force components acting on the poles. We continue the train of thought here by now considering the relative effect of the "A1" and "A2" force components which are caused by armature skew.

The concept behind skewing the armature is to reduce the total force on each of the poles to zero at all times. There are two principal reasons why skewing the armature does not result in a zero value of electromagnetically induced vibration.

(a) The effects of air ducts in the armature and fringing at the ends

of the poles mean that the total radial circumferential and moment forces on the poles are not zero. Wignall (A.1987) calculates that up to 7% of the "unskewed" force on the poles remains after skewing in some instances.

(b) The poles can respond to the armature forcing even when the total force on each individual pole is zero.

Item (b) above is of interest to us here.

Appendix 8 reviews the forcing caused to exist on poles due to straightline and herringbone skew and quantifies the components "A1" and "A2" of the fundamental slot-passing force and its harmonics. Table 9.3 below summarises the findings.

Skew-Type	FUNDAMENTAL			2nd HARMONIC		
	"A0"	"A1"	"A2"	"A0"	"A1"	"A2"
Straightline	0.0	0.66	1.0	0.0	0.27	0.0
Herringbone	0.0	0.0	0.85	0.0	0.0	0.34

Table 9.3 Coefficients of the Force Components "A1" and "A2"

9.3.1 The "A1" force components

Straightline skew of the armature produces force components in both "A1" and "A2" axial distributions. We noted in 9.2 that the stiffness of cylinder modes for which j=2 was considerably greater than the stiffness of the corresponding j=1 modes. Thus, in considering the vibration resulting from the electromagnetic excitation of a straightline skewed armature, it is only necessary to consider the "A1" components of the forcing.

Clearly, the "RAD_A1" component forces can be transmitted to the yoke without deforming the poles. The "MOM_A1" components by their nature attempt to twist the ends of the poles in opposite senses. The "CCF_A1" force components attempt to translate the ends of the poles circumferentially in opposite directions. However, because the pole is fixed to the yoke it cannot translate circumferentially without rotating about the center of the pole back at the same time. The torsional stiffness of the poles themselves in comparison with the stiffness of the pole-yoke joint ultimately determines the extent to which "CCF_A1" and "MOM_A1" are successful in vibrating the yoke. For the "RAD_A1" force components, precisely the same conditions govern the levels of transmitted force to the yoke as applied for the "RAD_A0" forces. Thus, we can state that a perfect straightline skew results in significantly less vibration from the "CCF" and "MOM" force components but only a modest reduction for the "RAD" force components.

9.3.2 The "A2" force components

When a herringbone skew is used, there are only "A2" components in the force (plus residual "A0" forces due to the ducts, fringing effects etc.). The "A2" forces can be dominant in determining vibration levels even in the case of machines having a relatively short yoke. This statement is borne out by the axial profiles of the operating shapes measured for machine **B** in chapter 8. Each of the "A2" forces must deform the pole if forces are to be transmitted to the yoke. Depending on the pole geometry, its material constants and the type of the force, the deformation may be primarily shear or extensional. "MOM_A2" forces attempt to twist the pole while "RAD_A2" forces deform the pole in the radial plane in a mixture of shear and bending.

Mainpoles of machines are invariably laminated and we can state with some confidence as a result of the investigation into the behaviour of laminated bodies that these poles are much more flexible as a result of being laminated. The shear modulus is reduced by a greater factor than the Youngs modulus. Torsion of the mainpoles can therefore be sufficient to allow a significant forcing to occur on the yoke as a result of "CCF" and "MOM" components.

The determinant of how much force is experienced by the yoke because of any of the "A2" forces is the ratio between the internal stiffness of the pole and the stiffness of the pole-yoke joint.

The internal stiffness of the pole for resisting the "RAD" components can

be judged from the first non-rigid-body resonance of the pole in that plane. By comparing the natural frequency of this mode with the characteristic frequency of pole radial translation (both illustrated in Fig. 9.3) the proportion of the radial force which will be transmitted to the yoke can be estimated. Where the "CCF" and "MOM" components are concerned, the 'internal stiffness' of the pole should not be interpreted to mean the stiffness of the associated mode. As stated before, circumferential stiffness of the pole-yoke joint is quite high relative to the torsional stiffness. (Strictly speaking, it is not valid to compare two quantities which do not have the same dimensions but a comparison of the characteristic frequency of pole rocking and pole circumferential translation is valid). The pole-backs tend not to move relative to the yoke, to the same extent as the poles will twist. Consequently, the 'internal stiffness' which should be considered for both "CCF" and "MOM" forces is the stiffness of the constrained torsional mode.

The reader is referred back to fig.s 8.29-8.34 for visual corroboration of the above statements.

Once the electromagnetic forces ("A0" and "A2") are known for a particular machine and operating condition, it is possible to assess relatively quickly which components of forcing will dominate the vibration produced. If it transpires that the "A0" forces are dominant, there is a case for distributing the ducts on the armature more carefully so that the "A0" components can be reduced. If, on the other hand, the "A2" forces dominate, thought may be given to stiffening the poles or stiffening the yoke against these deflections.

For a given yoke geometry, and given the approximate ratio of "A0"/"A2" for the forces, the ratio between the contribution from each can be assessed by the following procedure.

(1) Evaluate the expected "RAD_A2" and "MOM_A2" forces which will be transmitted to the yoke by considering the internal stiffness of the poles and the approximate stiffness of the pole-yoke joints.

(2) Evaluate the relation between rms yoke response to the four components, "RAD_A0", "MOM_A0", "RAD_A2", "MOM_A2". This relation would be taken from tables similar to table 9.2 and the equations preceding it.

(3) Combine (1) and(2) to produce expected levels of yoke vibration due to "RAD_A2" and "MOM_A2". Compare these levels with the results for "RAD_A0" and "MOM_A0"

When the mechanical symmetry of the machine is seriously disrupted by structural detail welded on the yoke, proper consideration of the skew can only be given by using the software.

§9.4 The Effect of Coils.

As a rule, the field coils of a machine have sufficient mass to

substantially affect the vibration of the machine. In order for this to happen, the connection between coils and poles must be sufficiently stiff for that inertia to be used to good effect.

The properties of the connection between the coil and the pole are important in determining the vibration especially that due to CCF_A0 and MOM_A0 force components. The connection would be expected to be relatively flexible in radial translation and in rotation about an axial line because each of these derives its stiffness from the shearing stresses set up between the pole and the insulation of the coil. The stiffness of the coil-pole connection in circumferential translation is expected to be higher. This stiffness is derived from normal strains in the coil insulation. When the pole rocks on the yoke, the back of the pole moves very little in the circumferential direction compared with the face. Thus, pole rocking translates the center of the pole in the circumferential direction and this generally involves a circumferential translation of the coil also.

It has not been possible to study the parameters of the coil-pole joint in a general way. Approximate values were obtained for machine A of chapter 8 by comparing the response of the machine with and without coils. Extrapolation of these values is not possible because the coil mounting on the pole varies from machine to machine.

If the operating shapes of the machine in the frequency range of most interest are dominated by exciation due to "CCF_A0" and/or "MOM_A0", the coils can play an important role in reducing the vibration.

If the slot-passing frequency of most interest to us is f, an optimum set of parameters can be computed for the coil-pole stiffness. If these parameters can be achieved in practice (heavily impregnating the pole+coil or the use of adhesives might make this possible), the coils will have been put to good use as vibration absorbers.

The computation of the optimum parameters is explained here. Fig. 9.4 illustrates the theoretical model using the usual symbols from the vibration literature. The system comprises two masses M_a and M_b. K_b is a pure spring and D_{ab} is a pure damping connection. (It seems likely that most of the vibration energy going into the coil-pole connection is dissipated.) The responses of the system - r_a and r_b are determined by . . .

$$-\omega^2 M_b r_b = (1-K_b r_b - i\ D_{ab} (r_b-r_a)) \qquad (9.18)$$

$$-\omega^2 M_a r_a = i\ D_{ab} (r_b-r_a) \qquad (9.19)$$

Solving these yields ...

$$r_b = 1/(K_b-\omega^2 M_b + i.D_{ab} (1+i.D_{ab}/(i.D_{ab}-\omega^2 M_a))) \qquad (9.20)$$

Substituting numbers gives an expression for easy differentiation to find the optimum D_{ab}.

§9.5 The Number of Armature Slots.

The number of armature slots is invariably an integer multiple of the number of pole-pairs of the machine. That integer may be even or odd. Current preference appears to lie with the odd. In this section we present a criterion by which a rational choice between the two may be made.

If the integer multiplier is even, the forces on adjacent mainpoles and compoles are in phase for the fundamental slot-passing force and all its harmonics. In this case, the modes of the magnet frame which are significantly excited are the i=0 modes and the $i=n_p$ modes using the notation for the modes of cylinders. Of course, the magnet frame is not a pure cylinder and other modes can also be excited. In particular, the presence of a split in the yoke which is flexible will mean that the i=0 extensional mode of the yoke is modified to a mode in which the two halves move together and apart almost like independent rigid bodies. There will also be some excitation of the i=2 mode due to the presence of the feet. Both the rotor and the stator will experience a torque pulsation at slot-passing frequency and the motion on each due to this force is governed primarily by the inertia of the rotor and stator. We can quantify the extent of vibrations of the above modes and compare them with the vibrations due to an armature having an even integer multiplier for the number of slots. Axial force distributions "A0" are considered in detail here. One must also consider the "A2" forces for a herringbone skewed machine but it is not feasible to do this analytically.

9.5.1 Excitation of the i=0 modes.

In the case of a machine whose yoke is unsplit, it is straightforward to compute the deflections due to the i=0 extensional mode responding to the "RAD_A0" forces. As usual, r_m is the mean radius of the yoke and d the radial thickness. The total mass of the yoke is $M_y=2\pi dr_m$. Let M_m be the mass per unit length of the mainpoles and M_c is the mass per unit length of the compoles. At slot-passing frequency, the stiffness of the pole-yoke joints is such that all poles move in unison with the frame. Then, the stiffness of this extensional mode is $K_e= E.d/r_m$ and the inertia of the mode is $M_e=n.(M_y+(M_m+M_c))$. For machine **B** of chapter 8 (without a split), K_e has a value of 1.53e10 N/m^2 and M_e equals 1.25e3 kg/m. The resonant frequency of the extension mode is 176 Hz.

For the i=0 torsional mode, the stiffness is zero and the inertia is $M_t=M_e$ as defined above.

The rms vibration of the yoke responding to one unit of "RAD_C1_A0" force at frequencies well below the extensional resonant frequency is $1/K_e$. At frequency "f" much higher than extensional resonance, the response is $1/(39.5\ M_e\ f^2)$. When f is greater than 1.41 times the extensional resonance (176 Hz for machine **B**), the dynamic stiffness of the mode is dominated by the inertia term and is greater than the static

stiffness.

The response of the torsional mode to one unit of "CCF_C1_A0" at frequency f, is given by $1/(39.5\ M_t\ f^2)$.

9.5.2 Excitation of the $i=n_p$ modes.

A yoke having no split has stiffness K_{f1} for the flexural mode $i=n_p$ given by (9.21) below.

$$K_{f1} = E\ \pi\ d^3\ (n_p^2-1)^2\ /\ (12\ r_m^3) \qquad (9.21)$$

Assuming that the mainpoles and compoles are rigid on the yoke, the inertia of this flexural mode "M_{f1}" is given approximately by (9.22).

$$M_{f1} = M_y/2 + n_p.(M_p + M_c) \qquad (9.22)$$

For machine **B**, K_{f1} = 8.17e11, M_{f1} =8.65e3 and the flexural resonance of this mode occurs at a frequency of 1545 Hz. The rated slot-passing frequency of this machine is 530.4 Hz.

9.5.3 Excitation of the $i = n_p/2$ modes.

Armatures having an odd integer multiplier for the number of slots

principally excite only the modes of one group, namely the $i = n_p/2$ modes. The simplest (and lowest frequency) of these modes is the j=0 mode. We have already developed the formula for the stiffness K_{f2} of this mode in §9.2.

$$K_{f2} = E \pi d^3 ((n_p/2)^2-1)^2 / (12 r_m^3) \qquad (9.23)$$

Now there are two 'versions" of this mode possible. In one, the mainpoles translate radially with the yoke and the compoles rock. In the other, compoles translate radially and the mainpoles rock. (Fig. 9.5). The inertia of the mainpoles has most effect in the latter case. However, the natural frequency of this mode is greater than the characteristic frequency of mainpole rocking. Thus, not all of the mainpole inertia is actually effective in this mode. We therefore consider only the version where mainpoles translate. The other must be considered using the software package. The inertia of this mode is given approximately by

$$M_{f2} = M_y/2 + nM_p \qquad (9.23)$$

For machine **B**, K_{f2} is calculated as 4.89e10 (much less than K_{f1}). The modal mass M is also less for this mode than previously and is calculated as 7.78e3. The natural frequency of this mode for machine **B** is then approximately 398.9 Hz.

The indication is that an <u>even</u> integer multiplier for the number of slots

of the armature of machine **B** will lead to lower vibration levels near the rated speed. These calculations have taken no account of the split which undoubtedly has a strong bearing on the modal stiffness of all modes. A full analysis would involve including this effect into a numerical model in DMS.

A full consideration of which integer multiplier to use for the number of slots must include an examination of the effects of the "A2" forces as well as the "A0" forces. If the machine is very short, it may be assumed that the "A0" forces will dominate the vibration and the choice of the suitable integer multiplier may be made on the basis of these forces alone.

In general, the modal mass of the i=0 modes and $i=n_p$ modes is substantially greater than the modal mass of at least one version of the $i= n_p/2$ modes. This suggests that in general, the default choice for the number of slots ought be the <u>even</u> integer multiple. The principle argument against using an <u>even</u> multiplier must be that at very low rotational speeds, the yoke displacement response to circumferential pole forces is inversely proportional to the frequency squared.

One final point worth noting is that circumferential forces have a much smaller effect on the yoke flexural vibration in the case of an <u>even</u> number of slots per pole-pair at normal running speeds because the $i=n_p/2$ mode is considerbly more flexible than the $i=n_p$ mode.

§9.6 Disruption of Symmetry.

Practical machine construction dictates that feet and other appendages associated with the cooling of the machine must be welded on to the yoke. These and the split in the yoke remove the rotational and axial symmetry which otherwise exists in the machine.

Measures such as skewing the armature and using an integer number of armature slots per pole-pair rely heavily on symmetry for their effectiveness. Assymetries introduced to the machine invariably have the effect of introducing what Mikina (A.1934) terms "auxiliary" modes to the machine vibration.

It is not possible to include a comprehensive study on the effects of assymetry on machine vibrations. Each case of assymetry is different and has significantly different influences at various bands of the frequency range.

For the present we shall be content to note that assymetry does introduce extra modes to the set of modes which are excitable by electromagnetic forces. This is illustrated for three very simple cases. In the case of a real machine, a full DMS analysis will inform of the expected effects.

9.6.1 Assymetry Case 1 :- Constraints at Feet.

This case illustrates the excitation of ring modes due to rotationally

symmetrical forcing where the ring is supported at two points at its middle-layer. It examines the effect of adding stiffness to a ring. The stiffness of the supports is varied to identify the effect. Fig. 9.6 shows the ring used and the three force sets applied. The model was prepared in DMS and has 24 equally spaced nodes at which forces can be applied. Response of the ring (radially at the uppermost node) is evaluated for each of the three force sets between 0 and 5kHz for the three joint stiffness values k=1.0e10, k=1.0e9, k=2.0e8. Figs. 9.7-9.9 shows the response to force-sets F6, F8 and F12.

The principal point worth noting here is that even when the pin joint support stiffness is not sufficient to significantly raise the first natural frequency of the ring, it is ample to excite some other important resonances which would not otherwise have been excited.

9.6.2 Assymetry Case 2 :- Yoke with Split.

The yoke of machine **B**, was modelled in two distinct ways (fig 9.10). One of these included the split while the other did not. Typical joint attributes (as derived from experiment in §6) were used for the split in one analysis and for checking purposes, the joints were set to be virtually rigid in another so that the results could be compared with those from the single-piece yoke. The response of the yoke to the force component "RAD_CP_C2_A0" was computed in each case. The actual response freedom examined was radial translation at the top ot the machine and this was computed over the frequency range 0-5 kHz. Fig. 9.11 contrasts the frequency response curves for the three cases.

It is not possible to generalise about the effect of this joint in machines except to observe from fig. 9.11 that the joint is sufficiently flexible to make a strong impression on the behaviour of the yoke in the vicinity of the split and that the tests reported in chapter 6 are therefore justified.

9.6.3 Assymetry Case 3 :- Yoke with Feet (Inertia Effect).

The same yoke (in one part) is used again to illustrate the effect of the feet in modifying the modes of the frame so that modes other than the "principal" one can be excited. The force component ("RAD_CP_C2_A0") was applied to this structure (as was applied to the split yoke above) and response computed at the same point. Fig. 9.12 shows the yoke with feet and the computed response curve.

§9.7 The Effect of Pole Root Flexibility on the Overall Dynamic Behaviour of the DC Magnet Frame.

In much of the previous literature, the poles of DC machines were considered to be rigidly affixed to the yoke of the machine. It has been shown that this is not the case where very small deflections are concerned and this investigation has provided a set of data for the approximate values of the flexibilities of the pole-yoke joint.

The root flexibility has two general effects.

(1) Forces acting on the poles are not transmitted directly to the yoke. There will be some attenuation of the force if the frequency of forcing is well removed from the appropriate characteristic pole-on-a-stiff-yoke resonance. On the other hand, there may also be some magnification of the transmitted force if the frequency of forcing happens to lie close to the appropriate resonance.

(2) The dynamic behaviour of the frame as a whole structure is modified. At freqencies well below, the lowest characteristic pole-on-a-rigid-yoke resonance, the frame will behave as though the poles were rigidly mounted. At frequencies well above the highest characteristic pole-on-a-stiff-yoke resonance, the frame will be able to vibrate significantly with only very small oscillations occurring on the poles. In this case, the stiffness of the pole-yoke joints acts to increase the stiffness of the yoke.

In the earlier sections of §6, we have seen that the force transmitted to the yoke is dependent on the pole-yoke joint stiffness especially for the "A2" force components. We do not pursue this further here.

The dynamic behaviour of the frame at frequencies between the two extremes mentioned above in item (2) is affected in some complex way by the pole stiffness. We demonstrate this fact but it is not possible to make general remarks on the effects of the pole root flexibility on the dynamic behaviour of the frame. Suffice it to say that the pole root flexibility is one of the principal determinants of the set of resonant

frequencies of a frame. If it is not known to reasonable accuracy, then important resonances will not be calculated correctly and the resulting errors in the estimation of response at individual frequencies can be very large.

The DMS model of the stator of machine **B** is used here to illustrate the effect of pole root flexibility on the behaviour. Six mainpoles are attached to the model of one half of the yoke and the assembly is excited by a point force acting at the top. Fig. 9.13 shows the arrangement. The joint stiffnesses are set to three different values . . .

Zero stiffness (poles are not attached at all)
Rigid Joints (poles not free to move at all wrt to the yoke)
Estimated True Value.

The comparison of the frequency response in each of the three cases is presented in Fig. 9.14.

§9.8 Acceptable Pole Spacing Tolerances.

Errors in pole spacing result in error forces coming to exist on the poles of the machine. A procedure has been established whereby the vibration resulting from such errors can be quantified. It comprises the following steps.

(1) Estimate the coefficients of the error force components acting on one of the poles as a result of the positional error. For

circumferential errors this is straightforward. For axial misalignment of the armature or an angular error in the position of the pole, an armature which is herringbone skewed will produce a component of "A1". See appendix 8 for the evaluation of this quantity.

(2) Apply the error force components to the theoretical model of the machine and compute the response over a range of frequencies of interest.

(3) Compare the computed error response with the computed normal response at a number of frequencies.

There is no general expression for the acceptable pole-spacing error but the above procedure provides a rational quantitative estimate of what levels of pole-spacing error can be tolerated without significantly increasing the overall machine vibration levels. The procedure was carried out for vibration of machine B (chapter 8) at fundamental slot-passing frequency and the allowable pole-spacing discrepancy corresponded to a slot-ripple phase-error of 13° ... equivalent to 1.5 mm at the bore of the yoke. Normal factory practice would generally ensure that this tolerance was met whether specified or not. For harmonics of slot-passing, the tolerance becomes proportionally finer.

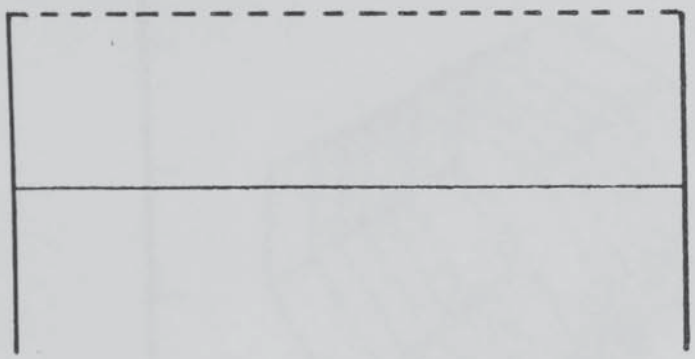

Axially-Uniform Pattern - "A0"

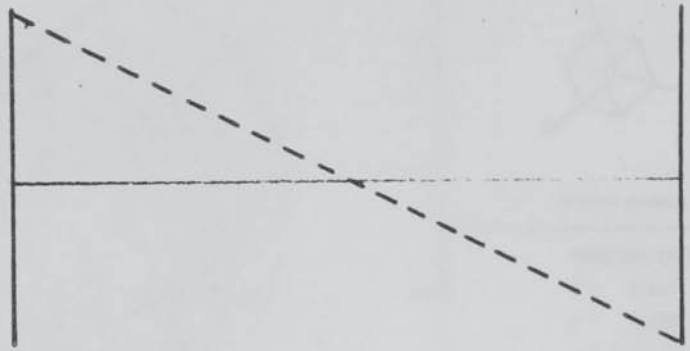

Axially Antisymmetrical Linear Pattern - "A1"

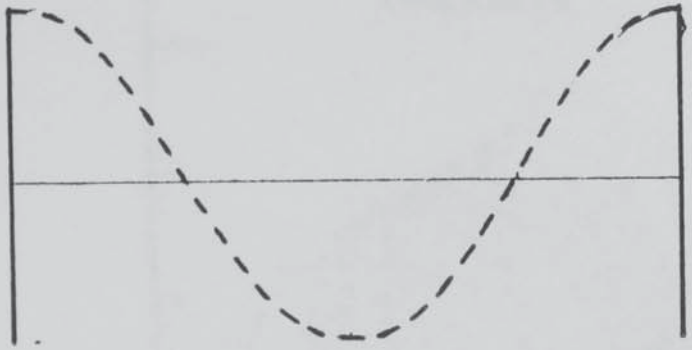

Axially Symmetrical Bending Pattern - "A2" (Cos Shape)

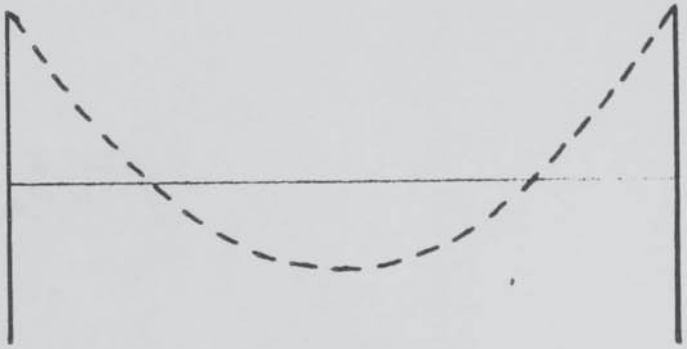

Axially Symmetrical Bending Pattern - "A2" (Parabolic)

Fig. 9.1 Axial Displacement Patterns.

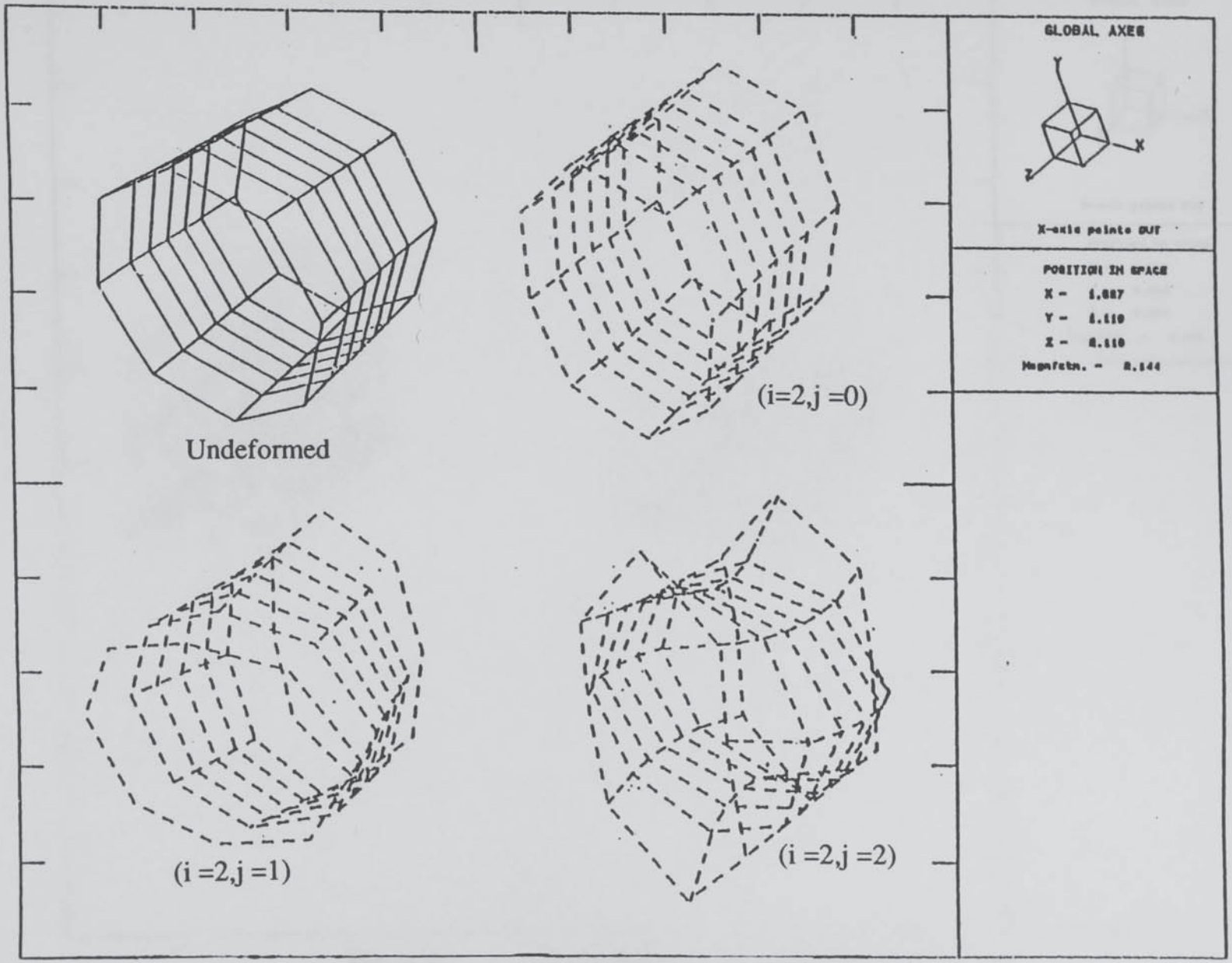

Fig. 9.2 **Differentiation Between Modes (i=2,j=0), (i=2,j=1) and (i=2,j=2)**

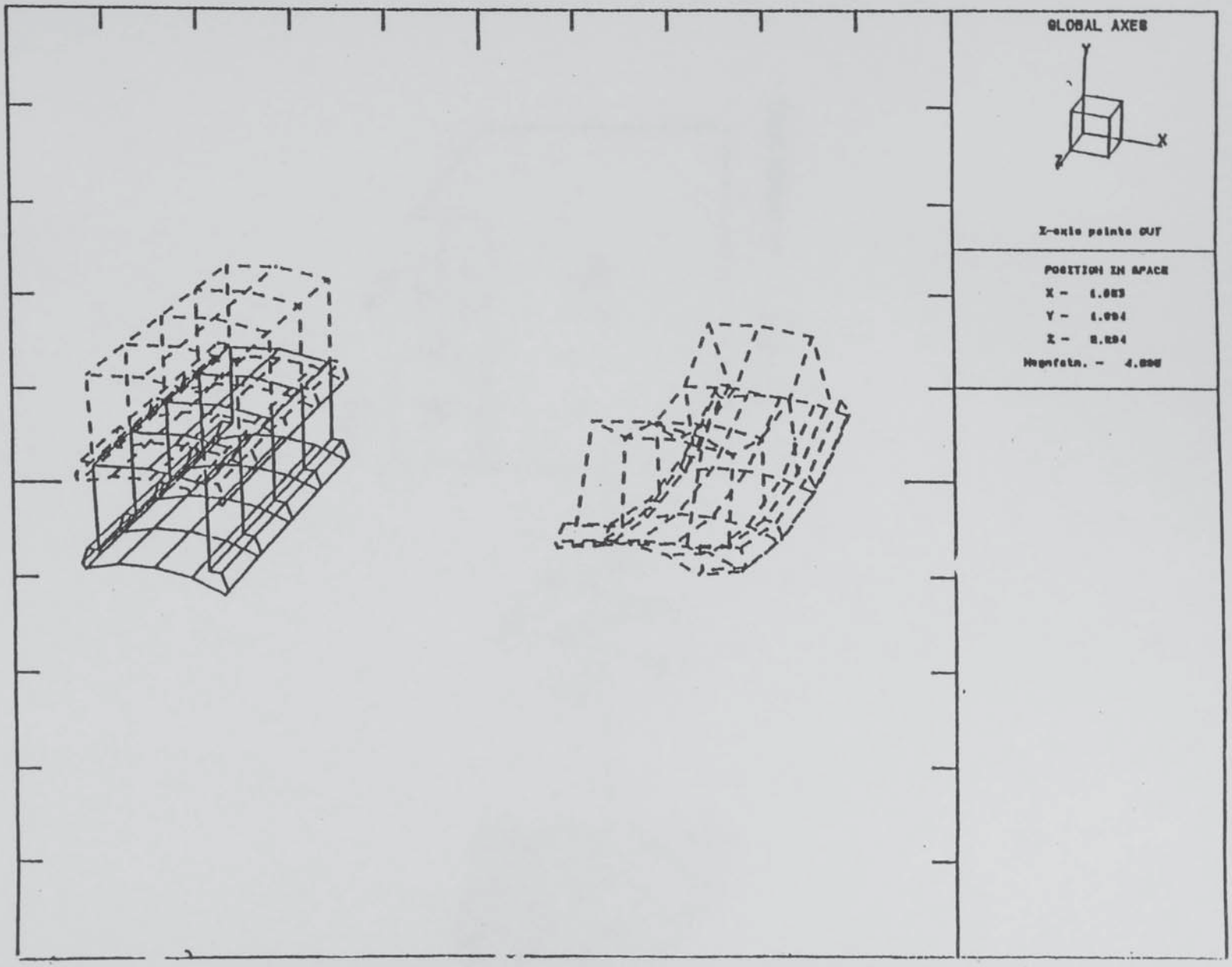

Fig. 9.3 **Translational and Bending Resonances of a Mainpole.**

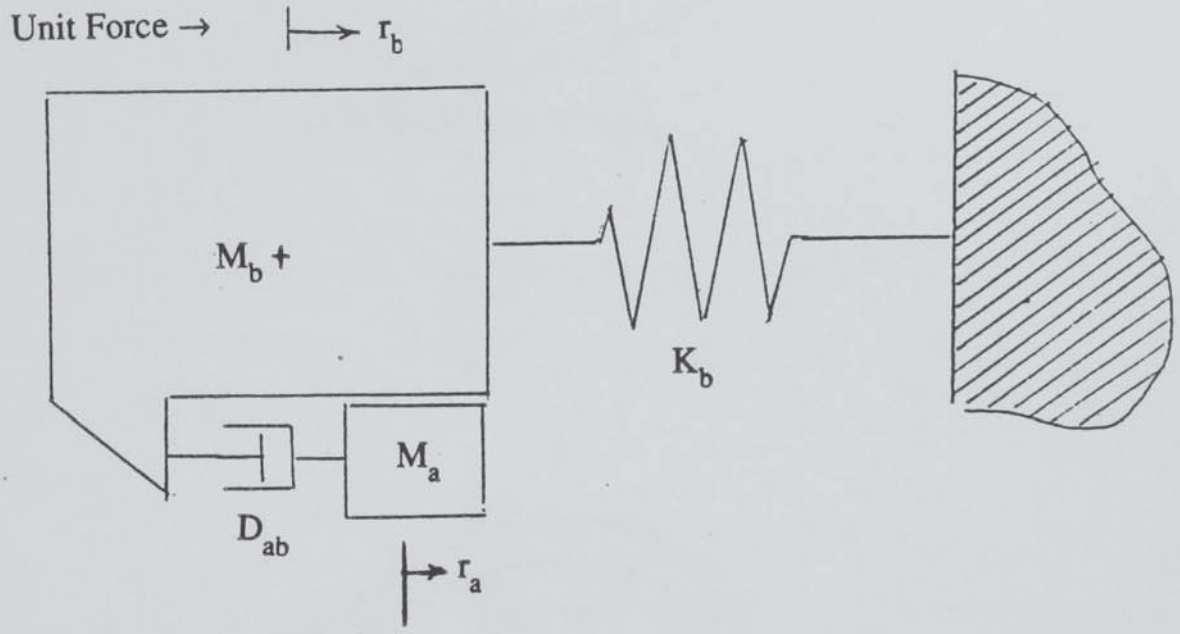

Fig. 9.4 **Theoretical Model for Derivation of Optimum Coil-Pole Connection Properties.**

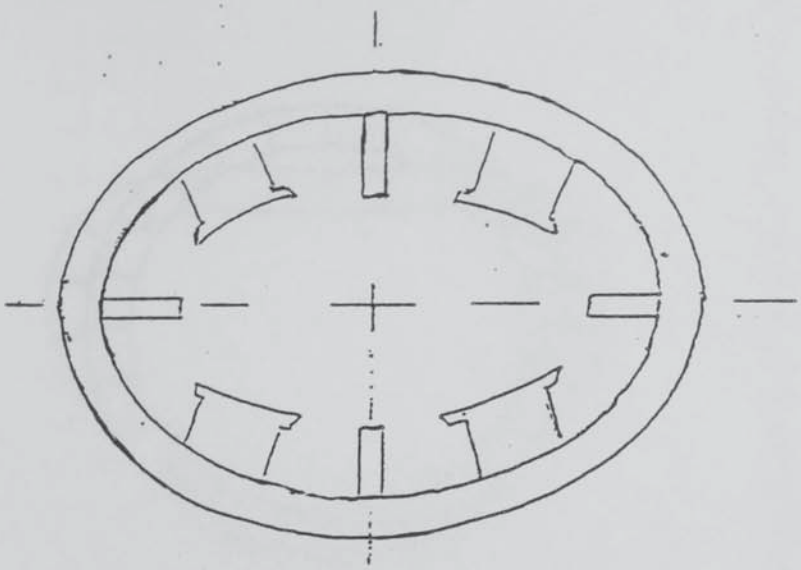

Low Frequency Version.

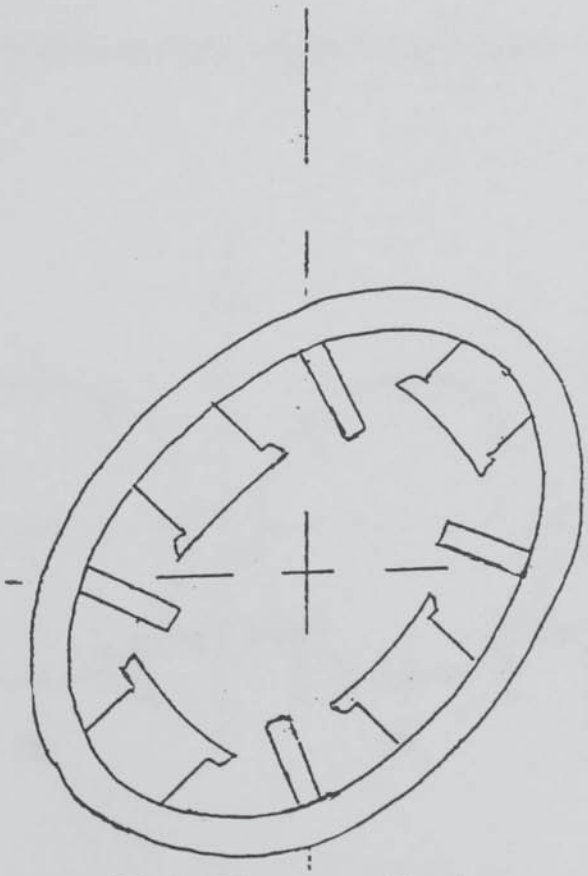

Higher Frequency Version.

Fig. 9.5 **Two Versions of the mode (i=n/2).**

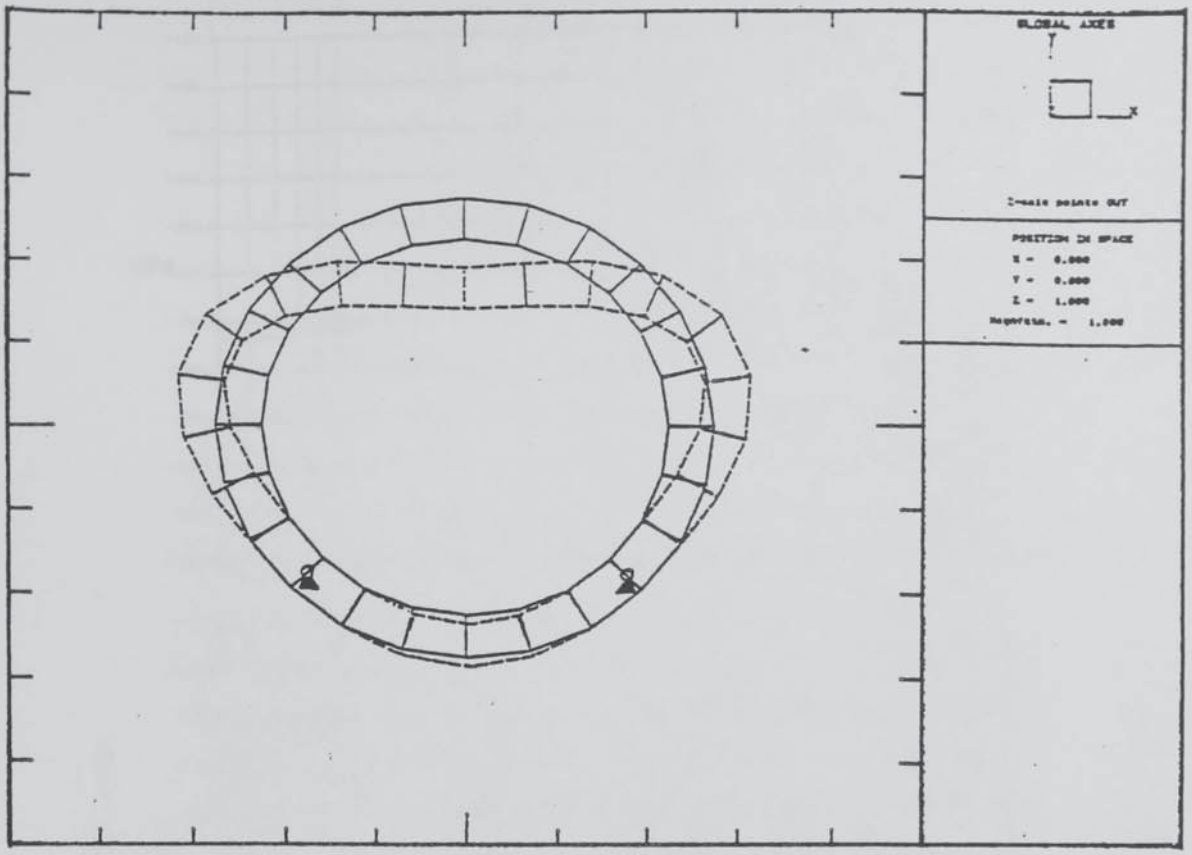

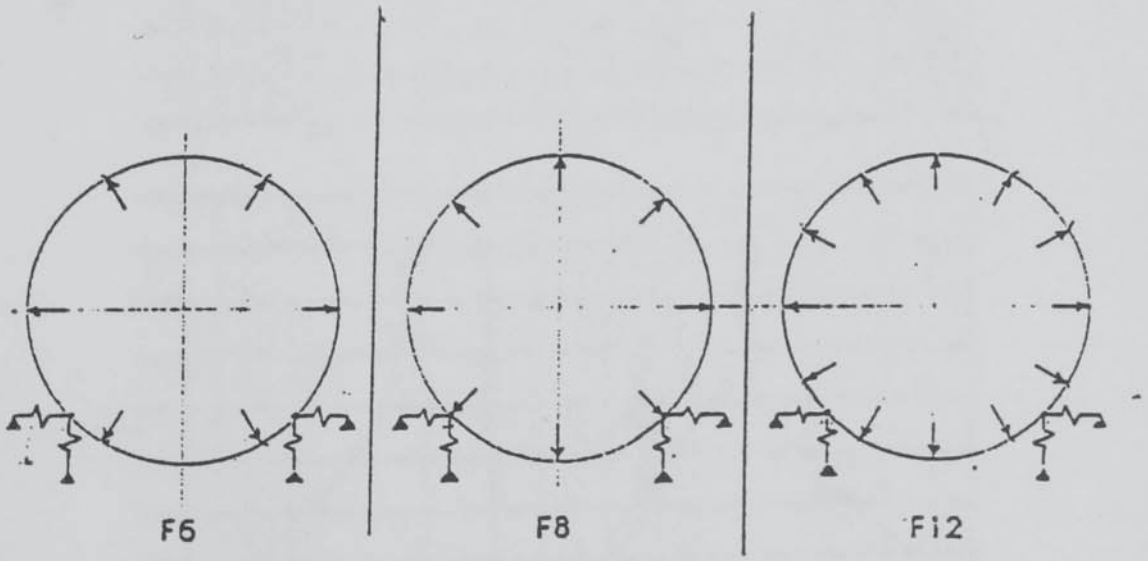

Fig. 9.6 **The Constrained Ring and Three Force Sets. F6 F8 F12**

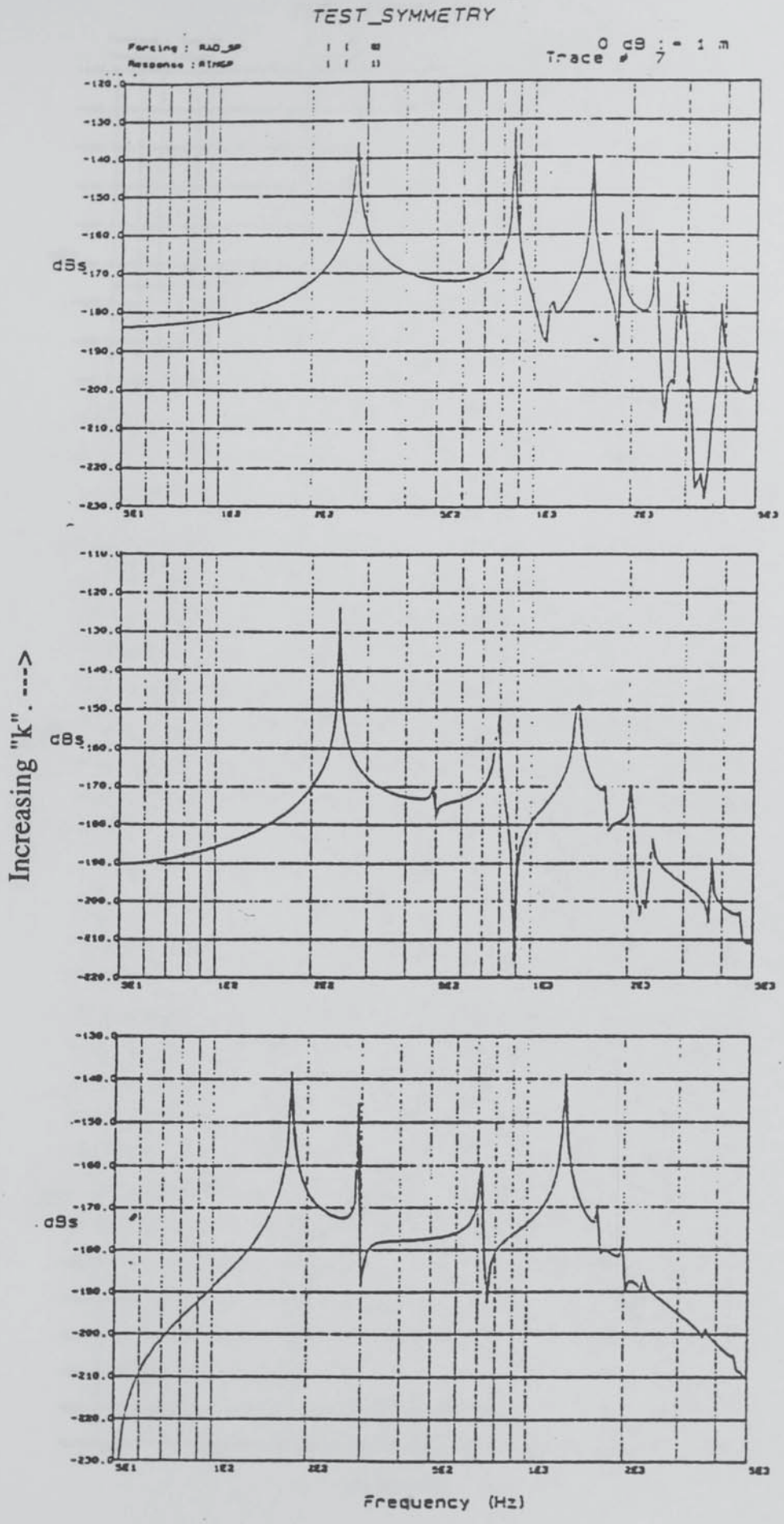

Fig. 9.7 **Response of Ring to F6 for k=1.0e10, 1.0e9 and 2.0e8 N/m.**

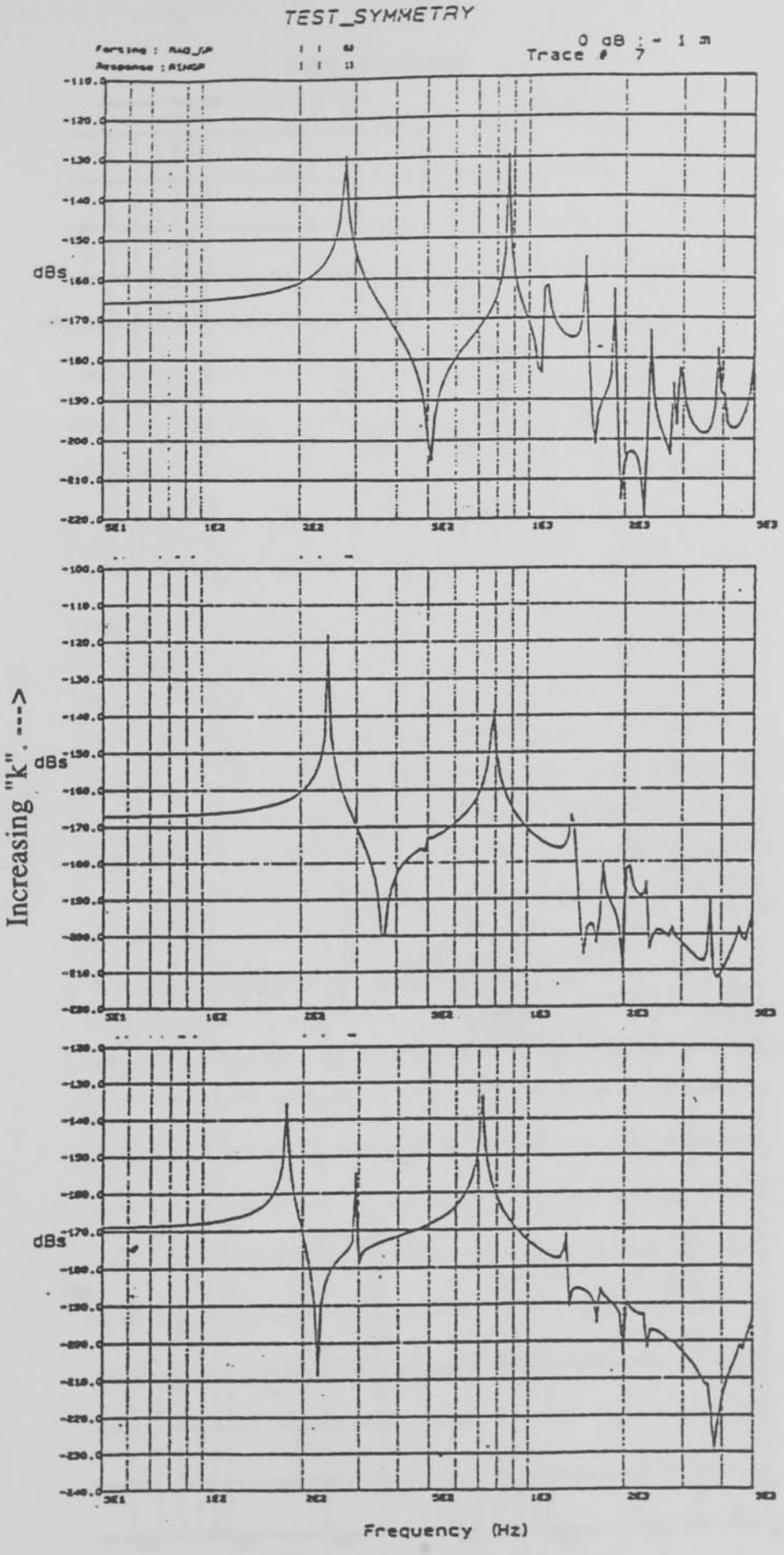

Fig. 9.8 **Response of Ring to F8 for k=1.0e10, 1.0e9 and 2.0e8 N/m.**

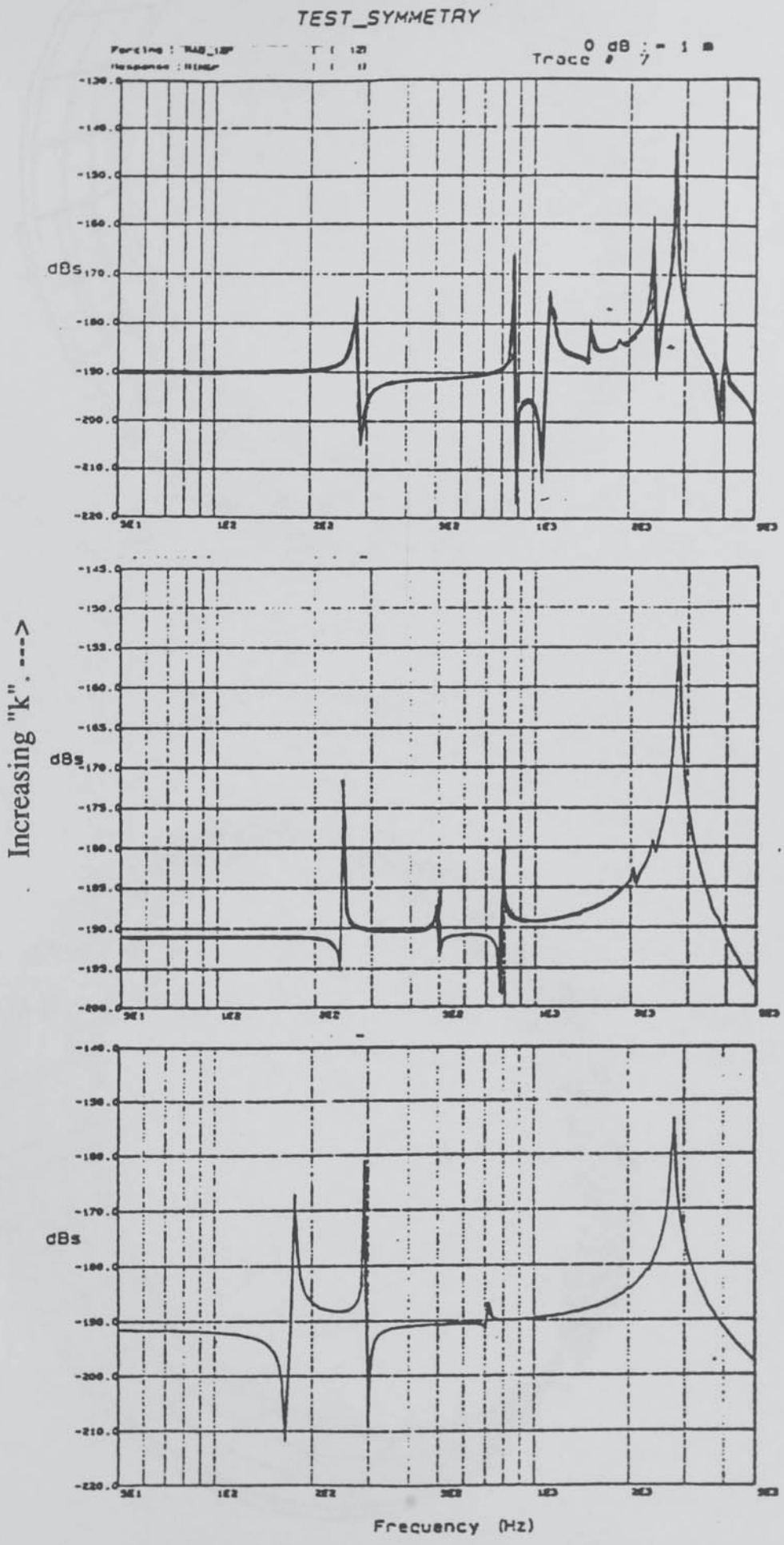

Fig. 9.9 **Response of Ring to F12 for k=1.0e10, 1.0e9 and 2.0e8 N/m.**

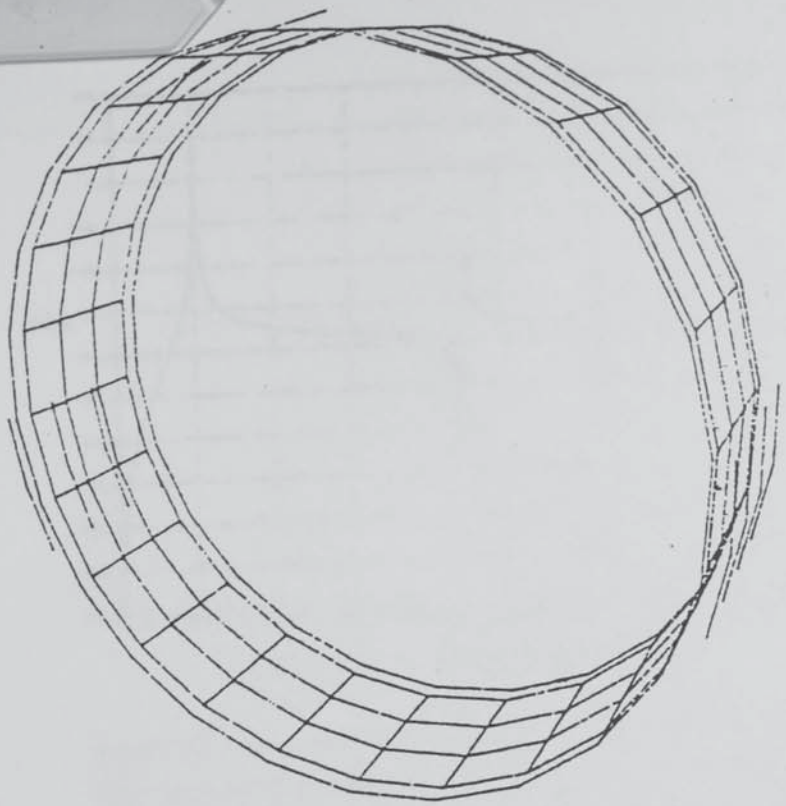

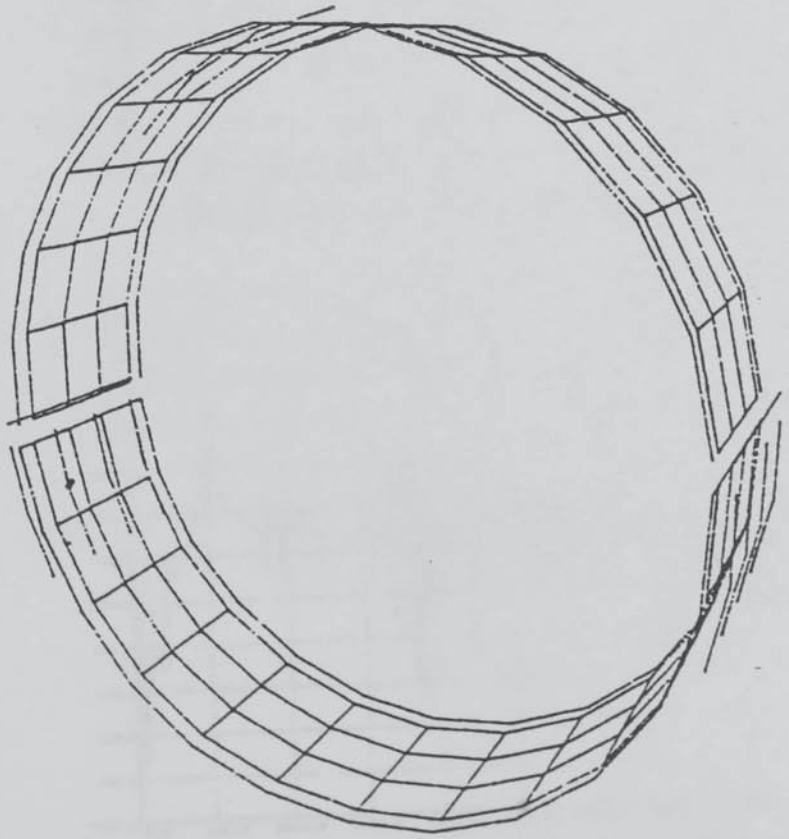

Fig. 9.10 **Yoke Modelled Whole and as Two Halves.**

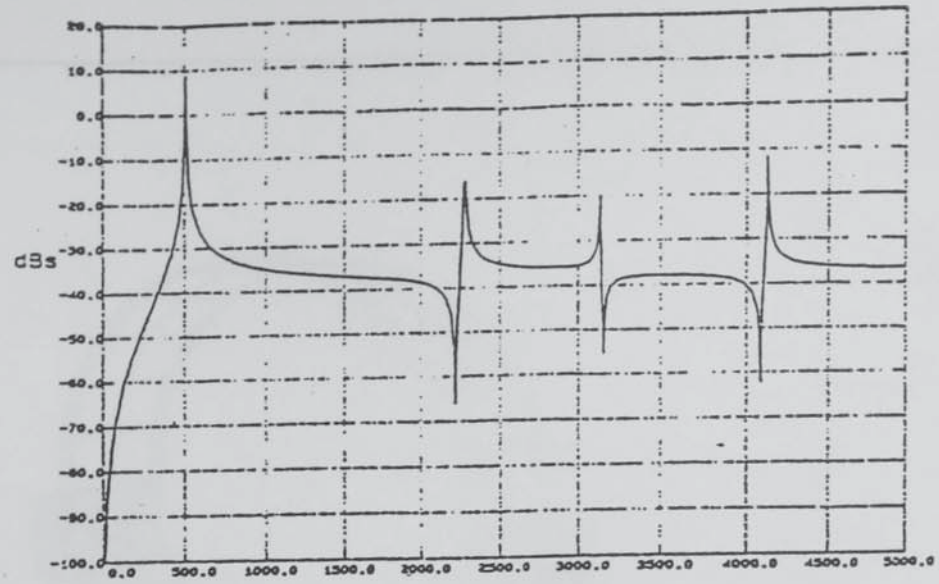

Response of Yoke without split.

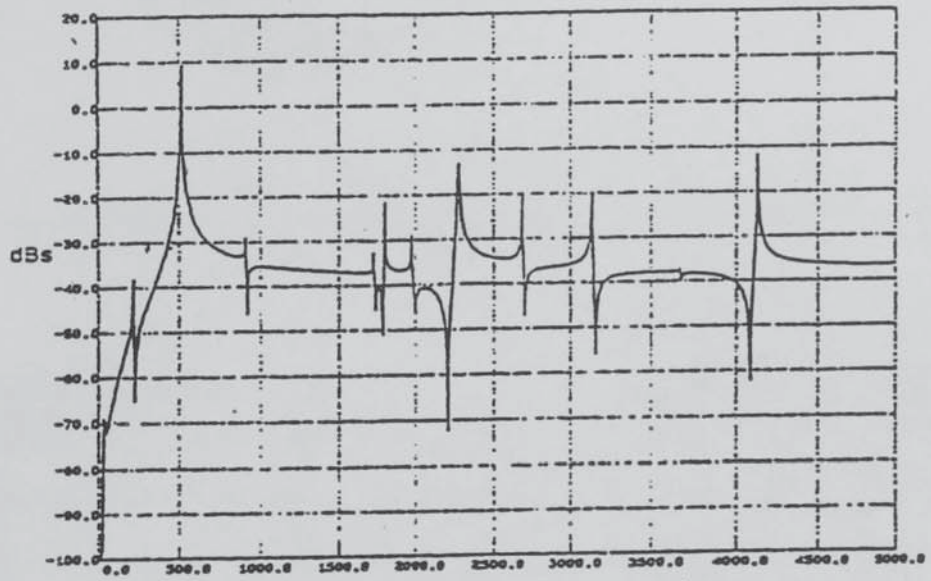

Response of Yoke with almost-rigid split.

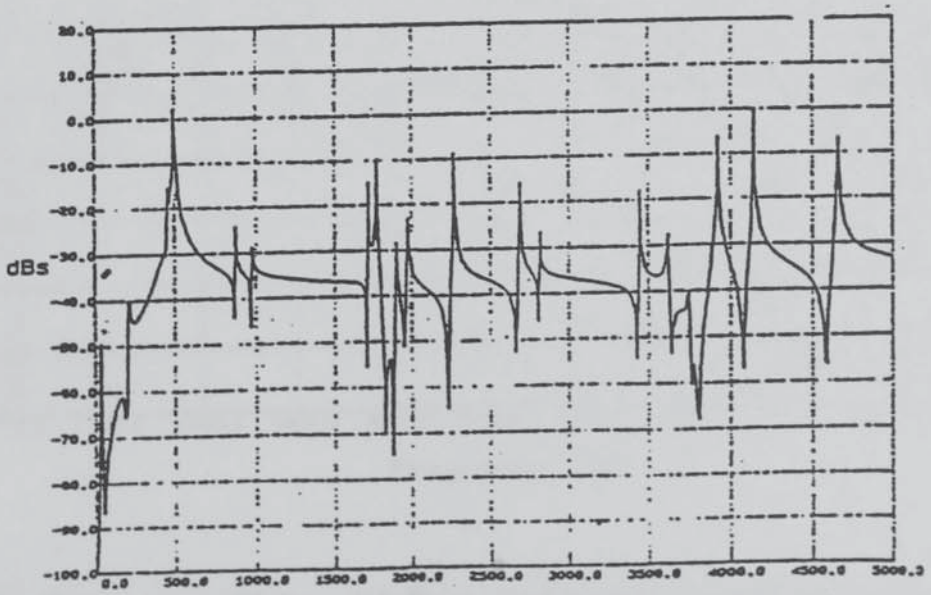

Response of Yoke with typical-stiffness split.

Fig. 9.11 **Effect of a Split on the Response of a Yoke to the Force Component "RAD_CP_C2_A0"**

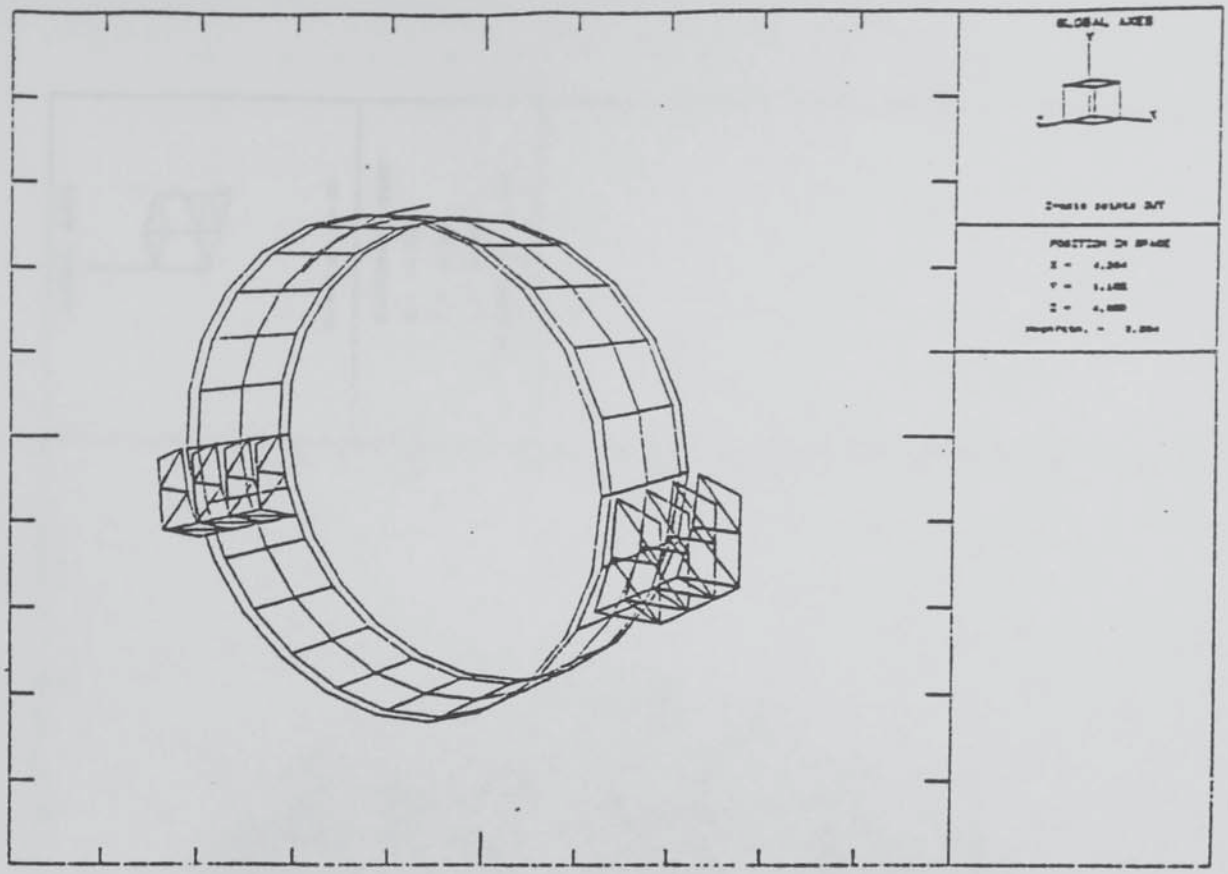

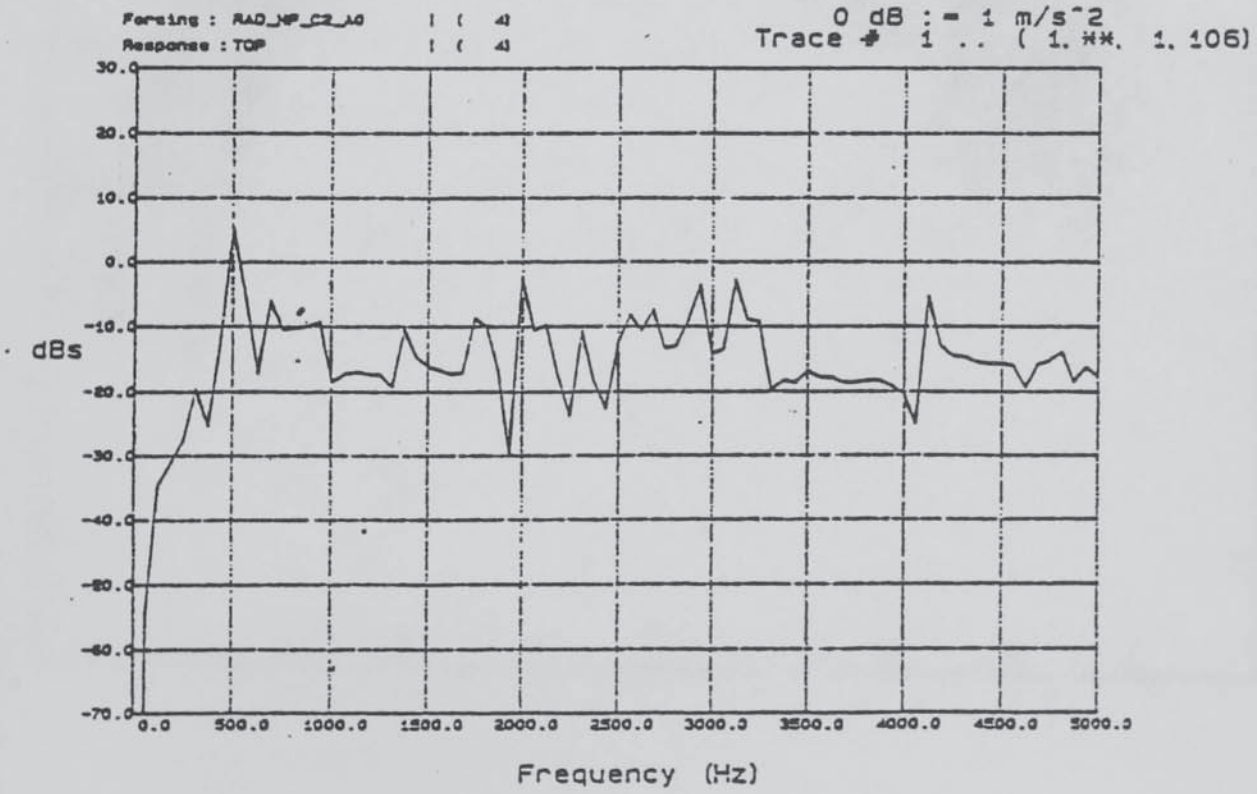

Fig. 9.12 **Yoke with Feet and its Frequency Response.**

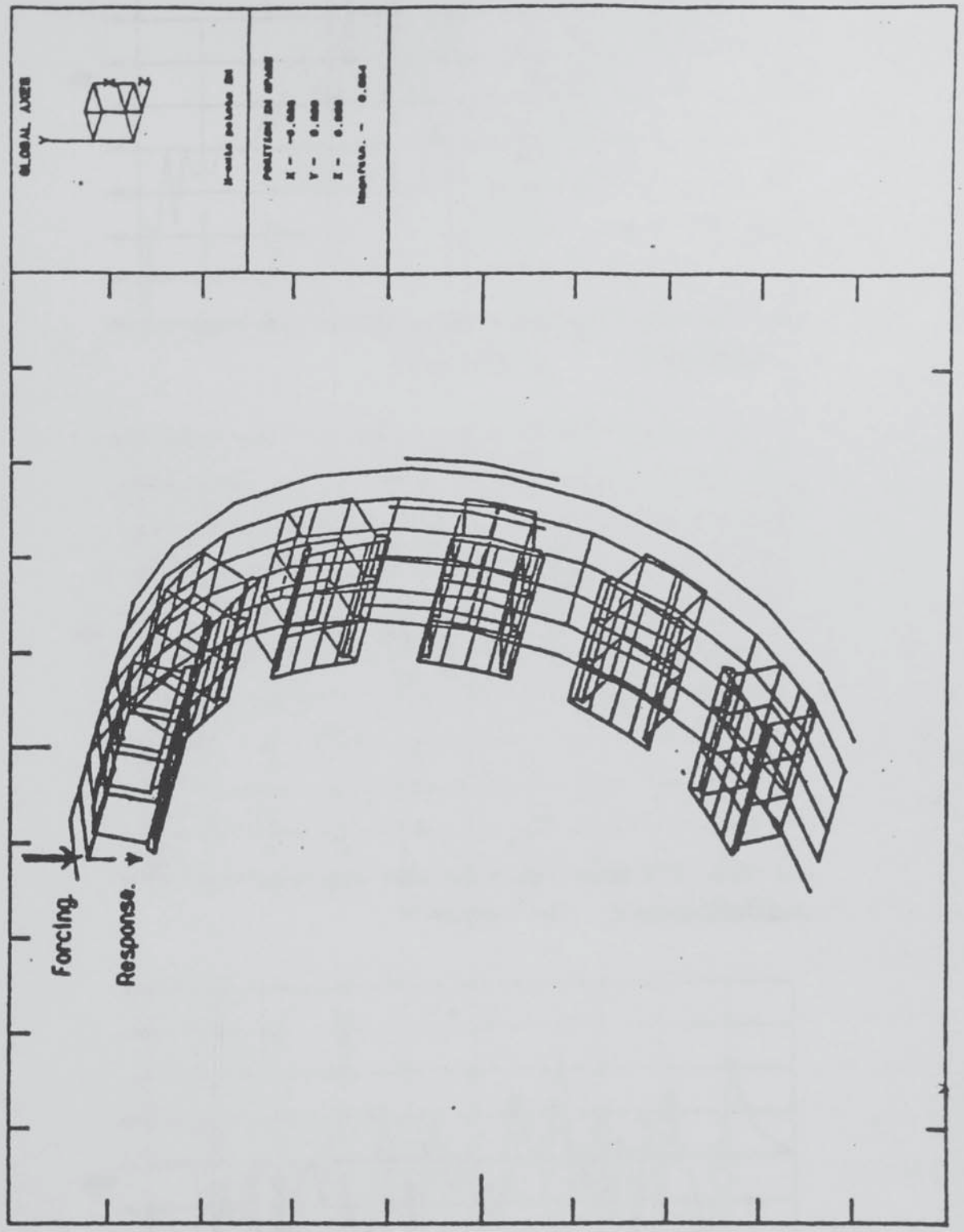

Fig. 9.13 **Symmetrical Half of Machine B with 6 Mainpoles.**

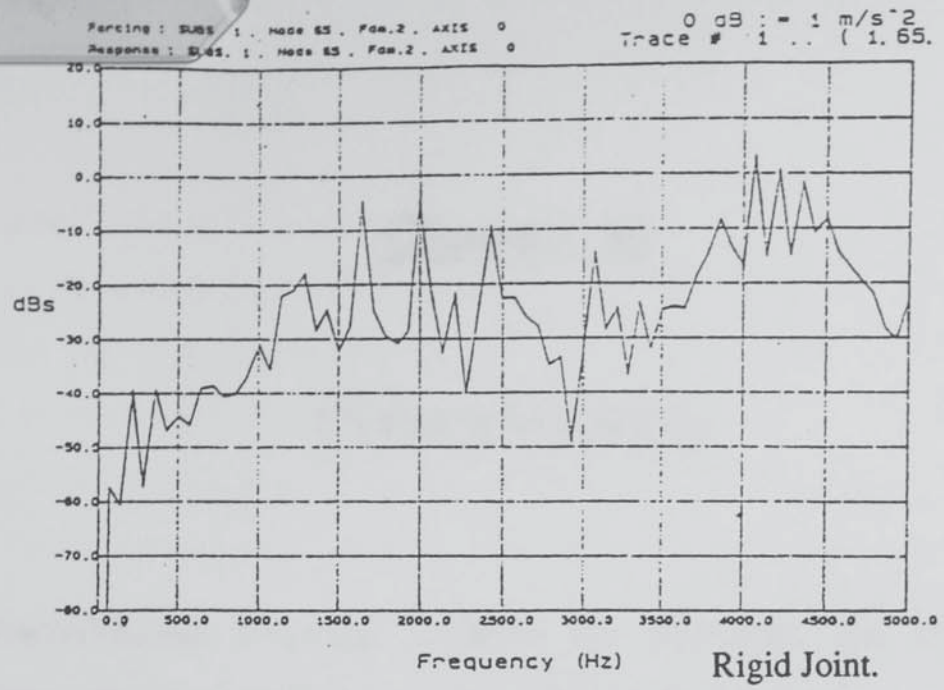

Rigid Joint.

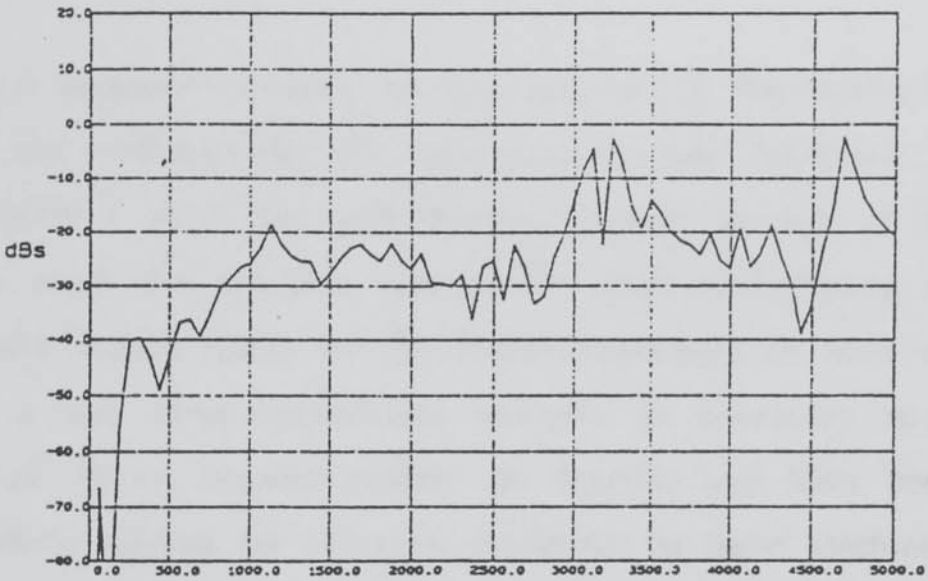

Normal Stiffness.

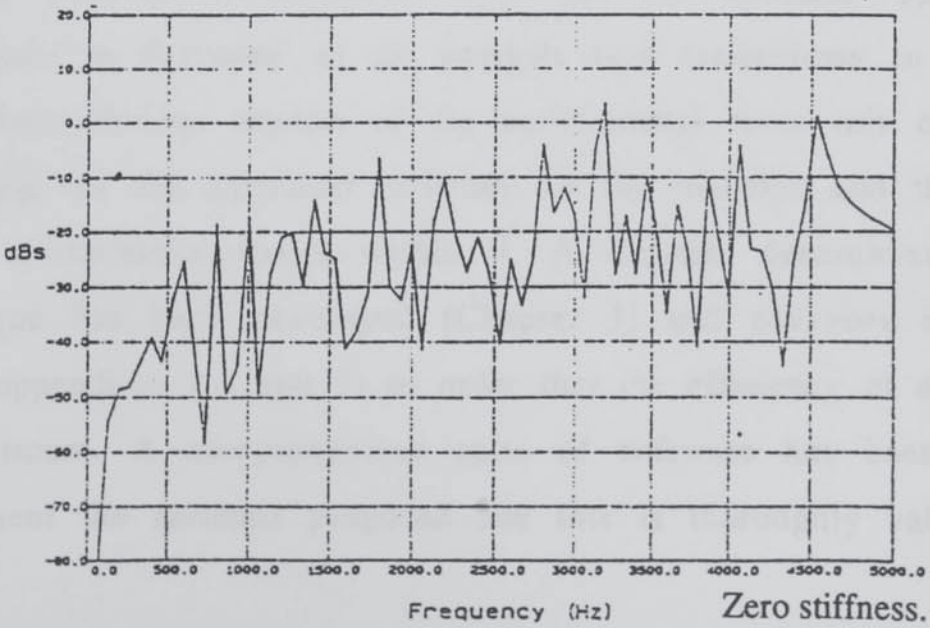

Zero stiffness.

Fig. 9.14 **Dynamic Behaviour of Stator under 3 conditions of Pole-Yoke Joint Stiffness.**

Chapter 10

CONCLUSIONS

The low-vibration electrical machine (in particular the DC machine) poses two distinct problems to the would-be modeller.

The first problem concerns the size (degrees of freedom) required for a model and consequently, the computational time consumed. It is shown in chapters 1 & 2 that conventional in-plane models of machines are useless when the machine incorporates such pole-spacing and skewing as would reduce many of the force-components to zero or near-zero. Thus, a full three-dimensional analysis is necessary to treat these machines. Finite element models are feasible and have been examined as a likely method for vibration prediction in these machines. However, computation times for a single analysis are prohibitivly high even for modest problem dimensions. The use of dynamic substructuring techniques is favoured as an analysis tool (sometimes in conjunction with finite-element models of the components) since this can take full advantage of the particular structure of the machine and the symmetry which exists/almost-exists within it. A suitable dynamic-substructuring technique has been developed (Chapter 3) and advances made in the field (appendices 1,2 and 3) in order that the efficiency of analysis is at a maximum. A comprehensive suite of software has been written to implement the methods proposed and this is thoroughly validated.

The other obstacle posed by the modelling of machines is that empirically-determined quantities must be used to realistically represent the pole-yoke joint, the bolted-flange joint, the properties of the laminated components and various other features of the machines. Chapters 5, 6 and 7 report the findings of investigations to determine three of the principal empirical properties required for the analsysis of the DC machine.

Chapter 5 contains a discussion on how a complete picture of the behaviour of a laminated stack may be obtained by measuring only two variables directly. The effects of laminated components in machine are explored and tables presented which relate the two necessary unknown properties of the stack to various conditions including clamping pressure and surface treatment.

In chapter 6, values are presented for a limited set of conditions of the pole-to-yoke joint together with extrapolation guidelines which enable the modeller to find good estimates of the torsional, shear and compression/extension stiffnesses of the joint for most practical pole-to-yoke joints.

In chapter 7, the effects of a split on the behaviour of a ring/cylinder are investigated and an approximate graph is presented at the end giving joint torsional siffness as a function of the joint preload.

Test procedures, model designs and interpretation methods are included in the respective chapters in order that further work in these areas can take place easily when necessary. The findings of these three sub-investigations are consistent with a number of single instances quoted in the literature and enable realistic values to be inserted by the modeller.

A system of dividing the electromagnetic force patterns into components has been formalised and used to make some elementary speculation on the likely effects of various design features on the machine's vibratory performance. These form the basis of a low-vibration machine design strategy. Generally, the effects of various features and modifications can only be accurately quantified by employing a full three-dimensional model.

The combination of substructuring-methods, software and empirical values has been tested on two machines and the findings are broadly as follows.

(i) The rms vibration levels of vibration of machines responding to "balanced" electromagnetic forcing can be consistently computed to very good accuracy. (6 dBs must be regarded as excellent in comparison with what might be expected from the previous in-plane models).

(ii) Impulse responses in which the primary modes of the machine are excited are also predicted with very good

accuracy.

(iii) The vibration levels of individual points cannot be reliably predicted. It is well known that there is a high degree of variance within the properties of joints. The machines have a large number of resonances within the range of frequencies over which one might require to compute response and consequently small variations in the properties can make dramatic changes to the machine response level. It has been demonstrated that other steelwork affixed to the outside of a machine yoke, and assymetries in general, can have a profound effect on the machine vibration at particular running speeds. The operating shapes measured and presented in chapter 8 (Figs. 8.16 - 8.18) for machine **B**, are highly irregular and give some indication of the true complexity of the problem being tackled.

REFERENCES A

DC Motor Vibration

Benhafsi, Y — Investigation into the Behaviour of the Bolted-Flange Joint in Cylinders. Report submitted as part fulfillment of requirements for Masters degree in CAD. University of Aston, 1986.

Chong, L.B. — Structural Excitation of Noise in DC Machines by Magnetic Forces. Honours Project Report. Herriot-Watt University, April, 1977.

Cocotelis, N. — Dynamic Behaviour of the Bolted Pole-Yoke joint in Large DC Machines. Report submitted as part fulfillment of requirement for Masters degree in CAE. University of Aston, 1986.

Den Hartog, J.P. — Vibration of the frames of electrical machines. Trans. ASME, 1928, Vol. 50, pp.1-6, 9-11.

Delves, B. — Investigation into Noise and Vibration on a CS.08 DC motor comprising part of a 5 M.V.A set in main test. Engineering Report S/NE u 82. Applied Mechanics Laboratory, Nelson Engineering Laboratories, Stafford. 1962

Delves, B. — Noise and Frame Vibrations of DC machines. Engineering Report S/NE u 110 , Applied Mechanics Laboratory, Nelson Engineering Laboratories, Stafford. 1964.

Design Dept. — D.C Frame - High Frequency Vibration. G.E.C Large Machines Ltd. , Internal Design-Calculation Sheet.

Dvoracek, A.I. Forces on teeth in DC macines. Trans. Am. IEE. Vol. 81, 1962

France, D. Investigation of a DC motor vibration problem. I.Mech.E 2nd Intnl. conf. - Vibration in rotating machinery, Cambridge, England. Sept 1-4, 1980 pp.83-90.

Garvey, S.D The Behaviour of Laminated Components In Machines. GEC Large Machines Ltd., Engineering Report #621.

Garvey, S.D The Prediction Vibration in Large DC Machines. GEC Large Machines Ltd., Engineering Report #661

Hamata, V. Magnetic noise of DC machinery ACTA tech. CSAV 1966(2) pp 202-226.

King, A.J. The Measurement and Suppresion of Noise with Special Reference to Electric Machines. Chapman and Hall. 1965.

Mikina, S.J. Effect of Skewing and Pole Spacing on the Magnetic Noise in Electrical Machinery. Scientific paper #729, Westinghouse Research Laboratories, East Pittsburgh, Pa. 1934.

Rothert, H Magnetisch erregte Schwingungen an Gleichstrommaschinen. VDI-Berichte, Bd. 24, !957. pp39-44.

Swales, P. Investigation into the Dynamic Characteristics of the Bolted-Flange joint in a Flat Plate. Report submitted as part fulfillment of requirements for Masters degree in C.A.D. University of Aston, 1985.

Wignall, A.N. Report on the Use of Finite-Element Methods to Predict the Electromagnetic Forces on the Poles of the DC Machine. Engineering Report # 684, GEC Large Machines Ltd., Rugby, 1987.

REFERENCES B

AC Motor Vibration

Alger, P.L. — Magnetic Noise in Polyphase Induction Motors. Trans AIEE, 1954, No. 73, Part IIIA, pp 118-125.

Belmans, R.
Vandenput, A.
Geysen, W. — CAE Techniques for Calculating Natural Frequencies of Machine Stators. NASA Scientific Workshop on Vibrations in Rotating Electrical Machines. Katholique Universistat Leuven. Belgium, 1986.

Binns, K.K. — Calculation of Some Basic Flux Quantities in Induction and other Double-Slotted Electric Machines. Proc. IEE. Vol 111,1964, pp. 1842-1858

Chen, Y.X.
Zhu, Z.Q. — Study of the Natural Frequencies and Modes of Stators of Electrical machines. International Conference on Electrical Machines. (1986)

Erdelyi, E., — Predetermination of Sound Pressure Levels of Magnetic Noise in Dynamo-Electric Machines. Trans. AIEE, 1955, No. 74, Part III, pp1269-1280

Erdelyi, E.,
Horvay, G. . — Vibration Modes of Stators of Induction Motors. Trans. ASME, Series E, Vol. 24, 1957, pp39-45

Ellison, A.J.,
Moore, C.J. — Acoustic Noise and Vibration of Rotating Electric Machines. Proc. Vol. 115, No. 11, November 1968.

Ellison, A.J.
Yang, S.J. — Natural Frequencies of Stators of Small Electrical Machines. Proc. IEE, Vol 118, Jan. 1974, pp185-190

Fertman, B.S. . Calculating the Detuning from Resonant Radial Vibrations of an Electric Machine Stator Frame. Elektroteknika, Vol. 47, No. 6, pp. 28-30, 1952

Finch, D. Vibration and Noise Response of Electrical Machine Stator Cores Excited By Magnetic Forces. PhD. Thesis. University of Aston, 1976.

Holzmann, F. Eigenfrequenzen des Blechpaketes von Drehstrommaschinen unter Berucksichtigung des Schwingungsverhaltens der Zahne. ETZ-A, Bd 93(1972), pp 82-85.

Jordan, H.
Rothert, H. Nutenzahlregeln und ihr Zusammenhang mit dem magnetischen Gerausch von Asynchronmaschinen. IBID., 1953, [A], 74, pp. 637-642.

Jordan, H.
Uner, Z. Berechnung der Eigenfrequenzen der Blechpakete Von Drehstrommaschinen, Konstruction, No. 16 (1964), Heft 3 pp 108-111

Nevelsteen, J. Vibration in large motors, causes and effects. IEEE Petroleum and Chemical Industries Conf. '78, pp. 213-217

Pavlovsky, H. Die Eigenfrequenzen der Standerblechpakete umlaufender elektrischer Maschinen. E. und M., 1971, Vol. 8, Heft II, pp 479-486

Verma, S.P.
Girgis, R.S. Resonant Frequencies and Vibration Behaviour of Stators of Electrical Machines as Affected by Teeth, Windings, Frame, and Laminations. IEEE Trans., Vol. PAS-98, 1979, pp1446-1455.

Verma, S.P.
Girgis, R.S.
Experimental Verification of Resonant Frequencies and Vibration Behaviour of Stators of Electrical Machines. IEE Proc-B, Vol. 128,1981, pp1-32.

Verma, S.P.
Girgis, R.S.
Resonant Frequencies of Electrical Machine Stators Having Encased Construction. Part I: Derivation of the General Frequency Equation. Trans IEEE, PAS(1973), pp1577-1585.

Watenabe,S.
Kenjo, S.
Ide, K.
Sato, F
Yamamoto, M
Natural Frequencies and Vibration Behaviour of Motor Stators. Trans. IEEE, Vol. PAS-102, No. 4, April 1983.

Yang, S.J.
Low Noise Induction Motors.
Clarendon Press, Oxford, 1981.

REFERENCES C

Dynamic Substructuring Methods

Bajan, R.L.
Feng, C.C
Free Vibration Analysis by the Modal Substitution Method. AAs paper 68-8-1, July 1968.

Bamford, R.M.
A Modal Combination Program for Dynamic Analysis of Structures. Tech. Memo. 33-290, Aug. 1966, Jet Propulsion Lab. Pasadena, Calif.

Bamford, R.M.
Wada, B.K.
Gayman, W.H.
"Equivalent Spring Mass System for Normal Modes." Tech. Memo. 33-380, Feb. 1971, Jet Propulsion Lab. Pasadena, Calif.

Benfield, W.A.
Hruda, R.F.
Vibration Analysis of Structures by Component Mode Substitution. AIAA Journal, Vol 9, No. 7, July, 1971, pp. 1255-1261.

Benfield, W.A.
Bodley, C.S.
Proceedings of Symposium on Substructure Treatment and Synthesis. Aug. 30, 1972, Marshall Space Flight Center, Huntsville, Ala.

Craig, R.R.
Chang, A.S.
Structure Coupling for Dynamic Analysis and Testing. NASA CR 2781 (1977).

Craig, R.R.
Pampton, M.C.C
Coupling of Substructures for Dynamic Analysis. Journal of the AIAA Vol 6, No. 7, 1968, pp. 1313-1319.

Garvey, S.D.
DMS User Manual. GEC Large Machines internal document. Dec, 1987.

Garvey, S.D.
Penny, J.E.
Gilbert, A.J.
The Reduction of Computational Effort in Krons Methods for Eigenvalue and Response Analyses of Large Structures. Paper submitted to Journal of the AIAA, June 1988. (Appendix 1)

Garvey, S.D.
Penny, J.E.
The Computation of the Eigen-states of Periodic Systems. Paper submitted to the International Journal of Numerical Methods. August 88. (Appendix 2)

Goldman, R.L.
Vibration Analysis by Dynamic Partitioning. Journal of the AIAA Vol 7, No. 6, 1969, pp. 1152-1154.

Gladwell, G.M.L.
Branch Mode Analysis of Vibrating Systems. Journal of Sound and Vibrations, Vol. 1, 1964, pp 41-59

Hou, S.N.
Review of Modal Synthesis Techniques and Approaches. The Shock and Vibration Bulletin, No. 40, Pt. 4, Naval Research Lab., Washington D.C., Dec 1969. pp. 25 - 39.

Hurty, W.C.
Component
Dynamic Analysis of Structural Systems Using Modes. Journal of the AIAA Vol 3, No. 4, 1965 pp. 678-684.

Hurty, W.C.
Collins, J.D.
Hart, C.H.
Dynamic Analysis of Large Structures By Modal Synthesis Techniques. Computers and Structures, Vol 1, pp.535-563. Pergammon Press 1971.

Kron, G.
Diakoptics. MacDonald & Company. London. 1963.

Kuhar, E.J.
Stahle, C.V.
Dynamic Transformation Method for Modal Synthesis. Journal of the AIAA Vol 12, No. 5. May 1974, pp. 672-678

MacKenzie, I.W. Computational Methods for the Eigenvalue Analysis of Large Structures by Component Synthesis. PhD thesis, Dept. of Aeronautics, Imperial College, London.

MacNeal, R.H. A Hybrid Method of Component Mode Synthesis. Computers and Structures, Vol 1, pp.581-601. Pergammon Press 1971.

Rubin, S. . Improved Component-Mode Representation For Structural Dynamic Analysis. Journal of the AIAA Vol 13, No. 8 1975 pp. 995-1006.

Sehmi, N.S. A Newtonian Procedure for the solution of the Kron's characteristic value problem. Journal of Sound and Vibration, 100(3), pp. 409-421. 1985

Simpson, A. Kron's Method: A Consequence of the Minimisation of the Primitive Lagrangian in the Presence of Displacement Constraints. Journal of Sound and Vibration. 27(3) 1973 pp. 377-386.

Simpson, A. The Kron Methodology and Practical Algorithms for Eigenvalue, Sensitivity and Response Analyses of Large Scale Structural Systems. Aeronautical Journal, 84, 1980 pp. 417-433.

Simpson, A., Tabarrok, B. On Kron's Eigenvalue Procedure and Related Methods of Frequency Analysis. Quart. Journ. Mech. and Applied Maths, Vol. XXI pt.I 1968.

Sykes, A. Calculating the Vibratory Response of a Mechanical Structure in Terms of the Properties of its Substructures. Trans. ASME, Paper # 85-DET-183.

Thomas, D.L., Dynamics of Rotationally Periodic Structures. International Journal for Numerical Methods in Engineering. Vol. 14, 81-102 (1979).

Turner, G.L., Milsted, M.G., Hanks, P The adaptation of Kron's method for use with Large Finite-element models. Trans. ASME, Paper # 85-DET-183.

Wittrick, W.H. Williams, F.W. A general algorithm for computing natural frequencies of elastic structures. QJ Mech. App. Math. XXIV. pt 3. pp263-284. 1971.

Zhao, X. An Extension of Krons Method to an Undamped Spinning Structure. Finite Element News, Issue No. 2, 1988.

REFERENCES D

Vibration of Components & Numerical Methods

Arnold, R.N.
Warburton, G.
The Flexural Vibrations of Thin Cylinders
Proc. I.Mech.E. , Series A, Vol. 167, 1953, pp. 62-80

Arnold, R.N.
Warburton, G.
Flexural Vibrations of the Walls of Thin Cylindrical Shells Having Freely Supported Ends.
Proc. Royal Society , Series A, Vol. 197, 1949.

Buckens, F.
Influence of the Radial Thickness of a Ring on its Natural Frequencies. Journal Acoustical Society of America, Vol. 22, No. 1, pp. 137-140

Gourlay, A.R
Watson. G.A.
Computational Methods for Matrix Eigenproblems.
John Wiley and Sons. 1973.

Guyan, R.J.
Reduction of Stiffness and Mass Matrices.
AIAA Journal Vol. 3, pp. 380 , 1965.

Irons, B.
Eigenvalue Economisers in Vibration Problems
J. R. Aero. Soc., 67, pp526-528, 1963.

Leissa,
The Vibration of Shells. NASA Scientific Paper #288.

Love, A.E.H.
A Treatise on the Mathematical Theory of Elasticity.
Dover Publications, New York. 4th Edition, 1944

Przemieniecke, J.S.
Theory of Matrix Structural Analysis.
McGraw Hill, New York, 1968.

Rao, S.S. Effects of Transverse Shear and Rotatory Inertia On the Coupled Twist-Bending Vibrations of Circular Rings. Journal of Sound and Vibration. 1971, Vol 16(4), pp. 551-566.

Seidel, B.S.
Erdelyi, E.A. On the Vibrations of a Thick Ring in its Own Plane. Trans. ASME, Journal of Engineering for Industry. Aug. 1964, pp. 240-244.

Timoshenko, S. Theory of Elasticity. Van Nostrand, Reinhold 1956. New York & London.

Walker, J.H.
Rogers, G.J.
Jackson, R.L. Pressing and Clamping Laminated Cores. Proc. IEE. Vol. 111, No.3. March 1964.

White, J.C. The Flexural Vibrations of Thin Laminated Cylinders. Trans. A.S.M.E., Paper No. 60-WA-6.

Wilkinson, J.H. The Algebraic Eigenvalue Problem. Clarendon Press, Oxford. 1965

Appendix 1

THE REDUCTION OF COMPUTATIONAL EFFORT IN KRONS METHODS FOR EIGENVALUE/RESPONSE ANALYSES OF LARGE STRUCTURES

This paper was accepted for publication by the Journal *Computers and Structures* in May 1989).

Appendix 2

THE COMPUTATION OF THE EIGENSTATES OF SYSTEMS COMPRISING A NUMBER OF IDENTICAL SUBSTRUCTURES IDENTICALLY CONNECTED.

This paper was resubmitted for publication to the
International Journal for Numerical Methods in Engineering
in June 1989 in a revised form bearing the modified title:
The Computation of the Eigenstates of Periodic Systems.

Appendix 3

AN OPTIMAL METHOD FOR THE SOLUTION OF THE CONSTRAINED EIGENVALUE/RESPONSE PROBLEM FOR LARGE STRUCTURES COMPRISING A NUMBER OF RIGIDLY-CONNECTED SUBSTRUCTURES.

This paper was submitted for approval in a revised form to the
International Journal for Numerical Methods in Engineering
in April 1989 bearing the modified title:
An Optimal Method for the Solution of the Constrained Eigenvalue/Response Problem for Large Structures Using Rigidly-Connected Substructures.

Appendix 4

CONVOLUTION INTEGRALS FOR THE GENERATING FUNCTIONS FROM THE LINE/TRIG./HYP. SET

The functions from this set have the advantage that the convolution integrals necessary for the mass, stiffness and damping matrices can be expressed in a closed form. A subset of the relevant convolution integrals is presented here which covers all cases in which the object has symmetry (i.e. that the interval [p,q] is symmetrical). (All of the components used in examples in chapter 4 have regular symmetrical boundaries). Because of the symmetry of the intervals, the convolution of an antisymmetrical function with a symmetrical one must always be zero. The integrals are derived using integration- by-parts.

$$\int_p^q 1.1.dx = q - p$$

$$\int_p^q x.x.dx = \frac{1}{3}\left(q^3 - p^3\right)$$

$$\int_p^q 1.\cos(ax).dx = \left[\sin(ax)\right]_p^q$$

$$\int_p^q x.\sin(ax).dx = \frac{1}{a}\left[\frac{\sin(ax)}{a} - x.\cos(ax)\right]_p^q$$

$$\int_p^q 1.\cosh(ax).dx = \frac{1}{a}\left[\sinh(ax)\right]_p^q$$

$$\int_p^q x.\sinh(ax).dx = \frac{1}{a}\left[x.\cosh(ax) - \frac{\sinh(ax)}{a}\right]_p^q$$

$$\int_p^q \cos(ax).\cos(bx).dx = \frac{1}{2}\left[\frac{\sin((a-b).x)}{(a-b)} + \frac{\sin((a+b).x)}{(a+b)}\right]_p^q \quad (a \neq b)$$

$$\int_p^q \cos^2(ax).dx = \frac{1}{2}\left[1 + \frac{\sin(2a.x)}{2a}\right]_p^q$$

$$\int_p^q \sin(ax).\sin(bx).dx = \frac{1}{2}\left[\frac{\sin((a-b).x)}{(a-b)} - \frac{\sin((a+b).x)}{(a+b)}\right]_p^q \quad (a \neq b)$$

$$\int_p^q \sin^2(ax).dx = \frac{1}{2}\left[1 - \frac{\sin(2a.x)}{2a}\right]_p^q$$

$$\int_p^q \cos(ax).\cosh(bx).dx = \frac{1}{\left(a^2 + b^2\right)}\left[a.\left(\sin(ax).\cosh(bx)\right) + b.\left(\cos(ax).\sinh(bx)\right)\right]_p^q$$

$$\int_p^q \sin(ax).\sinh(bx).dx = \frac{1}{\left(a^2 + b^2\right)}\left[b.\left(\sin(ax).\cosh(bx)\right) - a.\left(\cos(ax).\sinh(bx)\right)\right]_p^q$$

$$\int_p^q \cosh(ax).\cosh(bx).dx = \frac{1}{\left(a^2 - b^2\right)}\left[a.\left(\cosh(ax).\sinh(bx)\right) - b.\left(\sinh(ax).\cosh(bx)\right)\right]_p^q \quad (a \neq b)$$

$$\int_p^q \cosh^2(ax).dx = \frac{1}{2}\left[\frac{\left(\cosh(ax).\sinh(ax)\right)}{a} + x\right]_p^q$$

$$\int_p^q \sinh(ax).\sinh(bx).dx = \frac{1}{\left(a^2 - b^2\right)}\left[a.\left(\sinh(ax).\cosh(bx)\right) - b.\left(\cosh(ax).\sinh(bx)\right)\right]_p^q \quad (a \neq b)$$

$$\int_p^q \sinh^2(ax).dx = \frac{1}{2}\left[\frac{\left(\cosh(ax).\sinh(ax)\right)}{a} - x\right]_p^q$$

Appendix 5

EQUATIONS FOR STRAIN IN POLAR COORDINATES

In the derivation of expressions for stiffness and inertia in discs, cylinders and rings - and portions of these elements - it is necessary to use cylindrical-polar strain terms and to relate these to polar deflection coordinates. The equations below give the relations.

$$\varepsilon_{\theta\theta} = (1/r) \,.\, (u + (dv/d\theta)) \quad (1)$$

$$\varepsilon_{rr} = (du/dr) \quad (2)$$

$$\varepsilon_{zz} = (dw/dz) \quad (3)$$

$$\varepsilon_{\theta r} = (1/r).((dv/dr) - v + (du/d\theta)\,) \quad (4)$$

$$\varepsilon_{rz} = (du/dz) + (dw/dr) \quad (5)$$

$$\varepsilon_{z\theta} = ((dv/dz) + (dw/d\theta)/r) \quad (6)$$

Displacement coordinates u,v,w correspond to unit deflections in the radial, circumferential and axial directions respectively. Polar position coordinates r,θ,z have their usual meaning for a cylindrical polar coordinate set.

Appendix 6

THE STIFFNESS OF CYLINDERS OF FINITE LENGTH IN AXIALLY UNIFORM SHAPES OF DEFORMATION

Plane models of cylinders in vibration are restricted to the examintaion of deformation shapes for which the radial and circumferential displacements are dependent only on the angular position coordinate θ. When the cylinder is axially short, it is justifiable to assume that the normal stress σ_{zz} is zero throughout the cylinder at all times. The cylinder dimensions appropriate to the modelling of electrical motors do not generally satisfy the shortness criterion. Hence estimates of the stiffness of the deformations are lower than the real stiffness.

The extent of the error is evaluated here and a simple correction factor is presented which is dependent upon the material constants as well as the physical dimensions of the cylinder.

Consider a uniform cylinder with inside radius r_i, outside radius r_o, and length 2l. Two translations, U,V, and one rotation, W, are evaluated at the neutral layer ($r=r_n$). $U(z,\theta)$ is defined as the radial translation of the particle on the neutral layer at z,θ. $V(z,\theta)$ is defined as the circumferential translation of the particle on the neutral layer at z,θ. $W(z,\theta)$ is the rotation of the radial fibre at z,θ. W is positive when the outside end of the fibre moves in the direction of $+z$ at $\theta=0$. For simplicity, it is assumed that no extension occurs at the neutral layer of the cylinder and no shear deformation occurs in the r,θ or r,z planes. These assumtions themselves tend to break down as the radial thickness (r_o-r_i) and the n - the number of wave-lengths about the circumference - increases. If these assumptions are no longer valid then one might as well use a full cylinder model as attempt to incorporate the necessary extra generality to the ring model.

There are three position coordinates r, θ and z having the usual definitions for the cylindrical-polar coordinate system. The three point displacement coordinates u,v and w are translations of the material particle at r,θ,z in the radial, circumferential and axial directions respectively. We consider the simple case where . . .

$$u = U \cos(n\theta) \tag{1}$$

$$v = (V + (r-r_n).U/r_n).\ \sin(n\theta) \tag{2}$$

$$w = W.(z/l).((r-r_n)/(r_o-r_i)).\ \cos(n\theta) \tag{3}$$

The assumption of inextension at the neutral layer (in the circumferential direction) leads to an expression for V in terms of U and n .

$$V = -\ U/n \tag{4}$$

The normal stresses $\varepsilon_{\theta\theta}$ and ε_{zz} are simply . . .

$$\varepsilon_{\theta\theta} = U.n.((r-r_n)/r_n^2)\ \cos(n\theta) \tag{5}$$

$$\varepsilon_{zz} = W.\ ((r-r_n)/\ l.(r_o-r_i))\ \cos\ (n\theta) \tag{6}$$

The shear-stress ε_{rz} depends on W, z as . . .

$$\varepsilon_{rz} = W.\ z\ /\ l.(r_o-r_i) \tag{7}$$

Now, the stress-strain relations are defined as . . .

$$\sigma_{\theta\theta} = E_{\theta\theta}.\ \varepsilon_{\theta\theta} + E_{\theta z}.\ \varepsilon_{zz} \tag{8}$$

$$\sigma_{zz} = E_{\theta z}.\ \varepsilon_{\theta\theta} + E_{zz}.\ \varepsilon_{zz} \tag{9}$$

$$\sigma_{rz} = G_{rz}.\ \varepsilon_{rz} \tag{10}$$

The constants $E_{\theta\theta}$, $E_{\theta z}$ and E_{zz}. are the material elastic constants for normal stresses and strains. For isotropic materials, they are derived directly from the Young's modulus and Poisson's ratio. For laminated

stacks, a derivation is presented in chapter 5 relating the normal stress/strain constants to those of the solid material and a single property of the laminated stack. There are only two degrees of freedoms determining the cylinder deformed shape - U and W . The stiffness of the shape - K - can be simply derived using energy arguments by integrating the energy-per-unit-volume over the complete volume of the cylinder. The integral of $\cos^2(n\theta)$ over the interval $\theta=0,2\pi$ is simply π and it is convenient to define the integral I as . . .

$$I = \int r.(r-r_n)^2 \, dr \quad \text{. . . between limits } r_i \text{ and } r_o \text{ .} \qquad (11)$$

For the plane-stress (or "ring") model, there is an inbuilt assumption that σ_{zz} equals zero. In this case, the estimated strain energy $S.E._1$ of the deformation of the cylinder is given by

$$S.E._1 = I.2l.\pi.[E_{\theta\theta}\,(1-E_{qz}{}^2/(E_{\theta\theta}.E_{zz}))\;\;((n-1)/r_n{}^2)^2]\;U^2 \qquad (12)$$

For the more general "plane" model of the cylinder, the equation below gives the expression for the strain energy.

$$\begin{aligned} S.E._2 = I.2l.\pi.\; & [E_{\theta\theta}.((n-1)/r_n{}^2)^2\,U^2 \\ & + 2.E_{\theta z}.((n-1)/l.(r_o-r_i).r_n{}^2).U.W \\ & + E_{zz}.(1/l.(r_o-r_i))^2\,W^2] \\ & + (l.(r_o{}^2-r_i{}^2)\,\pi\,/\,3.(r_o-r_i)^2).\,G_{rz}.W^2] \end{aligned} \qquad (13)$$

This expression is useful in comparing the stiffness which would be estimated using a plane-stress model with that caluclated using a more general and correct model.

Utilising this expression in conjunction with the experimentally derived values for effective shear and compressive modulii of laminated stacks shows that in typical cases of laminated stator-cores for AC machines, a plane-stress model will be quite accurate for the axially-uniform modes of vibration where it would not be if the mechanical material properties of the core were similar to those of solid steel.

EXAMPLE: Consider a cylinder with dimensions and material constants (mild-steel) below.

r_o	= 0.55 m	$E_{\theta\theta}$	= 2.275e11 N/m^2
r_i	= 0.50 m	$E_{\theta z}$	= 6.483e10 N/m^2
r_n	= 0.5254 m	E_{zz}	= 2.275e11 N/m^2
l	= 0.25 m	G_{rz}	= 8.127e10 N/m^2

For the axially-uniform displacement pattern $u=\cos(2\theta)$, the strain energy of this shape would be calculated as $S.E._1$=94.2 MJ if the plane-stress assumption were used.

Now, relaxing the plane-stress assumption we get . . .

$$S.E._2 = 102.5e6 + 322.6e6\ W + 1.1481e9\ W^2 + 2.362e12\ W^2$$

(Terms from normal-stress & strain) (Term from shear stress & strain)

Differentiating to find the value of W which makes K a minimum gives. . .

$$W = -6.83e\text{-}6\ m, \qquad w(z,\theta) = -6.83e\text{-}6\ (z/l)\ \cos(2\theta)\ m$$

Hence $S.E._2$ =100.3e6 MJ.

The original estimate was too low by 6.1%. Had a plane-strain model been used instead of the plane-stress model, the computed stiffness would have been 102.5e6 N/m which would be too high by 2.2%.

Appendix 7

THE FLEXIBILITY ADDED BY SEGMENTATION

It is shown in chapter 5 that successive laminations in electrical machines can move with respect to each other (in a way that does not require them to 'slip') to such an extent that the properties of a stack of laminations differs vastly from those of solid steel. Ring theory applies directly to laminated stator-cores when each of the laminations is a complete ring. The optimum use of material (and physical limitations on the sizes of punch available to manufacturers) often dictate that the core be segmented as discussed in chapter 1. Each layer of segments overlaps the gaps left in the layer before and after it. In the light of the test results from chapter 5, one might expect that the flexibility of the laminated stack in shear would contribute to the flexural and extensional flexibility of the segmented laminated ring.. This appendix presents a simple approximate expression for the flexibility added by the segmentation. The evaluation of this expression for a typical set of values shows that in that particular case, segmentation makes very little difference. However, it is also clear that using shorter segment arcs and thicker laminations can lead to cases where the flexibility of a laminated ring in flexure is dominated by the segmentation effects.

Flexibility Added To The Circumferential Flexure.

Fig. 1 shows two overlapping segments **A** and **B**. We shall look at the two extreme cases of how these segments can deflect to yield an angle a at the 'free' ends of A and B .

CASE 1 : The 'pure-flexure' shape involves segments **A** and **B** bending in the plane. There is no relative motion between **A** and **B** in this case.

CASE 2 : The 'pure-shear' shape involves segments **A** and **B** rotating in the plane about the center-of-area of the common-area. There is no

deformation of either **A** and **B** in this case.

The following terms are used.

E	Youngs' modulus for the lamination steel. (N/m^2)
C	The constant relating shear stress at the interlaminar layer to the relative shear deflection. (N/m^3)
M_1	The moment at the segment ends :- case 1.
M_2	The moment at the segment ends :- case 2.
t	The thickness (m) of the laminations (the smallest dimension).
d	The radial depth (m) of the segments.
r	The mean radius (m) of the segments.
l	The mean circumferential length of the overlap.
θ_s	The angle of overlap of the segments.

$$l = r.\theta_s \qquad (1)$$

In deriving M_1, we consider the net stress at each point on the interface which acts in a direction normal to the line between the center of the overlap area and the point itself using straightforward second moment of area reasoning, the total restoring moment M_1 is computed as . . .

$$M_1 = 2\ C\ l.d\ ((d^2+l^2)/1^2)\ 2.\alpha \qquad (2)$$

In deriving M_2, we assume that the angle of deflection varies linearly between points 1 and 2. (ie. the moment in the section is constant). The rate of change of angle with respect to position on the middle line of the ring is $2.\alpha/l$ and the moment M_2 is given by . .

$$M_2 = 2\ E.t\ (d^3/12)\ 2.\alpha/l \qquad (3)$$

Now the ratio M_2/M_1 for any angle α, is a useful indication for the effect of segmentation. We call this ratio "S_{flex}".

$$S_{flex} = (E.t/C.l^2).(d^2/(d^2+l^2)) \qquad (4)$$

The stiffness of the ring as computed ignoring the segmentation effect is

divided by (1+ S_{flex}) to find the true stiffness. Small S_{flex} means that the segmentation has little effect.

Inserting the following real values, gives a sample of the value of S_{flex} which can be expected.

E= 209e9 N/m^2 X = 1.5e12 N/m^3 t= 6.5e-4 m
d= 0.1 m r= 0.4 m l= 0.42 m S_{flex}= 2.75e-5

Flexibility Added To The Circumferential Extension.

Now, the flexibility of a segmented laminated ring in extension is also affected. Again we examine two extreme cases. In one case the motion "δ" (see Fig. 1) at either side of the overlap is taken up by pure shear. In the other case, "δ" is taken up by pure extension of the segments. As before, case 1 involves no deformation of the segments. Case 2 involves deformation but no interlaminar shear. N_1 is the force which would exist in the segments if case 1 were to occur. N_2 would be the force if case 2 were to occur.

N_1 and N_2 can be derived in terms of the translation at the ends and the ratio N_2/ N_1 is called S_{ext}.

$$N_1 = 2 X\ d.l\ 2.\delta \qquad (5)$$

$$N_2 = 2\ E.t\ d\ \ 2.\delta / l \qquad (6)$$

$$S_{ext} = E.t / X\ l^2 \qquad (7)$$

For the above set of parameters, S_{ext} is evaluated to be 5.13e-4

As before, the extensional stiffness of the ring must be scaled down by $(1+S_{ext})$ to account for the segmentation. Clearly the effects of segmentation on the flexibility of laminated cores in both extensional and flexural deformations is negligible.

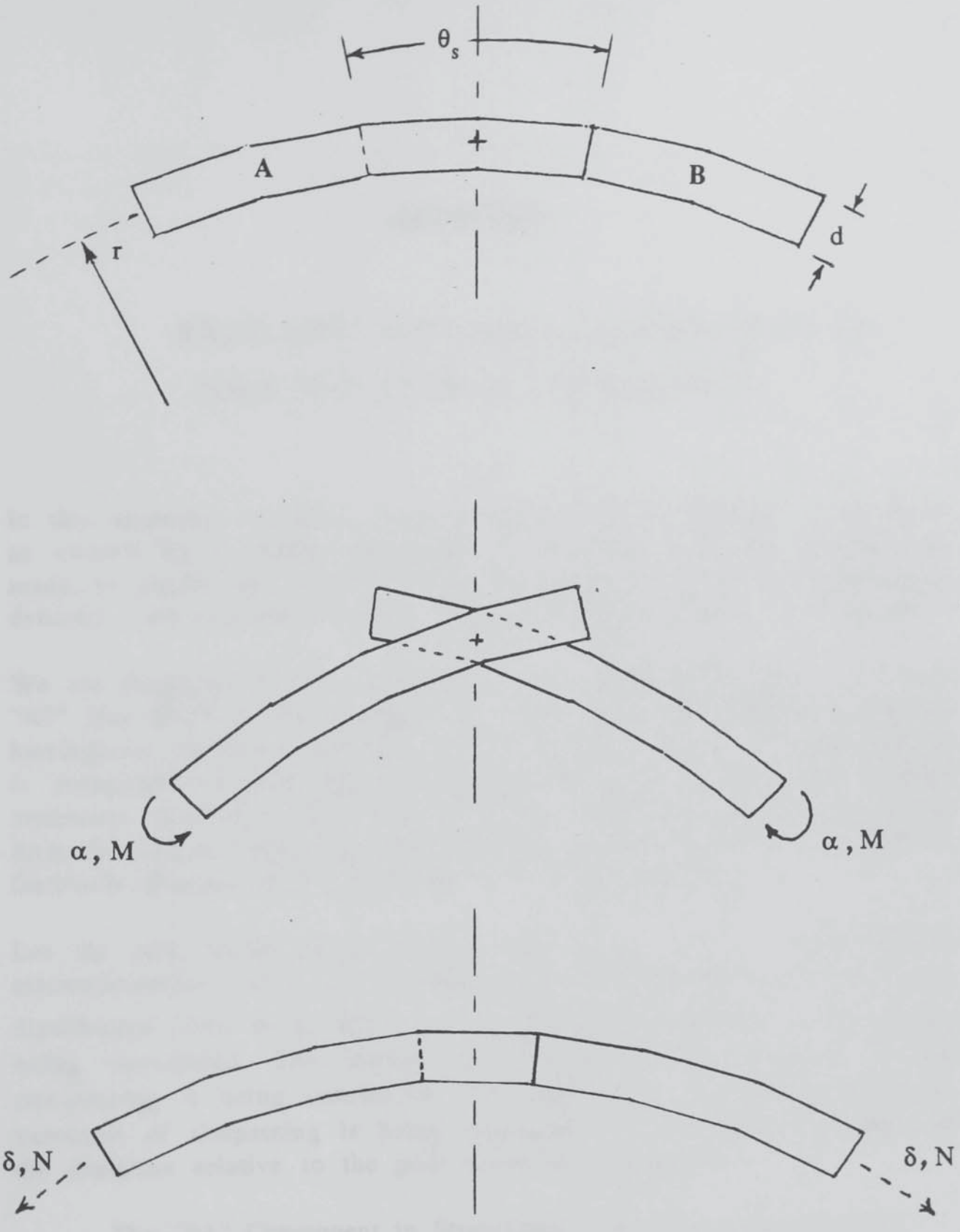

Fig. 1 Adjacent Pair of Segments.
(Showing Flexure and Extension Flexibility)

Appendix 8

RESOLVING THE AXIAL DISTRIBUTION OF POLE FORCES INTO COMPONENTS

In this appendix, we break down the forcing on a mainpole or compole as caused by a skewed armature. In keeping with the assumptions made to model the poles (i.e. that cross-sections do not themselves deform) , the resultant for each infinitesimal axial section is examined.

We are interested in three component axial distributions "A0", "A1" and "A2" (see §9.1). In the (unattainable) case where the skewing is perfect, herringbone skewed armatures produce a force pattern on poles which is composed of two pure sinusoid forms while straightline skewed armatures produce a force pattern which comprises a single sinusoidal form. In each of these cases, the component of "A0" is zero. Thus "A0" is forthwith dropped from consideration in this appendix.

Let the pole length be l. The force-per-metre (be it a radial force, circumferential force or moment) is F_0. The phase of the force distribution itself is θ, and z is the axial position of the cross-section being considered. The integer m indicates which harmonic of the slot-passing is being considered. The angle θ is determined by which harmonic of slotpassing is being examined and the angular position of the armature relative to the pole under consideration.

The "A1" Component in Straightline Skew Force Distributions.

Only the straightline skew is capable of producing the component "A1" to a 'first-order' extent. An unskewed or herringbone-skewed armature can produce small components of "A1" if the pole alignment is not

perfectly axial but this is not considered here. Fig. 1 shows the force distribution over a pole due to the straightline skew for four instances of armature angle. At the instant in time when the forcing of "A1" is a maximum, the force at any section z, is given by (1) below.

$$F(z) = F_o \sin(2m \pi z / l) \qquad (1)$$

Integer m is the number of slot-pitches by which the armature is skewed (or in other words, m is the number of waves of the force distribution along the length of the pole).

The coefficient of "A1" in this distribution is given by (2).

$$\text{Coefficient-of-"A1"} = \int (z/l).\sin(2m \pi z/l)\, dz \; / (l^2/3) \qquad (2)$$

The integral is evaluated using integration by parts and the general result is obtained for an integer value of m

$$\text{Coefficient-of-"A1"} = (3/(\pi.m)) \qquad (3)$$

The sign is "+" for <u>odd</u> values of m and "-" for <u>even</u> values of m.
The table below gives the results for various values of m.

m	Coefficient-of-"A1
1	0.955
2	0.477
3	0.318
4	0.239

Coefficients of the axial distribution "A1"
from straightline skew (m slot-pitches).

The "A2" Component in Herringbone Skew Force Distributions.

Fig. 2 shows the force patterns caused by a herringbone skewed armature at two instants in time. Only the second of these has a component of the "A2" distribution. The force acting on any section z at this instant, is given by (4) below.

$$F(z) = F_0 \sin(-4m\pi z/l) \quad \ldots \text{if } z > 0$$
$$= F_0 \sin(+4m\pi z/l) \quad \ldots \text{if } z < 0 \qquad (4)$$

The coefficient of "A2" is defined by (5).

$$\text{Coefficient-of-"A2"} = \int \cos(\alpha)\ \sin(2m\alpha)\ .d\alpha\ /\ (\pi/2) \qquad (5)$$

Evaluating this for various values of m gives the table below.

m	Coefficient-of-"A2"
1	0.849
2	0.440
3	0.218
4	0.162

Coefficients of "A2" from the Herringbone Force Distribution.

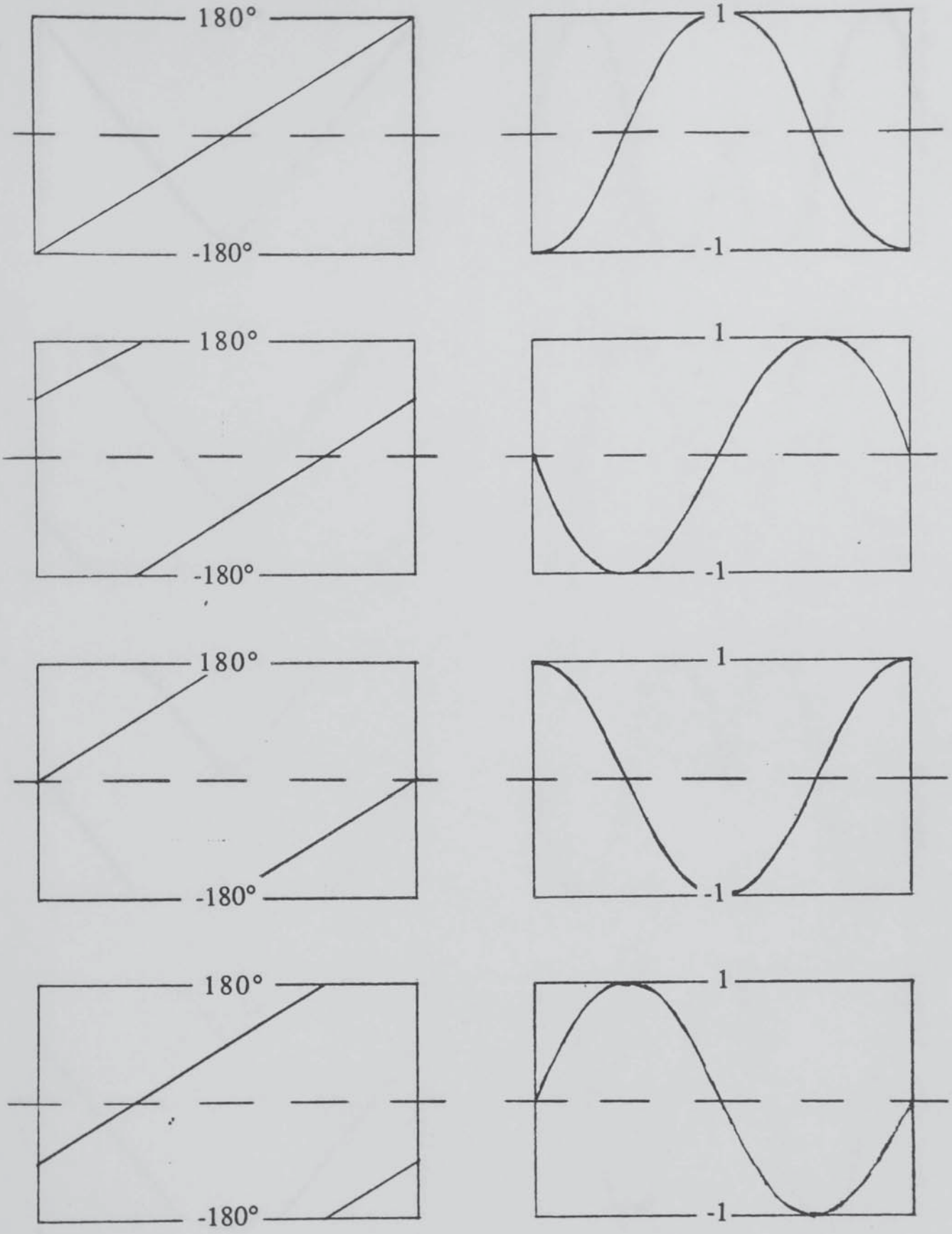

Fig. 1 Phase Angle of Forcing and Actual Value of the Force at 4 Equally-Spaced Instants STRAIGHTLINE SKEW.

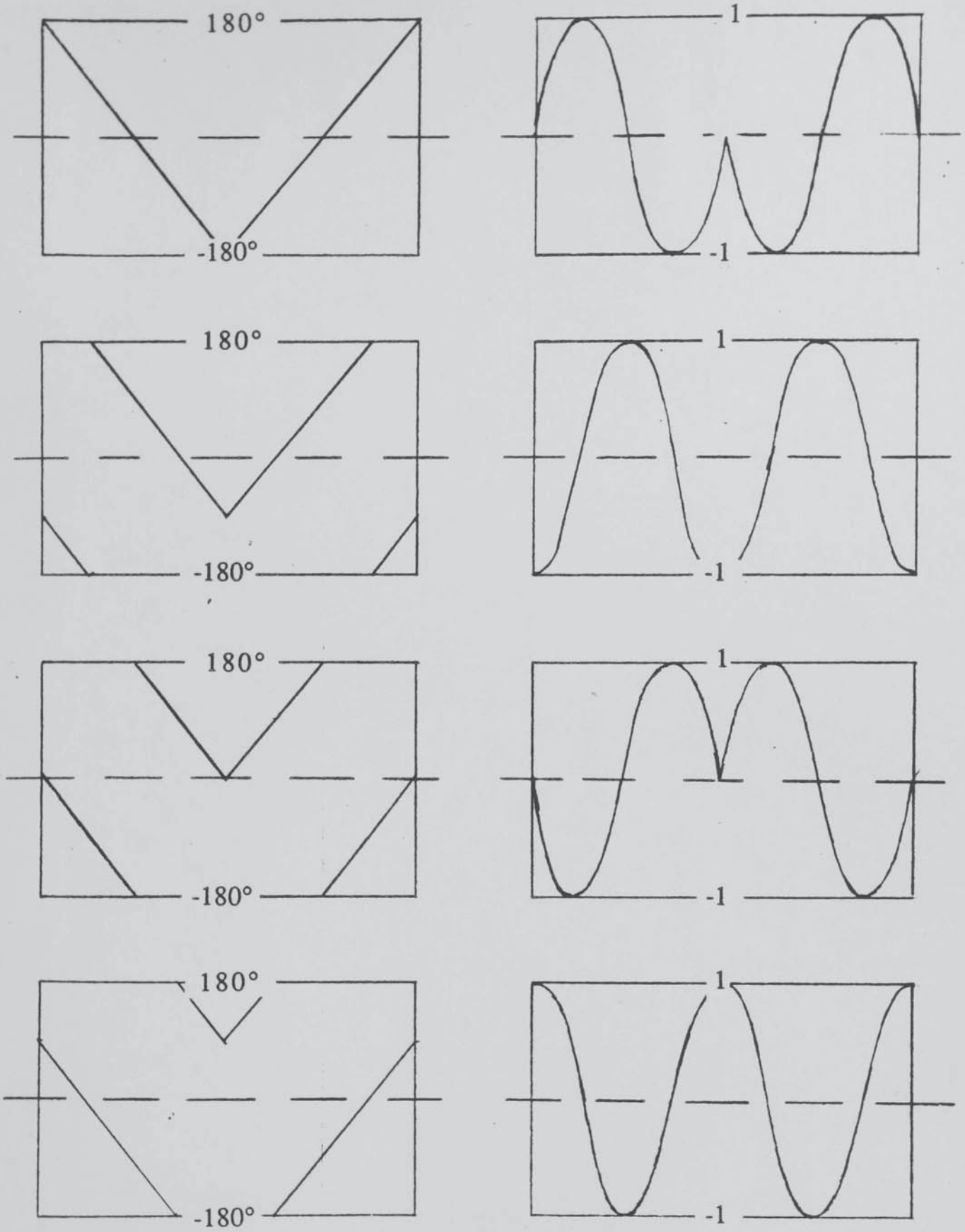

Fig. 2 Phase Angle of Forcing and Actual Value of the Force at 4 Equally-Spaced Instants HERRINGBONE SKEW.